



US Army Corps  
of Engineers

AD-A230 279



TECHNICAL REPORT GL-87-14

2

# SEISMIC STABILITY EVALUATION OF FOLSOM DAM AND RESERVOIR PROJECT

## REPORT 4

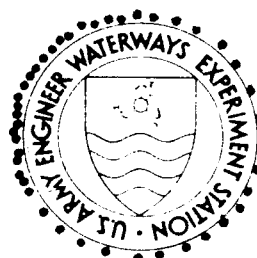
### MORMON ISLAND AUXILIARY DAM - PHASE I

by

Mary E. Hynes, Ronald E. Wahl  
Robert T. Donaghe, Takashi Tsuchida

Geotechnical Laboratory

DEPARTMENT OF THE ARMY  
Waterways Experiment Station, Corps of Engineers  
3909 Halls Ferry Road, Vicksburg, Mississippi 39180-6199



December 1990

Report 4 Update



Approved for Public Release; Distribution Unlimited

Prepared for US Army Engineer District, Sacramento  
Sacramento, California 95814

When this report is no longer needed return it to  
the originator.

The findings in this report are not to be construed as an  
official Department of the Army position unless so  
designated by other authorized documents.

The contents of this report are not to be used for  
advertising, publication, or promotional purposes.  
Citation of trade names does not constitute an  
official endorsement or approval of the use of such  
commercial products.

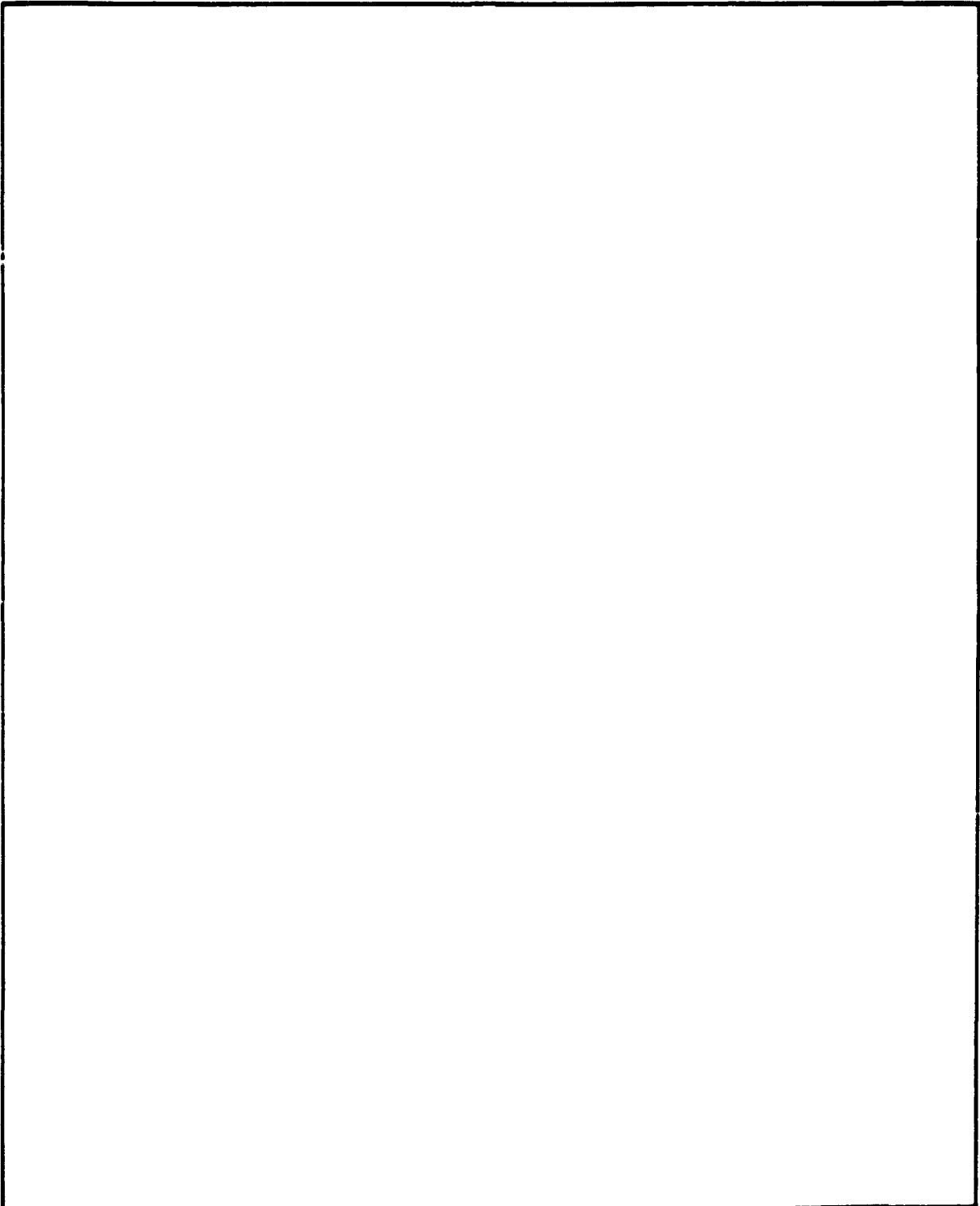
Unclassified

Form Approved  
OMB No. 0704-0188

1a. REPORT SECURITY CLASSIFICATION Unclassified			1b. RESTRICTIVE MARKINGS		
2a. SECURITY CLASSIFICATION AUTHORITY			3. DISTRIBUTION / AVAILABILITY OF REPORT Approved for public release; distribution unlimited.		
2b. DECLASSIFICATION / DOWNGRADING SCHEDULE					
4. PERFORMING ORGANIZATION REPORT NUMBER(S) Technical Report GL-87-14			5. MONITORING ORGANIZATION REPORT NUMBER(S)		
6a. NAME OF PERFORMING ORGANIZATION USAEWES Geotechnical Laboratory		6b. OFFICE SYMBOL (If applicable) WESGH	7a. NAME OF MONITORING ORGANIZATION		
6c. ADDRESS (City, State, and ZIP Code) 3909 Halls Ferry Road Vicksburg, MS 39180-6199			7b. ADDRESS (City, State, and ZIP Code)		
8a. NAME OF FUNDING / SPONSORING ORGANIZATION US Army Engineer District, Sacramento		8b. OFFICE SYMBOL (If applicable) SPKED	9. PROCUREMENT INSTRUMENT IDENTIFICATION NUMBER		
8c. ADDRESS (City, State, and ZIP Code) 650 Capital Mall Sacramento, CA 95814			10. SOURCE OF FUNDING NUMBERS		
			PROGRAM ELEMENT NO.	PROJECT NO.	TASK NO.
			WORK UNIT ACCESSION NO.		
11. TITLE (Include Security Classification) SEISMIC STABILITY EVALUATION OF FOLSOM DAM AND RESERVOIR PROJECT; Report 4: Mormon Island Auxiliary Dam - Phase I					
12. PERSONAL AUTHOR(S) Hynes, Mary E., Wahl, Ronald E., Donaghe, Robert T. and Tsuchida, Takashi					
13a. TYPE OF REPORT Report 4 of a Series		13b. TIME COVERED FROM 1982 TO 1988		14. DATE OF REPORT (Year, Month, Day) December 1990	
				15. PAGE COUNT 319	
16. SUPPLEMENTARY NOTATION Available from National Technical Information Service, 5285 Port Royal Road, Springfield, VA 22161.					
17. COSATI CODES			18. SUBJECT TERMS (Continue on reverse if necessary and identify by block number)		
FIELD	GROUP	SUB-GROUP			
			Folsom Dam (Calif.)		
			Earthquakes and hydraulic structures		
			Dam safety		
19. ABSTRACT (Continue on reverse if necessary and identify by block number) The man-made water retaining structures at the Folsom Dam and Reservoir Project, located on the American River about 20 miles upstream of the City of Sacramento, Calif., have been evaluated for their seismic safety in the event of a Magnitude 6.5 earthquake occurring on the East Branch of the Bear Mountains Fault Zone at a distance of about 15 km. This report documents the Phase I study of Mormon Island Auxiliary Dam, one of the zoned embankment dams at the Folsom Project. The evaluation process involved extensive review of construction records, field and laboratory investigations, and analytical studies. It has been determined that Mormon Island Auxiliary Dam will not perform satisfactorily. Remedial or hazard-mitigating action is recommended. A Phase II study which consists of additional field investigation and analyses to determine the lateral extent of remedial action necessary is documented in Report 8 of this series.					
20. DISTRIBUTION / AVAILABILITY OF ABSTRACT <input checked="" type="checkbox"/> UNCLASSIFIED / UNLIMITED <input type="checkbox"/> SAME AS RPT <input type="checkbox"/> DTIC USERS			21. ABSTRACT SECURITY CLASSIFICATION Unclassified		
22a. NAME OF RESPONSIBLE INDIVIDUAL			22b. TELEPHONE (Include Area Code)		22c. OFFICE SYMBOL

Unclassified

SECURITY CLASSIFICATION OF THIS PAGE



Unclassified

SECURITY CLASSIFICATION OF THIS PAGE



## PREFACE

The US Army Engineer Waterways Experiment Station (WES) was authorized to conduct this study by the US Army Engineer District, Sacramento (SPK), by Intra-Army Order for Reimbursable Services Nos. SPKED-F-82-2, SPKED-F-82-11, SPKED-F-82-34, SPKED-F-83-15, SPKED-F-83-17, SPKED-F-84-14, and SPKED-D-85-12. This report is one in a series of reports which document the seismic stability evaluations of the man-made water retaining structures of the Folsom Dam and Reservoir Project, located on the American River in California. The Reports in this series are as follows:

- Report 1: Summary
- Report 2: Interface Zone
- Report 3: Concrete Gravity Dam
- Report 4: Mormon Island Auxiliary Dam - Phase I
- Report 5: Dike 5
- Report 6: Right and Left Wing Dams
- Report 7: Upstream Retaining Wall
- Report 8: Mormon Island Auxiliary Dam - Phase II

ADA 201328

The work on these reports is a joint endeavor between SPK and WES. Messrs. John W. White and John S. Nickell, of Civil Design Section 'A', Civil Design Branch, Engineering Division (SPKED-D) at SPK were the overall SPK project coordinators. Messrs. Gil Avila and Matthew G. Allen, of the Soil Design Section, Geotechnical Branch, Engineering Division (SPKED-F) at SPK, made critical geotechnical contributions to field and laboratory investigations. Support was also provided by the South Pacific Division Laboratory. The WES Principal Investigator and Research Team Leader was Dr. Mary E. Hynes of the Earthquake Engineering and Geophysics Division (EEGD), Geotechnical Laboratory (GL), WES. Primary Engineers on the WES team for the portion of the study documented in this report were Mr. Ronald E. Wahl, (EEGD) and Mr. Takashi Tsuchida, on temporary assignment to WES from the Port and Harbour Research Institute, Yokosuka, Japan. Geophysical support was provided by Mr. Jose Llopis, EEGD. Additional engineering support was provided by Mr. Richard S. Olsen, EEGD. Large-scale laboratory investigations were conducted by Mr. Robert T. Donaghe of the Soil Mechanics Division (SMD), GL, WES. Laboratory instrumentation services were provided by Mr. Thomas V. McEwen, of the Data Acquisition Section, Instrumentation Services Division.

Mr. W. L. Hanks, (SMD), Mr. C. Schneider, (SMD), Mr. B. L. Washington of the Engineering Geology and Rock Mechanics Division (EGRMD), GL, WES, Mr. M. H. Seid (EEGD), and Mr. T. Cho (EEGD) assisted in preparation of figures. Key contributions also were made by Dr. Leslie F. Harder, Jr., of Sacramento, California; Professor Shobha Bhatia, Syracuse University; and Professor David Elton, Auburn University.

Professors H. Bolton Seed, Anil K. Chopra, and Bruce A. Bolt of the University of California, Berkeley; Professor Clarence R. Allen of the California Institute of Technology; and Professor Ralph B. Peck, Professor Emeritus of the University of Illinois, Urbana, served as Technical Specialists and provided valuable guidance during the course of the investigation.

Overall direction at WES was provided by Dr. A. G. Franklin, Chief, EEGD, and Dr. W. F. Marcuson III, Chief, GL.

COL Larry B. Fulton, EN, is Commander and Director of WES. Dr. Robert W. Whalin is Technical Director.

<b>Accession For</b>	
NTIS GRA&I	<input checked="" type="checkbox"/>
DTIC TAB	<input checked="" type="checkbox"/>
Unannounced	<input type="checkbox"/>
Justification	
By	
Distribution/	
Availability Codes	
Dist	Avail and/or Special
A-1	



# CONTENTS

	<u>Page</u>
PREFACE.....	1
CONVERSION FACTORS, NON-SI TO SI (METRIC)	
UNITS OF MEASUREMENT.....	5
PART I:    INTRODUCTION.....	6
General.....	6
Project History.....	7
Hydrology and Pool Levels.....	7
Description of Mormon Island Auxiliary Dam.....	8
Site Geology.....	9
Dredging Deposition Process.....	10
Seismic Hazard Assessment.....	11
Seismological and geological investigations.....	11
Selection of design ground motions.....	14
PART II:    REVIEW OF CONSTRUCTION RECORDS.....	16
General.....	16
Exploration and Sampling During Original Design and	
Initial Construction.....	16
Foundation Preparation at Mormon Island Auxiliary Dam.....	17
Laboratory Tests During Original Design and Initial	
Construction.....	19
Embankment Materials.....	21
PART III:    FIELD INVESTIGATIONS PERFORMED FOR THIS STUDY.....	22
General.....	22
SPT Results in Core and Filter Zones.....	22
Geophysical Tests.....	23
Surface vibratory tests.....	24
Crosshole tests and interpreted velocity profiles.....	25
Test Pits in Foundation Gravels.....	27
Test Shaft in Downstream Shell.....	29
Becker Hammer Tests.....	29
Summary.....	31
PART IV:    LABORATORY INVESTIGATIONS AND	
ESTIMATES OF CYCLIC STRENGTH.....	33
General.....	33
Estimates of Cyclic Strength from In Situ Tests.....	33
Empirical procedure to estimate cyclic strength.....	33
Cyclic strength estimate for shell gravels, Zones 1 and 2....	34
Cyclic strength estimates for foundation gravels.....	35
Cyclic strength estimates of Zone 3 filter	
and Zone 4 core materials.....	36
Relative Cyclic Strength Behavior from Laboratory	
Investigations.....	37
Adjustments to cyclic strength and residual excess	
pore pressures.....	37
Selection of laboratory gradations and densities.....	38
Effective stress strengths and cyclic strength estimates.....	39

	<u>Page</u>
Adjustment factors $K_\sigma$ and $K_\alpha$ .....	40
Comparison of in situ and laboratory cyclic strengths.....	40
Safety factors against liquefaction and residual excess pore pressures.....	41
PART V:     STATIC FINITE ELEMENT ANALYSIS.....	43
General.....	43
Section Idealization and Static Finite Element Inputs.....	43
Results of Static Analysis.....	45
PART VI:     DYNAMIC FINITE ELEMENT ANALYSIS.....	47
General.....	47
Description of FLUSH.....	47
Inputs to FLUSH.....	47
Dynamic Response Results.....	49
PART VII:    LIQUEFACTION POTENTIAL EVALUATION.....	52
General.....	52
Safety Factors Against Liquefaction in Embankment Shell and Foundation.....	52
Residual Excess Pore Pressures.....	53
Liquefaction Potential Evaluation of Zone 4 Core and Zone 3 Filter Materials.....	54
Effective Stress Response and Liquefaction Potential Analyses....	54
Summary.....	54
PART VIII:   STABILITY EVALUATION.....	55
Postearthquake Slope Stability.....	55
Permanent Deformation Estimates.....	56
Stability Evaluation.....	57
PART IX:     SUMMARY AND CONCLUSIONS.....	58
REFERENCES.....	60
TABLES 1-7	
FIGURES 1-81	
APPENDIX A:   EVALUATION OF BECKER PENETRATION TESTS PERFORMED AT MORMON ISLAND AUXILIARY DAM IN 1983.....	A1
APPENDIX B:   LABORATORY TESTS ON GRAVEL SPECIMENS.....	B1

CONVERSION FACTORS, NON-SI TO SI (METRIC)  
UNITS OF MEASUREMENT

Non-SI units of measurement used in this report can be converted to SI (metric) units as follows:

<u>Multiply</u>	<u>By</u>	<u>To Obtain</u>
acre-feet	1,233.489	cubic metres
cubic feet	0.02831685	cubic metres
cubic yards	0.7645549	cubic metres
degrees (angle)	0.01745329	radians
feet	0.3048	metres
feet per mile	0.1893935	metres per kilometre
inches	2.54	centimetres
kips (force) per square foot	47.88026	kilopascals
miles (US statute)	1.609347	kilometres
pounds (force) per square foot	47.88026	pascals
pounds (force) per square inch	6.894757	kilopascals
square miles	2.589998	square kilometres
yards	0.9144	metres

## SEISMIC STABILITY EVALUATION OF FOLSOM DAM AND RESERVOIR PROJECT

### Report 4: Mormon Island Auxiliary Dam - Phase I

#### PART I: INTRODUCTION

##### General

1. This report is one of a series of reports that documents the investigations and results of a seismic stability evaluation of the man-made water retaining structures at the Folsom Dam and Reservoir Project, located on the American River in Sacramento, Placer and El Dorado Counties, California, about 20 airline miles\* northeast of the City of Sacramento. This seismic safety evaluation was performed as a cooperative effort between the US Army Engineer Waterways Experiment Station (WES) and the US Army Engineer District, Sacramento (SPK). Professors H. Bolton Seed, Anil K. Chopra, and Bruce A. Bolt of the University of California, Berkeley, Professor Clarence R. Allen of the California Institute of Technology, and Professor Ralph B. Peck, Professor Emeritus of the University of Illinois, Urbana, served as Technical Specialists for the study. This report documents Phase I of the seismic stability studies of Mormon Island Auxiliary Dam, a zoned embankment dam at the Folsom project. A location map and plan of the project are shown in Figures 1 and 2.

2. Mormon Island Auxiliary Dam may be divided into three segments according to foundation conditions -- the core is founded on rock along the entire length of the dam, but the shells are founded either on rock, on undisturbed alluvium, or on very loose dredged tailings. The Phase I study consists of a detailed review of construction records, field and laboratory investigations, and analytical studies of the segment of the dam with shells founded on dredged tailings to estimate the response of the embankment dam and its foundation to earthquake shaking, to determine the susceptibility of the soils to liquefaction, and to assess the stability of the dam slopes during and immediately after the design seismic event. These studies and the

---

\* A table of factors for converting non-SI units of measurement to SI (metric) units is presented on page 5.

conclusions drawn concerning the seismic stability of the dam are documented in this report.

3. From these Phase I studies, it has been concluded that the portion of Mormon Island Auxiliary Dam with shells founded on dredged tailings will probably not be stable during and after the design earthquake and, if this is so, sudden loss of the pool may be expected to occur. Immediate remedial or hazard mitigating action is recommended. The Phase II study, documented in Report 8 of this series, provides additional in situ test data for the dredged tailings and examines the segment of Mormon Island Auxiliary Dam with shells founded on undisturbed alluvium to determine whether this segment of the dam needs to be included in the remedial work as well.

### Project History

4. The Folsom project was designed and built by the Corps of Engineers in the period 1948 to 1956, as authorized by the Flood Control Act of 1944 and the American River Basin Development Act of 1949. Upon completion of the project in May 1956, ownership of the Folsom Dam and Reservoir was transferred to the US Bureau of Reclamation for operation and maintenance. As an integral part of the Central Valley Project, the Folsom Project provides water supplies for irrigation, domestic, municipal, industrial and power production purposes as well as flood protection for the Sacramento Metropolitan area, and extensive water related recreational facilities. Releases from the Folsom Reservoir are also used to provide water quality control for project diversions from the Sacramento-San Joaquin Delta, maintain fish-runs in the American River below the dam, and help maintain navigation along the lower reaches of the Sacramento River.

### Hydrology and Pool Levels

5. Folsom Lake impounds the runoff from 1,875 square miles of rugged mountainous terrain. The reservoir has a storage capacity of 1 million acre-ft at gross pool and is contained by approximately 4.8 miles of man-made water retaining structures that have a crest elevation of 480.5 ft\* above sea

---

\* In this report, elevations are in feet, National Geodetic Vertical Datum (NGVD) of 1929.

level. At gross pool, el 466, there is 14.5 ft of freeboard. This pool level was selected for the safety evaluation, based on a review of current operational procedures and hydrologic records (obtained for a 29-year period, from 1956 to 1984) for the reservoir which shows that the pool typically reaches el 466 about 10 percent of the time during the month of June and considerably less than 10 percent of the time during the other months of the year. Under normal operating conditions, the pool is not allowed to exceed el 466. Hydrologic records show that emergency situations which would cause the pool to exceed el 466 are extremely rare events.

#### Description of Mormon Island Auxiliary Dam

6. Mormon Island Auxiliary Dam was constructed in the Blue Ravine, an ancient channel of the American River, that is about 1 mile wide at the dam site. For about 1,650 ft of its width, the Blue Ravine is filled with auriferous, gravelly alluvium of Pleistocene age. The maximum thickness of the channel gravels is approximately 65 ft. The gravels have been dredged for their gold content in the deepest portion of the channel, and the tailings were placed back into the partially water-filled channel. The replacement process tended to deposit the tailings in a very loose condition with finer materials near the base of the channel and coarser materials near the top. The remaining undisturbed alluvium is crudely stratified and slightly cemented.

7. Mormon Island Auxiliary Dam is a zoned embankment dam 4,820 ft long and 165 ft high from core trench to crest at maximum section. The shells are constructed of compacted gravel from the dredged tailings in the Blue Ravine. The narrow, central impervious core is a well compacted clayey mixture founded directly on rock over the entire length of the dam to provide a positive seepage cutoff. After some placement of earth fill the foundation rock was grouted. Two transition zones, each 12 ft wide, flank both the upstream and downstream sides of the core. The transition zones in contact with the core are composed of well compacted decomposed granite which classifies as a silty sand according to the Unified Soils Classification System (USCS). The second transition zones are constructed of the -2 in. fraction of the dredged tailings; these zones are also well compacted. A plan and typical sections of the dam are shown in Figures 3 and 4.



8. From the right end of the dam, sta 412+00, to approximately sta 437+00 and from sta 458+00 to the left end of the dam, sta 460+75, all zones are founded on rock. Between sta 437+00 and 440+50, the downstream shells are founded on undredged alluvium and the upstream shells are founded on rock. The foundation report indicates that between sta 441+50 and 456+50, the undisturbed and dredged alluvium was excavated to obtain slopes of 1V:2H to found the core and most of the filter zones on rock, but the shells are founded on alluvium. The dredged portion of the alluvium begins approximately at sta 446 and continues approximately to sta 455. The slopes of the dam vary according to the foundation conditions, with the flattest slopes in the vicinity of the dredged tailings. The downstream slopes of the dam vary between 1V:2H and 1V:3.5H and the upstream slopes vary between 1V:2H and 1V:4.5H.

#### Site Geology

9. At the time of construction, the geology and engineering geology concerns at the site were carefully detailed in the foundation report by US Army Engineer District, Sacramento (1953). This foundation report from construction records and a later paper by Kiersch and Treasher (1955) are the sources for the summary of site geology provided in this section. Figure 5 shows a geologic map of the project area.

10. The Folsom Dam and Reservoir Project is located in the low, western-most foothills of the Sierra Nevada in central California, at the confluence of the North and South Forks of the American River. Relief ranges from a maximum of 1,242 ft near Flagstaff Hill located between the upper arms of the reservoir to 150 ft near the town of Folsom just downstream of the Concrete Gravity Dam. The North and South Forks entered the confluence in mature valleys up to 3 miles wide, but further downcutting resulted in a V-shaped inner valley 30 to 185 ft deep. Below the confluence, the inner canyon was flanked by a gently sloping mature valley approximately 1.5 miles wide bound on the west and southeast by a series of low hills. The upper arms of the reservoir, the North and South Forks, are bound on the north and east by low foothills.

11. A late Pliocene-Pleistocene course of the American River flowed through the Blue Ravine and joined the present American River channel downstream of the town of Folsom. The Blue Ravine was filled with late

Pliocene-Pleistocene gravels, but with subsequent downcutting and headward erosion, the Blue Ravine was eventually isolated and drainage was diverted to the present American River Channel.

12. The pertinent formations at the damsite are: a weathered quartz diorite granite which forms the foundation at the Concrete Gravity Dam, Wing Dams, and Saddle Dikes 1 through 7; metamorphic rocks of the Copper Hill volcanics\* which form the foundation at Mormon Island Auxiliary Dam and Saddle Dike 8; the Mehrten Formation, a deposit of cobbles and gravels in a somewhat cemented clay matrix which caps the low hills that separate the saddle dikes and is part of the foundation at Dike 5; and the alluvium that fills the Blue Ravine at Mormon Island Auxiliary Dam.

13. Between Dikes 7 and 8 there is a change in the bedrock from weathered quartz diorite granite to the metamorphic rock of the Copper Hill volcanics. The Copper Hill volcanics consist predominantly of schists, quite weathered in some locations, with numerous dioritic and diobasic dikes.

#### Dredging Deposition Process

14. The dredging process and the procedures used in the Folsom area were documented by Aubury (1905). Figure 6 is a drawing of a Bucyrus type of dredge typically used in the Folsom area. In the field, the dredge was surrounded by a small pond. Complete coverage of the area to be dredged was accomplished by periodically moving the spuds that anchor the dredge. In the dredging process, the alluvium was excavated below the water level of the dredge pond with a chain of closely connected buckets that had a capacity of approximately 5 to 13 ft<sup>3</sup> per bucket. The excavated material was typically sorted on a shaking screen with holes 3/8 in. in size. The coarse tailings (greater than 3/8-in. diam) were deposited by a conveyor belt to the edges of the dredge pond in windrows. After sluicing and processing the fine tailings (less than 3/8-in. diam) on the gold-saving tables (where mercury was used for amalgamation), the dredge crew then dumped this material back into the dredge pond. The coarse tailings slopes around the edge of the pond were generally marginally stable to unstable, and slope failures occurred often, mixing slide debris with the finer tailings in the pond. The gold-bearing gravels in the

---

\* Formerly referred to as the Amador Group.

Folsom area were characteristically described as "a very clean wash," which meant that there was little or no clay present.

### Seismic Hazard Assessment

#### Seismological and geological investigations

15. Detailed geological and seismological investigations in the immediate vicinity of Folsom Reservoir were performed by Tierra Engineering Consultants, Inc. to assess the potential for earthquakes in the vicinity, estimate the magnitudes these earthquakes might have, and assess the potential for ground rupture at any of the water-retaining structures. (See Tierra Engineering Consultants, Inc. (1983) for comprehensive report.) The 12-mile-wide by 35-mile-long study area centered on the Folsom Reservoir was extensively investigated using techniques such as areal imagery analysis, ground reconnaissance, geologic mapping, and detailed fault capability assessment. In addition, studies by others relevant to the geology and seismicity of the area around Folsom were also compiled. These additional literature sources include numerous geologic and seismologic studies published through the years, beginning with the "Gold Folios" published by the US Geological Survey in the 1890's, the engineering geology investigations for New Melones and the proposed Marysville and Auburn Dams, studies performed for the Rancho Seco Nuclear Power Plant as well as unpublished student theses and county planning studies. As described in this section, the East Branch of the Bear Mountains fault zone is the seismic source of concern.

16. Figure 7 shows a generalized geologic map of north central California and identifies the location of the 12-mile by 35-mile study area. Figure 8 shows a close-up of the study area as it surrounds the Folsom Project. Figure 9 shows the regional geology and highlights the basement rocks in the study zone. The western edge of the study zone contains Quaternary and Tertiary deposits of the Great Valley. The central and eastern portions of the study zone contain primarily metamorphic rock with granitic, gabbroic, and ultramafic intrusives.

17. Figure 9 also shows the major faults in the area. In the investigation of faults, shears, and lineaments, five features within the study area were selected for more detailed study -- (a) the West Branch of the Bear

Mountains fault zone, (b) the Bass Lake fault, (c) the Linda Creek lineament, (d) the Mormon Island fault, and (e) the Scott Road lineament. The East Branch of the Bear Mountains fault zone is located near the boundary of the study area. The characteristics of this fault zone were fully examined and reported in the above-mentioned references. This fault zone was not investigated further as part of this study by Tierra Engineering Consultants, Inc. Characteristics of this fault zone are discussed later in this section. The five features that were selected for further study are identified on the regional lineament map in Figure 10. On the basis of review of available data, geologic mapping, and imagery analysis, it was determined that the Bass Lake fault is more than 168 million years old and shows no evidence of movement in recent geologic time. Consequently, the fault is not considered capable. Based on the seismological studies for Auburn Dam, it was determined that the Linda Creek lineament also does not represent a capable fault (by Corps criteria). The Scott Road lineament was determined to be of erosional origin and is not considered to be a fault. The remaining two faults, the West Branch of the Bear Mountains fault zone and the Mormon Island fault, required additional studies.

18. The detailed lineament analyses, geomorphic analyses, geologic mapping, and trenching at selected locations indicated that the West Branch of the Bear Mountains fault zone is overlain by undisplaced soils more than 60 to 70 thousand years old. There were no geomorphic indications of Holocene faulting along the zone; therefore, it was concluded that the West Branch of the Bear Mountains fault zone is not a capable fault. Studies of the Mormon Island fault showed that the lineament zone associated with the fault dies out before reaching Mormon Island Auxiliary Dam. A review of the dam construction reports and trenching of the Mormon Island fault south of Mormon Island Auxiliary Dam revealed no evidence of faulting of quaternary alluvium in this ancestral channel of the American River. Based on the observation of undisplaced colluvium and weathering profiles more than 65,000 years old that overlies the sheared bedrock, as well as the lack of geomorphic indicators of Holocene faulting in this zone, it was concluded that the Mormon Island fault is not a capable fault and does not pass through the foundation of Mormon Island Auxiliary Dam (Tierra Engineering Consultants, Inc. 1983).

19. Tectonic studies of the Folsom Project show it is located in the Sierran block. Within the Sierran block there is a very low level of

seismicity. The more seismically active areas are located along the eastern and southern edges of the block. Figure 11 shows epicentral locations for the western United States. On this map, the Sierra Nevada and Great Basin areas are identified. Tectonic studies of the Sierran block indicate an extensional stress regime which suggests that major stress buildup and release sequence associated with large earthquakes is unlikely in the central or northern Sierran block.

20. Figure 12 shows epicentral locations in north central California from data accumulated between 1910 and 1981. As indicated in the previous discussion, a low level of seismicity can be observed in the vicinity of the Folsom Project. The nearest highly active areas are the Calaveras Hayward-San Andreas System located 70 to 100 miles to the west of the study area, or the Genoa Jack Valley zone located more than 70 miles to the east. Table 1 summarizes the characteristics of the capable fault zones near the Folsom Project. Although these two highly active zones are capable of generating maximum earthquake magnitudes in excess of  $M = 7$ , the ground motions generated by such earthquakes would be significantly attenuated by the time the motions arrived at the Folsom Reservoir.

21. The closest capable fault is the East Branch of the Bear Mountains fault zone which has been found to be capable of generating a maximum magnitude  $M = 6.5$  earthquake. The tectonic and seismicity studies also indicated that it is unlikely that Folsom Lake can induce major macroseismicity. Faults that underlie the water retaining structures at the Folsom Project were found to be noncapable; thus, seismic fault displacement in the foundations of the water retaining structures is judged to be highly unlikely.

22. Determination that the East Branch of the Bear Mountains fault zone is a capable fault came from the Auburn Dam earthquake evaluation studies in which it was concluded that this fault was capable of generating a maximum magnitude earthquake of 6 to 6.5. The minimum distance between the East Branch of the Bear Mountains fault zone and Mormon Island Auxiliary Dam is 8 miles, and the minimum distance between this fault zone and the Concrete Gravity Dam is 9.5 miles. The focal depth of the earthquake is estimated to be 6 miles. This hypothetical maximum magnitude earthquake would cause more severe shaking at the project than earthquakes originating from other known potential sources.

### Selection of design ground motions

23. The seismological and geological investigations summarized in the Tierra report were provided to Professors Bruce A. Bolt and H. B. Seed to determine appropriate ground motions for the seismic safety evaluation of the Folsom Dam Project. The fault zone of concern is the East Branch of the Bear Mountains fault zone located at a distance of about 15 km from the site. This fault zone has an extensional tectonic setting and a seismic source mechanism that is normal dip-slip. The slip rate from historic geomorphic and geological evidence is very small, less than  $10^{-3}$  cm per year with the most recent known displacement occurring between 10,000 and 500,000 years ago in the late Pleistocene period.

24. Based on their studies of the horizontal ground accelerations recorded on an array of accelerometers normal to the Imperial Valley fault during the Imperial Valley earthquake of 1979, as well as recent studies of a large body of additional strong ground motion recordings, Bolt and Seed (1983) recommend the following design ground motions:

Peak horizontal ground acceleration = 0.35 g

Peak horizontal ground velocity = 20 cm/sec

Bracketed Duration ( $\geq 0.05$  g)  $\approx$  16 sec

Because of the presence of granitic plutons at the site, it is expected that the earthquake accelerations might be relatively rich in high frequencies. Bolt and Seed (1983) provided two accelerograms that are representative of the design ground motions expected at the site as a result of a maximum magnitude earthquake of 6.5 occurring on the East Branch of the Bear Mountains fault zone. The accelerograms are designated as follows (Bolt and Seed 1983):

M6.5 - 15K - 83A. This accelerogram is representative of the 84-percentile level of ground motions that could be expected to occur at a rock outcrop as a result of a magnitude 6.5 earthquake occurring 15 km from the site. It has the following characteristics:

Peak acceleration = 0.35g

Peak velocity  $\approx$  25 cm/sec

Duration  $\approx$  16 sec

M6.5 - 15K - 83B. This accelerogram is also representative of the 84-percentile level of ground motions that could

be expected to occur at a rock outcrop as a result of a magnitude 6.5 earthquake occurring 15 km from the site. It has the following characteristics:

Peak acceleration = 0.35g

Peak velocity  $\approx$  19.5 cm/sec

Duration  $\approx$  15 sec

Figure 13 shows plots of acceleration as a function of time for the two design accelerograms. Figure 14 shows response spectra of the motions for damping ratios of 0, 2, 5, 10, and 20 percent damping.

## PART II: REVIEW OF CONSTRUCTION RECORDS

### General

25. Detailed construction records were kept to document the initial site reconnaissance, selection of borrow areas, foundation preparation, and construction sequence for the dam. Pertinent information from these construction records are summarized in this part. This information provides (a) key background data used in development of an idealized section for analysis, (b) detailed descriptions of foundation and embankment materials and the geometry of excavated areas, important to the planning of field investigations and interpretation of results, and (c) initial values for material properties of foundation and embankment materials.

### Exploration and Sampling During Original Design and Initial Construction

26. Mormon Island Auxiliary Dam may be divided into three different segments according to foundation conditions: an approximately 900-ft-long segment (sta 446 to 455) that has shells founded on dredged alluvium, an approximately 600-ft-long segment (sta 441+50 to 446, and sta 455 to 456+50) that has shells founded on undisturbed alluvium, and the remaining length of the dam (sta 412 to 441+50, and sta 456+50 to 460+75) is the segment founded on weathered bedrock. The undisturbed alluvial deposit consists generally of sands and gravels overlain by silty and clayey soils. In the dredged alluvium, the coarser tailings are distributed throughout the thickness of the deposit (but are somewhat more concentrated in the top portion) and the finer tailings (approximately the fraction finer than 3/8 in.) are found mainly in the lower portion of the deposit. The boring logs from the exploration and sampling efforts prior to construction are summarized in Figure 3. The undredged portion of the alluvial foundation was explored by one churn drill hole, four 6-in.-diam rotary core drill holes, and three test pits from which undisturbed and disturbed samples were obtained. The dredged portion of the foundation was explored by four churn drill holes in which an effort was made to obtain 5-in.-diam undisturbed push tube samples. Undisturbed sampling of the gravels was generally unsuccessful due to the large particle sizes. The



weathered schist foundation was investigated with 6-in.-diam rotary core drill holes and test pits from which undisturbed samples were obtained.

#### Foundation Preparation at Mormon Island Auxiliary Dam

27. At Mormon Island Auxiliary Dam, the Blue Ravine is more than 1 mile wide. The foundation rock consists of nonuniformly weathered metamorphic rock with isolated, relatively fresh blocks surrounded by highly weathered material to a considerable depth. From the right abutment, sta 412+00, to sta 441+50, a 1- to 16-ft thickness of overburden was removed to found the core and shells of the dam on blocky, moderately hard schist bedrock. Stripping depths averaged 4 ft (range 1 to 10 ft) from sta 412+00 to 439+00 and 8 ft (16 ft maximum) from sta 439+00 to 441+50.

28. From sta 441+50 to 458+00 the channel was filled with auriferous gravelly alluvium of Pleistocene age. The maximum thickness of the channel gravels is approximately 65 ft. The gravels have been dredged for their gold content in the deepest portion of the channel, from sta 446+10 to 455+00, and the tailings were placed back into the partially water-filled channel. The replacement process tended to deposit the tailings in a very loose condition with finer materials (less than 3/8-in. size) near the base of the channel and coarser materials (greater than 3/8-in. size) near the top. The remaining undisturbed alluvium is crudely stratified and, in some areas, slightly cemented according to the foundation report.

29. The undisturbed and dredged alluvium and any other overburden present were excavated along the entire length of the core to found the core on the blocky, somewhat weathered schist. The remaining foundation was stripped to found the shells on suitable materials. During stripping and core trench excavation of the undisturbed alluvium, it was observed that some portions were somewhat cemented; whereas, others were soft and somewhat plastic. Consequently, a zone of several feet of undisturbed alluvium was stripped from the foundation area. It was decided that an average of 18 ft of overburden and undisturbed alluvium would have to be excavated between sta 441+50 and 446+10 since this material was a relatively loose clayey and silty material and unsuitable as a foundation for the embankment shells. A minimum of 12 ft was excavated near sta 445+25 and a maximum of 24 ft was excavated near sta 446+00. The undisturbed channel gravels were excavated to have a

slope of 1V:2H along the sides of the core trench. The average thickness of undisturbed alluvium left in place between sta 441+50 and 446+10 was approximately 20 ft.

30. The construction records (US Army Engineer District, Sacramento 1953) indicate that the dredged tailing piles (located from sta 446+10 to 455+00) were leveled off at approximately el 390 to receive embankment material, and that the slope of this material was 1V:2H along the sides of the core trench. Kiersch and Treasher (1955) reported that the dredged channel gravels were cut back on a gentle slope of 1V:5H due to an unstable condition caused by an abundance of clay lenses.\*

31. Kiersch and Treasher (1955) also reported that the core trench slopes were compacted by passes of a Caterpillar tractor before placing earth fill. This field practice was not mentioned in the construction records, which describe placement of cobbles and gravel on the core trench slopes to collect incoming drainage and divert it away from the core trench as the core material was being placed and compacted. The construction record did state that, away from the core trench, the pervious fill was compacted by such equipment as moved across the fill during construction operations.\*\* Both references stated that exposure of the top of the schist bedrock revealed numerous springs, and a large quantity of water was seeping into the core trench, and had to be pumped out for construction to continue.

32. From sta 455+00 to 456+10, an average of 8 ft of undisturbed channel alluvium was stripped prior to placement of embankment fill. Finer alluvium (sand, silt, and clay) exposed from sta 456+10 to 458+00 was considered to be unsuitable as a foundation for the embankment, and was removed to expose schist bedrock. Approximately 18 ft of material was excavated near sta 456+10, and 4 to 6 ft of material was excavated near sta 458+00.

---

\* The Becker Hammer field investigation results presented in Part III of this report and additional results presented in Report 8 of this series are generally consistent with the construction record description of stripping and excavation in this area, and do not confirm the excavated slopes and abundant presence of clay lenses reported by Kiersch and Treasher (1955).

\*\* The Becker Hammer field investigation results presented in Part III and Report 8 of this series indicate there is some increase in energy- and overburden-corrected blowcounts in the dredged foundation gravels beneath the slopes compared with the dredged gravels downstream of the toe of the dam.

Approximately 3 ft of overburden was stripped from the foundation from sta 458+00 to 460+75 to expose the hard, blocky schist bedrock.

33. To drain the area for construction, the water that normally flowed through the Blue Ravine channel was diverted so that most of the water drained into the South Fork. There was a need for water from the Blue Ravine in the downstream area to serve dredge ponds, domestic, and irrigation purposes. To provide water downstream, a bypass tunnel was constructed through the left abutment of Mormon Island Auxiliary Dam. The 6 x 6-1/2-ft tunnel was approximately 1,300 ft long. The metamorphic rock encountered during tunneling was extensively weathered, blocky with numerous clayey seams, and required timbering for support, except for a 311-ft-long section near the middle of the tunnel. The rock in this unsupported section of the tunnel was typically hard, blocky schist. The bypass tunnel was plugged once construction was completed. After some placement of earth fill, the foundation rock was grouted.

#### Laboratory Tests During Original Design and Initial Construction

34. The laboratory test results reported in this section were used in the original design of the dam. The design and initial construction data were used to assist in characterizing the site and formulating an idealized section for the seismic safety evaluation. These design values for material properties were used as initial estimates for comparison with material property values determined in the field and laboratory investigations reported in Parts III and IV and Appendixes A and B performed as part of the seismic safety study. Index tests on the materials obtained from the dredged and undisturbed alluvium during this preconstruction period indicated they are a mixture of gravel, sands, and silty and clayey fines. Specific gravities ranged from 2.72 to 3.03. An average specific gravity of 2.82 was adopted for both the dredged and undredged alluvial materials and for both the +No. 4 and -No. 4 (sieve) particle sizes. Specific gravity of the bedrock ranged from 2.77 to 2.89 and averaged 2.84.

35. The in situ dry density of the dredged tailings was estimated to vary from 83 to 117 pcf. The average was estimated to be 108.5 pcf with an average in situ water content of 23.8 percent in the finer dredge tailings which were estimated to extend from approximately 10 ft below ground surface

to bedrock (based on examination of push-tube samples), a maximum distance of 55 ft. The adopted (for initial design purposes) dry density of the coarser dredged tailings located from 0 to 10 ft below the ground surface was 125.0 pcf.\* This is the same density that was adopted during design for the dredge tailing gravel fill that was compacted in the embankment shells.\*

36. In situ dry density of the undredged alluvial foundation varied from 80.0 to 117.5 pcf. The average dry density was estimated to be 100.0 pcf with an in situ moisture content of approximately 19.7 percent. For the coarser undisturbed alluvium, the in situ dry density varied from 108.0 to 133.7 pcf with a weighted average of 122.6 pcf and an average moisture content of 11.1 percent. In situ measurements of the density of the weathered bedrock varied from a dry density of 101.6 to 118.7 pcf with an average of 107.5 pcf. The in situ moisture content of the weathered bedrock averaged 18.6 percent.

37. Permeability tests were run on block samples of the undisturbed alluvium and ranged from  $0.07 \times 10^{-4}$  to  $40 \times 10^{-4}$  cm/sec in the vertical direction. In the horizontal direction permeability ranged from  $0.02 \times 10^{-4}$  to  $10 \times 10^{-4}$  cm/sec. Permeability tests were not run on the dredge tailings since they were so pervious.

38. The shear strength of the undredged and dredged alluvium was determined from consolidated-drained direct shear tests on remolded specimens of -No. 4 fraction and large-scale (12-in. diam) consolidated-undrained triaxial tests on remolded samples. The results of both types of shear tests were used to determine the adopted design shear strengths summarized in Table 2. In addition to the laboratory work, the shear strength of the dredged tailings was estimated by assuming that the tailing slopes that existed in the field prior to dam construction had a safety factor of 1. The average value of  $\tan \phi'$  required to hold the section in equilibrium was determined. The back-calculated friction angles ranged from about 24 deg to 26 deg. A value of  $\phi'$  equal to 24 deg ( $\tan \phi'$  equal to 0.45) was adopted for design. Shear tests were not performed on the weathered and decomposed schist.

---

\* Test pit results presented in Part III indicate that the average in situ dry density of the dredge tailings in the upper 7 ft of the foundation downstream of the toe of the dam was 117.5 pcf, and in the downstream shell of the embankment the dry density averaged 143.7 pcf.

### Embankment Materials

39. The Mormon Island Auxiliary Dam cross section consists of four zones. Zone 1 is constructed of dredged gravels and forms the upstream and downstream shells. These gravels came from Borrow Area 5, the Blue Ravine itself. Zone 2 is a 12-ft-wide transition zone constructed upstream and downstream between the central zones and embankment shell. Zone 2 consists of the -2 in. fraction of the dredge tailings, and was also obtained from Borrow Area 5. Zone 3 consists of impervious decomposed granite from Borrow Area 1. Zone 4 consists of impervious material (clayey sand) from Borrow Area 6. Zone 3 was added due to the fact that insufficient clayey material was available in Borrow Area 6 to construct Zone 4 as wide as originally planned. The specifications for placement of these zones are summarized in Table 3. The locations of the borrow areas are shown in Figure 2.

40. Figures 15 through 21 are photos from construction records which show key features of foundation preparation and construction procedures. Figure 15 was taken on 10 April 1951 and shows the foundation preparation in progress. The view was taken from the left abutment, facing the right abutment. The dredged tailing windrows are shown in the foreground, and the cleared bedrock schist foundation is shown in the background. Figure 16 was taken from sta 421+00 facing the right abutment and shows the cleared bedrock schist foundation for this portion of the dam. Figure 17 was taken from sta 440+00 facing the right abutment and shows core trench excavation through the undredged portion of the alluvium. Figure 18 was taken from sta 440+00 looking toward the left abutment and shows core trench excavation as it approached the dredged section. Figure 19 was taken on 26 September 1951 and was taken from the left abutment facing the right abutment. This photo shows the completed core trench excavation. Figure 20 was taken at sta 458+00 facing the right abutment and shows placement of Zones 2, 3, and 4 materials in the excavated core trench. Figure 21 was taken at sta 421+50 facing the right abutment and shows compacted Zone 1 material in the upstream shell.

### PART III: FIELD INVESTIGATIONS PERFORMED FOR THIS STUDY

#### General

41. Field investigations were conducted in the embankment and foundation materials at Mormon Island Auxiliary Dam to obtain index information about these materials as well as strength and other input parameter values for the seismic stability analyses. The program consisted of Standard Penetration Tests (SPT), disturbed and undisturbed sampling, geophysical tests, test pits and shafts (to obtain disturbed samples and determine in situ densities), and Becker Hammer testing. Field investigations were concentrated at the tallest section of the dam where the dredge tailings form the foundation for the shells. Field investigation of the shell and foundation tailings was confined to the downstream area. It is assumed that the information observed downstream is also generally representative of the material upstream of the core of the dam. This assumption appears to be supported by observations during core trench excavation in the original construction. With the exception of limited surface geophysical testing, the undisturbed alluvium was excluded from the investigations. The locations of the various field investigations are shown in Figures 22, 23, and 24. The results of these investigations are discussed in this chapter.

#### SPT Results in Core and Filter Zones

42. Two pair of holes were drilled at the crest of the dam in the vicinity of sta 447+75. Each pair consisted of a hole for undisturbed sampling, denoted US in Figure 22, and an SPT hole, denoted SS in Figure 22, spaced 10 ft apart along the dam axis. Borings US-6 and SS-6 were drilled through the Zone 4 core materials at the dam center line, and borings US-7 and SS-7 were drilled at the downstream edge of the crest, mainly in Zone 3 compacted decomposed granite. SPT samples were obtained with trip hammer equipment and drilling fluid, and undisturbed samples were obtained with a Denison sampler. The blowcounts measured in SS-6 and SS-7 are shown in Figure 25.

43. Record samples show the core is a well-compacted mixture of clay, sand, and gravel with an average gradation of about 7 percent gravel, 57 percent sand, and 36 percent plastic fines, an average plasticity index of

20, and an average liquid limit of 40. Mechanical analyses and Atterberg limit tests were performed on a total of 17 samples from borings US-6 and SS-6. These index tests on core material indicate an average gravel content of 7 percent, an average sand content of 61 percent, and an average fines content of 32 percent. The average liquid limit was 43 percent and the average plasticity index was 21 percent. The material generally classified as a clayey sand (SC), according to the USCS. Blowcounts in the core ranged from a minimum of 10 blows per ft at a depth of about 30 ft to more than 50 blows per ft at depths greater than 160 ft. The weathered schist bedrock was encountered at a depth of 168 ft in Boring SS-6 and at a depth of 173 ft in Boring US-6. These two borings were extended approximately 25 ft into the weathered schist bedrock to a total depth of 197 ft.

44. Six record samples of the Zone 3 decomposed granite show an average gradation of 7 percent gravel, 73 percent sand, and 20 percent silty fines with no to low plasticity, typically a liquid limit (LL) of 28 and a plasticity index (PI) of 4. Index tests on 129 samples from Borrow Area 1 (the source for Zone 3) showed an average silty fines content of 30 percent, and 15 index tests on record samples of the core of the Left Wing Dam, also from Borrow Area 1, showed an average fines content of 25 percent. Consideration of the small number of record samples used to estimate average fines content from Zone 3 and comparison with the data from Borrow Area 1 and the Left Wing Dam suggest that the average fines content of Zone 3 is actually greater than 20 percent, more typically 25 percent, like the Left Wing Dam. Index tests were not performed on samples from US-7 and SS-7 drilled through Zone 3 decomposed granite. Blowcounts in the decomposed granite filter zone ranged from 23 blows per ft at a depth of 6 ft to more than 50 blows per ft at depths deeper than 40 ft. Drilling in borings US-7 and SS-7 was stopped at a depth of about 50 ft.

#### Geophysical Tests

45. The geophysical investigations consisted of surface vibratory, surface refraction seismic, crosshole, and uphole tests (Llopis 1983 and Llopis 1984). The geophysical investigations measure in situ shear-wave velocities ( $V_s$ ) and compression-wave velocities ( $V_p$ ) as a function of depth within the embankment and the underlying foundation materials. Since  $V_p$  profiles

were estimated from the cross-hole tests rather than the surface refraction seismic tests, the latter are omitted from this summary.

#### Surface vibratory tests

46. The surface vibratory test is used to measure the surface Rayleigh-wave velocity  $V_R$  which is typically about 10 percent (or less) slower than  $V_s$ . Rayleigh waves are generated by a surface vibrator which is swept through a range of discrete frequencies, and arrival times are measured by geophones placed at selected intervals along a straight line on the surface of the ground. Wave velocities are approximately average values for an effective depth of one-half the wave length corresponding to the vibrator frequency (Ballard 1964). The locations of the surface vibratory tests are shown in Figure 23.

47. Vibratory lines V-9, V-10, V-11, V-12, V-15, and V-16 were 200 ft in length, vibratory line V-13 was 160 ft in length, and vibratory line V-14 was 130 ft in length. Vibratory lines V-9 and V-10 were run along the crest of the dam approximately between sta 446 and 450. The  $V_R$  determined from these lines averaged approximately 790 to 900 fps, as shown in the  $V_R$  profile in Figure 26. The depth of investigation ranged from approximately 5 to 55 ft. Vibratory lines V-11 and V-12 were run along the toe of the dam between sta 425 and 429. The depth of investigation varied from approximately 5 to 45 ft and the  $V_R$  averaged approximately 700 fps, as shown in Figure 27. A high velocity zone was detected at a depth of approximately 17 ft in line V-11, possibly indicating a cemented zone in the undisturbed alluvium. Vibratory lines V-11 and V-12 are the only field measured geophysical data obtained in the Phase I study for the undisturbed Blue Ravine alluvium.

48. Vibratory lines V-15 and V-16 were run along the toe of the dam between sta 446+75 and 450+75. At this location, velocities decreased from approximately 620 fps to 550 fps between depths of 7 and 12 ft. At this point, the observed velocities increased steadily with depth to approximately 750 fps at 44 ft. The  $V_R$  profiles measured at vibratory lines V-15 and V-16 are plotted in Figure 28. Vibratory lines V-13 and V-14 were also run along the downstream toe of the dam near the left abutment between sta 455+90 and 450+80. The observed  $V_R$  increased from approximately 720 fps at a depth of 7 ft to 780 fps at a depth of 41 ft. This velocity profile is shown in Figure 29. Based on the observed  $V_R$  shown in Figures 26 through 29, the following corresponding  $V_s$  have been estimated: 900 to 1,000 fps in the core (to a



depth of about 70 ft), 1,000 to 1,200 fps in the undisturbed alluvium, and about 600 to 750 fps in the dredged alluvium. These surface vibratory test results were considered in the evaluation of the crosshole test results and development of recommended  $V_s$  profiles for the dynamic analyses.

#### Crosshole tests and interpreted velocity profiles

49. Crosshole tests were conducted with a downhole vibrator which was swept through a range of frequencies to find one that propagated well through the soil and transmitted a high amplitude signal to the receiver geophone lowered to the same depth as the downhole vibrator. Borehole deviation surveys were conducted to eliminate source-to-receiver distance errors in the reduction of the data. Exploding bridge-wire detonators were used as the compression-wave source for the  $V_p$  crosshole tests. Measurements for  $V_s$  and  $V_p$  velocities were made at 5-ft-depth intervals. The range of frequencies used in the  $V_s$  measurements was 50 to 500 Hz.

50. Figure 22 shows five locations where crosshole measurements were made. These tests were performed in the Zone 4 core material, the Zone 3 filter material, in the downstream shell (Zone 1), and in the dredged alluvium at two locations, in the vicinity of sta 449 and in the vicinity of sta 454. The core and filter borings were cased with 4-in. ID PVC pipe and grouted with a special grout that sets up with a consistency of soil. The borings in the core are US-6 and SS-6. The borings in the filter zone are US-7 and SS-7.

51. Due to the gravelly nature of the embankment shell and the foundation alluvium, the borings for the other crosshole location were steel-cased holes drilled with Odex equipment. The Odex system consists of a downhole pneumatic hammer with an expanding bit that pulls a steel casing behind the bit. When the casing is in place, the bit can be retracted and withdrawn through the casing. The steel casing used in these investigations had an ID of 5 in. The Odex system was selected for installation of cased holes for subsurface geophysical testing because it did not require grouting of the gravels, and several holes could be installed within a single work day. Unfortunately, this system does not provide satisfactory samples of the subsurface materials.

52. The  $V_s$  zones interpreted from the crosshole data in the vicinity of sta 447+75 are shown in Figure 30. The  $V_s$  in the core ranged from 1,000 fps to 1,350 fps. To a depth of approximately 50 ft, the  $V_s$  measured in the

compacted decomposed granite filter zone ranged from 900 to 1,325 fps. In the downstream slope the  $V_s$  measured in the downstream embankment shell was approximately 825 fps in the first 10 ft, and 1,200 fps from depths of 10 ft to 42.5 ft. The dredged tailings below this point had a  $V_s$  of 625 fps. Material below a depth of 87 ft had a  $V_s$  of 2,900 fps. Downstream of the toe of the dam, very low  $V_s$  were measured in approximately the top 40 ft of the dredge tailings. From ground surface to 37.5 ft, the  $V_s$  of the dredge tailings ranged from 475 to 400 fps. From 37.5 ft to 52.5 ft, the estimated  $V_s$  is 875 fps. At this depth, there is an abrupt increase in the  $V_s$  to 2,350 fps.

53. Figure 31 shows  $V_s$  profiles measured beyond the toe of the dam, in the downstream flat area near sta 449 and 454.  $V_s$  measured in the dredge tailings in the vicinity of sta 454 increase steadily with depth from 525 fps in the top 30 ft to 925 fps to a depth of approximately 60 ft. The  $V_s$  of the weathered schist bedrock ranged from 2,900 fps measured in the dredge tailings area to 3,150 fps measured underneath the center line of the dam.

54. The  $K_2$  value is a modulus coefficient which is a material characteristic independent of confining stress. It is computed as follows:

$$K_2 = \frac{G}{1,000(\sigma'_m)^{1/2}} \quad (1)$$

where

$G$  = shear modulus, psf

$\sigma'_m$  = mean effective confining stress, psf

At low shear strain levels,  $G_{\max}$  and  $K_{2\max}$  can be estimated from  $V_s$  as follows:

$$G_{\max} = V_s^2 \rho \quad (2)$$

$$K_{2\max} = \frac{V_s^2 \rho}{1,000(\sigma'_m)^{1/2}} \quad (3)$$

where  $\rho$  is mass density. Any consistent units may be used in Equation 2, but in Equation 3, the units must be feet, pounds, and seconds. From the field-measured  $V_s$ , it was estimated that the  $K_{2max}$  values for the embankment material ranged from approximately 110 to 125, and, for the loosest portion of the dredged alluvium, the  $K_{2max}$  value was approximately 25.

55. The interpreted  $V_p$  zones are shown in Figures 32 and 33. The  $V_p$  data are used to distinguish between materials that have very low or very high levels of saturation. The interpreted  $V_p$  zones shown in Figures 32 and 33 indicate that the zone of saturation\* in the core material begins at approximately a depth of 45 ft below the crest. The downstream shell  $V_p$  data indicate the zone of saturation begins approximately at the interface between the embankment shell material and the dredge tailings. The  $V_p$  data obtained in the dredge tailings downstream of the toe of the dam indicate that the zone of saturation begins approximately at the surface of the dredge tailings. Figure 34 from Allen et al. (1980) shows the relationship between  $V_p$  and degree of saturation. The pool level during the time the geophysical tests were performed ranged from a minimum of el 433.3 to a maximum of el 444.5. No observations of water levels in borings at the site were made. The Mormon Island Auxiliary Dam is not instrumented with piezometers.

#### Test Pits in Foundation Gravels

56. Two series of test pits were excavated in the dredged foundation gravels to determine in situ densities and to obtain disturbed samples for laboratory testing. Approximate test pit locations are shown in Figure 22. In the first series, the in situ moist densities from nine tests ranged from 115 to 152 pcf. The depth interval of the tests was typically 0 to 2.5 ft since the water table was encountered at a depth of 4 to 4.5 ft. The excavated material from all of the 4-ft diam water ring density tests was mixed together and the average gradation is shown in Figure 35. This average gradation was scalped to a maximum particle size of 3 in. to obtain a gradation for preliminary laboratory testing. This preliminary laboratory gradation is also shown in Figure 35.

---

\* Materials are assumed to be within the zone of saturation if the degree of saturation,  $S$ , equals or exceeds 99.95 percent. For this case,  $V_p$  will generally equal or exceed 3,500 fps (Allen et al. 1980).

57. Consideration of the wide range of in situ moist densities observed in the first test pit series suggested that gradation had a significant effect on measured in situ density, so, for the next test pit series, the gradation for each ring density test specimen was determined. The observed range is shown in Figure 36. This figure excludes the gradation of a sand lens encountered in one of the test pits. The sand lens was estimated to be of limited extent since it was not observed at other test pits. Further investigation of this individual lens was not pursued because it did not appear to be a controlling factor in the seismic performance of the dam.

58. Dewatering efforts at the site allowed the test pits to reach a maximum depth of about 7 ft in the dredged tailings. In this series, test pits were located in the downstream flat area near sta 449 and 454. The excavated materials were oven-dried to determine in situ dry densities. Several of the observed gradations were reconstructed in the laboratory to determine maximum and minimum dry densities. Because no well established procedure exists to determine these values for gravels, an extensive study was conducted to determine them. The study included both impact and vibratory loads applied to samples in a range of mold sizes from 11 in. to 36 in. in diameter. In some cases, the impact loads were severe enough to cause particle breakage and increase the percent passing the No. 4 sieve by as much as 15 percent. The laboratory estimates of maximum and minimum density are shown in Figure 37a. Since several of the measured in situ dry densities in the shell material, described next, exceeded the laboratory maximum values, it was concluded that laboratory procedures consistently lead to underestimates of maximum density. As in situ relative densities greater than 100 percent have no meaning, the maximum dry density was estimated as an envelope of all the data. Less difficulty was encountered in determining consistent minimum dry densities in the laboratory. The relationship between maximum and minimum dry densities and gradation, expressed by the uniformity coefficient,  $C_u$ , is shown in Figure 37b. It is estimated that the in situ relative density of the dredged tailings is about 35 percent. Specific gravity tests were performed on the gravel (portion which is coarser than the No. 4 sieve) and sand (portion passing the No. 4 sieve) fractions. Both fractions had an average  $G_s$  equal to 2.83. The average fines content of the foundation gravel was 6 percent (LL = 33, and PI = 15) for the first test pit series and 2.9 percent (LL = 29, and PI = 11) for the second.

### Test Shaft in Downstream Shell

59. A 19-ft-deep shaft was excavated in the downstream shell near sta 446+50 to measure in situ densities and gradations of the Zone 1 gravels. Figure 22 shows the location of the test shaft. Sixteen samples were obtained. The range of these gradations is shown in Figure 38. The average of the foundation gradations was almost identical to the average of the shell gradations. This combined average gradation, scalped to a maximum particle size of 3 in., was used in subsequent laboratory tests. The maximum and minimum density bounds discussed previously indicate the in situ relative density of the shell gravel is approximately 70 percent (the average of the 16 tests was computed to be 71 percent), as shown in Figures 39a and 39b. The fines were found to be somewhat plastic, with average plasticity index of 11 and liquid limit of 28. The average fines content was 5 percent. Both the gravel and the sand fractions had an average  $G_s$  equal to 2.83.

### Becker Hammer Tests

60. Becker Hammer blowcounts,  $N_B$ , were measured in the downstream embankment shell and the foundation material to provide in situ penetration data from which cyclic strength can be estimated. The field drilling was performed by Becker Drills, Inc. in October 1983. Figure 40 shows the Becker rig which is used to drive a double-walled steel pipe into the ground with a double-acting diesel hammer. Two types of soundings were made, closed-bit soundings (BDT) to measure  $N_B$  and open-bit soundings (BH) during which samples are taken in addition to  $N_B$  measurement. (In the drawings, BH-9 and BDT-3 etc. will be used.) For the closed-bit soundings, an 8-tooth crowd-out bit with a 6-5/8-in. OD and a 4-1/4-in. ID (plugged at the end) was used with 6-5/8-in. OD casing. These bits are shown in Figure 41.

61. The open-bit soundings were made with a Felcon bit which is a 3-web crowd-in bit for 6-5/8-in. casing but has an enlarged diameter near the bit (7-1/4-in. OD) and an inner casing ID of 3-7/8 in. In the open-bit sound, air is forced into the annular space between the two casings and material is forced up into the inner casing and is collected at the surface. One closed-bit and two open-bit soundings were driven through the downstream shell into the foundation gravel, and the remaining soundings, eight open-bit and

two closed-bit, were driven in the downstream flat area. A more detailed description of the Becker Hammer field work is given by Allen (1984).

62. The  $N_B$  values were translated into equivalent SPT  $N_{60}^*$  and  $(N_1)_{60}^{**}$  values using recently developed techniques (Harder and Seed 1986). (See report by Harder provided in Appendix A.) Translation of the Becker blowcounts to SPT blowcounts depends upon combustion conditions (throttle and supercharger settings, temperature, and altitude), and the equipment used (type of bit, size of casing, and drill rig). Hammer energy readings were collected with the blowcount data so that  $(N_1)_{60}$  values could be estimated.

63. The  $N_B$  and equivalent  $N_{60}$  values are plotted in Figures 42 and 43 for the soundings through the slope, and Figures 44-46 for the downstream flat area. The  $(N_1)_{60}$  contours on these figures were determined from the static finite element analyses discussed later, and the  $C_n$  curve shown in Figure 47. The work by Bieganousky and Marcuson (1977) indicates that the  $C_n$  overburden correction factor is closer to unity as  $D_{50}$  increases. This trend is shown in Figures 48a and 48b. By extrapolating this trend to gravel sizes, an adjusted  $C_n$  curve was estimated (Figure 47). The  $C_n$  data were extrapolated to estimate  $C_n$  for a  $D_{50}$  of 40 mm. The  $D_{50}$  observed in the test pits ranged from 18 to 85 mm.

64. Occasional instances of zero blowcounts were measured with open-bit soundings in the downstream flat area (Figure 46). These zero blowcounts were not confirmed by nearby closed-bit soundings (Figure 44). According to Harder and Seed (1986), this may indicate that finer-grained pockets were encountered, but due to the circulation system of the Becker equipment, accurate blowcounts could not be measured with open-bit soundings.

65. The index test results from the Becker Hammer samples are summarized in Figure 49. Within the depth of the test pits, the index tests on Becker samples indicate a higher fines content, typically 15 percent, and a lower gravel content, typically 50 percent, than do the test pit results. Scalping of larger gravel particles is expected since the bit ID is only 3+7/8 in. However, since the average fines content (percent passing the No. 200 sieve) from the Becker samples is 15 percent, and the averages from

---

\*  $N_{60}$  denotes SPT blowcount corresponding to an energy efficiency of 60 percent.

\*\*  $(N_1)_{60}$  denotes SPT blowcount corresponding to an effective confining stress of 1 tsf and an energy efficiency of 60 percent.

the test pits are 6 percent (first test pits) and 2.9 percent (second test pits), it is concluded that the Becker sample gradations are unreliable indicators of the gradations in this deposit. The Atterberg limits are consistent with the test pit results.

66. Figures 42 and 43 show the  $(N_1)_{60}$  values for the shell gravel typically range from 15 to over 35. An average value of 23 was selected to represent the shell gravels. In the downstream flat area, the  $(N_1)_{60}$  values are quite low, and typically range from 4 to 10. A value of 6.5 was selected as representative of the dredged tailings beyond the upstream and downstream toes of the dam. Beneath the dam, an increase in  $(N_1)_{60}$  with depth was observed in the dredged foundation gravels (Figures 42 and 43). It is thought that these dredged foundation gravels have higher values of  $(N_1)_{60}$  due to compaction by construction activities and equipment traffic, densification under the embankment load, and aging effects. A similar observation of an increase in blowcounts in gravelly dredge tailings and stream deposits beneath the shells of a dam was reported by Seed, Idriss, and Arango (1983) for Camanche Dam, California. The effect at Mormon Island Auxiliary Dam was most pronounced in the closed-bit sounding, BDT-3. In an effort to best represent the field conditions, this strength increase was included in the characterization of the dredged foundation gravels beneath the embankment shells. The higher dredged foundation blowcounts observed in BDT-3 were extrapolated to other locations beneath the shells by consideration of the vertical effective stress contours from the static finite element analyses. Table 4 lists the estimated  $(N_1)_{60}$  values and Figure 50 shows the assumed distribution of  $(N_1)_{60}$  values throughout the dredged foundation gravels.

#### Summary

67. The field investigations at Mormon Island Auxiliary Dam consisted of undisturbed sampling and SPT borings, surface and subsurface geophysical testing, test pits and shafts, and Becker Hammer soundings. The undisturbed and SPT borings provided information about the Zone 4 core and Zone 3 compacted decomposed granite for index test correlation and estimates of cyclic strength. The geophysical investigations provided shear-wave velocity profiles which are key input parameters for the dynamic response analyses discussed later. The test pits and shafts provided in situ density measurements

for use in the static and dynamic finite element analyses as well as material for laboratory testing. The Becker soundings provided blowcount data from which corrected blowcounts,  $(N_1)_{60}$ , could be estimated. These estimated corrected blowcounts could then be related to cyclic strength of the embankment shell and foundation materials by means of Seed's empirical procedure (Seed, Idriss, and Arango 1983 and Seed et al. 1984). The use of this field information in the analyses is described later in this report.



## PART IV: LABORATORY INVESTIGATIONS AND ESTIMATES OF CYCLIC STRENGTH

### General

68. In addition to the index tests described in the previous part, an extensive laboratory testing program was conducted on reconstructed specimens of gravel from the Blue Ravine to estimate effective strength parameters, the relative change in cyclic strength with confining stress ( $K_\sigma$ ) and consolidation stress anisotropy ( $K_\alpha$ ), and residual excess pore pressure as a function of factor of safety against liquefaction. The cyclic strength of the shell and dredged foundation gravels at Mormon Island Auxiliary Dam was estimated from a combination of the in situ and laboratory test results. This part contains descriptions of the procedures for estimating cyclic strength from in situ data, the cyclic strength thus determined from Becker Hammer soundings, and the laboratory investigations designed to determine the relative strength and pore pressure generation behavior of gravels subjected to cyclic loads. Tests performed on undisturbed specimens of compacted decomposed granite and index tests on all materials are reported in US Army Engineer Laboratory, South Pacific Division (1986).

### Estimates of Cyclic Strength from In Situ Tests

#### Empirical procedure to estimate cyclic strength

69. The cyclic strength of the shell and dredged foundation gravels were determined by Seed's empirical procedure (Seed, Idriss and Arango 1983, and Seed et al. 1984). The 1984 cyclic strength chart from Seed's work is shown in Figure 51. This chart relates measured  $(N_1)_{60}$  values to estimated cyclic stress ratios at several sites which have been subjected to earthquake shaking from a  $M = 7.5$  seismic event. The lines on the chart distinguish safe combinations of  $(N_1)_{60}$  and cyclic stress ratios from unsafe combinations based on whether or not surface evidence of liquefaction was observed in the field. This chart is interpreted to relate  $(N_1)_{60}$  to the cyclic stress ratio required to generate 100 percent residual excess pore pressure. Figure 51 provides data for clean and silty sands with different fines contents, expressing the cyclic stress ratio causing liquefaction, for a confining pressure of about

1 tsf and level ground conditions and for earthquakes with  $M = 7.5$ , as a function of the  $N_1$ -value of a soil corrected to a 60 percent energy level,  $(N_1)_{60}$ . Seed's work (Seed et al. 1983, and Seed et al. 1984) shows that, for  $M = 6.5$  events, the cyclic loading resistance is about 20 percent higher, for any value of  $(N_1)_{60}$ , than for  $M = 7.5$  earthquakes. Figure 52 shows the cyclic strength curves for relatively clean sands for several values of  $M$  as suggested by Koester and Franklin (1985).

Cyclic strength estimate for  
shell gravels, Zones 1 and 2

70. The representative  $(N_1)_{60}$  values used to enter the cyclic strength chart shown in Figure 51 were determined from the Becker Hammer field investigations described in Part III. The equivalent SPT  $N_{60}$  values determined from Becker Hammer soundings in the downstream embankment shell at Mormon Island Auxiliary Dam are shown in Figures 42 and 43. Superimposed on these plots of  $N_{60}$  with depth are contours of  $(N_1)_{60}$ . The equivalent blowcounts range from approximately 8 to more than 60 blows per ft. The one closed sounding through the shell indicated occasional layers of relatively low blowcounts, values of  $(N_1)_{60}$  of approximately 8 to 17. However, the open-bit soundings located nearby and well away from the closed-bit sounding indicate that these low blowcounts are in an isolated, discontinuous zone.

71. The open- and closed-bit equivalent  $N_{60}$  values were averaged with depth over 10-ft intervals. Within each interval the average equivalent  $(N_1)_{60}$  value was 23 blows per ft. This is the value of  $(N_1)_{60}$  used to enter Seed's 1984 cyclic strength chart shown in Figure 51. The fines contents observed in the test shaft samples ranged from 3 percent to 7 percent with an average of 5 percent. The test shaft reached a maximum depth of 19 ft in the downstream shell at Mormon Island Auxiliary Dam. Samples from the Becker soundings at depths of 0 to 40 ft in the shell material had fines contents that ranged from 10 to 28 percent with an average of 15 percent. The cyclic strength for the shell gravel was obtained from Seed's 1984 chart with an assumed average fines content of 8 percent. The strength determined from the chart was then increased by 20 percent to represent a magnitude 6.5 earthquake. This resulted in a cyclic stress ratio of 0.35 required to generate 100 percent excess pore pressure in eight cycles (representative of the magnitude 6.5 earthquake) in level ground at a vertical effective stress of 1 tsf.

72. Due to the similarity of the Zone 2 transition gravel to the Zone 1 shell gravel in terms of gradation, fines content and plasticity, and method of placement, it was concluded that the Zone 2 gravel could reasonably be assumed to have the same cyclic strength as the Zone 1 shell. Zone 2 is treated as part of Zone 1 in the rest of the analyses. The cyclic strength value of 0.35 for the Zones 1 and 2 embankment shell material was appropriately corrected to allow for overburden pressures greater than 1 tsf and to allow for nonlevel ground confining stress conditions based on the laboratory test results in order to evaluate the liquefaction potential of this gravel. (See Figure 53 for a schematic description of the cyclic strength computation procedure.)

#### Cyclic strength estimates for foundation gravels

73. Figures 42 through 46 show Becker Hammer blowcounts and equivalent  $N_{60}$  blowcounts plotted with depth for several locations in the foundation gravel beneath the downstream shell and in the level ground area beyond the downstream shell. In the downstream flat area, the equivalent  $N_{60}$  blowcounts from closed-bit soundings (Figures 44 and 45) had  $(N_1)_{60}$  values that ranged from about 5 to 12 blows/ft. The index tests on Becker Hammer samples indicate an average fines content of about 15 to a depth of 55 ft and about 35 percent below 55 ft. The liquid limit is typically 40 at any depth and the plasticity index is typically 15 at any depth. Although the two closed-bit soundings plotted in Figure 49 with the index test data indicate a slightly stronger zone over the depth interval 28 to 40 ft, the open bit soundings do not indicate the presence of a continuous higher strength zone at this depth. (The average  $(N_1)_{60}$  within this zone is 9 blows/ft). Based on examination of these figures, it was estimated that a value of  $(N_1)_{60} = 6.5$  was a representative average value at any depth within the dredged foundation downstream of the toe of the dam.

74. The soundings in the foundation gravel beneath the downstream shell indicate higher  $(N_1)_{60}$  values than in the free field area. The trend for higher blowcounts with depth was more evident in the closed soundings than in the open soundings. In order not to be overly conservative and to best represent the foundation material beneath the embankment shell, these higher  $(N_1)_{60}$  values were assigned to different zones within the foundation beneath the embankment. It is estimated that these higher  $(N_1)_{60}$  values are due to

compression of the foundation tailings during and after construction as well as aging affects. The higher blowcounts were distributed throughout the foundation material based on the vertical effective stress contours determined in the static finite element analyses described in Part V. This distribution of blowcounts is shown in Figure 50.

75. The fines contents (defined as percent passing the No. 200 sieve) observed in test pits in the downstream flat area ranged from 1 to 6 percent with an average of 3 percent. These test pits did not reach depths deeper than 7 ft. The description of the dredging deposition process indicated that the fines content (defined as percent passing the 3/8-in. sieve) of the gravel in the dredged area is higher at greater depths. The construction records also indicated that finer gravels existed at greater depths. The Becker test samples indicated a relatively uniform fines content (defined as percent passing the No. 200 sieve) of about 15 percent to a depth of 55 ft, and an average of about 35 percent below 35 ft. The blowcounts shown in Figure 50 were associated with cyclic strengths from Seed's 1984 chart shown in Figure 51 with an assumed fines content of 10 percent. The chart's cyclic strengths were then increased by 20 percent to determine strengths representative of a magnitude 6.5 earthquake. These strengths are listed in Table 4.

#### Cyclic strength estimates of Zone 3 filter and Zone 4 core materials

76. The cyclic strength of the compacted decomposed granite in Zone 3 was estimated in a similar manner. Although no index tests were run on samples from borings US-7 or SS-7, information from construction records indicates that the average fines content is about 20 to 25 percent. This material comes from Borrow Area 1 as did the core material for the Left Wing Dam which had an average fines content of about 25 percent. The field measured blowcounts plotted in Figure 25 were corrected to a confining stress of 1 tsf by means of the factor  $C_N$  for a relative density of 60 to 80 percent shown in Figure 54. Since the blowcounts were measured with a trip hammer, they were increased by 30 percent to correct the measured blowcounts to a 60 percent energy level. At depths greater than 30 ft (below the estimated phreatic surface) the computed  $(N_1)_{60}$  values exceed 30 blows/ft. Examination of Figure 51 shows that, for materials with  $(N_1)_{60}$  values that exceed 30 blows/ft and that have fines contents of 20 to 25 percent, the cyclic strength is extremely high and these materials are not susceptible to liquefaction. Due to the

plasticity of the fines, the high fines content, the method of material placement, and the high degree of compaction of Zone 4, this material was not considered susceptible to liquefaction.

#### Relative Cyclic Strength Behavior from Laboratory Investigations

##### Adjustments to cyclic strength and residual excess pore pressures

77. Laboratory tests reported in Appendix B were used to estimate effective strength parameters ( $\sigma'$  and  $c'$ ), the change in cyclic strength with confining stress ( $K_\sigma$ ) and consolidation stress anisotropy ( $K_\alpha$ ), and residual excess pore pressure as a function of factor of safety against liquefaction. The factor  $K_\sigma$  adjusts the cyclic stress ratio for the nonlinear increase in cyclic strength with confining stress. The factor  $K_\sigma$  is determined from a plot of cyclic shear stress,  $\tau_c$ , versus effective normal stress on the failure plane,  $\sigma'_{fc}$ . Cyclic stress ratios are computed as the ratio of  $\tau_c$  to  $\sigma'_{fc}$  to develop a plot of  $\tau_c/\sigma'_{fc}$  versus  $\sigma'_{fc}$ . The cyclic stress ratios are then divided by the cyclic stress ratio for a confining stress of 1 tsf to determine  $K_\sigma$  as a function of  $\sigma'_{fc}$ :

$$\left( \frac{\tau_c}{\sigma'_{fc}} \right)_{\sigma' \neq 1} = K_\sigma \left( \frac{\tau_c}{\sigma'_{fc}} \right)_{\sigma' = 1} \quad (4)$$

78. The adjustment factor  $K_\alpha$  accounts for the increase in cyclic strength with the presence of initial shear stresses on the failure plane. The ratio of initial shear stress,  $\tau_o$ , to effective normal stress on the failure plane,  $\sigma'_{fc}$ , is defined as  $\alpha$ . Level ground conditions correspond to  $\alpha = 0$ . The normal effective stress on the failure plane in the laboratory,  $\sigma'_{fc}$ , is equivalent to the vertical effective stress in the field,  $\sigma'_v$ . A family of cyclic strength envelopes (plots of  $\tau_c$  or  $\tau_c/\sigma'_{fc}$  versus  $\sigma'_{fc}$ ) can be developed for different values of  $\alpha$ . At a given confining stress, the cyclic strengths for  $\alpha > 0$  are normalized by the cyclic strength at  $\alpha = 0$ , to determine  $K_\alpha$  as a function of  $\alpha$ :

$$\left( \tau_c \right)_{\alpha \neq 0} = K_\alpha \left( \tau_c \right)_{\alpha = 0} \quad (5)$$

79. Fortunately,  $K_\alpha$  does not vary with confining stress ( $\sigma'_{fc}$ ) and  $K_\sigma$  does not vary with  $\alpha$  (as determined from the laboratory tests on the Folsom gravels), so the cyclic strength at any value of  $\sigma'_{fc}$  or  $\sigma'_v$  and  $\alpha$  can be computed from the cyclic strength at a confining stress of 1 tsf with  $\alpha = 0$  :

$$\left( \frac{\tau_c}{\sigma'_v} \right)_{\substack{\sigma'_v=1 \\ \alpha \neq 0}} = K_\sigma K_\alpha \left( \frac{\tau_c}{\sigma'_v} \right)_{\substack{\sigma'_v=1 \\ \alpha=0}} \quad (6)$$

80. A computed safety factor of 1.0 against liquefaction,  $FS_L$ , corresponds to a residual excess pore pressure ratio,  $R_u$ , of 100 percent. As values of  $FS_L$  increase, the corresponding values of  $R_u$  decrease. This relationship was roughly estimated from the laboratory data. Values of  $FS_L$  less than 1.0 are interpreted as the development of  $R_u = 100$  percent during the earthquake rather than toward the end of the earthquake.

#### Selection of laboratory gradations and densities

81. Two laboratory gradations were used to construct test specimens representative of the foundation. One gradation is the average gradation observed in the first series of test pits, scalped to a maximum particle size of 3 in. The full-scale and scalped average gradations from the first test pit series are shown in Figure 35. The second gradation is the average gradation observed in both the test pits in the foundation (in the second test pit series) and the test shaft in the downstream shell, scalped to a maximum particle size of 3 in. It was observed that the average gradation of the samples from the second test pit series in the foundation was almost identical to the average gradation of the shell test shaft samples. The second laboratory gradation is thus the average of these two average gradations scalped to a maximum particle size of 3 in. The two laboratory gradations are shown in Figure 55. Only the second gradation, denoted as the combined gradation in Figure 55, was used to construct laboratory specimens representative of the embankment shell.

82. To demonstrate that the laboratory gradations and densities are representative of actual field conditions, they are compared with the

gradations and in situ density tests from test pits in the foundation and the test shaft in the shell in Figures 35 through 39. The laboratory gradations generally fall within the observed gradation ranges shown in Figure 36 for the dredged foundation gravel and Figure 38 for the embankment shell. In situ dry density was observed to change with variations in gradation. The in situ dry densities from the test pit data are plotted versus the corresponding uniformity coefficient ( $C_u$ ) from the individual in situ density test gradations in Figure 39 for the foundation and Figure 37 for the shell.

83. Maximum and minimum densities were estimated from laboratory tests for several gradations with different values of  $C_u$ . Compaction molds of 18- and 36-in. diam were used in these tests for gradations with maximum particle sizes of 3 and 6 in., respectively. Both vibratory and impact compaction methods were used for maximum laboratory density. It was found that the laboratory compaction results underestimated maximum dry density, since a few in situ dry densities exceeded the laboratory maximum estimates. More representative values of maximum dry density were estimated as the envelope of all laboratory and in situ results. Figure 37 indicates that the average relative density of the foundation material within the relatively shallow depth of the test pits (7 ft) is about 35 percent. Figure 37 shows a slight trend toward higher relative density for more well-graded soils (higher values of  $C_u$ ). The deeper foundation soils are expected to have more sand and fines contents, and may be at a slightly higher relative density, on the order of 40 percent. Figure 39 indicates that the average relative density of the shell (Zone 1) is about 70 percent. A laboratory target dry density of 134 pcf was selected to model relative densities observed in the gravel shell and a target dry density of 125 pcf was selected to model the foundation. For the laboratory gradations, these densities correspond to estimated target relative densities of 64 and 40 percent, respectively.

#### Effective stress strengths and cyclic strength estimates

84. The laboratory triaxial tests were performed on 15-in. diam, 38.5-in.-high, hand-compacted specimens. The stress-controlled cyclic triaxial tests performed on these specimens are listed in Tables 5 and 6. Detailed test results are given in Appendix B of this report. Consolidated-undrained and consolidated-drained triaxial compression tests on laboratory compacted specimens show that the shell gravels have an effective friction

angle of approximately 43 deg ( $c' = 0$ ) before and after cyclic loading and the foundation has an effective friction angle of approximately 41 deg ( $c' = 0$ ) before and after cyclic loading. A series of cyclic triaxial tests on isotropically and anisotropically consolidated laboratory compacted specimens was performed to develop the cyclic strength curves shown in Figures 56 and 57. The failure criterion is 30 percent measured residual excess pore water pressure response,  $R_u$ , normalized by the normal effective consolidation stress on the failure plane,  $\sigma'_{fc}$ , achieved in eight loading cycles,  $N$ . The eight cycles correspond to the magnitude 6.5 earthquake event predicted for this site. This failure criterion also corresponds to a permanent axial strain of about 2.5 percent. Membrane compliance corrections show that a measured excess pore pressure response of about 30 percent in a laboratory test specimen corresponds to 100 percent response in a truly undrained test with no compliance (Evans 1987).

#### Adjustment factors $K_\sigma$ and $K_\alpha$

85. From these test results,  $K_\sigma$  and  $K_\alpha$  adjustments were determined to extrapolate the level ground strength at 1 tsf from the Becker work to higher and lower confining stresses and sloping-ground stress conditions. The  $K_\sigma$  curve developed from the laboratory data is shown in Figure 58. This curve is applicable to both the shell and foundation relative densities. The  $K_\alpha$  curve for the shell is shown in Figure 59. Since the foundation soils are so loose, it was not considered appropriate to apply  $K_\alpha$  adjustments to the cyclic strengths.

#### Comparison of in situ and laboratory cyclic strengths

86. In laboratory cyclic triaxial tests on specimens representative of the shell gravel, the cyclic stress ratio required to develop  $R_u = 30$  percent in eight cycles for a confining stress of 1 tsf and isotropic consolidation was 0.38. To account for the fact that isotropic consolidation and triaxial tests do not truly represent level ground conditions, this strength was multiplied by the factor  $C_r = 0.60$ , as suggested by Banerjee, Seed, and Chan (1979) for the analysis of Oroville Dam, which was also constructed of compacted dredged tailings gravels. Thus, the level ground cyclic strength of the shell gravels (at 1 tsf) as determined from the laboratory is 0.23. The difference between the cyclic strengths determined from field and laboratory tests implies a factor of 1.5 is needed to account for field conditions which



affect in situ cyclic strengths that cannot be represented by reconstructed laboratory specimens. For the Folsom Dam shell material, the most important of these factors is probably aging. Since the Folsom Project is approximately 10,000 days old, the aging factor could range from 1.45 to 1.75, according to the data presented by Banerjee, Seed, and Chan (1979) shown in Figure 60. The laboratory cyclic strength (cyclic stress ratio) of the foundation gravels for 100 percent  $R_u$ , level ground conditions, confining stress of 1 tsf, and eight equivalent cycles (magnitude 6.5) was 0.12, based on a laboratory failure criterion of 30 percent measured  $R_u$  due to membrane compliance effects. This value also corresponds to the in situ estimated strength from Becker Hammer soundings, discussed previously. Evidently, aging effects (and other factors that cannot be accurately represented by reconstructed laboratory specimens) for this material are negligible at the low relative density and confining stress in the downstream flat area.

Safety factors against liquefaction and residual excess pore pressures

87. Evans' work (1987) also indicated that relative pore pressure development behavior for isotropically consolidated specimens can be observed in test results that are not corrected for membrane compliance effects. Cyclic stress levels before the failure level (observed or extrapolated to 100 percent in the membrane compliance affected test) at eight cycles can be associated with lower excess pore water pressures. These lower cyclic stress levels determined in tests on the shell gravels are normalized by the failure level to yield safety factors and are plotted with their corresponding residual excess pore pressure ratios in Figure 61. Laboratory test results on anisotropically consolidated specimens not corrected for membrane compliance effects indicate higher residual excess pore water pressures at a given factor of safety against liquefaction than isotropically consolidated test results. Evans' work (1987) shows that these higher pore pressures are not observed in anisotropically consolidated test results that are corrected for membrane compliance effects. The test results from specimens at the foundation density indicate that the relationship between  $R_u$  and safety factor against liquefaction was about the same as that for the shell gravels with  $\alpha$  equal to zero. The pore pressure curve for  $\alpha = 0$  shown in Figure 61 was used to estimate  $R_u$  for the foundation gravels. Figure 61 also shows a relationship between  $FS_L$  and  $R_u$  for  $\alpha = 0.32$ . For the shell,  $R_u$  was increased by

interpolation of the curves shown in Figure 61 according to the  $\alpha$  value computed in the static stress analysis.

## PART V: STATIC FINITE ELEMENT ANALYSES

### General

88. A static finite element analysis was performed to determine the preearthquake vertical effective stresses and the initial static shear stresses on horizontal planes throughout the dam and foundation. This information was used to calculate values of  $\alpha$ , the ratio of initial horizontal shear-stress to initial vertical effective stress, so that the appropriate cyclic strength can be associated with each element. The idealized section selected for the finite element analysis represents nearly the entire width of the dredged section, since the depth to bedrock and the thickness of the dredged alluvium are fairly constant in this area. In this Phase I study, only the section through the dredged tailings was investigated since it was anticipated that it would be the most critical. A comprehensive analysis of sections through Mormon Island Auxiliary Dam founded on undisturbed alluvium and on rock is reported in Report 8 of this series as part of the Phase II seismic stability investigations.

89. The computer program FEADAM84 developed by Duncan et al. (1984) was used to calculate the initial effective stresses in the foundation and shells of the dam. This program is a two-dimensional, plane strain, finite element solution for determining static stresses, strains, and displacements in earth and rock-fill dams and their foundations. The program uses a hyperbolic constitutive model developed by Duncan et al. (1984) to estimate the nonlinear, stress history dependent, stress-strain behavior of soils. The hyperbolic constitutive model requires 9 parameters. The program performs incremental calculations to simulate the addition of layers of fill during construction of an embankment. A description of the constitutive model, procedures for evaluating the parameters, and the data base for typical parameter values are included in Duncan et al. (1980).

### Section Idealization and Static Finite Element Inputs

90. The segment of Mormon Island Auxiliary Dam with shells founded on dredged tailings was idealized as a two-dimensional section typical of the section in the vicinity of sta 450. This assumption for numerical simplicity

should be satisfactory inasmuch as the height from the core trench to the crest is approximately 165 ft, the thickness of the dredged tailings is approximately 65 ft, the width of the dredged area is approximately 900 ft, and this area is fairly remote from the abutments.

91. Table 7 contains a summary of the hyperbolic constitutive model parameter values for each of the materials in the Mormon Island Auxiliary Dam cross section. The parameter values listed in Table 7 were determined from consideration of several different sources of information -- drained and undrained triaxial shear tests, comparison with soils of similar characteristics from a data base of over 150 soils, and geophysical test results.

92. The finite element mesh used to represent the dam cross section is shown in Figure 62. This mesh was used for both the static and dynamic finite element analyses. It contains 381 elements and 399 nodal points. The mesh was constructed giving consideration to the distribution of materials in the cross section, the shear-wave velocities measured in the field, and specific criteria for dynamic finite element meshes (Lysmer et al. 1983). Consequently, the mesh is a compromise between the needs of the dynamic and the static finite element computations. Element heights were varied throughout the mesh to meet the Lysmer criteria, as described in the next part. The resulting mesh had a maximum element height of 12 ft, and the aspect ratio (length:height) did not exceed 4 for any element.

93. Eight material types are represented in the finite element mesh. The properties and hyperbolic parameters for each of these material types are listed in Table 7. The embankment was represented by five materials: (a) submerged gravel shells, (b) moist gravel shell, (c) central impervious core, (d) submerged transition zone, and (e) dry transition zone. The foundation materials were represented by three material zones: (a) submerged foundation gravels (dredge tailings), (b) dry foundation gravels (dredge tailings), and (c) clayey gravels (a layer just above the level of the bed-rock). Submerged material zones (those below the phreatic surface) had the same properties as their nonsubmerged counterparts except that buoyant unit weights rather than total unit weights were used in the static stress calculations. The gravel filter zone, Zone 2, was assumed to have the same properties as the embankment shell, Zone 1.

94. The construction sequence of the dam was modeled in two steps. First, the foundation was constructed in seven lifts leaving a notch for the

core trench. Second, the embankment was constructed by filling in the core trench and building the shells over the preexisting foundation elements in 16 construction increments. A construction increment was typically one element high. In the analysis it was assumed that the entire differential head imposed by the reservoir was lost in the Zone 4 core material and that no head was lost in the pervious embankment shells. This situation imposes unbalanced hydrostatic pressures on the upstream face of the core, as depicted in the sketch in Figure 63. The unbalanced hydrostatic pressure distribution acting on the upstream side of the impervious core was simulated in FEADAM84 by an equivalent system of forces applied to the nodes on the upstream face of the core and acting in the downstream direction. These forces were applied after the dam was numerically "constructed." FEADAM84 was then used to compute the states of stress occurring in the embankment and foundation under these conditions.

#### Results of Static Analysis

95. Contours of vertical effective stress, horizontal effective stress, shear stresses on horizontal planes and alpha developed from the FEADAM84 static stress computations are shown in Figures 64 through 67. The contours of vertical effective stress shown in Figure 64 reflect the effect of submergence since the vertical effect of stresses in the upstream portion of the dam and foundation are lower than those at corresponding points on the downstream portion of the dam. This plot also shows some evidence of arching across the impervious core, because the vertical stresses are significantly lower in the impervious core than vertical stresses at corresponding elevations in the shell just outside the core trench. Some arching is expected inasmuch as the shell materials are significantly stiffer than the core materials. The vertical effective stresses are highly concentrated in the embankment and foundation materials immediately upstream and downstream of the impervious core in the lower portion of the cross section. These stress concentrations are expected since the stiffness of the embankment materials are significantly greater than the dredged gravel foundation.

96. The stiffness contrast between the highly compressible foundation and the fairly stiff embankment gravel also affects the horizontal effective stresses and the shear stresses acting on horizontal planes. The lateral

stresses shown in Figure 65 do not follow the surface contour of the dam in the central section of the cross section, and the lateral stress levels are low. During the numerical "construction", the nodal points in the upstream and downstream shells have moved down and away from the dam's center line due to compression of the loose dredged gravel foundation. This spreading effect tends to reduce lateral stresses.

97. Figure 66 shows contours of shear stresses on horizontal planes. In the central portion of the cross section, the horizontal shear-stress contours generally follow the slope of the core trench. Figure 67 shows contours of alpha throughout the cross section. The absolute values of the alpha contours range from 0 to 0.25. In the upstream portion of the cross section, alpha is approximately equal to 0.10 throughout most of the shell and foundation beneath the embankment shell. In the downstream portion of the cross section the alpha values are higher and range in absolute value from 0.10 near the core trench to slightly greater than 0.25 near the slope and toe of the downstream portion of the dam.

98. These static stress results are used in various portions of the seismic stability study. They are used to estimate overburden correction factors for interpretation of the equivalent SPT blowcounts from Becker Hammer soundings, extrapolate in situ measurements to other portions of the cross section (such as geophysical results and blowcount results), and determine the appropriate cyclic strength for each portion of the embankment, as cyclic strength varies with vertical effective stress and alpha value.

## PART VI: DYNAMIC FINITE ELEMENT ANALYSIS

### General

99. A two-dimensional dynamic finite element analysis was performed with the computer program FLUSH (Lysmer et al. 1973) to calculate the dynamic response of the idealized cross section to the specified motions. The objectives of this analysis were to determine dynamic shear stresses, maximum accelerations at selected points in the cross section, earthquake-induced strain levels, and the fundamental period of the idealized cross section.

### Description of FLUSH

100. FLUSH is a finite element computer program developed at the University of California Berkeley by Lysmer et al. (1973). The program solves the equations of motion with the complex response technique under the assumption of total stress conditions. Nonlinear soil behavior is approximated with an equivalent linear constitutive model which relates shear modulus and damping ratio to the dynamic strain level developed in the material. In this approach, FLUSH solves the wave equation in the frequency domain and uses an iterative procedure to determine the appropriate modulus and damping values compatible with the developed level of strain. FLUSH assumes plane-strain conditions. As a two-dimensional, total stress, equivalent linear solution, FLUSH does not account for possible pore water pressure generation or dissipation during the earthquake. Each element in the mesh is assigned properties of unit weight, shear modulus, and strain-dependent modulus degradation and damping ratio curves. FLUSH input parameters for the various zones in the Mormon Island Auxiliary Dam cross section are described in the next section.

### Inputs to FLUSH

101. The same mesh from the static analysis was used in the dynamic analysis. The static finite element solution computes static stresses, vertical effective stress, horizontal effective stress, and initial shear stress on horizontal planes for the centroid of each element. The dynamic finite element analysis computes the dynamic shear stress history for the centroid of

each element. The same mesh is used in both the static analysis and the dynamic analysis so that the locations of the computed static stresses exactly match the locations of the computed dynamic stresses.

102. The finite element mesh was designed to propagate ground motions in the frequency range of interest. The maximum element height was determined from Equation 4 as suggested by Lysmer et al. (1973):

$$h_{\max} = (1/5) \times V_e \div f_c \quad (7)$$

where

$h_{\max}$  = maximum element height

$V_e$  = lowest degraded shear wave velocity in that zone of the cross section after the iteration process

$f_c$  = highest frequency of interest in the analysis

In the design of this mesh,  $f_c$  was limited to 8 Hz and the maximum element height was varied according to the  $V_s$  distribution in the dam cross section.  $V_s$  zones are shown in Figure 68. The  $V_s$  measured from geophysical tests was assumed to degrade to half the low strain value as a result of the earthquake shaking. In the Mormon Island Auxiliary Dam cross section, the lowest measured  $V_s$  was 400 fps. The layer of elements in the finite element mesh that corresponds to this low velocity zone has a maximum element height as shown below:

$$h_{\max} = (1/5) \times (400/2) \div 8 = 5 \text{ ft} \quad (8)$$

Elements throughout the remainder of the cross section were similarly sized in accordance with the measured shear wave velocities.

103. The earthquake-induced dynamic shear stresses were computed with Accelerogram B since preliminary SHAKE (a one-dimensional dynamic response code, Schnabel, Lysmer, and Seed 1972) analyses indicated that Accelerogram B resulted in about the same to slightly higher dynamic stresses than Accelerogram A. To develop appropriate input ground motions, Accelerogram B, a rock outcrop record, was input to SHAKE to compute corresponding bedrock ground motions at the base of a free field soil column taken from the first column of elements in the finite element mesh.



104. The key material properties for each element were unit weight and  $V_s$ . The unit weights required are total unit weight. Total unit weights were distributed throughout the cross section as defined in the static finite element analyses. The  $V_s$  results were estimated to be distributed throughout the cross section as shown in Figure 68. The in situ geophysical measurements were made in the downstream area. In the extrapolation of these results to the upstream shell and foundation, the reduced confining stress due to the presence of the reservoir was not considered. In the downstream dredged tailings beyond the toe of the dam, the low velocity layer of 400 fps was not included in the dynamic response analyses because it did not appear to be continuous across the dredged area and because its effect on the calculations would be to reduce the computed dynamic shear stresses.

105. The modulus degradation and damping curves used in the FLUSH computations were the average curves for sand from Seed and Idriss (1970). Seed et al (1984b) recently published a new curve for gravelly soils which is lower than that for sand. The degradation curves observed in the laboratory tests on Folsom gravels fell within the range of gravel data reported by Seed et al (1984b). This comparison is shown in Figure 69. The consequence of using the sand curve rather than the lower gravel curve is that the computed dynamic shear stresses will generally be slightly higher. The difference is most significant when the shear strains equal  $10^{-2}$  percent and less significant when the shear strains exceed the  $10^{-1}$  percent level.

#### Dynamic Response Results

106. The FLUSH program computes the dynamic response history for the centroid of each element in the finite element mesh. From these calculations, the maximum earthquake-induced horizontal cyclic shear stress computed for each element over the entire time period of shaking was determined from the finite element results and this value was then multiplied by 0.65 to determine the average cyclic stress imposed by the earthquake. Contours of average earthquake-induced dynamic shear stresses are plotted on the cross section shown in Figure 70. These average dynamic shear stresses ranged from approximately 0.5 ksf in the near surface layer of the foundation in the upper portion of the embankment to 4.0 ksf in the lower portion of the core trench.

Safety factors against liquefaction in the embankment shell and foundation are calculated with these dynamic shear stresses, as described in Part VII.

107. The program FLUSH computes accelerations for each of the nodal points in the finite element mesh. Figure 71 shows accelerations computed for several nodal points in the dam cross section. The rock outcrop record had a peak acceleration of 0.35 g. The SHAKE computations showed that this rock outcrop record would be modified to have a peak acceleration of 0.34 g if a layer of soil representative of the free field were placed on top of the rock. When these motions are propagated through the free field column, the peak acceleration at the ground surface is 0.26 g. Underneath the center line of the dam at the contact of the bedrock and the core, the peak acceleration of the incoming earthquake motions is 0.32 g. When these motions are propagated up through the core of the dam, the computed crest acceleration is 0.31 g. In general, the finite element analysis results indicate that the incoming earthquake ground motions will be attenuated as they propagate through the foundation and embankment materials.

108. During earthquake shaking, the embankment and foundation materials undergo shear straining. Consequently, the shear modulus is reduced in the manner indicated in Figure 69. Figure 72 shows typical effective shear strain (single amplitude) levels computed for various zones of the cross section. The strain levels shown in Figure 72 are effective cyclic strain levels determined with FLUSH, and are equal to 65 percent of the maximum cyclic shear strains. The effective cyclic shear strain levels were typically 0.05 to 0.06 percent in the embankment shells and 0.6 to 0.7 percent in the foundation materials. These shear strain levels are quite high, and, in this shear strain region, the difference between the degradation curve for sand and the degradation curve for gravel has little or no effect on the computed response.

109. Prior to the earthquake, the fundamental period of this section, estimated by Sarma's technique (Sarma 1979) for an idealized two-dimensional section on a foundation layer of limited thickness is 0.53 sec. The chart for computing this fundamental period is shown in Figure 73. The average  $V_s$  for the embankment is estimated to be 1,250 fps and the average  $V_s$  for the foundation is estimated to be 900 fps.

110. As the shear modulus reduces due to earthquake-induced straining, the fundamental period of the dam increases. The fundamental period of the idealized two-dimensional section at the strain levels induced by the seismic

safety evaluation earthquake was 1.72 sec, determined from the FLUSH output. The initial fundamental period of 0.53 sec and the fundamental period of 1.72 sec effective during the earthquake are compared with the response spectra for Accelerogram B in Figure 74. As the dredged portion approaches the undisturbed alluvium at sta 446+10, there is a gentle 10-ft rise in the bedrock elevation. The idealized two-dimensional fundamental period at sta 446 is estimated to be 0.45 sec. This is the minimum fundamental period for any location within the dredged area. The geometry at sta 446+10 is representative of less than 1/10 of the width of the valley. The section selected for analysis is considered to provide more representative response in the dynamic finite element calculations than section at sta 446+10.

111. The initial fundamental period for sta 446+10 is also shown in Figure 74. This figure demonstrates that the initial fundamental period for the section of Mormon Island Auxiliary Dam founded on dredged tailings is somewhat larger than the predominant range of periods of Accelerogram B. Earthquake shaking will (temporarily) further reduce the fundamental period of the section, as demonstrated by the value computed with FLUSH.

## PART VII: LIQUEFACTION POTENTIAL EVALUATION

### General

112. The cyclic strengths estimated from the in situ Becker Hammer tests and the laboratory studies were compared with the average earthquake-induced shear stresses to compute safety factors against liquefaction throughout the embankment shell (Zones 1 and 2) and the dredged foundation. Based on the laboratory studies, a relationship between safety factor against liquefaction and residual excess pore pressure was developed. This relationship was used to estimate the residual excess pore pressure field in the shell and foundation as a result of earthquake shaking. The results of these computations are described in this chapter. As described in Part IV, it has been determined that the Zone 3 compacted decomposed granite filter and the Zone 4 compacted clayey core are not susceptible to liquefaction and no significant excess pore pressures are expected to develop in these zones.

113. The residual excess pore pressure field estimated in this chapter for the shell and foundation is used in the next chapter to compute postearthquake stability. These results are compared with effective stress, one-dimensional dynamic response analyses to confirm the liquefaction potential evaluation drawn from the more extensive FLUSH analyses. The effective stress column analyses incorporated the effects of possible pore pressure generation and dissipation during the earthquake shaking.

### Safety Factors Against Liquefaction in Embankment Shell and Foundation

114. As described in an earlier chapter, it was estimated that the embankment shells had a normalized cyclic strength (shear stress ratio required to develop 100 percent residual excess pore pressure in eight cycles at a confining stress of 1 tsf for a magnitude 6.5 event) of 0.35 which corresponds to an average relative density of the embankment shell material of about 70 percent. The cyclic strength of the foundation was varied from a normalized value of 0.30 in the foundation material nearest the base of the core trench to 0.12 in the dredged tailings upstream and downstream of the toes of the dam. The cyclic strength for each element was determined with the

appropriate values of vertical effective stress,  $\alpha$ ,  $K_\sigma$ ,  $K_\alpha$ , and the normalized cyclic strength. Figure 53 schematically shows the procedure for computing cyclic strength. Due to the extremely loose condition of the foundation, it was assumed that  $K_\alpha$  was equal to 1.0 for all foundation elements. The safety factor against liquefaction is equal to the available cyclic shear strength divided by the average earthquake-induced cyclic shear stress. Contours of safety factor against liquefaction,  $FS_L$ , are plotted on the cross section shown in Figure 75. The shaded areas indicate  $FS_L$  values less than or equal to unity.

115. These safety factor contours indicate that the safety factors against liquefaction in the upstream embankment shell material are  $\geq 1.5$ . The embankment materials at the contact between the embankment and the alluvial foundation in the core trench had safety factors against liquefaction of approximately 1.0. Safety factors against liquefaction in the downstream shell were not computed since this material is not saturated. Foundation materials in the central portion of the cross section generally had safety factors against liquefaction  $> 1.0$ . Foundation material from about mid-slope to the toes of the dam had safety factors  $< 1.0$  and in the free field beyond the upstream and downstream toes of the dam safety factors against liquefaction were considerably  $< 1.0$ .

#### Residual Excess Pore Pressures

116. Based on the relationship between safety factor against liquefaction and residual excess pore pressure developed in the laboratory (shown in Figure 61), the computed safety factors against liquefaction in the dam cross section were translated into residual excess pore pressures. Contours of residual excess pore pressure are plotted on the cross section shown in Figure 76. Portions of the dam with safety factors against liquefaction  $\leq 1.0$  and correspondingly with residual excess pore pressure ratios of 1.0 are shaded. These contours show that residual excess pore pressures in the upstream shell may be significant and generally range from about 0.25 to 0.50. In the foundation materials near the core trench, the residual excess pore pressures also range from approximately 0.25 to 0.50. From about mid-slope to beyond the upstream and downstream toes of the dam, the pore pressures in the foundation are much higher and equal 1.0 for the zones with safety factors against

liquefaction  $\leq 1.0$ . This residual excess pore pressure field is used in the next chapter to compute safety factors against sliding in effective stress postearthquake stability calculations.

#### Liquefaction Potential Evaluation of Zone 4 Core and Zone 3 Filter Materials

117. Due to the plasticity of the fines, the high fines content, the method of material placement, and the high degree of compaction of Zone 4, this material was not considered to be susceptible to liquefaction and no significant excess pore pressures are expected to develop in the core. The Zone 3 decomposed granite filter is also well compacted, has a large fines content (typically 20 to 25 percent), and has high  $(N_1)_{60}$  values. It was determined that safety factors against liquefaction in these materials would be  $\gg 1.0$  and no significant excess pore pressures are expected to develop.

#### Effective Stress Response and Liquefaction Potential Analyses

118. In an effort to estimate whether sufficient pore pressure dissipation could occur during the earthquake to avoid liquefaction, a few effective stress, one-dimensional column analyses with DESRA-2 were performed (Bhatia 1986). These analyses estimated effective stress material properties from strain controlled cyclic tests on Folsom gravel specimens. Though approximate, these computations still indicated 100 percent residual excess pore pressure response in the foundation near and beyond the upstream and downstream toes of the dam.

#### Summary

119. In this part, the dynamic finite element results were compared with the cyclic strengths for the embankment and foundation materials. It was generally found that the embankment materials had safety factors against liquefaction that averaged about 1.5. In the foundation materials beyond mid-slope, the safety factor against liquefaction was typically  $< 1.0$ . Based on these studies, extensive liquefaction is expected in the free field and in the dredged alluvium beneath the upstream and downstream shells of the dam.

## PART VIII: STABILITY EVALUATION

### Postearthquake Slope Stability

120. The safety factor contours from Figure 75 were associated with corresponding residual excess pore water pressure ratios,  $R_u$ , from Figure 61. Contours of estimated residual excess pore pressure ratios are shown in Figure 76. The residual strength of the liquefied soils was estimated from  $(N_1)_{60}$  values from Seed's chart (Seed 1986), shown in Figure 77. For the portions of the embankment with safety factors against liquefaction  $>1.0$ , the residual excess pore pressures were used to estimate the available effective strength. The section was zoned with the strength parameters shown in Figures 78 and 79 for postearthquake slope stability analyses with UTEXAS2 (Wright 1985), which solves the slope stability problem with Spencer's method.

121. Both upstream and downstream failure surfaces were investigated. No cracks were incorporated in the computations. Since several surfaces have safety factors against sliding  $<1.0$  for both upstream and downstream slopes, the objective in the search was to find the approximate location of potential failure surfaces with safety factors against sliding equal to unity, and thus estimate the volume of material involved in initial postearthquake sliding.

122. Figure 80 shows two postearthquake failure surfaces computed for the upstream slope. The safety factors against postearthquake sliding ( $F_{PES}$ ) are 0.96 and 0.63. Surfaces passing through materials above and upstream of the surface with  $F_{PES} = 0.96$  have safety factors against sliding of  $<1.0$ . Surfaces that are deeper and involve materials further downstream of the surface with  $F_{PES} = 0.96$  have safety factors against sliding  $>1.0$ . The surface with  $F_{PES} = 0.96$  deeply cuts into the core and exits approximately at the pool elevation on the downstream slope. For general information purposes, static safety factors against sliding before the earthquake ( $F_{STA}$ ) for the same surfaces are also shown.

123. Figure 81 shows similar information for the downstream slope. Surfaces that intercept material upstream of the postearthquake sliding surface marked  $F_{PES} = 1.02$  have safety factors against sliding  $>1.0$ . Surfaces that pass through materials shallower and downstream of the surfaces marked  $F_{PES} = 1.02$  have safety factors  $<1.0$ . The static (preearthquake) safety factors are also shown. The critical surface,  $F_{PES} = 1.02$ , does not cross the

core, but intercepts the downstream slope at about the same location as the upstream critical surface.

124. Since the safety factors against liquefaction of the gravels are so low, it is estimated that 100 percent  $R_u$  will be reached during the earthquake, thus adding earthquake-induced inertial forces to the unstable slopes. The amount of permanent deformation cannot be exactly determined within the current state of the art. A lower bound deformation can be estimated from consideration of other slopes that have failed due to liquefaction, such as Upper San Fernando Dam (Seed et al. 1973). This dam experienced about 15 percent shear strain in the development of residual strength in liquefied soils. For Mormon Island Auxiliary Dam, 15 percent lateral distortion in the liquefied soils (the liquefied deposit is approximately 65 ft thick) corresponds roughly to 10 ft of lateral displacement ( $65 \text{ ft} \times 0.15 = 10 \text{ ft}$ ). Due to the inertial effects, the displacements should exceed 10 ft both upstream and downstream.

125. The remaining pyramid of soil left behind after upstream and downstream sliding can, in a very approximate manner, be thought of as a remnant embankment. The tip of this remnant consists of gravel and has an elevation of about 466 ft, the pool elevation. Zone 3 filter material, compacted decomposed granite, is first encountered at an elevation of about 443 ft, and Zone 4 core material is first encountered at an elevation of about 420 ft. It is unrealistic to expect zero slumping, no further sliding, and perfect retention of the pool with this remnant embankment. Among other events in a postearthquake failure scenario, the pool could quickly erode the gravelly section, leading to complete and catastrophic failure.

#### Permanent Deformation Estimates

126. Significant levels of excess pore water pressure are expected to develop in the foundation and embankment soils upstream and downstream of the core below el 370 and in the upstream shell of Mormon Island Auxiliary Dam. In these locations, Newmark-type permanent deformation estimates are inappropriate. The Phase II permanent deformation studies for the portions of Mormon Island Auxiliary Dam found on rock (sta 412+00 to 441+50 and 456+50 to 460+75) and on undisturbed alluvium (sta 441+50 to 446+10, and sta 455+00 to 456+50) are presented in Report 8 of this series. These Phase II studies indicate no



liquefaction and permanent displacements of about 1 ft or less for sections of Mormon Island Auxiliary Dam founded on rock or undisturbed alluvium.

### Stability Evaluation

127. Mormon Island Auxiliary Dam is 4,820 ft long. From the right end of the dam to sta 441+50, and from sta 456+50 to the left end of the dam, the embankment dam is founded on rock. The Phase II studies documented in Report 8 of this series indicate that these portions of Mormon Island Auxiliary Dam founded on rock will perform well during and immediately after the earthquake. Liquefaction is not expected in the embankment materials. Although some excess pore pressures may develop in saturated portions of the shells, they do not pose a stability problem. Permanent deformations computed for this section are expected to be tolerable, <1 ft.

128. The Phase II study includes analysis of the portion of the dam with shells founded on undisturbed alluvium (sta 441+50 and sta 455+00 to 456+10). Initial fundamental periods for these sections are estimated to range from 0.25 to 0.4 sec. This range brackets the peak of the response spectra for Accelerogram B. Further field investigations, complementary laboratory work, and analyses to determine whether the remedial work needs to include the undisturbed alluvium in addition to the dredged tailings are reported in the Phase II part of this study documented in Report 8 of this series. The Phase II studies indicate no liquefaction will occur in the foundation or embankment. Permanent deformation estimates for this portion of the dam founded on undisturbed alluvium are expected to be tolerable, <1 ft. Consequently, no remedial action is necessary for this portion of Mormon Island Auxiliary Dam.

129. From sta 446+10 to sta 455+00, the channel alluvium has been dredged for its gold content, and this dredged material forms the foundation for the upstream and downstream shells of the dam. Extensive liquefaction and slope instability would be likely in this portion of the dam and foundation. Catastrophic loss of the reservoir could well occur. To prevent these occurrences, remedial or hazard-mitigating measures should be enacted immediately.

## PART IX: SUMMARY AND CONCLUSIONS

130. This report has documented the Phase I study of the seismic stability evaluation of Mormon Island Auxiliary Dam at the Folsom Dam and Reservoir Project, located on the American River, about 20 miles northeast of the City of Sacramento, California. The review of the site geology and the seismic hazard assessment indicated that no active faults are present immediately beneath any of the man-made water retaining structures at the site. The most severe earthquake shaking was determined to come from the East Branch of the Bear Mountains Fault Zone, which is considered capable of producing a maximum magnitude earthquake of  $M = 6.5$ . The shortest distance between the fault zone and the Folsom Project is 8 miles to Mormon Island Auxiliary Dam and 9.5 miles to the Concrete Gravity Dam. The design ground motions for the site are  $a_{\max} = 0.35 \text{ g}$ ,  $V_{\max} = 20 \text{ cm/sec}$ , and duration ( $\geq 0.05 \text{ g}$ ) = 16 sec.

131. The seismic stability study of Mormon Island Auxiliary Dam has consisted of a review of construction records, field and laboratory investigations, static and dynamic stress analyses, liquefaction potential evaluation, and postearthquake slope stability analyses. Mormon Island Auxiliary Dam was constructed in the Blue Ravine, an ancient channel of the American River, that was partially filled with auriferous gravels. The underlying bedrock is weathered schist of the Copper Hill volcanics. The review of construction records showed that the core of the dam is founded on rock along its entire 4,820-ft length, but the foundation conditions for the shells of the dam vary. The dam may be divided into three segments according to foundation conditions for the shells: a 900-ft-long segment that has shells founded on dredged alluvium, a 600-ft-long segment that has shells founded on undisturbed alluvium, and the remaining length of the dam is the segment founded on weathered rock.

132. This Phase I study focused on the segment of the dam with shells founded on dredged alluvium. The Phase II study documented in Report 8 focuses on the portion of the dam with shells founded on rock or on undisturbed alluvium; these studies indicate that this segment of the dam does not pose a stability problem.

133. The Mormon Island Auxiliary Dam's cross section selected for the Phase I study consists of (a) Zone 1 shell gravels (fairly well graded, sandy gravel from the Blue Ravine, with maximum particle size of about 6 in., and

finer content of about 8 percent, placed in 18-in. lifts and compacted with one complete coverage of a Caterpillar tractor, in situ  $D_r \approx 70$  percent); (b) Zone 2 transition gravel (the same as Zone 1 but scalped to a maximum particle size of 2 in., and placed in the same manner as Zone 1); (c) Zone 3 compacted decomposed granite (decomposed granite that classifies as SM by USCS, approximately 95 percent of modified effort maximum density); (d) Zone 4 core (clayey, gravelly sand also compacted to approximately 95 percent of modified effort maximum density); and (e) dredged foundation gravel (similar to Zone 1, possibly increasing in fines content with depth, and extremely loose, with in situ  $D_r \approx 35$  to 40 percent).

134. Based on empirical liquefaction evaluation procedures developed by Professor H. B. Seed and his colleagues at the University of California, Berkeley, the cyclic strengths of the embankment and foundation materials were estimated from in situ tests, mainly Becker Hammer and SPT soundings. Relative cyclic strength and pore pressure generation behavior were determined in laboratory tests. The cyclic strengths were compared with the earthquake-induced cyclic stresses computed with FLUSH to determine safety factors against liquefaction and to estimate the excess pore pressures developed due to shaking. Postearthquake slope stability calculations were then performed with this excess pore pressure field.

135. The Phase I study shows that extensive liquefaction would probably occur in the dredged gravel foundation and to some extent in the portion of the embankment shells in the core trench. The upstream shell may develop residual excess pore pressure ratios of about 25 to 50 percent. No significant excess pore pressures are expected to develop in Zones 3 and 4 or in the downstream shell of the embankment. The postearthquake slope stability studies indicate that sliding could occur in both the upstream and downstream slopes and that catastrophic loss of the reservoir could result. Remedial or hazard mitigating measures should be enacted immediately.

## REFERENCES

- Allen, M. G. 1984. "Liquefaction Potential Investigation of Mormon Island Auxiliary Dam, Folsom Project, California", Soil Design Section, US Army Engineer District, Sacramento, CA.
- Allen, N. F., Richart, F. E., Jr., and Woods, R. D. 1980. "Fluid Wave Propagation in Saturated and Nearly Saturated Sands," Journal of the Geotechnical Engineering Division, American Society of Civil Engineers, Vol 106, No. GT3, pp 235-254.
- Aubury, Lewis E. 1905. "Gold Dredging in California." The California State Mining Bureau, San Francisco, CA.
- Ballard, R. F., Jr. 1964. "Determination of Soil Shear Moduli at Depth by In-Situ Vibratory Technique," Miscellaneous Paper 4-691, US Army Engineer Waterways Experiment Station, Vicksburg, MS.
- Banerjee, N. G., Seed, H. B. and Chan, C. K. 1979. "Cyclic Behavior of Dense Coarse-Grained Materials in Relation to the Seismic Stability of Dams," Report No. EERC 79-13, Earthquake Engineering Research Center, University of California, Berkeley, CA.
- Bhatia, S. 1986. "Dynamic Effective Stress Analysis, Folsom Project," unpublished WES Contract Report, Vicksburg, MS.
- Bieganousky, W. A. and Marcuson, W. F., III. 1976. "Liquefaction Potential of Dams and Foundations - Report 1: Laboratory Standard Penetration Test on Reid Bedford Model and Ottawa Sands," Report S-76-2, US Army Engineer Waterways Experiment Station, Vicksburg, MS.
- Bolt, B. A., and Seed, H. B. 1983. "Accelerogram Selection Report for Folsom Dam Project, California." Contract Report DACW 05-83-Q-0205, US Army Engineer District, Sacramento, CA.
- Duncan, J. M., Byrne, P., Wong, K. S., and Mabry, P. 1980. "Strength, Stress-Strain and Bulk Modulus Parameters for Finite Element Analyses of Stresses and Movements in Soil Masses," Report No. UCB/GT/80-01, Geotechnical Engineering, Department of Civil Engineering, University of California, Berkeley, CA.
- Duncan, J. M., Seed, R. B., Wong, K. S., and Ozawa, Y. 1984. "FEADAM84: A Computer Program for Finite Element Analysis of Dams," Research Report No. SU/GT/84-03, Stanford University, Stanford, CA.
- Evans, M. 1987. "Undrained Cyclic Triaxial Testing of Gravels - The Effect of Membrane Compliance," PhD Thesis in Engineering, University of California, Berkeley, CA.
- Harder, L. F. 1986. "Evaluation of Becker Penetration Tests Performed at Mormon Island Auxiliary Dam in 1983," Contract Report, US Army Engineer Waterways Experiment Station, Vicksburg, MS.
- Harder, L. F., and Seed, H. B. 1986. "Determination of Penetration Resistance for Coarse-Grained Soils Using the Becker Hammer Drill," UCB/EERC Report No. 86/06, Earthquake Engineering Research Center, University of California, Berkeley, CA.

- Kiersch, G. A., and Treasher, R. C. 1955. "Investigations, Areal and Engineering Geology - Folsom Dam Project, Central California," Economic Geology, Vol 50, No. 3, pp 271-310.
- Koester, J. P., and Franklin, A. G. 1985. "Current Methodologies for Assessing the Potential for Earthquake-Induced Liquefaction in Soils," NUREG/CR-4430, US Nuclear Regulatory Commission, Washington, DC.
- Llopis, J. L. 1983 (Jul). "Preliminary Results of an In-Situ Seismic Investigation of Folsom Dam, California," Draft Letter Report to US Army Engineer District (CESPK-ED-F), Sacramento, California, from US Army Engineer Waterways Experiment Station, Vicksburg, MS.
- Llopis, J. L. 1984 (Sep). "Preliminary Results of In-Situ Surface Vibratory Tests of Folsom Dam, California," Letter Report to Commander, US Army Engineer District (CESPK-ED-F), Sacramento, California, from US Army Engineer Waterways Experiment Station, Vicksburg, MS.
- Lysmer, J., Udaka, T., Tsai, C. F., and Seed, H. B. 1973. "FLUSH: A Computer Program for Approximate 3-D Analysis of Soil-Structure Interaction Problems," Report No. EERC 75-30, Earthquake Engineering Research Center, University of California, Berkeley, CA.
- Newmark, N. M. 1965. "Effects of Earthquakes on Dams and Embankments," Geotechnique, Vol 15, No. 2, pp 139-160.
- Sarma, S. K. 1979. "Response and Stability of Earth Dams During Strong Earthquakes," Miscellaneous Paper GL-79-13, US Army Engineer Waterways Experiment Station, Vicksburg, MS.
- Schnabel, P. B., Lysmer, J., and Seed, H. B. 1972. "SHAKE, A Computer Program for Earthquake Response Analysis of Horizontally Layered Sites," Report No. EERC 72-12, Earthquake Engineering Research Center, University of California, Berkeley, CA.
- Seed, H. B. 1979. "19th Rankine Lecture: Considerations in the Earthquake Resistant Design of Earth and Rockfill Dams," Geotechnique, Vol 29, No. 3, pp 215-263.
- \_\_\_\_\_. 1983. "Earthquake-Resistant Design of Earth Dams," Presented at the American Society of Civil Engineers Spring Convention, May 1983, Philadelphia, PA.
- \_\_\_\_\_. 1986. "Design Problems in Soil Liquefaction," UCB/EERC Report No. 86/02, Earthquake Engineering Research Center, University of California, Berkeley, CA.
- Seed, H. B., and Idriss, I. M., 1970. "Soil Moduli and Damping Factors for Dynamic Response Analyses," Report No. EERC 70-10, Earthquake Engineering Research Center, University of California, Berkeley, CA.
- Seed, H. B., Idriss, I. M., and Arango, I. 1983. "Evaluation of Liquefaction Potential Using Field Performance Data," Journal of the Geotechnical Engineering Division, American Society of Civil Engineers, Vol 109, No. GT3, pp 458-482.
- Seed, H. B., Lee, K. L., Idriss, I. M., and Makdisi, F. 1973. "Analysis of the Slides in the San Fernando Dams During the Earthquake of February 9, 1971," Report No. EERC 73-2, Earthquake Engineering Research Center, University of California, Berkeley, CA.

Seed, H. B. and Peacock, W. H. 1971. "Test Procedures for Measuring Soil Liquefaction Characteristics," Journal of the Soil Mechanics and Foundations Division, American Society of Civil Engineers, Vol 97, No. SM8, pp 1099-1119.

Seed, H. B., Tokimatsu, K., Harder, L. F., and Chung, R. M. 1984a. "The Influence of SPT Procedures in Soil Liquefaction Resistance Evaluations," UCB/EERC Report No. 84-15, University of California, Berkeley, CA.

Seed, H. B., and Whitman, R. V. 1970. "Design of Earth Retaining Structures for Dynamic Loads," American Society of Civil Engineers Specialty Conference, Lateral Stresses in the Ground and Design of Earth Retaining Structures, pp 103-147.

Seed, H. B., Wong, R. T., Idriss, I. M., and Tokimatsu, K. 1984b. "Moduli and Damping Factors for Dynamic Analyses of Cohesionless Soils," Report No. EERC 84-14, Earthquake Engineering Research Center, University of California, Berkeley, CA.

Tierra Engineering Consultants, Inc. 1983. "Geologic and Seismologic Investigations of the Folsom, California Area," Contract Report DACW 05-82-C-0042, US Army Engineer District, Sacramento, CA.

US Army Corps of Engineers. 1985. "Earthquake Analysis and Response of Concrete Gravity Dams," Engineer Technical Letter (ETL) 1110-2-303, Washington, DC.

US Army Engineer District, Sacramento. 1953. "Foundation Report, American River, California, Mormon Island Auxiliary Dam, Folsom Project." Sacramento, CA.

US Army Engineer Laboratory, South Pacific Division. 1986. "Report of Soil Tests, Folsom Dam Laboratory Program," Sausalito, CA.

Whitman, R., and Liao, S. 1985. "Seismic Design of Gravity Retaining Walls," Miscellaneous Paper GL-85-1, US Army Engineer Waterways Experiment Station, Vicksburg, MS.

Wright, S. G. 1985. "UTEXAS2 (University of Texas Analysis of Slopes - Version 2), A Computer Program for Slope Stability Calculations," Contract Report, Report No. Instructional Report GL-87-1, US Army Engineer District, Fort Worth, TX.

Table 1

Estimated Seismic Characteristics of Capable Faults\*

Name of Fault Zone	Minimum Distance To Site miles	Type of Faulting	Maximum Earthquake Magnitude**	Approximate Slip Rate†	Most Recent Displacement Known††
San Andreas	102	Strike-slip	8	1-2 cm/yr	Historic
Hayward	85	Strike-slip	7	0.5 cm/yr	Historic
Calaveras	77	Strike-slip	7	0.25 cm/yr	Historic
Genoa Jack Valley	70+	Normal-slip	7.25	0.01-0.02‡	Holocene
West Walker River	85	Normal-slip	7.25	0.01‡	Historic
Melones	16.5	Normal-slip	6.5	0.0006-0.0001‡	Pleistocene ±100,000
East Branch Bear Mountains	8.0	Normal-slip	6.5‡‡	0.0006-0.0001‡	Pleistocene ±100,000

\* Capable fault, under criteria used by Tierra Consultants, Inc., is one that exhibited displacement at or near the ground surface within the past 35,000 years, recurrent movement within the past 500,000 years, exhibits creep movement, and/or exhibits aligned macro ( $M \geq 3.5$ ) seismicity determined from instruments.

\*\* Maximum earthquake estimate on rupture length of continuous strands, type of faulting, fault displacement, historic earthquakes, seismic moment, experience and judgment.

† Slip rates estimated from historic, geomorphic, or geologic evidence.

†† Late Pleistocene displacement may be as old as 500,000 years ago or as young as 10,000 years ago.

‡ Slip rate in units of cm/yr assumed.

‡‡ Hypothetical value (acceptance based on USBR Auburn Dam studies).

Table 2  
Adopted Design Shear Strengths from Construction Records

Material	Dry Unit Weight pcf	Moist Unit Weight pcf	Saturated Unit Weight pcf	Buoyant Unit Weight pcf	Effective Friction, tan $\phi'$	Effective Cohesion c', psf
Dredged tailings below el 369	108.5	125.5	132.2	69.8	0.45	0
Dredged tailings above el 369	125	133.0	143.8	81.4	0.84	0
Zone 1 shell	125	133.0	143.8	81.4	0.84	0
Zone 2 transition	125	133.0	143.8	81.4	0.84	0
Zone 3 filter*	(123.4)	(134.0)	(140.0)	(77.6)	(0.70)	(0)
Zone 4 core**	108.5	125.5	132.2	69.8	0.55	0

\* Zone 3 was assumed to have the same strengths as Zone 4. Tabulated information is from Wing Dams for 95 percent modified effort compacted density.

\*\* Zone 4 was compacted to 82 percent modified effort compacted density.

Table 3  
Placement Specifications for Embankment Materials

Zone	Source	Compaction Equipment	No. of Passes	Maximum Lift Thickness in.
1 (Gravel shell)	Borrow No. 5	D-8 Caterpillar tractor	3*	24
2 (Gravel transition)	Borrow No. 5 (-2 in. fraction)	D-8 Caterpillar tractor	3*	12
3 (Decomposed granite filter)	Borrow No. 1	Sheepsfoot roller	8	12
		Pneumatic-tired roller	4	18
4 (Clayey core)	Borrow No. 6	Sheepsfoot roller	10	8
		Pneumatic-tired roller	4	8

\* One complete coverage with a D-8 Caterpillar tractor with standard width treads was specified. One complete coverage is estimated to correspond to 3 or 4 passes.



Table 4  
Cyclic Strengths Estimated from Becker Data  
and Seed's 1984 Chart

Material	$(N_1)_{60}$	Vertical Stress ksf	Cyclic Stress Ratio	Residual Strength psf
Shell gravels	23	--	0.356	1200
Foundation gravels	6.5	0-5.2	0.12	100
	12	5.2-6.8	0.19	440
	15.5	6.8-8.0	0.24	800
	17	8.0-8.8	0.26	1060
	20	8.8-	0.30	1200

Table 5

## Stress-Controlled Cyclic Triaxial Tests (First Test Pit Gradation)

Test No.	Minor Effective Consolidation Stress $\sigma_{3c}$ , psi	Consolidation Stress Ratio $K_c = \frac{\sigma_{vc}}{\sigma_{hc}}$	Dry Unit Weight After Consolidation $\gamma_{dc}$ , pcf	Relative Density* $D_R$ , percent	Cyclic Stress Ratio $\pm \frac{\sigma_{dc}}{2 \sigma_{3c}}$
1	20	1.0	129.85	45.6	0.21
2	20	1.0	129.52	44.8	0.29
3	20	1.0	129.26	44.2	0.24
4	10	1.0	129.41	44.5	0.35
5**	20	1.0	127.95	41.0	0.28

\*  $\gamma_{dmax} = 158.0$  pcf,  $\gamma_{dmin} = 113.0$  pcf.

\*\* Periphery of specimen covered with thin coating of plastic modeling clay to mitigate membrane compliance.

Table 6

## Stress-Controlled Cyclic Triaxial Tests (Combined Representative Gradation)

Test No.	Minor Effective Consolidation Stress $\sigma_{3c}$ , psi	Consolidation Stress Ratio $K_c = \frac{\sigma_{vc}}{\sigma_{hc}}$	Dry Unit Weight After Consolidation $\gamma_{dc}$ , pcf	Relative Density* $D_R$ , percent	Cyclic Stress Ratio $\pm \frac{\sigma_{dc}}{2 \sigma_{3c}}$
1	15	1.0	125.9	42.8	0.29
2	15	1.0	124.6	39.0	0.25
3	15	1.0	125.4	41.3	0.25
4	40	1.0	126.6	44.6	0.30
5	40	1.0	125.9	42.8	0.20
6	15	2.0	125.7	42.3	0.25
7	15	2.0	124.7	39.4	0.40
8	40	2.0	125.6	42.1	0.30
9	40	2.0	125.1	40.5	0.20
10	80	2.0	125.5	41.7	0.50
11A	15	1.0	133.0	61.1	0.20
11B	15	1.0	133.0	61.1	0.50
12	15	1.0	131.4	57.2	0.35
13	40	1.0	132.7	60.5	0.50
14	40	1.0	132.6	60.3	0.30
15A	15	2.0	134.7	65.3	0.50

(Continued)

\*  $\gamma_{dmax} = 151.0$  pcf,  $\gamma_{dmin} = 112.0$  pcf.

Table 6 (Concluded)

Test No.	Minor Effective Consolidation Stress $\sigma_{3c}$ , psi	Consolidation		Dry Unit Weight After Consolidation $\gamma_{dc}$ , pcf	Relative Density* $D_R$ , percent	Cyclic Stress Ratio $\pm \frac{\sigma_{dc}}{2 \sigma_{3c}}$
		$K_c = \frac{\sigma_{vc}}{\sigma_{hc}}$	Stress Ratio $\frac{\sigma}{\sigma_{hc}}$			
15B	15	2.0		134.7	65.3	0.60
15C	40	2.0		137.7	65.3	0.60
16	40	2.0		131.3	56.9	0.45
17	80	1.0		134.4	64.6	0.25
18	20	1.5		127.6	47.4	0.50
19	20	1.5		127.5	47.0	0.35
20	80	1.5		129.0	51.1	0.25
21	80	1.5		130.3	54.4	0.29
22	40	1.5		135.2	66.4	0.50
23	40	1.5		137.4	71.6	0.65
24	40	2.0		137.7	72.2	0.99
25	20	1.0		~135	~64	0.99



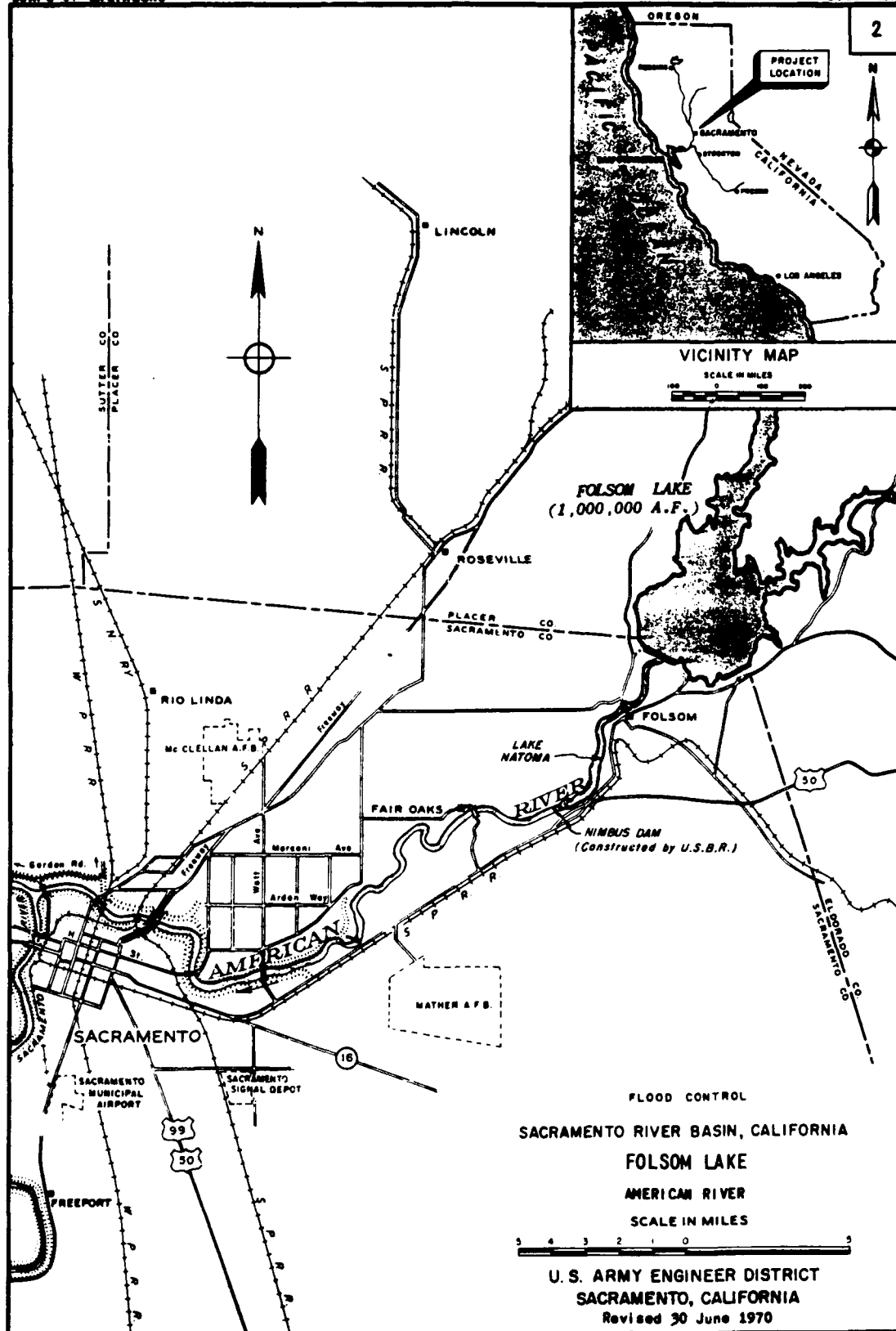


Figure 1. Location of Folsom Dam and Reservoir Project

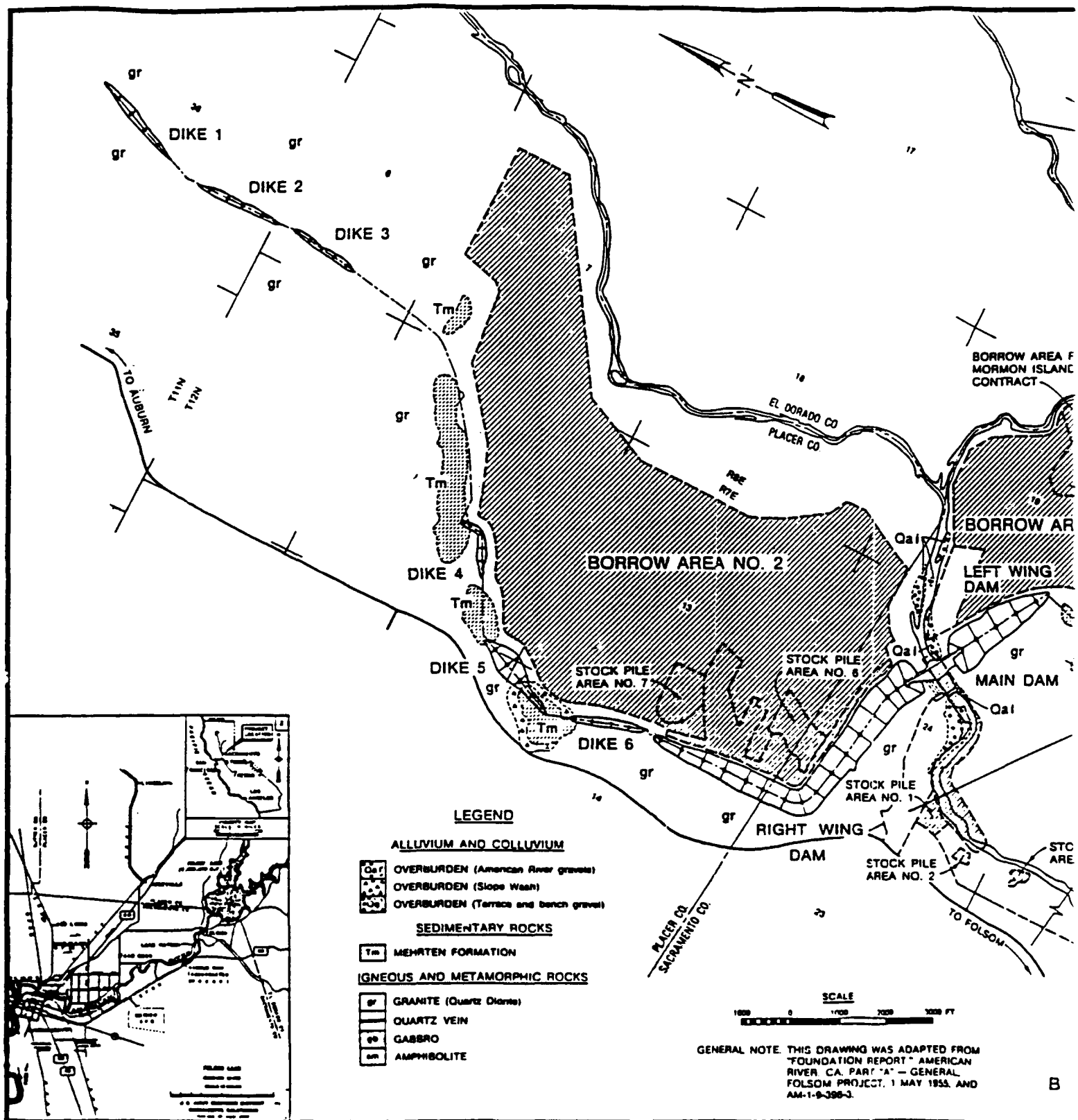
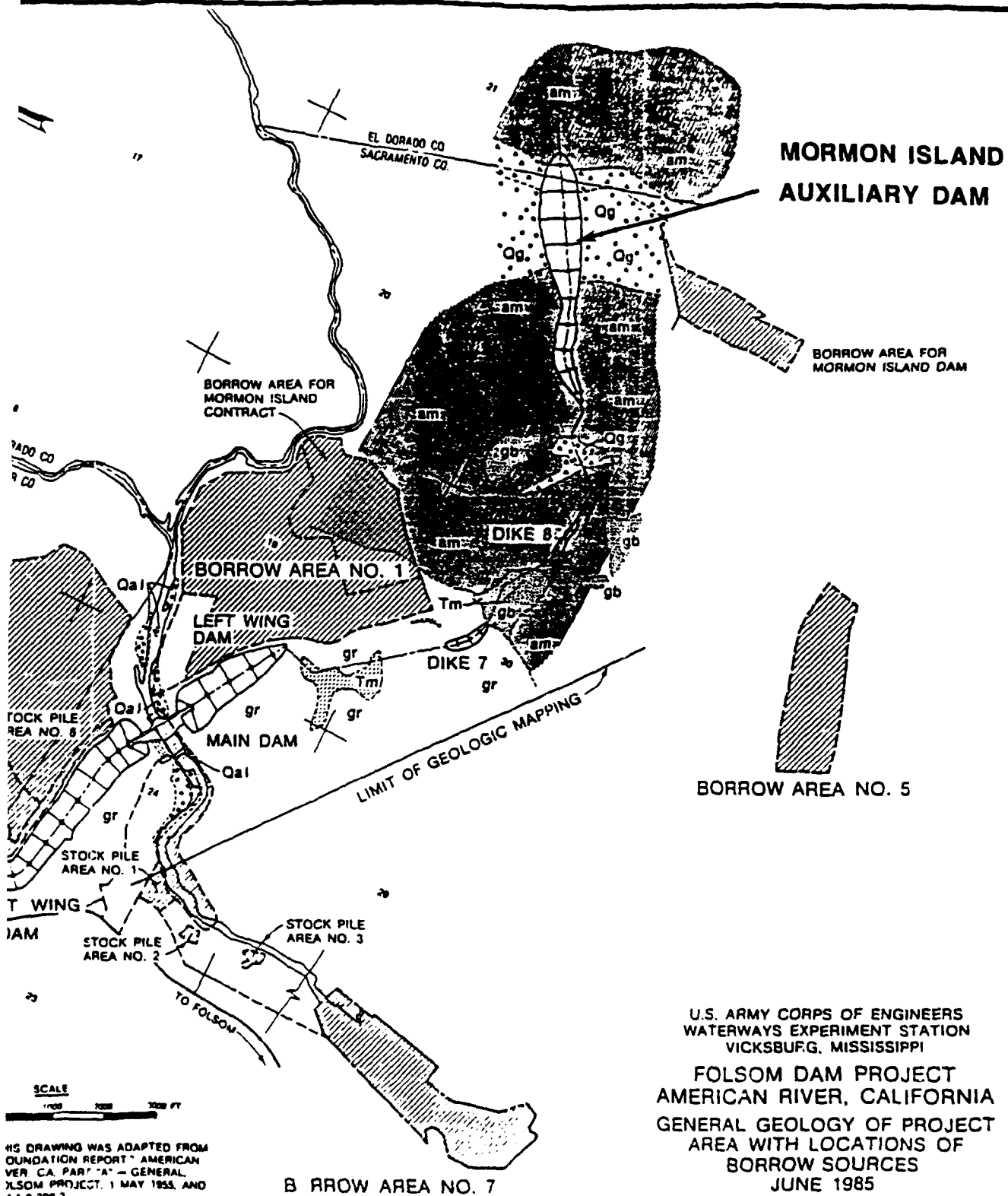


Figure 2. Plan of man-made retaining structures at Folsom Dam Project



ing structures at Folsom Dam Project



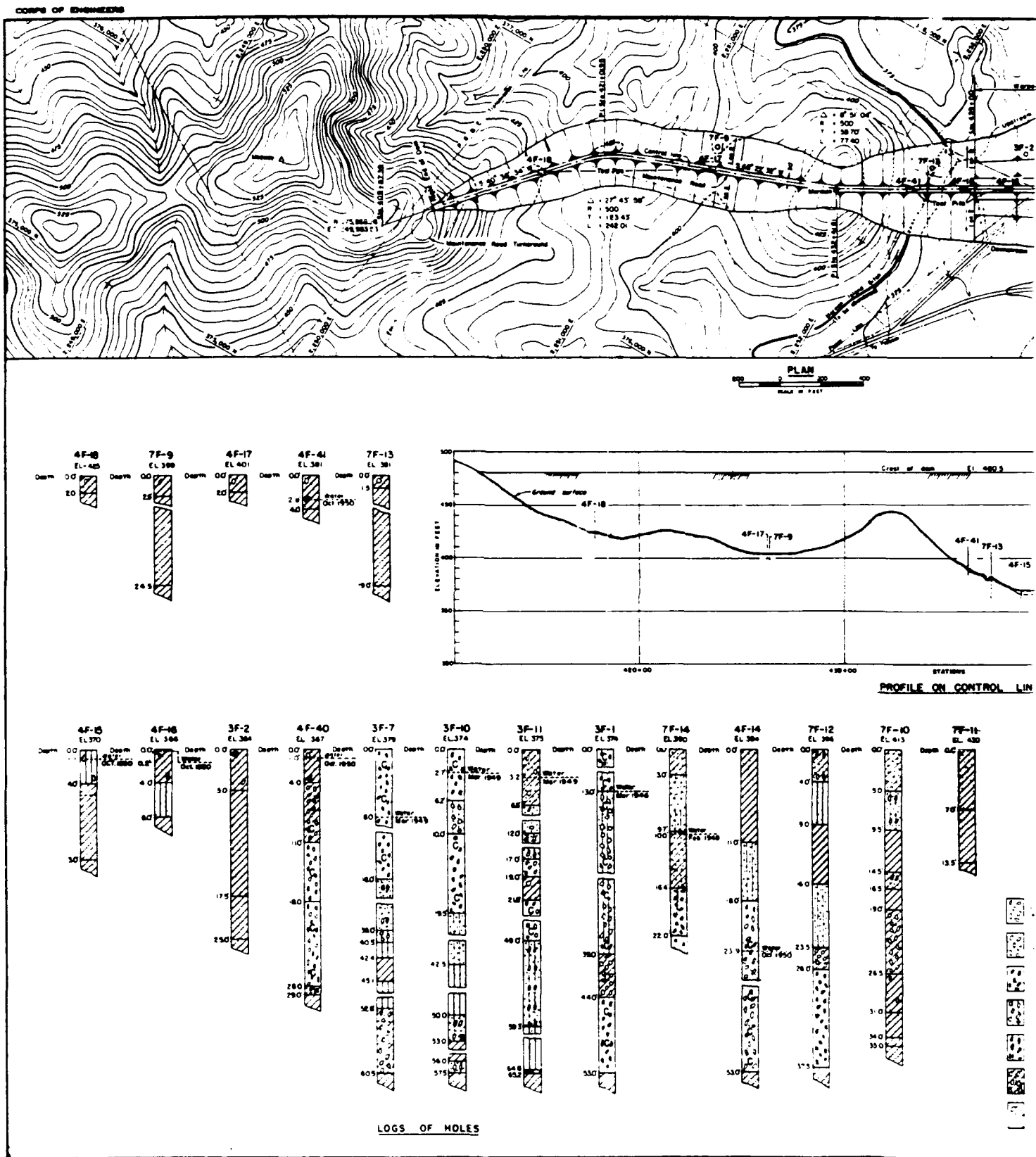
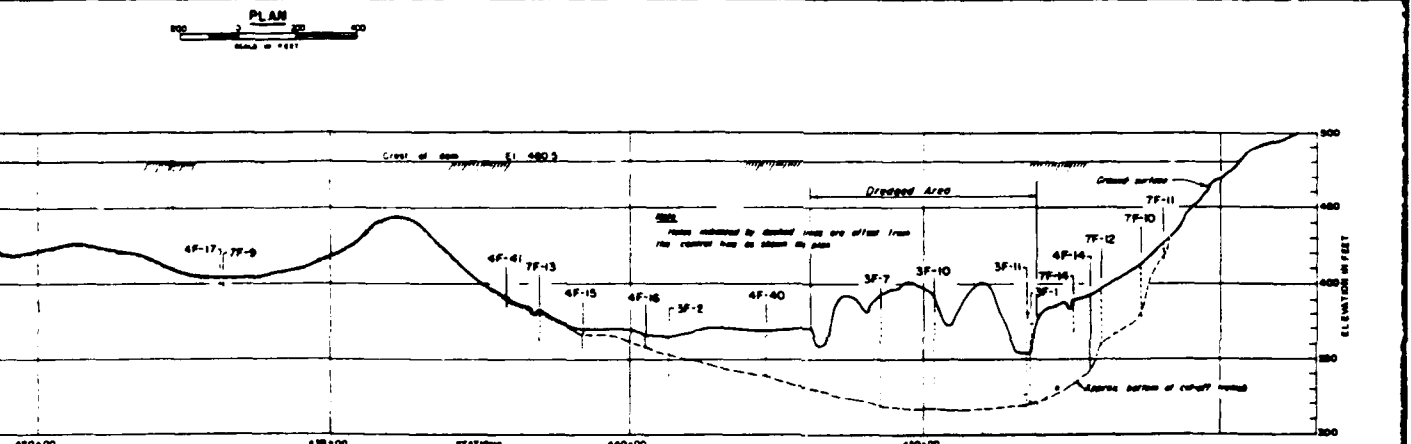
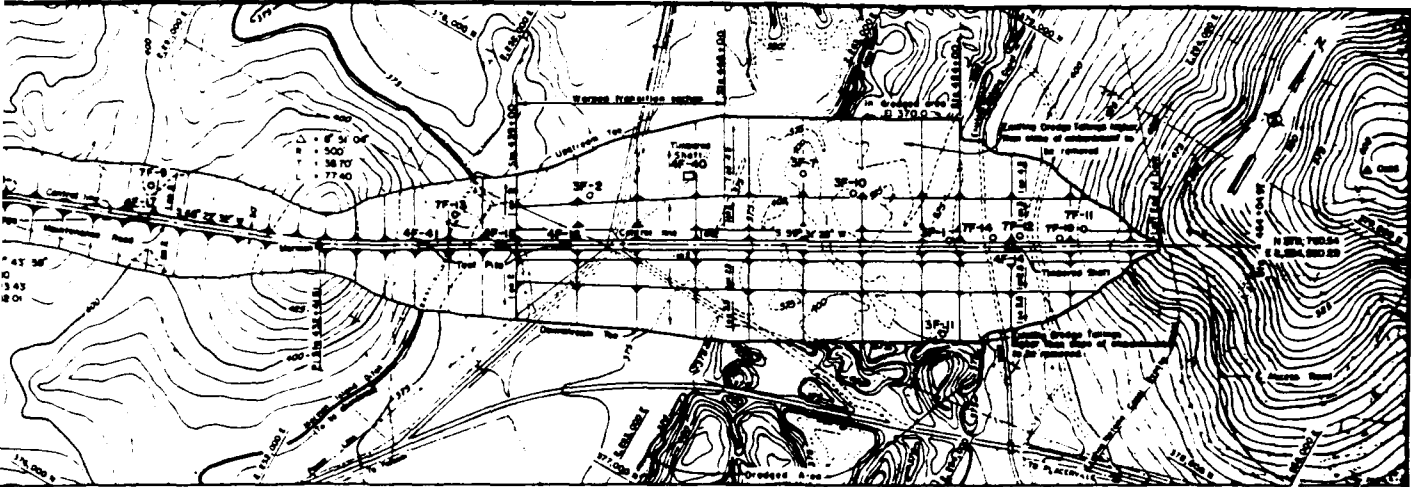
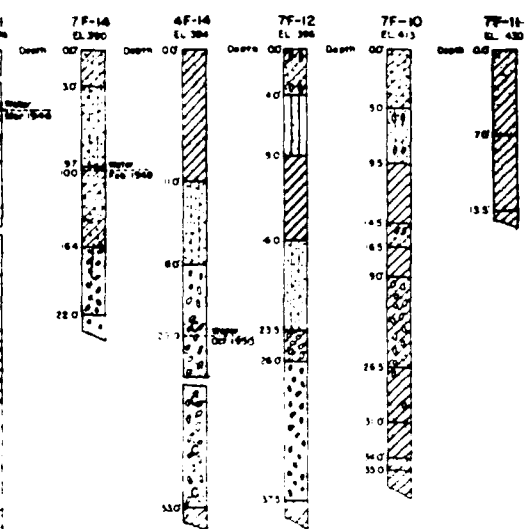


Figure 3. Plan and axial section of Mormon Island Auxiliary Dam



PROFILE ON CONTROL LINE



LEGEND

Gravel, well graded	Silty gravelly sand	Gravelly clay
Sandy gravel, well graded	Silty sand	Gravelly sandy clay
Sandy gravel, poorly graded	Clayey gravelly sand	Sandy clay
Silty gravel	Clayey sand	Lean clay
Silty gravel	Gravelly sandy silt	Fat clay
Clayey sandy gravel	Sandy silt	Heavy silt, silty clay
Gravelly sand	Cobbles	

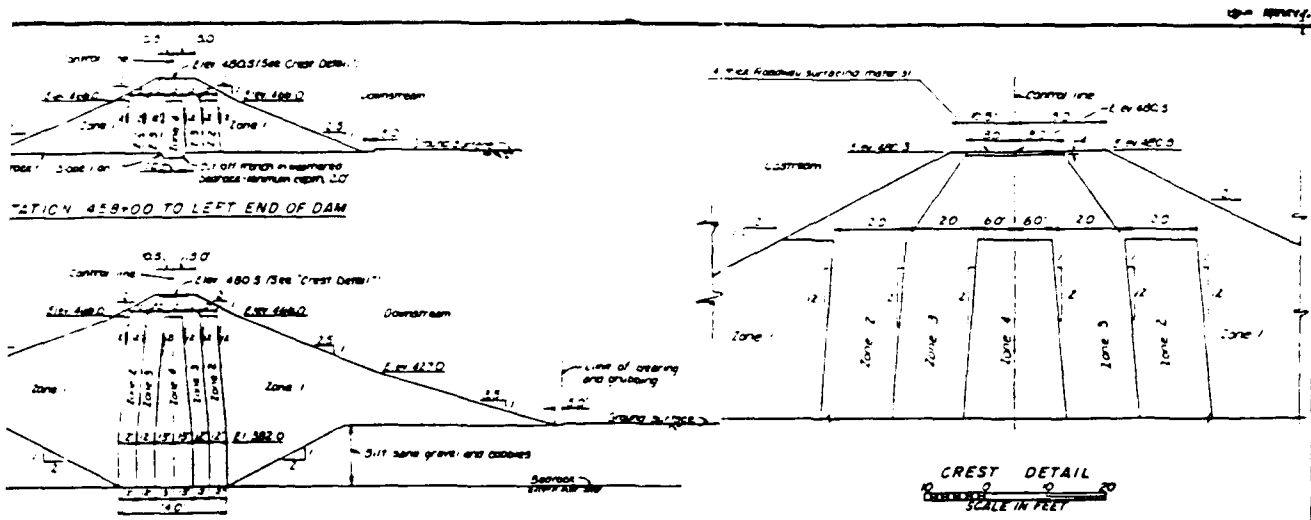
NOTES

1. Datum is Sea Level Datum of 1929.
2. Elevations shown on logs are ground surface elevations.
3. Laboratory classification shown for all materials, according to the Corps of Engineers' Uniform Soils Classification, except those shown in logs of holes 3F-1, 3F-2, 7F-13 and 7F-14, which are field classifications.
4. Holes 3F-1 and 3F-2 were drilled with a 12" churn drill. Holes 3F-7, 3F-10 and 3F-11 were drilled with a 10" churn drill. Samples were taken with a power auger and push tube sampler, where possible.
5. All 4F holes are open pits or shafts.
6. All 7F holes were drilled with a Folsom drilling rig using a 7" diameter rotary core drill.
7. Typical embankment sections shown on Sheet No. 357/7.
8. Limit of contractor's work areas including waste areas are shown on drawing Sheet No. 357/2.
9. Slopes of warped transition very uniformly from Station 439+00 to 446+00.
10. The term gravel, under the classification system used for this drawing, applies to grain sizes larger than the No. 10 sieve.
11. The term cobbles includes material from 3" to 18" in size and the presence of some is indicated by the letter "C" in the logs.
12. This drawing was taken from As-Constructed sheet no. 357/3, File No. AM-1-7-557.

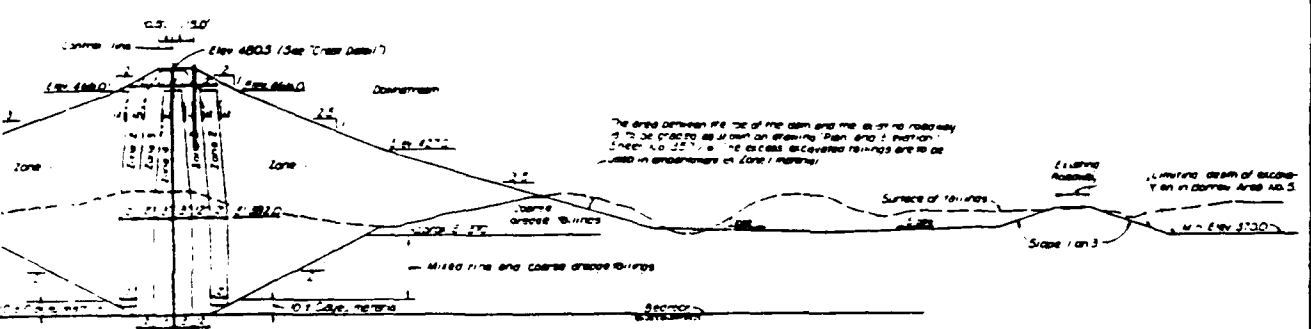
AMERICAN RIVER BASIN DEVELOPMENT CALIFORNIA  
FOLSOM RESERVOIR PROJECT  
AMERICAN RIVER  
MORMON ISLAND AUXILIARY DAM  
FOUNDATION EXPLORATION  
PLAN, PROFILE AND LOGS OF HOLES

axial section of Mormon Island Auxiliary Dam

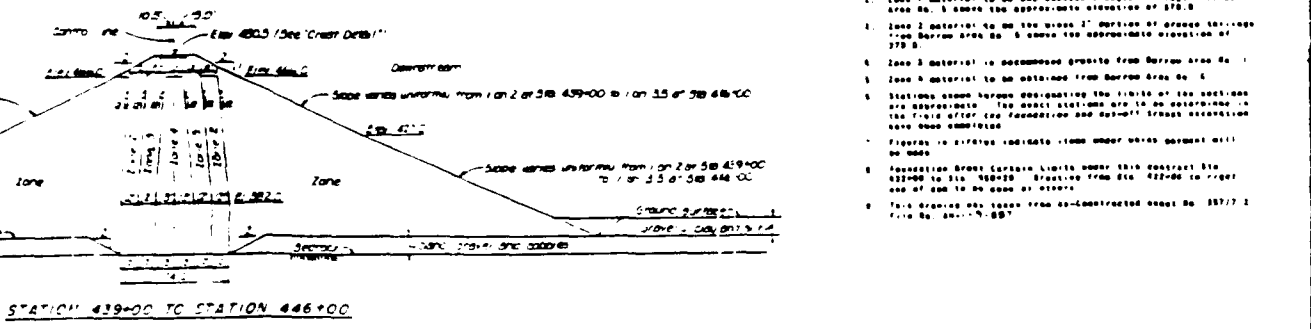
**Figure 4. Typical embankment sections, Mormon Island Auxiliary Dam**



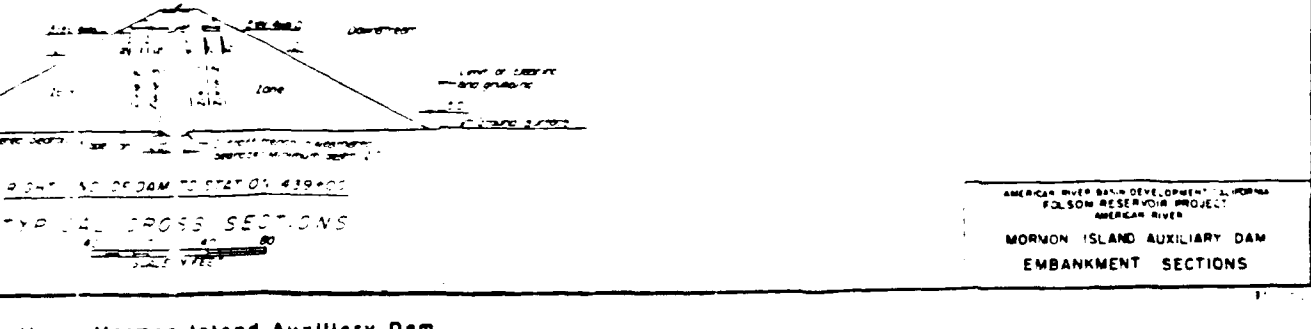
STATION 459+00 TO LEFT END OF DAM



STATION 454+00 TO STATION 459+00



STATION 446+00 TO STATION 454+00



STATION 439+00 TO STATION 446+00

TYPICAL CROSS SECTIONS

NOTES

1. Refer to Sea Level Datum of 1929
2. Zone 1 material to be processed dredged tailings from Barron Area No. 5 above the approximate elevation of 370.0
3. Zone 2 material to be the waste 1" portion of dredged tailings from Barron Area No. 5 above the approximate elevation of 370.0
4. Zone 3 material to be processed granite from Barron Area No. 1
5. Zone 4 material to be obtained from Barron Area No. 4
6. Stations shown herein designating the limits of the sections are approximate. The exact stations are to be determined in the field after the foundation and abutment structure excavation have been completed.
7. Figures in figures indicate zone number which payment will be made.
8. Foundation Brack Corrosion Limits under this contract are 425+00 to Sta. 460+00. Brackings from Sta. 425+00 to proper end of dam to be done at owner's expense.
9. To be Brackings may taken from co-constructed abutment No. 357/7.2 from Sta. 460+00 to 460+00.

AMERICAN RIVER BASIN DEVELOPMENT - CALIFORNIA  
FOLSOM RESERVOIR PROJECT  
AMERICAN RIVER  
MORMON ISLAND AUXILIARY DAM  
EMBANKMENT SECTIONS

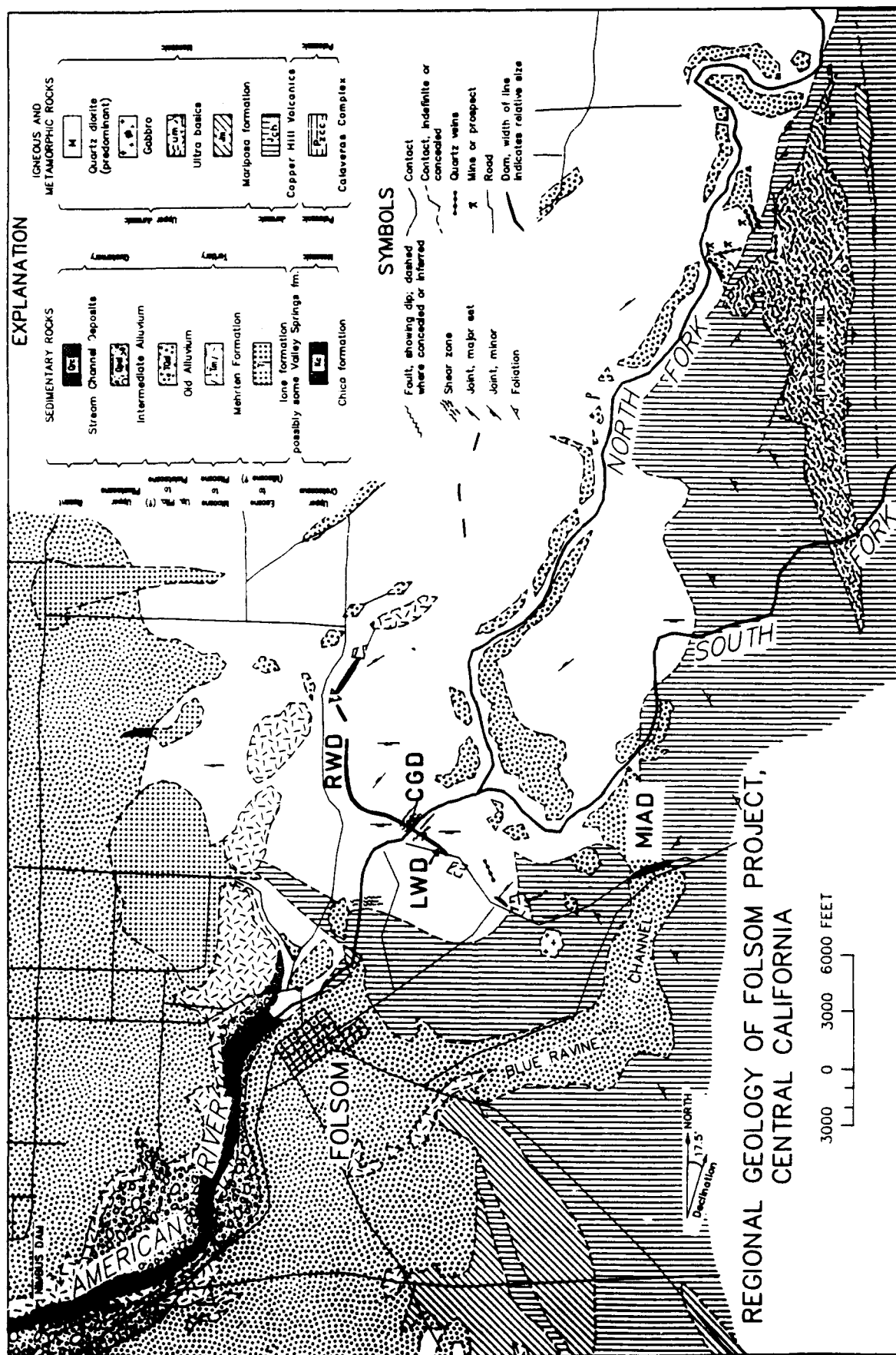


Figure 5. Geologic map, parts of the Folsom and Auburn quadrangles

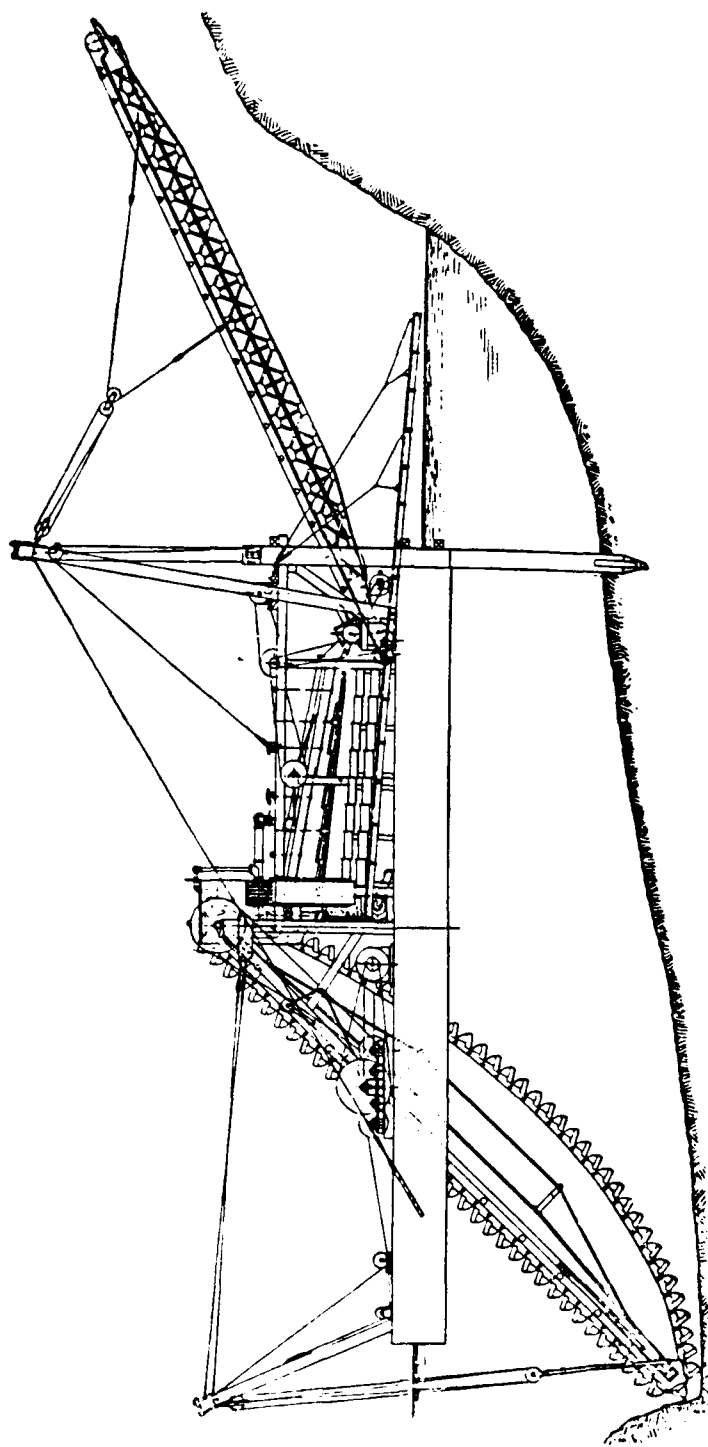


Figure 6. Bucyrus type of dredge, with close-connected buckets, shaking screens, belt conveyor, and spuds (from Aubury 1905)

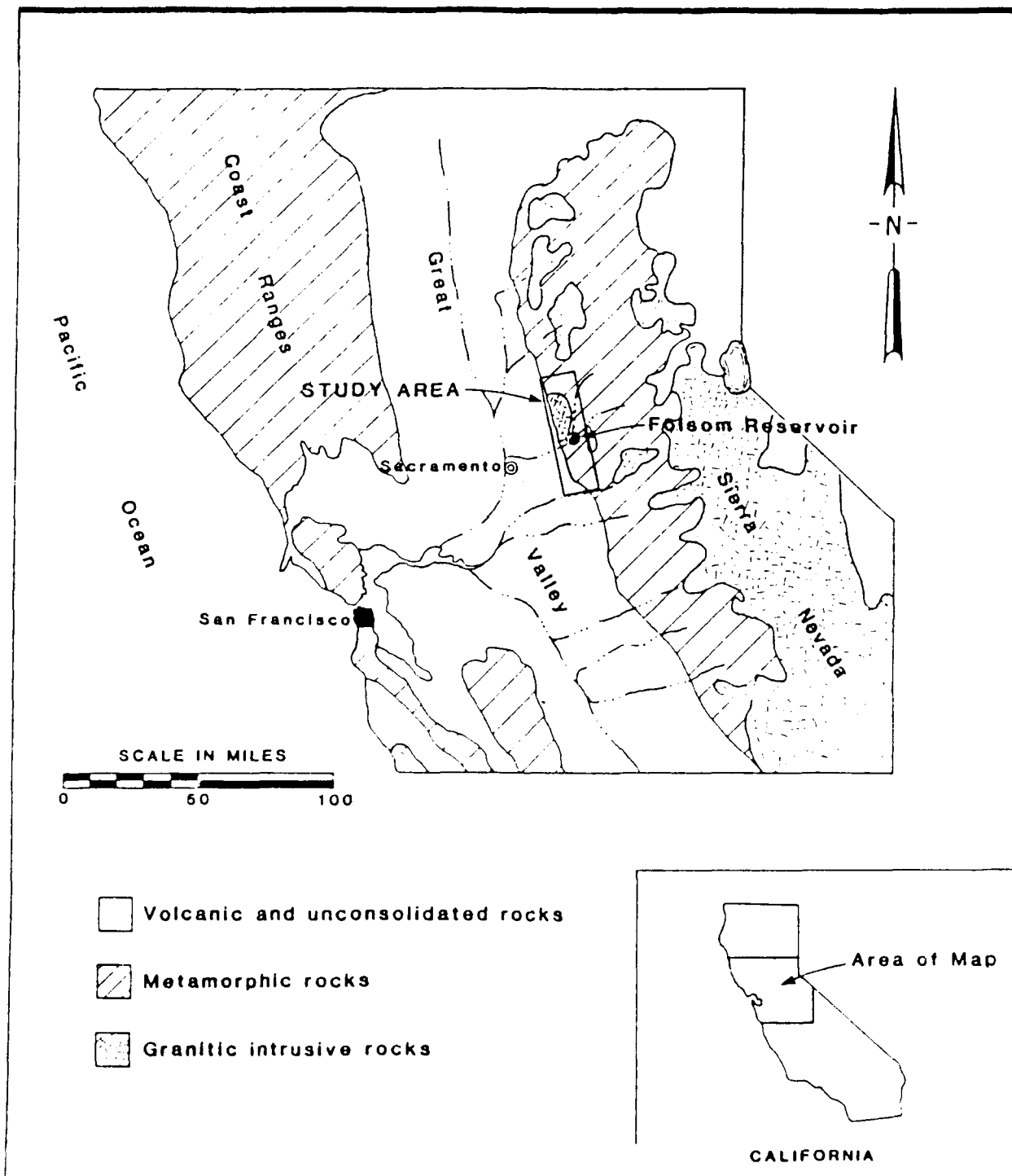


Figure 7. Regional geologic map (after Tierra Engineering Consultants 1983)

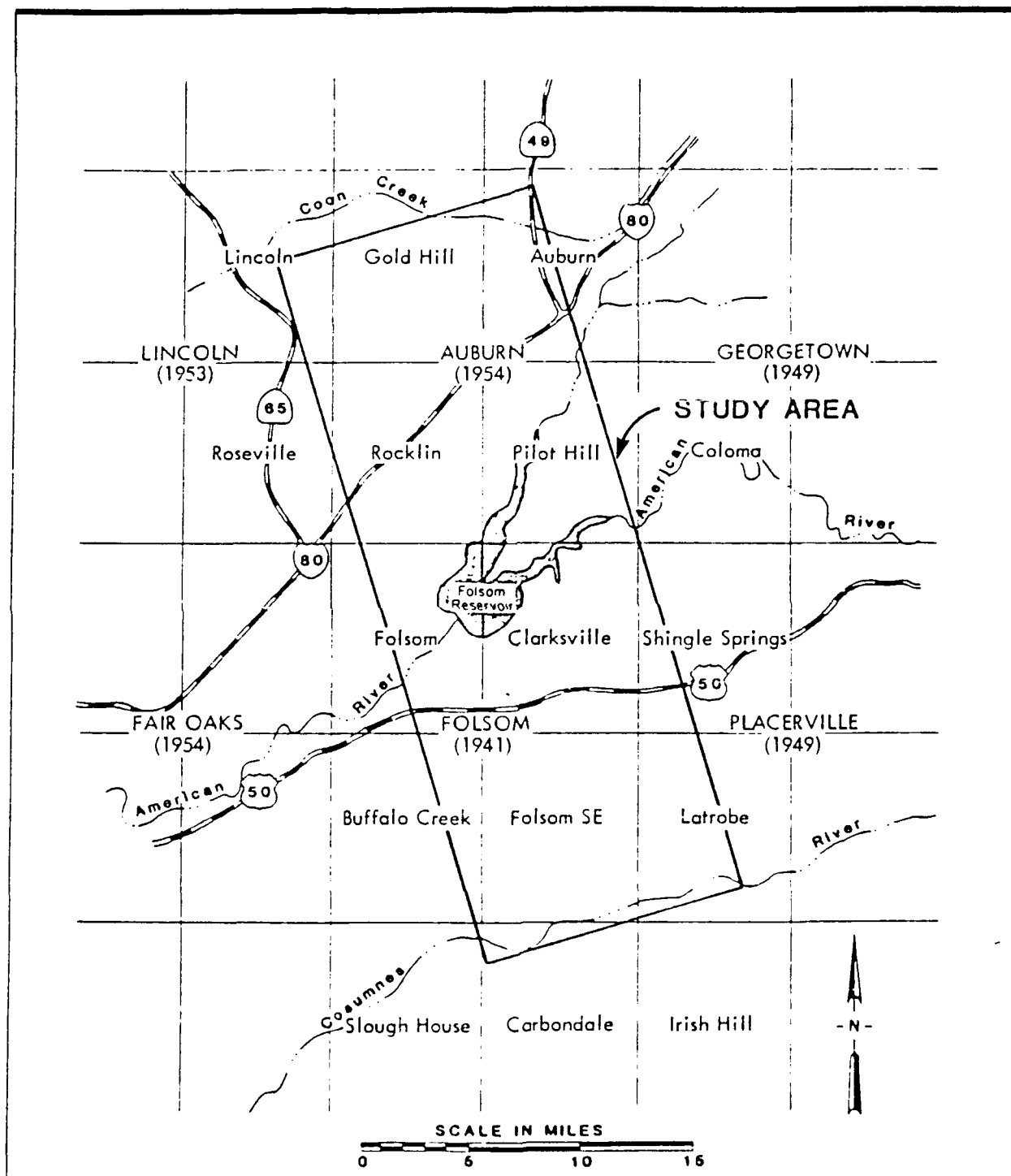


Figure 8. Identification of study area (from USGS 7.5 and 15 ft topographic maps, after Tierra Engineering Consultants 1983)



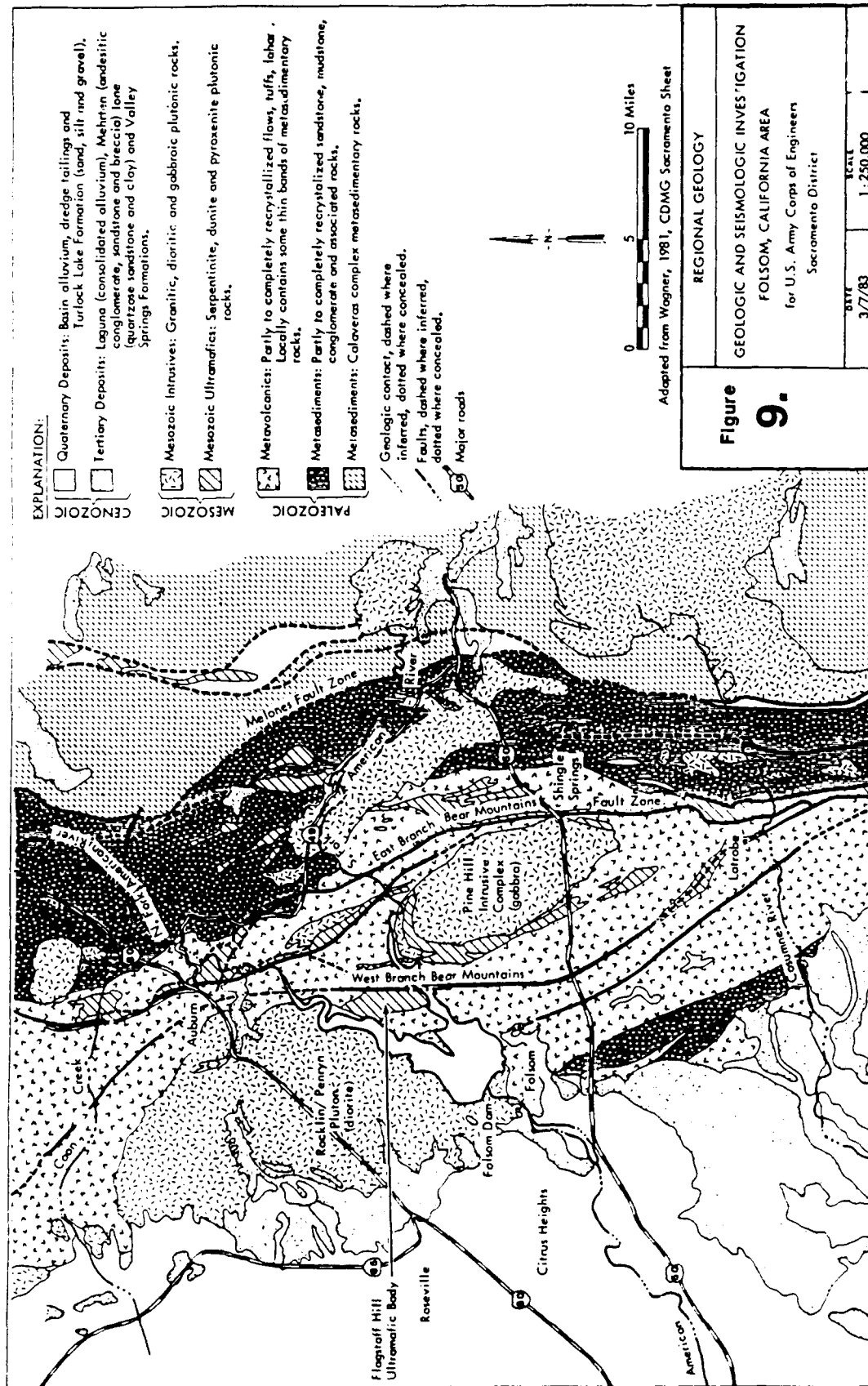


Figure 9. Regional geology in vicinity of Folsom Dam and Reservoir (after Tierra Engineering Consultants 1983)

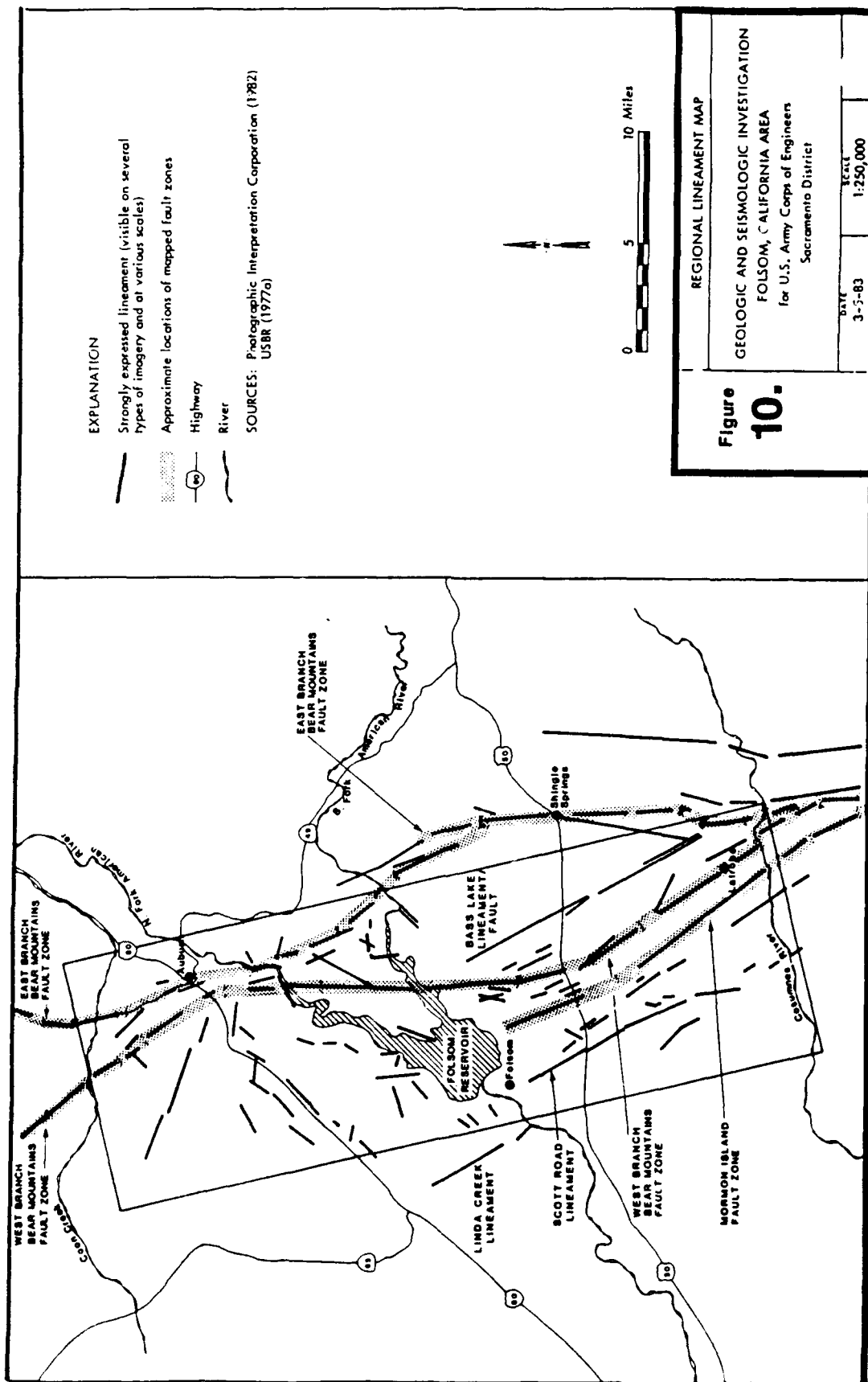
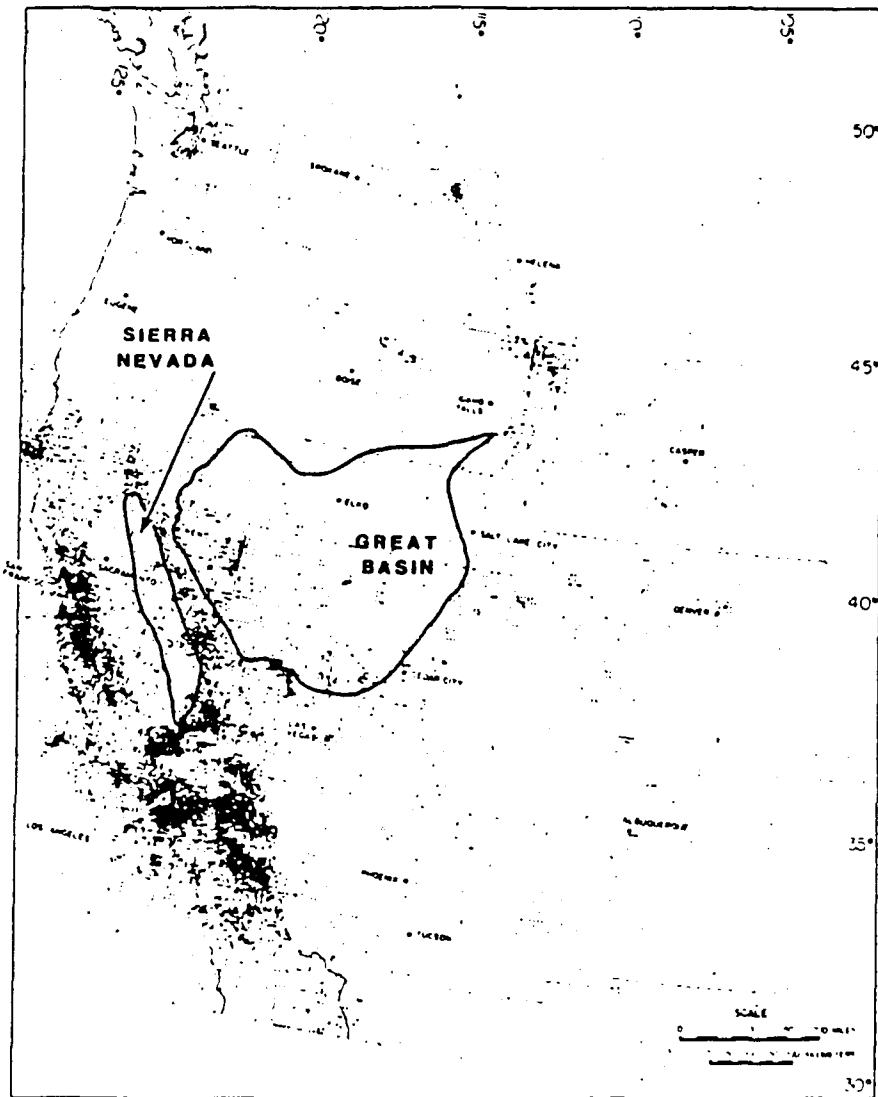


Figure 10. Regional lineament map (after Terra Engineering Consultants 1983)



SOURCE: Adapted from Smith 1978

Figure 11. Epicenter map of western United States (after Tierra Engineering Consultants 1983)

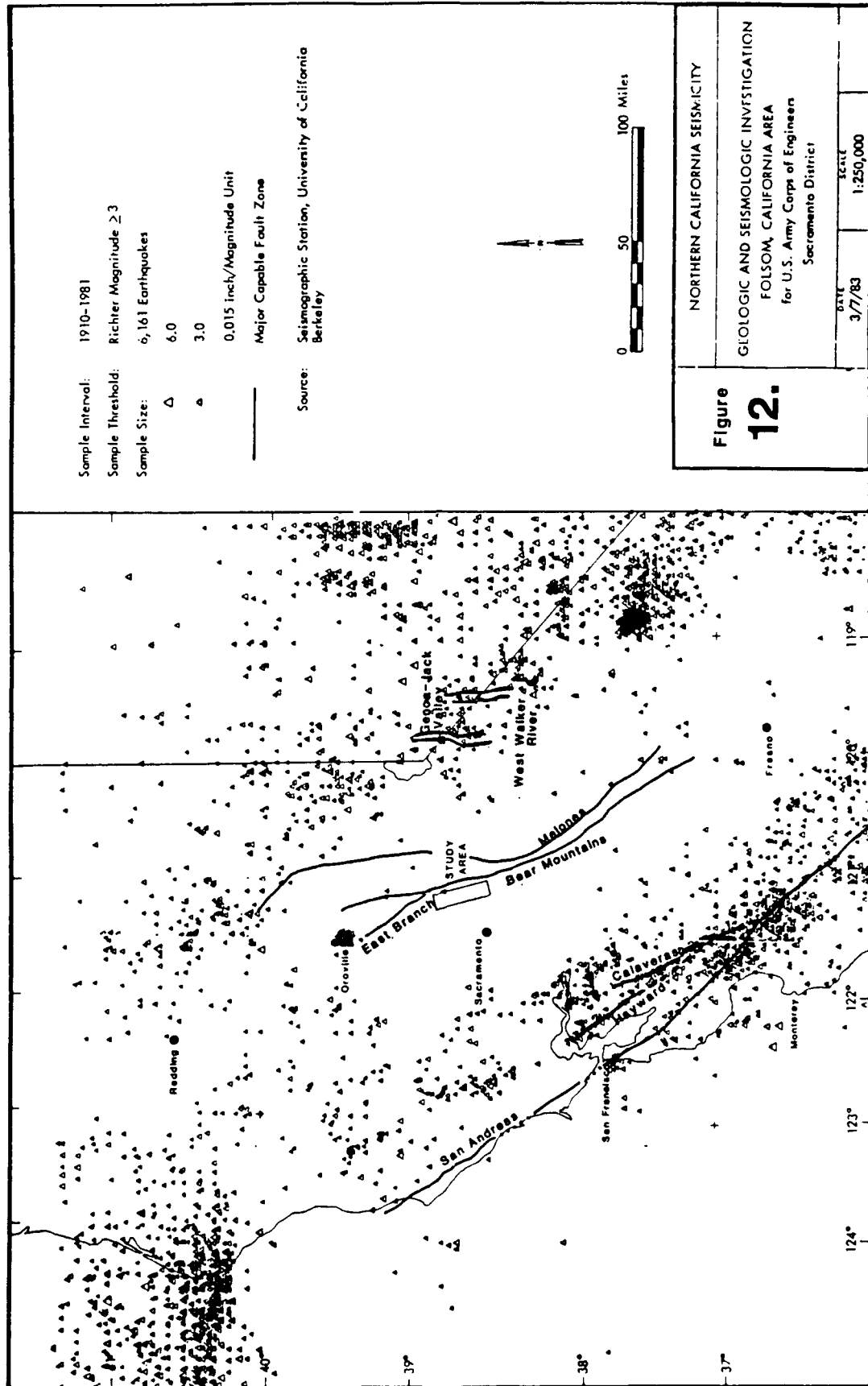


Figure 12. Seismicity map for northern California (after Tierra Engineering Consultants 1983)

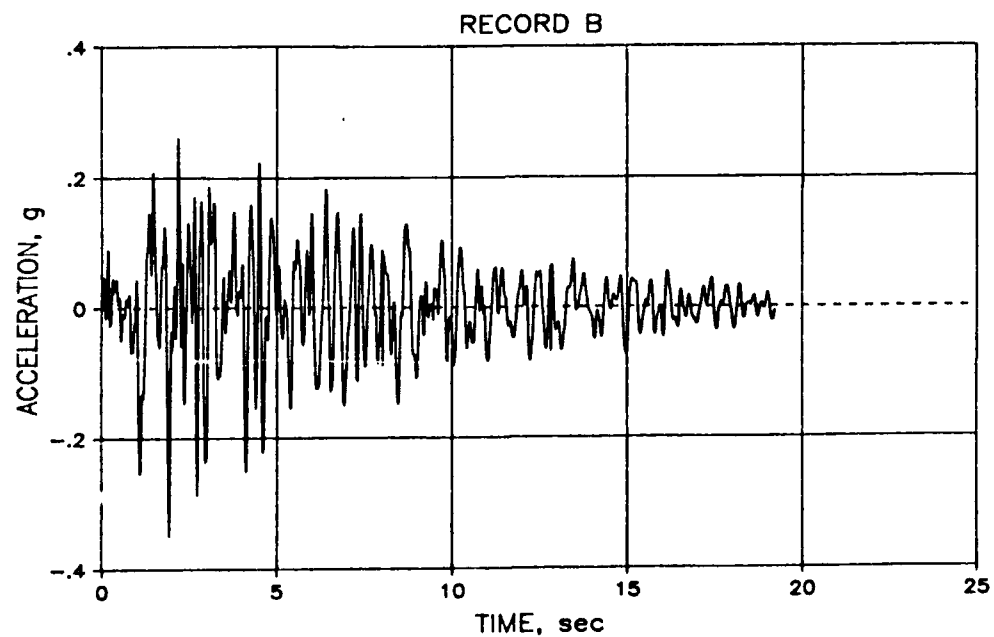
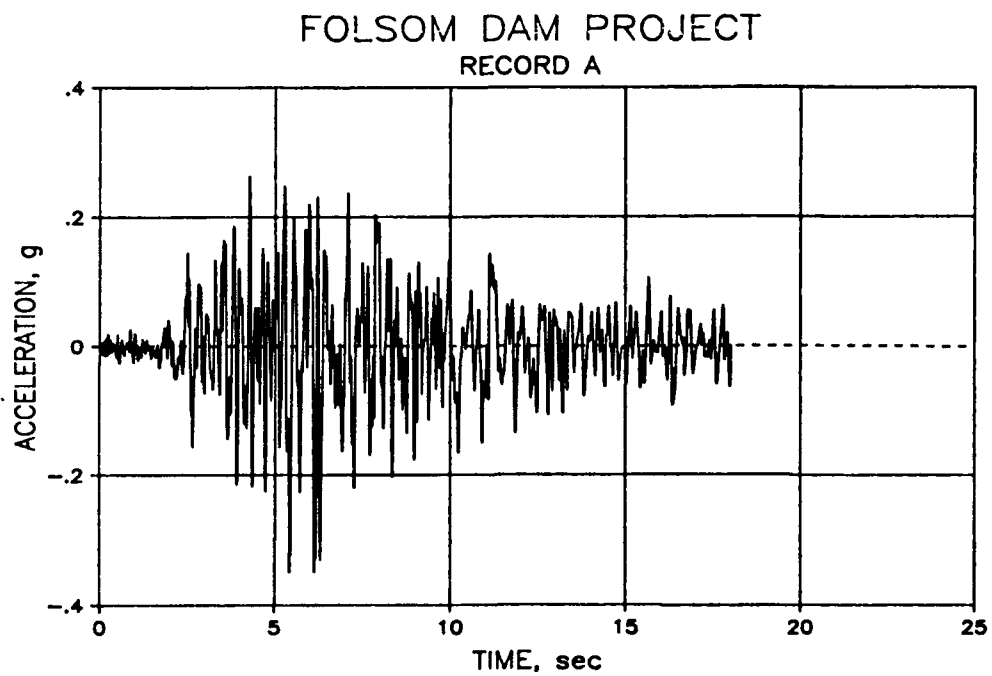


Figure 13. Acceleration histories used in the analysis

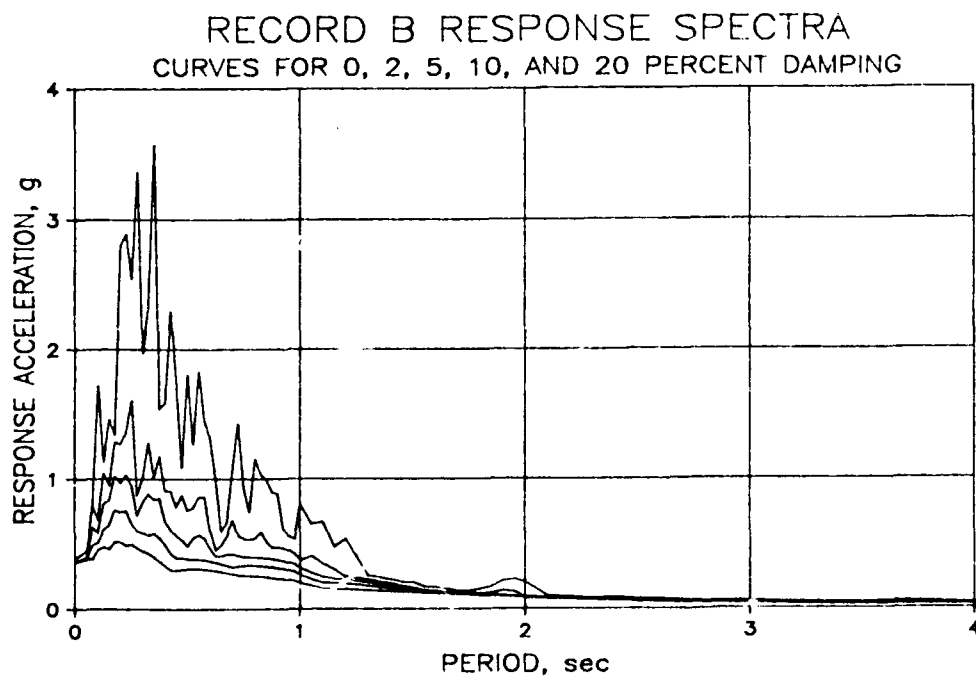
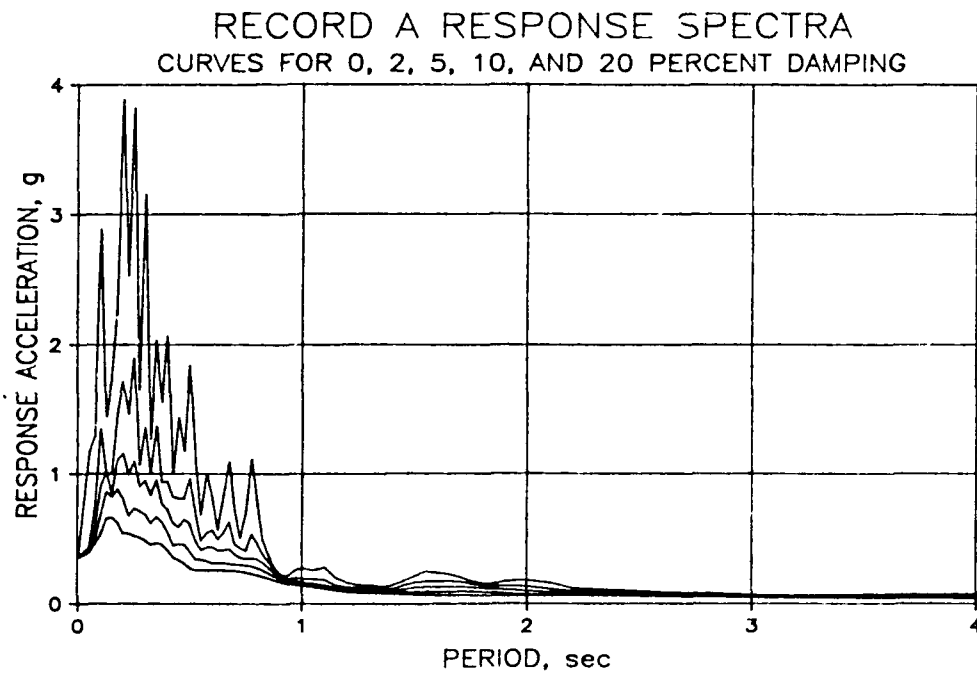


Figure 14. Response spectra of records A and B



Figure 15. View of Mormon Island Auxiliary Dam foundation preparation, looking southwest from left abutment to right abutment (FOL-476, 4/10/51)



Figure 16. Foundation preparation for portion of Mormon Island Auxiliary Dam founded on rock, looking southwest from sta 421+00 to right abutment (FOL-490, 4/11/51)



Figure 17. Core trench excavation through undisturbed alluvium, looking southwest from sta 440+00 to right abutment (FOL-544, 6/25/51)



Figure 18. Core trench excavation in alluvium, looking northeast from sta 440+00 to left abutment (FOL-538, 6/26/51)





Figure 19. Completed core trench excavation, looking southwest from left abutment to right abutment  
(FOL-619, 9/26/51)



Figure 20. Placement of zone materials in core trench, looking southwest from sta 458+00 to right abutment  
(FOL-633, 10/30/51)



Figure 21. Placement of Zone 1 upstream shell, looking southwest from sta 421+50 to right abutment (FOL-528)

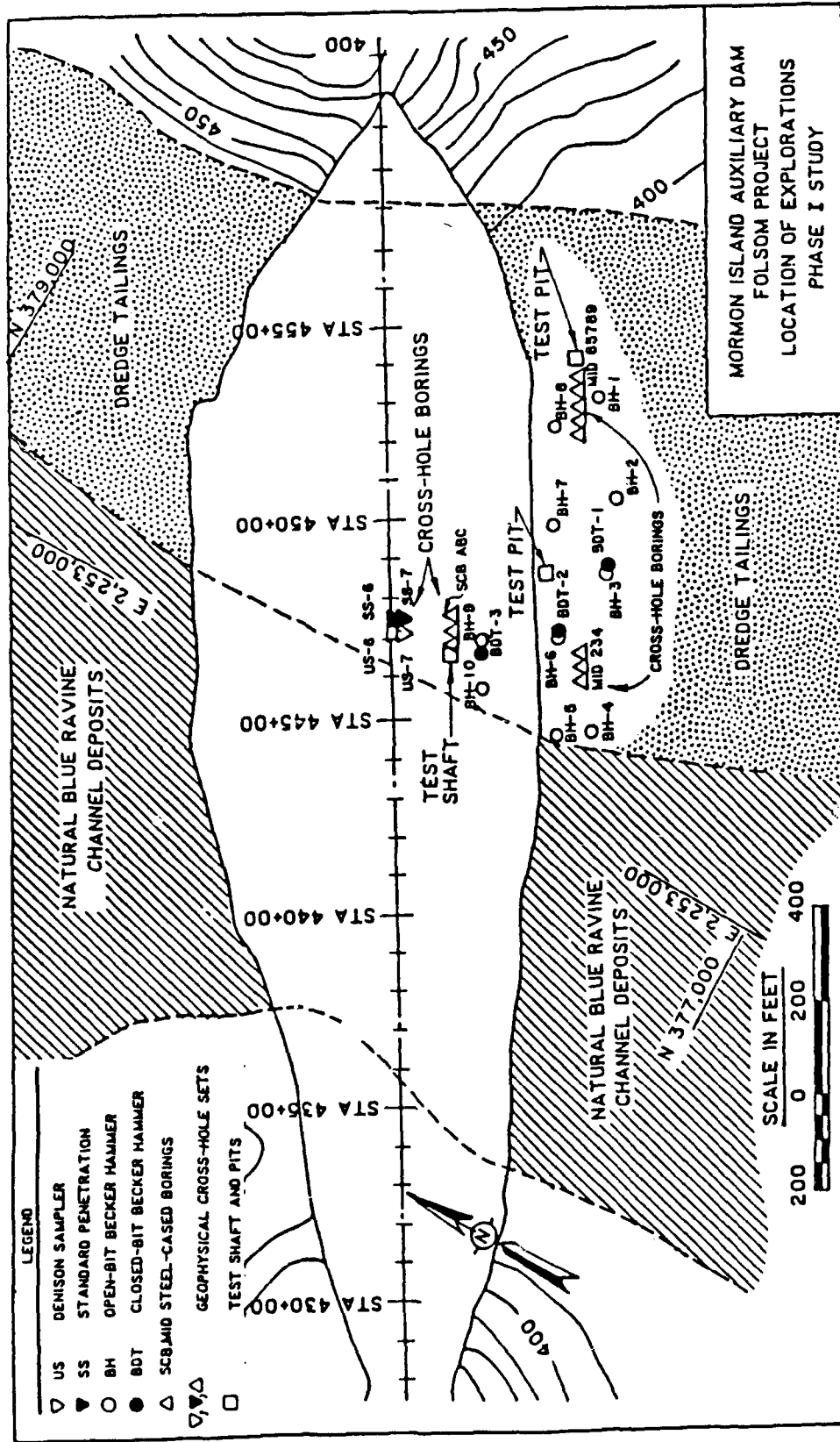


Figure 22. Plan view of field investigations at Mormon Island Auxiliary Dam

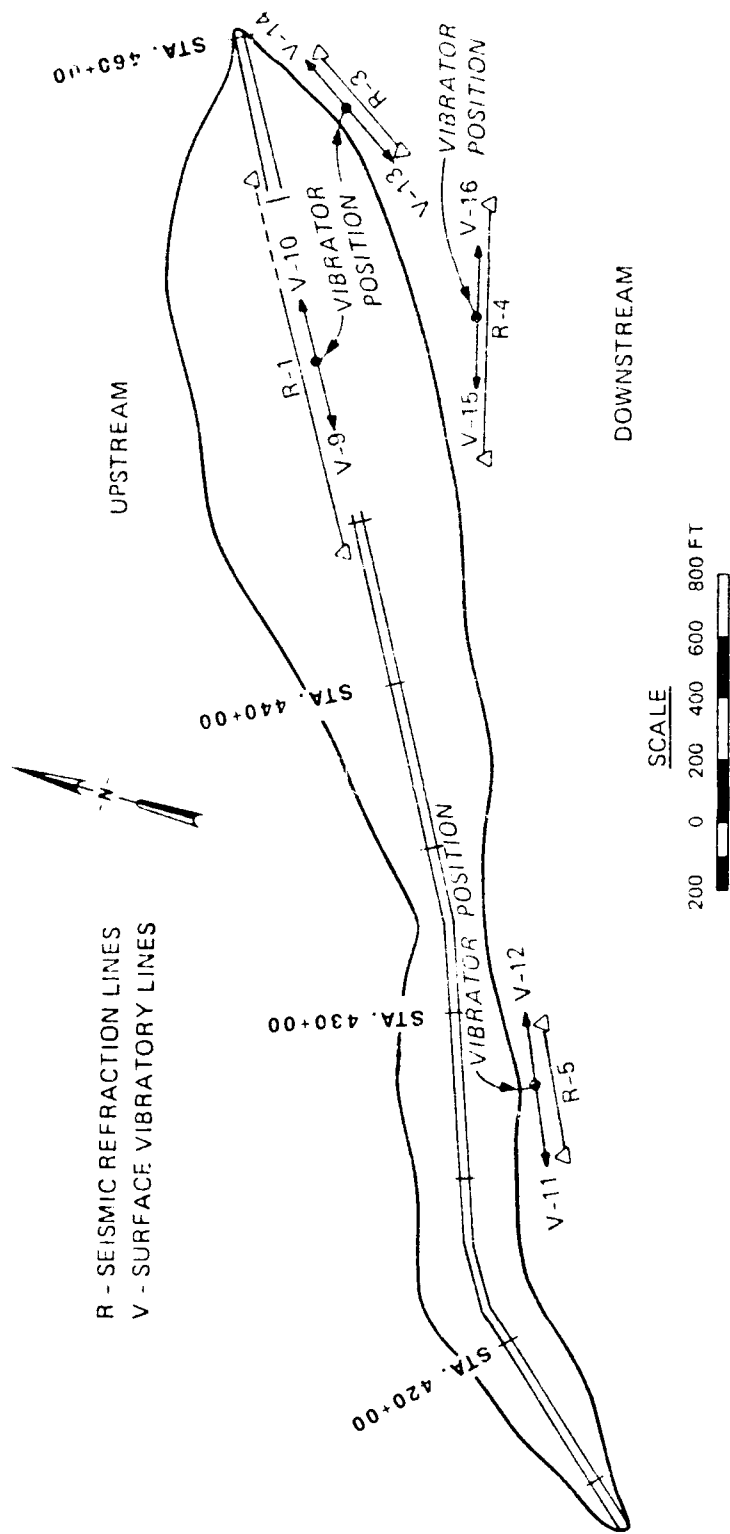


Figure 23. Plan of surface geophysical investigations at Mormon Island Auxiliary Dam

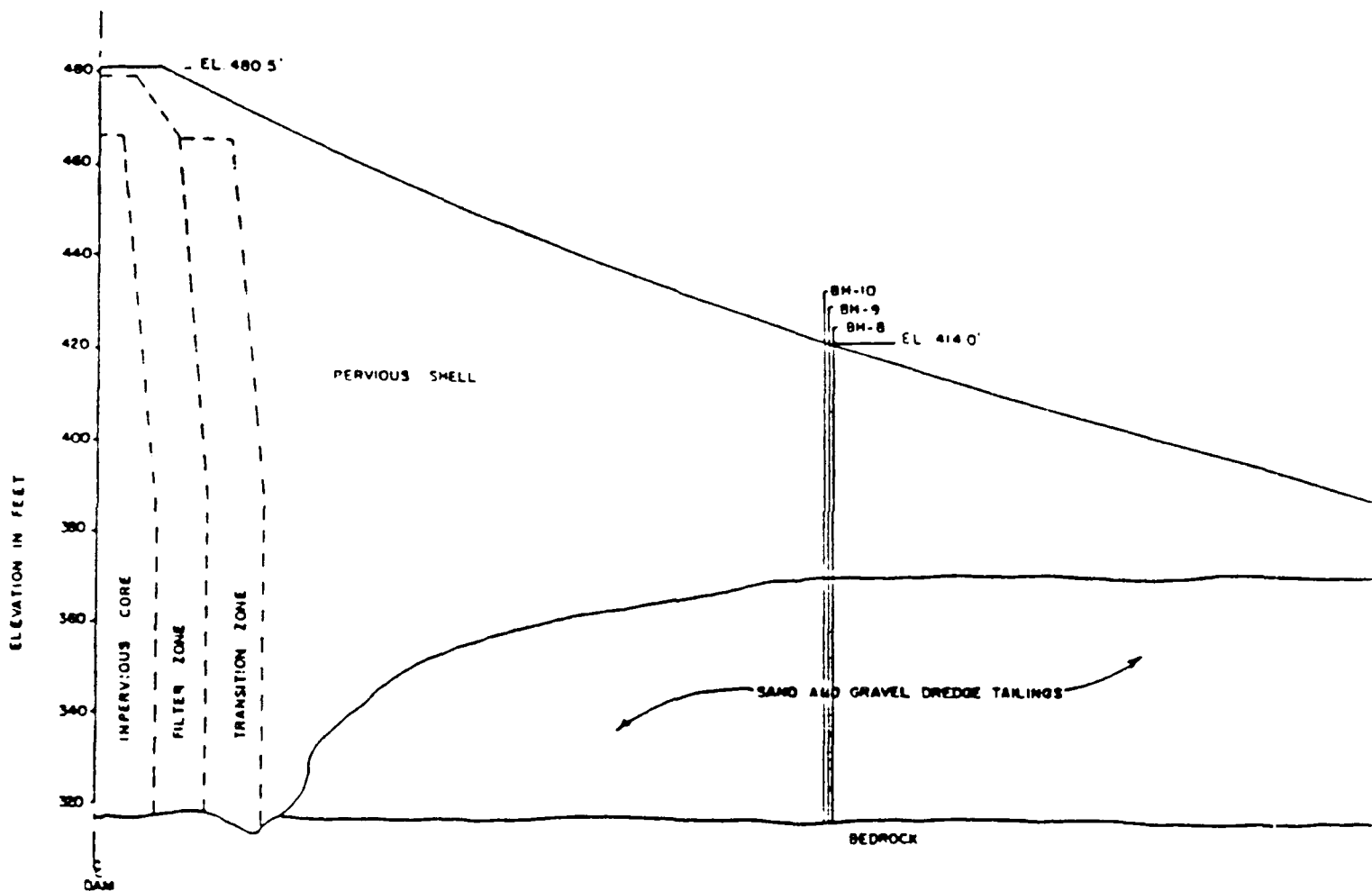
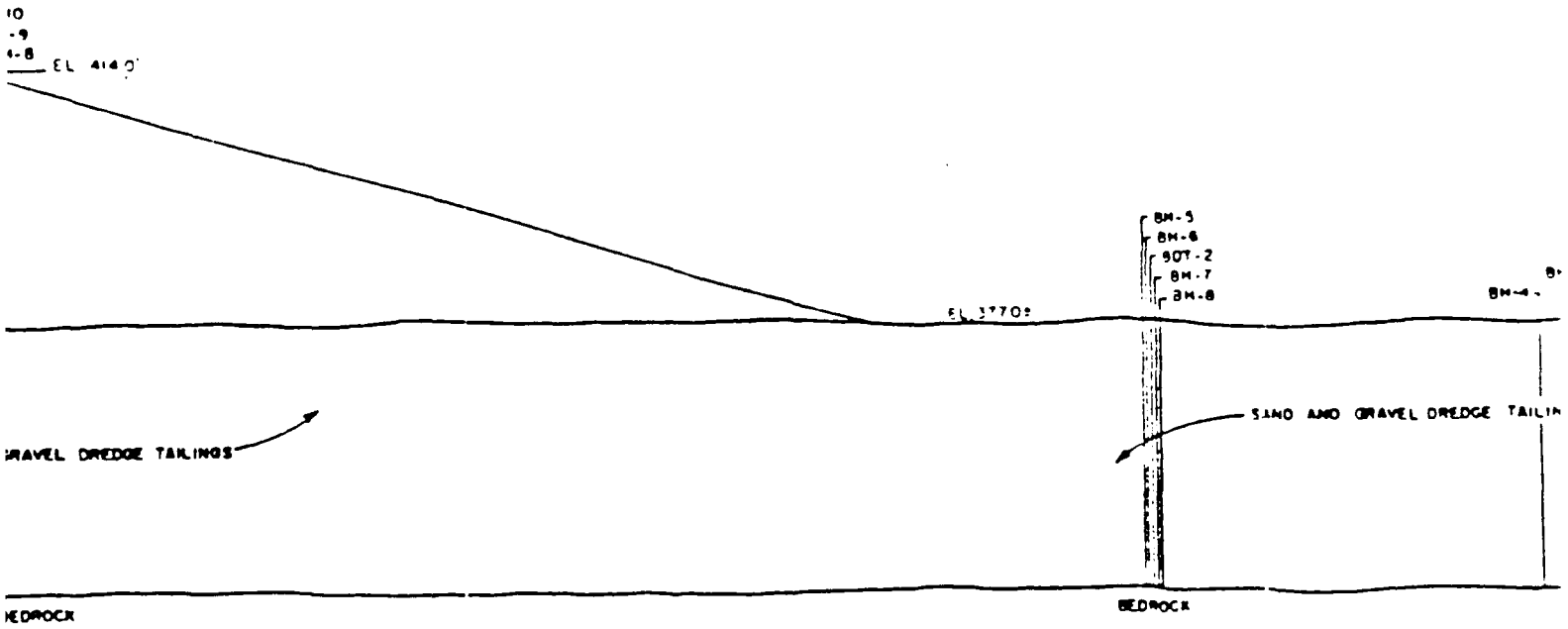


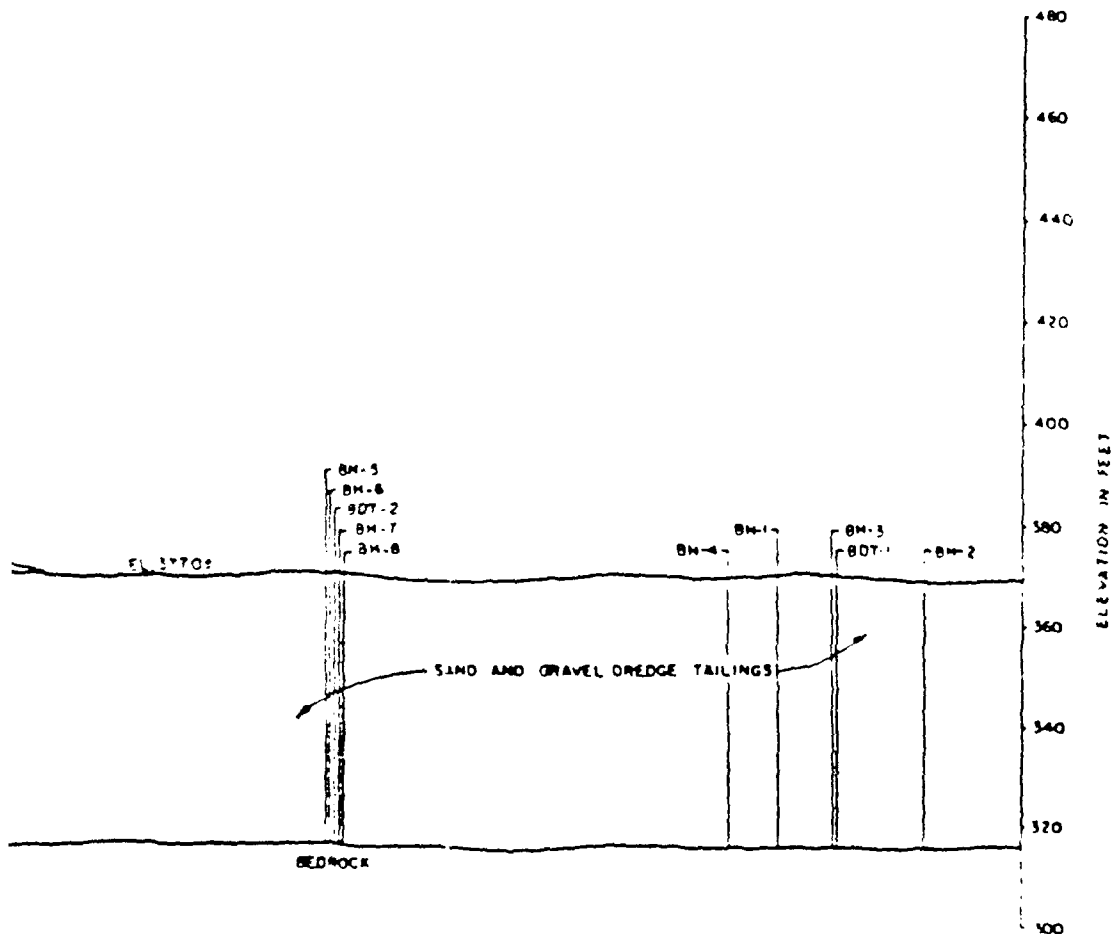
Figure 24. Section of Mormon Island Auxiliary Dam in the vicinity of sta 4

107



liary Dam in the vicinity of sta 447 showing materials sampled with Becker Hammer sound

293



Materials sampled with Becker Hammer soundings

393

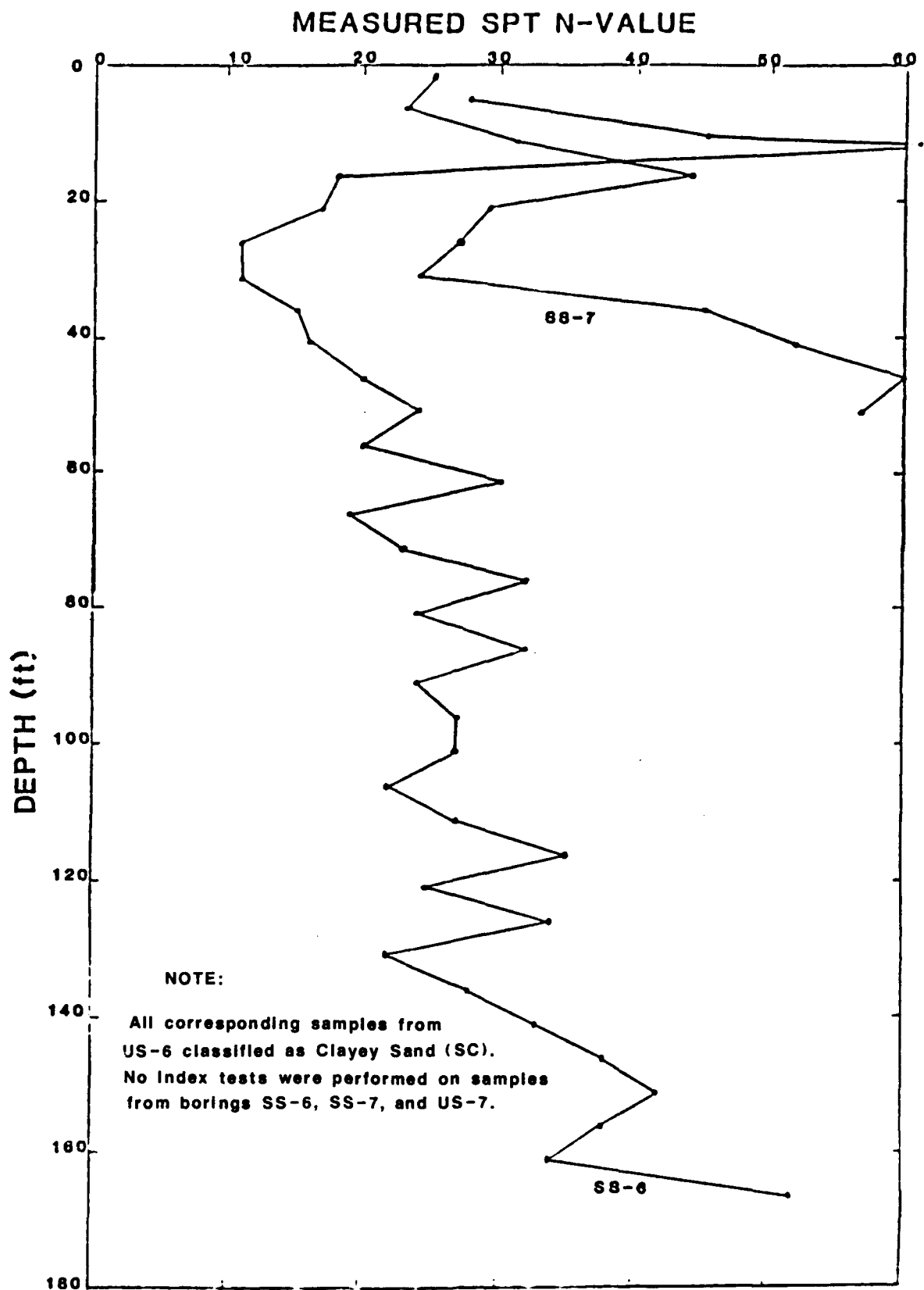


Figure 25. SPT blowcounts measured in core (Zone A, Boring 38-6) and filter (Zone 3, Boring 88-7) materials



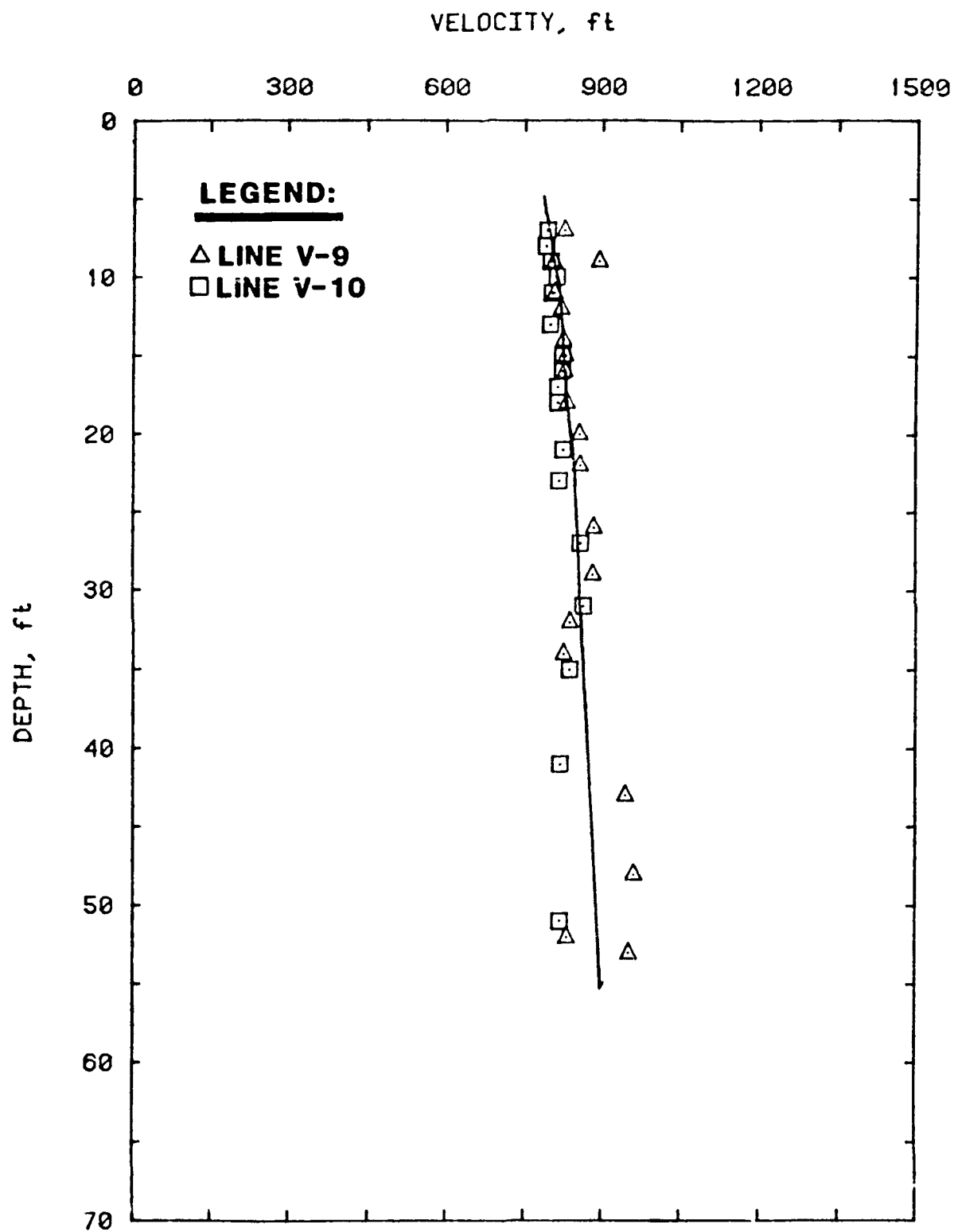


Figure 26.  $V_R$  versus depth for lines V-9 and V-10, measured along crest of Mormon Island Auxiliary Dam

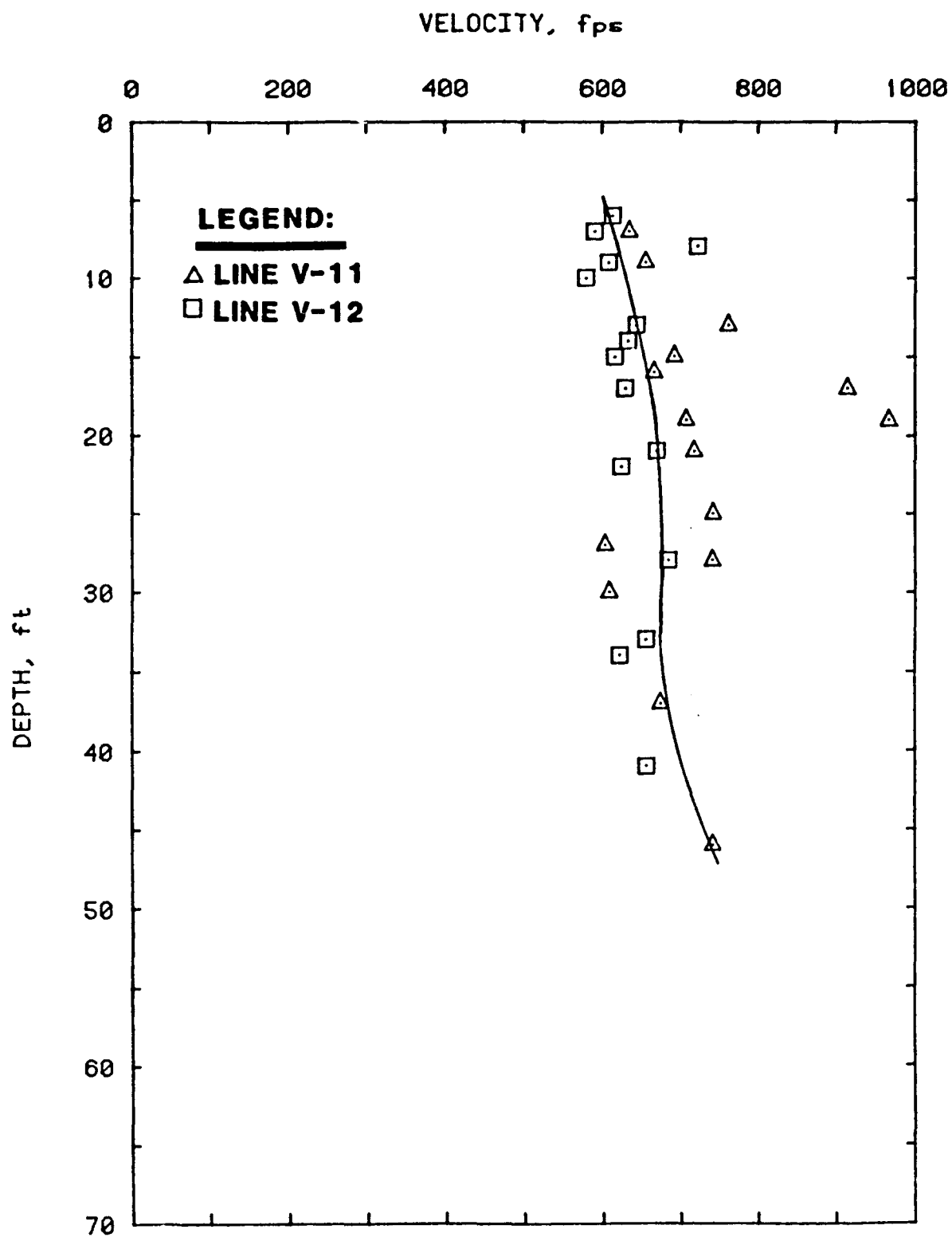


Figure 27.  $V_R$  versus depth for lines V-11 and V-12, measured along toe of Mormon Island Auxiliary Dam

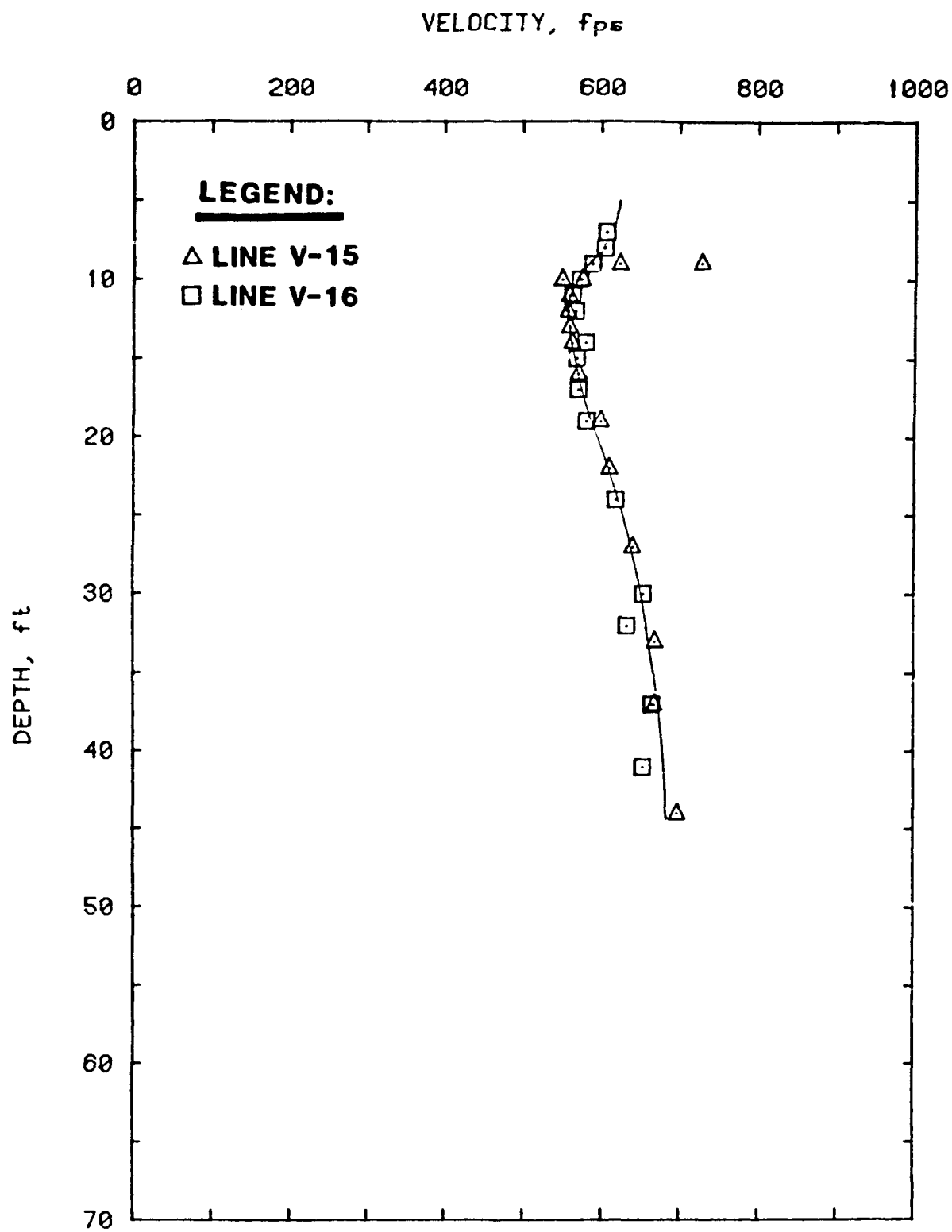


Figure 28.  $V_R$  versus depth for lines V-15 and V-16, measured along toe of Mormon Island Auxiliary Dam

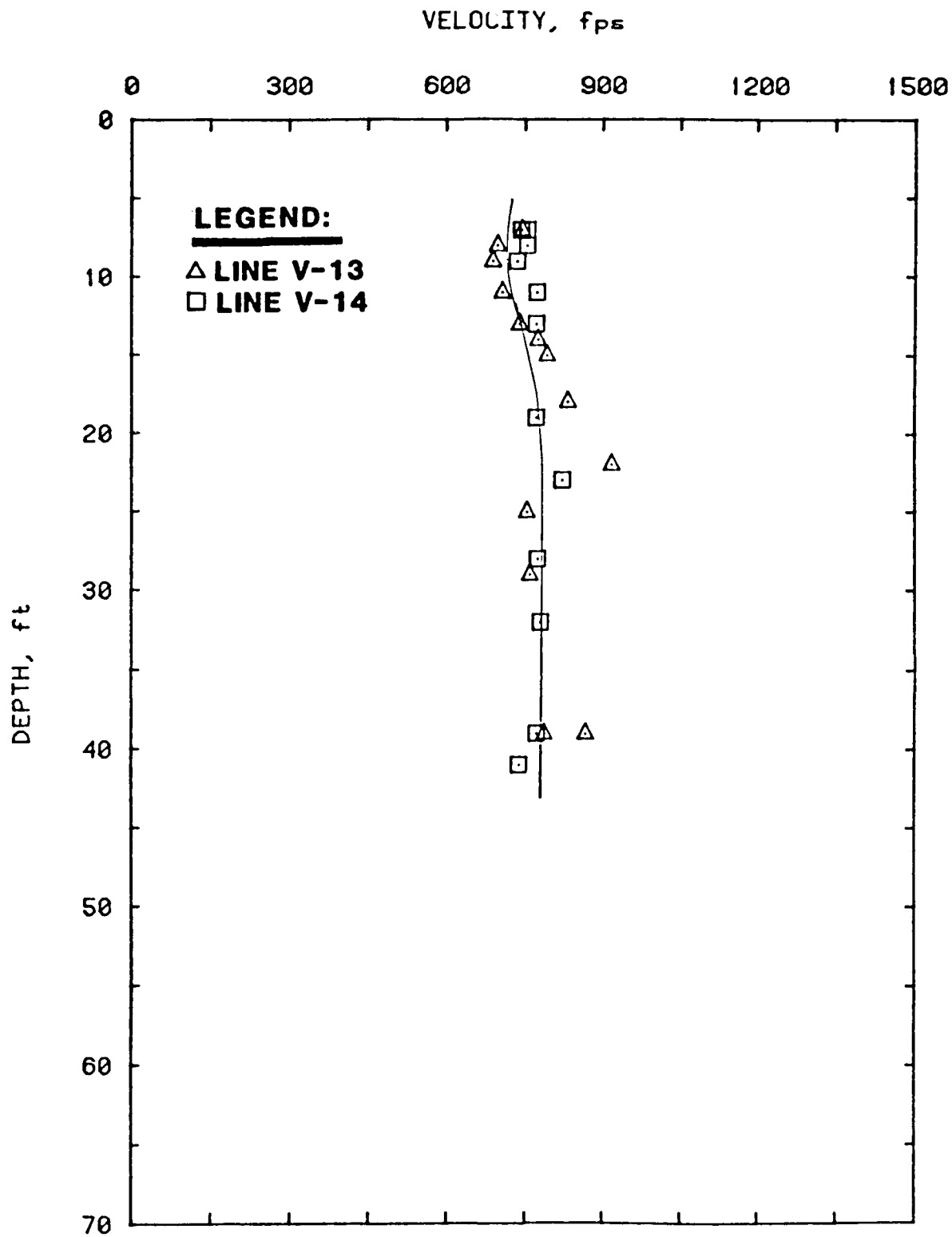


Figure 29.  $V_R$  versus depth for lines V-13 and V-14, measured along toe of Mormon Island Auxiliary Dam

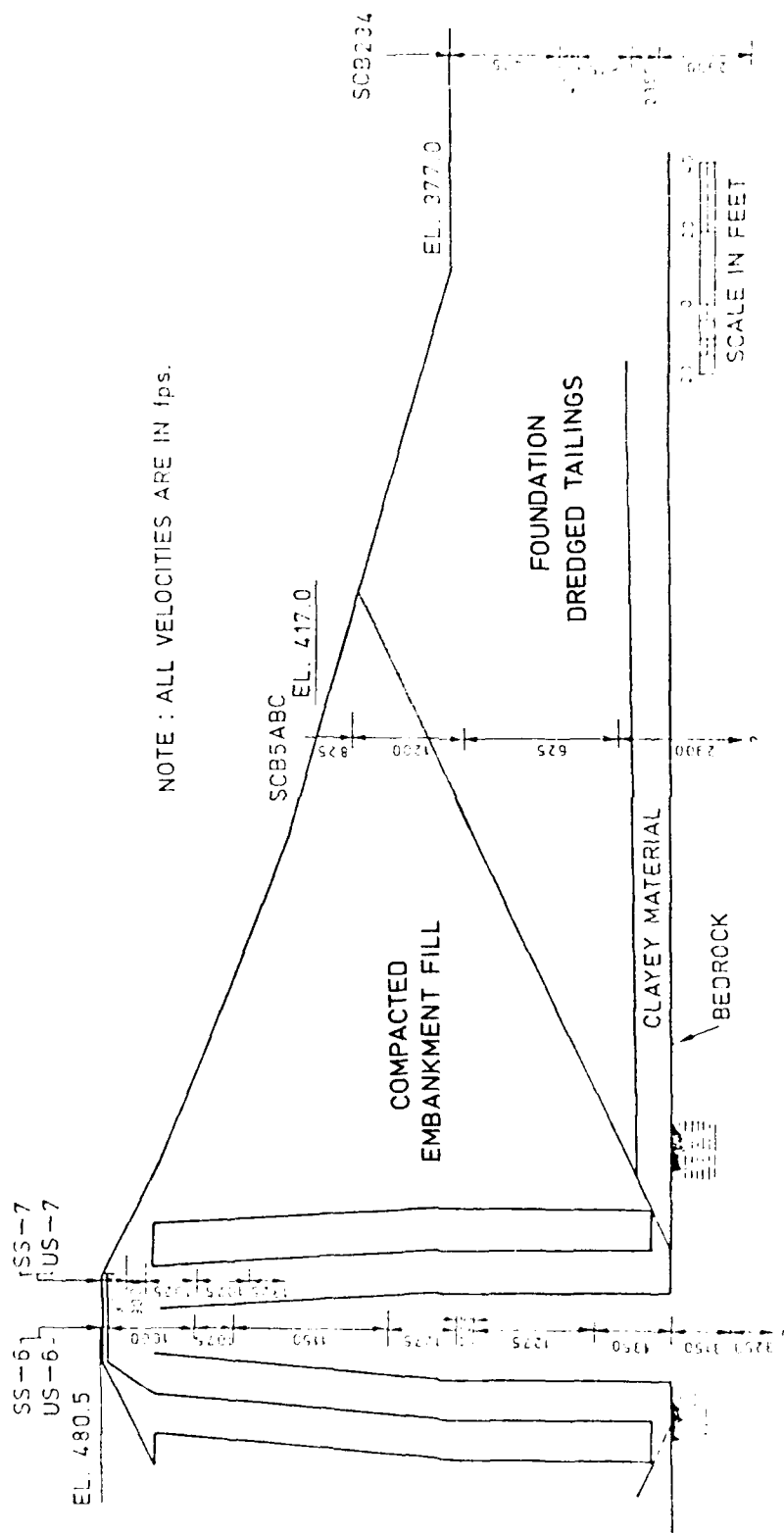
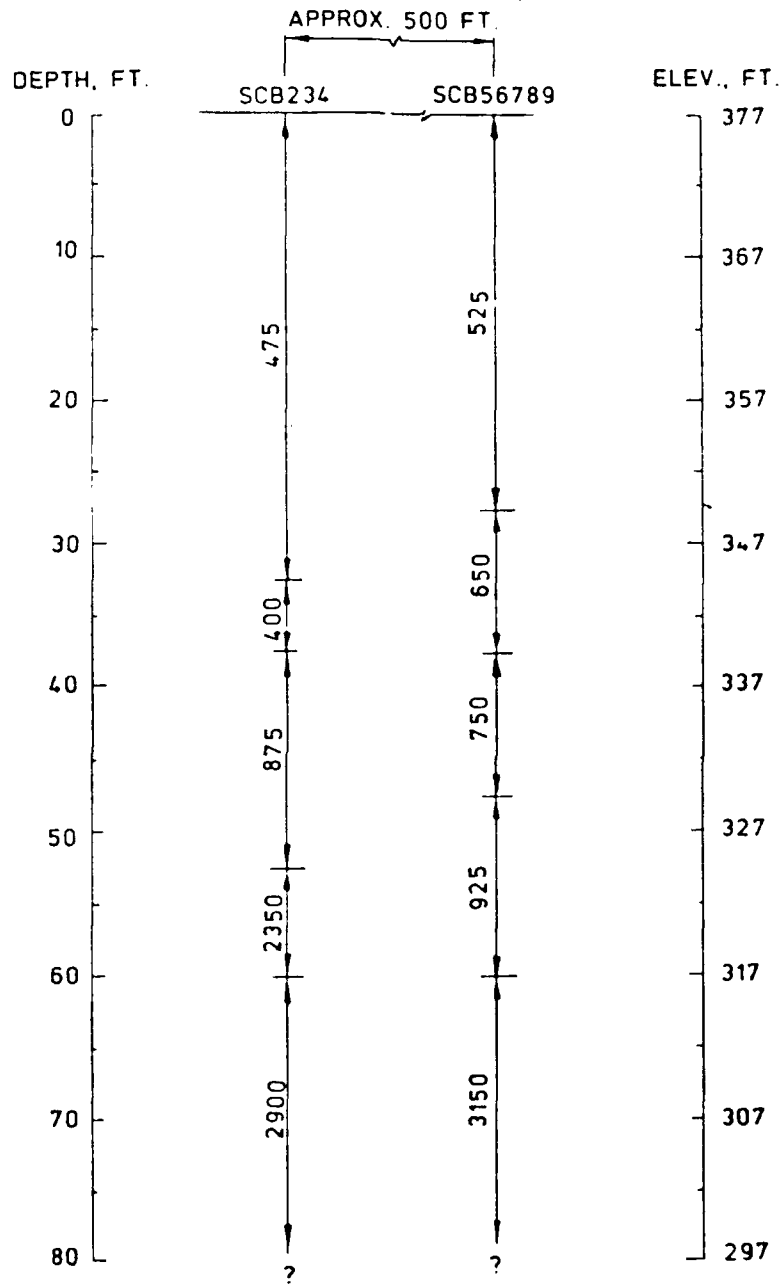


Figure 30.  $V_s$  zones interpreted from geophysical crosshole tests for section near sta 447+75, Mormon Island Auxiliary Dam



NOTE : ALL VELOCITIES ARE IN fps.

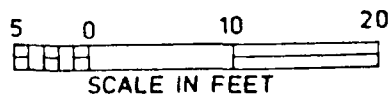


Figure 31.  $V_s$  zones measured in crosshole tests along downstream toe of Mormon Island Auxiliary Dam

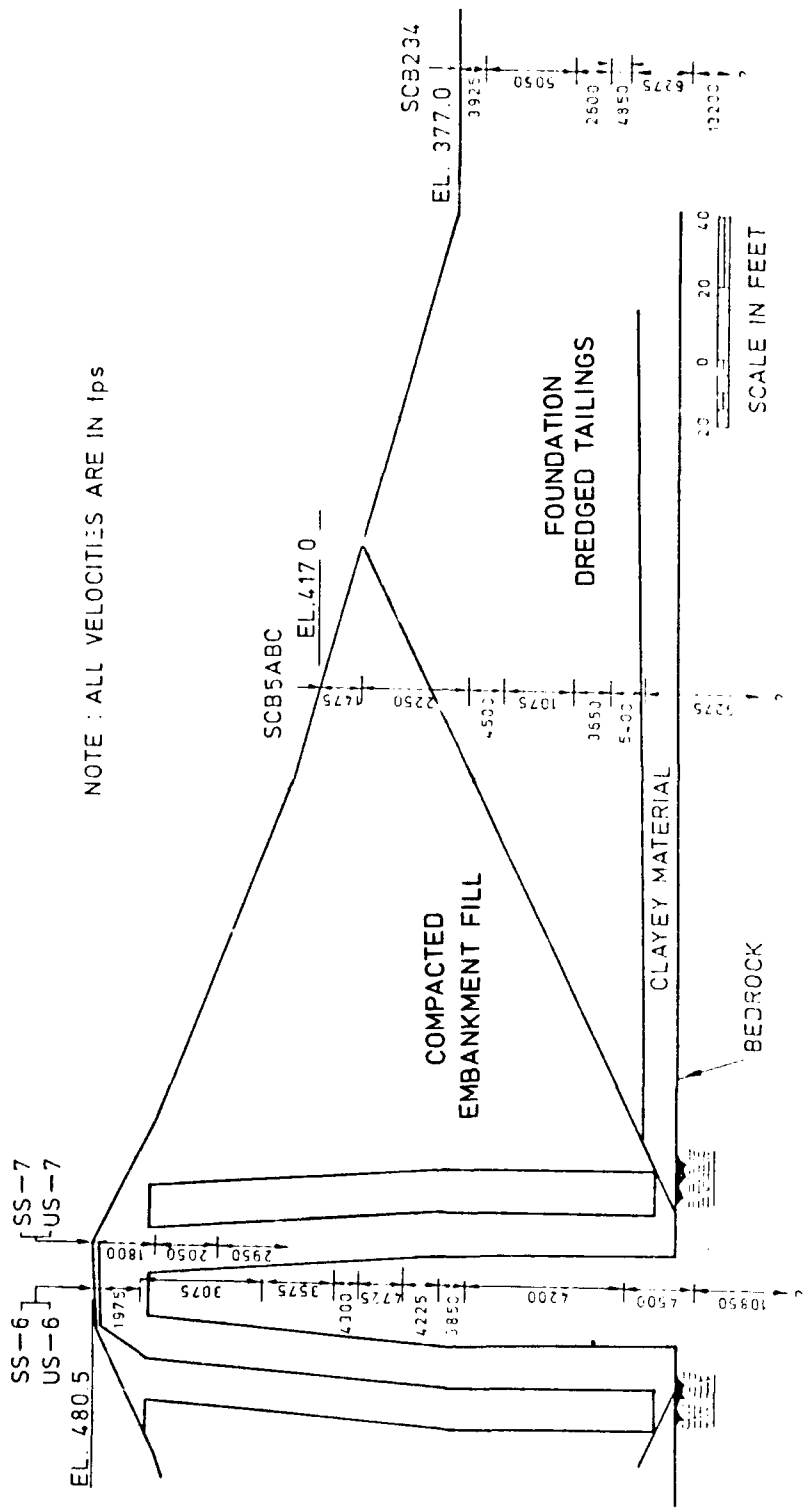
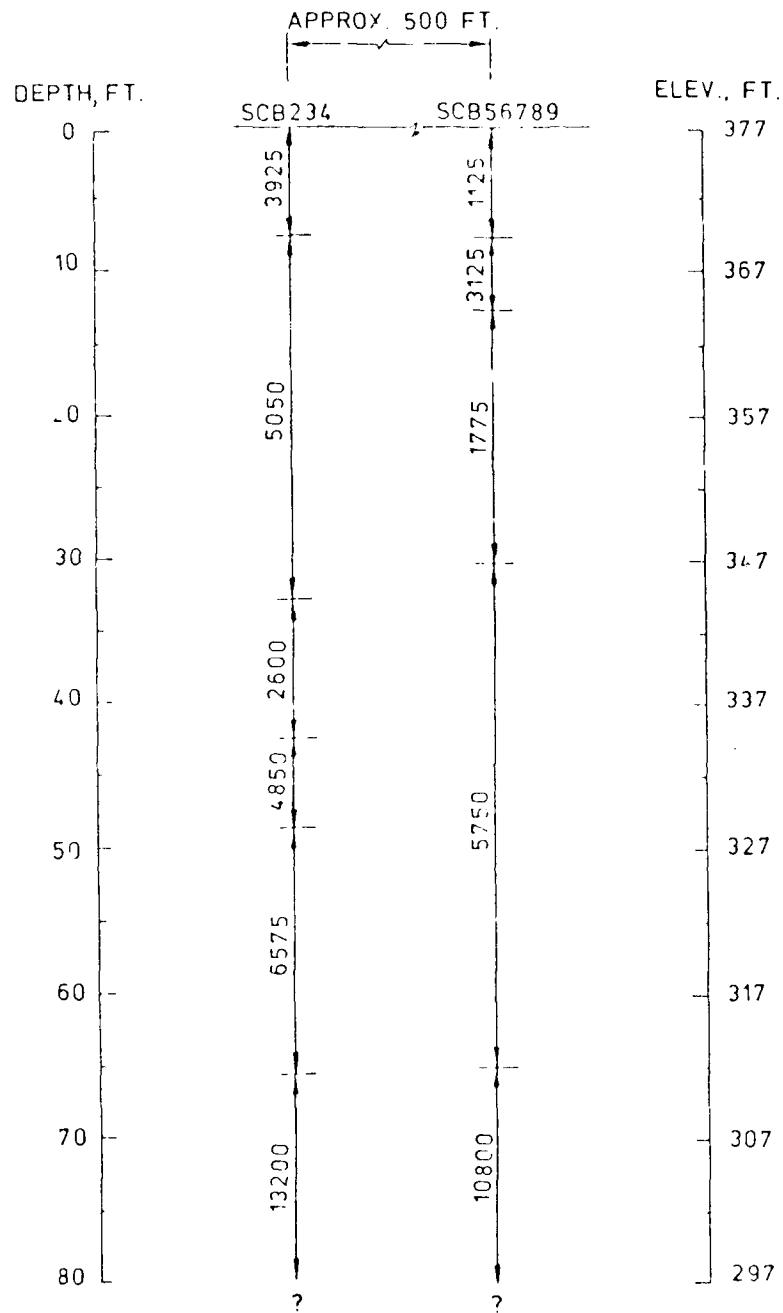


Figure 32.  $V_p$  zones interpreted from geophysical crosshole tests for section near sta 447+75, Mormon Island Auxiliary Dam



NOTE : ALL VELOCITIES ARE IN f/s

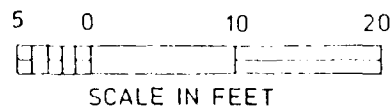


Figure 33.  $V_p$  zones measured in crosshole tests along downstream toe of Mormon Island Auxiliary Dam



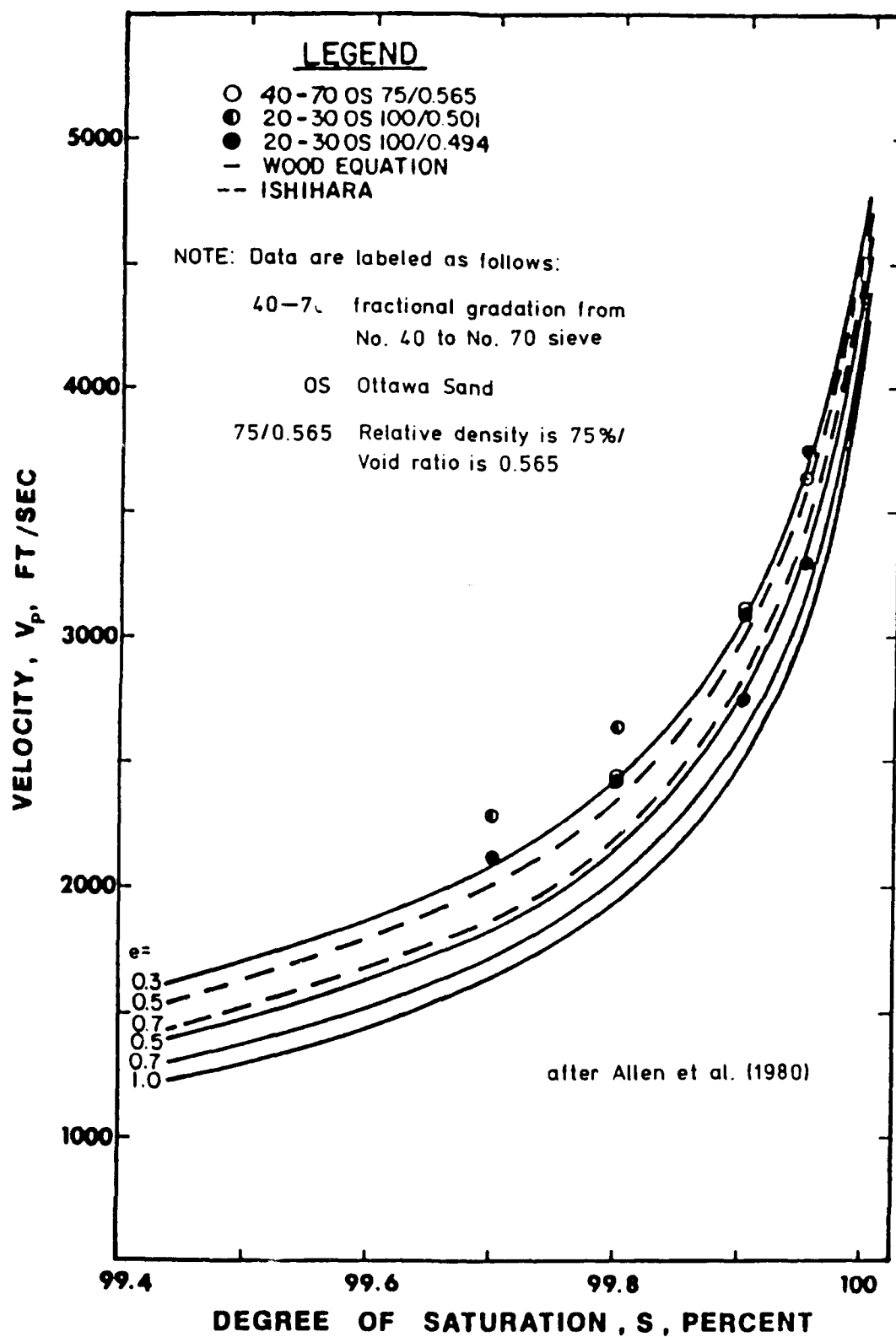


Figure 34. Theoretical and measured relationships between  $V_p$  and degree of saturation for saturated and partially saturated sand

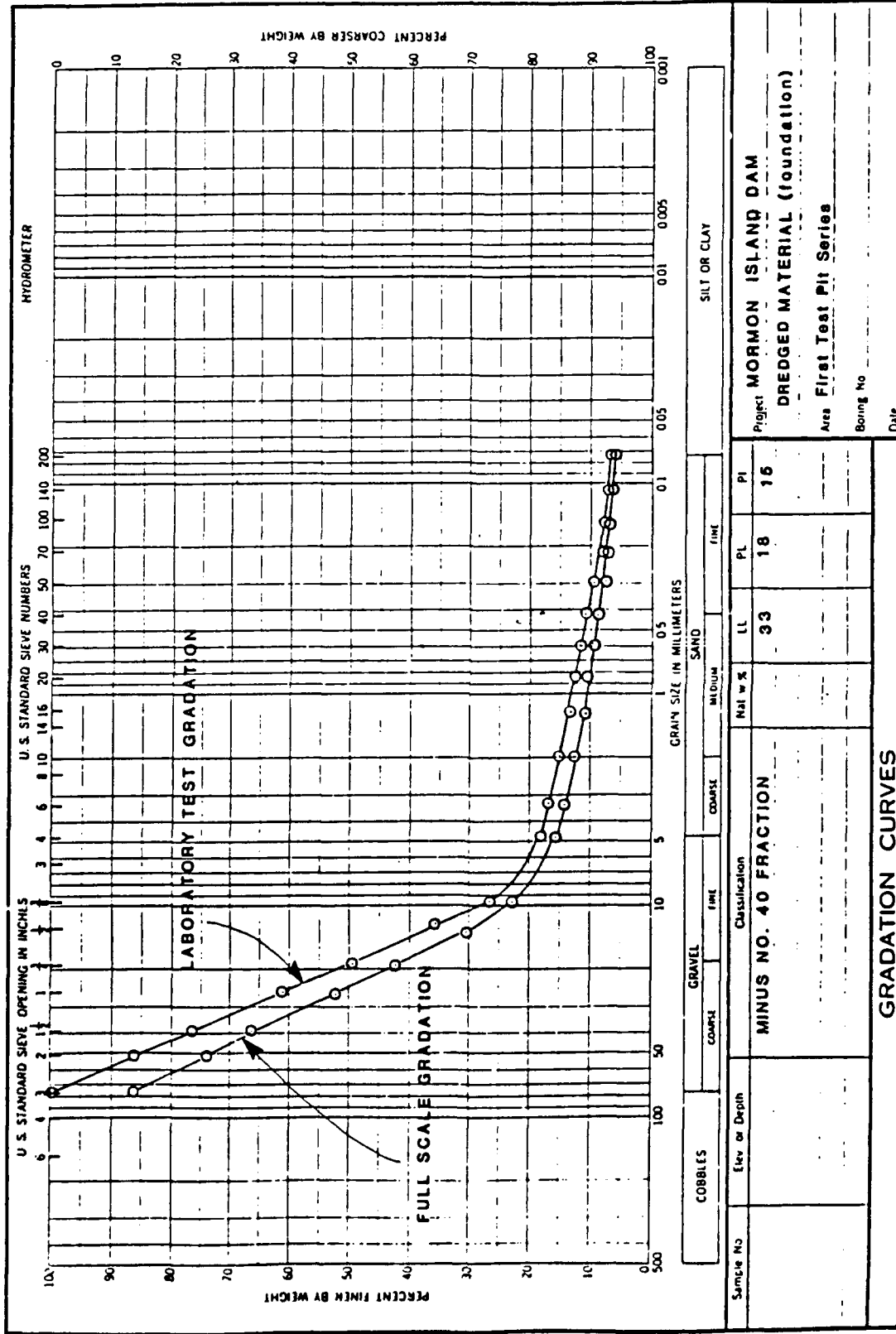


Figure 35. Average full-scale and scalped (3-in. maximum) gradations observed in first test pit series in dredged gravel foundation at Mormon Island Auxiliary Dam. Full-scale gradation scalped to 3-in. maximum particle size used in laboratory tests

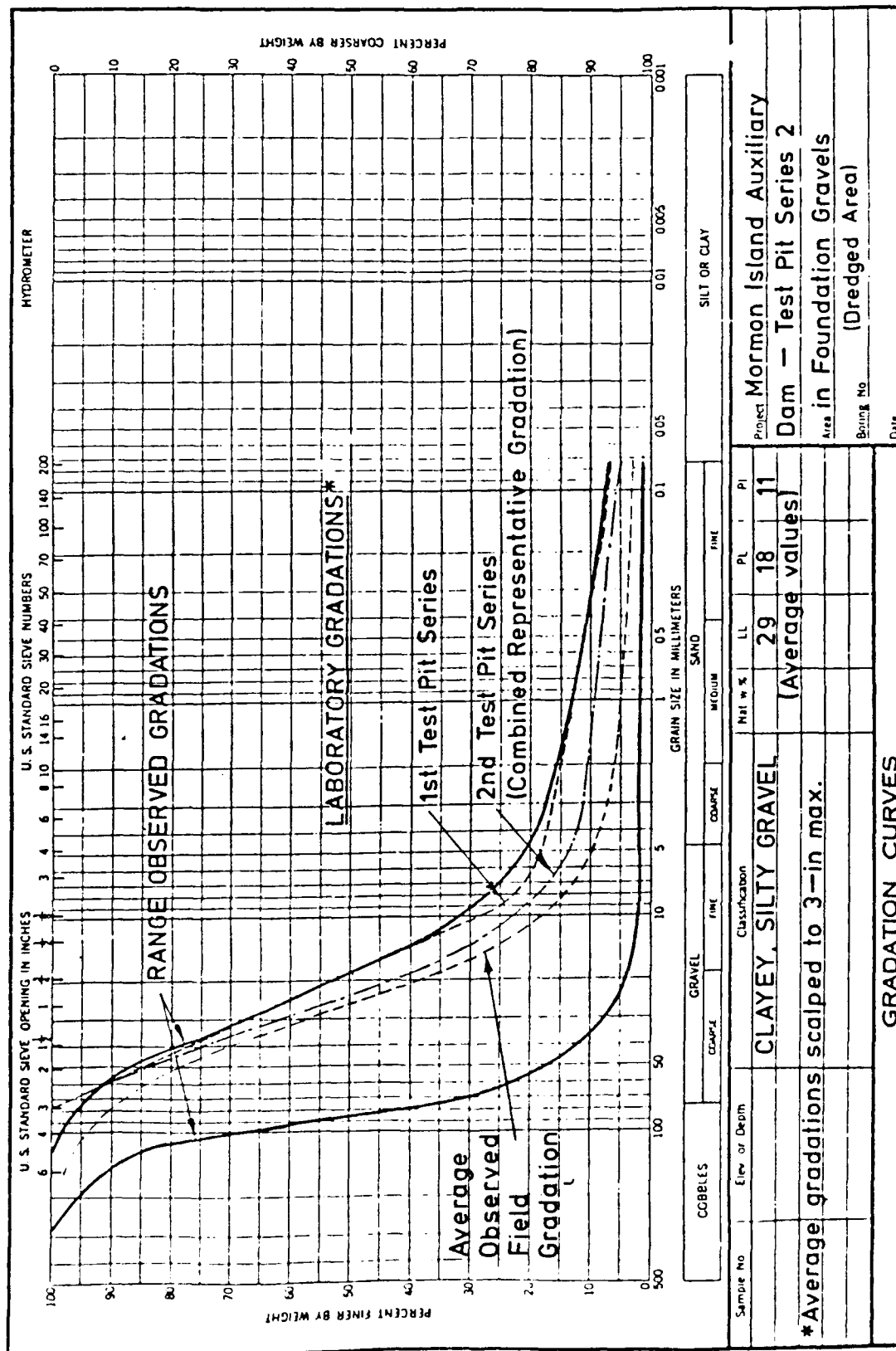


Figure 36. Range of gradations observed in second test pits excavated in dredged foundation gravel at Mormon Island Auxiliary Dam, compared with two laboratory gradations

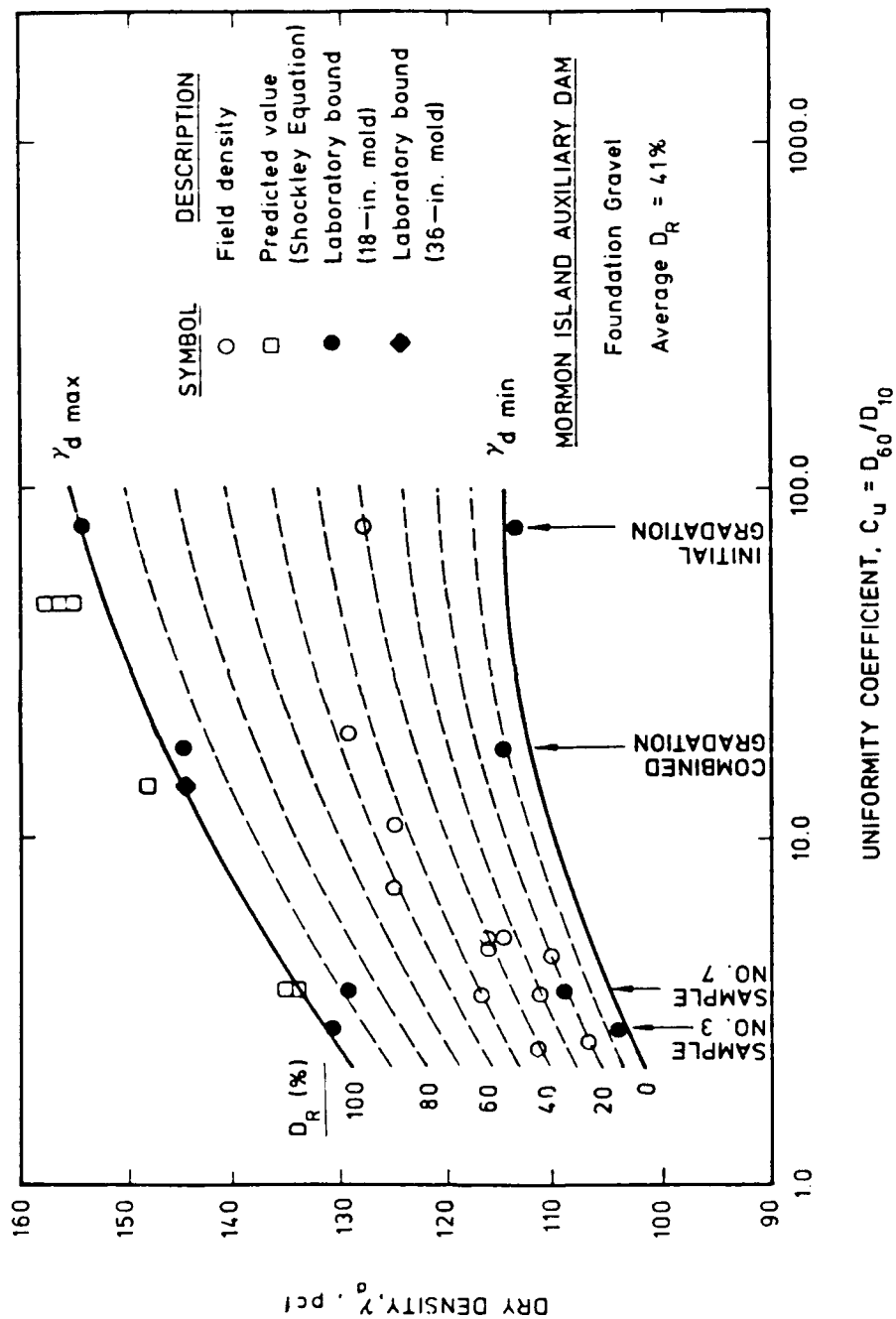
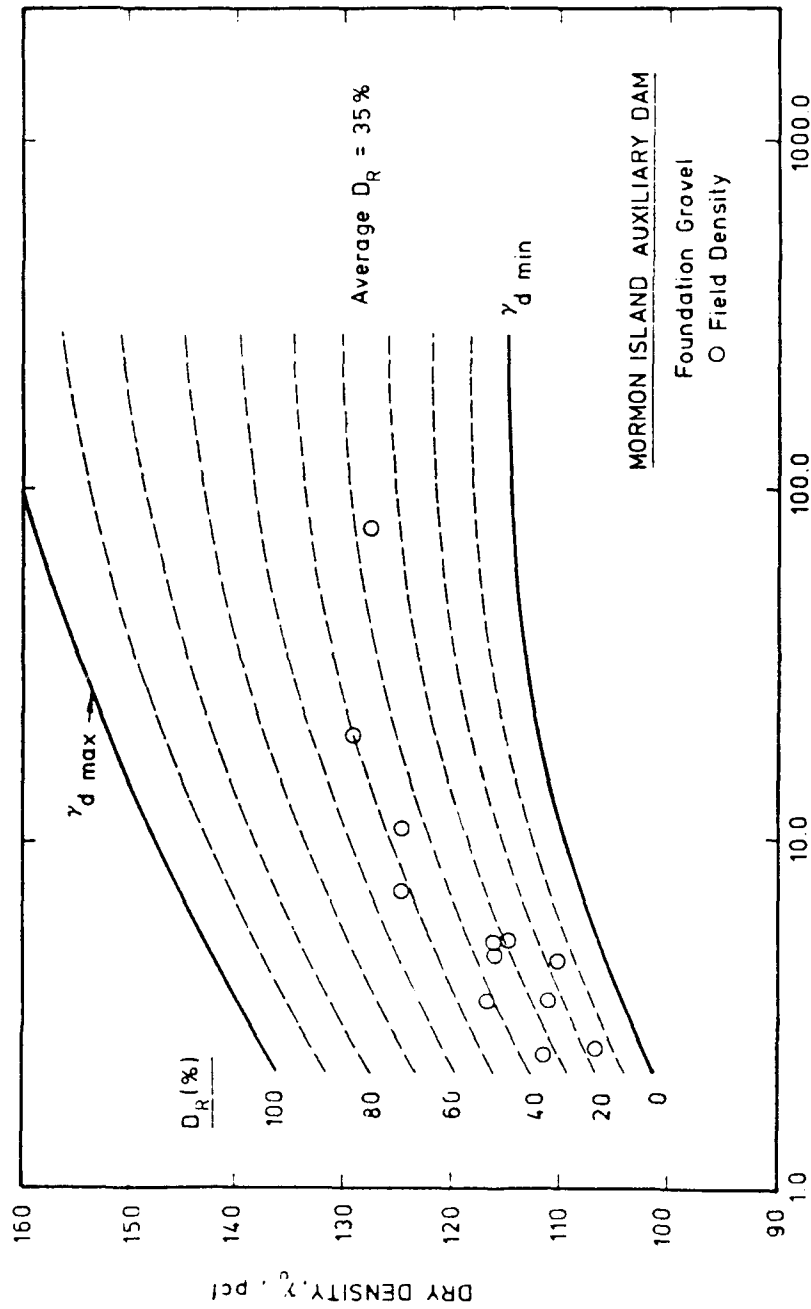


Figure 37a. Relative density of dredged foundation gravel at Mormon Island Auxiliary Dam based on in situ density measurements and  $\gamma_{dmin}$  and  $\gamma_{dmax}$  from laboratory tests



UNIFORMITY COEFFICIENT,  $C_u = D_{60}/D_{10}$

Figure 37b. Relative density of dredged foundation gravel at Mormon Island Auxiliary Dam based on in situ density tests. Bound for  $\gamma_{dmin}$  determined from laboratory tests. Bound for  $\gamma_{dmax}$  estimated as envelope of laboratory and field data



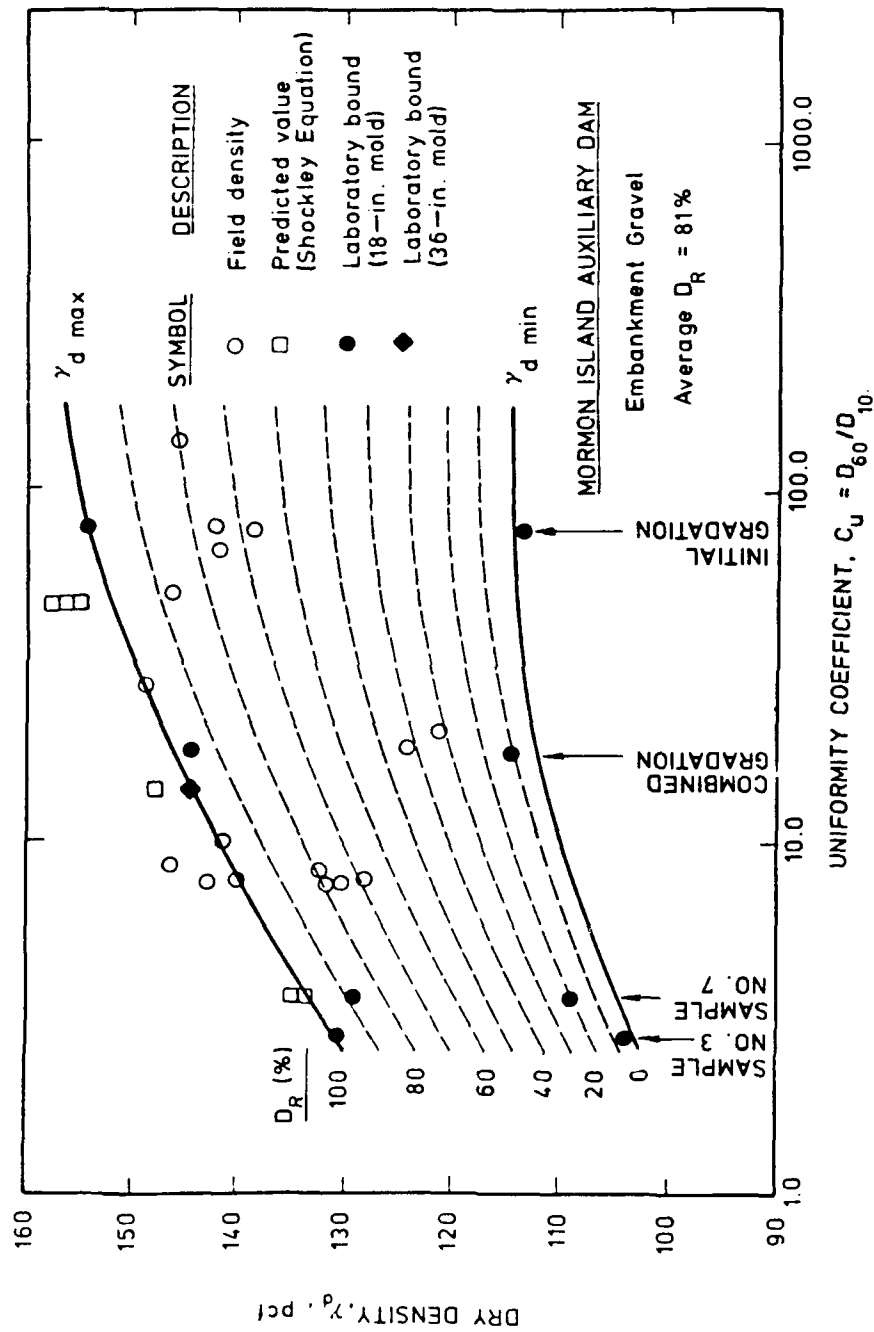


Figure 39a. Relative density of embankment gravel at Mormon Island Auxiliary Dam based on in situ density measurements and  $\gamma_{dmin}$  and  $\gamma_{dmax}$  from laboratory tests

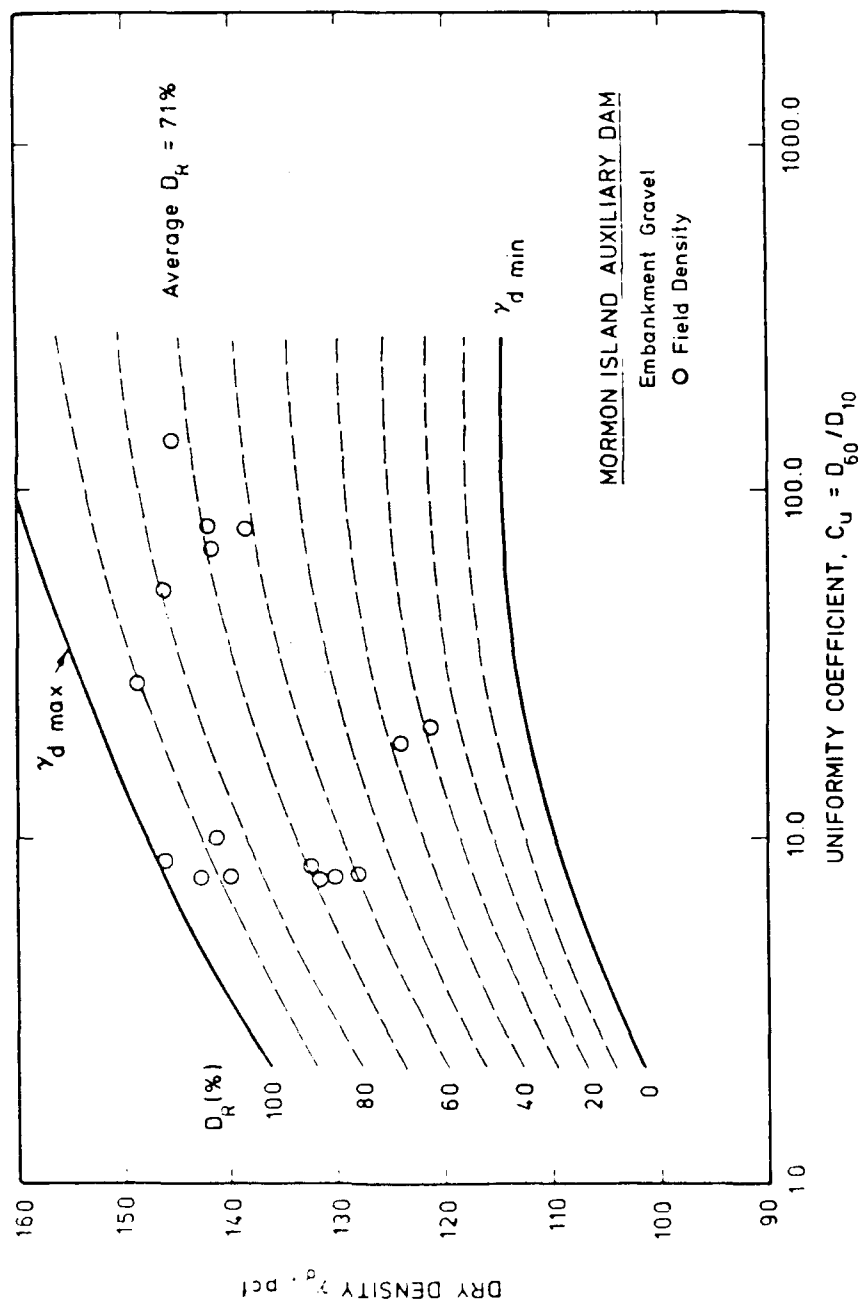


Figure 39b. Relative density of embankment gravel at Mormon Island Auxiliary Dam based on in situ density measurements. Bound for  $\gamma_{d \min}$  determined from laboratory tests. Bound for  $\gamma_{d \max}$  estimated as envelope of laboratory and field data



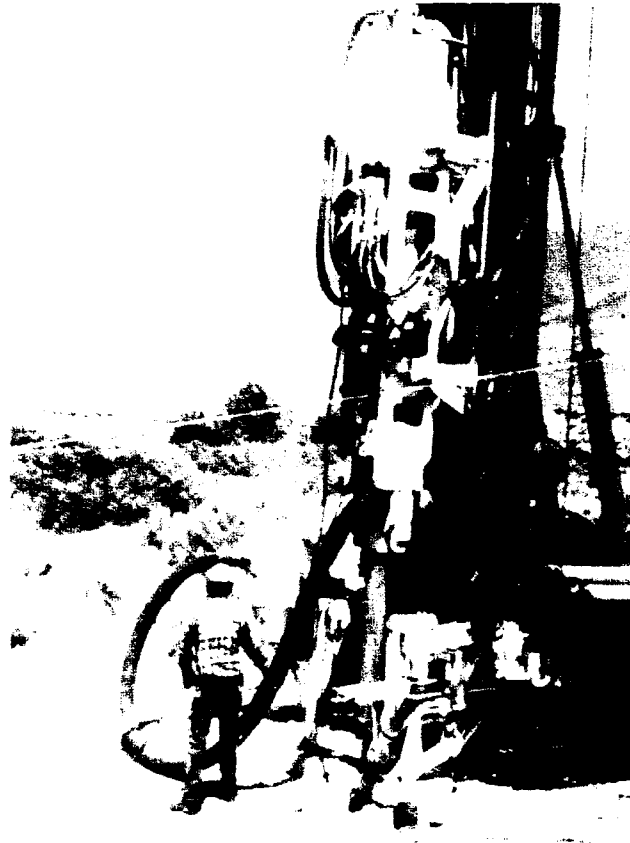


Figure 40. Becker Hammer drilling rig



Figure 41. Three-web crowd-in Felcon bit for open-bit penetration testing and sampling, and eight-tooth crowd-out bit (used plugged) for closed-bit penetration testing

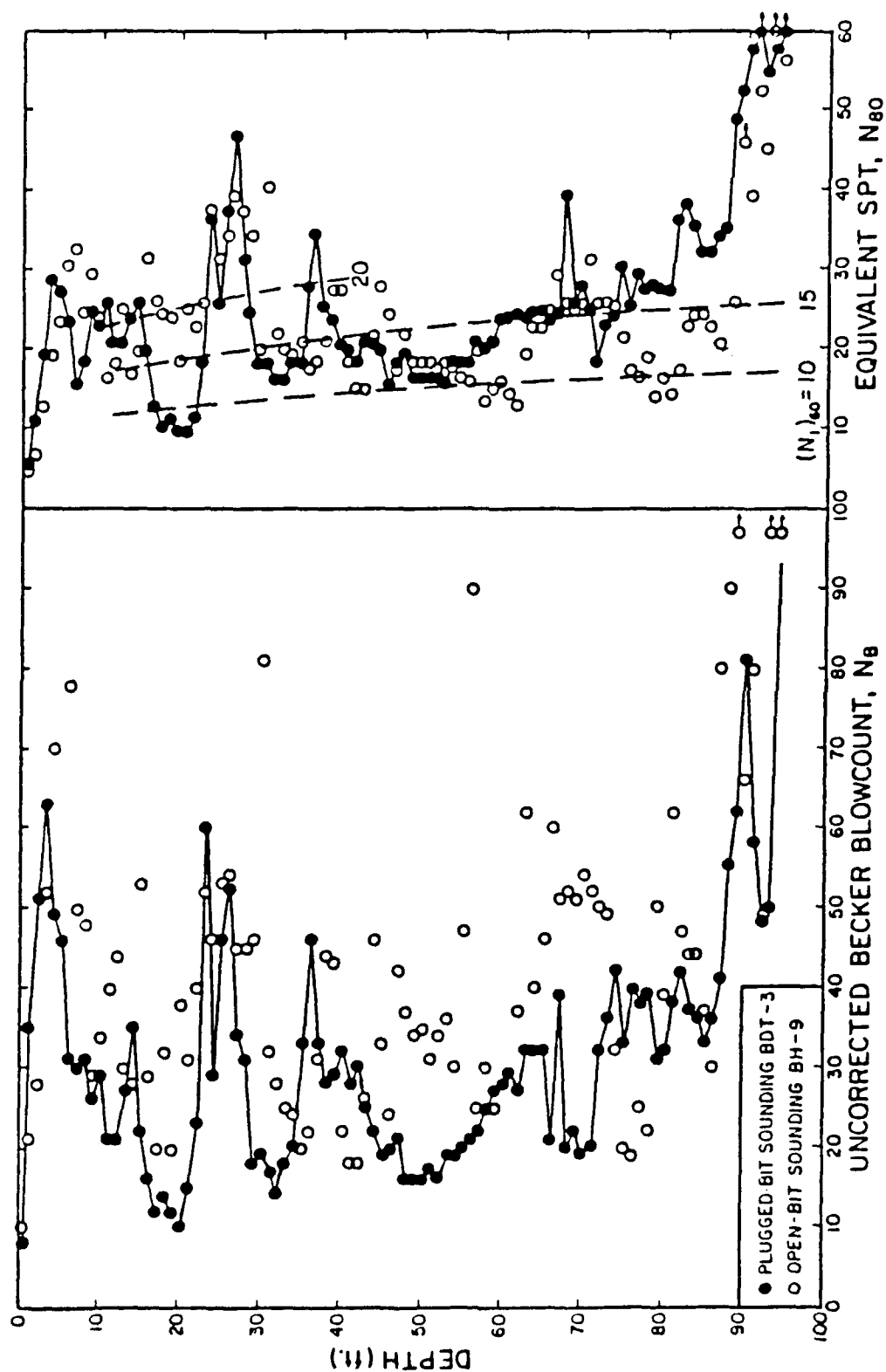


Figure 42. Uncorrected Becker and equivalent SPT blowcounts for soundings BH-9 and BDT-3 performed through downstream slope, Mormon Island Auxiliary Dam (from Harder 1986)

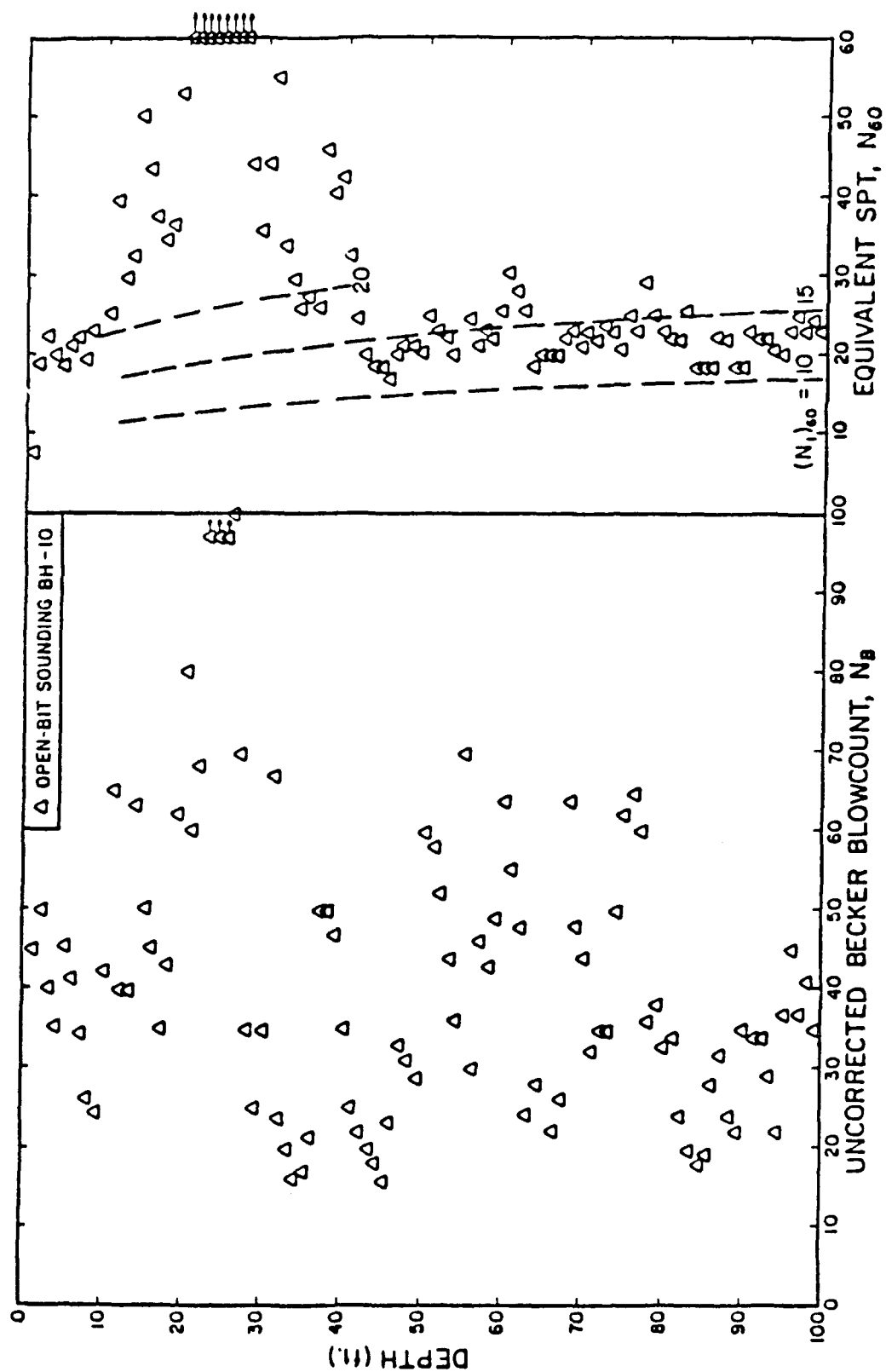


Figure 43. Uncorrected Becker and equivalent SPT blowcounts for sounding BH-10 performed through downstream slope, Mormon Island Auxiliary Dam (from Harder 1986)

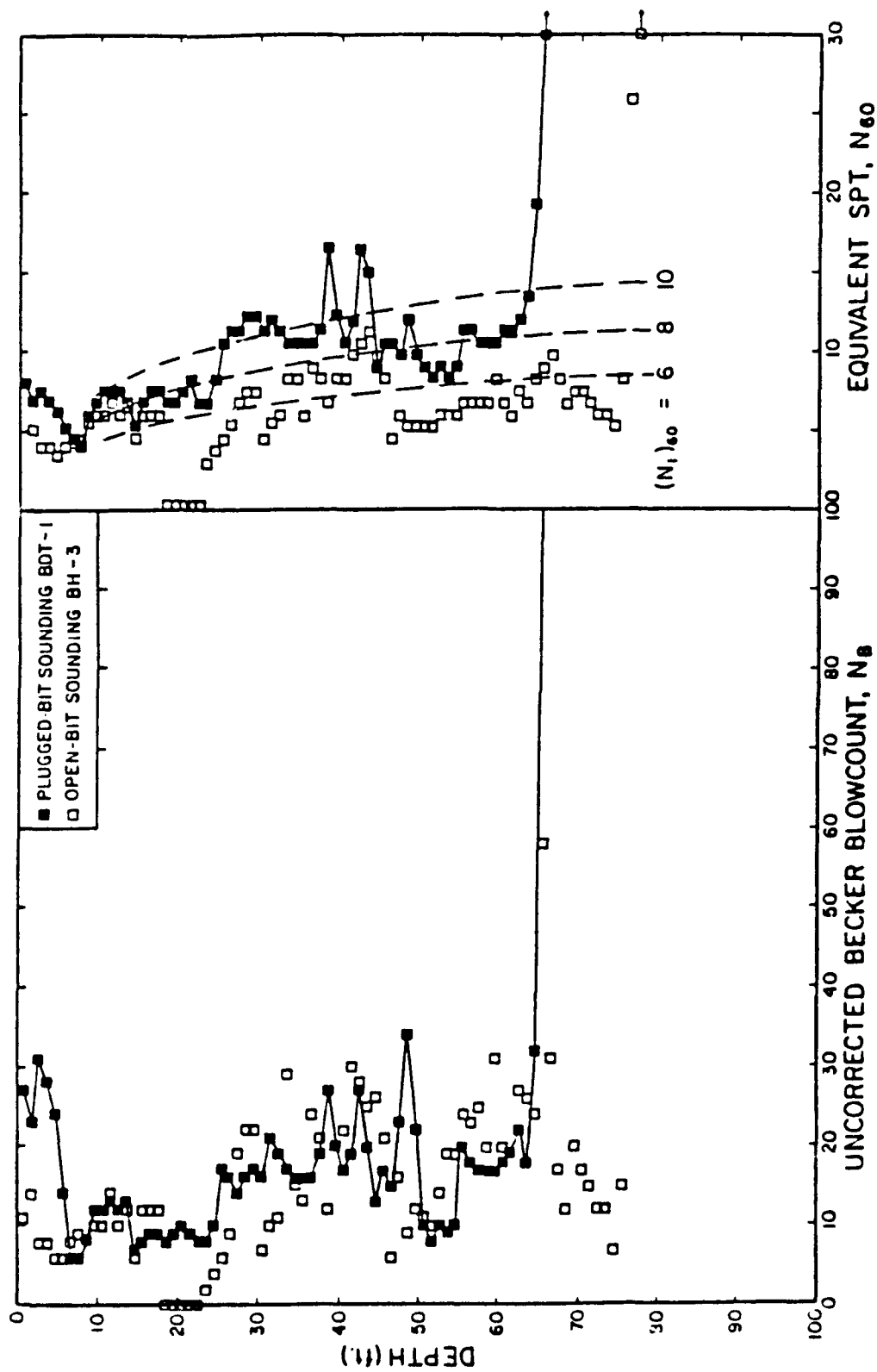


Figure 44. Uncorrected Becker and equivalent SPT blowcounts for sounding BH-3 and BDT-1 performed in the downstream flat area, Mormon Island Auxiliary Dam (from Harder 1986)

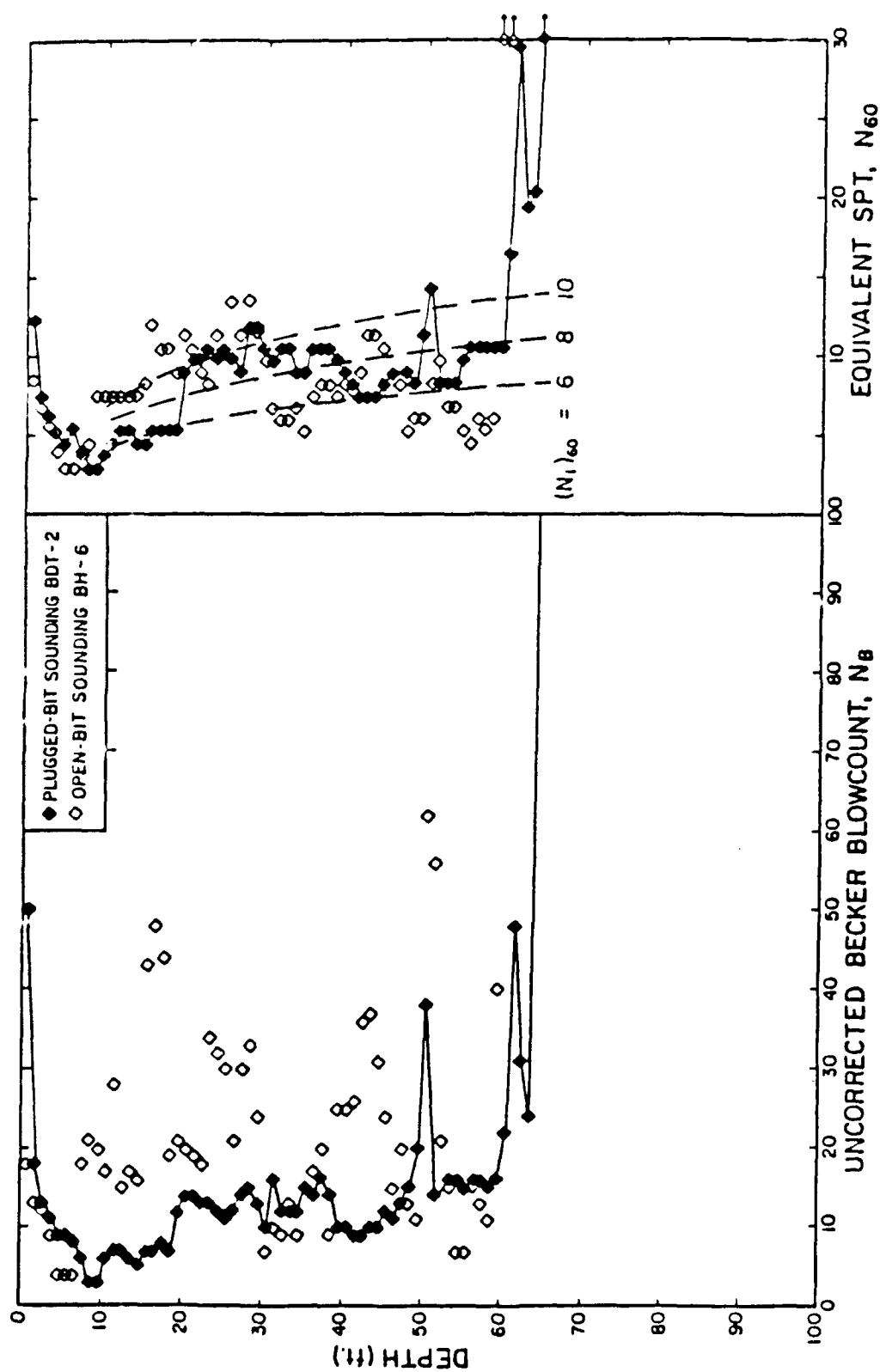


Figure 45. Uncorrected Becker and equivalent SPT blowcounts for sounding BH-6 and BDT-2 performed in the downstream flat area, Mormon Island Auxiliary Dam (from Harder 1986)

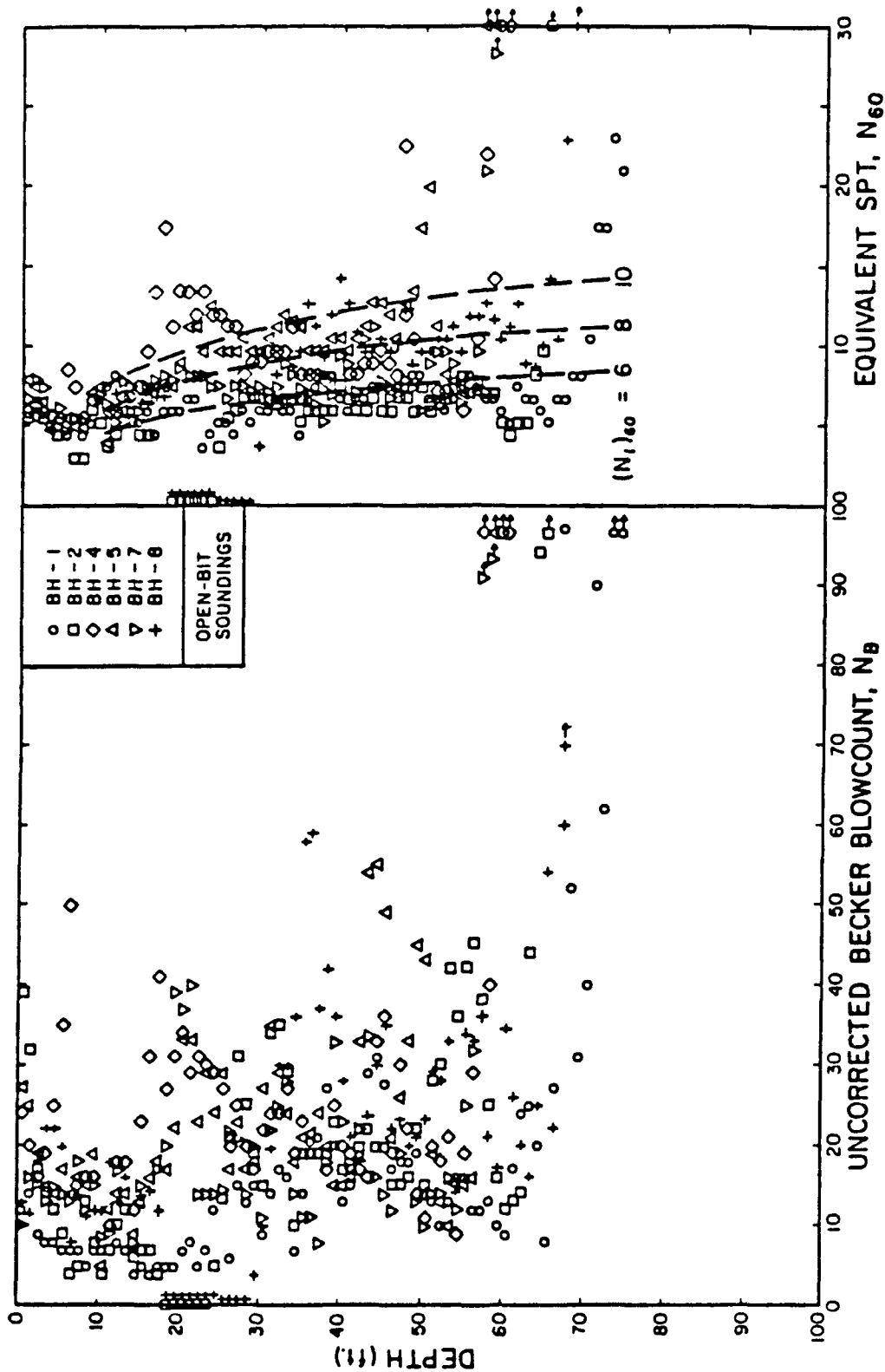


Figure 46. Uncorrected Becker and equivalent SPT blowcounts for soundings BH-1, 2, 4, 5, 7, and 8 performed in the downstream flat area, Mormon Island Auxiliary Dam (from Harder 1986)

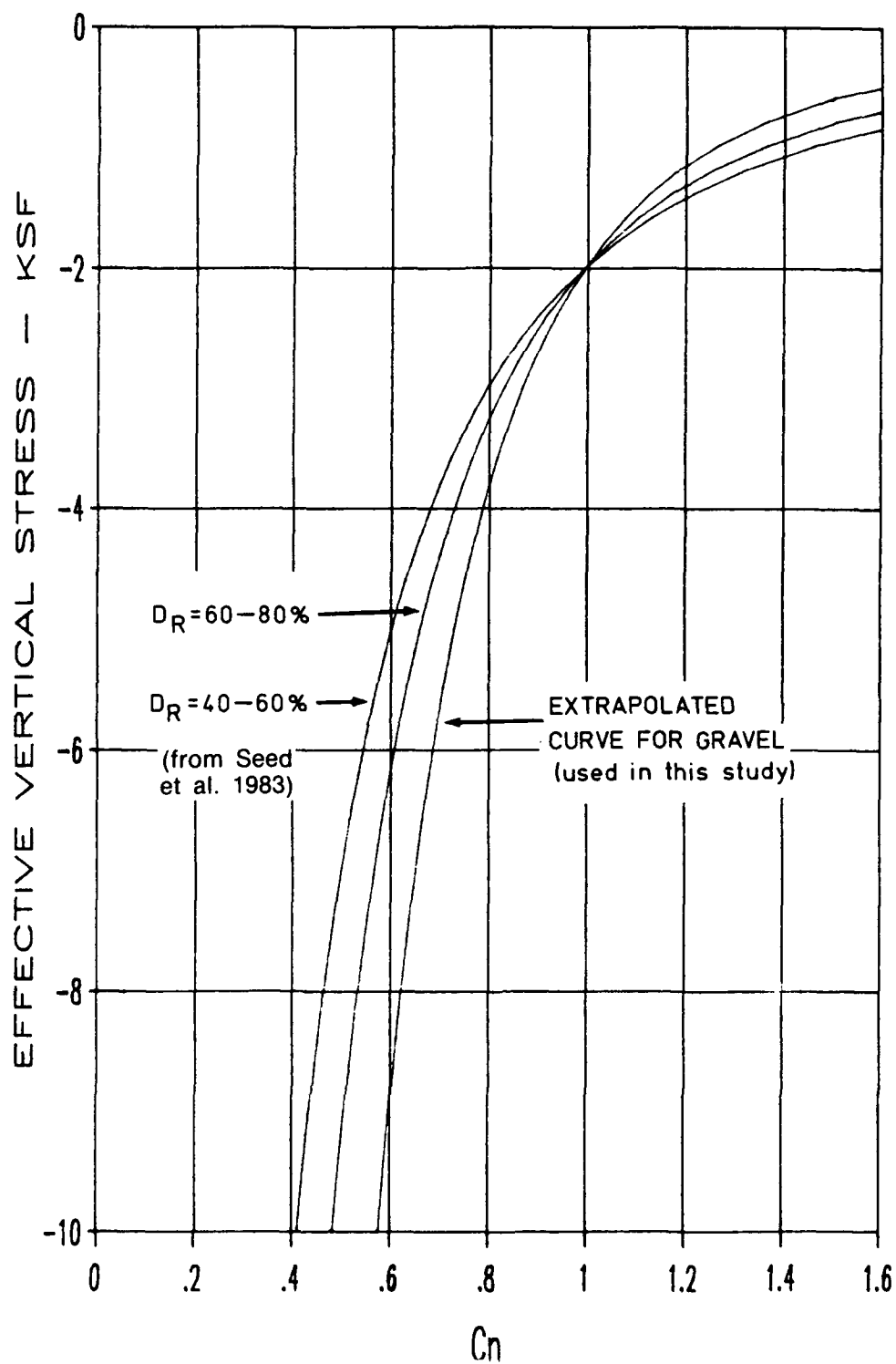


Figure 47. Comparison of overburden correction factors  $C_n$  recommended by Seed et al. (1983) and extrapolated values for Folsom gravel



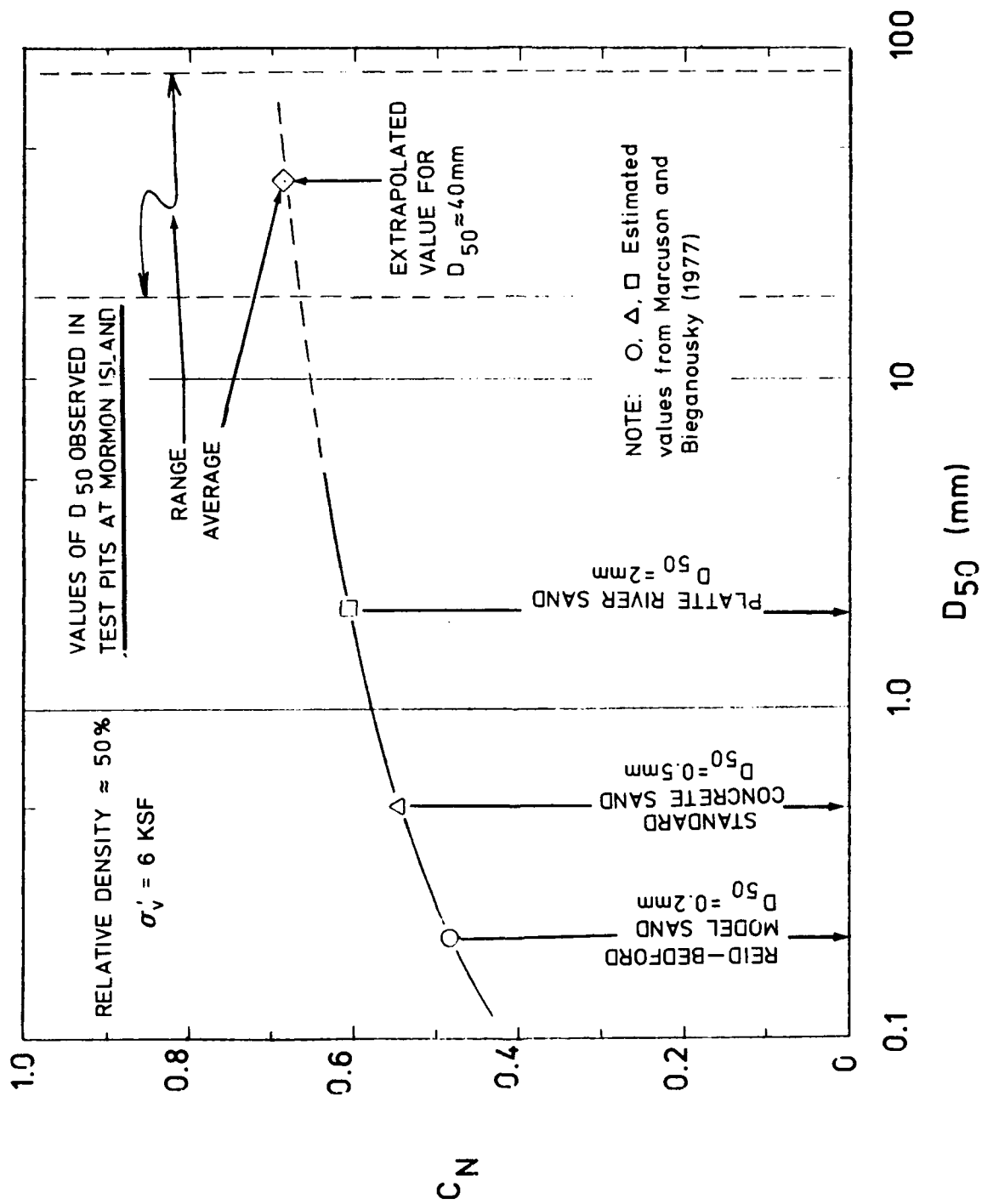


Figure 48a. Relationship between  $C_N$  and for an overburden pressure of 6 ksf,  $D_{50}$  based on data from Marcuse and Bieganousky (1977)

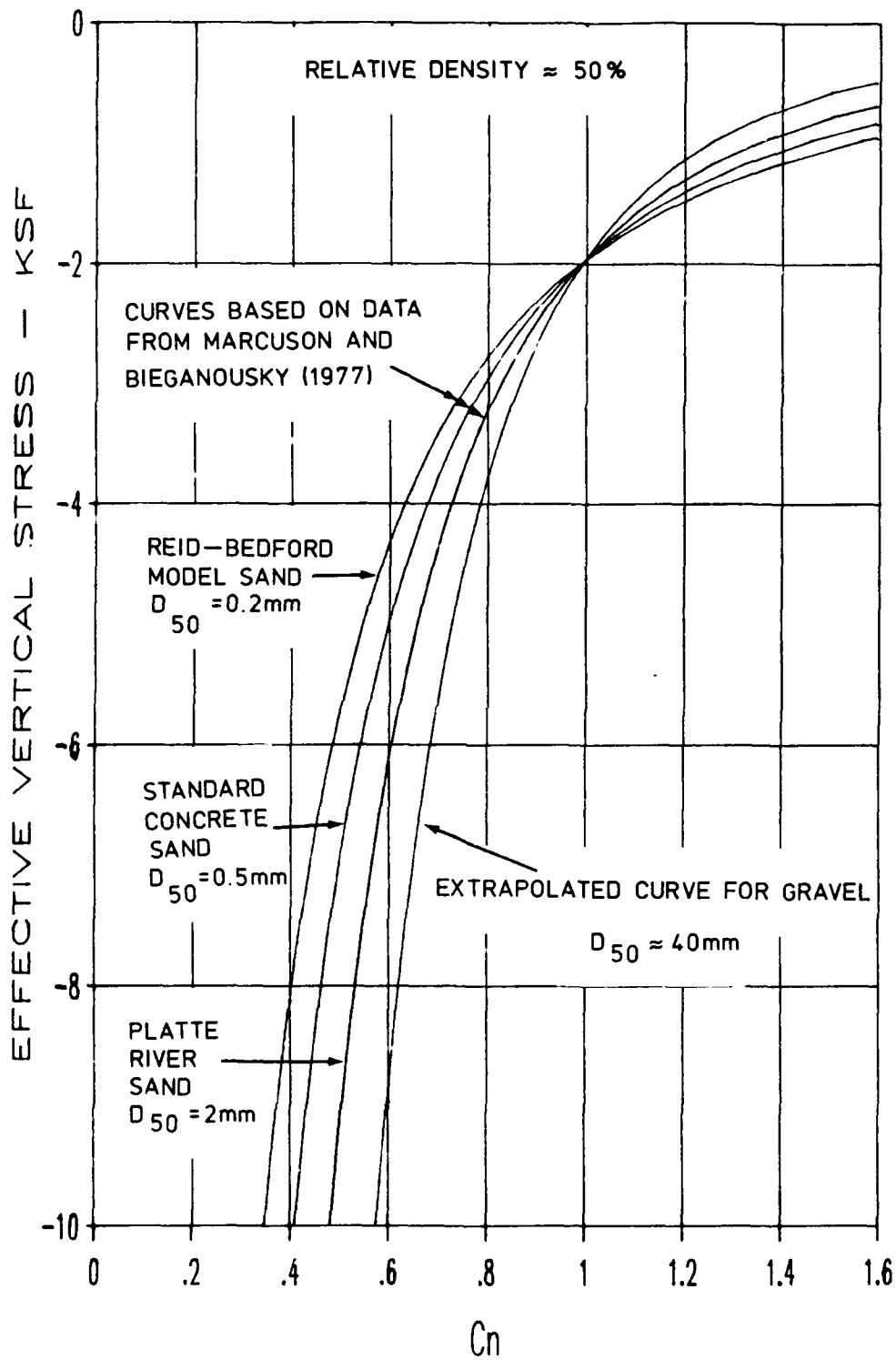


Figure 48b. Relationship between  $C_n$  and overburden pressure as a function of  $D_{50}$  based on data from Marcuson and Bieganousky (1977)

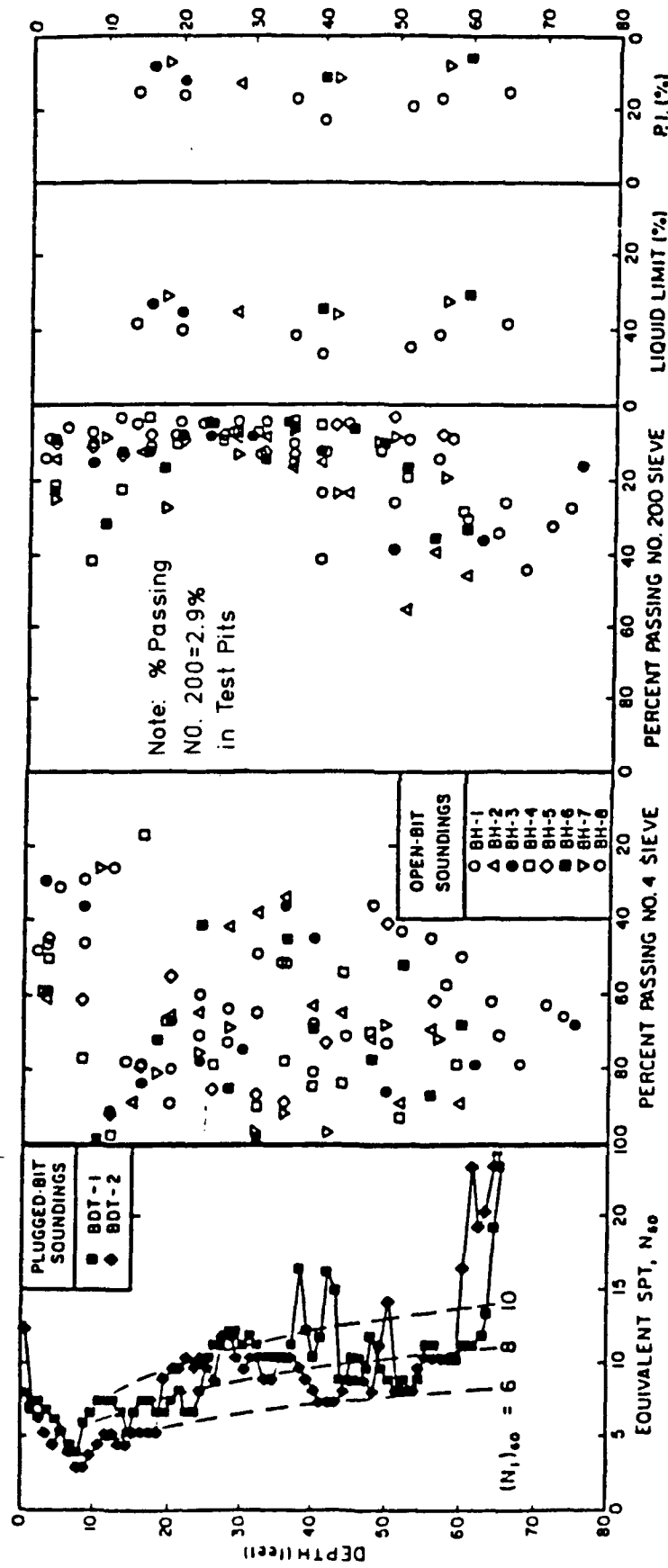


Figure 49. Equivalent SPT blowcounts and classification test data from soundings performed in the downstream flat area, Mormon Island Auxiliary Dam (from Harder 1986)

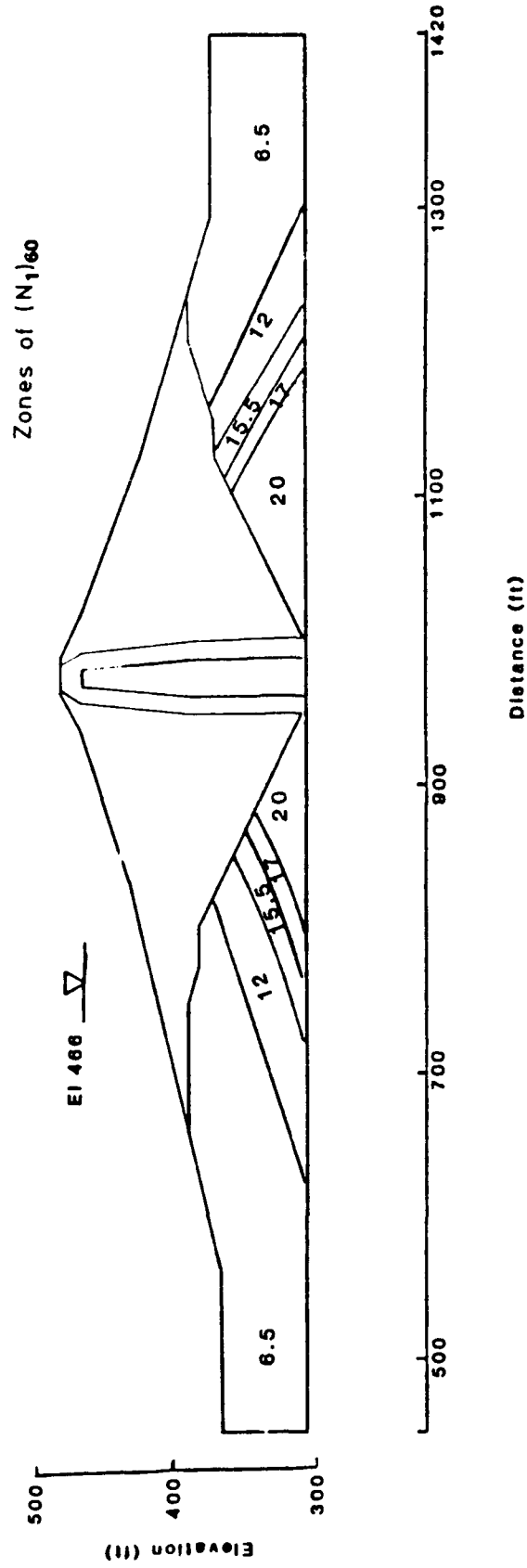


Figure 50. Zones of  $(N_1)_{60}$  for foundation gravels at Mormon Island Auxiliary Dam estimated from Becker Hammer soundings and computed vertical effective stresses from static finite element analyses

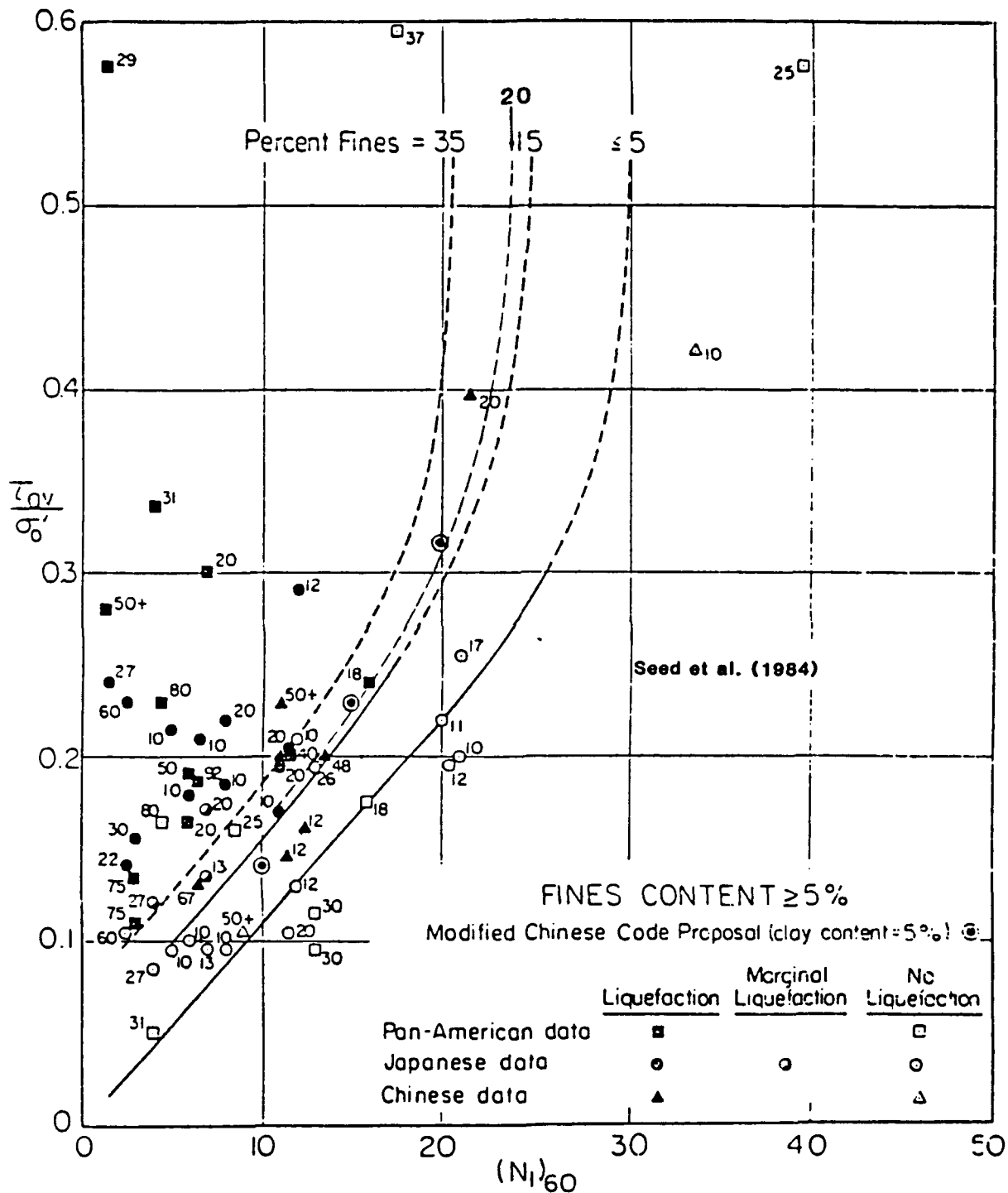


Figure 51. Relationships between stress ratio causing liquefaction and  $(N_1)_{60}$  - values for silty sands for  $M = 7\frac{1}{2}$  earthquakes from Seed, Tokimatsu, Harder, and Chung 1984)

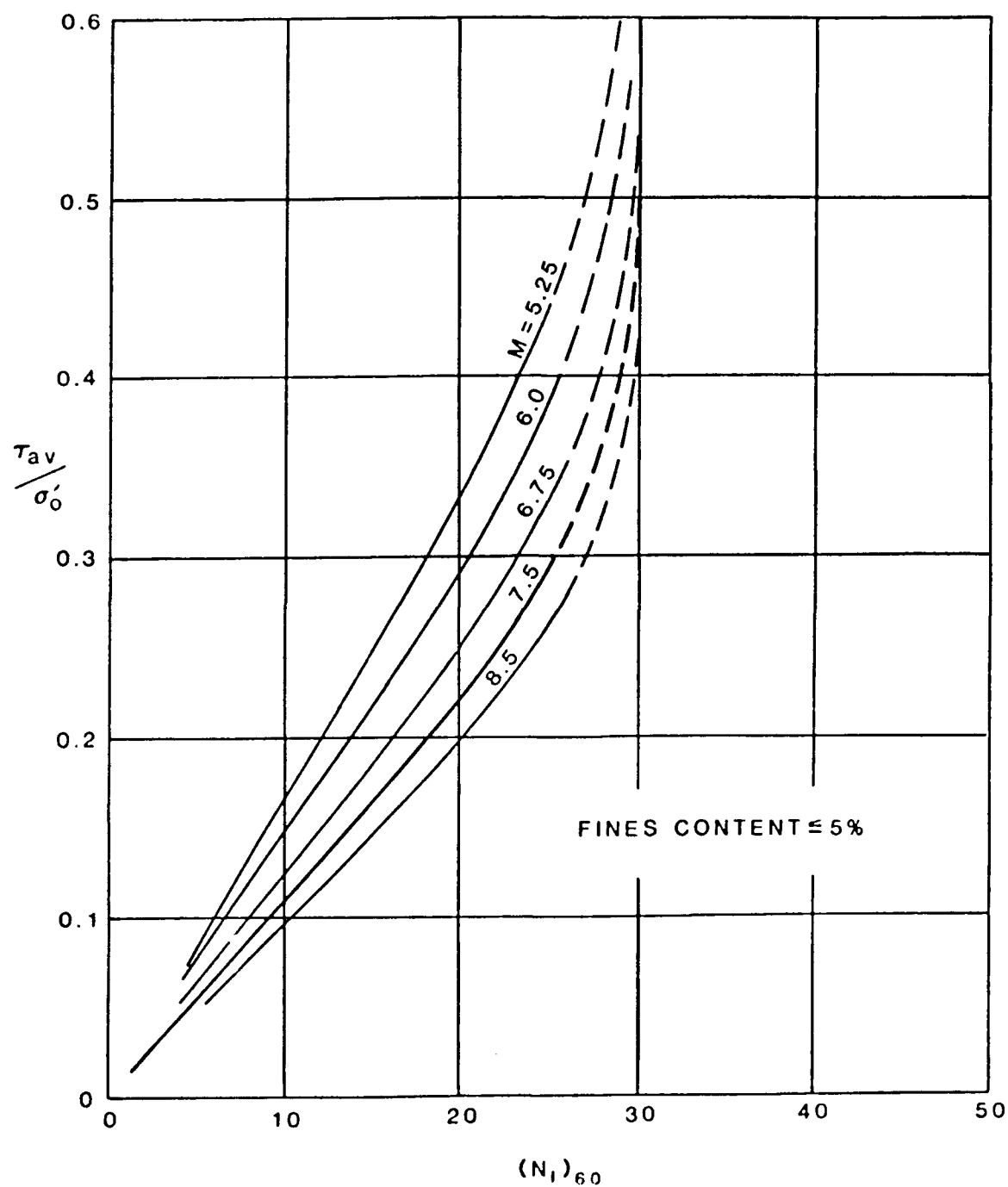
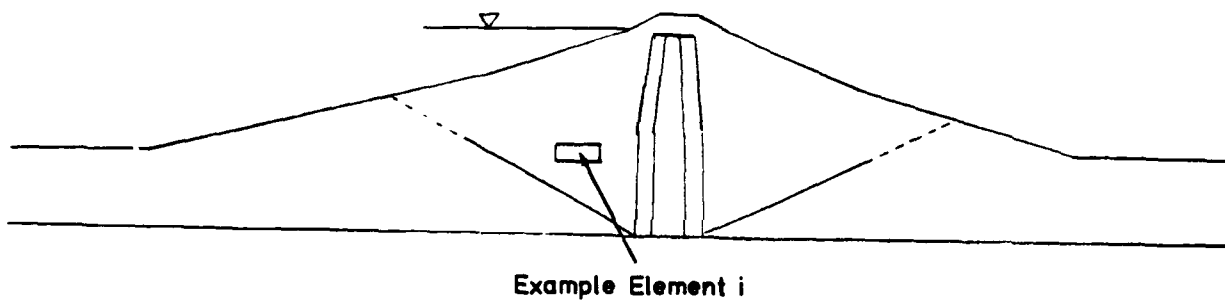


Figure 52. Chart for estimation of liquefaction resistance of clean sands using SPT data, for earthquakes of various Richter Magnitudes (from Koester and Franklin 1985)

## Determination of Appropriate Cyclic Strength for Example Element

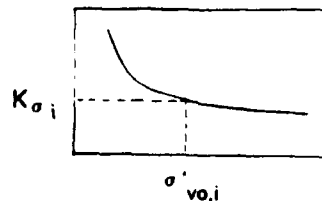


1. Analysis of Becker Penetration Test results and application of Seed's empirical procedure shows:

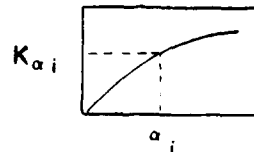
$$(N_1)_{60} \approx 23 \quad \text{for embankment gravel}$$

$$\left( \frac{\tau_{CAVE}}{\sigma'_{vo}} \right) \approx 0.35 \quad \text{for } M_L = 6.5, \sigma'_{vo} = 1 \text{ tsf, and } \alpha = 0$$

2. Static FEM yields  $\sigma'_{vo,i}$  and  $\alpha_i$  for element i.
3.  $K_{\sigma i}$  is determined from chart with  $\sigma'_{vo,i}$



4.  $K_{\alpha i}$  is determined from chart with  $\alpha_i$  :



5. Cyclic strength,  $\tau_{ci}$ , for element i is:

$$\tau_{ci} = \left( \frac{\tau_{CAVE}}{\sigma'_{vo}} \right)_{\substack{\alpha=1 \\ \alpha=0}} \times K_{\sigma i} \times K_{\alpha i} \times \sigma'_{vo,i}$$

$$= (0.35) \times K_{\sigma i} \times K_{\alpha i} \times \sigma'_{vo,i}$$

Figure 53. Schematic representation of procedure for calculating the appropriate cyclic strength for elements in idealized embankment section

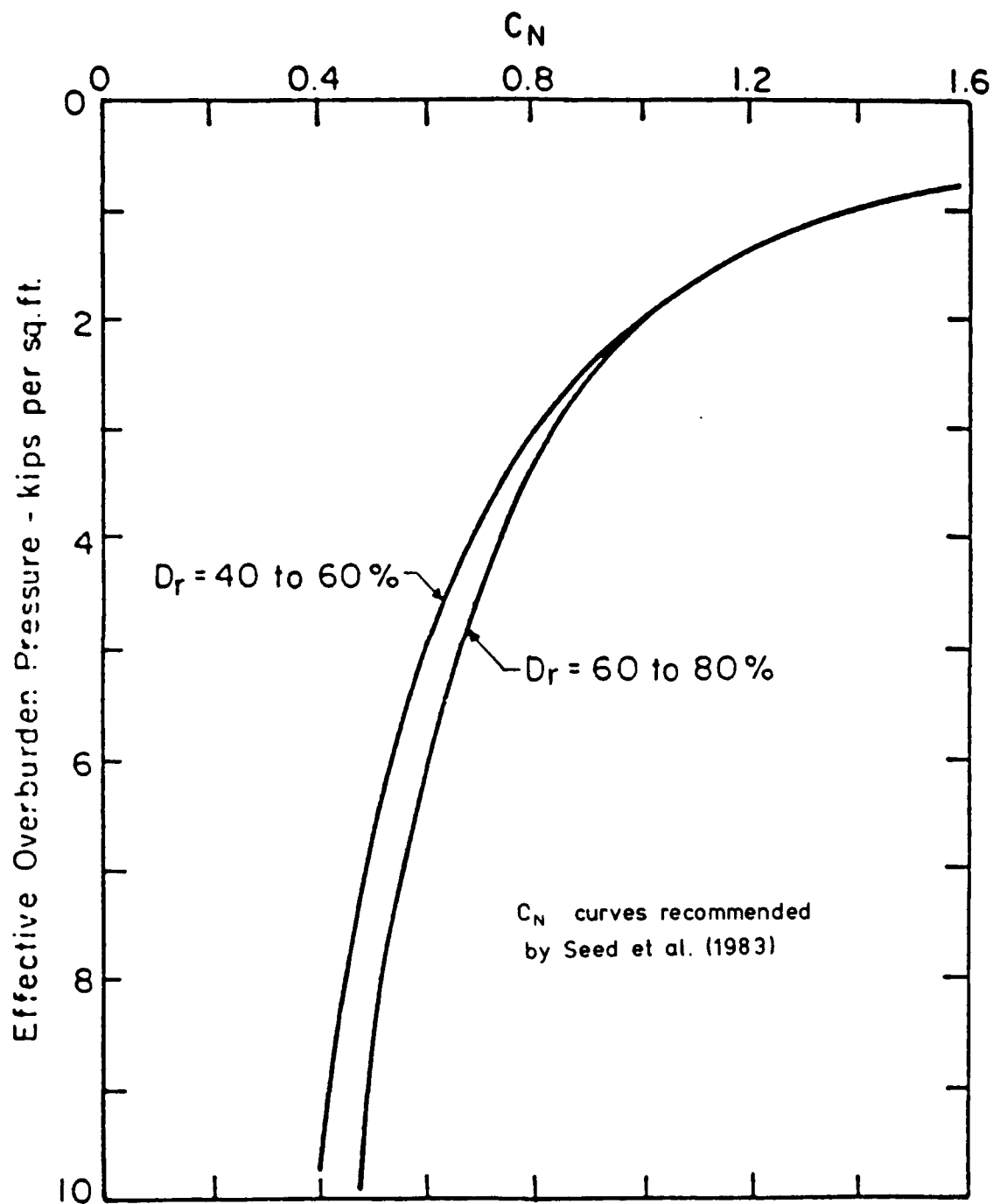


Figure 54. Normalization factor  $C_N$  to adjust SPT blow-counts to a confining stress of 1 tsf (from Bieganousky and Marcuson 1976)



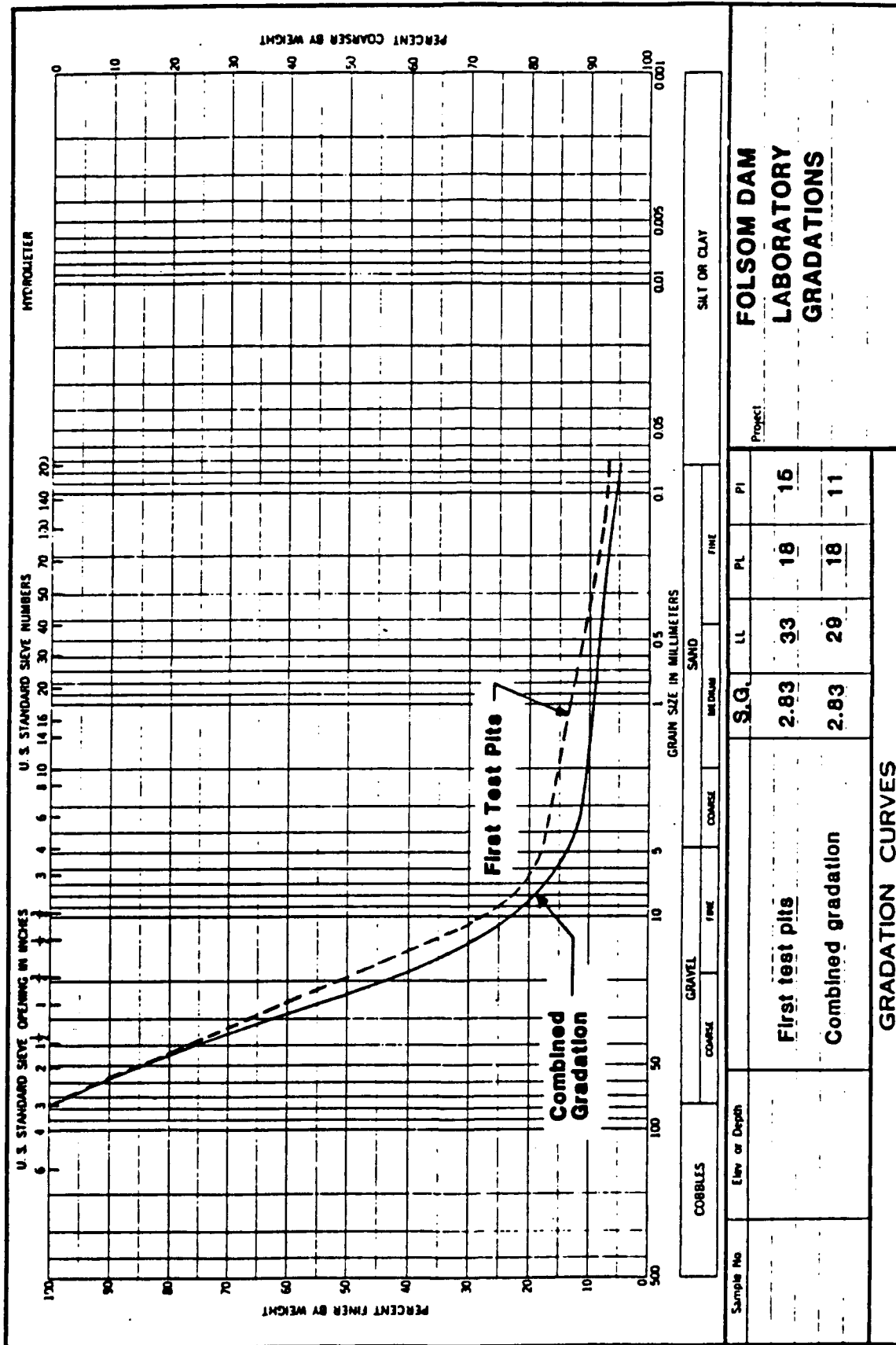


Figure 55. Folsom gravel gradations used in laboratory testing

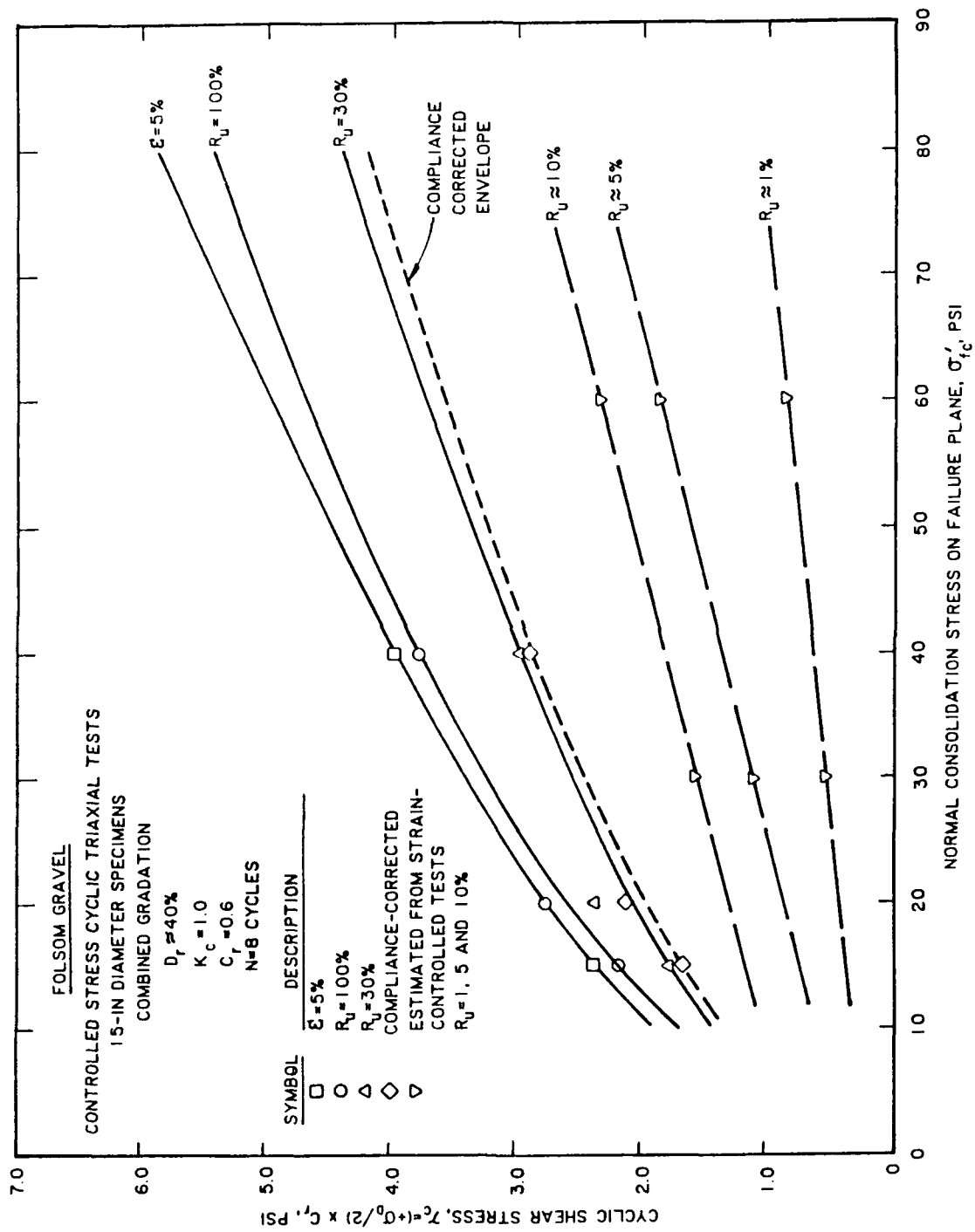


Figure 56. Cyclic strength envelopes for dredged foundation gravel determined from cyclic triaxial laboratory tests

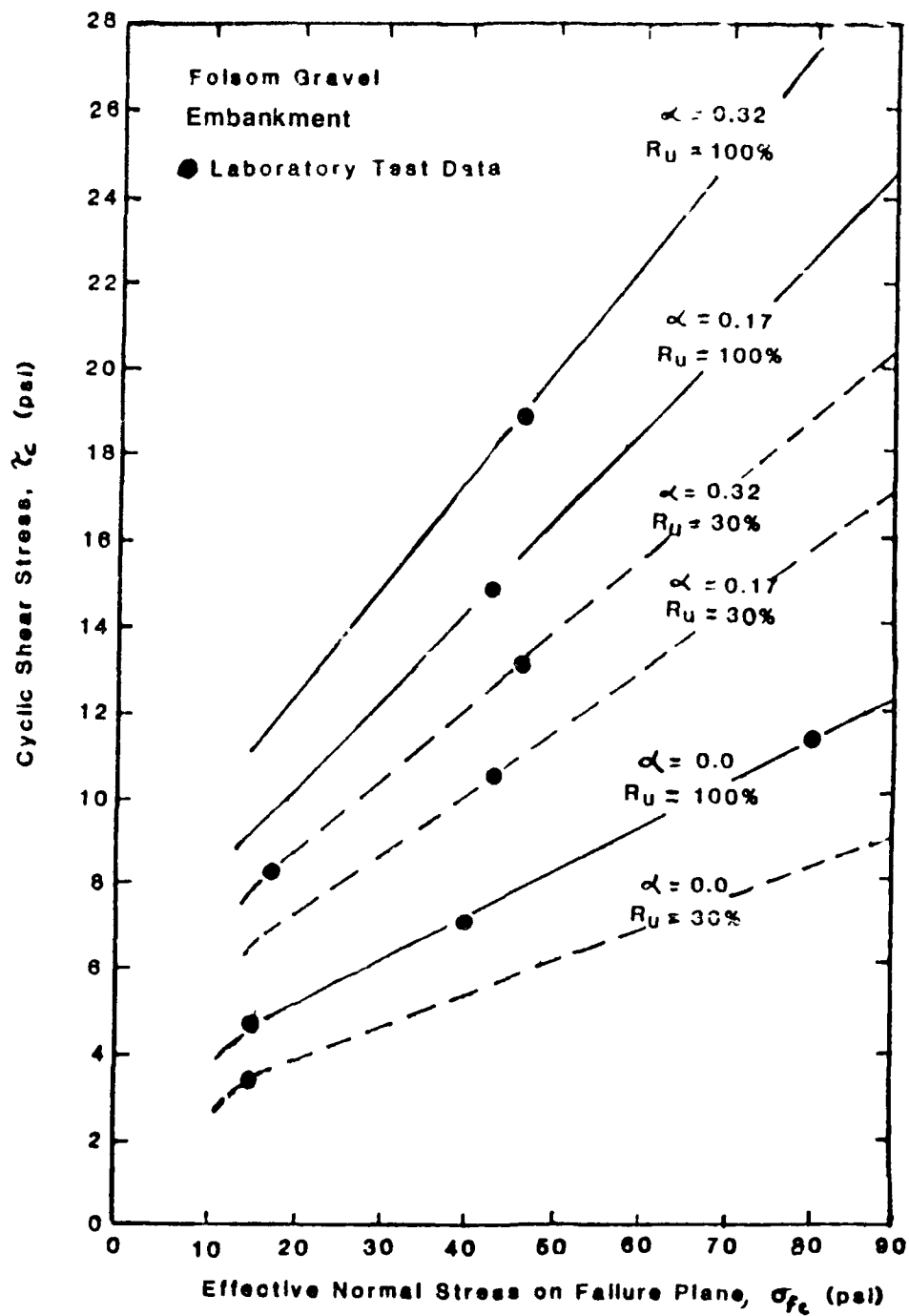


Figure 57. Cyclic strength envelopes for Folsom Dam shell gravels determined from cyclic triaxial laboratory tests

# ADJUSTMENT FACTOR

$K_G$  versus Vertical Effective Stress

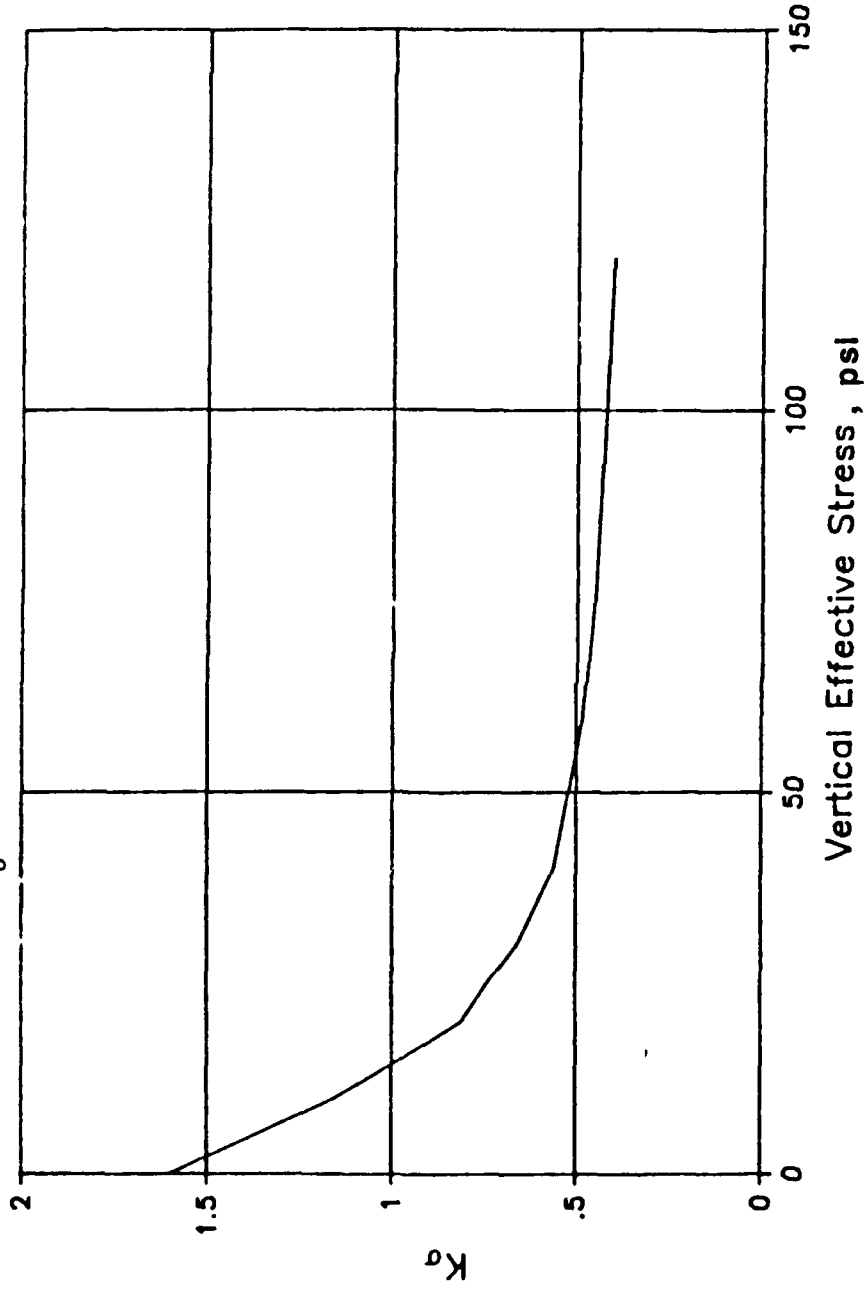


Figure 58. Adjustment factor,  $K_G$ , for change in cyclic stress ratio required to cause  $R_u = 100$  percent with change in effective normal stress, determined from laboratory tests on Folsom gravels

# ADJUSTMENT FACTOR

$K_\alpha$  versus  $\alpha$  Ratio

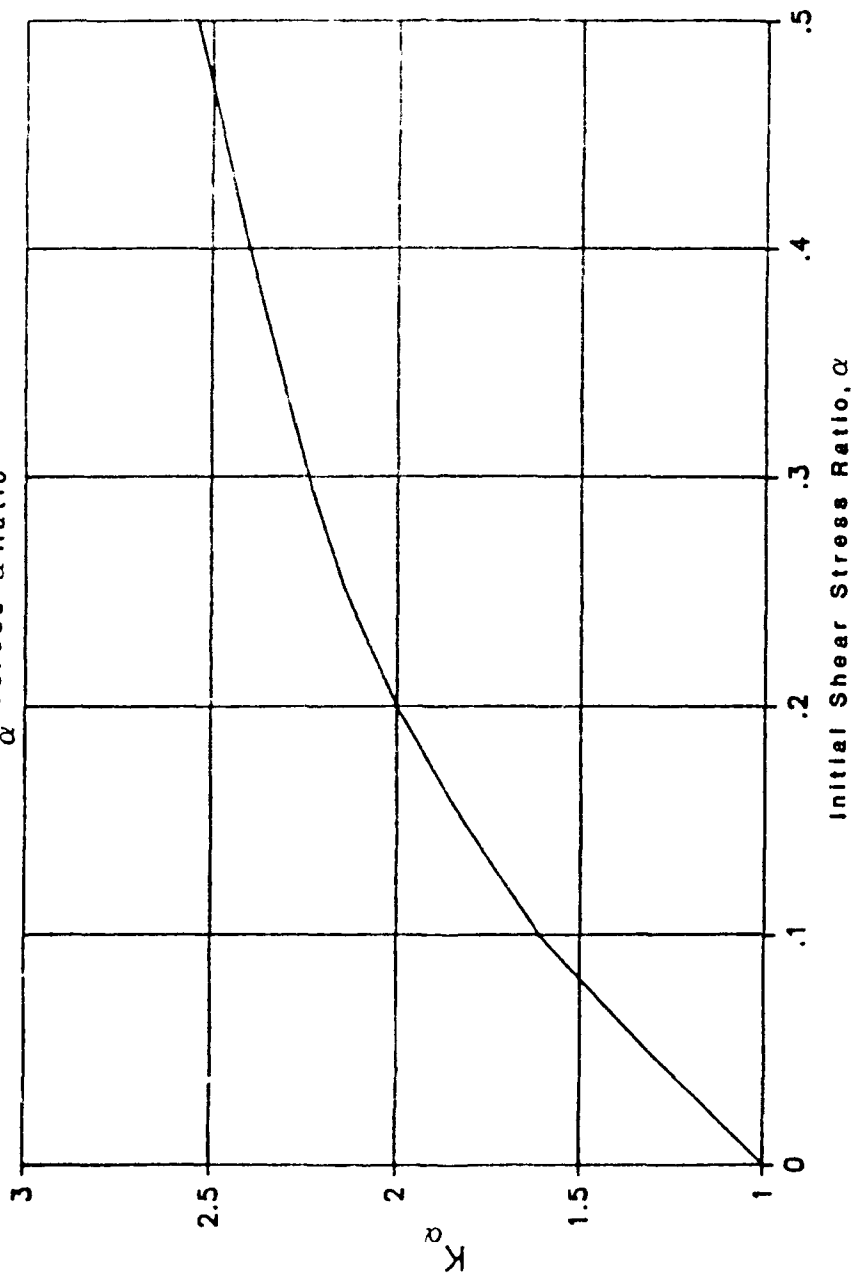


Figure 59. Adjustment factor,  $K_\alpha$  for change in cyclic stress ratio required to cause  $R_u = 100$  percent with change in initial shear stress ratio,  $\alpha$ , determined from laboratory tests on Folsom gravels

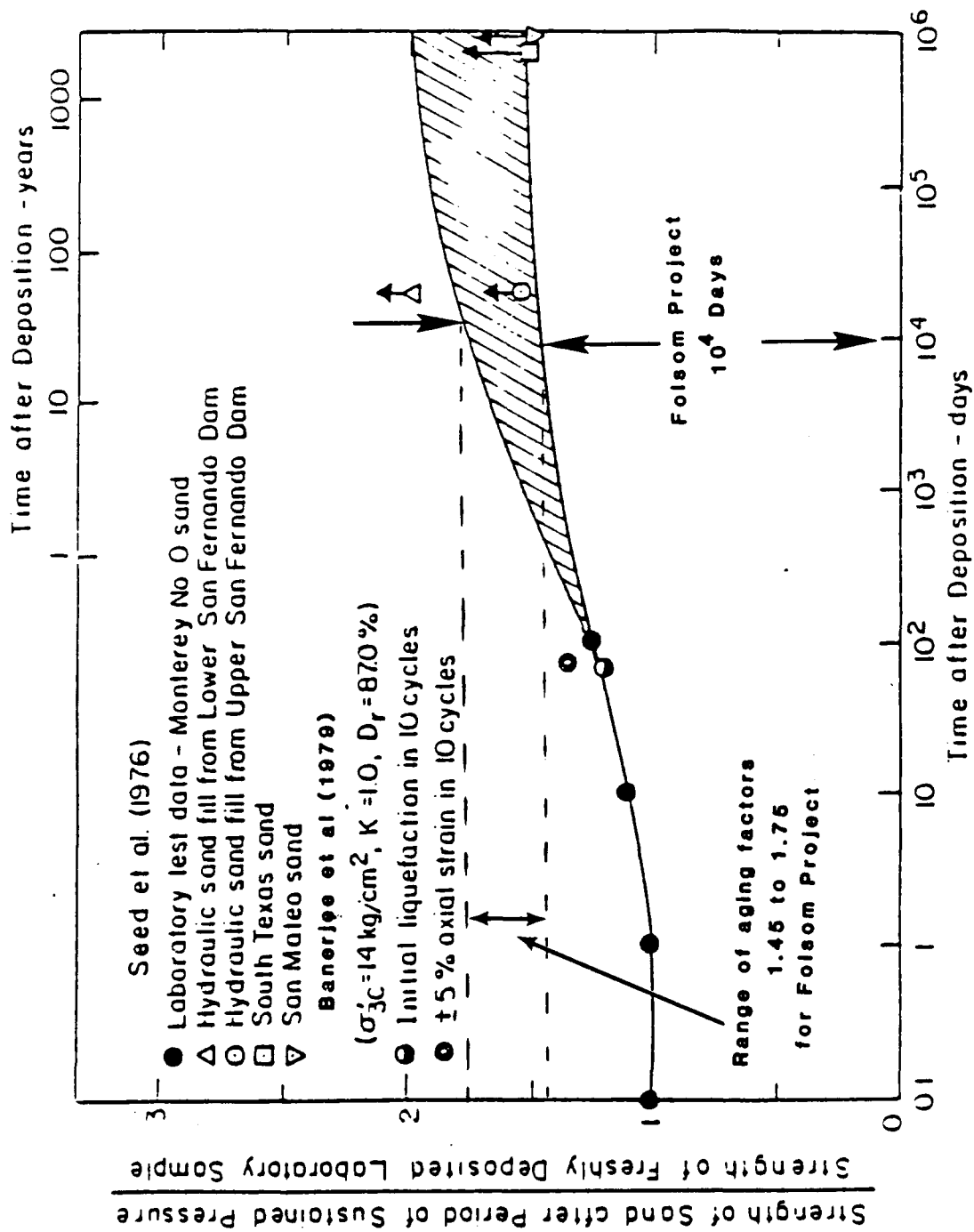


Figure 60. Influence of period of sustained pressure on stress ratio required to cause pore-water pressure of 100 percent or 2.5 to 5.0 percent strain in ten cycles (from Banerjee, Seed, and Chan 1979)

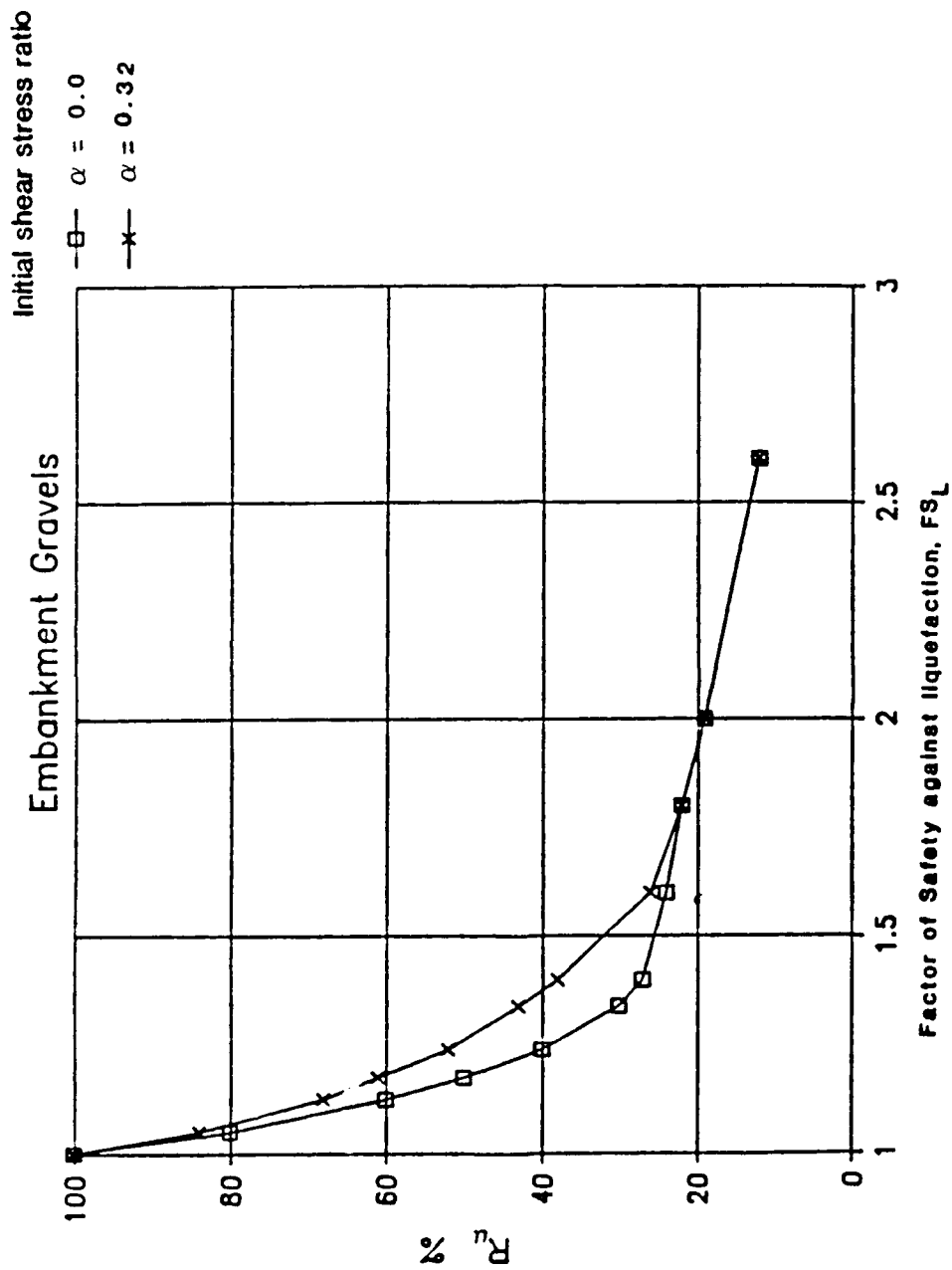


Figure 61. Residual excess pore pressure ratio,  $R_u$ , and corresponding values of Factors of Safety against liquefaction,  $FS_L$ , estimated from laboratory tests on Folsom gravels, for initial shear stress ratios of  $\alpha = 0.0$  and  $\alpha = 0.32$

**381 ELEMENTS**  
**399 NODAL POINTS**

**NOTE: ALL ELEMENTS BELOW DARK LINE ARE SUBMERGED.**

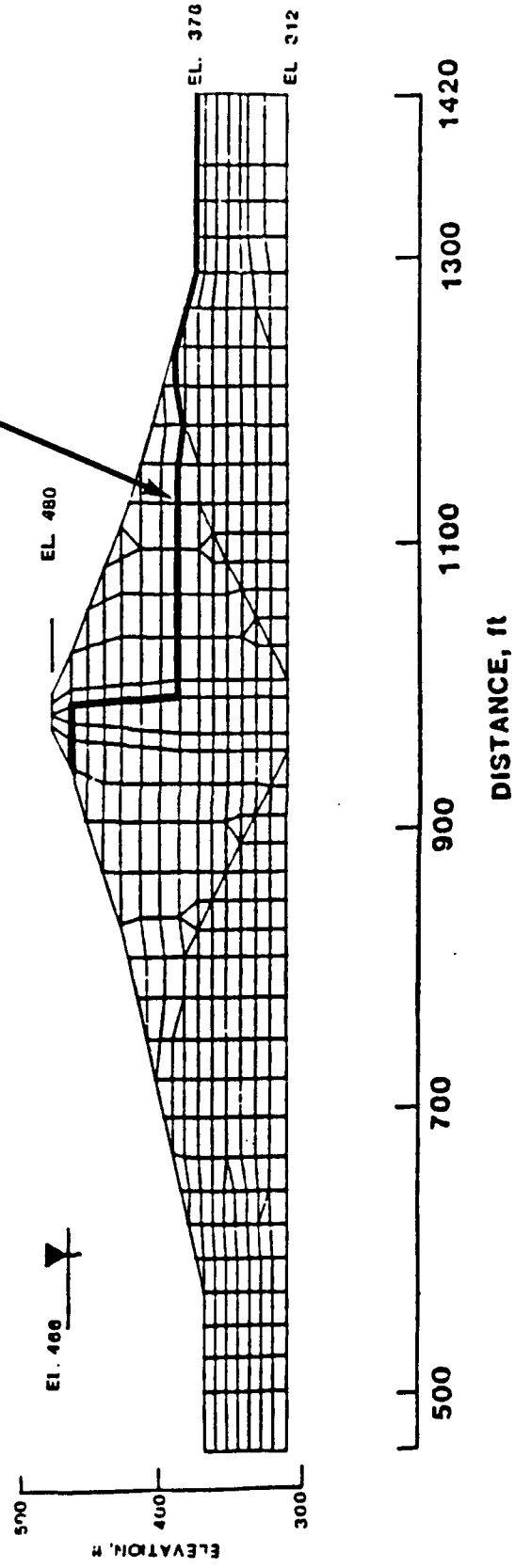


Figure 62. Finite element mesh of representative section of Mormon Island Auxiliary Dam



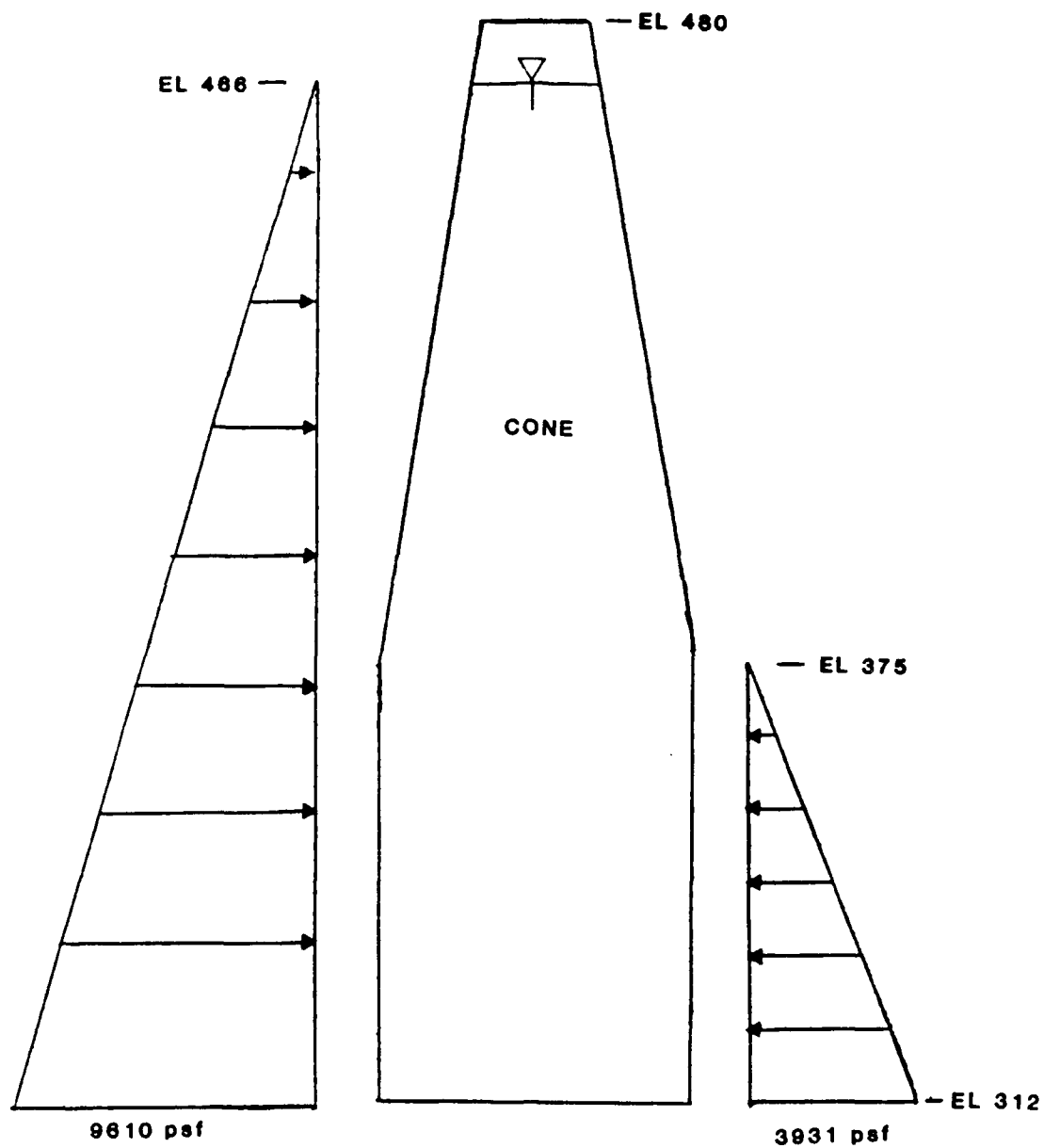


Figure 63. Hydrostatic pressure distribution acting on impervious core of Mormon Island Dam for static finite element analysis

Note: Units are in ksf

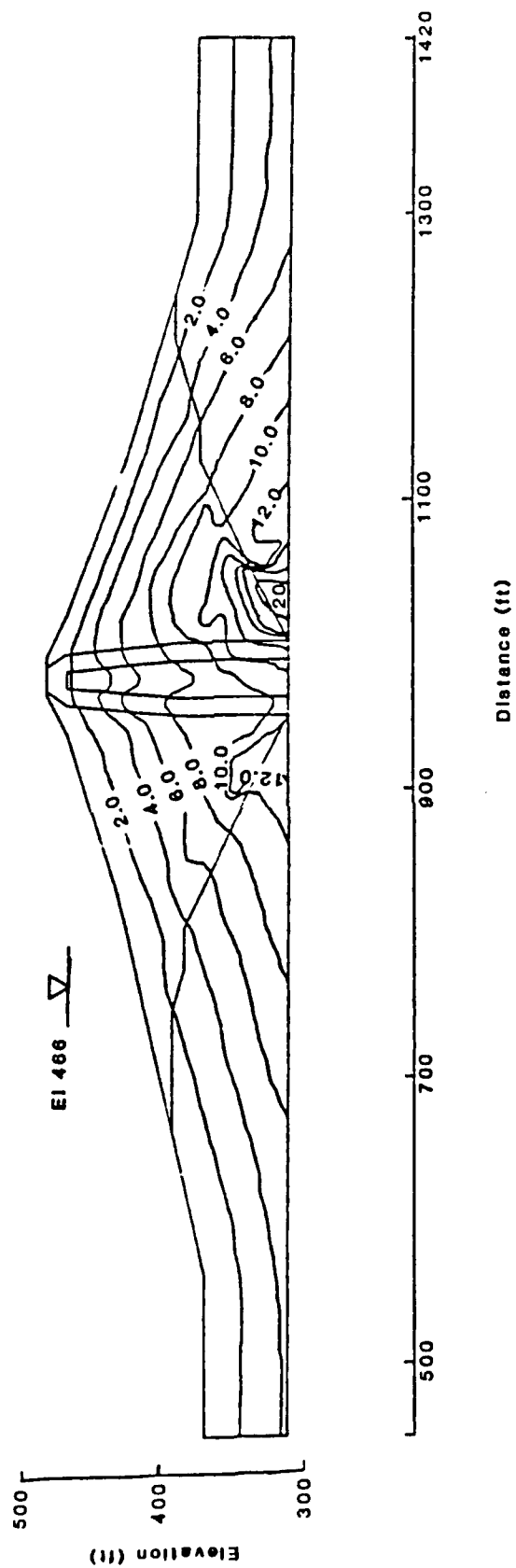


Figure 64. Contours of vertical effective stress

Note: Units are in kaf

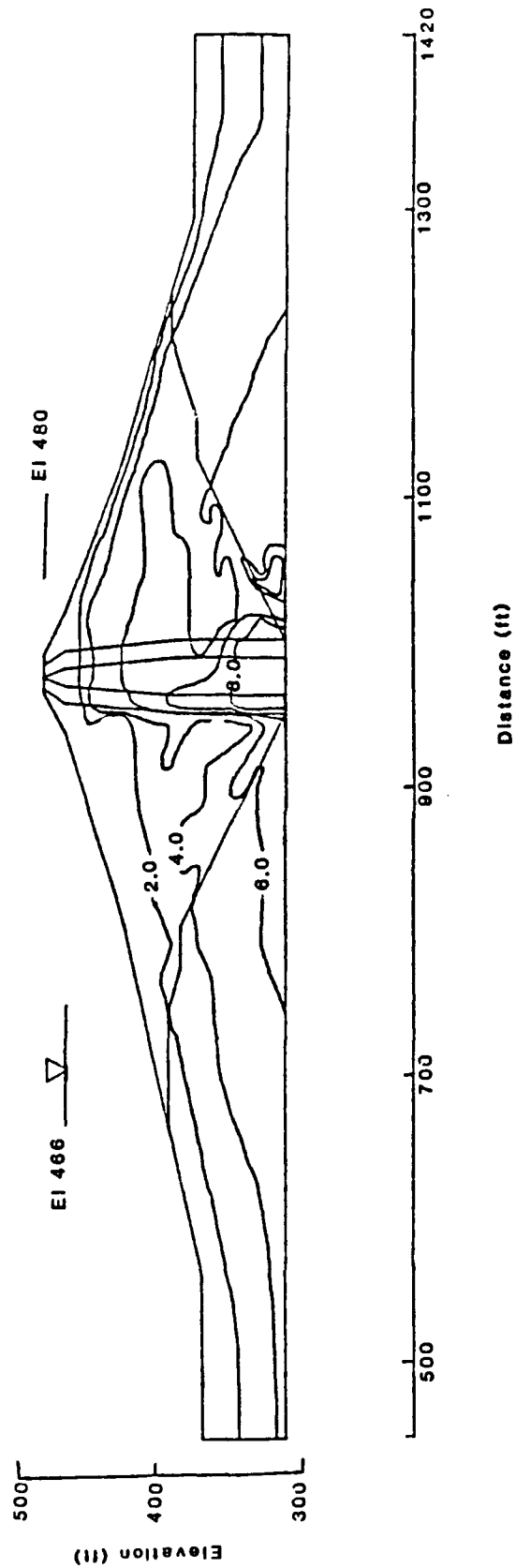


Figure 65. Contours of horizontal effective stress

Note: Units are in ksf

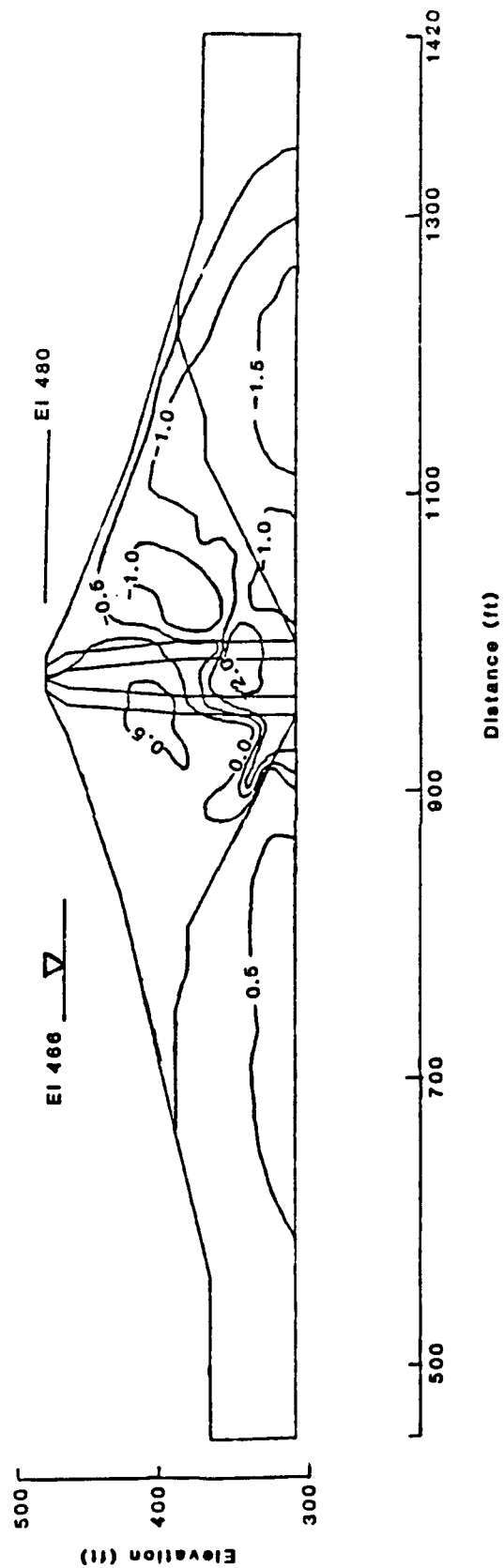


Figure 66. Contours of static shear stresses on horizontal planes

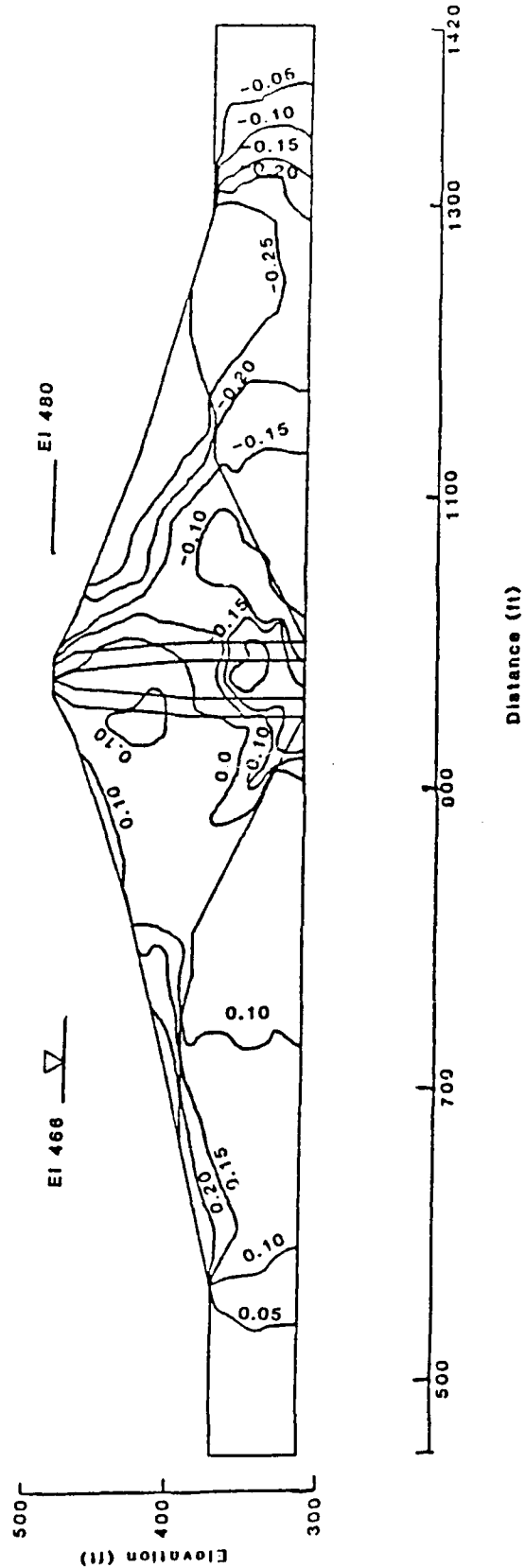


Figure 67. Contours of  $\alpha = \frac{\tau_{xy}}{\sigma'_v}$

NOTE: VELOCITIES ARE IN fps

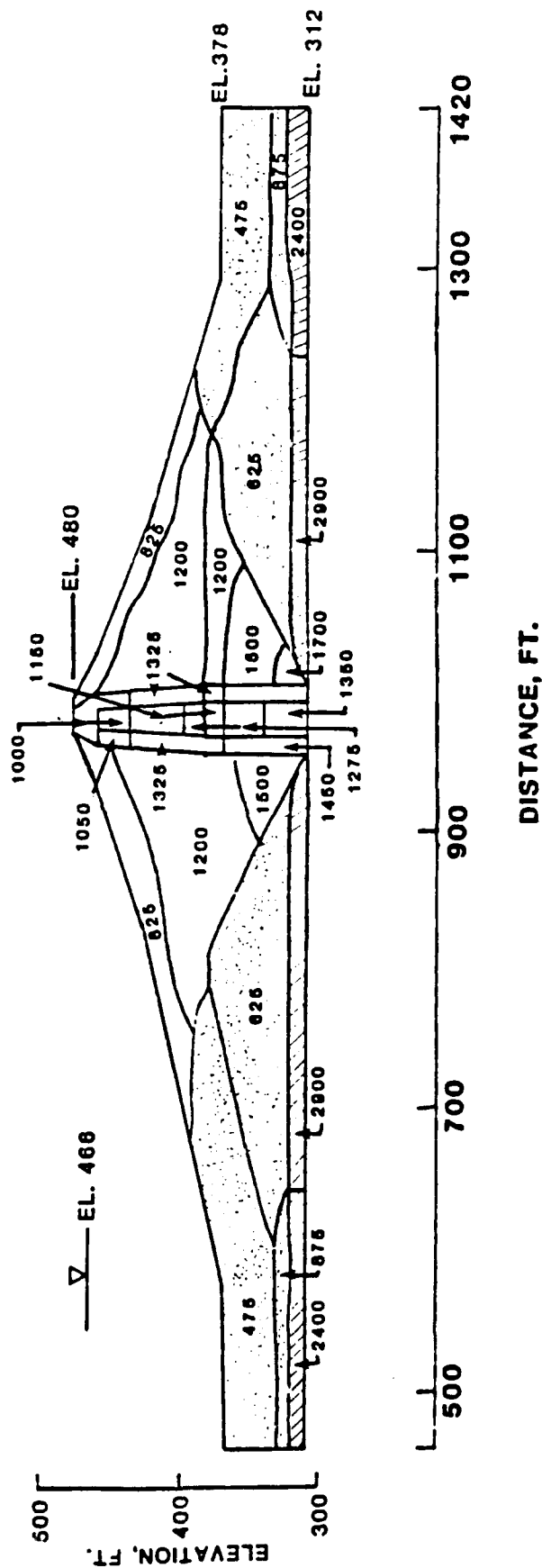
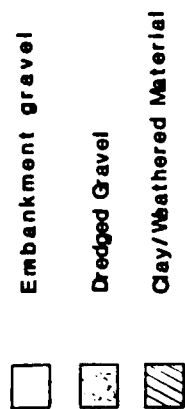
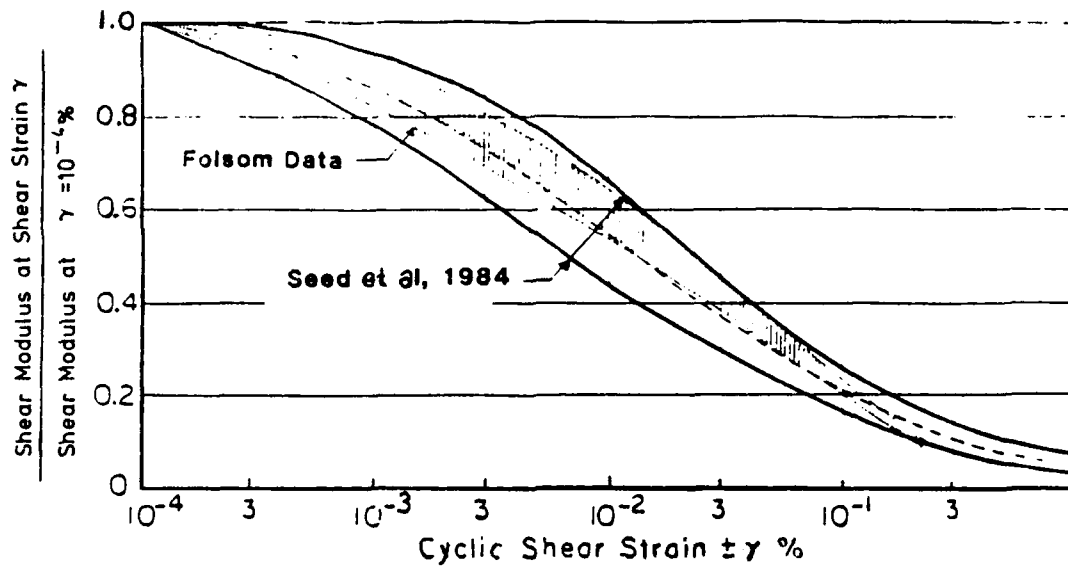
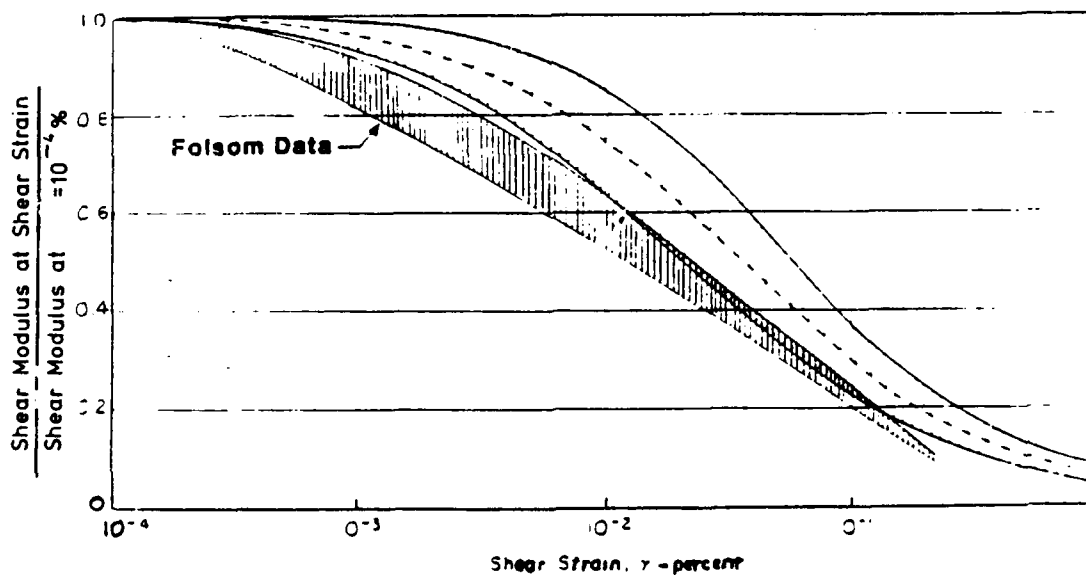


Figure 68. Shear wave velocity distribution for FLUSH analysis of Mormon Island Auxiliary Dam



a. Variation of shear modulus with shear strain for gravelly soils



b. Variation of shear modulus with shear strain for sands (after Seed and Idriss 1970)

Figure 69. Comparison of shear modulus degradation curves from Seed et al. (1984b) and Seed and Idriss (1970) with laboratory test data on Folsom gravels

$$\tau_{\text{FLUSH}} = 0.65 \cdot \tau_{\text{MAX}}$$

UNITS ARE IN ksf

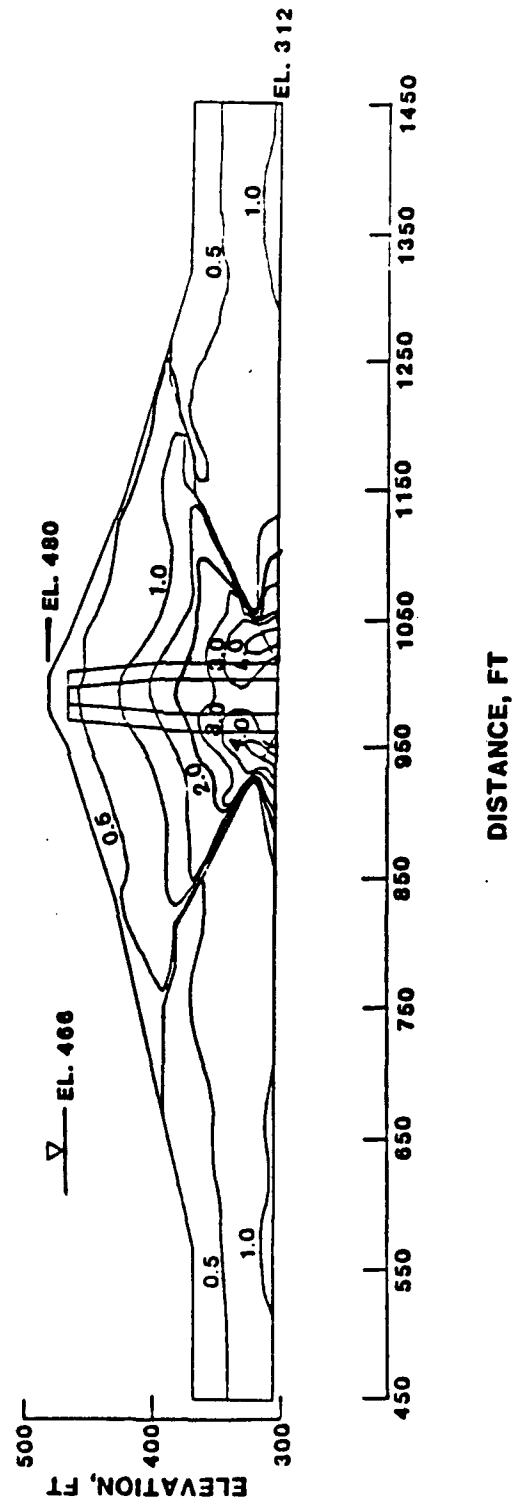


Figure 70. Contours of average dynamic shear stress,  $\tau_{\text{FLUSH}}$ , computed with FLUSH and Accelerogram B for Mormon Island Auxiliary Dam



**FUNDAMENTAL PERIOD = 1.72 sec.**

**Note: Accelerations are in g**

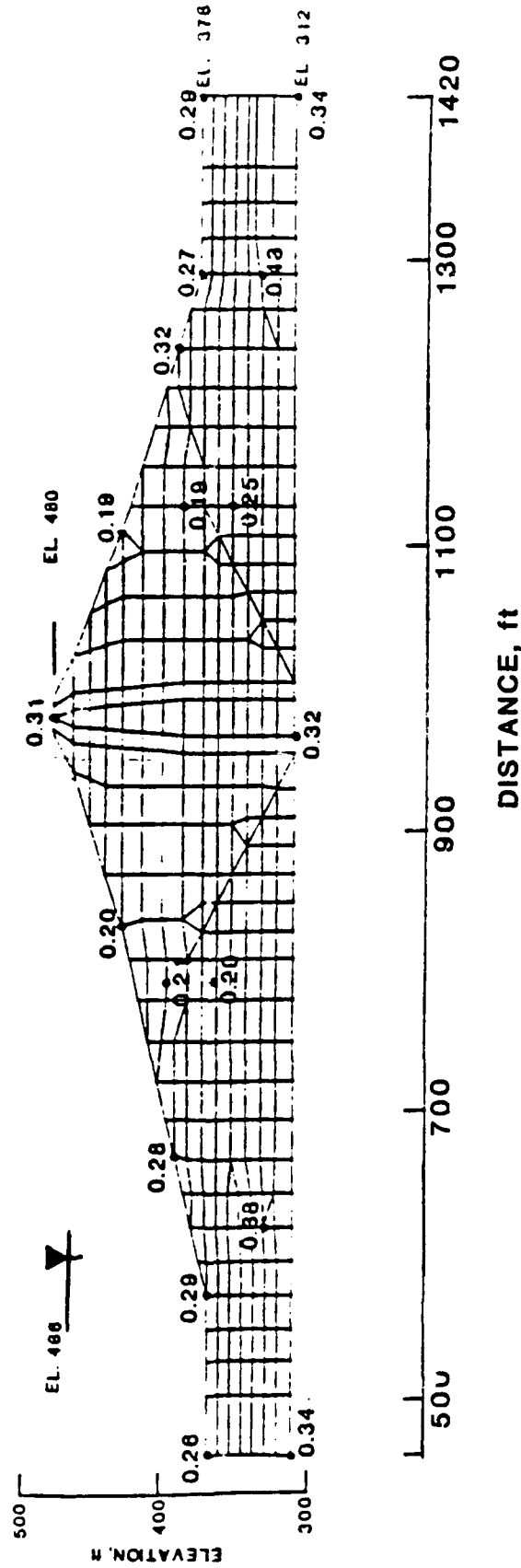


Figure 71. Maximum accelerations computed with FLUSH and Accelerogram B for selected nodal points, Mormon Island Auxiliary Dam

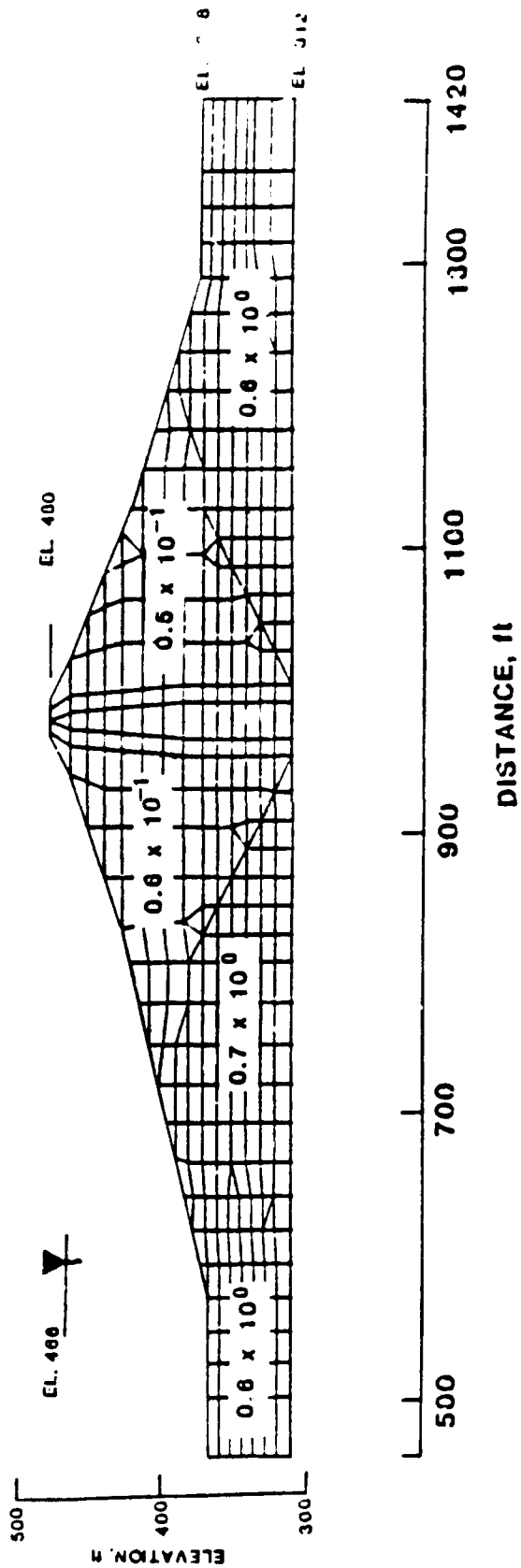


Figure 72. Effective shear strains in percent computed with FLUSH and Accelerogram B for Mormon Island Auxiliary Dam

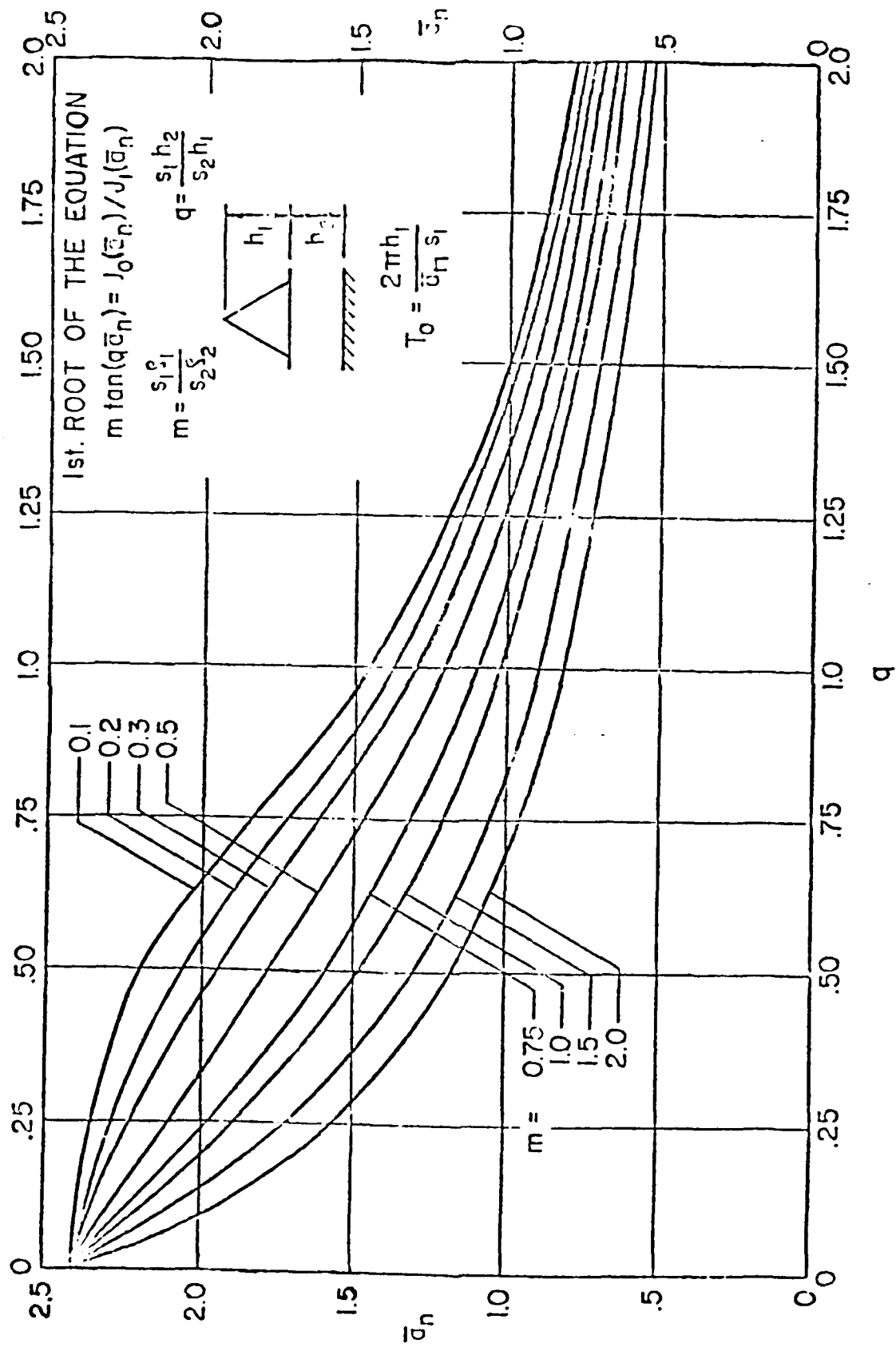
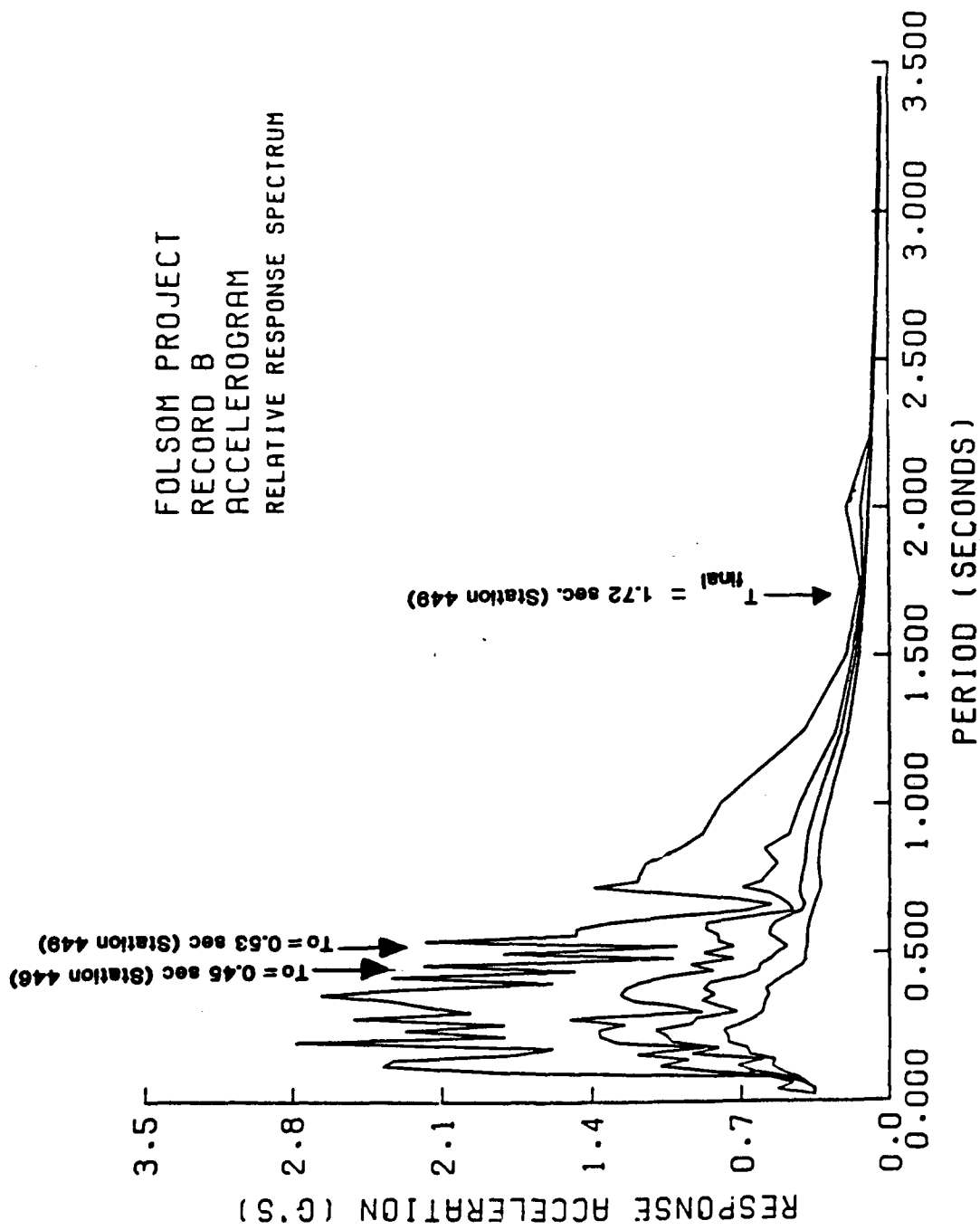


Figure 73. Fundamental period calculation chart



CURVE FOR 0.2.5 AND 10 PERCENT DAMPING

Figure 74. Initial (low strain) and final (high strain) fundamental periods for Mormon Island Auxiliary Dam compared with response spectra for Accelerogram B

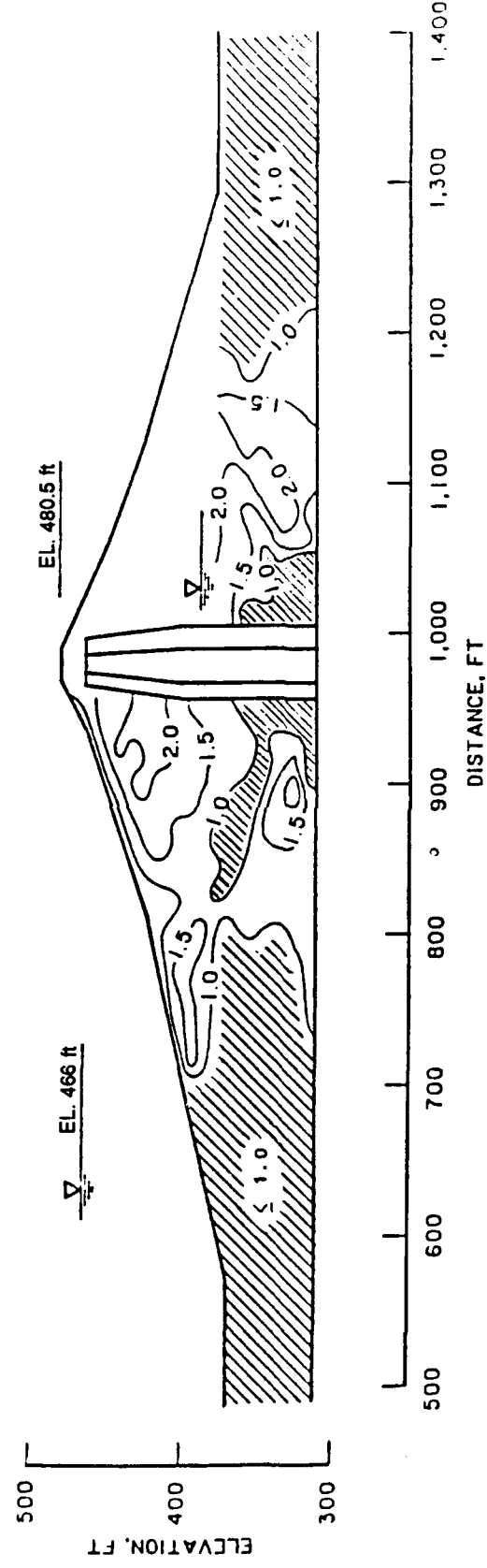


Figure 75. Contours of factors of safety against liquefaction for Mormon Island Auxiliary Dam

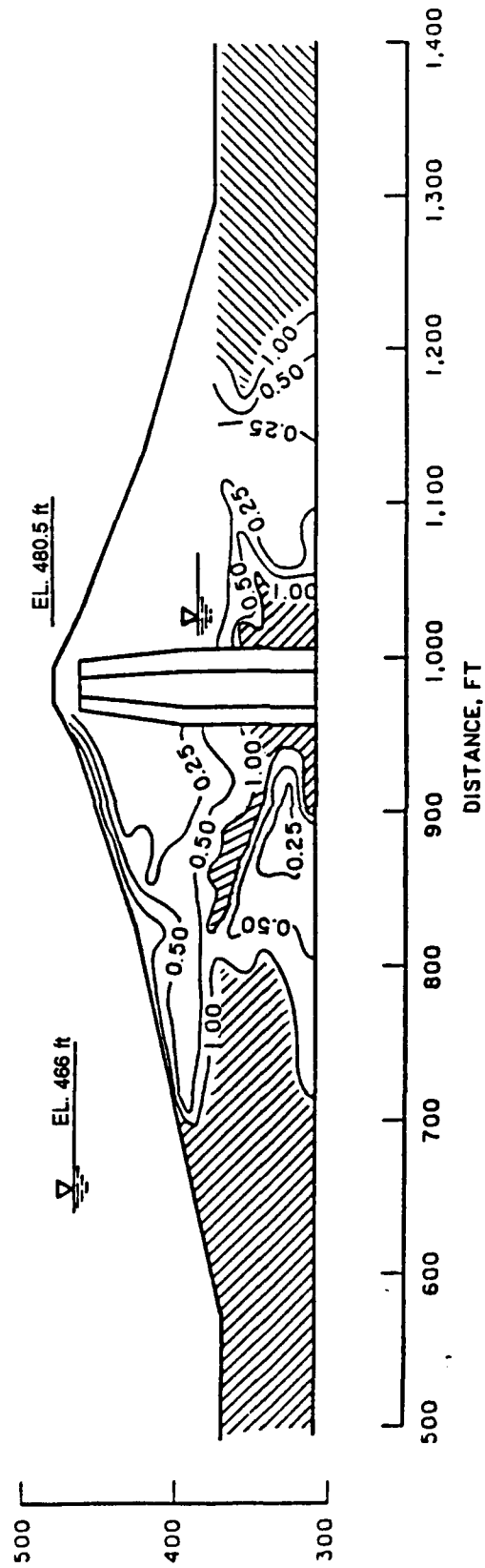


Figure 76. Contours of residual excess pore pressure ratio,  $R_u$  (percent), for Mormon Island Auxiliary Dam

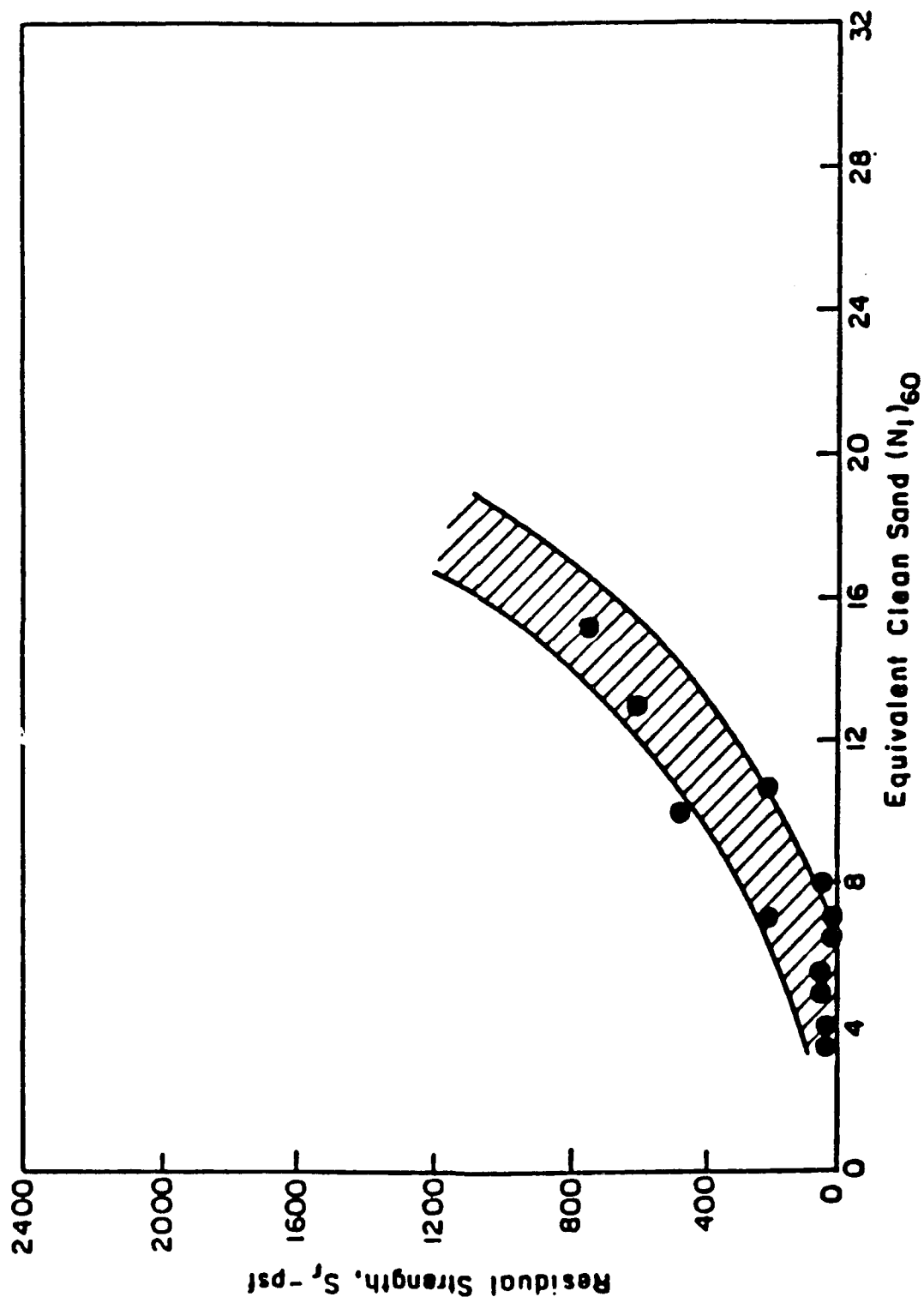


Figure 77. Relationship between residual strength and SPT N-values for sands  
(after Seed 1986)

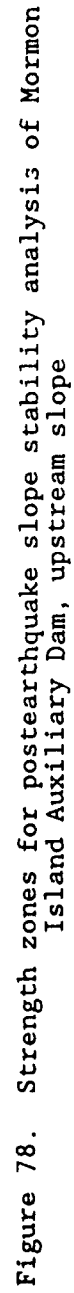


Figure 78. Strength zones for postearthquake slope stability analysis of Mormon Island Auxiliary Dam, upstream slope



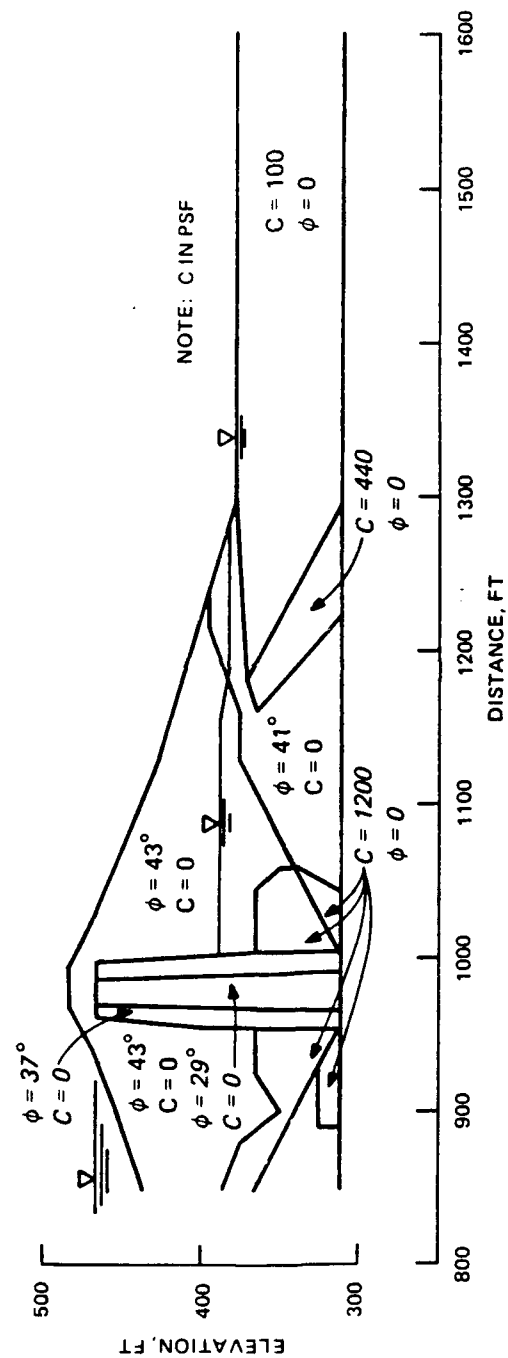


Figure 79. Strength zones for postearthquake slope stability analysis of Mormon Island Auxiliary Dam, downstream slope

$F_{PES}$  = Post-earthquake safety factor against sliding

$F_{STA}$  = Initial safety factor against sliding

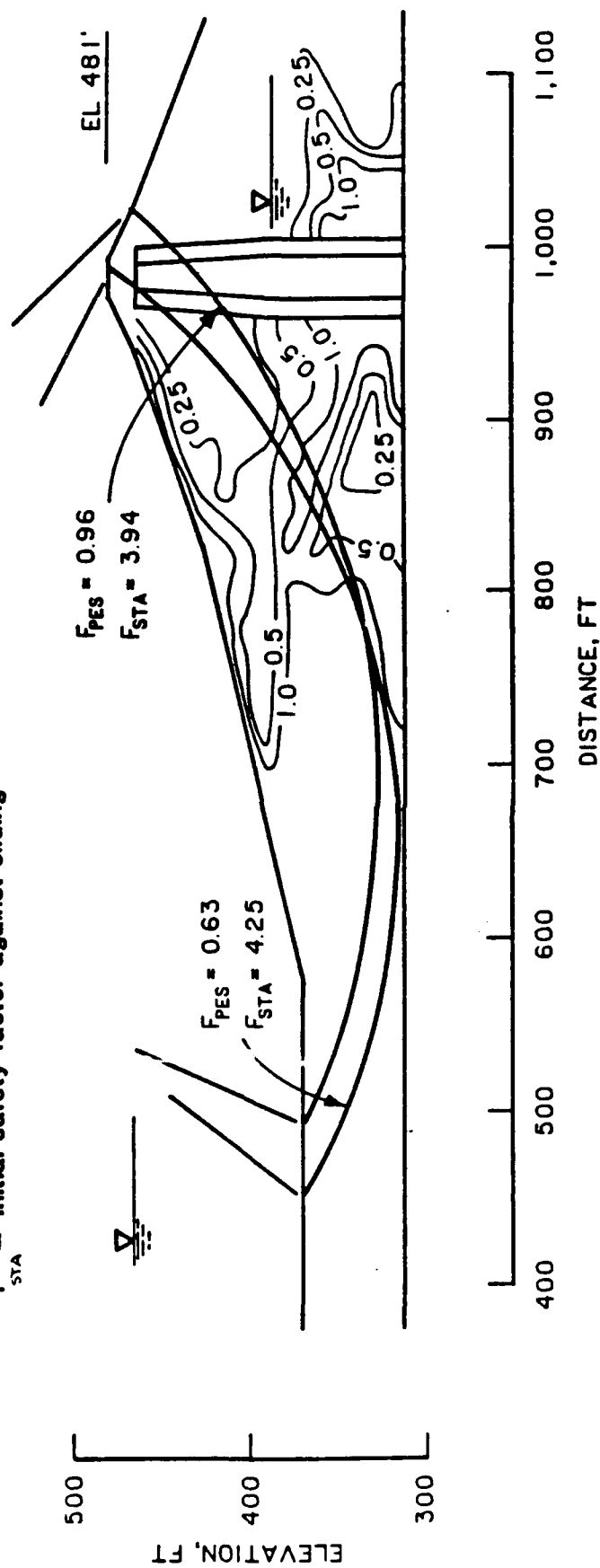


Figure 80. Postearthquake slope stability of Mormon Island Auxiliary Dam, upstream slope

$F_{PES}$  = Post-earthquake safety factor against sliding

$F_{STA}$  = Initial safety factor against sliding

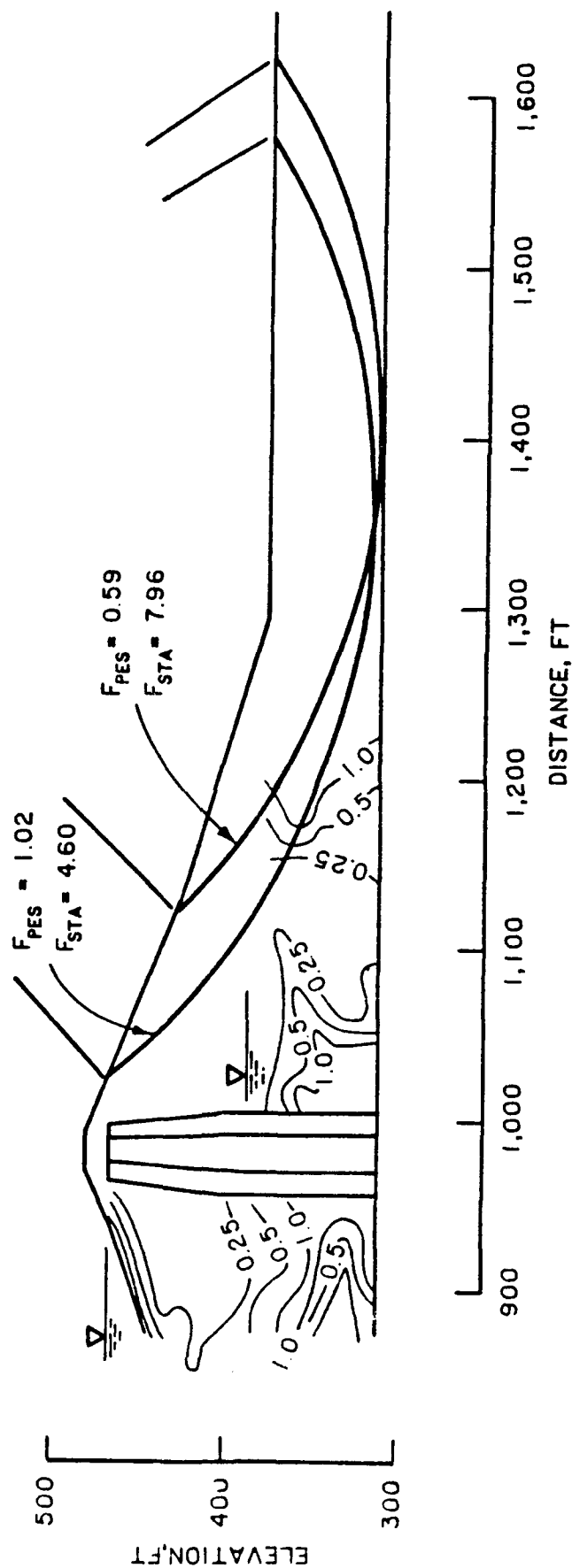


Figure 81. Postearthquake slope stability for Mormon Island Auxiliary Dam, downstream slope

APPENDIX A: EVALUATION OF BECKER PENETRATION TESTS  
PERFORMED AT MORMON ISLAND AUXILIARY DAM IN 1983

Contract Report by Dr. Leslie F. Harder, Jr.

October 1986

## Table of Contents

	<u>Page</u>
SECTION 1: INTRODUCTION	A7
Background	A7
Scope of Work	A8
SECTION 2: DETERMINATION OF EQUIVALENT SPT BLOWCOUNTS	A13
1983 Mormon Island Becker Penetration Tests	A13
Corrections to Becker Penetration Resistance for Combustion Energy	A15
Corrections to Becker Penetration Resistance for Drill Rig Type	A19
Conversion of Becker Blowcounts into Equivalent SPT Blowcounts	A23
SECTION 3: ACCOUNTING FOR OVERBURDEN PRESSURE	A25
Correction to 1 tsf Overburden Pressure	A25
Effect of Sloping Ground Conditions on Overburden Correction Factor	A28
SECTION 4: PRESENTATION OF RESULTS AND DETERMINATION OF CYCLIC STRENGTH	A31
Presentation of Results	A31
Effect of Fines Content	A38
Determination of Cyclic Strength	A42
SECTION 5: SUMMARY OF FINDINGS	A45
SECTION 6: REFERENCES	A47

## List of Figures

<u>Title</u>	<u>Page</u>
A1. Schematic Diagram of Becker Sampling Operation (after Harder and Seed, 1986)	A9
A2. Plan View of Mormon Island Auxiliary Dam Showing Location of Becker Soundings Performed in 1983 (after U.S. Army Corps of Engineers, Sacramento Dist.)	A10
A3. Section View of Mormon Island Auxiliary Dam Showing Location of Becker Soundings Performed in 1983 (after U.S. Army Corps of Engineers, Sacramento Dist.)	A11
A4. Typical Relationship Between Becker Blowcount and Bounce Chamber Pressure (after Harder and Seed, 1986)	A17
A5. Idealization of How Diesel Hammer Combustion Efficiency Affects Becker Blowcounts (after Harder and Seed, 1986)	A18
A6. Correction Curves Adopted to Correct Becker Blowcounts to Constant Combustion Curve Adopted for Calibration (after Harder and Seed, 1986)	A20
A7. Effect of Drill Rig on Corrected Becker Blowcount (after Harder and Seed, 1986)	A22
A8. Correlation Between Corrected Becker and SPT Blowcount (after Harder and Seed, 1986)	A24
A9. Relationship Between $C_N$ Correction and Overburden Pressure	A27
A10. Uncorrected Becker and Equivalent SPT Blowcounts for Soundings BH-1, 2, 4, 5, 7, and 8 (Performed in the Downstream Flat Area)	A32
A11. Uncorrected Becker and Equivalent SPT Blowcounts for Soundings BH-3 and BDT-1 (Performed in the Downstream Flat Area)	A33
A12. Uncorrected Becker and Equivalent SPT Blowcounts for Soundings BH-6 and BDT-2 (Performed in the Downstream Flat Area)	A34
A13. Uncorrected Becker and Equivalent SPT Blowcounts for Soundings BH-9 and BDT-3 (Performed through Downstream Slope)	A35
A14. Uncorrected Becker and Equivalent SPT Blowcounts for Sounding BH-10 (Performed through Downstream Slope)	A36

## List of Figures

<u>Title</u>	<u>Page</u>
A15. Relationship Between Corrected SPT Blowcount and Average Cyclic Stress Ratio Causing Liquefaction for M = 7.5 Earthquakes (after Seed et al., 1985)	A39
A16. Equivalent SPT Blowcounts and Classification Test Data from Soundings Performed in the Downstream Flat Area	A41

## List of Tables

<u>Title</u>	<u>Page</u>
A1. 1983 Becker Penetration Soundings Performed at Mormon Island Auxiliary Dam	A14
A2. Determination of Overburden Pressure Corrections for Soundings Performed through Downstream Face	A30
A3. Determination of Overburden Pressure Corrections for Soundings Performed through Beyond Downstream Toe	A30
A4. Summary of Mormon Island Cyclic Strengths	A43



## 1. INTRODUCTION

### Background

The Mormon Island Auxiliary Dam is part of the Folsom Dam and Reservoir Project and is located approximately 20 miles northeast of Sacramento, California. As part of a seismic safety evaluation of the Folsom project, the sands and gravels which make up the embankment's shells and foundation are being studied for their potential to liquefy and lose strength during earthquake shaking.

For sandy soils, evaluations of liquefaction potential usually employ the Standard Penetration Test (SPT). This test consists of driving a standard 2-inch O.D. split spoon sampler into the bottom of a borehole for a distance of 18 inches. The SPT blowcount, or N value, is defined as the number of blows required to drive the sampler the last 12 inches. Based on the performance of sites which have sustained strong earthquake shaking, researchers have developed correlations between the cyclic strength of sands and the SPT blowcount (Seed et al. 1983, Seed et al. 1985).

Unfortunately, the large gravel and cobble particles present in the embankment's shell and foundation precluded the use of the SPT at the Mormon Island Auxiliary Dam. Any SPT blowcounts obtained would have given a misleadingly higher blowcount due to the 2-inch sampler simply bouncing off the large particles, or by having a large gravel particle block the opening of the sampler's shoe and resulting in the sampler being driven as a solid penetrometer. As an alternative to the SPT, a larger penetration test was selected to explore the site. This test, known as the Becker Penetration Test (BPT), is generally used

with a 6.6-inch O.D. double-walled casing and is driven into the ground with a diesel pile hammer. The Becker Penetration Test consists basically of counting the number of hammer blows required to drive the casing one foot into the ground. By counting the blows for each foot of penetration, a continuous record of penetration resistance can be obtained for an entire profile. The casing can be driven with an open bit and reverse air circulation to obtain disturbed samples (Figure A1), or with a plugged bit and driven as a solid penetrometer.

An exploration program was performed with a Becker Hammer drill rig at the Mormon Island Auxiliary Dam in October 1983. A total of 13 open and plugged-bit soundings were conducted on the downstream face and beyond the downstream toe of the embankment (Figures A2 and A3). The purpose of this report is to evaluate these Becker soundings and determine the cyclic strength of the deposits explored.

#### Scope of Work

The principal approach was to convert the Becker blowcounts into equivalent SPT blowcounts, and then use the correlation between SPT blowcount and liquefaction potential developed by Seed et al. (1985) to obtain an estimate of the cyclic strength. The conversion of Becker blowcounts into equivalent SPT blowcounts was performed using the procedures outlined by Harder and Seed (1986). Because the Becker Penetration Test is a non-standard test, and because the effect of overburden pressure on blowcount had to be accounted for, there were several intermediate steps prior to the final determination of cyclic strength. In summary, the steps of the process are presented below:

1. Because the diesel hammer can be run at a wide variety of combustion conditions, all of the Becker Penetration Test blowcounts were corrected to blowcounts obtained with a standard set of constant combustion conditions (Section 2).

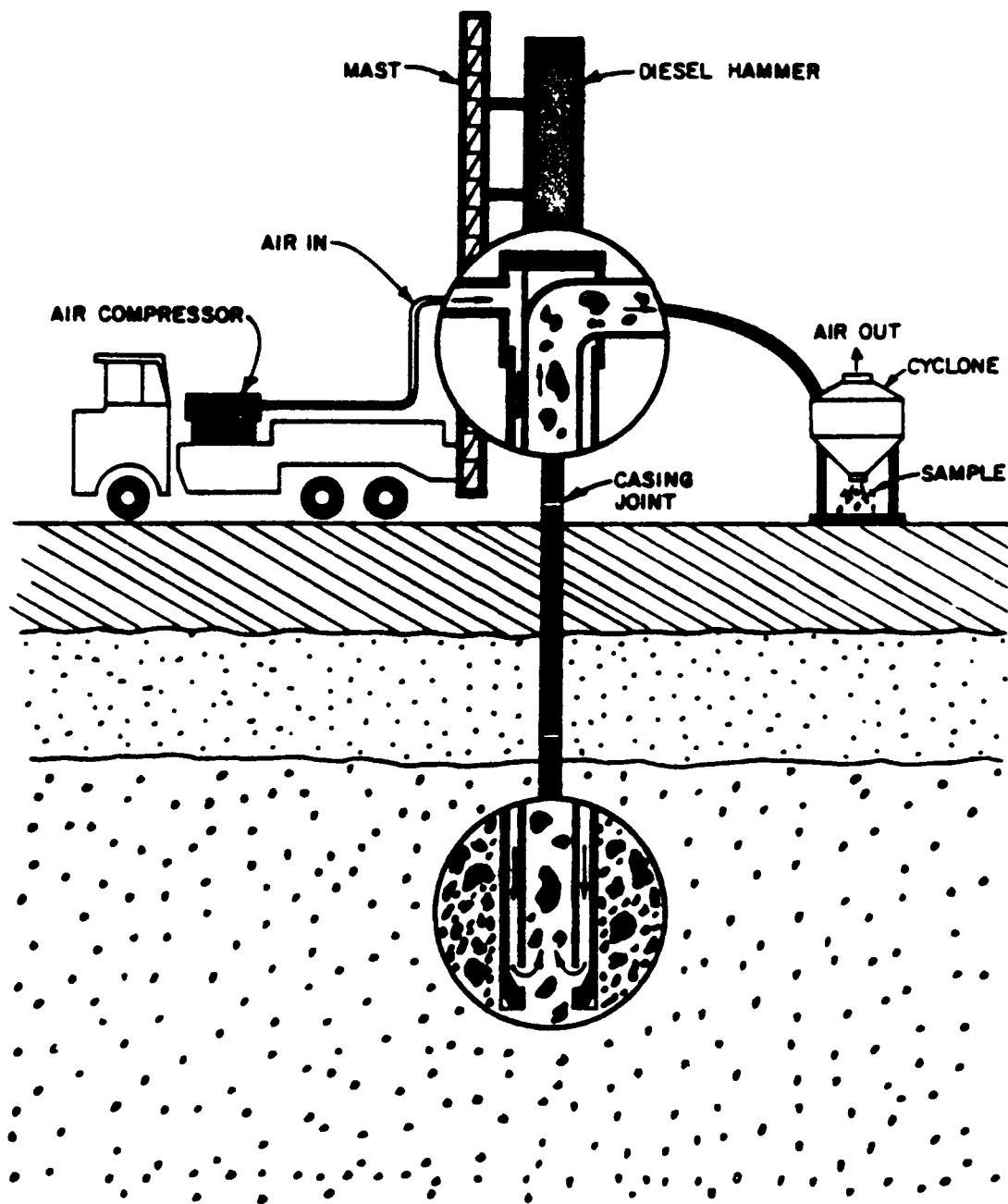
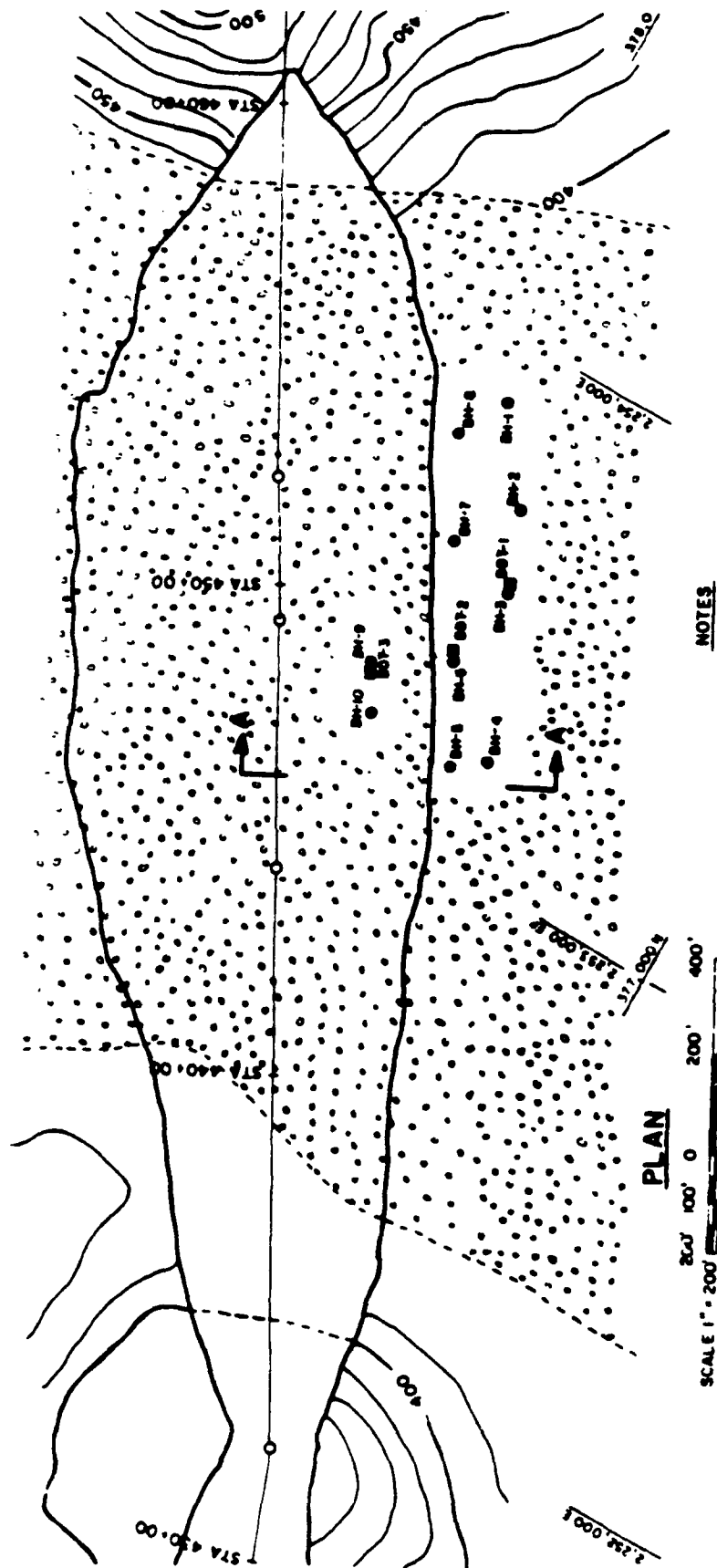


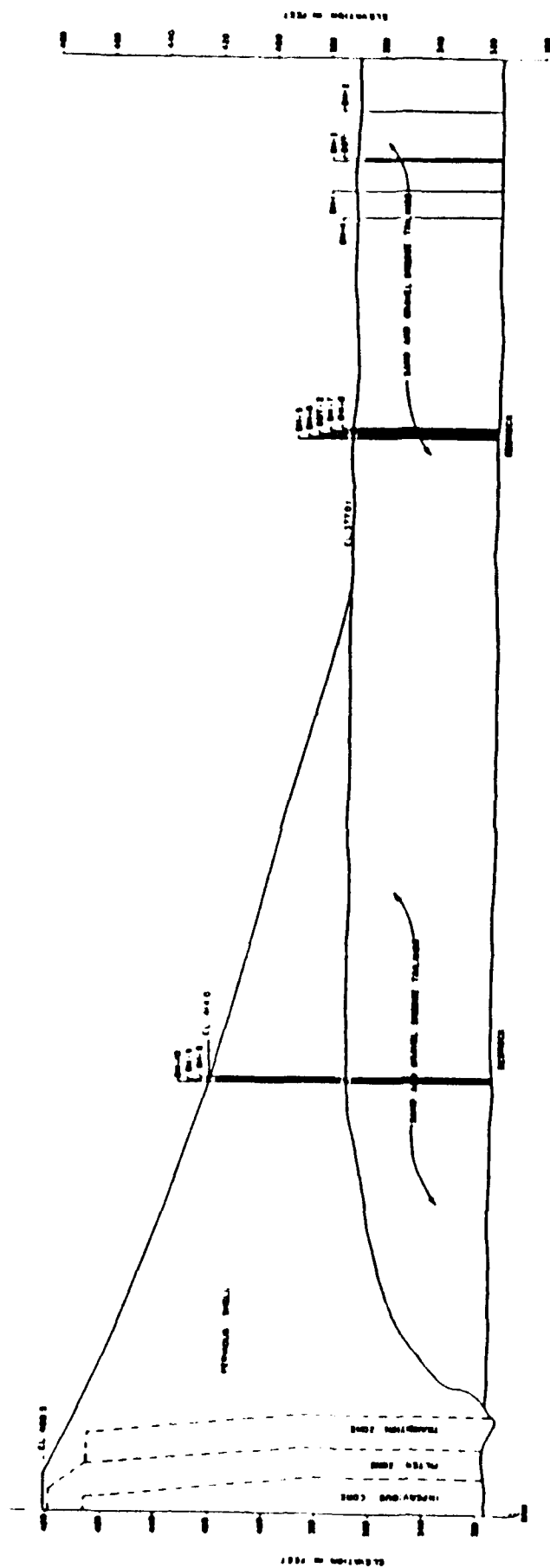
Figure A1. Schematic diagram of Becker sampling operation  
(after Harder and Seed, 1986)



#### NOTES

- 1) BH PREFIX DENOTES A BECKER SOUNDING PERFORMED WITH A 7.3-INCH O.D. OPEN FELCON BIT.
- 2) BDT PREFIX DENOTES A BECKER SOUNDING PERFORMED WITH A 6.6-INCH O.D. PLUGGED 8-TOOTH BIT.
- 3) SECTION A-A SHOWN IN FIGURE 3.

Figure A2. Plan view of Mormon Island Auxiliary Dam showing location of Becker Soundings performed in 1983 (after U.S. Army Corps of Engineers, Sacramento Dist.)



2. Because the Becker drill rig used at Mormon Island (Rig No. 11) is more efficient than the type of rig adopted for the correlation by Harder and Seed (1986), the Becker blowcounts had to be adjusted upward for this effect (Section 2).
3. Using the correlation developed by Harder and Seed (1986), the corrected Becker blowcounts were converted into equivalent SPT blowcounts (Section 2).
4. Using effective stress values determined from finite element analyses, the equivalent SPT values from different depths and stress levels were normalized to those that would have been obtained in the same material under level ground conditions with an effective overburden stress of 1 tsf (Section 3).
5. Using the correlation developed by Seed et al. (1985), the normalized equivalent SPT blowcounts were used to obtain an estimate of cyclic strength of the gravelly embankment shell and foundation for the locations tested (Section 4).
6. A summary of results is also presented (Section 5).

The sources of the basic data used in this report were the listings and plots showing uncorrected Becker data, testing depths, and classification test results featured in a preliminary report by the U. S. Army Corps of Engineers Sacramento District (Reference 8). The stress results from finite element analyses used to normalize the equivalent SPT results to 1 tsf overburden pressure were supplied by Ron Wahl of the Geotechnical Laboratory, Waterways Experiment Station. Additional information regarding the gradations obtained from field density test pits were obtained from Mary Ellen Hynes-Griffin.

This report was prepared under Contract No. DACW 39-86-M-2923.

## 2. DETERMINATION OF EQUIVALENT SPT BLOWCOUNTS

### 1983 Mormon Island Becker Penetration Tests

Thirteen Becker soundings were performed at the Mormon Island Auxiliary Dam during the period of October 10-21, 1983. All of the soundings were performed with 6.6-inch O.D. double-walled casing and were driven by an ICE Model 180 diesel pile hammer mounted on a Becker B-180 Drill Rig (No. 11). Ten of the soundings, designated with the prefix BH, employed an open Felcon crowd-in bit together with air-recirculation to obtain disturbed samples of penetrated soil. This open bit has a 7.3-inch O.D. and a 3.8-inch I.D. The 7.3-inch O.D. extends from the tip of the bit for a distance of about 8.5 inches before reducing down to the same outside diameter (6.6 inches) that the drill casing has.

The remaining 3 soundings, given the prefix BDT, used a plugged 8-tooth crowd-out bit. This plugged bit had the same 6.6-inch O.D. as did the casing. Details and photographs of the two bit types are available in Reference 1. The details of the 1983 Mormon Island soundings are presented in Table A1.

At three locations at the Mormon Island Auxiliary Dam, an open-bit sounding was performed about 10 feet away from a closed-bit sounding. This was done in order to make comparisons between the blowcounts obtained with the two different types of bits. Thus, open-bit sounding BH-3 was performed in the same proximity as plugged-bit sounding BDT-1, open-bit sounding BH-6 was performed in the same proximity as plugged-bit sounding BDT-2, and open-bit sounding BH-9 was performed in the same proximity as plugged-bit sounding BDT-3 (Figure A2).

Table A1: 1983 Becker Penetration Soundings Performed at Mormon Island Auxiliary Dam (from Reference 8)

Sounding	Location	Approximate Ground Surface Elev.(ft)	Bit Configuration	Bit O.D. (in)	Maximum Depth (ft)
BH- 1	Downstream Flat	377	Open	7.3	74.5
BH- 2	Downstream Flat	377	Open	7.3	66.
BH- 3	Downstream Flat	377	Open	7.3	78.
BH- 4	Downstream Flat	377	Open	7.3	61.
BH- 5	Downstream Flat	377	Open	7.3	59.
BH- 6	Downstream Flat	377	Open	7.3	61.
BH- 7	Downstream Flat	377	Open	7.3	59.
BH- 8	Downstream Flat	377	Open	7.3	69.
BH- 9	Downstream Face	414	Open	7.3	95.
BH-10	Downstream Face	414	Open	7.3	102.
BDT- 1	Downstream Flat	377	Plugged	6.6	66.
BDT- 2	Downstream Flat	377	Plugged	6.6	65.
BDT- 3	Downstream Face	414	Plugged	6.6	95.

NOTE: Open-bit sounding BH-3 was performed in the same proximity as plugged-bit sounding BDT-1, open-bit sounding BH-6 was performed in the same proximity as plugged-bit sounding BDT-2, and open-bit sounding BH-9 was performed in the same proximity as plugged-bit sounding BDT-3 in order to make comparisons between the blowcounts obtained from the two different types of bits.



## Corrections to Becker Penetration Resistance for Combustion Energy

Constant energy conditions are not a feature of the double-acting diesel hammers used in the Becker Penetration Test. One reason for this is that the energy is dependent upon combustion conditions; thus anything that affects combustion, such as fuel quantity, fuel quality, air mixture and pressure all have a significant effect on the energy produced. Combustion efficiency is operator-dependent because the operator controls a variable throttle which affects how much fuel is injected for combustion. On some rigs, the operator also controls a rotary blower which adds additional air to the combustion cylinder during each stroke. This additional air is thought to better scavenge the cylinder of burnt combustion gases and has been found to produce higher energies (Reference 1).

To monitor the level of energy produced by the diesel hammer during driving, use is made of the bounce chamber pressure. For the ICE Model 180 diesel hammers used on the Becker drill rigs, the top of the hammer is closed off to allow a smaller stroke and a faster driving rate. At the top, trapped air in the compression cylinder and a connected bounce chamber acts as a spring. The amount of potential energy within the ram at the top of its stroke can be estimated by measuring the peak pressure induced in the bounce chamber. Although calibration charts between potential energy and bounce chamber pressure are available from the manufacturer of the hammer, studies by Harder and Seed (1986) have shown that they are unable to predict the change in Becker blowcount for different levels of bounce chamber pressure.

Another reason why the energy is not a constant with the Becker Hammer Drill is that the energy developed is dependent on the

blowcount of the soil being penetrated. As blowcounts decrease, the displacement of the casing increases with each stroke. With increasing casing displacement, a larger amount of energy from the expanding combustion gases is lost to the casing movement rather than being used to raise the ram for the next stroke. Thus, as blowcounts decrease, the energy developed by the hammer impact on subsequent blows also decreases. Conversely, if the blowcounts increase, then there is less casing displacement per blow and more of the combustion energy is directed upward in raising the ram for the next stroke. Figure A4 shows a curve illustrating a typical relationship between Becker blowcounts and bounce chamber pressure for constant combustion conditions (Reference 1). This curve is designated as a constant combustion rating curve and is just one member of a family of such curves that can be produced by a given drill rig and hammer.

Studies by Harder and Seed (1986) have shown that diesel hammer combustion efficiency significantly affects the Becker blowcount. Presented in Figure A5 are typical results obtained for different combustion efficiencies. In the upper plot, three combustion rating curves representing three different combustion efficiencies are shown. With different combustion conditions, the resulting blowcounts from tests performed in the same materials can be radically different. Consequently, tests in the same material at a depth of 40 feet can give a Becker blowcount of 14 when the hammer is operated at high combustion efficiency (throttle and blower on full), but give blowcounts of 26 and 50 at succeeding reductions of combustion energy.

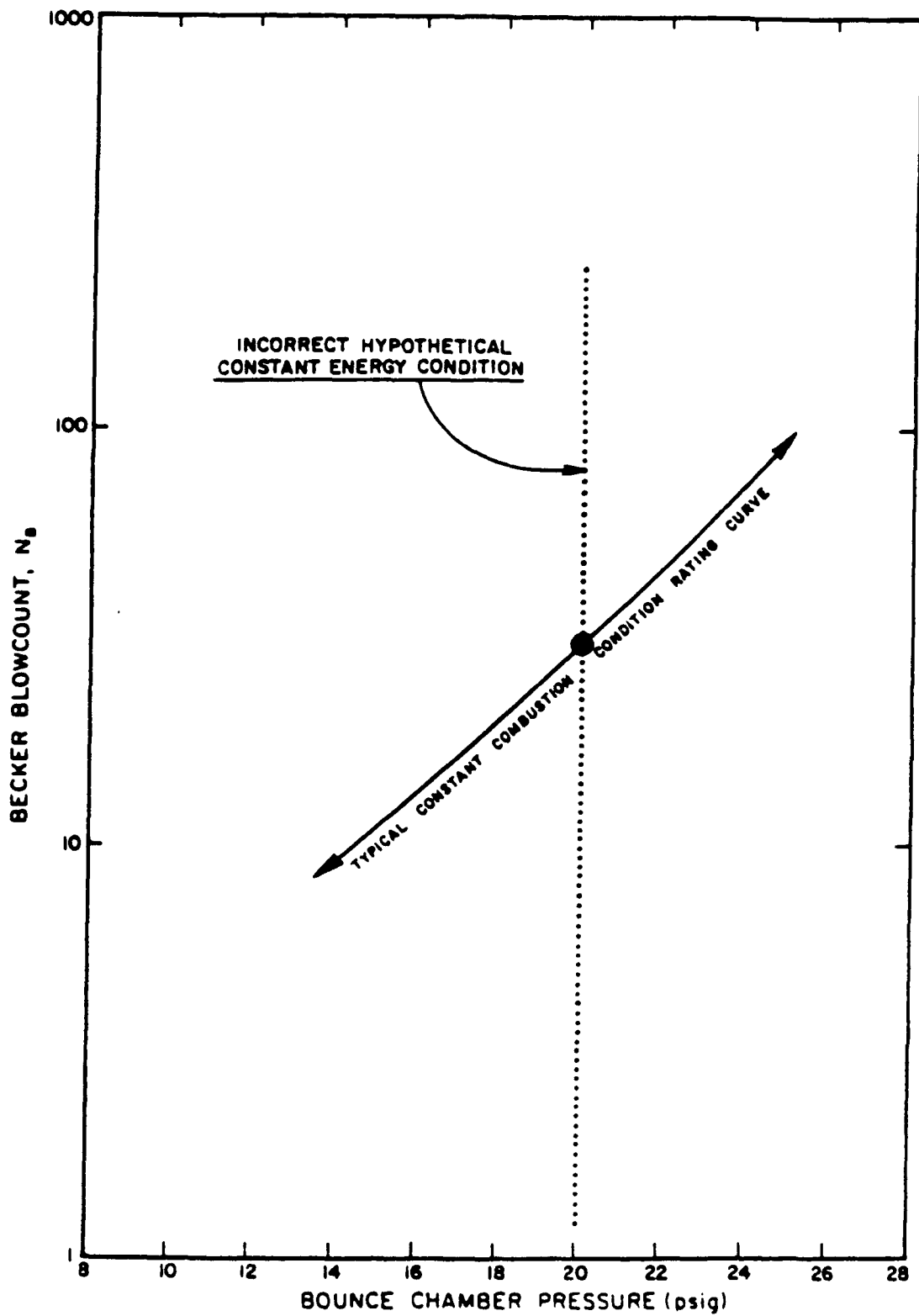


Figure A4. Typical relationship between Becker blowcount and Bounce Chamber pressure (after Harder and Seed, 1986)

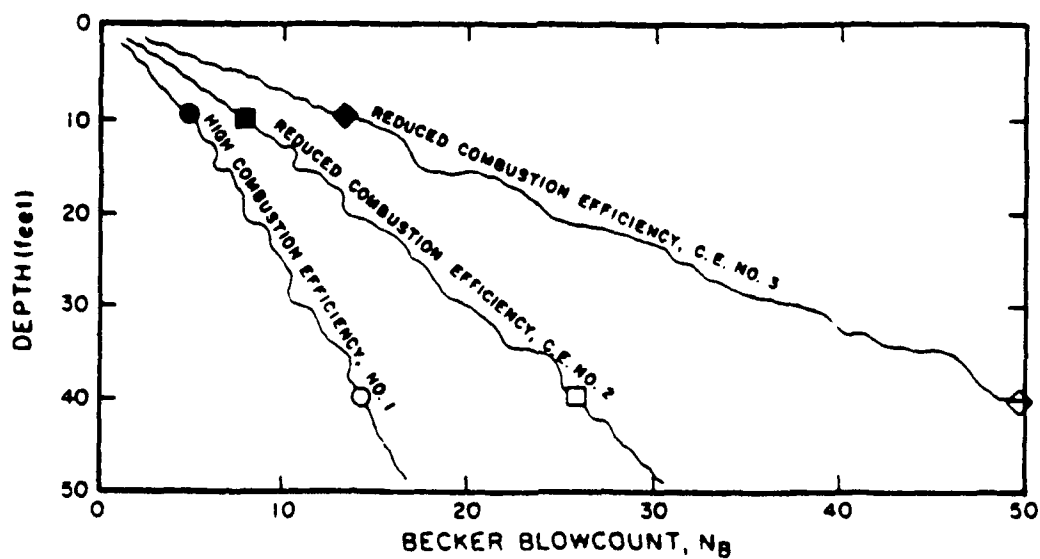
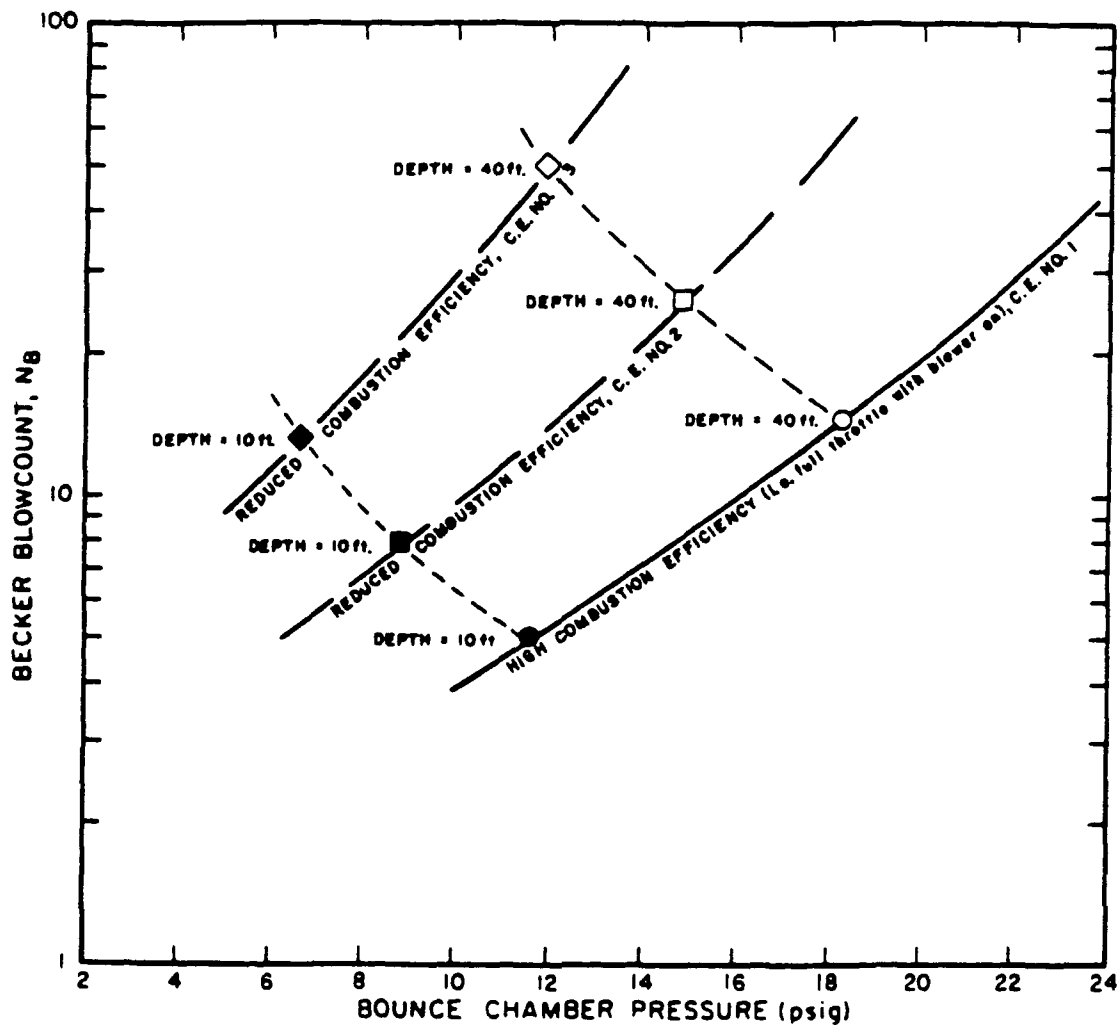


Figure A5. Idealization of how diesel hammer combustion efficiency affects Becker blowcount (after Harder and Seed, 1986)

To account for combustion effects, it is necessary to adopt a standard combustion efficiency and make corrections to the blowcount for different combustion conditions. For the corrections of the 1983 Mormon Island data, the curve marked in Figure A6 with the symbols AA was selected. This curve was chosen because it was the curve used by Harder and Seed (1986) to correct Becker data before correlating Becker blowcounts to SPT blowcounts. Also shown in Figure A6 are correction curves that are used to reduce measured Becker blowcounts to corrected Becker blowcounts when reduced combustion levels were employed during testing.

To use the correction curves, it is simply necessary to locate each uncorrected test result on the chart shown in Figure A6, using both the uncorrected blowcount and the bounce chamber pressure, and then follow the correction curves down to the standard rating curve AA, to obtain the corrected Becker blowcount, denoted as  $N_{BC}$ . For example, if the uncorrected blowcount was 44 and it was obtained at sea level with a bounce chamber pressure of 18 pounds per square inch-gauge (psig), then the corrected Becker blowcount would be 30 (Figure A6).

Because the combustion rating curve AA that was adopted represents a high combustion level compared with combustion levels achieved at the Mormon Island Dam, almost all of corrections of the Mormon Island data for combustion effects required reducing the measured blowcounts.

#### Corrections to Becker Penetration Resistance for Drill Rig Type

Becker Drills, Inc. employs principally two types of drill rigs to perform the Becker Penetration Test. The older rig is designated the B-180 drill rig (it is also known as the HAV-180 rig) and a newer model, developed in the mid-70's, which is designated the AP-1000 drill

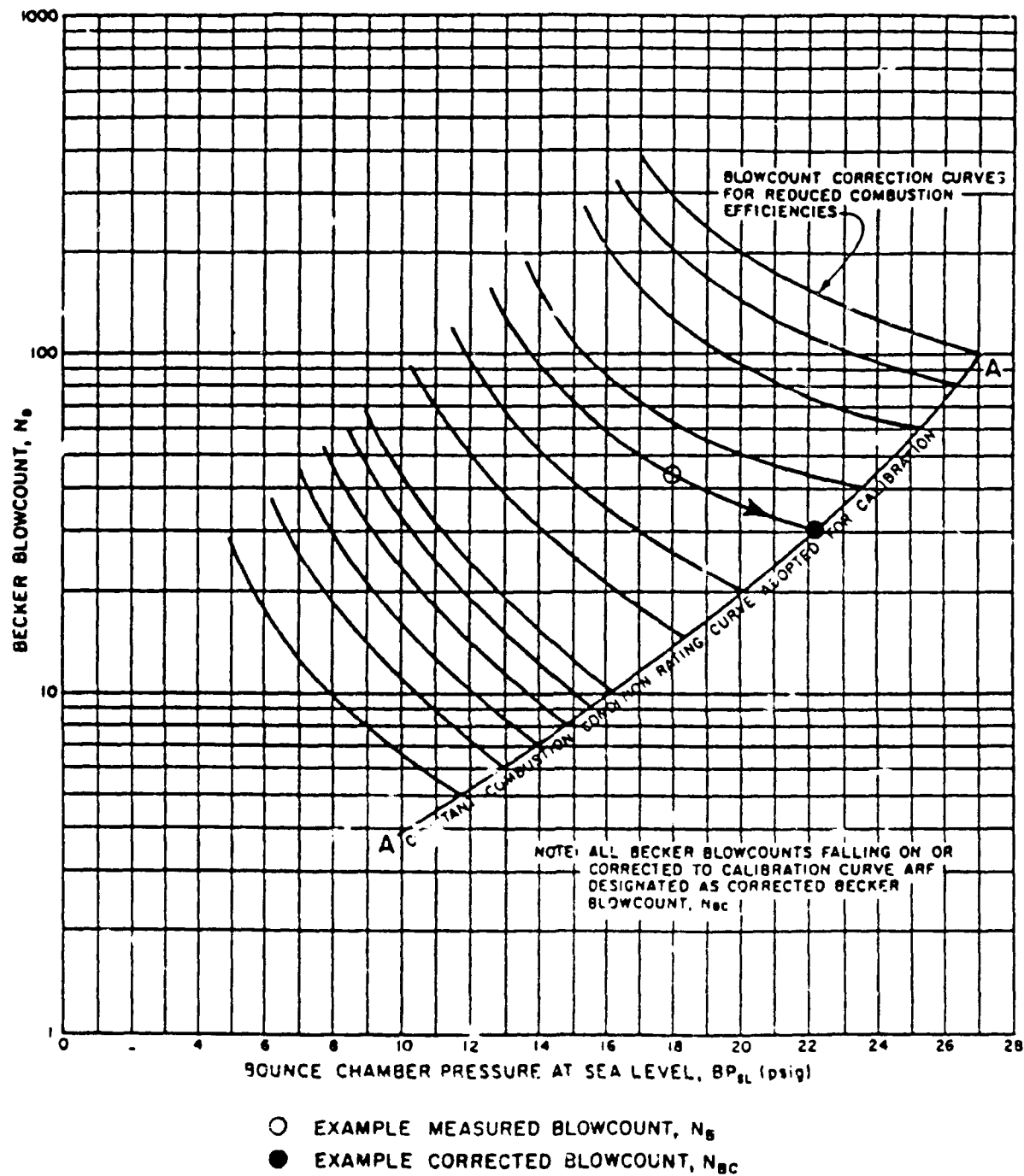


Figure A6. Correction curves adopted to correct Becker blowcounts to constant combustion curve adopted for calibration (after Harder and Seed, 1986)

rig. Both rigs employ the same model of diesel hammer, an ICE Model 180. The main difference between the two types of drill rigs is that the mast of the newer AP-1000 rig is more elaborate and the way the hammer is connected to the mast is more complicated. Based on the results of comparison tests by Harder and Seed (1986), it was observed that the older style B-180 rigs are more efficient (i.e. give lower blowcounts in the same material) than the newer AP-1000 drill rig. The apparent explanation is that the added cables on the AP-1000 rig restrict the ability of the hammer frame to follow the casing during driving. This apparently results in the cable support system absorbing some of the hammer energy. After correcting the measured Becker blowcounts to the standard combustion rating curve, corrected Becker blowcounts from an AP-1000 rig have been found to be roughly 50 percent higher than those from a B-180 drill rig (Figure A7).

Because of the effect of drill rig type, the Becker blowcounts obtained during the 1983 exploration program were increased by 50 percent after they were corrected for combustion effects. This was because the drill rig used in 1983 at Mormon Island was a B-180 type and the drill rig used to obtain most of the data in the Harder and Seed (1986) correlation between Becker blowcounts and SPT blowcounts generally employed an AP-1000 drill rig. It should be noted that at one of the the test sites used by Harder and Seed (1986) to develop their correlation, the San Diego Test Site, the Becker drill rig used was the exact same B-180 drill rig (Rig No. 11) that was used in 1983 at Mormon Island. In their correlation between corrected Becker blowcounts and SPT blowcounts, Harder and Seed (1986) also increased the Becker blowcounts for the San Diego Test Site by 50 percent after correcting for combustion effects.

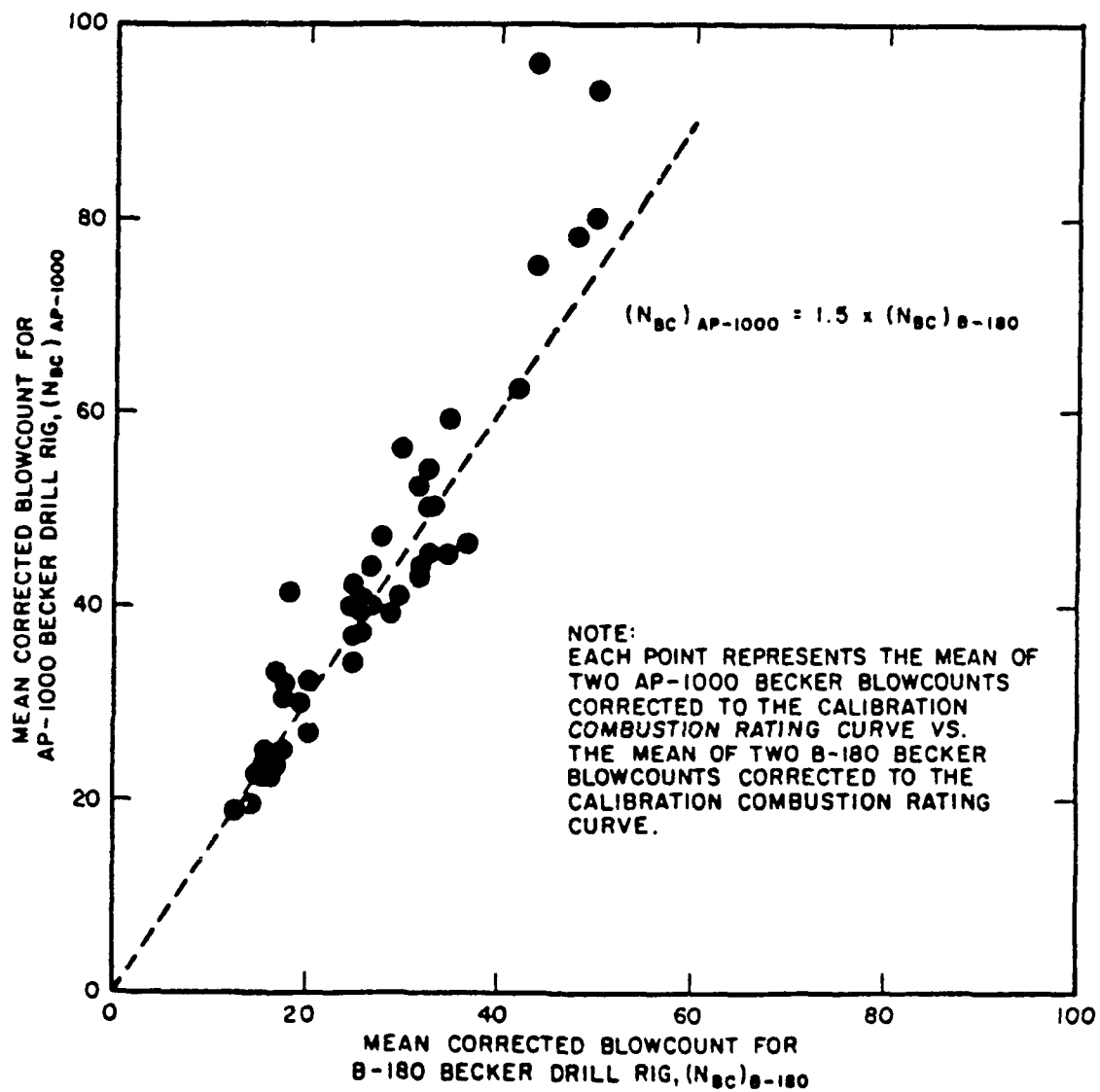


Figure A7. Effect of drill rig on corrected Becker blowcounts  
(after Harder and Seed, 1986)



### Conversion of Becker Blowcounts into Equivalent SPT Blowcounts

The correlation curve and the data used by Harder and Seed (1986) to generate the relationship between corrected Becker blowcounts and equivalent SPT blowcounts are presented in Figure A8. As detailed above, the corrections to measured Becker data that are required before using this correlation are as follows:

1. Correction of measured data for combustion effects.
2. Correction for drill rig type.

After these two corrections were made, all of the 1983 Mormon Island Becker data were converted into equivalent SPT blowcounts, denoted by the symbol  $N_{60}$ .

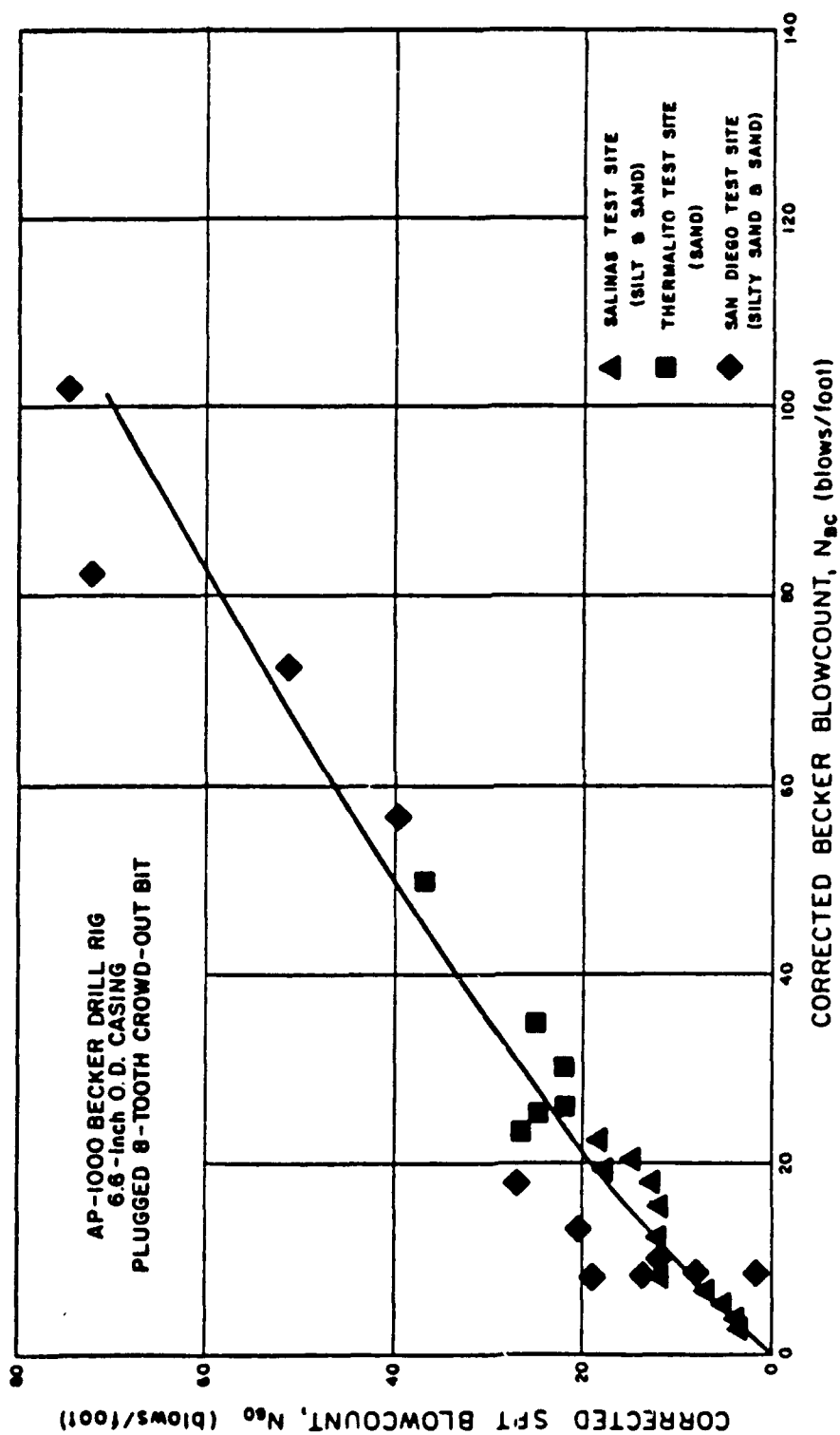


Figure A8. Correlation between corrected Becker and SPT blowcounts (after Harder and Seed, 1986)

### 3. ACCOUNTING FOR OVERBURDEN PRESSURE

#### Correction to 1 tsf Overburden Pressure

Penetration test results are affected by both soil properties and by the effective pressures confining the soil. Thus, a loose soil at great depth and confinement can have a high blowcount and a dense soil tested at shallow depth and small confinement can have a low blowcount. To account for the effect of confinement, penetration tests are usually normalized to the blowcount that would result if the soil was tested at a depth corresponding to 1 tsf of overburden pressure. This normalization is accomplished by multiplying a measured blowcount,  $N$ , by a correction factor,  $C_N$ , to obtain the normalized blowcount,  $N_1$  (Reference 5). Because the equivalent SPT blowcounts derived from Becker blowcounts using the correlation by Harder and Seed (1986) are in terms of  $N_{60}$  values (the SPT blowcount that would be obtained with a SPT hammer producing 60 percent of the free-fall energy of a 140-lb hammer falling 30 inches), the formula for normalizing to 1 tsf overburden pressure is as follows:

$$(N_1)_{60} = C_N * N_{60}$$

where  $(N_1)_{60}$  = Normalized and corrected SPT blowcount used with correlation by Seed et al. (1985) to predict cyclic strength.

$N_{60}$  = Corrected or equivalent SPT blowcount derived from Becker Penetration Tests

$C_N$  = Factor for correcting blowcounts to 1 tsf overburden pressure under level ground conditions

Studies have found that the  $C_N$  correction factor can vary as a function of both relative density and soil gradation. For overburden pressures greater than 1 tsf, the effect of the  $C_N$  correction is to reduce the blowcount. The studies by Marcuson and Bieganousky (1977a,b) indicate that as the soil becomes denser or the gradation becomes coarser, the magnitude of this reduction for higher overburden pressures decreases. In Figure A9 are two plots showing  $C_N$  overburden corrections indicated by Marcuson and Bieganousky's tests for three sands having a relative density of about 50 percent. The value of 50 percent was chosen because it was intermediate between values of 45 and 65 percent determined from density tests in the Mormon Island foundation and embankment shell material (Reference 2). As Figure A9 illustrates, the magnitude of the overburden correction for a particular stress level significantly decreases as the  $D_{50}$  of the sand increases from 0.2 to 2 mm.

According to gradation tests of recovered Becker samples, the average  $D_{50}$  of the foundation soils appeared to be about 2 mm, whereas the average  $D_{50}$  for the embankment shell soils was roughly 5 mm (Reference 8). However, gradations from density pit samples indicated  $D_{50}$  values for both materials that were generally between 20 and 40 mm (Reference 2). Although the density pits could only sample materials near the surface and, therefore, may not be able to obtain representative gradings, it should be noted that the 3.8-inch I.D. Becker bit may have scalped off some large particles. Accordingly, for the purposes of selecting an appropriate  $C_N$  curve, the overall  $D_{50}$  of the Mormon Island soils sampled has been assumed to be between 5 and 20 mm. However, the highest  $D_{50}$  of the three

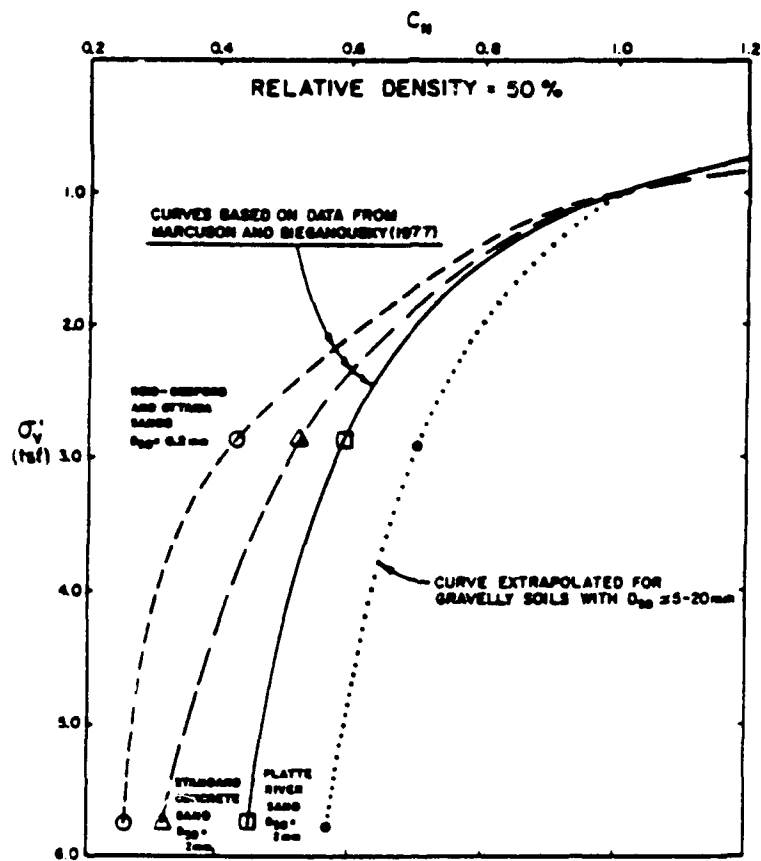
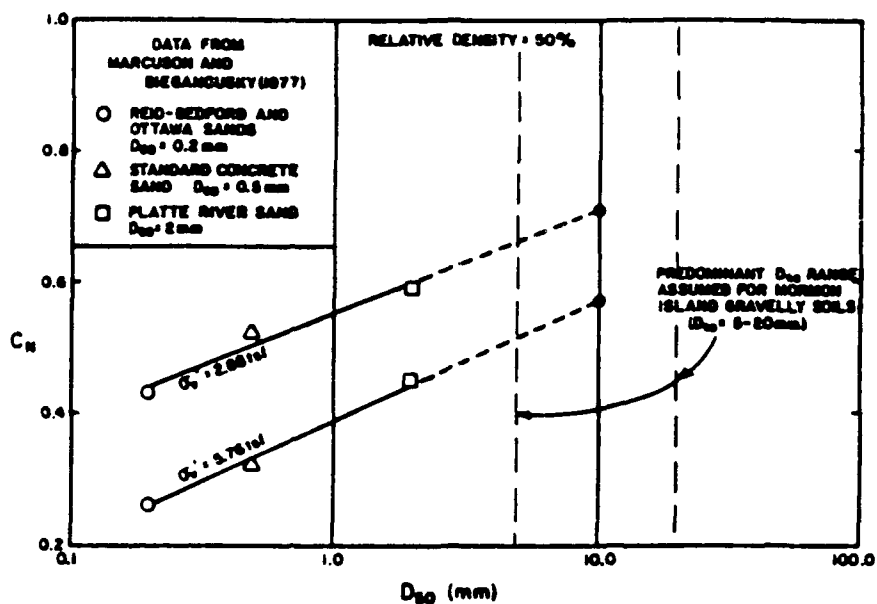


Figure A9. Relationship between  $C_N$  correction and overburden pressure

sands tested by Marcuson and Bieganousky is only 2 mm. Therefore, a new  $C_N$  curve was developed by extrapolating from the three curves based on test data. The extrapolation process is illustrated in the upper plot shown in Figure A9 and the resulting  $C_N$  curve is shown as a dotted line in the lower plot in Figure A9. This extrapolated curve was used for normalizing the equivalent SPT blowcounts obtained from the 1983 Mormon Island Becker data.

#### Effect of Sloping Ground Conditions on Overburden Correction Factor

The  $C_N$  overburden corrections shown in Figure A9 have been developed for level ground conditions. Level ground conditions for normally-consolidated materials usually have effective mean normal stresses that are approximately equal to 60 percent of the vertical effective overburden pressure. This is equivalent to having a coefficient of lateral earth pressure at rest,  $K_0$ , equal to 0.4. However, soils under sloping ground conditions often have higher lateral stresses due to the driving forces imparted by the weight of the slope material. This leads to mean normal stresses that may be equal to as much as 90 percent of the vertical overburden pressure. Several studies (e.g. Marcuson and Bieganousky, 1977a; Seed et al., 1975) have indicated that penetration resistance increases with increases in lateral confinement. Consequently, with increased mean confinement, a blowcount performed in soil under sloping ground conditions could be significantly greater than a blowcount conducted at the same vertical effective stress in the same soil under level ground conditions. Thus, the use of only the vertical overburden pressure with the curves in Figure A9 would lead to unconservative corrections for tests performed under sloping ground conditions.

Since the Becker tests performed at Mormon Island were located through or adjacent to sloping ground, it is necessary to account for higher mean confinement. The method adopted to correct the data was to use an equivalent level ground vertical effective pressure for use with the extrapolated  $C_N$  curve shown in Figure A9. This equivalent vertical effective pressure is set equal to 1.67 times the effective mean confinement at the depth where the penetration test was performed. In this way, the equivalent level ground vertical effective stress represents the overburden pressure that a soil element in level ground would have if that soil element had the same mean confinement that was present in sloping ground (i.e. the mean confinement is equal to 60 percent of the equivalent level ground vertical effective stress).

To determine the equivalent vertical stresses to be used with the adopted  $C_N$  curve, the results from non-linear static finite element analyses (Reference 10) were employed to calculate the mean confining pressures at the locations where Becker soundings were performed. Because the finite element stress analyses employed two-dimensional plane strain models, the mean confining pressure was calculated using the following formula:

$$\sigma'_m = ( \sigma'_y + \sigma'_x ) * ( 1. + \nu ) * 0.333$$

where  $\sigma'_m$  = mean effective confining pressure  
 $\sigma'_y$  = effective vertical pressure in 2-D plane  
 $\sigma'_x$  = effective horizontal pressure in 2-D plane  
 $\nu$  = Poisson's ratio - assumed equal to 0.3

The elements, stresses, equivalent level ground overburden pressures, and resulting  $C_N$  values are presented in Tables A2 and A3.

Table A2: Determination of Overburden Pressure Corrections for Soundings Performed through Downstream Face

Element	Depth (ft)	Vertical Stress (ksf)	Horizontal Stress (ksf)	Poisson's Ratio	Mean Stress (ksf)	Equiv. Level Ground Vertical Stress (ksf)	CN
331	10.7	1.865	2.134	0.3	1.733	2.888	0.88
309	24.9	3.731	2.592	0.3	2.740	4.567	0.76
275	38.7	6.928	3.375	0.3	4.465	7.441	0.65
242	50.6	6.603	3.198	0.3	4.247	7.079	0.65
203	60.5	7.258	3.443	0.3	4.637	7.729	0.64
156	70.5	8.003	3.912	0.3	5.163	8.605	0.62
116	80.5	8.906	4.365	0.3	5.751	9.585	0.60
74	90.6	9.395	4.683	0.3	6.100	10.167	0.59
32	101.7	10.276	5.236	0.3	6.722	11.203	0.57

Table A3: Determination of Overburden Pressure Corrections for Soundings Performed Beyond Downstream Toe

Element	Depth (ft)	Vertical Stress (ksf)	Horizontal Stress (ksf)	Poisson's Ratio	Mean Stress (ksf)	Equiv. Level Ground Vertical Stress (ksf)	CN
250	11.1	0.857	0.728	0.3	0.687	1.145	1.29
211	19.3	1.447	1.103	0.3	1.105	1.842	1.04
164	27.2	2.094	1.464	0.3	1.542	2.570	0.92
124	33.7	2.530	1.660	0.3	1.816	3.026	0.87
83	42.3	3.239	1.909	0.3	2.231	3.718	0.81
40	56.3	4.409	2.473	0.3	2.982	4.970	0.74

Notes: 1) Stresses presented in tables above are effective stresses.

2) Vertical and Horizontal stresses obtained from 2-D non-linear finite element analyses, Reference 8.



#### 4. PRESENTATION OF RESULTS AND DETERMINATION OF CYCLIC STRENGTH

##### Presentation of Results

Shown in Figures A10 through A14 are the uncorrected blowcounts obtained from the 1983 Becker Soundings performed at Mormon Island. Also shown are the equivalent SPT  $N_{60}$  blowcounts together with dashed lines representing different levels of blowcount normalized for overburden pressure. Figures A10 through A12 present results obtained in the downstream flat area. Figures A13 and A14 show results from the three soundings conducted through the downstream slope of the embankment. As already discussed in Section 2, there were three locations where an open-bit sounding was performed in close proximity to a plugged-bit sounding. At these three locations, the spacings between the two types of soundings was generally about 10 feet. The data in Figures A11 through A13 are arranged so that the blowcounts from the pairs of open-bit and plugged-bit soundings performed at the same locations can be compared.

One significant point that requires noting is that the correlation developed by Harder and Seed (1986) between Becker and SPT blowcounts is for use with plugged Becker bits having outside diameters of 6.6-inches. Of the thirteen soundings performed in 1983 at Mormon Island, only 3 soundings fit this description. The other ten soundings employed open bits with 7.3-inch outside diameters. The blowcount from a 6.6-inch O.D. open bit is believed to be about the same as that obtained from a 7.3-inch O.D. open bit. However, the blowcount from a plugged bit can be significantly higher than that from an open bit. This is because the air reverse-circulation used with open bits often

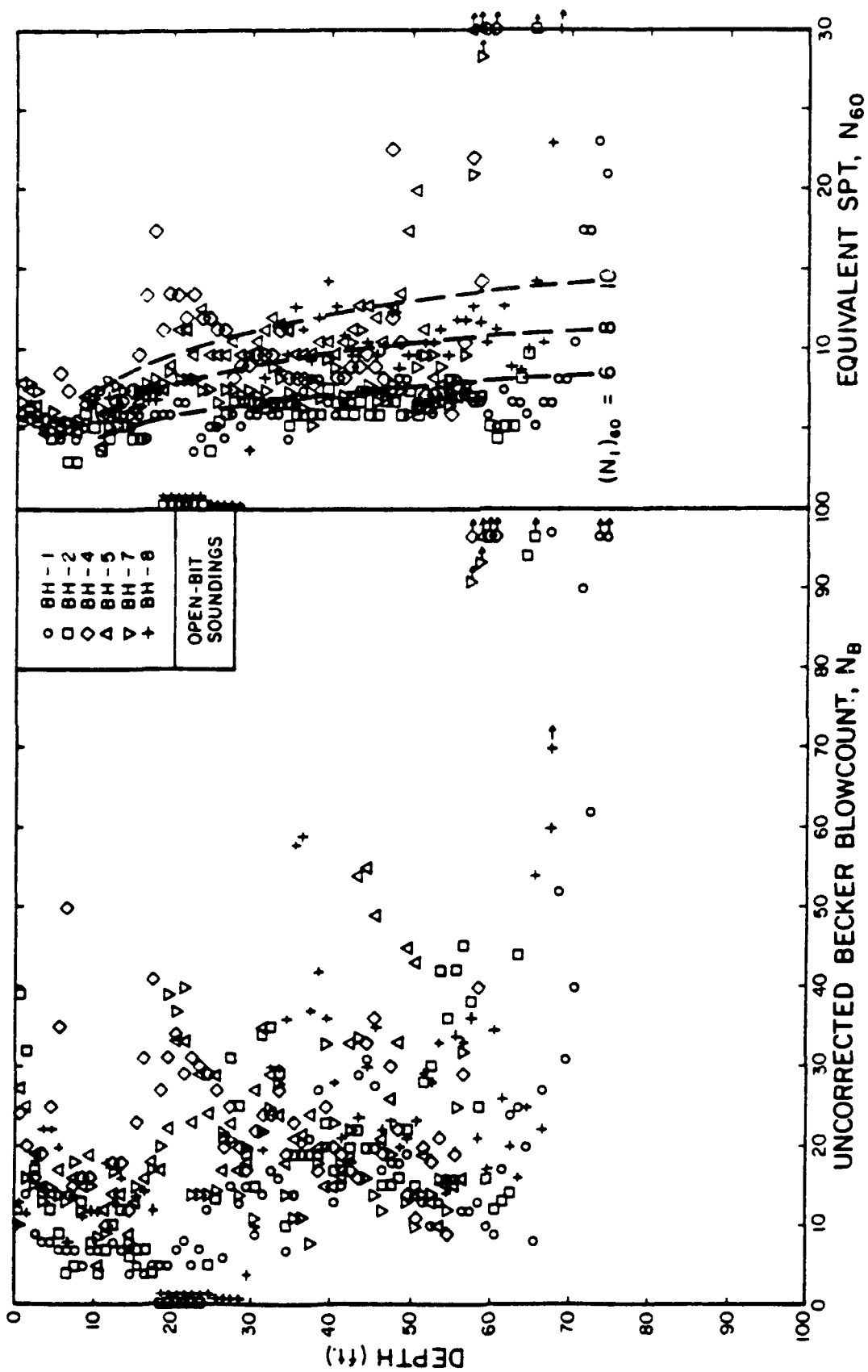


Figure A10. Uncorrected Becker and equivalent SPT blowcounts for soundings BH-1, 2, 4, 5, 7, and 8 (performed in the downstream flat area)

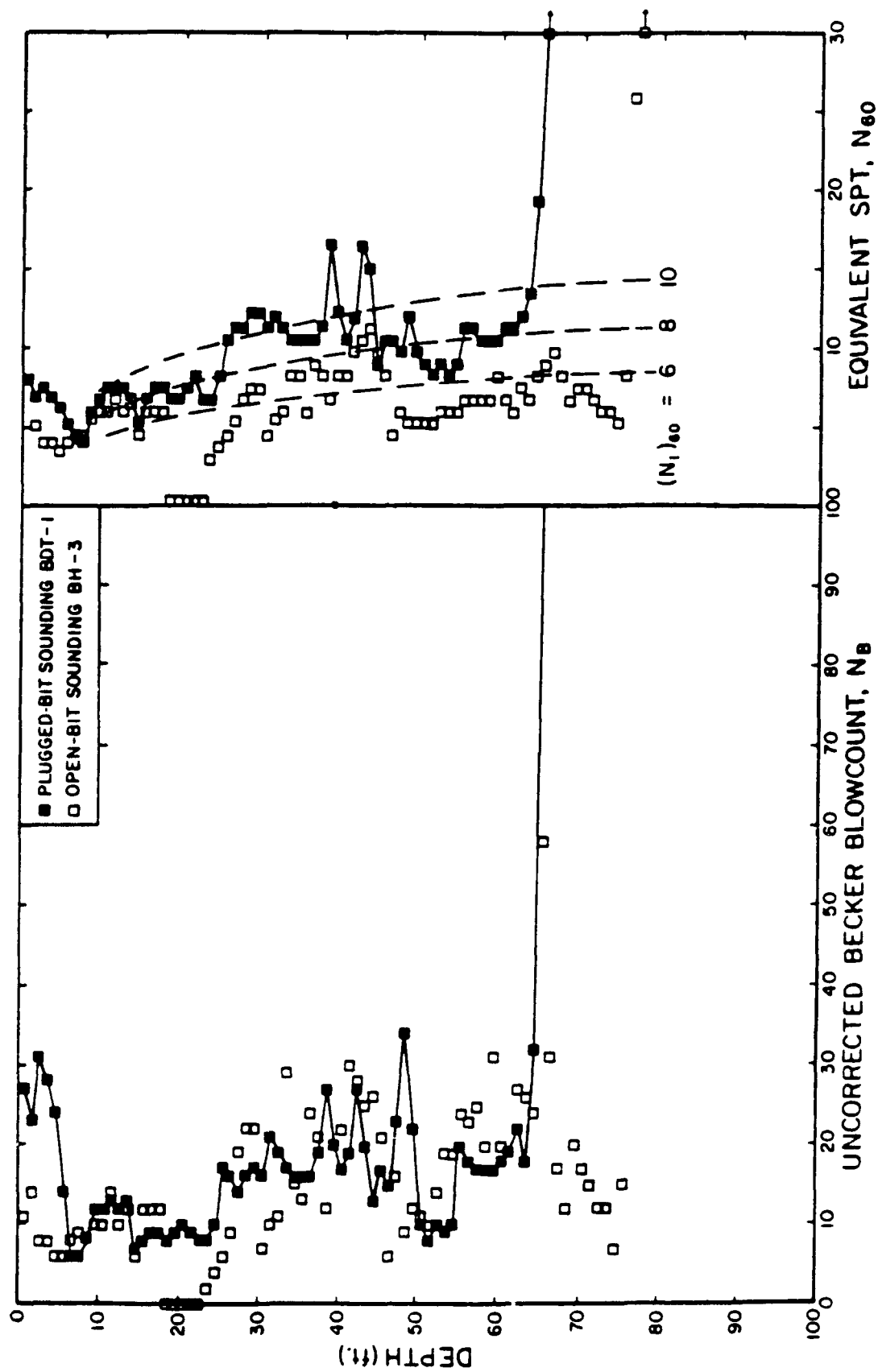


Figure A11. Uncorrected Becker and equivalent SPT blowcounts for soundings BH-3 and BDT-1  
(performed in the downstream flat area)

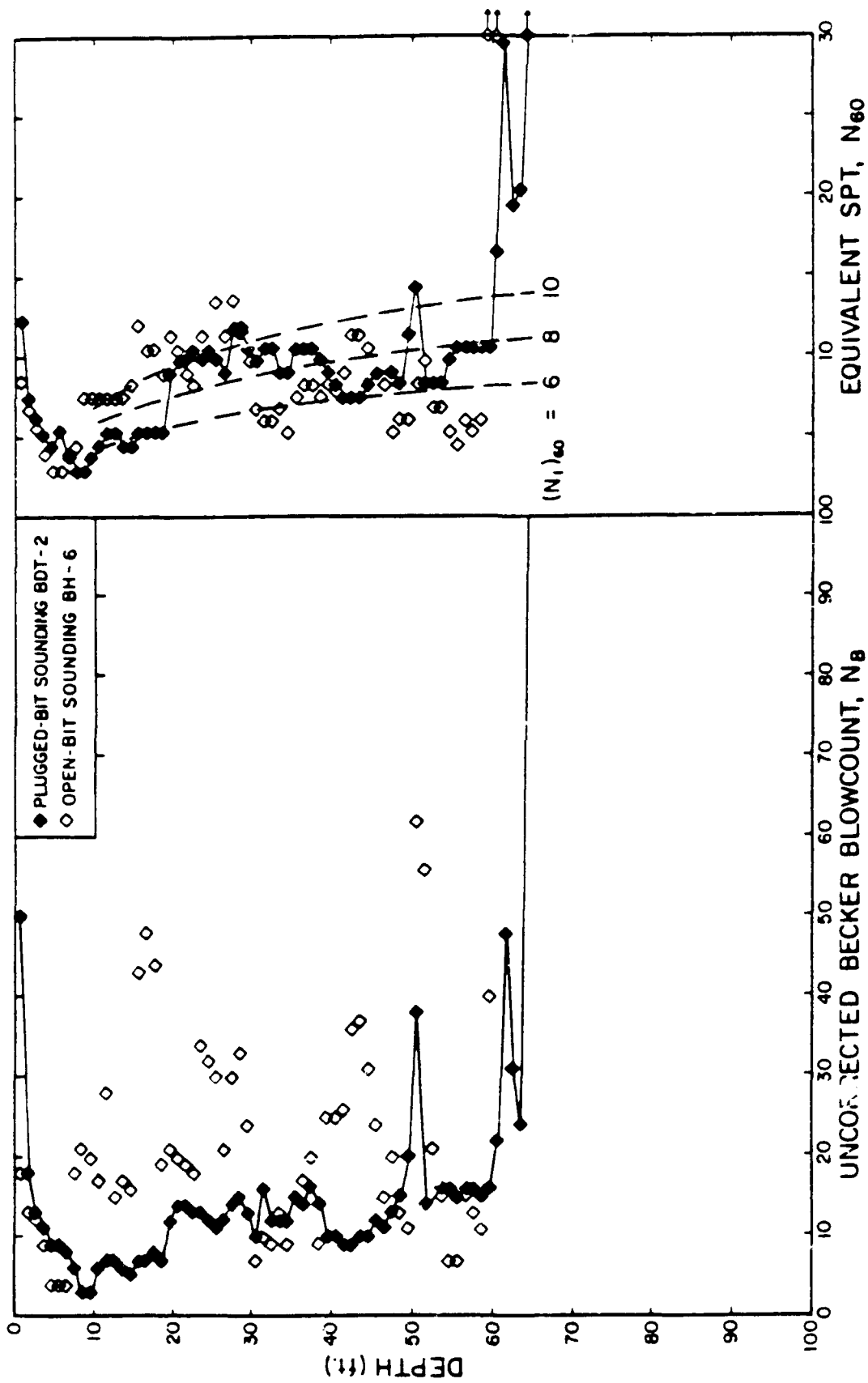


Figure A12. Uncorrected Becker and equivalent SPT blowcounts for soundings BH-6 and BDT-2 (performed in the downstream flat area)

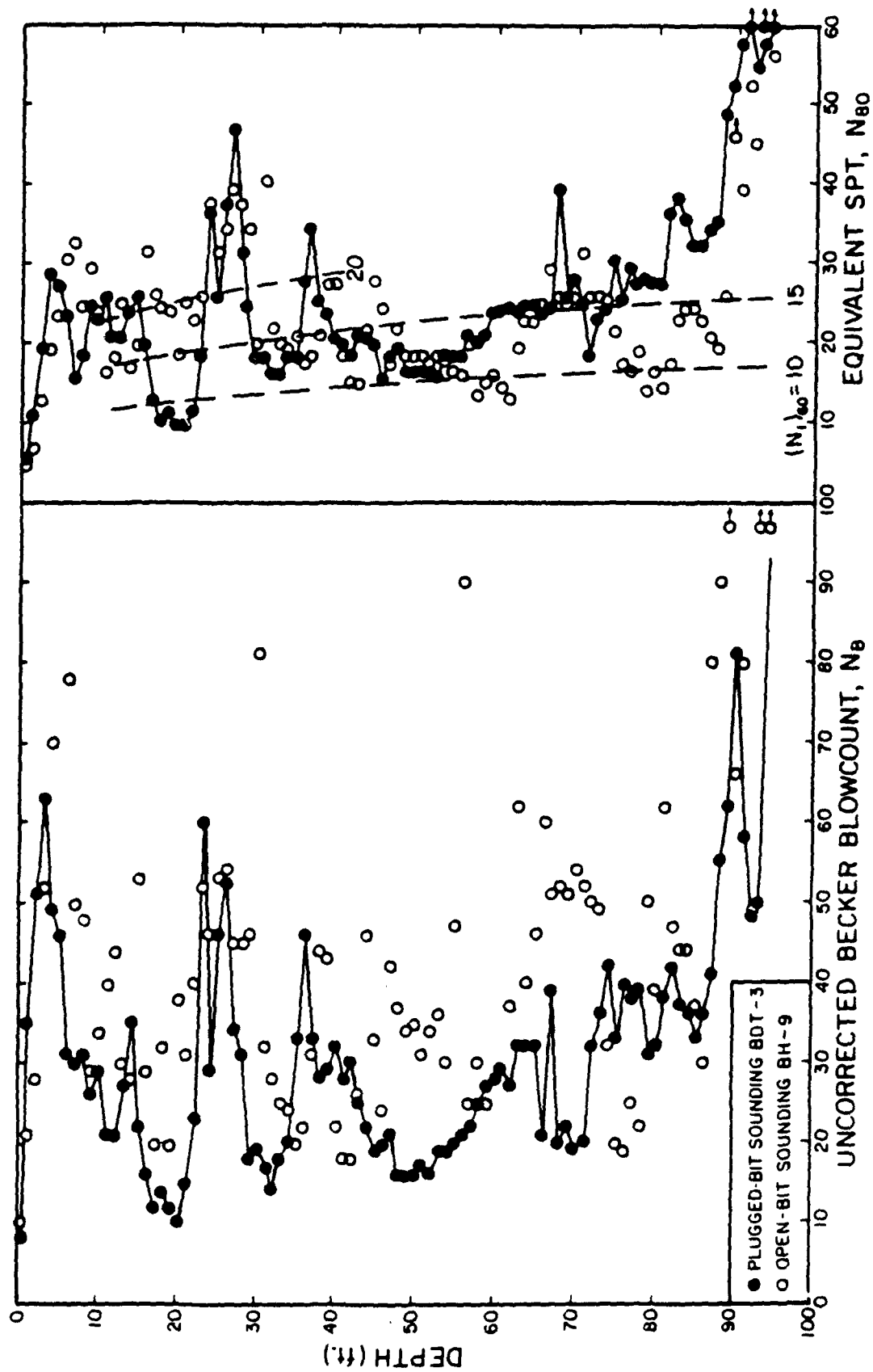


Figure A13. Uncorrected Becker and equivalent SPT blowcounts for soundings BH-9 and BDT-3 (performed through downstream slope)

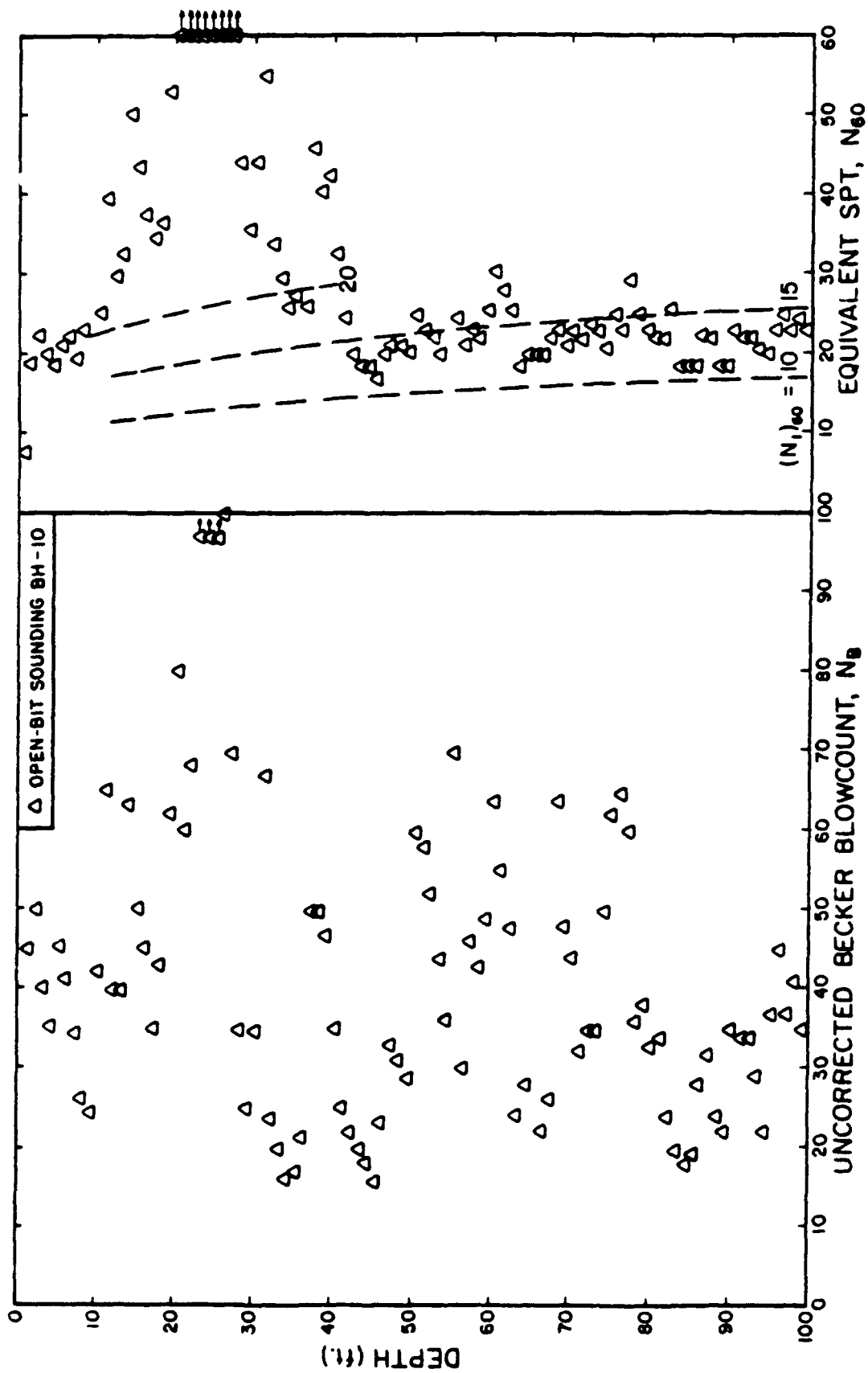


Figure A14. Uncorrected Becker and equivalent SPT blowcounts for sounding BH-10  
(performed through downstream slope)

draws up excessive amounts of soil and water from ahead of the bit and into the casing. When this happens, the loosening and removal of material ahead of the bit leads to a relatively low blowcount. Although this effect appears to be most significant in saturated sands, it is sometimes important in gravelly soils as well.

Instances of open-bit soundings giving misleadingly low values appear to have occurred in the data from the foundation material at Mormon Island. In general, the results show that the open-bit BH soundings gave comparable but somewhat lower equivalent SPT blowcounts than did the plugged-bit BDT soundings (Figures A11 through A13). In some cases, the open-bit BH soundings actually gave zero blowcounts. However, the plugged-bit soundings performed in the same material at the same depth always had at least some resistance. Because of the heave problem apparently present in limited degree for the Mormon Island open-bit soundings, the equivalent blowcounts from plugged-bit soundings are considered more reliable indicators of cyclic strength. Accordingly, it is judged that the blowcounts from open-bit soundings should be used only as estimates of the lower bound of cyclic strength (i.e. the strength could actually be higher than what the open-bit blowcounts indicate).

Figures A11 and A12 indicate that the equivalent normalized SPT blowcount,  $(N_1)_{60}$ , obtained from plugged-bit Becker soundings in the gravelly foundation in the downstream flat area is generally between 6 to 10 blows per foot. Since the open-bit soundings in Figures A10 through A12 show comparable or lower blowcounts for tests in the flat, the 6 to 10 blowcount range is judged appropriate for the foundation soils in this area.

Figures A13 and A14 show the results from the three soundings through the downstream face. At this location, the contact between the gravel shell and the gravelly foundation is roughly at a 37-foot depth. The results from both the open and plugged-bit soundings in Figures A13 and A14 show that the equivalent  $(N_1)_{60}$  blowcounts in the shell material (above 37 feet in this figure) have a significant scatter, but average out somewhere between 20 to 25 blows per foot. The equivalent  $(N_1)_{60}$  blowcounts obtained from both open and plugged-bit soundings in the foundation material beneath the slope (below 37 feet in Figures A13 and A14) have much less scatter and range generally between 10 and 15 blows per foot. This latter range indicates that the gravelly foundation is significantly stronger beneath the embankment slope than it is beyond the downstream toe (i.e. equivalent SPT blowcounts of 10-15 versus 6-10). The only immediate, obvious reasons why this might be so are that construction activities and/or the weight of the embankment possibly densified the material to some degree, or that the effect of the stresses in the foundation beneath the slope add an additional effect that is not adequately accounted for with our present knowledge. It should also be noted that the quantity of data is relatively small to draw large conclusions.

#### Effect of Fines Content

After obtaining the equivalent  $(N_1)_{60}$  values, cyclic strength is determined using the correlation by Seed et al. (1985) between SPT blowcount and cyclic strength. This correlation is presented in Figure A15 and gives the cyclic strength in terms of an average cyclic stress ratio,  $(\tau_a / \sigma'_o)$ . In this figure, three different curves are available for determining cyclic strength. The proper curve is



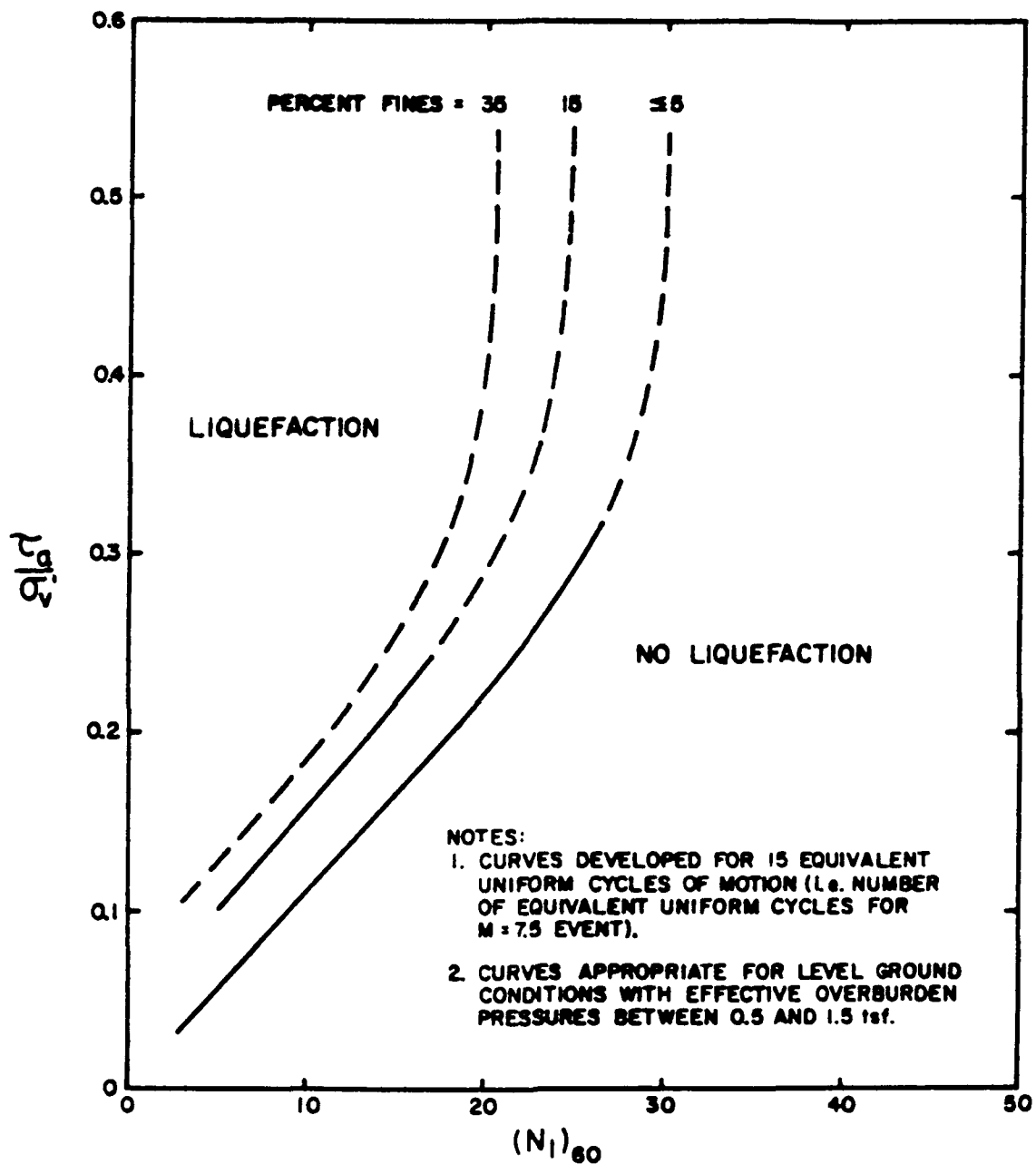


Figure A15. Relationship between corrected SPT blowcount and average cyclic stress ratio causing liquefaction for M = 7.5 earthquakes (after Seed et al., 1985)

selected by determining how high a fines content (i.e. percent finer than the No. 200 sieve size) is present in the soil. For the same blowcount, an increase in fines content also increases the cyclic strength. Shown in Figure A16 are the results of classification tests conducted for foundation samples recovered from the open-bit soundings performed in the downstream flat area (Reference 8). For most of the tests, the fines content appears to range generally between 5 and 15 percent with an overall average of roughly 10 percent. There were also two test pits excavated into the foundation to depths of approximately 8 feet. The soil samples obtained from one test pit had fines contents ranging from 1 to 6 percent with an approximate average of 3 percent. The average fines content from the second test pit was found to be about 7 percent (Reference 2).

Figure A16 also shows that the results from a limited number of Atterberg limit tests indicate that the fines from some of the Becker samples are predominantly clayey. Although some clayey soils may undergo significant straining during cyclic loading, unless certain conditions such as very high water content, clay content below 15 percent, and low plasticity characteristics are present, such soils are often regarded as being non-liquefiable (Reference 5). For the foundation below Mormon Island Auxiliary Dam, however, only below approximately the 50-foot depth does the amount of fines apparently increase to a level where the soil might begin to meet the conditions required for being considered non-liquefiable. Furthermore, many of the samples which were not given Atterberg limit tests were field-classified as having predominantly silt fines (Reference 8). Consequently, the foundation soils above the 50-foot depth should be

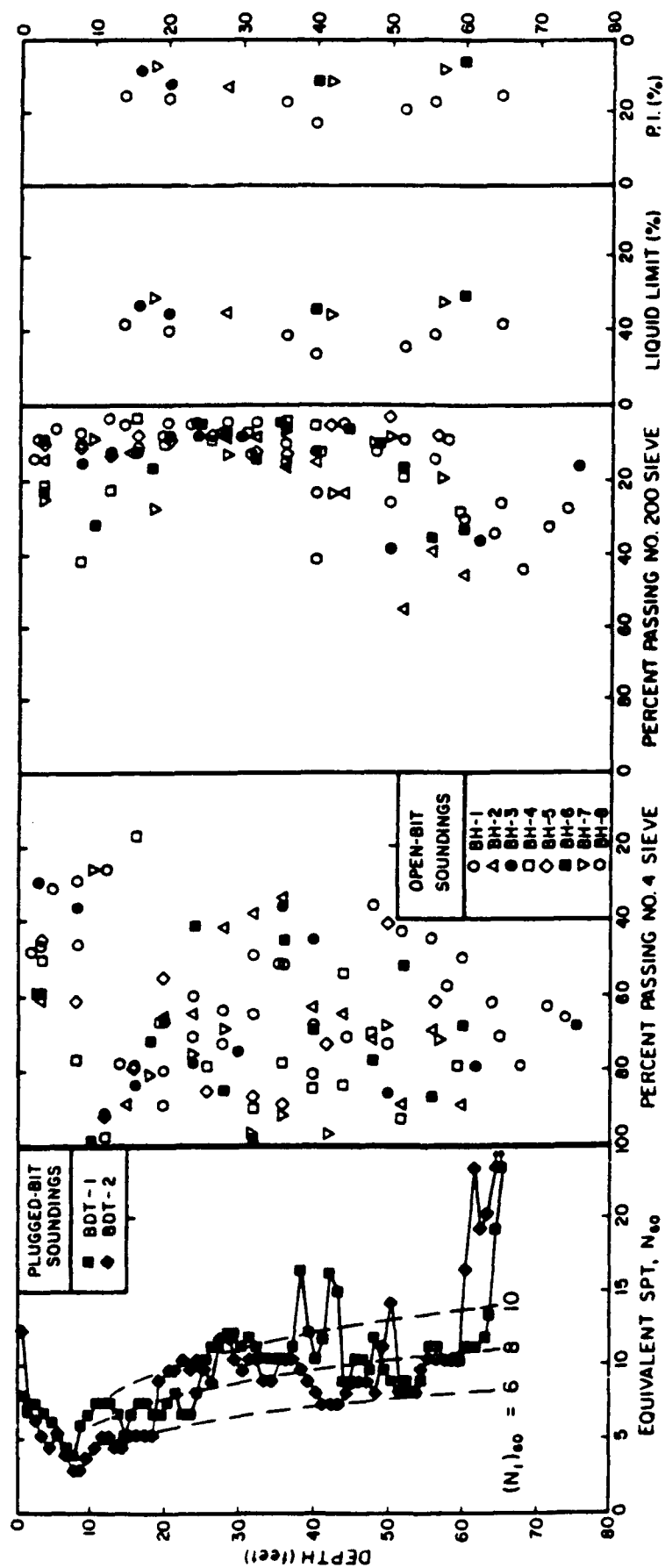


Figure A16. Equivalent SPT blowcounts and classification test data from soundings performed in the downstream flat area

considered liquefiable. For the finer soils that apparently lie below 50 feet, there is insufficient information to determine if they meet the requirements for being considered non-liquefiable. However, the conservative approach would be to assume that the deeper foundation soils are indeed liquefiable.

For the embankment shell, samples from the Becker soundings performed in the downstream slope had an approximate average fines content of 15 percent (Reference 8). However, samples were also obtained from a density test pit that extended 15 feet down into the embankment shell. These samples had fines contents ranging from 3 to 7 percent with an approximate average of 5 percent (Reference 2).

For both the embankment shell and the foundation soils, there remains a discrepancy between the fines content determined from shallow test pits and those obtained from the recovered Becker samples. As discussed in Section 3, there are limitations to the applicability of both sets of gradation data. The test pit samples were obtained only at relatively shallow depths and, therefore, are not necessarily representative of the whole depth profile. However, the 3.8-inch I.D. Becker bit may have scalped off larger particles and, thus, may have yielded a higher fines content than what actually exists in the ground. Consequently, for the purposes of this study, the results from both sets of data were roughly averaged to obtain a value of 10 percent for the fines content in both the embankment shell and foundation soils.

#### Determination of Cyclic Strength

Figure A15 presented correlations between corrected SPT blowcount, fines content, and cyclic stress ratio. This cyclic stress ratio is a normalized cyclic strength that is consistent with about 15 equivalent

uniform cycles of shaking (assuming an average amplitude equal to 65 percent of the peak motion). Fifteen equivalent uniform cycles is the number that would be produced by a magnitude 7.5 earthquake. However, the critical earthquake for the Mormon Island Auxiliary Dam has only a 6.5 Richter magnitude (Reference 2). A 6.5 magnitude earthquake has only about 8 equivalent uniform cycles of motion (Reference 5). Therefore, for the same peak amplitude, a 6.5 magnitude earthquake is less severe than a 7.5 magnitude earthquake. This means that the curves shown in Figure A15 will underpredict the appropriate average cyclic stress ratio for a postulated 6.5 magnitude earthquake. To correct for the lower magnitude, Seed et al. (1983) recommend increasing the cyclic stress ratio by approximately 20 percent. Accordingly, this correction was used to obtain the average cyclic stress ratio appropriate for the postulated Mormon Island 6.5 magnitude earthquake.

Shown in Table A4 are the equivalent SPT  $(N_1)_{60}$  values, fines contents, and cyclic stress ratios determined for the gravelly soils tested at Mormon Island.

Table A4: Summary of Mormon Island Cyclic Strengths

SOIL	$(N_1)_{60}$ (blows/foot)	FINES CONTENT (%)	CYCLIC STRESS RATIO	
			$(\tau_a / \sigma_o')$ <sub>M=7.5</sub>	$(\tau_a / \sigma_o')$ <sub>M=6.5</sub>
Foundation				
(D/S Flat)	6 - 10	10	0.085 - 0.13	0.10 - 0.16
(D/S Slope)	10 - 15	10	0.13 - 0.19	0.16 - 0.23
Embankment Shell				
(D/S Slope	20 - 25	10	0.25 - 0.35	0.30 - 0.42

It should be noted that the cyclic stress ratio represents the normalized strength for the following stress conditions:

1. Level ground conditions with a lateral earth pressure at rest coefficient,  $K_0$ , equal to about 0.4.
2. Overburden pressures between 0.5 and 1.5 tsf.

For stress conditions other than those above, corrections are available to modify the cyclic stress ratio. However, it should also be noted that one of the corrections for cyclic strength often used to increase strength for the presence of a static shear stress on the horizontal plane,  $K_{\alpha}$ , may not be appropriate for the loose foundation soil (corrected blowcounts less than 10) found in the downstream flat area. This is because studies by Vaid and Chern (1983) and others have found that the cyclic strength of very loose soil does not appear to increase with the presence of this static shear stress.

## 5. SUMMARY OF FINDINGS

1. The open-bit Becker soundings generally gave a somewhat lower range of blowcounts in the foundation soil after correction than did the plugged-bit Becker soundings. For the one pair of soundings performed within the embankment shell, the two types of bits gave about the same blowcount after correction. Because of the heave problem associated with open-bit soundings, the equivalent SPT blowcounts obtained from open-bit soundings should only be used to obtain a lower bound estimate of strength. In addition, the presence of this heave problem means that the occasional zero blowcounts produced by some open-bit soundings within the foundation soils should be discounted.
2. The equivalent SPT ( $N_1$ )<sub>60</sub> blowcounts for the gravelly soils in the foundation and embankment shell were found to be as follows:  

Foundation (D/S Flat):	6 - 10	blows/foot
Foundation (D/S Slope):	10 - 15	blows/foot
Emb. Shell (D/S Slope):	20 - 25	blows/foot
3. The cyclic strengths of the soils, expressed as an average cyclic stress ratio for a Richter magnitude 6.5 earthquake, were estimated (using an assumed average fines content of 10 percent) to be as follows:  

Foundation (D/S Flat):	0.10 - 0.16
Foundation (D/S Slope):	0.16 - 0.23
Emb. Shell (D/S Slope):	0.30 - 0.42

4. The very low blowcounts and strengths determined for the foundation soils in the downstream flat area may preclude increasing the cyclic strength of this material to account for static shear stresses present on the horizontal plane.
5. Although there are limited data, there appears to be a higher fines content, with more clayey fines, in roughly the bottom 10 to 15 feet of the foundation. With more fines, especially clayey fines, the actual cyclic strength of this deeper material may be much higher than that estimated above for the foundation soils.



## 6. REFERENCES

1. Harder, Jr., Leslie F. and Seed, H. Bolton (1986), "Determination of Penetration Resistance for Coarse-Grained Soils Using the Becker Penetration Test," University of California, Berkeley, EERC Report No. UCB/EERC-86-06, May, 1986.
2. Hynes-Griffin, Mary Ellen, (1986), Geotechnical Laboratory, Waterways Experiment Station, U.S. Army Corps of Engineers, personal communication.
3. Marcuson, W. F., III and Bieganousky, W. A. (1977a), "Laboratory Standard Penetration Tests on Fine Sands," Journal of the Geotechnical Engineering Division, American Society of Civil Engineers, Vol 103, No. GT6, June, 1977.
4. Marcuson, W. F., III and Bieganousky, W. A. (1977b), "SPT and Relative Density in Coarse Sands," Journal of the Geotechnical Engineering Division, American Society of Civil Engineers, Vol 103, No. GT11, November, 1977.
5. Seed, H. Bolton, Idriss, I. M. and Arango, Ignacio (1983), "Evaluation of Liquefaction Potential Using Field Performance Data," Journal of the Geotechnical Engineering Division, ASCE, Vol. 109, No. 3, March, 1983.
6. Seed, H. Bolton, Mori, Kenji, and Chan, Clarence K. (1975), "Influence of Seismic History on the Liquefaction Characteristics of Sands," University of California, Berkeley, Report No. EERC 75-5, August, 1975.
7. Seed, H. Bolton, Tokimatsu, K., Harder, L.F., and Chung, Riley M. (1984), "Influence of SPT Procedures in Soil Liquefaction Resistance Evaluations," Journal of the Geotechnical Engineering Division, ASCE, Vol. 111, No. 12, December, 1985.
8. U.S. Army Corps of Engineers, Sacramento District (1984), "Preliminary Evaluation of Liquefaction Potential at Mormon Island Auxiliary Dam", Draft Report.
9. Vaid, Y. P. and Chern, J. C. (1983), "Effect of Static Shear Stress on Resistance to Liquefaction," Soils and Foundations, Vol. 23(1).
10. Wahl, Ron (1986), Results of Finite Element Static Stress Analysis (Program FEADAM) of Mormon Island Auxiliary Dam, Geotechnical Laboratory, Waterways Experiment Station, U.S. Army Corps of Engineers, personal communication, 1986.

APPENDIX B: LABORATORY TESTS ON GRAVEL SPECIMENS

## APPENDIX B: LABORATORY TESTS ON GRAVEL SPECIMENS

### General

1. A laboratory testing program on compacted gravel specimens was performed to provide effective stress strength parameters and relative cyclic strength behavior of the gravels in the shell and foundation of Mormon Island Auxiliary Dam. This appendix contains descriptions of the testing equipment, specimen preparation, and testing procedures. The individual test results are then presented in graphical form.

### Testing Equipment

2. A photo of the large-scale triaxial testing station used in the investigation is given in Figure B1 and a schematic diagram of the pressure control and measurement system is shown in Figure B2. All pressures were controlled by pneumatic pressure regulators. Detailed descriptions of the testing equipment are given in the following paragraphs.

3. The cast-aluminum split mold shown in Figure B3 was used to form specimens. The mold was attached to the specimen base platen with bolts. The inner surface of the mold was formed by a 0.025-in.-thick latex membrane held in place against the mold sides by a vacuum acting through an underlying thin porous plastic liner. The membrane was sealed to the base platen with an O-ring. Nominal specimen dimensions were 15-in. diam by 38.5-in. height.

4. The top and base platens were made of steel and contained 3-in.-diam porous stone inserts located over holes to ports where 3/8-in.-ID nylon drainage tubes were connected.

5. Specimens were encased in at least two membranes. The inner membrane was the 0.025-in.-thick membrane forming the inner surface of the mold and the outer membrane was usually a 0.050-in.-thick latex membrane placed over the specimen after the specimen was positioned and secured on the actuator piston and the mold was removed. Additional 0.050-in.-thick membranes were placed over the specimen for tests at the higher confining pressures or when an inspection of the specimen periphery indicated the possibility of gravel particles puncturing the membranes at lower confining pressures. Inner

membranes were purposely punctured in several places with an ice pick to ensure air was not trapped between the membranes.

6. The triaxial chamber is shown in Figure B4. The chamber was designed for a working pressure of 500 psi and was sealed at the top and bottom with 3/8-in.-diam O-rings placed in compression using the weight of the chamber and eighteen 1-in.-diam bolts. The actuator piston, upon which the specimen base platen was secured, passed through the bottom of the chamber and extended into a pit below floor level. A shaft, rigidly attached to an annular load cell mounted on the specimen cap, was used to transfer applied axial forces from the specimen to the top of the chamber, thereby allowing the chamber to serve as a reaction frame. The shaft passed through a hole in the top of the chamber and was secured with a large nut to permit application of forces to place specimens in extension during cyclic loading. The hole was sealed by an O-ring between a shoulder on the shaft and the bottom surface of the chamber top.

7. The actuator piston for applying axial forces was controlled by an electro-hydraulic closed-loop system (MTS Systems, Inc.) and had a 270-kip capacity. The MTS system has options for two modes to apply axial force to specimens, a controlled load mode and a controlled stroke mode. In both modes, two commands are available, one from a manually adjusted set point and the other from a manually adjusted span setting. In the controlled load mode, the actuator piston moves until the output from the load cell equals the command from both the set point and span setting. For example, in a controlled cyclic stress test, the set point is used to apply the axial force about which the force cycles and the span control is used to control the amplitude of the cyclic force.

8. In the controlled stroke mode, the actuator piston moves until the output from the actuator linear variable differential transformers (LVDT) matches the set point and span setting. In the case of a controlled cyclic strain test, the set point is used to control the piston position about which the piston movement cycles and the span control is used to control the amplitude of the cyclic movement. Axial deformations were measured by LVDT's attached to the actuator piston or, in the case of the controlled cyclic strain tests, attached to vertical rods mounted inside the chamber on the specimen base platen so movement of the top platen relative to the base platen

could be measured. A photo of the internal axial deformation system is shown in Figure B5.

9. Induced pore water pressures were measured at the bottom of the specimen with an electronic differential pressure transducer which sensed the difference between the back pressure required for saturation and the total pore water pressure in the specimen. Chamber pressures were measured at the base of the chamber using an electronic pressure transducer.

10. The volume of water entering or leaving the specimen during saturation and consolidation phases of the tests was determined by measuring the change in water level in 3-in.-diam aluminum tubes serving as burettes and connected to the specimen by high pressure hoses. The changes in water level in the tubes were measured with high-sensitivity electronic differential pressure transducers which detected the difference between the pneumatic pressure (back pressure) acting on the water in the tubes and the total pressure at the bottom of the tubes.

11. The outputs of the electronic sensors were monitored by digital voltmeters and recorded by analog recorders (Hewlett-Packard Model 79046A X-Y-Y recorder and Model 7700, stylus heat, 8-channel strip chart recorder). The electronic sensors were selected on the basis of their calibrated accuracy and range such that measured values of stress, strain, and pressures were accurate to the decimal places given. The data acquisition equipment and MTS System controls for the testing are shown in Figure B6.

#### Specimen Preparation

12. Specimens were compacted in six equal weight layers using sufficient impact effort to achieve the desired density. Overcompaction of the lower layers of the specimens was avoided by deliberately undercompacting lower layers and allowing effort applied to succeeding layers to bring the lower layers to the target density as the specimen preparation was completed. The degree of initial undercompaction was greatest for the first or lowermost layer and was decreased with each succeeding layer.

13. Each layer was batched separately to prevent any variation in gradation among layers. To decrease the tendency for migration of the finer material to the bottom of the specimen during compaction, layer batches were prepared by thoroughly mixing the required minus No. 4 sieve material with

sufficient water to bring the mixture to approximately its bulk water content and then allowing the material to cure for at least 16 hr. The plus No. 4 sieve material (gravel) for each batch was prepared by combining the air-dry portion (by weight) of gravel required for each sieve size. Immediately prior to compaction, the minus No. 4 fraction was thoroughly mixed with the plus No. 4 material.

14. Figures B7 through B10 are photos taken during compaction of a specimen. The material for each layer was placed in the mold (Figure B7) and tamped to the desired height using the hand-held rammer shown in Figure B8. The distance from the top of the mold to the soil surface was periodically measured at several points to determine when the layer was compacted to the desired height (Figure B9). The surface of each completed layer, except the top layer, was scarified before compaction of the subsequent layer. After tamping the top layer of the specimen to within about 1/4 in. above the top of the mold, the specimen top platen was placed on the soil and struck vertically with the end surface of a heavy steel bar to bring the soil layer flush with the top of the mold (Figure B10). This provided a good seat between the platen and specimen, a requirement for the controlled cyclic strain tests. A bubble level was used during the procedure to assure that the soil surface remained horizontal.

15. Following compaction, the latex membrane lining the mold was pulled up over the top platen and secured with an O-ring. Next, the mold and specimen were placed on the actuator piston at the base of the triaxial chamber and a vacuum was applied to the specimen through the 3/8-in. drainage tube to the bottom platen. After puncturing the inner membranes with an ice pick (this did not relieve the vacuum in the specimen significantly), the outer membrane(s) was placed over the specimen and secured with O-rings.

#### Specimen Dimension Measurements

16. Specimen dimensions were determined while the specimens were under vacuum. Specimen height was taken as the average of four measurements at 90-deg intervals around the circumference of the specimen with a metal scale reading to 0.01 in. Diameter measurements were taken at the top, middle, and bottom quarter points of the specimen using a "PI" tape reading to the nearest 0.001 in. A "PI" tape is a thin and narrow flexible metal scale graduated and

verniered so that the diameter may be read when the tape is drawn around the circumference of the specimen. The diameter of the specimen was taken as the weighted average of the sum of the top reading, twice the center reading, and the bottom reading. A value of twice the thickness of the membrane(s) was subtracted from each reading before computing the weighted average.

17. After the specimen initial dimensions were determined, the triaxial chamber was assembled and the piston actuator was raised with the MTS controller in the controlled load mode until the shaft attached to the specimen top platen contacted the chamber top. The shaft was then secured to the chamber top with a large nut and an initial piston LVDT reading was taken. The MTS controller remained in the controlled load mode during saturation and consolidation so that the axial force could be adjusted to maintain desired stress conditions. Subsequent actuator piston LVDT readings were used to determine the change in height of the specimen during saturation and consolidation. After the initial LVDT readings were obtained, the chamber was filled with tap water to within approximately 12-in. of the top of the chamber. The resulting air pocket was formed to allow subsequent movement of the actuator piston into or out of the chamber could occur without affecting the chamber pressure. The presence of the air pocket did not produce problems with air passing from the chamber fluid through the membranes and into the specimen pore water because of the relatively thick membranes and short times of testing.

#### Saturation

18. Saturation of the specimens was initiated while a full vacuum remained applied to the top of the specimen by allowing deaired water (produced by a Nold deaerator) to percolate slowly from the bottom to the top of the specimen under a differential vacuum head. During this procedure, the vacuum acting on the bottom of the specimen was regulated so that the differential vacuum between top and bottom of the specimen never exceeded 5.0 psi. When water appeared in the tube through which a high vacuum was being maintained at the top of the specimen, valves to the top and bottom of the specimen were closed and the tube to the top of the specimen still under full vacuum was filled with deaired water. The valve to the top of the specimen was then opened and the vacuum acting on the tube was slowly decreased with a simultaneous equivalent increase in chamber pressure.

19. Accurate control of the chamber pressure during this and subsequent stages of the test was made possible by including a pneumatic volume booster relay in the line to the top of the specimen. When the vacuum had been decreased to zero, i.e., atmospheric pressure (and the chamber pressure increased to approximately 14 psi), back-pressure saturation was initiated. Back pressure was applied to the specimen pore water by simultaneously increasing the chamber pressure and the pressure acting through the burette in communication with the top of the specimen. To avoid undesirable prestressing of the specimen while applying back pressure, the pressures were applied slowly to avoid pore water pressure gradients within the specimen. After the estimated total back pressure required for saturation was applied, a check of the Skempton pore pressure "B" parameter was made. The "B" check was accomplished by closing the valve to the top of the specimen and increasing the chamber pressure by 10.0 psi. If the induced pore pressure was 9.5 psi or greater, i.e., a "B" value equal to 0.95 or greater, the specimen was assumed to be saturated. If the "B" value was less than 0.95, the back pressure was increased and "B" checks made until the 0.95 requirement was satisfied.

#### Consolidation

20. After saturation, specimens were isotropically consolidated by increasing the chamber pressure, with valves to the top and bottom of the specimen closed, to the desired consolidation stress (the desired difference between chamber and back pressure) and then opening the drainage valves to the top and bottom of the specimen to allow water from the specimen to enter a tube. In cases where specimens were anisotropically consolidated, the desired consolidation stress ratio was achieved by increasing the axial force to the required level immediately after the drainage valves were open. To check for completion of consolidation, specimen drainage valves were closed and the pore water pressure was observed over an interval of approximately 1 min. If the increase in pore pressure was less than 1 percent of the consolidation stress, consolidation was assumed to be complete.



## Shear Procedures

21. Brief descriptions of procedures employed during shear for the various types of tests are given in the following paragraphs.

### Drained triaxial tests

22. Upon completion of consolidation, the MTS loading system was changed from the controlled load to the controlled stroke mode and shear was initiated at a rate of axial deformation of 0.067-in. per minute. Specimen drainage valves to the top and bottom of the specimen were open to a single 3-in.-diam tube and the volume of water entering or leaving the specimen during shear was determined using readings from a differential pressure transducer which measured the difference between the back pressure and the total pressure at the bottom of the tube. The change in axial force during shear was measured with a 50,000-lb-capacity load cell attached to the specimen cap. Actuator piston movement was used to determine axial deformation. Sensor outputs were recorded with the x-y-y recorder. Specimens were sheared until the total axial deformation was approximately 6 in. This produced a total axial strain slightly in excess of 15 percent.

### Undrained triaxial tests

23. After consolidation, specimen drainage valves were closed and specimens were sheared with the MTS system in the controlled load mode. Axial force was applied to the specimens at a rate of 50,000 lb per hour. During shear, changes in axial force were measured with a 50,000-lb capacity load cell attached to the specimen cap and the induced pore water pressure was measured with a differential pressure transducer which measured the difference between the specimen pore water pressure and the initial back pressure. Actuator piston movement was used to determine axial deformation. Sensor outputs were recorded using a x-y-y recorder. Shear was continued until the q-p' stress path indicated an adequate definition of the failure envelope.

### Controlled cyclic stress tests

24. Following consolidation, specimen drainage valves were closed and the span control on the MTS actuator controller was adjusted to the proper setting to achieve the desired cyclic stress ratio. Cyclic shear was then initiated at a rate of 1 cycle per min using a sinusoidal load waveform. The induced pore water pressure and axial force were monitored during shear in the same manner as for the undrained triaxial test. Axial deformation was

measured using the LVDT attached to the actuator piston. Sensor outputs were recorded on the 8-channel strip chart recorder and the x-y-y recorder. Shear was continued until the MTS actuator was unable to maintain the desired waveform or until the residual pore pressure became essentially constant with increasing cycles of loading.

#### Controlled cyclic strain tests

25. Upon completion of consolidation, the MTS load controller was changed to the controlled stroke mode and the span control was adjusted to the required setting for the desired cyclic strain amplitude. Cyclic shear was then initiated at a rate of 1 cycle per min using a sinusoidal deformation waveform. The standard 16-in. stroke actuator piston LVDT used in the MTS control loop was replaced with a 2-in. stroke LVDT to achieve the desired low strain amplitudes. To avoid including apparatus deflection in axial deformation measurements, two LVDT's attached to steel rods on each side of the specimen were used to obtain direct measurement of movement between the specimen cap and base (see Figure B5). The LVDT's were chosen so that deformation measurements were accurate to 0.0001 in., thus providing accurate shear strain measurements as low as 0.0005 percent.

26. Possible errors in axial deformation measurements due to tilt of the specimen cap during loading were minimized by summing and averaging the LVDT readings. Some tilt of the cap occurred because of nonuniform specimen conditions even though the loading piston at the top of the specimen was rigidly attached to the specimen cap and the chamber top. Sensors and recording devices were the same as those described for the controlled stress cyclic tests except for the internal LVDT's and the volume change measurement device used for drained portions of the tests. For portions of tests where cyclic strains were applied under drained conditions, volume changes were measured in the same manner as for the controlled strain drained triaxial tests except a nominal 1-in.-diam tube was used in lieu of the standard 3-in.-diam tube. The 1-in.-diam tube was calibrated so that measured volume changes were accurate to within 0.5 cc.

27. For the test performed to verify whether axial deformation measured by the internal LVDT's was actually being transferred to the specimen rather than being partially absorbed by seating of the specimen on the specimen cap and base, two lightweight lucite platforms were glued to the outer membrane at quarter points along the specimen height. LVDT's attached to a single

vertical steel rod mounted on the specimen base were then used to measure the axial deformation occurring between the platforms (over the central third of the specimen) to determine shear strains to compare with those from the test on an identical specimen where shear strains were measured with the standard internal system. Photos of the test set up for this test are given in Figure B11. Procedures employed during shear were the same as those for the test with the standard internal axial deformation measurement system.

#### Post-Shear

28. Upon completion of the shear portion of the tests, a vacuum was reapplied to the specimen and the chamber was removed. Photos of the specimen were taken and then the entire specimen was placed in a container to be dried for an accurate determination of the specimen dry weight.

#### Membrane Compliance Test

29. For the test performed to measure the extent of membrane compliance, procedures for specimen preparation, saturation, and consolidation were the same as those for shear tests performed in the investigation. The test was performed in three stages. In each stage the specimen was isotropically consolidated to a given stress level and then rebounded in steps to an effective stress of 10 psi by increasing the back pressure. Consolidation stresses were 30, 50, and 60 psi and were chosen so that increases in back pressure necessary to obtain the 10-psi-effective stress encompassed the range of expected pore-water pressure changes during undrained testing in the study. During each stage, specimen drainage valves were open to a nominal 1-in.-diam tube serving as a burette and the volume of water expelled from the specimen was determined using readings from a differential pressure transducer which measured the difference between the back pressure and the total pressure at the bottom of the tube. The tube was calibrated so that measured volume changes were accurate to within 0.5 cc. Volume changes determined in this manner reflect those due to both membrane relaxation and structural rebound of the specimen.

30. Changes in specimen dimensions during each stage were used to determine volume changes due to structural rebound of the specimen. Changes

in specimen height and diameter were determined from measurements obtained with actuator piston LVDT and girth gages, respectively. The actuator LVDT readings were corrected for apparatus deflection to obtain valid specimen axial deformation values. Three girth gages were placed around the specimen at quarter points along the specimen height to determine changes in specimen diameter. Each gage formed nine chords around the specimen's circular cross-section. During each stage, the change in length of one chord on each gage was measured with an LVDT having a 0.2-in. stroke. LVDT readings were summed and averaged to determine the average change in diameter for the specimen.

31. Additional information on girth gages and procedures for determining membrane compliance may be found in University of California, Berkeley (Banerjee, Seed, and Chan 1979).\*

#### Large-Scale Cyclic Triaxial Laboratory Test Results

32. Stress-controlled cyclic triaxial tests were conducted on specimens of Folsom Dam gravel compacted to relative densities representative of the in situ dam shell and dredged foundation material to assess the following:

- a. The variation in cyclic strength with confining stress,  $K_\sigma$ .
- b. The increase in cyclic strength with initial static shear stress ratio,  $K_\alpha$ .
- c. The residual excess pore pressure ratios to associate with factors of safety against liquefaction  $\geq 1$ .

33. Cyclic strengths for eight load cycles were assessed for measured residual excess pore pressures,  $R_u$ , of 100 percent and 30 percent at confining stress levels of 15 to 80 psi, and consolidation stress ratios,  $K_c = \sigma'_{vc}/\sigma'_{hc}$ , of 1.0 to 2.0. As recommended by Seed et al. (1984), eight load cycles were selected to correspond to the design earthquake at the Folsom Project which is a magnitude 6.5 event. The test conditions are summarized in Tables B1, B2, and B3. Table B1 lists tests representative of the foundation gravels ( $D_R \approx 40$  percent), Table B2 lists tests representative of the embankment gravels ( $D_R \approx 64$  percent), and Table B3 lists tests at an intermediate relative density ( $D_R \approx 45$  percent). The test results are presented in this section along with comparisons of these results with cyclic strengths of Blue Ravine gravels estimated from Becker hammer tests performed in situ at Mormon

---

\* References in this appendix are cited at the end of the main text.

Island Auxiliary Dam, and laboratory test results on other gravels at similar relative densities.

Reduction and interpretation of laboratory data

34. The following guidelines were adopted in the reduction and interpretation of the cyclic triaxial test data, mainly to deal with difficulties caused by membrane compliance effects:

- a. The laboratory cyclic strength envelope for  $R_u = 30$  percent was determined to correspond to the laboratory cyclic strength at  $R_u = 100$  percent corrected for membrane compliance effects.
- b. Measured  $R_u$  values were extrapolated to 100 percent for most tests to obtain reasonable pore pressure development ( $N/N_L$ ) curves, which were used to extrapolate test results in a consistent manner to develop contours of  $R_u$  on plots of cyclic stress ratio and number of load cycles,  $N$ .
- c. Factors of safety against  $R_u = 100$  percent in the compliant laboratory specimens are associated with lower values of  $R_u$  to develop a relationship between  $FS_L$  and  $R_u$  since Evan's work shows these curves are unaffected by membrane compliance.
- d. Individual test results were adjusted slightly by the ratio of the as-consolidated relative density to the target relative density to remove accountable variability from the data.

35. Within these guidelines, laboratory cyclic strength envelopes were developed for  $D_R = 40$  percent and 64 percent, and also values of  $K_o$  and  $K_a$  were determined.

Laboratory tests on specimens at  $D_R = 64$  percent

36. Table B2 lists the tests which were constructed to relative densities most representative of the embankment shell gravels. These are tests on samples 11-17 and 22-25. Seven test groups with different consolidation stress conditions defined by  $K_c$  and  $\sigma'_{hc}$ , were investigated with one or more tests. The tests groups are:

Group	$K_c$	$\sigma'_{hc}$ , psi	Tests	Figures
1	1.0	15	11, 12	B12-B18
2	1.0	40	13, 14	B19-B25
3	1.0	80	17	B26-B32
4	1.5	40	22, 23	B33-B39
5	2.0	15	15a, 15b	B40-B41
6	2.0	20	25	B42-B44
7	2.0	40	15c, 16, 24	B45-B51

37. For each test group, data plots were prepared (in accordance with the sufficiency of the data) which show:

- a. Residual excess pore pressure development for each load cycle,  $R_u$  versus  $N$ .
- b. Residual excess pore pressure ratio contours on a plot of cyclic stress ratio versus load cycle number,  $N$ .
- c. Peak to peak strain or permanent axial strain (for isotropically or anisotropically consolidated specimens, respectively) for each load cycle,  $\epsilon$  versus  $N$ .
- d. Strain contours on plots of cyclic stress ratio versus load cycle,  $N$ .
- e. Residual excess pore pressure ratio plotted against normalized load cycles,  $N/N_L$ , where  $N_L$  is the number of cycles to achieve  $R_u = 100$  percent at the test cyclic stress ratio.
- f. Strain plotted against normalized load cycles,  $N/N_f$ , where  $N_f$  is the number of load cycles to achieve a failure strain level of 2.5 percent permanent axial or single amplitude (5 percent peak to peak) cyclic axial strain at the test cyclic stress ratio.
- g. Residual excess pore pressure ratio plotted as a function of safety factor against liquefaction (liquefaction defined as  $R_u = 100$  percent in eight load cycles, which roughly also correspond to permanent axial strain = 2.5 percent, or peak cyclic axial strain = 5 percent).

38. In the data reduction and analysis, the residual excess pore pressure ratio  $R_u$  is defined as the ratio of residual excess pore pressure to the initial consolidation stress normal to the failure plane,  $\sigma'_{fc}$ . In the isotropically consolidated tests, the cyclic stress ratio is computed as the ratio of the cyclic deviator stress to two times the initial consolidation stress,  $\sigma'_{hc}$ . At a later stage, when cyclic strength envelopes were determined for several  $K_c$  values, a factor  $C_R = 0.6$  was applied to the isotropic cyclic stress ratio values in order to correct the results to simple shear stress conditions. For the anisotropically consolidated tests, the cyclic stress ratio is computed as the ratio of the cyclic shear stress on the failure plane to the consolidation stress normal to the failure plane (no  $C_R$  factor is applied to the anisotropically consolidated test results).

39. The figures that correspond to each test group are listed above. These data were used to develop the cyclic strength envelopes for  $R_u = 30$  percent in eight cycles shown in Figure B52 for the gravel specimens compacted to a relative density of 64 percent, representative of the compacted embankment shell. From these cyclic strength envelopes, the  $K_v$  and  $K_a$  curves shown

in Figures B53 and B54 were determined. It was found that the shape of the  $K_\sigma$  curve does not change with  $\alpha$  ( $K_\sigma = (\text{cyclic strength at } \sigma)/(\text{cyclic strength at } \sigma = 1 \text{ tsf})$ ). It was also found that the shape of the  $K_\alpha$  curve does not change with  $\sigma$  ( $K_\alpha = (\text{cyclic strength at } \alpha)/(\text{cyclic strength at } \alpha = 0)$ ).

40. The cyclic stress ratio requires to develop  $R_u = 30$  percent (in a compliant specimen) in eight cycles at  $\sigma = 1$  tsf and  $\alpha = 0$  for  $D_R \approx 64$  percent determined in these laboratory tests on compacted Folsom gravel specimens was 0.23. Figure B55 compared this cyclic strength with other laboratory test results on gravels for  $N = 10$  cycles, at relative densities that range from 20 percent to 84 percent. Figure B55 shows data for strain and pore pressure definitions of failure, and for measured and membrane-compliance corrected strength. The data shown in Figure B55 indicate that the laboratory cyclic strength determinations in this study are generally consistent with strengths determined by other researchers on other gravels compacted to about the same relative densities.

41. Figure B56 compares the  $K_\sigma$  curve shown in Figure B53 with data for sands compiled by Dr. Leslie F. Harder. Generally, the  $K_\sigma$  curve determined in this study for gravel lies below the curve for sand, which results in a more severe reduction in cyclic stress ratio as confining stress increases. The gravel and sand curves merge at high confining stress. The  $K_\alpha$  curve shown in Figure B54 is compared in Figure B57a with several relationships for sand at  $D_R = 55$  percent. The  $K_\alpha$  curve for Folsom gravel lies in the middle of the band of relationships for sand data.

Comparison of laboratory and Becker  
hammer strengths,  $D_R \approx 64$  percent

42. The cyclic stress ratio required to generate  $R_u = 30$  percent in eight cycles in a membrane compliant specimen consolidated to a confining stress of 1 tsf is estimated to be 0.23 from Figure B52. The Becker hammer blowcounts indicate that the cyclic stress ratio required to cause 100 percent excess pore pressure in the compacted shell gravels in the dam is approximately 0.35 at a confining stress of 1 tsf and  $N = 8$  cycles. Within the laboratory data interpretation guidelines, this implies a factor of 1.5 to account for field conditions which affect in situ cyclic strength that cannot be represented by reconstructed laboratory specimens. For the Folsom Dam shell material, the most important of these factors is probably aging. Since the

Folsom Project is approximately 10,000 days old, the aging factor could range from 1.45 to 1.75, according to the data presented by Banerjee, Seed, and Chan (1979). Thus, a factor of 1.5 appears to be quite reasonable, and has been applied to the laboratory strengths derived from the  $R_u = 30$  percent failure criterion to compute a cyclic strength consistent with that determined by in situ testing.

Safety factors against  
liquefaction and residual excess  
pore pressures,  $D_R \approx 64$  percent

43. The figures of  $R_u$  contours on plots of cyclic stress ratio versus load cycle number were used to associate residual excess pore pressures with factors of safety against liquefaction,  $FS_L$ , greater than or equal to 1. These data were presented for test groups 1-7. From this data, the relationship shown in Figure B58 was estimated for  $N = 8$  cycles and  $\alpha = 0$  and 0.32. The laboratory data from this study indicated there was a slight increase in residual excess pore pressure at a given  $FS_L$  for soil elements with initial shear stresses present. These pore pressure curves were compared with data on gravels at  $D_R = 42$  percent from Evans (1987), who found a similar relationship for  $\alpha = 0$ , but no increase for higher  $\alpha$  values. Evidently, the higher  $R_u$  values resulted from membrane compliance effects. These data and data on sand from several other researchers are shown in Figure B59. Evan's data clearly show that, for isotropically consolidated tests, the same relationship between  $R_u$  and  $FS_L$  results from membrane-compliant specimens as it does from noncompliant specimens.

Residual excess pore pres-  
sure and  $N/N_L$ ,  $D_R \approx 64$  percent

44. For the individual tests,  $R_u$  was extrapolated to 100 percent to estimate  $N_L$ . The individual  $N/N_L$  curves were presented earlier, and a summary plot is shown in Figure B60 for  $\alpha = 0$ . For  $\alpha = 0$ , the curves fall within a relatively narrow band, and there is no consistent trend with confining stress. These curves are higher than similar curves for sand.

45. In an attempt to relate pore pressure buildup with cyclic strains, Figure B61 was developed from the peak to peak cyclic strain values observed in each cycle. Usually, a cyclic strain failure level of 5 percent required no extrapolation of the test data. The number of cycles to the failure level of 5 percent is denoted as  $N_f$ . The curves of peak to peak cyclic axial



strain and  $N/N_f$  shown in Figure B61 have the same general shape as the  $R_u$  and  $N/N_L$  curves of Figure B60, but there is more scatter.

46. Figures B62 and B63 show the effect of  $\alpha$  on  $R_u$  and permanent axial strain, respectively, as they increase with normalized cycle number. At low values of  $N/N_L$ , higher  $R_u$  values are observed with higher  $\alpha$ . This was also reflected in the  $R_u$  and  $FS_L$  curves shown in Figure B58 for  $\alpha = 0.32$ . This effect of  $\alpha$  shown in Figure B62 may also be due to membrane compliance errors. At  $N/N_L > 0.5$ ,  $\alpha$  has no effect on  $R_u$ . Even if  $\alpha$  effects are ignored, the curves of Figure B62 fall within a relatively narrow band that is higher than that for sand. The value of  $\alpha$  has a more pronounced effect on the permanent axial strain and  $N/N_f$  curves shown in Figure B63. The failure strain for the anisotropically consolidated specimen is defined as 2.5 percent permanent axial strain.

Laboratory tests on specimens  
compacted to  $D_R \approx 40$  percent

47. Table B1 lists the tests on samples which were constructed to relative densities most representative of the dredged foundation gravels. These are tests on samples 1-10 and 18-21. Seven test groups with different consolidation stress conditions defined by  $K_c$  and  $\sigma'_{hc}$  were investigated with one or more tests. The test groups for the low density specimens are:

Group	$K_c$	$\sigma'_{hc}$ , psi	Tests	Figures
1	1.0	15	1, 2, 3	B64-B70
2	1.0	40	4, 5	B71-B75
3	1.5	20	18, 19	B76-B78
4	1.5	80	20, 21	B79-B81
5	2.0	15	6, 7	B82-B84
6	2.0	40	8, 9	B85-B86
7	2.0	80	10	B82-B83

48. For each test group, data plots were prepared (in accordance with the sufficiency of the data) in the same manner as they were for the tests on specimens compacted to  $D_R \approx 64$  percent. These plots show:

- a. Residual excess pore pressure development for each load cycle,  $R_u$  versus  $N$ .
- b. Residual excess pore pressure ratio contours on a plot of cyclic stress ratio versus load cycle number,  $N$ .
- c. Peak to peak strain or permanent axial strain (for isotropically or anisotropically consolidated specimens, respectively) for each load cycle,  $\epsilon$  versus  $N$ .

- d. Strain contours on plots of cyclic stress ratio versus load cycle,  $N$ .
- e. Residual excess pore pressure ratio plotted against normalized load cycles,  $N/N_L$ , where  $N_L$  is the number of cycle to achieve  $R_u = 100$  percent at the test cyclic stress ratio.
- f. Strain plotted against normalized load cycles,  $N/N_f$ , where  $N_f$  is the number of load cycles to achieve a failure strain level of 2.5 percent permanent axial or single amplitude (5 percent peak to peak) cyclic axial strain at the test cyclic stress ratio.
- g. Residual excess pore pressure ratio plotted as a function of safety factor against liquefaction (liquefaction defined as  $R_u = 100$  percent in eight load cycles, which roughly also correspond to permanent axial strain = 2.5 percent, or peak cyclic axial strain = 5 percent).

49. In the data reduction and analysis of these lower density tests, the residual excess pore pressure ratio  $R_u$  is defined in the same manner as before, as the ratio of residual excess pore pressure to the initial consolidation stress normal to the failure plane,  $\sigma'_{fc}$ . In the isotropically consolidated tests, the cyclic stress ratio is computed as the ratio of the cyclic deviator stress to two times the initial consolidation stress,  $\sigma'_{hc}$ , multiplied by the factor  $C_R = 0.6$  in order to correct the results to simple shear stress conditions. All plots for these isotropically consolidated low density tests correspond to cyclic stress ratios corrected to level ground stress conditions. For the anisotropically consolidated tests, the cyclic stress ratio is computed as the ratio of the cyclic shear stress on the failure plane to the consolidated stress normal to the failure plane (no  $C_R$  factor is applied to the anisotropically consolidated tests results).

50. The figures that correspond to each test group are listed above. These data were used to develop the cyclic strength envelopes for  $R_u = 30$  percent in eight cycles shown in Figure B87 for the gravel specimens compacted to a relative density of 40 percent, representative of the loose dredged tailings foundation. From these cyclic strength envelopes, the  $K_\sigma$  and  $K_\alpha$  curves shown in Figures B88 and B89 were determined.

51. The cyclic stress ratio required to develop  $R_u = 30$  percent (in a compliant specimen) in eight cycles at  $\sigma = 1$  tsf and  $\alpha = 0$  for  $D_R = 40$  percent determined in these laboratory tests on compacted Folsom gravel specimens was 0.12. Figure B55 compared this cyclic strength with other laboratory test results on gravels for  $N = 10$  cycles, at relative densities that range from 20 percent to 84 percent. Figure B55 shows data for

strain and pore pressure definitions of failure, and for measured and membrane-compliance corrected strength. The data shown in Figure B55 indicate that the laboratory cyclic strength determinations in this study are generally consistent with strengths determined by other researchers on other gravels compacted to about the same relative densities.

52. Figure B90 compared the  $K_\alpha$  curve shown in Figure B88 with data for sands compiled by Dr. Leslie F. Harder. Generally, the  $K_\sigma$  curve determined in this study for loose gravel lies below the curve for sand, slightly above the  $K_\sigma$  curve for Folsom gravel compacted to  $D_R \approx 64$  percent. This results in a more severe reduction in cyclic stress ratio as confining stress increase for gravels, loose or dense, than for sand. The loose and dense gravel curves merge with the sand curves at high confining stress.

53. The  $K_\alpha$  curve shown in Figure B89 is compared in the same figure with laboratory test data from Evans (1987) for gravel compacted to a similar relative density. In this figure, the failure criterion is a permanent axial strain of 5 percent or peak to peak strain of 5 percent, whichever was greater. For this failure criterion, the Folsom data show a slightly lower  $K_\alpha$  curve than Evans found for his gravels. As defined earlier, failure strain for this study is defined as 2.5 percent permanent axial strain for anisotropically consolidated samples. With this definition,  $K_\alpha$  is approximately equal to unity for any  $\alpha$  value. This is shown in Figure B91 which compared cyclic strength envelopes for several different strain failure criteria. The two lowest curves are consistent with the failure criteria selected for this study. These two lowest failure envelopes, permanent axial strain of 2.5 percent or single amplitude cyclic strain of 2.5 percent, indicate no increase in strength with higher  $\alpha$  values.

54. Figure B92 shows a comparison of the  $K_\alpha$  curves from Figure B89 with several relationships for sand at  $D_R = 35-43$  percent. The  $K_\alpha$  curve for loose Folsom gravel based on the failure criteria of 5 percent strain lies well above the band of relationships for sand data, but with the failure criteria of 2.5 percent strain, the Folsom results are similar to the sand data. Upon examination of this data, it was decided that application of a  $K_\alpha$  increase to the cyclic strength of the foundation gravels was inappropriate.

Comparison of laboratory and Becker  
Hammer strengths,  $D_R \approx 40$  percent

55. The cyclic stress ratio required to generate  $R_u \approx 30$  percent in eight cycles in a membrane compliant specimen consolidated to a confining stress of 1 tsf is estimated to be 0.12 for the loose foundation gravel from Figure B87. The Becker Hammer blowcounts indicate that the cyclic stress ratio required to cause 100 percent excess pore pressure in the loose dredged gravels upstream and downstream of the dam is approximately 0.12 at a confining stress of 1 tsf and  $N = 8$  cycles. Within the laboratory data interpretation guidelines, this implies a factor of 1.0 to account for field conditions which affect in situ cyclic strength that usually are not represented by reconstructed laboratory specimens. For the loose Blue Ravine dredged tailing, it appears that aging effects have not significantly changed this deposit, probably due to the very loose nature of the materials, the lack of significant fines, and the relatively low confining stresses that exist upstream and downstream of the dam. However, beneath the dam shells, a significant increase in strength was indicated by the field tests. This strength increase is too large to be accounted for by densification effects alone (due to construction activity and increased confining stress due to the presence of the shells). It appears that the confining stress in this location is sufficient for aging effects to improve the material. A similar example of this increase in cyclic strength and penetration resistance of dredged and alluvial gravel deposits was observed at Comanche Dam, reported by Seed (1983).

Safety factors against  
liquefaction and residual excess  
pore pressures,  $D_R \approx 40$  percent

56. The figures of  $R_u$  contours on plots of cyclic stress ratio versus load cycle number were used to associate residual excess pore pressures with factors of safety against liquefaction,  $FS_L$ , greater than or equal to 1. These data were presented for test groups 1-7. From this data, the relationship shown in Figure B93 was estimated for  $N = 8$  cycles and  $\alpha = 0$  and 0.32. These pore pressure curves were compared with data on gravels at  $D_R = 42$  percent from Evans (1987), who found a similar relationship (for  $\alpha = 0$ ). Data on sand from several other researchers are also shown in Figure B93. Evans data clearly show that for isotropically consolidated tests, the same relationship

between  $R_u$  and  $FS_L$  results from membrane-compliant specimens as does from noncompliant specimens.

Laboratory tests on  
specimens at  $D_R \approx 45$  percent

57. Table B3 lists test conditions for five samples which were constructed to a relative density of about 45 percent with material from the first test pit series in the dredged tailings foundation at Mormon Island Auxiliary Dam. All five samples were isotropically consolidated. The data plots in Figures B94-B98 are similar to those shown for the other two test groups. This test group gives a well-defined relationship between  $R_u$  and  $FS_L$ , shown in Figure B98, and compared with the gravel data from Evans (1987) and the sand data from others.

Summary and conclusions

58. The cyclic strength of the compacted shell gravel in the embankment dams at the Folsom Dam and Reservoir Project has been estimated from cyclic triaxial tests on reconstructed gravel specimens compacted to a target relative density of 64 percent to represent in situ conditions. The cyclic stress ratio required to generate a residual excess pore pressure ratio,  $R_u$ , of 30 percent in eight cycles in a laboratory specimen with membrane compliance is defined as failure since Evan's work (1987) indicates this level approximately corresponds to  $R_u$  of 100 percent in laboratory specimens with no membrane compliance. The resulting laboratory failure stress ratio at a confining stress of 1 tsf is 0.23. Becker Hammer test results indicate an in situ failure stress ratio of 1 tsf is 0.35, which implies a factor of 1.5 to account for in situ conditions not represented in laboratory specimens, most notably aging. The relative changes in cyclic strength with confining stress and initial stress ratio,  $K_\sigma$  and  $K_\alpha$ , have been determined from the laboratory tests. In a study of residual excess pore pressures and corresponding factors of safety against liquefaction, it is concluded that  $FS_L$  must be greater than or equal to approximately 1.4 in order to have  $R_u$  values less than 25 percent.

59. The cyclic strength of the loose dredged tailings foundation gravel upstream and downstream of the dam has been estimated from cyclic triaxial tests on reconstructed gravel specimens compacted to a target relative density of 40 percent to represent in situ conditions. The cyclic stress ratio required to generate a residual excess pore pressure ratio,  $R_u$ , of

30 percent in eight cycles in a laboratory specimen with membrane compliance is defined as failure since Evan's work (1987) indicates this level approximately corresponds to  $R_u$  of 100 percent in laboratory specimens with no membrane compliance. The resulting laboratory failure stress ratio at a confining stress of 1 tsf is 0.12. Becker Hammer test results indicate an in situ failure stress ratio at 1 tsf is 0.12, which implies aging is not a factor in this loose deposit which is not confined by high stresses. The relative changes in cyclic strength with confining stress and initial stress ratio,  $K_\sigma$  and  $K_\alpha$ , have been determined from the laboratory tests. The  $K_\sigma$  curve for the loose gravel is very similar to that for the dense gravel. The adopted failure criterion of 2.5 percent permanent axial or peak single amplitude strain results in no strength increase as  $\alpha$  increases. This is consistent with tests performed on sands. In a study of residual excess pore pressures and corresponding factors of safety against liquefaction, it is concluded that  $FS_L$  must be greater than or equal to approximately 1.4 in order to have  $R_u$  values less than 20 percent.

Table 81

Test Conditions for Stress-Controlled Cyclic Triaxial Tests on 15-In. Diameter Specimens of Folsom Gravel Combined Laboratory Gradation,  
Relative Density = 40 Percent

Test No.	Initial Conditions			After Consolidation (1)					Cyclic Shear				
	Dry Unit Weight, $\gamma_d$ , pcf	Relative Density, $D_R$ , %	Drainage, $z$	Vertical Effective Stress, $\sigma_v$ , pcf	Horizontal Effective Stress, $\sigma_h$ , pcf	Normal Stress on Failure Plane, $\sigma_c$ , pcf	Initial Shear Stress on Failure Plane, $\tau_c$ , pcf	Initial Shear Stress Ratio, $\tau_c/\sigma_c$	Cyclic Deviator Stress Ratio, $\tau_d/\sigma_c$	Cyclic Stress Ratio During Test, $\tau_c/\sigma_c$	Cyclic Stress Ratio Adjusted to $D_R = 40\%$ , $\tau_c/\sigma_c$	Cycle Number, $N$	Rate of Cycling, cycles/sec
1	125.45	41.51	125.92	42.81	15.0	15.0	0	0	0.34	3.06	0.204	1-3	1/10
2	124.09	37.72	124.56	39.04	15.0	15.0	0	0	0.25	2.25	0.150	1-9	1/17
3	124.82	39.76	125.37	41.29	15.0	15.0	0	0	0.25	2.25	0.150	1-6	1/60
4	125.58	41.88	126.57	44.57	40.0	40.0	0	0	0.30	7.20	0.180	1-3	1/60
5	124.95	40.13	125.93	42.84	40.0	40.0	0	0	0.20	4.80	0.120	1-6	1/60
6a	125.37	41.29	125.72	42.26	30.0	15.0	5.66	0.32	0.25	2.83	0.161	1-10	1/60
6b	--	--	--	--	--	--	--	--	0.22	2.49	0.142	11-35	1/1
6c	--	--	--	--	--	--	--	--	0.24	2.72	0.155	36-49	1/2
6d	--	--	--	--	--	--	--	--	0.40	4.53	0.258	50-81	1/1
7a	124.45	38.74	124.70	39.44	30.0	15.0	5.66	0.32	0.40	4.53	0.258	1-11	1/60
7b	--	--	--	--	--	--	--	--	0.41	4.64	0.264	12-75	1/1
8a	125.38	41.32	125.66	42.08	80.0	40.0	15.09	2.32	0.29	8.75	0.187	1-20	1/60
8b	--	--	--	--	--	--	--	--	0.30	9.06	0.193	21-75	1/1
9a	124.50	38.88	125.09	40.51	80.0	40.0	15.09	0.32	0.20	6.04	0.127	1-20	1/60
9b	--	--	--	--	--	--	--	--	0.21	6.34	0.135	21-83	1/1
10	123.29	35.46	125.52	41.71	160.0	80.0	30.19	0.32	0.48	29.98	0.309	1-3	1/60
18	126.15	43.42	127.63	47.40	30.0	20.0	3.77	0.17	0.50	7.55	0.348	1	1/60
19	126.18	43.50	127.48	47.00	30.0	20.0	3.77	0.17	0.35	5.28	0.243	1-8	1/60
20	126.24	43.66	129.03	51.10	120.0	80.0	15.09	0.17	0.25	15.09	0.174	1-60	1/60
21	126.35	43.98	130.30	54.38	120.0	80.0	15.09	0.17	0.29	17.51	0.202	1-7	1/60

(1) All B-values exceeded 0.95.

(2) Computed with field envelope values,  $\gamma_{dmax} = 151$  pcf,  $\gamma_{dmin} = 112$  pcf.

(3)  $q'_c = q'_h (1 + (K_c - 1) \cos^2 \theta)$ ,  $\theta = 45^\circ + \phi'/2$ ,  $\phi' = 41^\circ$ .

(4)  $\tau'_c = (K_c - 1) q'_h \cos \theta \sin \theta$ ,  $\theta = 45^\circ + \phi'/2$ ,  $\phi' = 41^\circ$ .

(5)  $\sigma'_c = \tau'_c / q'_c$ .

(6) For anisotropically consolidated samples ( $K_c \neq 1$ ):  $\tau'_c = \sigma'_h \cos \theta \sin \theta$ ,  $\theta = 45^\circ + \phi'/2$ .  
For isotropically consolidated samples ( $K_c = 1$ ):  $\tau'_c = (\sigma'_h/2) \cdot C_R$ ,  $C_R = 0.6$  (after Banerjee et al. 1979).

(7) For isotropically consolidated samples:  $\tau'_c / q'_c = C_R \times \sigma'_h/2 \cdot q'_h$ ,  $C_R = 0.6$ .  
For anisotropically consolidated samples:  $\tau'_c / q'_c = \frac{\sigma'_h \cos \theta \sin \theta}{q'_h (1 + (K_c - 1) \cos^2 \theta)}$ ,  $\theta = 45^\circ + \phi'/2$ .

(8) Cyclic stress ratios adjusted by ratio of relative densities:  $\tau'_c / q'_c$  (adjusted to  $D_R = 40\%$ ) =  $(\tau'_c / q'_c \text{ during test}) \times (0.40/D_R)$ ,  $D_R$  = relative density of specimen after consolidation.

Table B2  
Test Conditions for Stress-Controlled Cyclic Triaxial Tests on 15-in. Diameter Specimens of Fulsom Gravel Combined Laboratory Gradation,  
Relative Density  $\approx 64$  Percent

Test No.	Initial Conditions			After Consolidation (1)										Cyclic Shear			
	Dry Unit Weight $\gamma_d$ , pcf	Relative Density $D_R$ , %	Dry Unit Weight $\gamma_d$ , pcf	Vertical Effective Stress $\sigma'_v$ , psi	Horizontal Effective Stress $\sigma'_h$ , psi	Normal Stress on Failure Plane (3) $q'_c$ , psi	Initial Shear Stress on Failure Plane (4) $\tau'_c$ , psi	Initial Shear Stress Ratio (5) $\alpha$	Cyclic Deviator Stress Ratio During Test $\pm \sigma'_d/2q'_c$	Cyclic Stress on Failure Plane During Test (6) $\tau_c$ , psi	Cyclic Stress Ratio During Test (7) $\tau_c/q'_c$	Cyclic Stress Ratio to $D_R \approx 64\%$ (8)	Cycle Number N	Rate of Cycling cycles/sec			
11a	132.66	60.29	133.00	61.13	15.0	15.0	3	0	0.20	1.80	0.12	0.126	1-10	1/50			
11b	--	--	--	--	--	--	--	--	0.19	1.71	0.11	0.119	11-75	1/1			
11c	--	--	--	--	--	--	--	--	0.50	4.50	0.30	0.314	76-86	1/50			
12	130.78	55.60	131.43	57.25	15.0	15.0	0	0	0.35	3.15	0.21	0.235	1-40	1/60			
13	131.82	58.23	132.73	60.47	40.0	40.0	0	0	0.50	12.00	0.30	0.318	1-2	1/60			
14	131.65	57.80	132.65	60.27	40.0	40.0	0	0	0.30	7.20	0.18	0.191	1-9	1/60			
15a	133.98	63.51	134.73	65.33	30.0	15.0	2.0	17.38	5.48	5.38	0.31	0.303	1-10	1/60			
15b	--	--	--	--	--	--	--	--	0.60	6.58	0.38	0.371	11-20	1/60			
15c	--	--	134.73	65.33	80.0	40.0	2.0	46.36	14.63	17.55	0.38	0.371	1-11	1/60			
16	130.80	55.66	131.29	56.89	80.0	40.0	2.0	46.36	14.63	12.87	0.28	0.313	1-69	1/60			
17	133.10	61.38	134.44	64.62	80.0	80.0	1.0	80.0	0	12.0	0.150	0.149	1-8	1/60			
22a	134.03	63.64	135.19	66.41	60.0	40.0	1.5	43.18	7.31	14.63	0.339	0.327	1-19	1/60			
22b	--	--	--	--	--	--	--	--	0.53	15.50	0.359	0.346	20	1/30			
22c	--	--	--	--	--	--	--	--	0.50	14.63	0.339	0.327	21	1/300			
23	136.16	68.70	137.41	71.60	60.0	40.0	1.5	43.18	7.31	19.02	0.440	0.393	1-8	1/300			
24	135.87	68.02	137.67	72.20	80.0	40.0	2.0	46.36	14.63	28.96	0.625	0.554	1-3	1/60			
25	~135	~64	~135	~64	40.0	20.0	2.0	23.18	7.31	14.627	0.631	~0.63	1-8	1/300			

(1) All  $B$ -values exceeded 0.95.

(2) Computed with field envelope values,  $\gamma_{dmax} = 151$  pcf,  $\gamma_{dmin} = 112$  pcf.

(3)  $q'_c = q'_c (1 + (K_c - 1) \cos^2 \theta)$ ,  $\theta = 45^\circ + \phi'/2$ ,  $\phi' = 41^\circ$ .

(4)  $\tau'_c = (K_c - 1) q'_c \cos \theta \sin \theta$ ,  $\theta = 45^\circ + \phi'/2$ ,  $\phi' = 41^\circ$ .

(5)  $\alpha = \tau'_c/q'_c$ .

(6) For anisotropically consolidated samples ( $K_c \neq 1$ ):  $\tau_c = q_c \cos \theta \sin \theta$ ,  $\theta = 45^\circ + \phi'/2$ .

For isotropically consolidated samples ( $K_c = 1$ ):  $\tau_c = (q_c/2) \times C_R$ ,  $C_R = 0.6$  (after Banerjee et al. 1979).

(7) For isotropically consolidated samples:  $\tau_c/q'_c = C_R \times q_c/2 q'_c$ ,  $C_R = 0.6$ .

For anisotropically consolidated samples:  $\frac{\tau_c}{q'_c} = \frac{q_c \cos \theta \sin \theta}{q'_c (1 + (K_c - 1) \cos^2 \theta)}$ ,  $\theta = 45^\circ + \phi'/2$ .

(8) Cyclic stress ratios adjusted by ratio of relative densities:  $\tau_c/q'_c$  (adjusted to  $D_R \approx 64\%$ ) =  $(\tau_c/q'_c \text{ during test}) \times (0.64/D_R)$ ,  $D_R$  = relative density of specimen after consolidation.



Table B3  
Test Conditions for Stress - Controlled Cyclic Triaxial Tests on 15-in. Diameter Specimens  
of Folsom Dam Gravel, Laboratory Gradation from First Test Pits

Test No.	Initial Conditions				(1) After Consolidation						Cyclic Stress Ratio	
	Water Content %	Void Ratio e	Dry Unit Weight $\gamma_d$ pcf	Relative Density $D_r$ %	Number and Thickness of Membranes	Void Ratio e	Dry Unit Weight $\gamma_{dc}$ pcf	Relative Density $D_r$ % (2)	Vertical Effective Stress $\sigma'_{vc}$ psi	Horizontal Effective Stress $\sigma'_{hc}$ psi	Cyclic Stress Ratio During Test $\pm \sigma'_d / 2 \sigma'_{hc}$	Cyclic Stress Ratio Adjusted to $D_r$ 45%
1	4.7	0.361	129.76	45.36	2 membranes (0.05 in., 0.05 in.)	0.360	129.85	45.56	20.0	20.0	1.0	0.207
2	4.7	0.365	129.40	44.49	2 membranes (0.05 in., 0.05 in.)	0.363	129.52	44.78	20.0	20.0	1.0	0.291
3	4.2	0.368	129.07	43.71	2 membranes (0.025 in., 0.05 in.)	0.366	129.26	44.16	20.0	20.0	1.0	0.245
4	4.0	0.365	129.33	44.34	2 membranes (0.05 in., 0.05 in.)	0.365	129.41	44.52	10.0	10.0	1.0	0.354
5	4.0	0.383	127.67	40.35	2 membranes (0.025 in., 0.025 in.) clay coating between membranes (clay 0.04 in.)	0.380	127.95	41.03	20.0	20.0	1.0	0.307

(1) All B values exceeded 0.95.

(2) Computed with field envelope values,  $\gamma_{dmax} = 158$  pcf and  $\gamma_{dmin} = 113$  pcf.



Figure B1. WES large-scale triaxial testing station

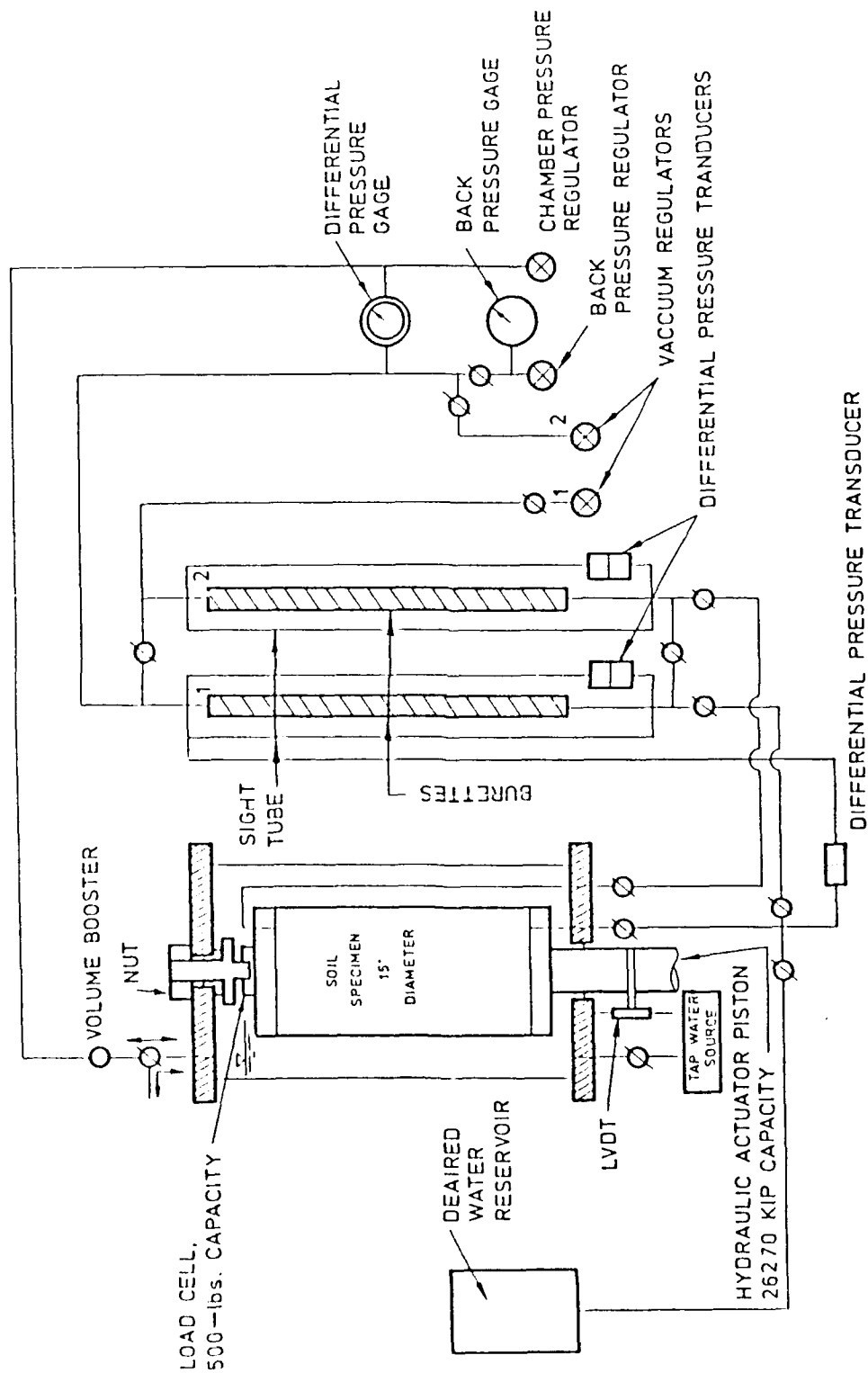


Figure B2. Schematic diagram of pressure control and measurement system, large-scale testing equipment



Figure B3. Cast aluminum split mold for construction of 15-in. diam specimens

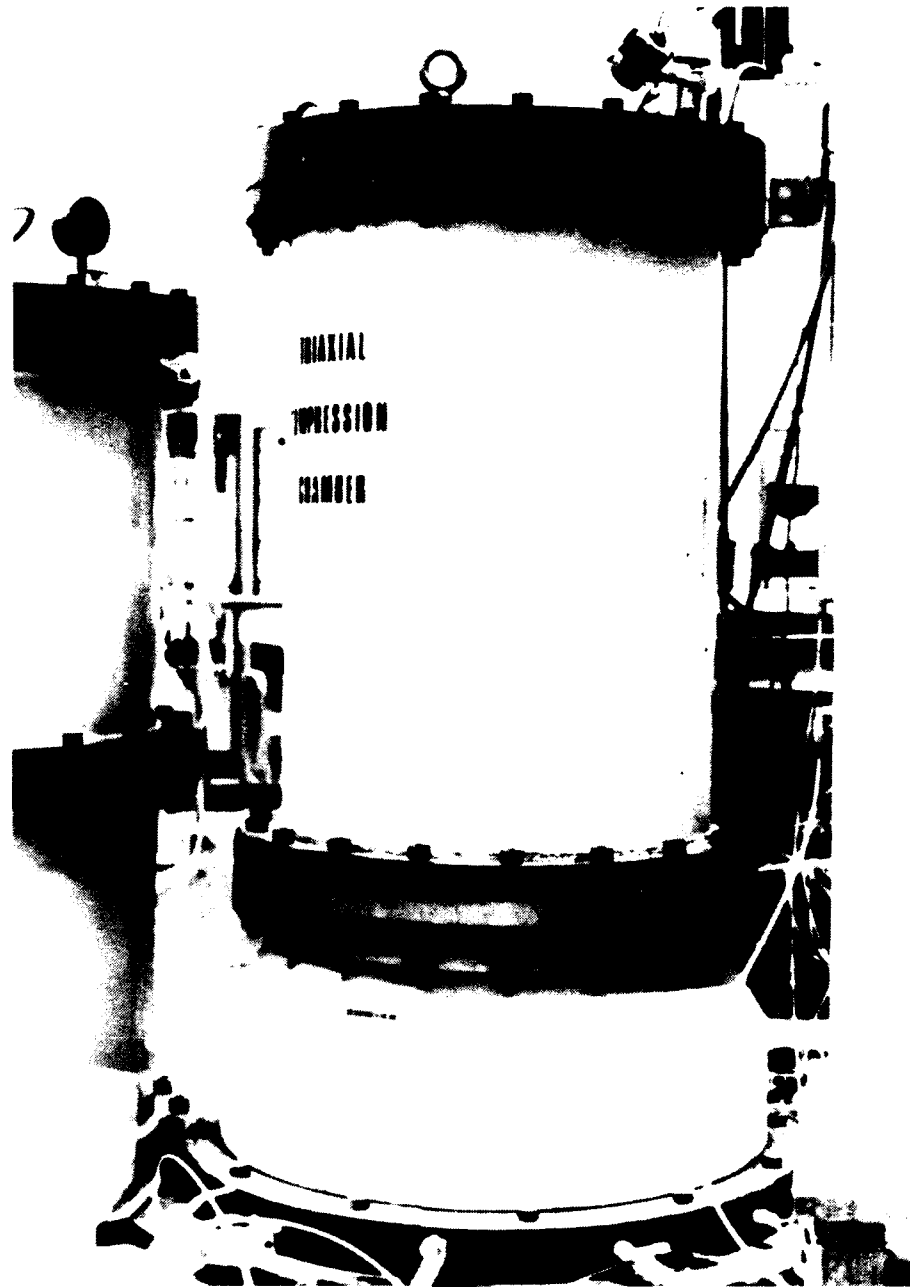


Figure B4. Confining chamber for large-scale testing station

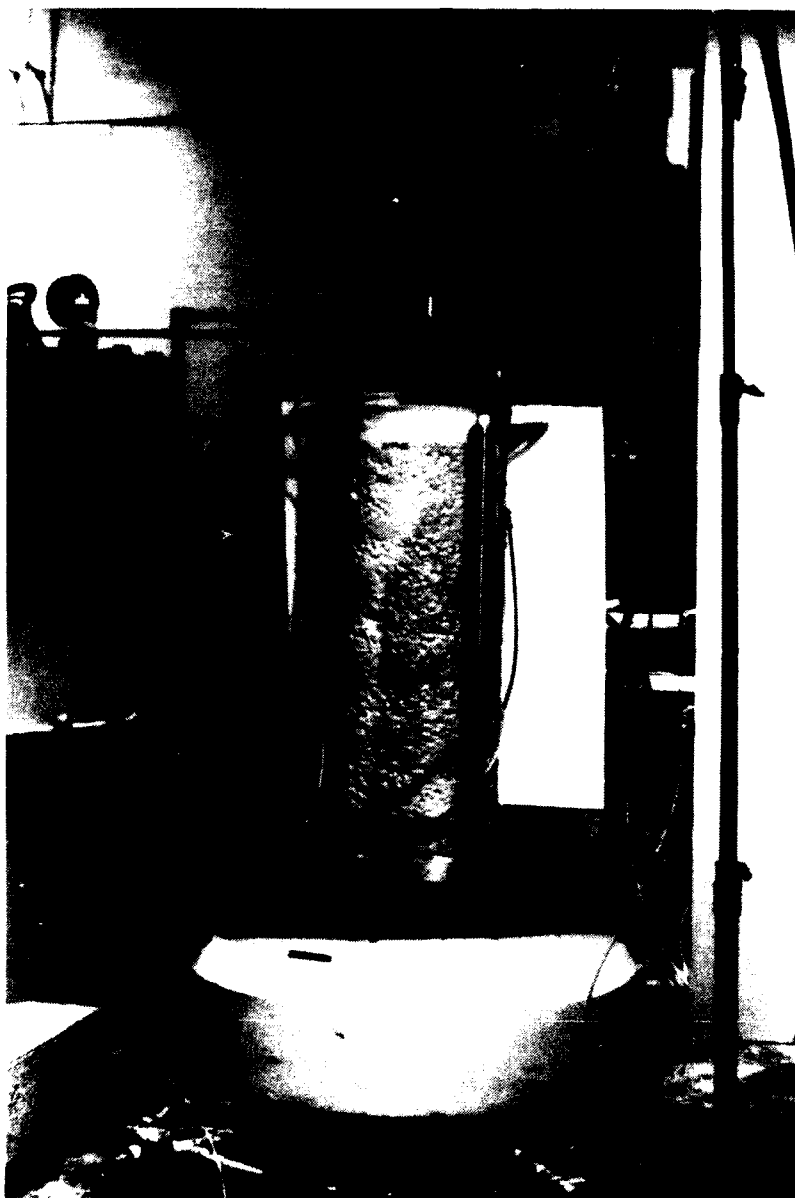


Figure B5. Internal axial deformation measurement instrumentation

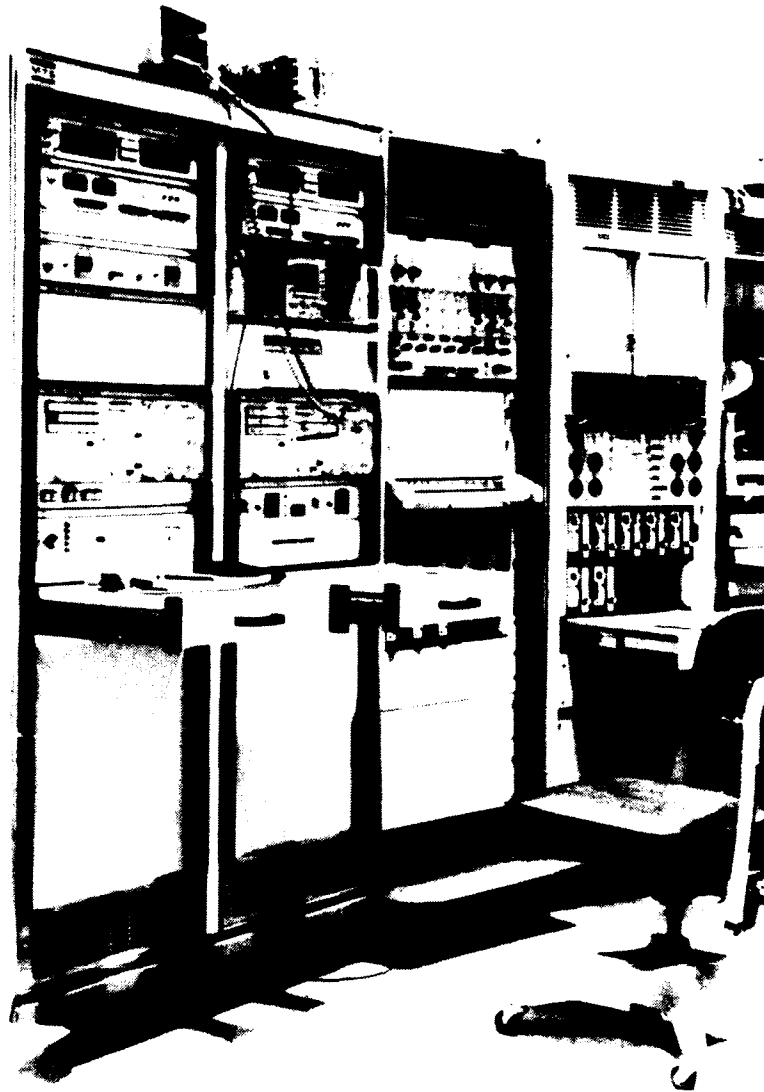


Figure B6. MTS system controls and data acquisition equipment

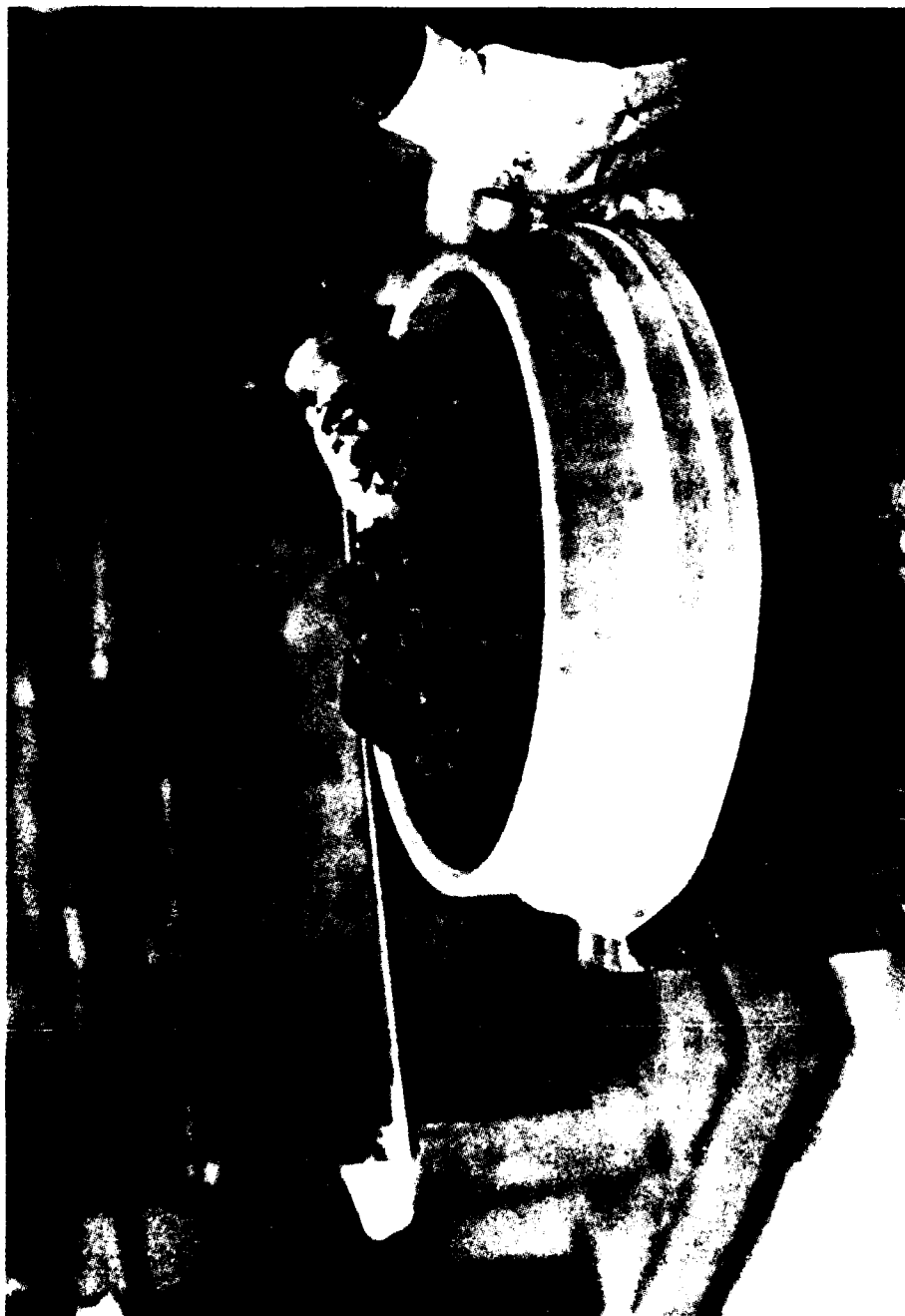


Figure B7. Placement of gravel in membrane-lined compaction mold



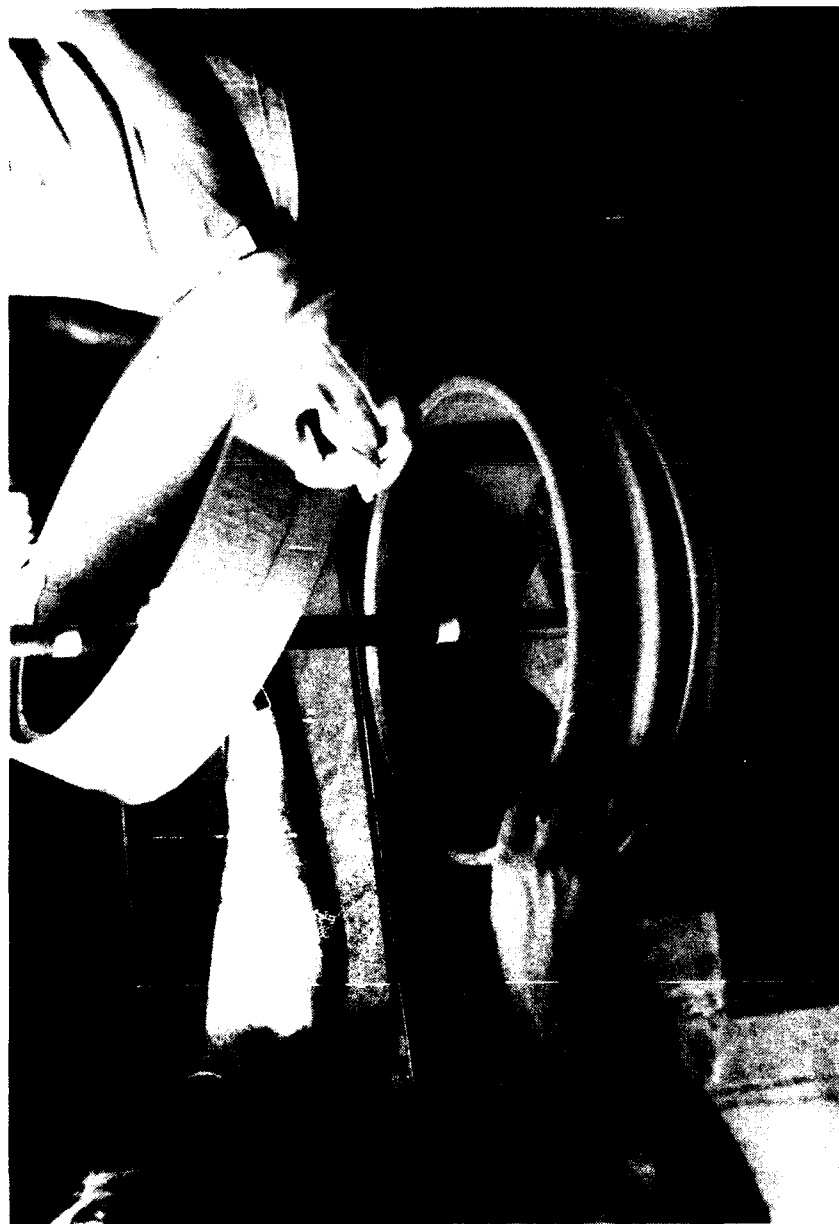


Figure B8. Compaction of gravel in membrane-lined mold with wedge-shaped tamper



Figure B9. Measurement of layer height after compaction

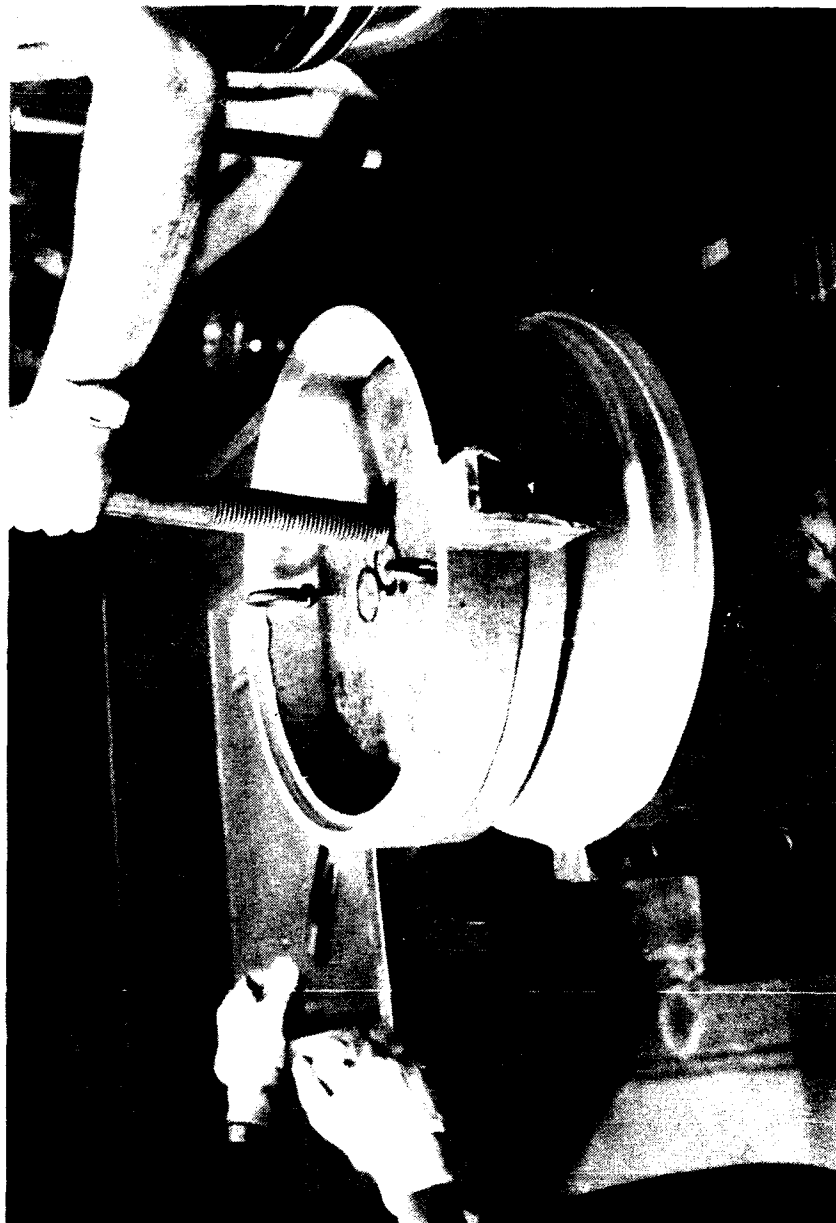
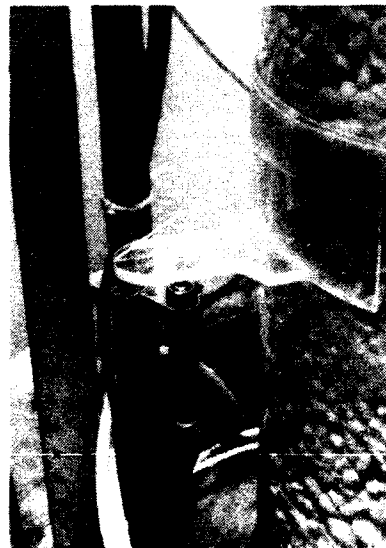


Figure B10. Compaction of top layer of specimen in 15-in. diam mold



a. Fully instrumented specimen



b. Close-up of LVDT instrumentation

Figure B11. Instrumented specimen to measure strain over full specimen height and within middle third of specimen

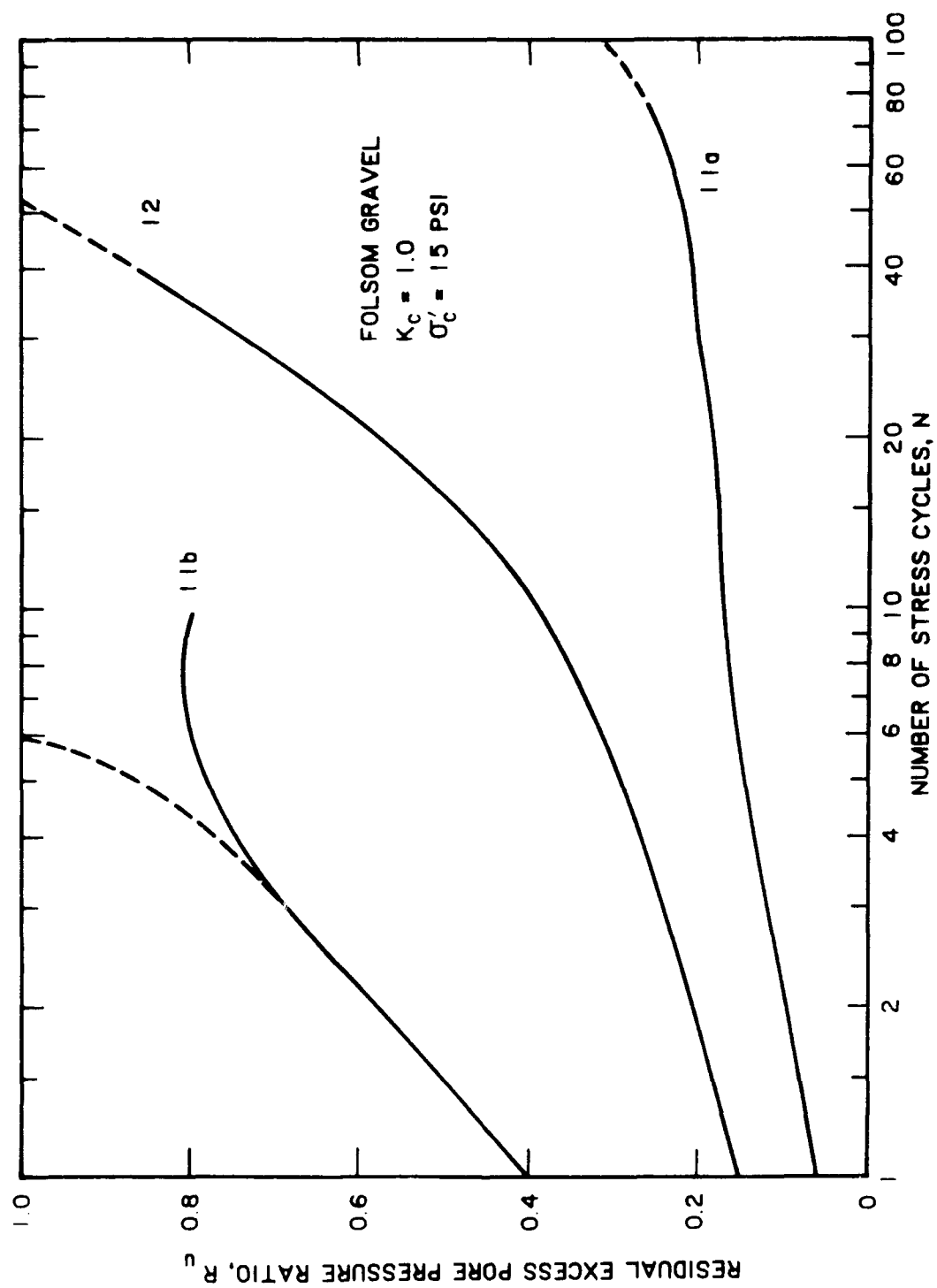


Figure B12. Development of residual excess pore pressure with each cycle

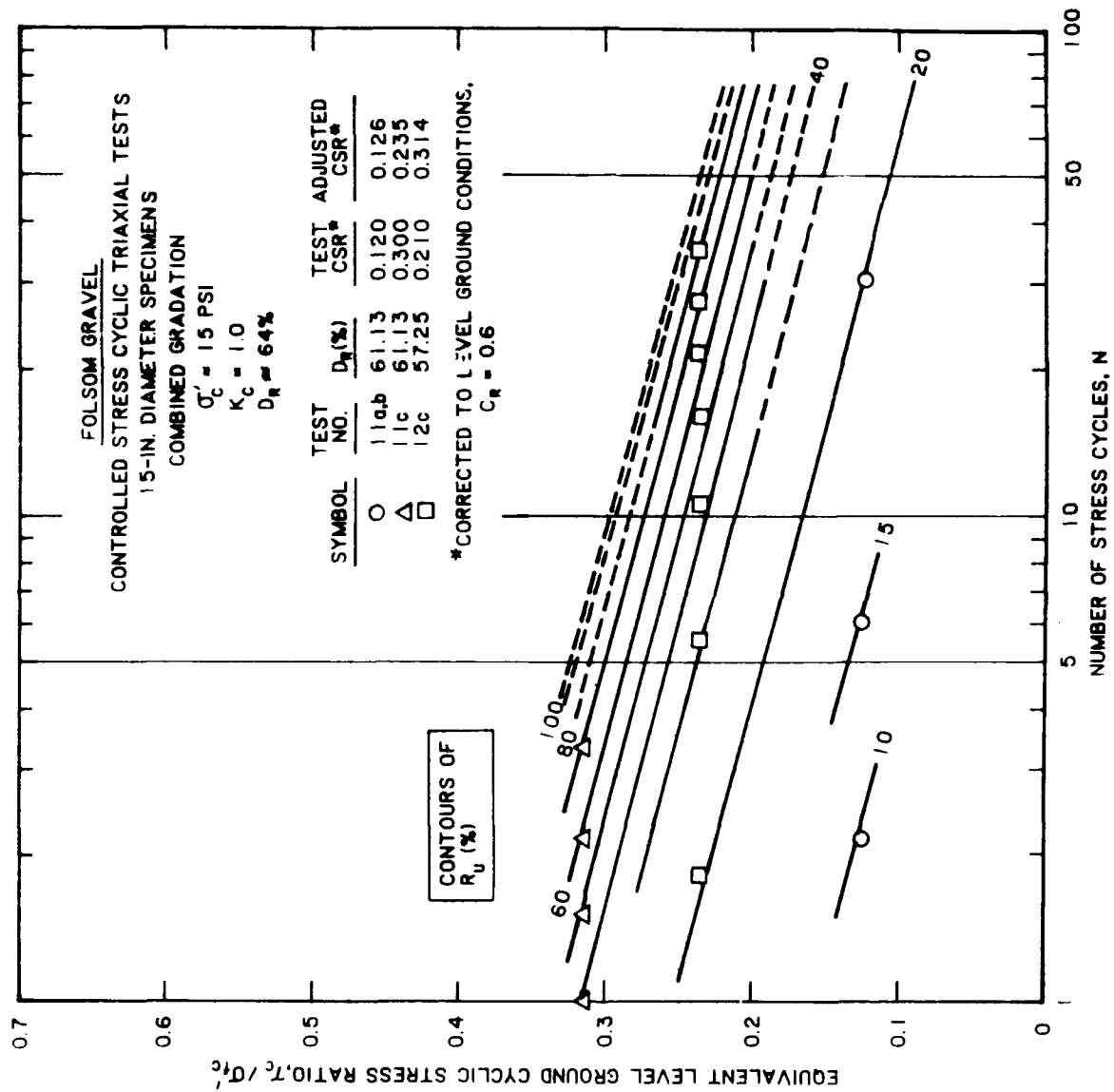


Figure B13. Contours of  $R_u$

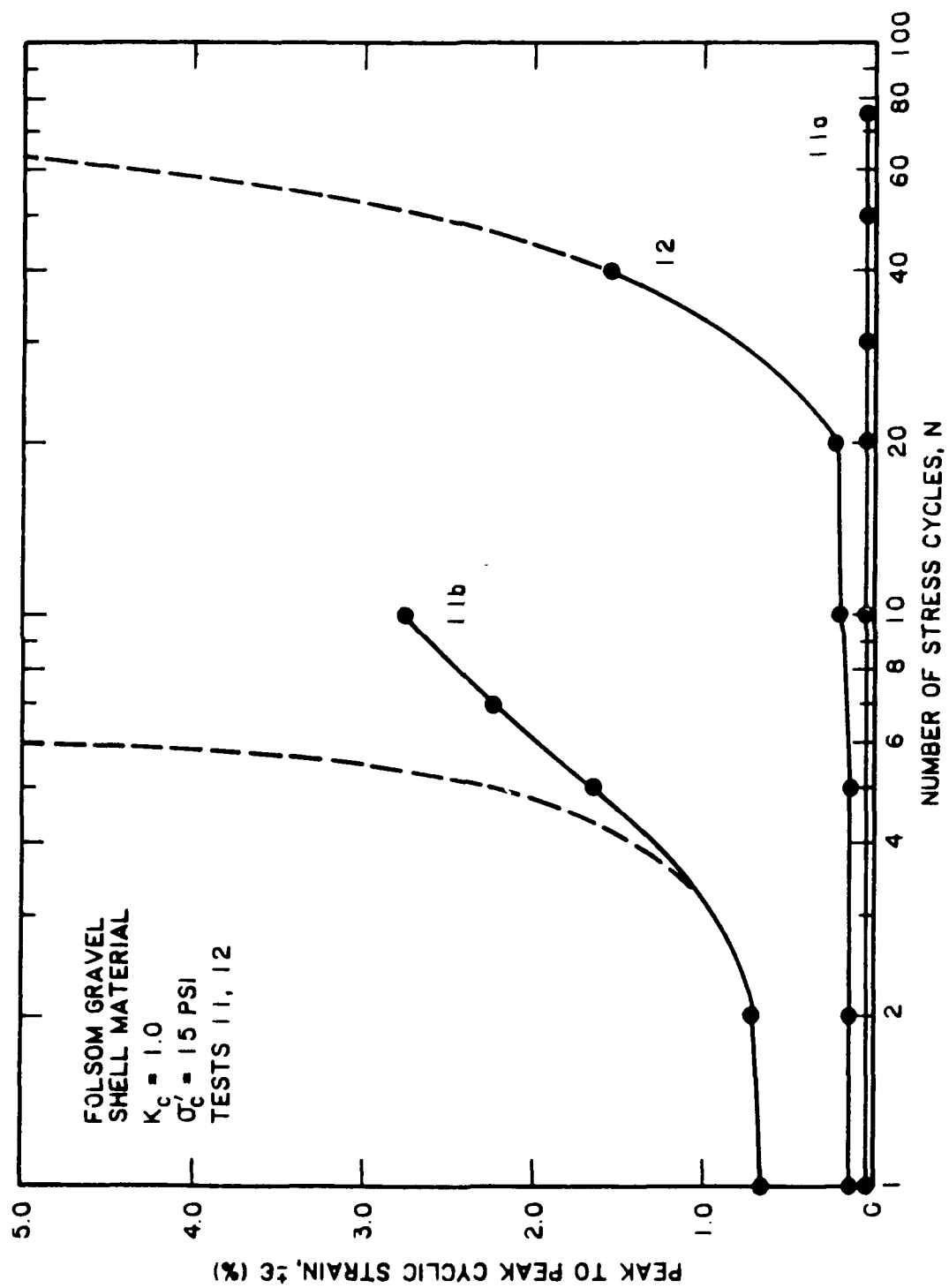


Figure B14. Development of cyclic strain with each stress cycle

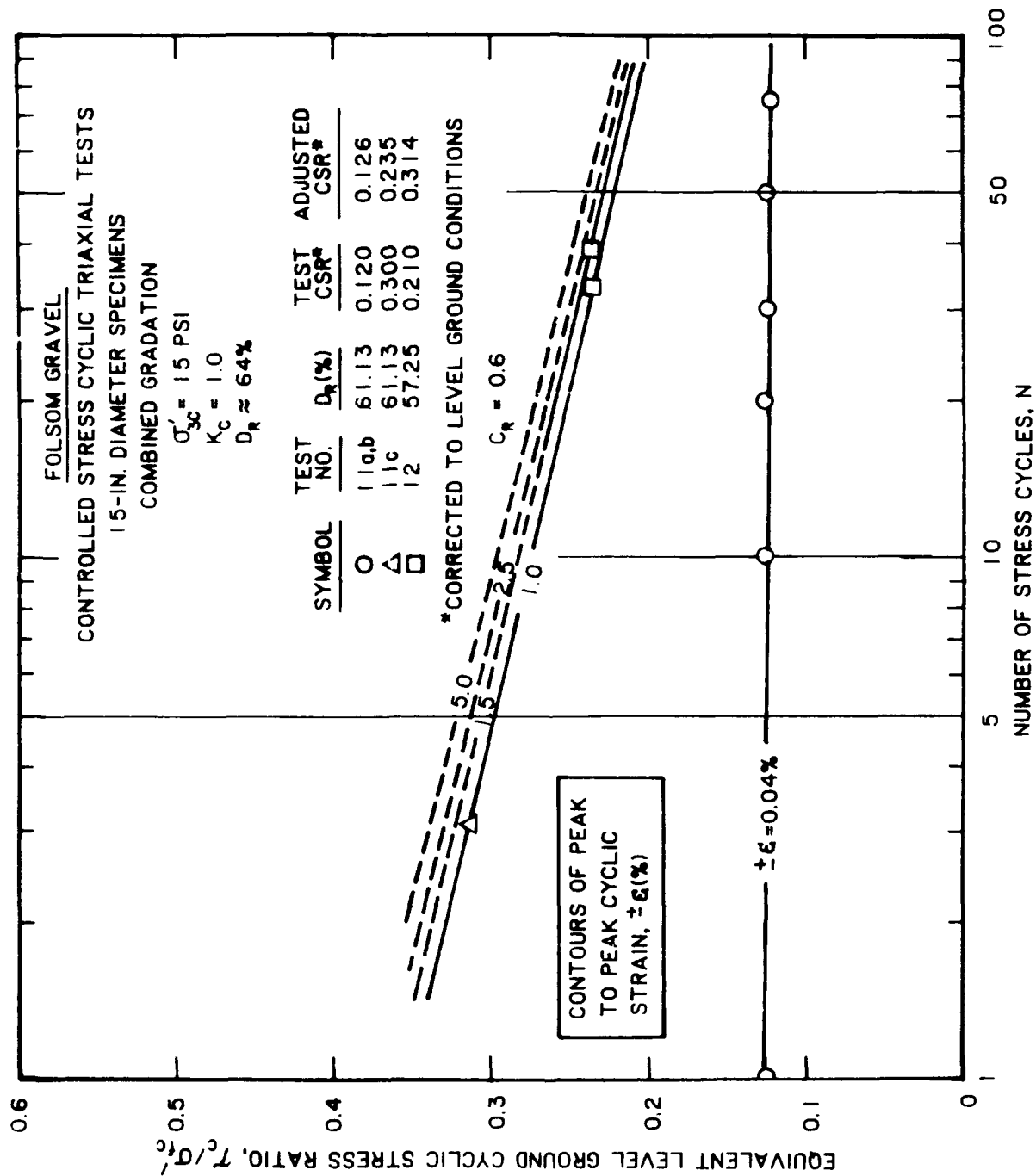


Figure B15. Contours of peak to peak cyclic strain



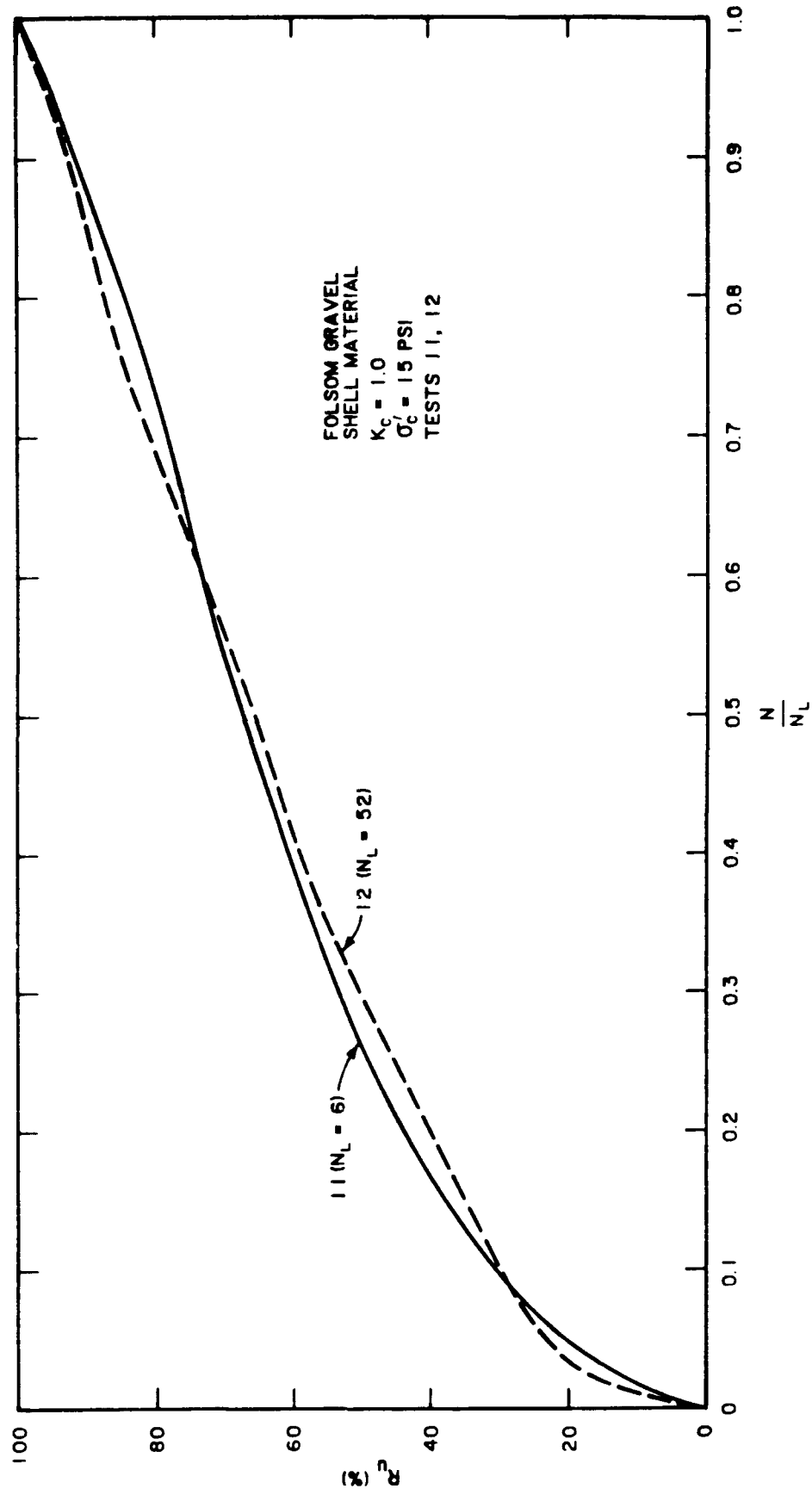


Figure B16. Residual excess pore pressure ratio versus normalized cycle number

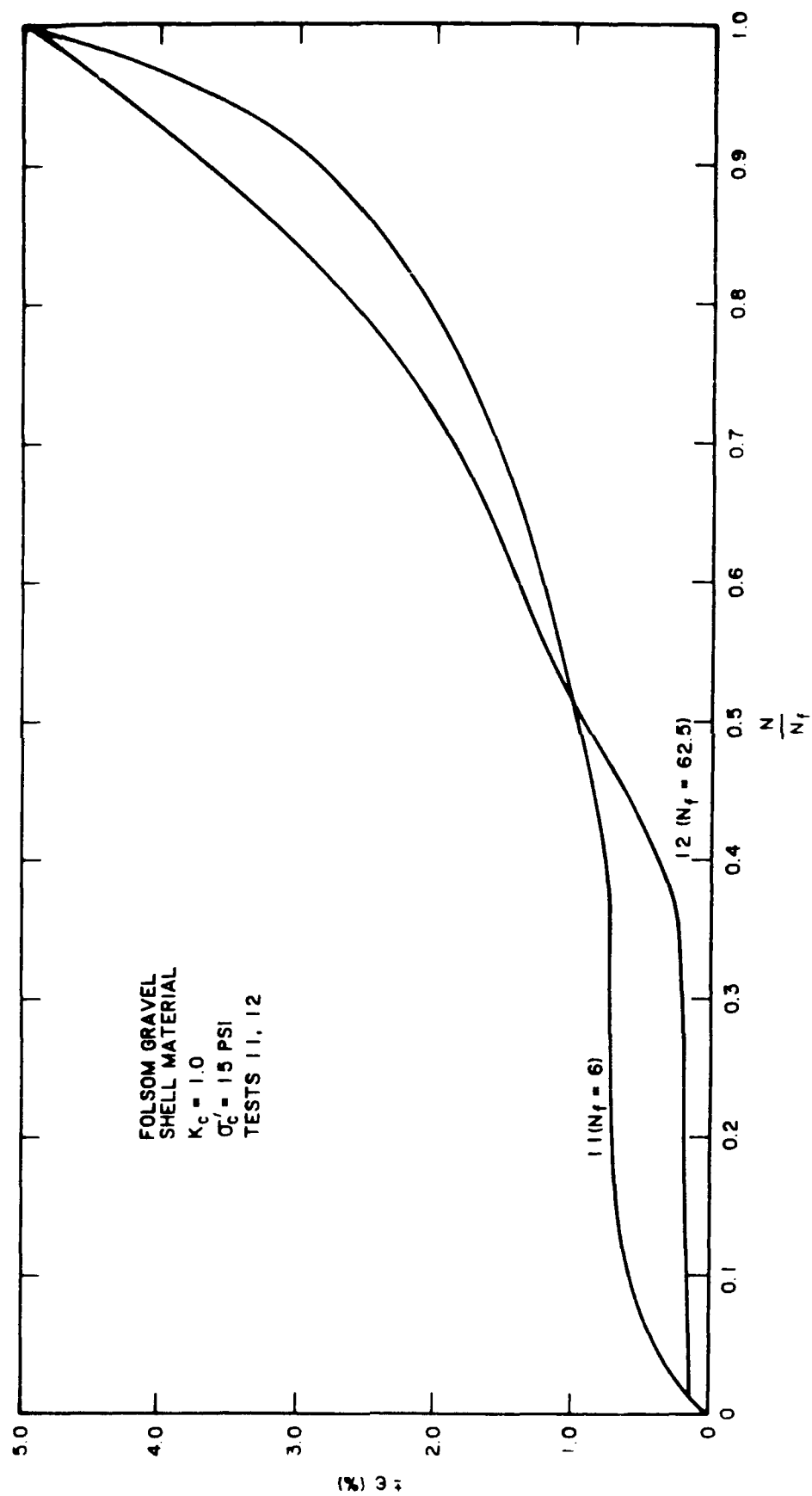


Figure B17. Peak to peak cyclic strain versus normalized stress cycle (Note:  $N_f$  = cycle at which  $\pm \epsilon = 5$  percent)

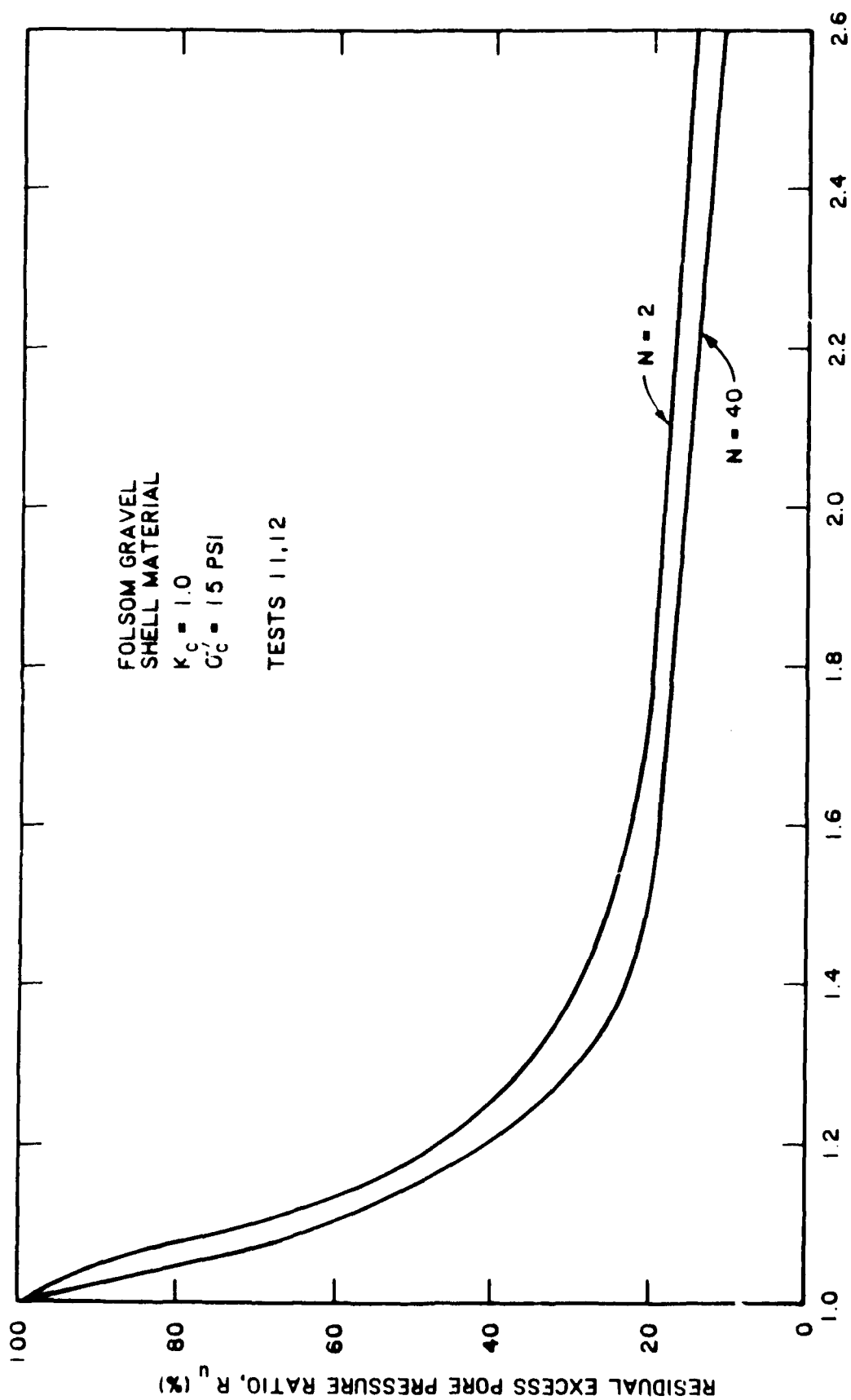


Figure B18. Relationship between residual excess pore pressure ratio and safety factor against  $R_u = 100$  or  $\pm\epsilon = 5$  percent

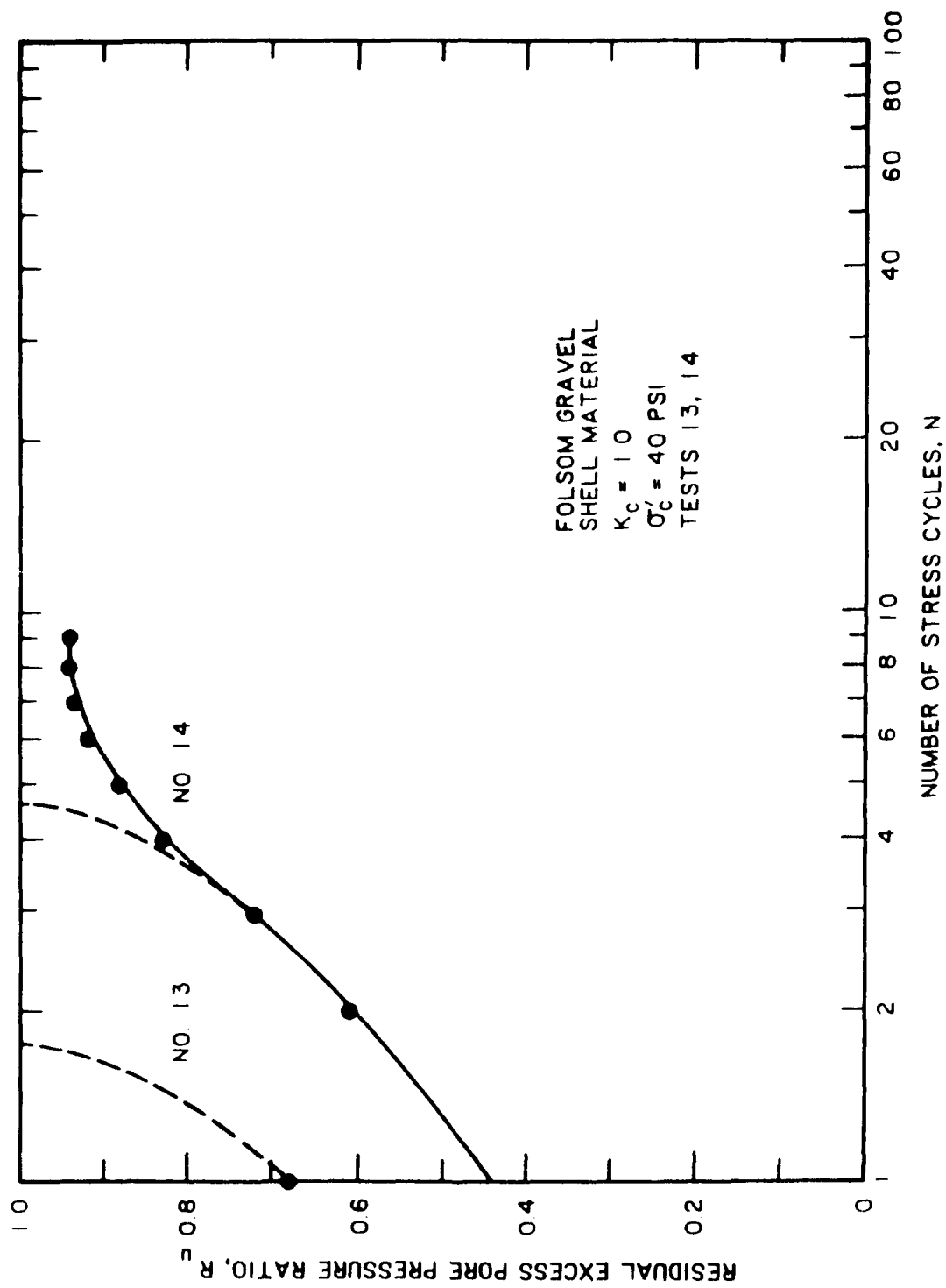


Figure B19. Development of residual excess pore pressure with each stress cycle

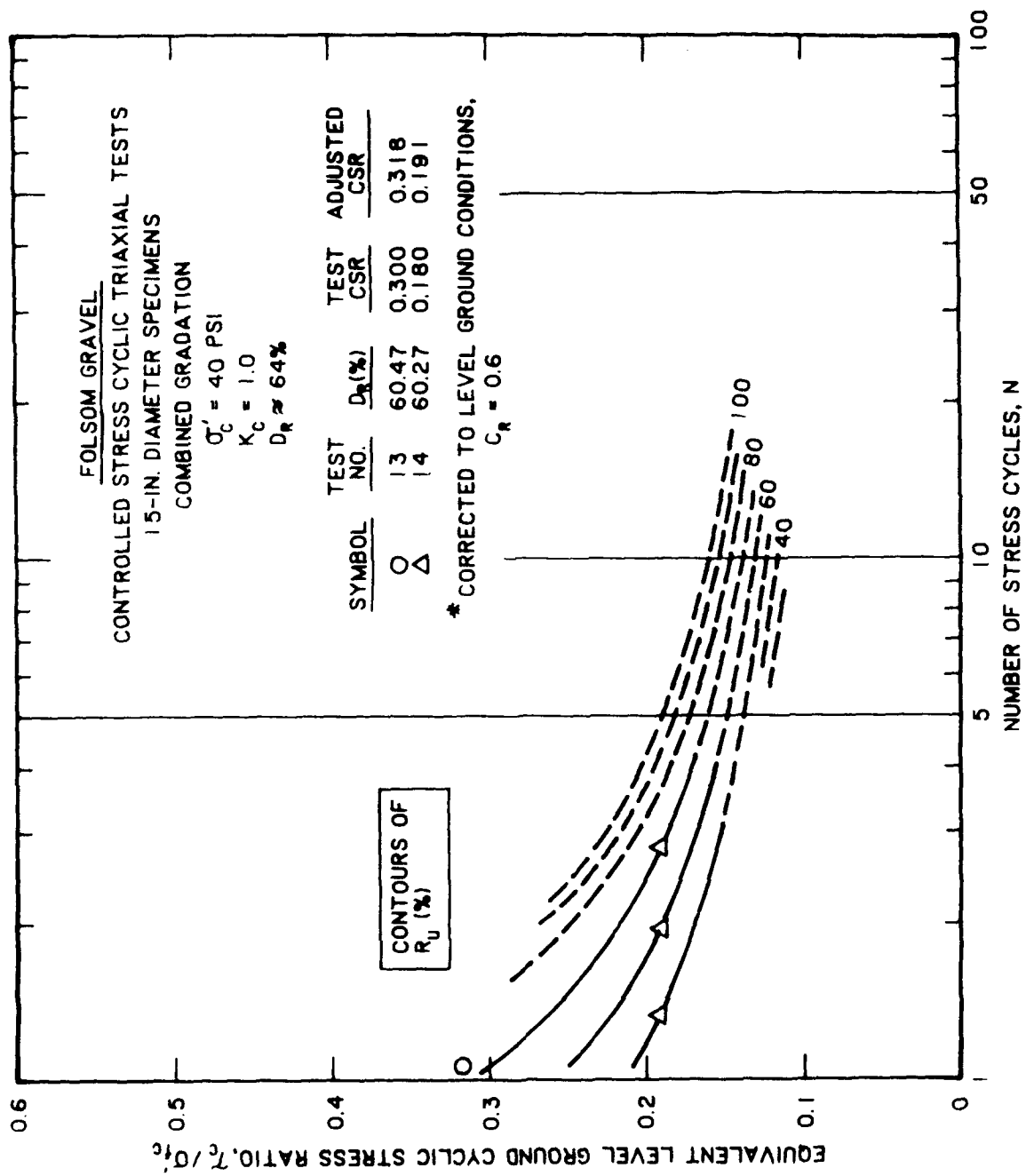


Figure B20. Contours of residual excess pore pressure ratio

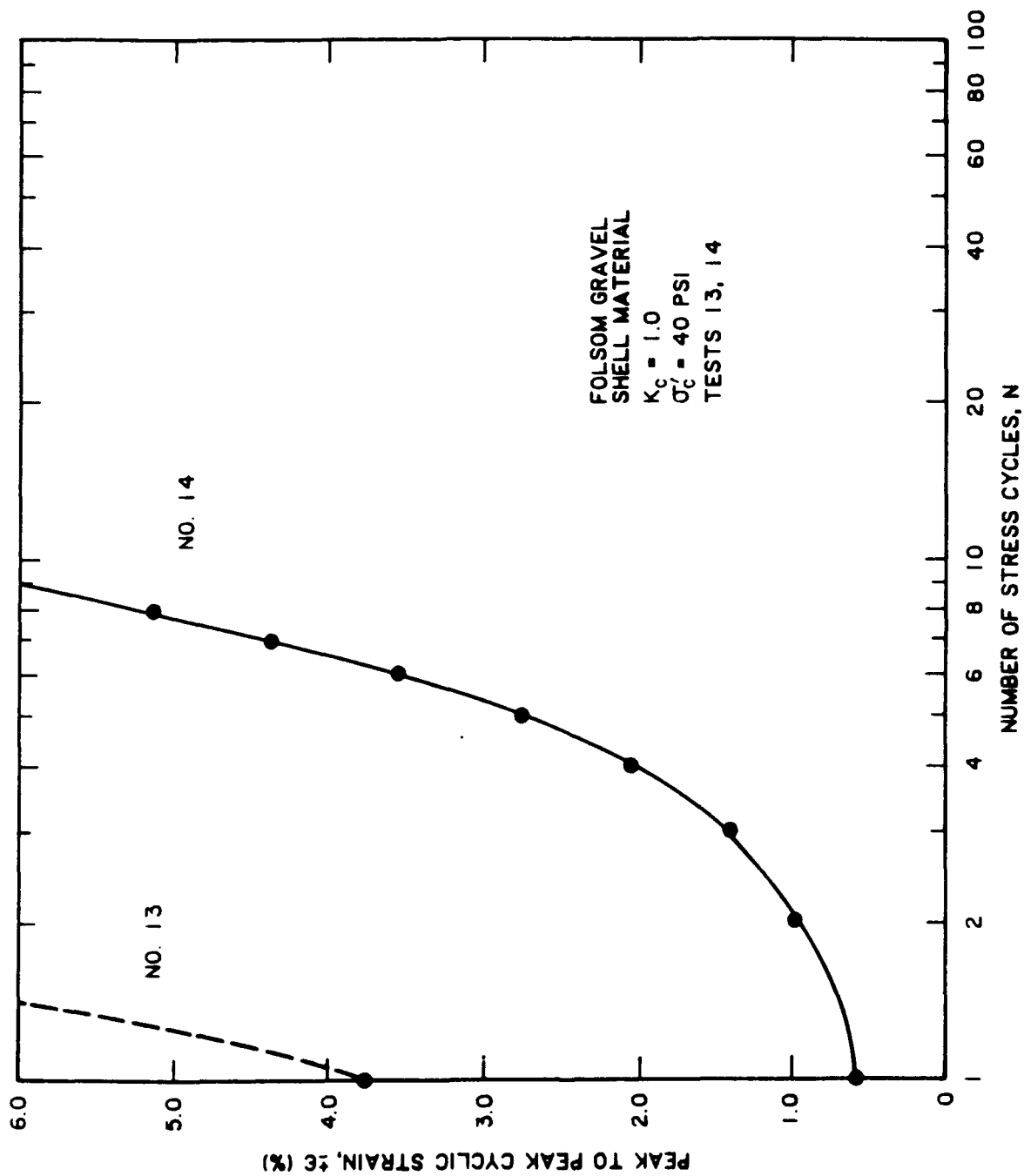


Figure B21. Development of peak to peak cyclic strain with each stress cycle

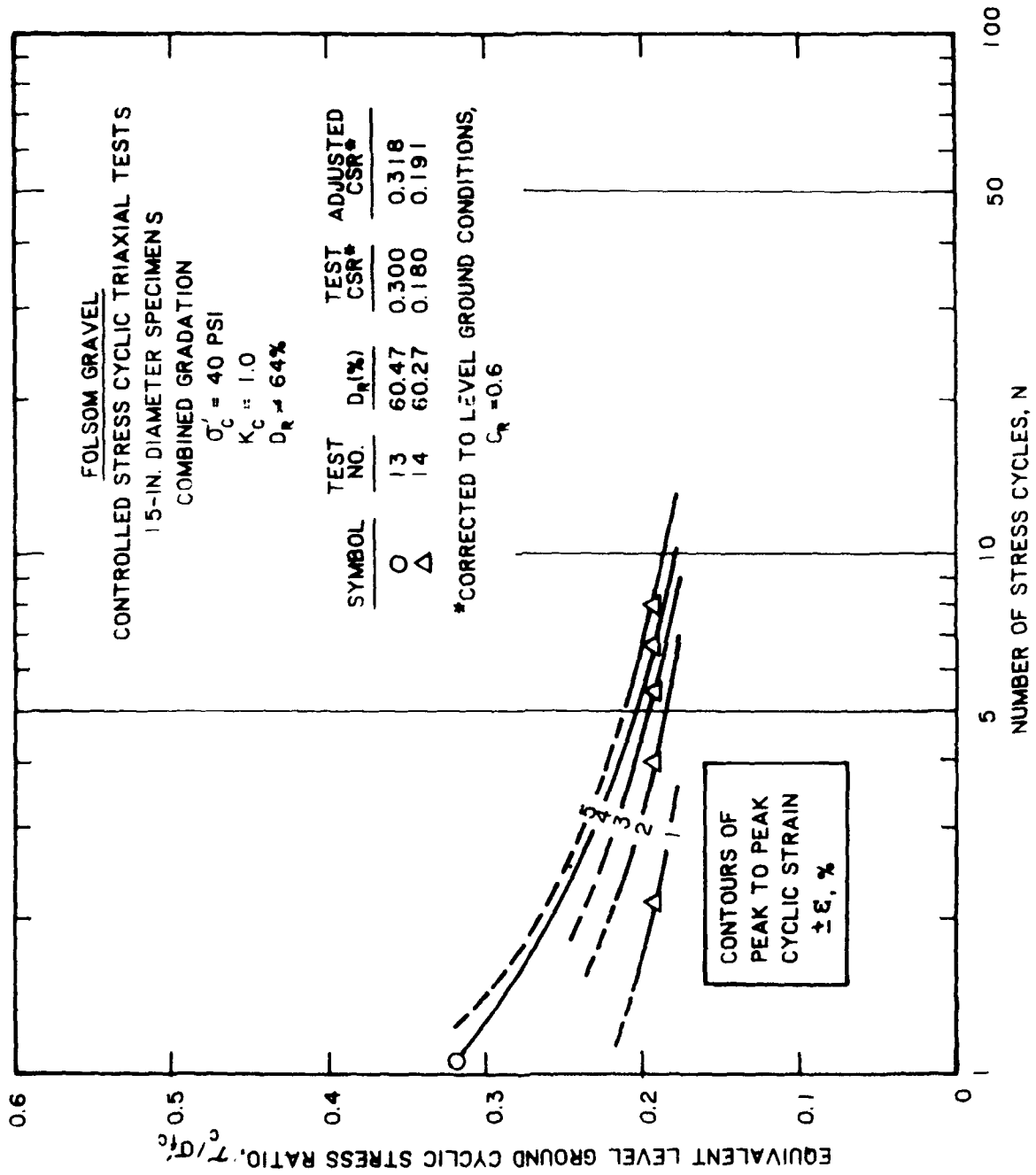


Figure B22. Contours of peak to peak cyclic strain

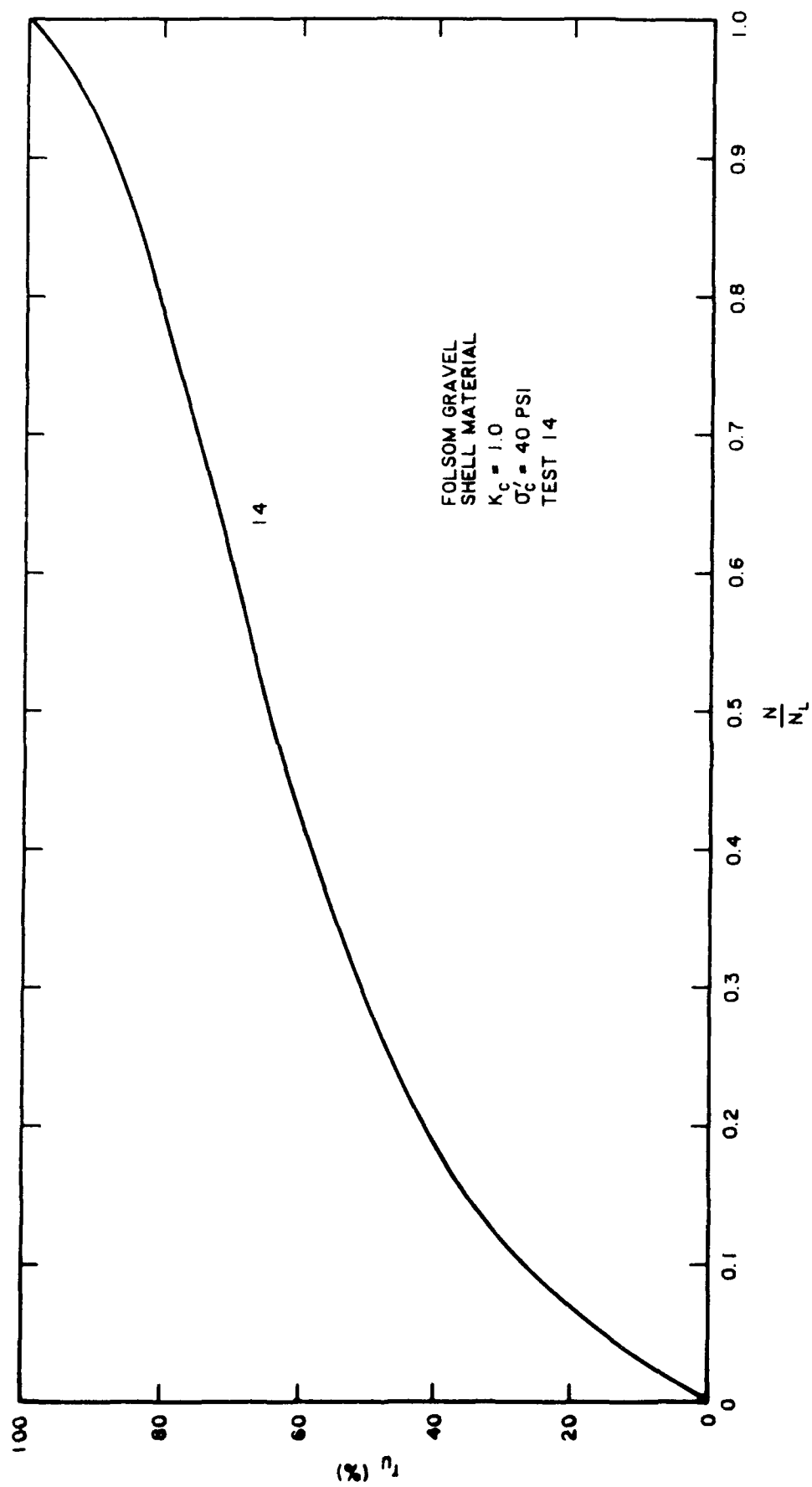


Figure B23. Residual excess pore pressure ratio versus normalized stress cycle



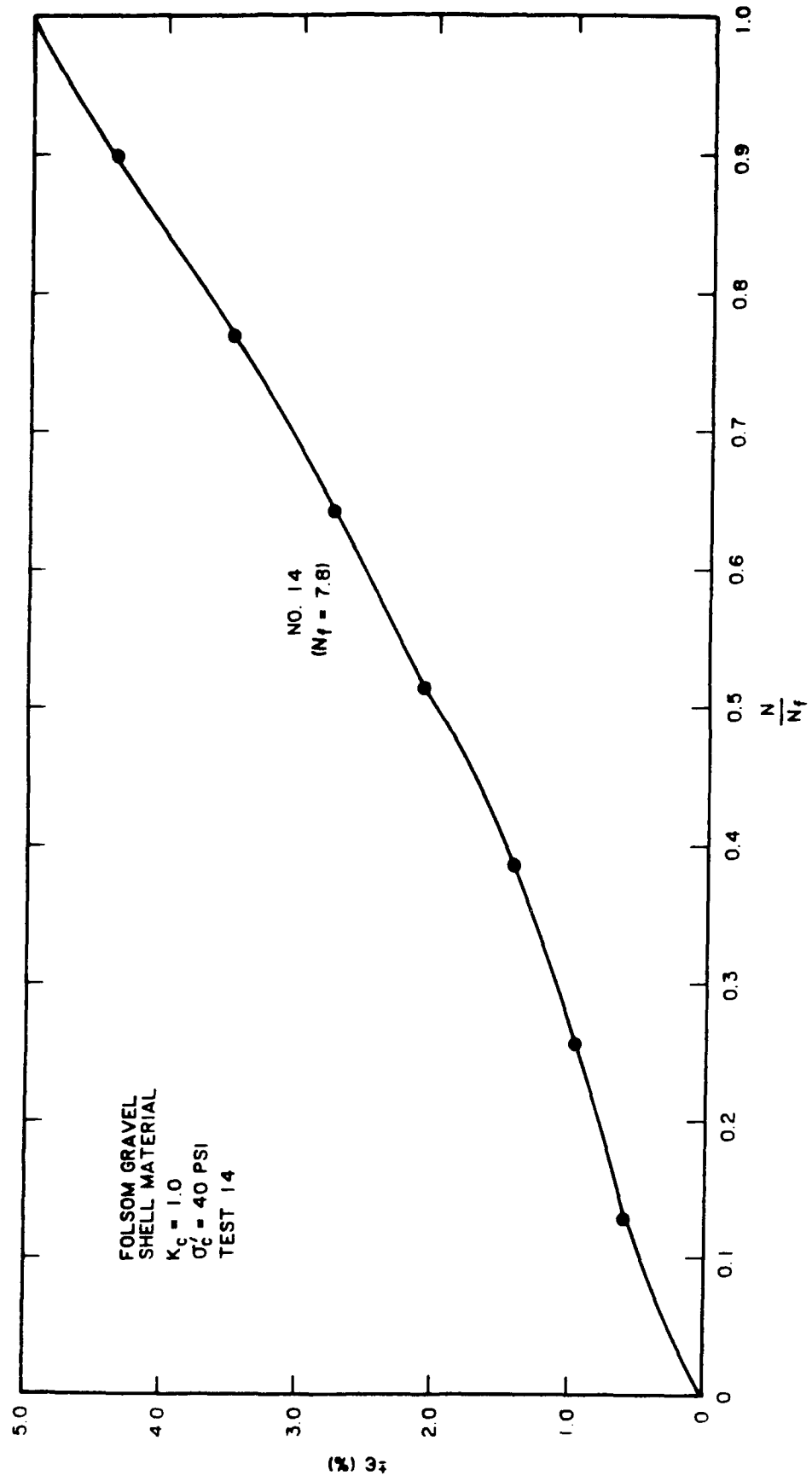


Figure B24. Peak to peak cyclic strain versus normalized stress cycle (Note:  $N_f$  = cycle at which  $\pm \epsilon = 5$  percent)

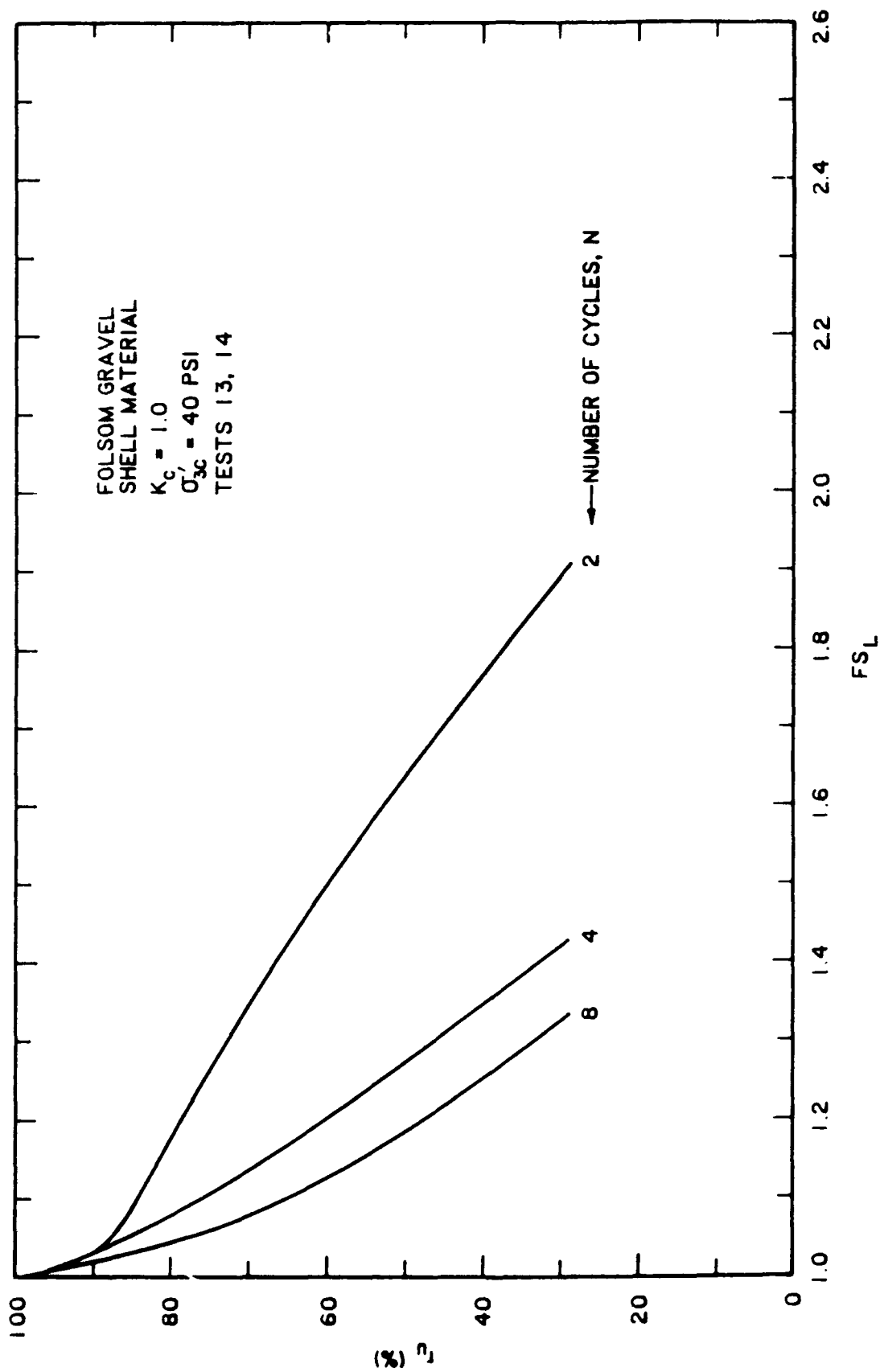


Figure B25. Relationship between residual excess pore pressure ratio and factor of safety against liquefaction

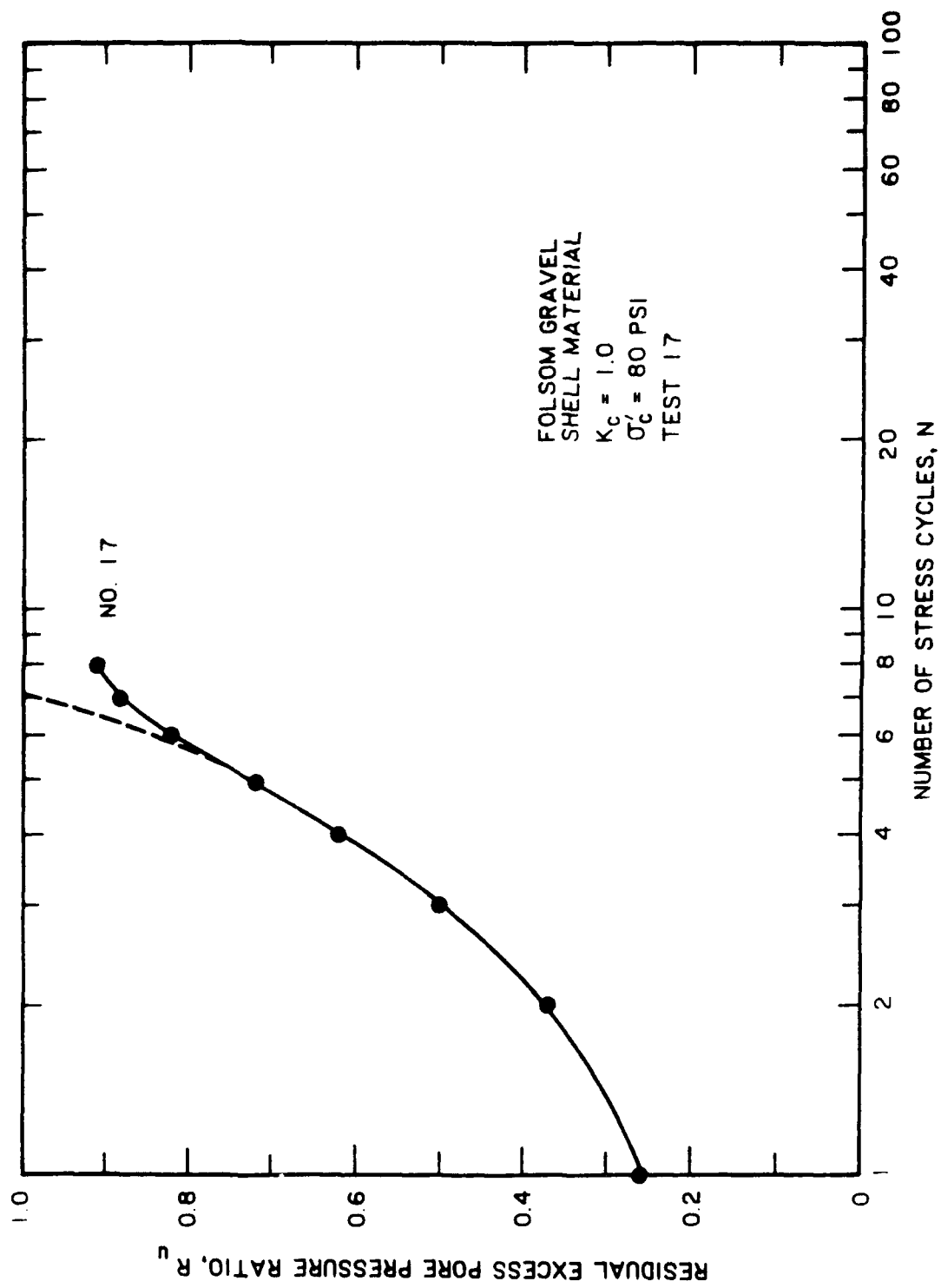


Figure B26. Development of residual excess pore pressure with each stress cycle

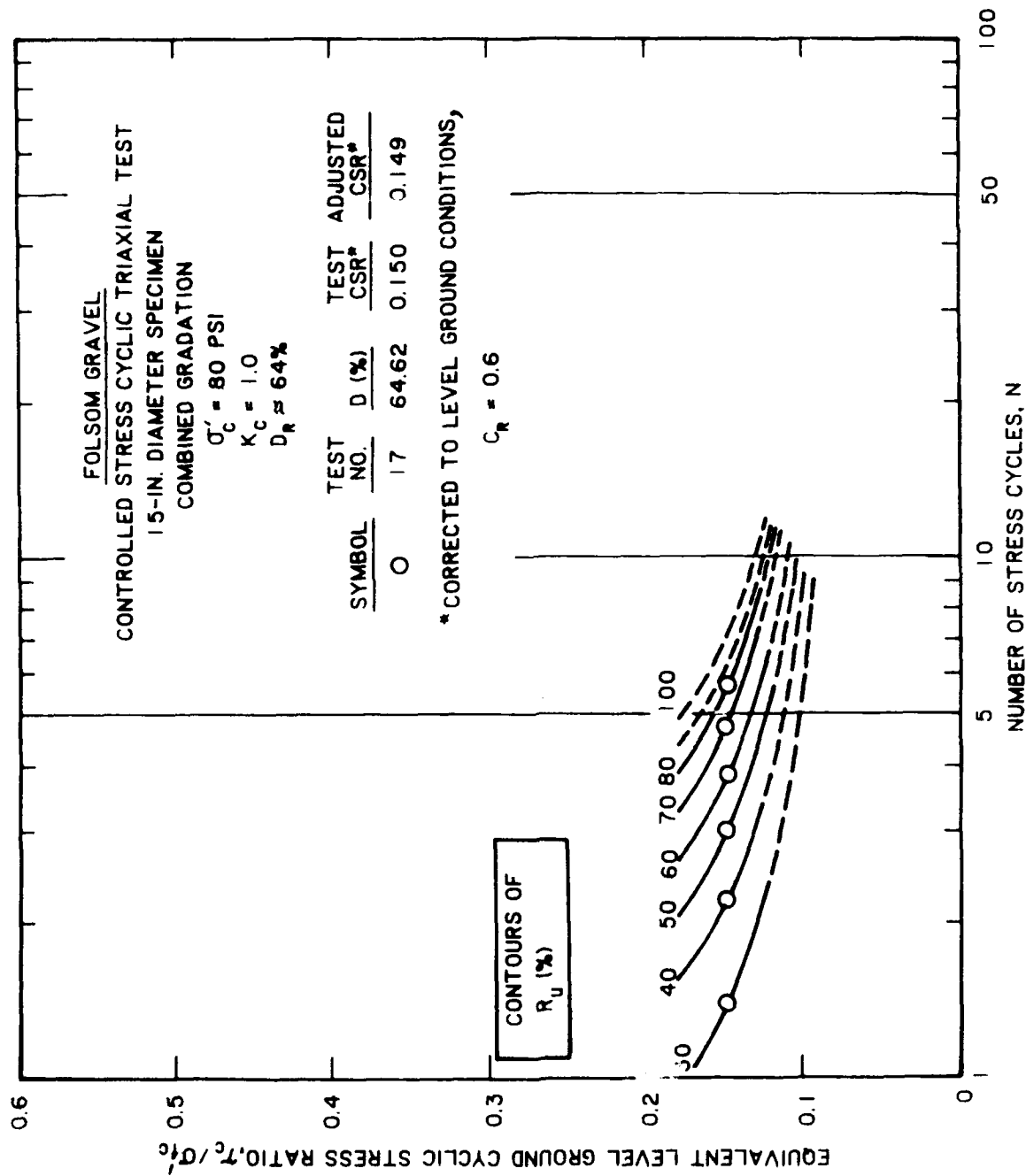


Figure B27. Contours of residual excess pore pressure ratio

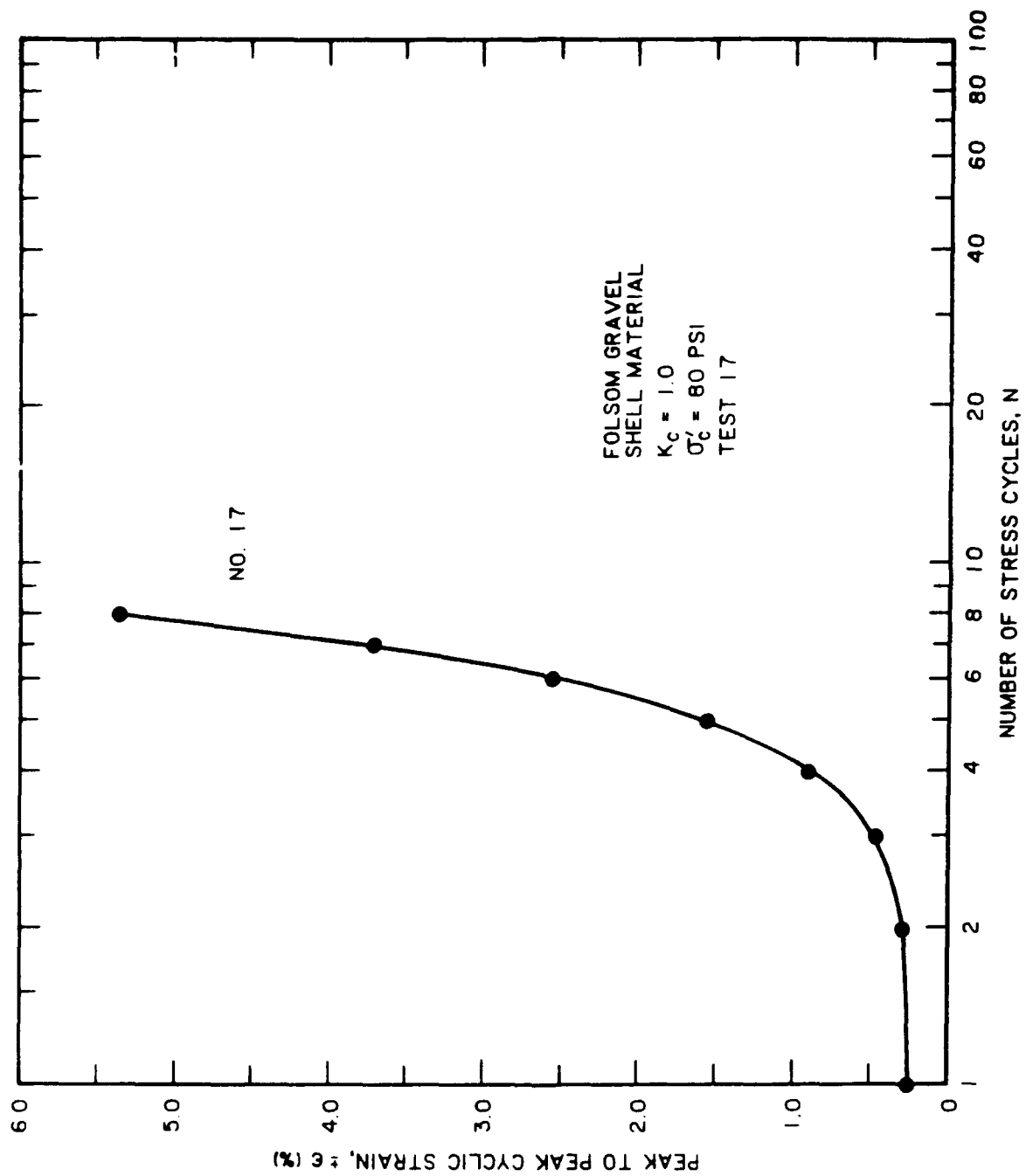


Figure B28. Development of peak to peak cyclic strain with each stress cycle

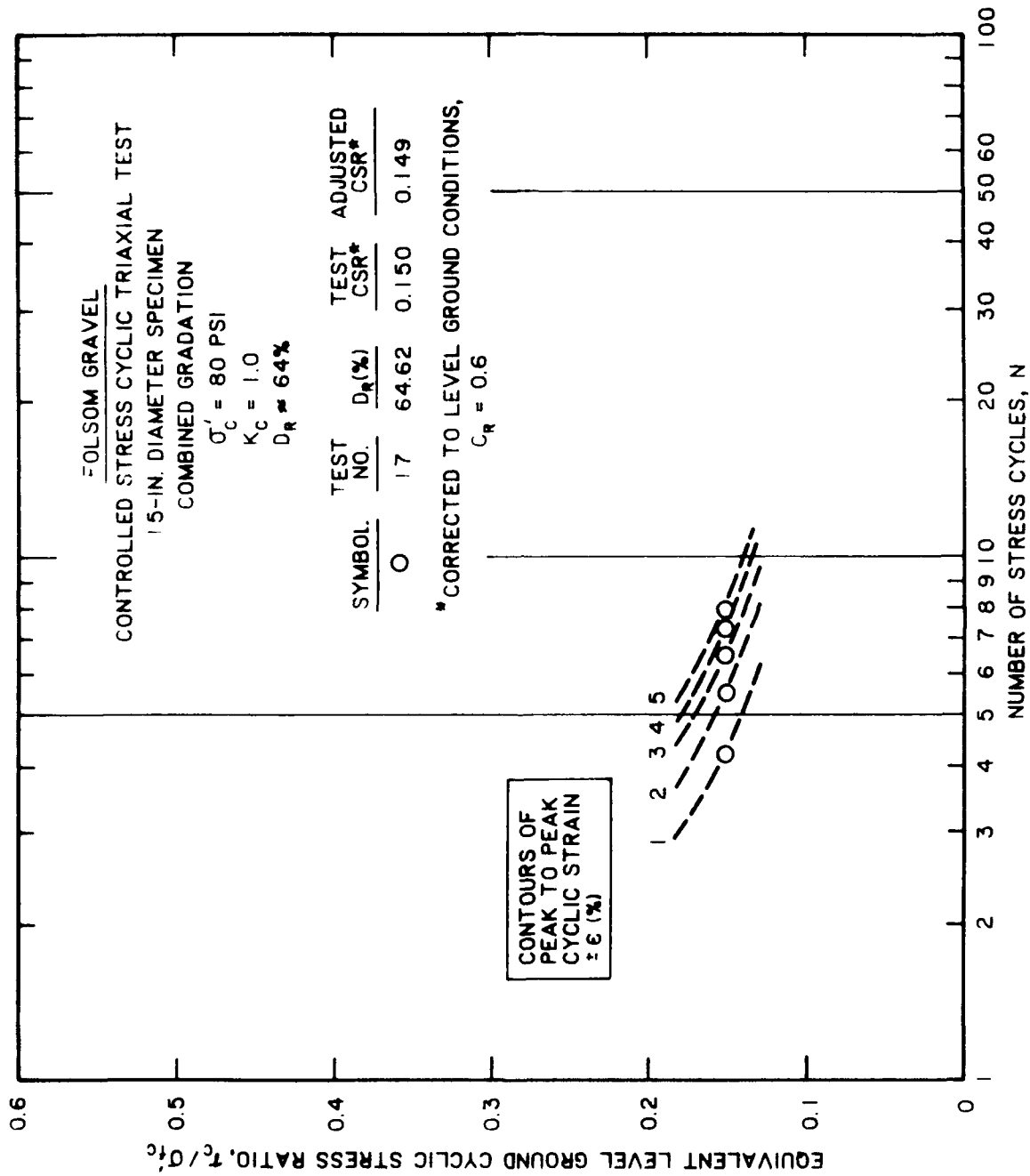


Figure B29. Contours of peak to peak cyclic strain

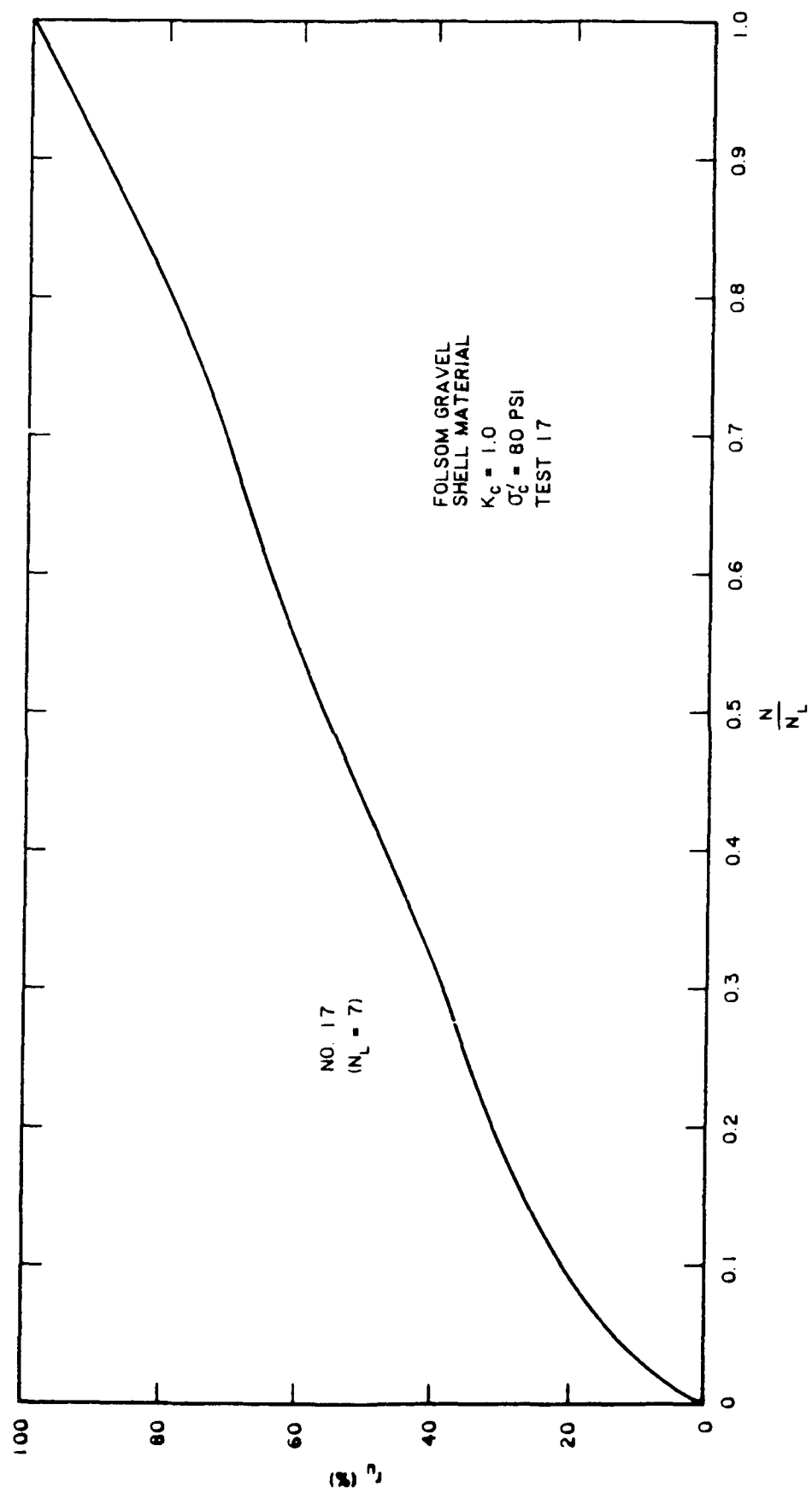


Figure B30. Residual excess pore pressure ratio versus normalized stress cycle

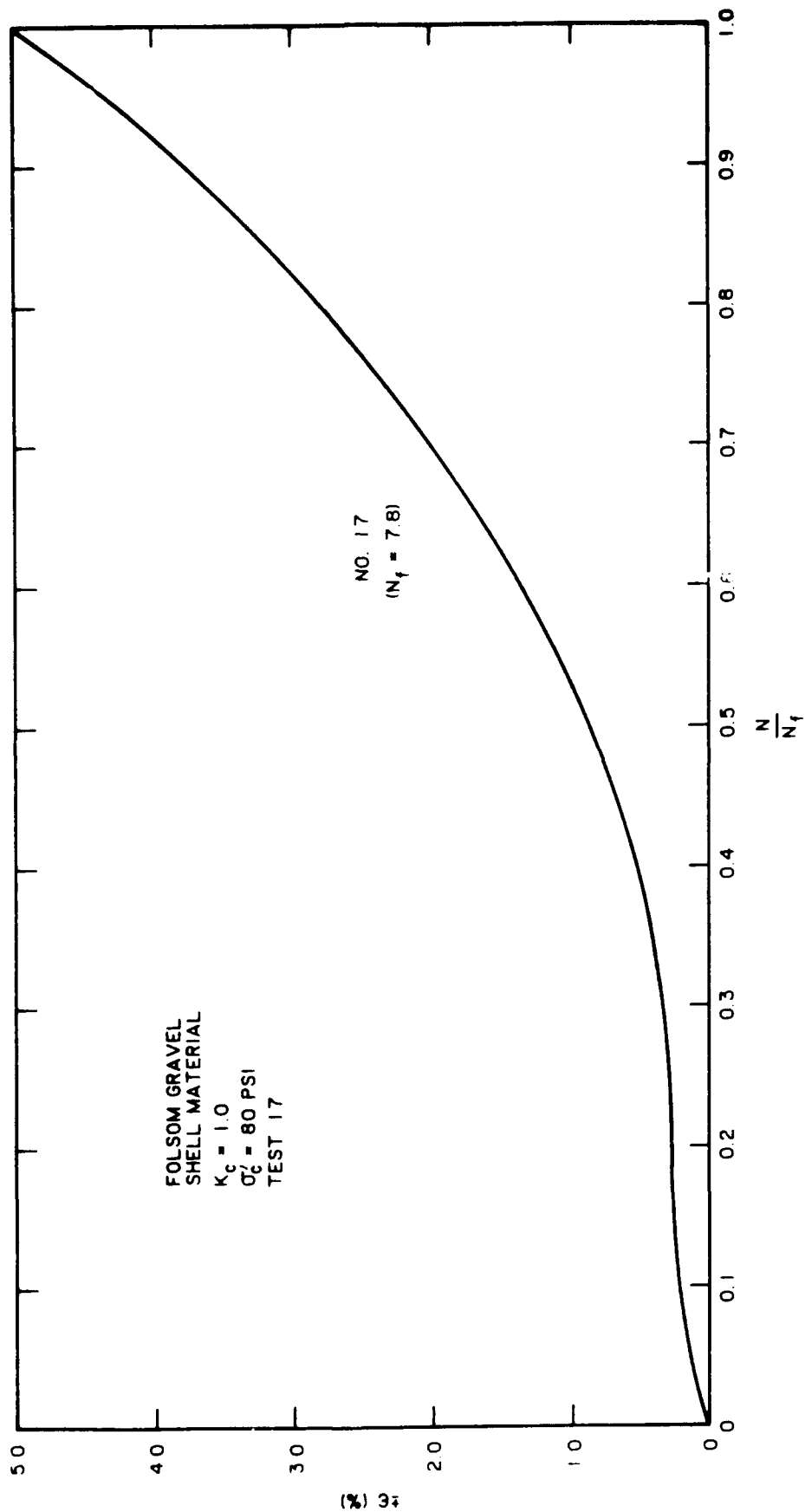


Figure B31. Peak to peak cyclic strain versus normalized stress cycle (Note:  $N_f$  = cycle at which  $\pm\epsilon = 5$  percent)



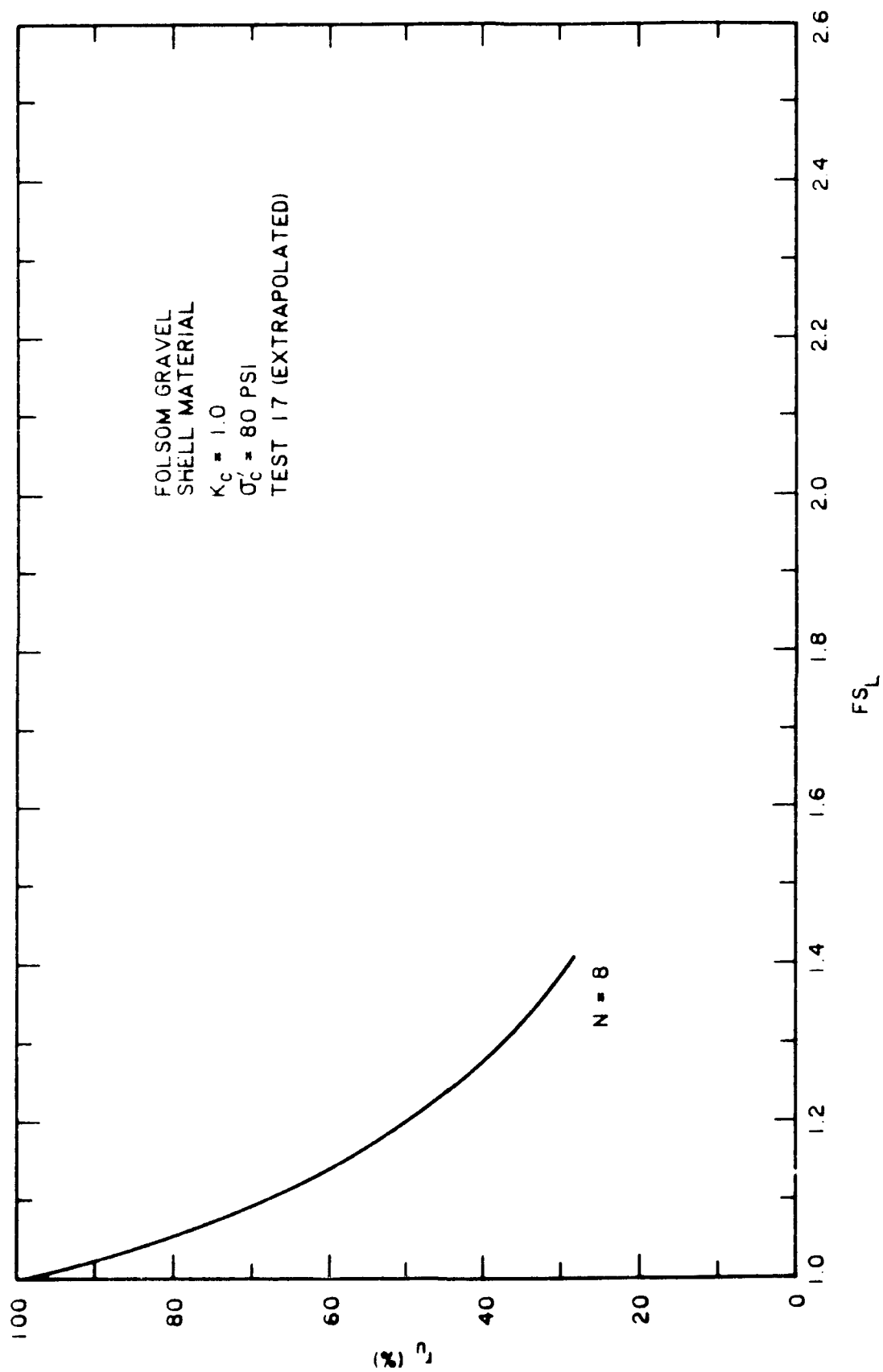


Figure B32. Relationship between residual excess pore pressure and factor of safety against liquefaction

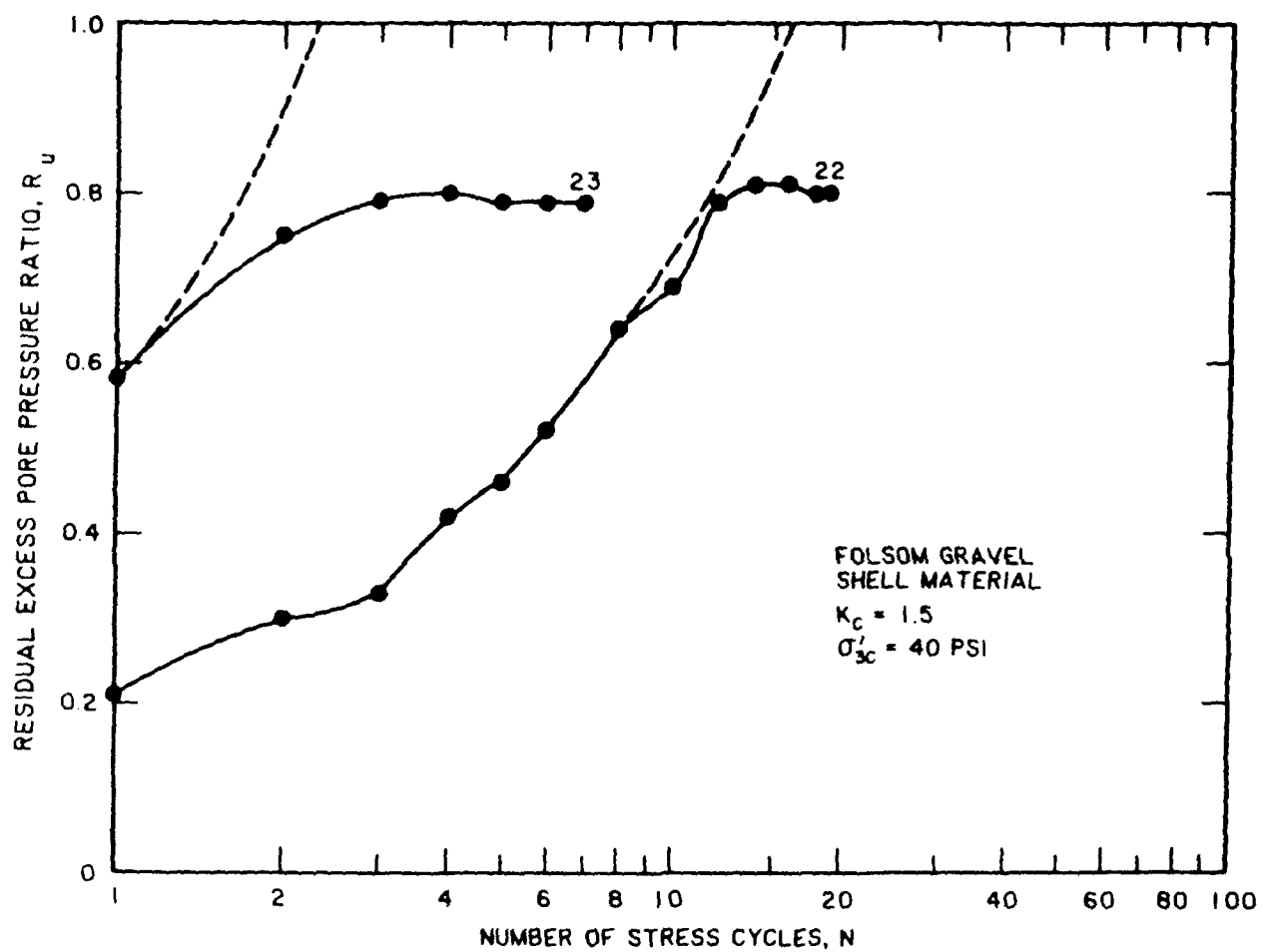


Figure B33. Development of residual excess pore pressure with each stress cycle

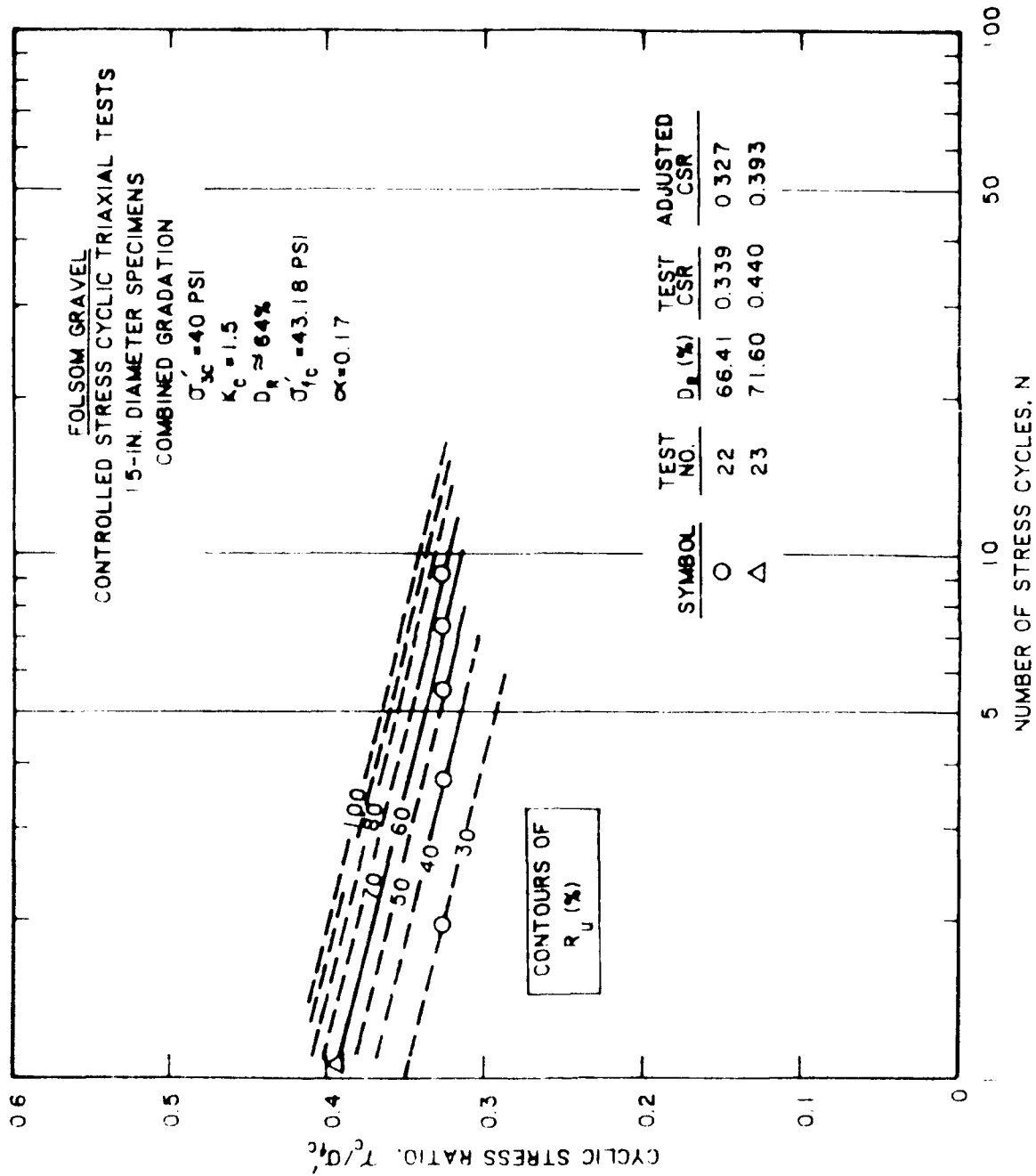


Figure B34. Contours of residual excess pore pressure ratio

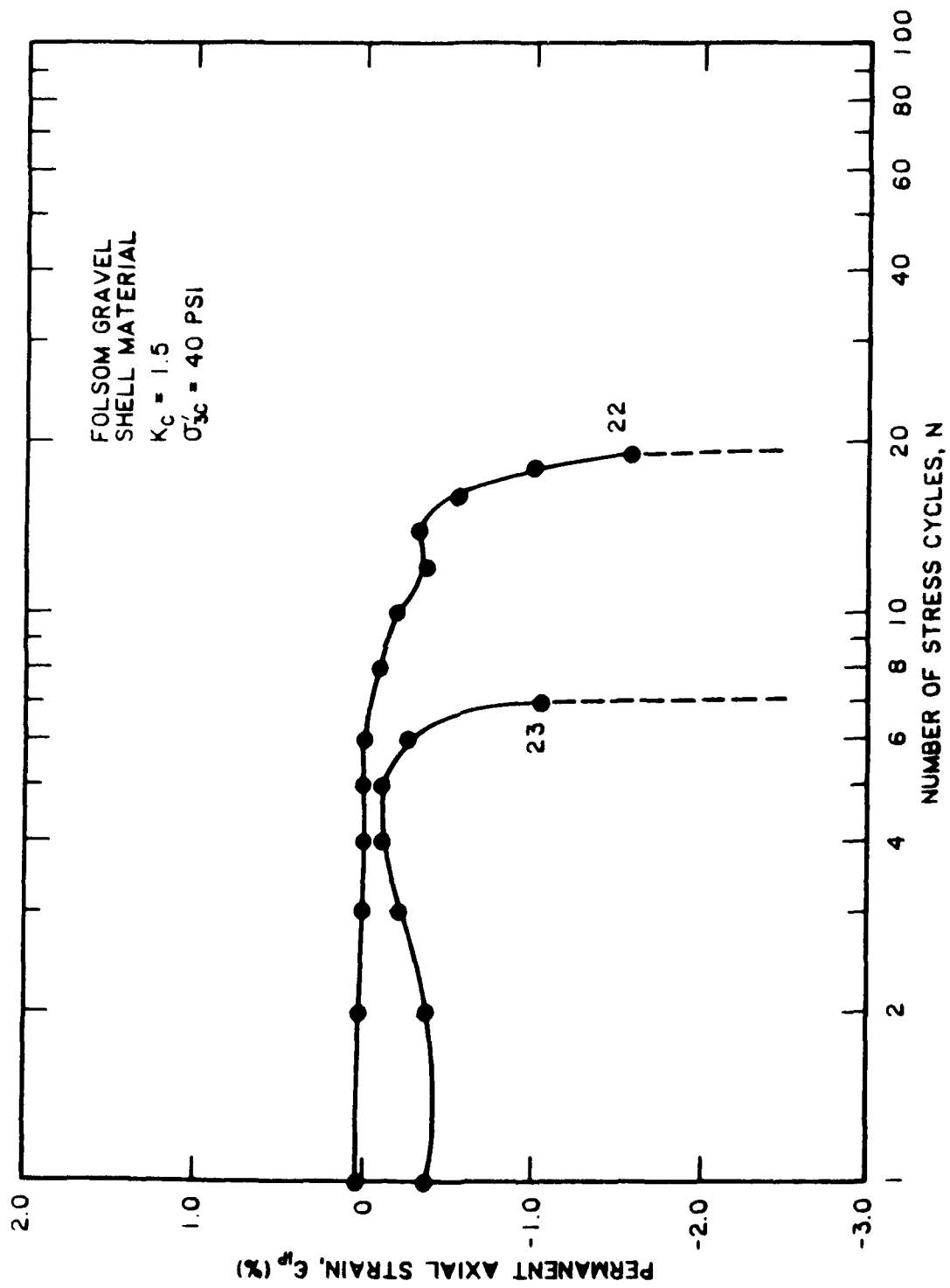


Figure B35. Development of permanent axial strain with each stress cycle

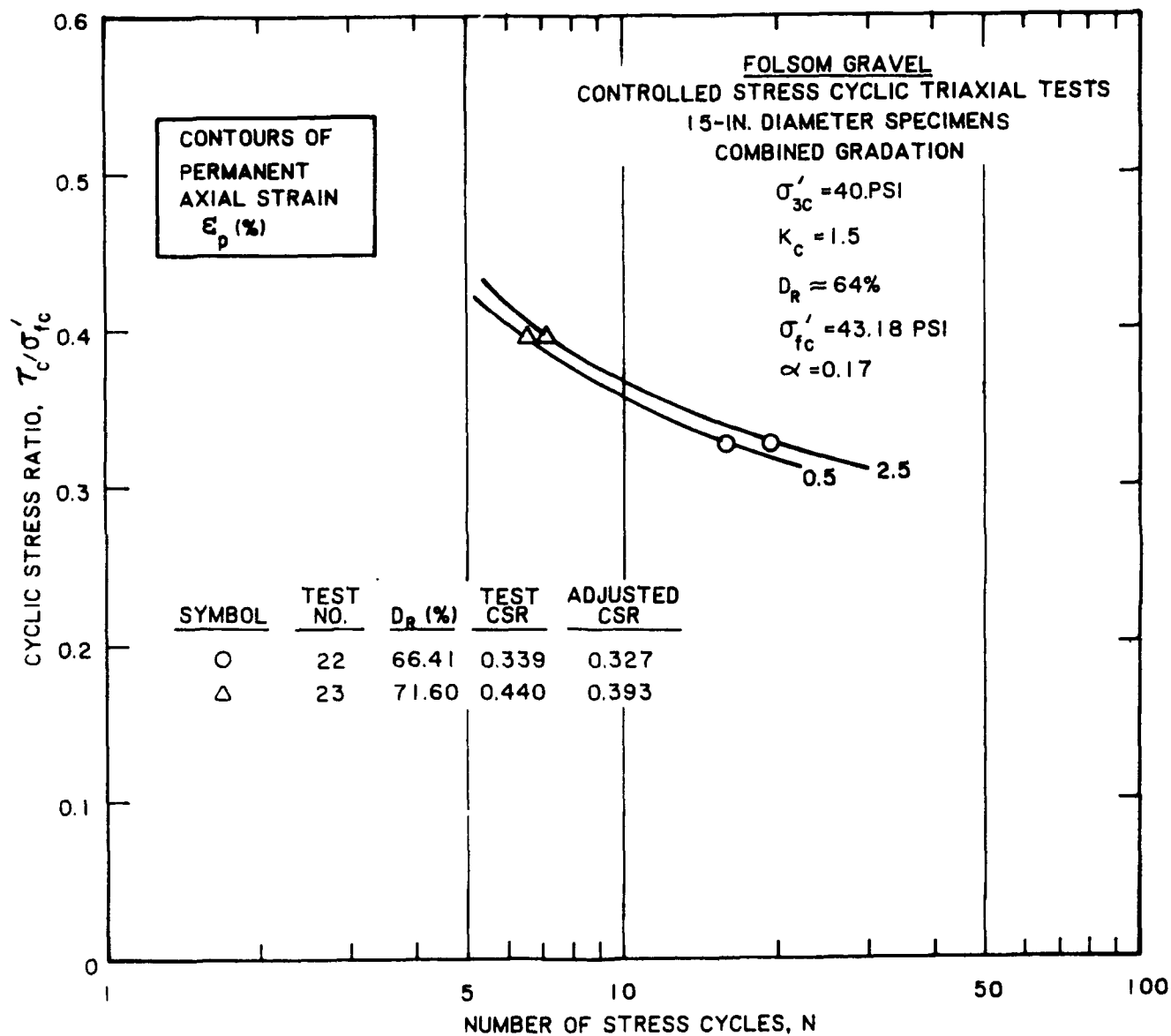


Figure B36. Contours of permanent axial strain

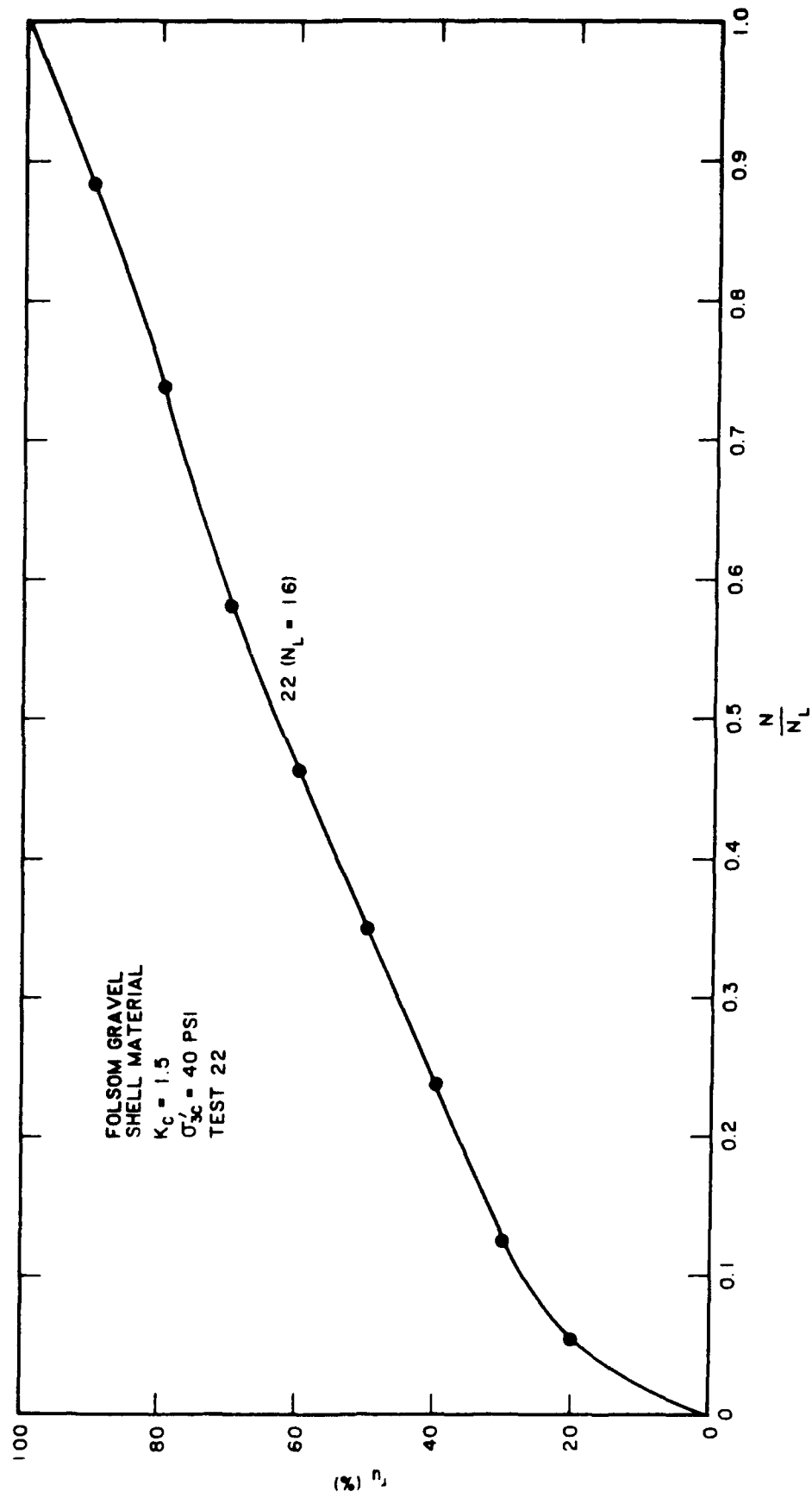


Figure B37. Residual excess pore pressure ratio versus normalized stress cycle

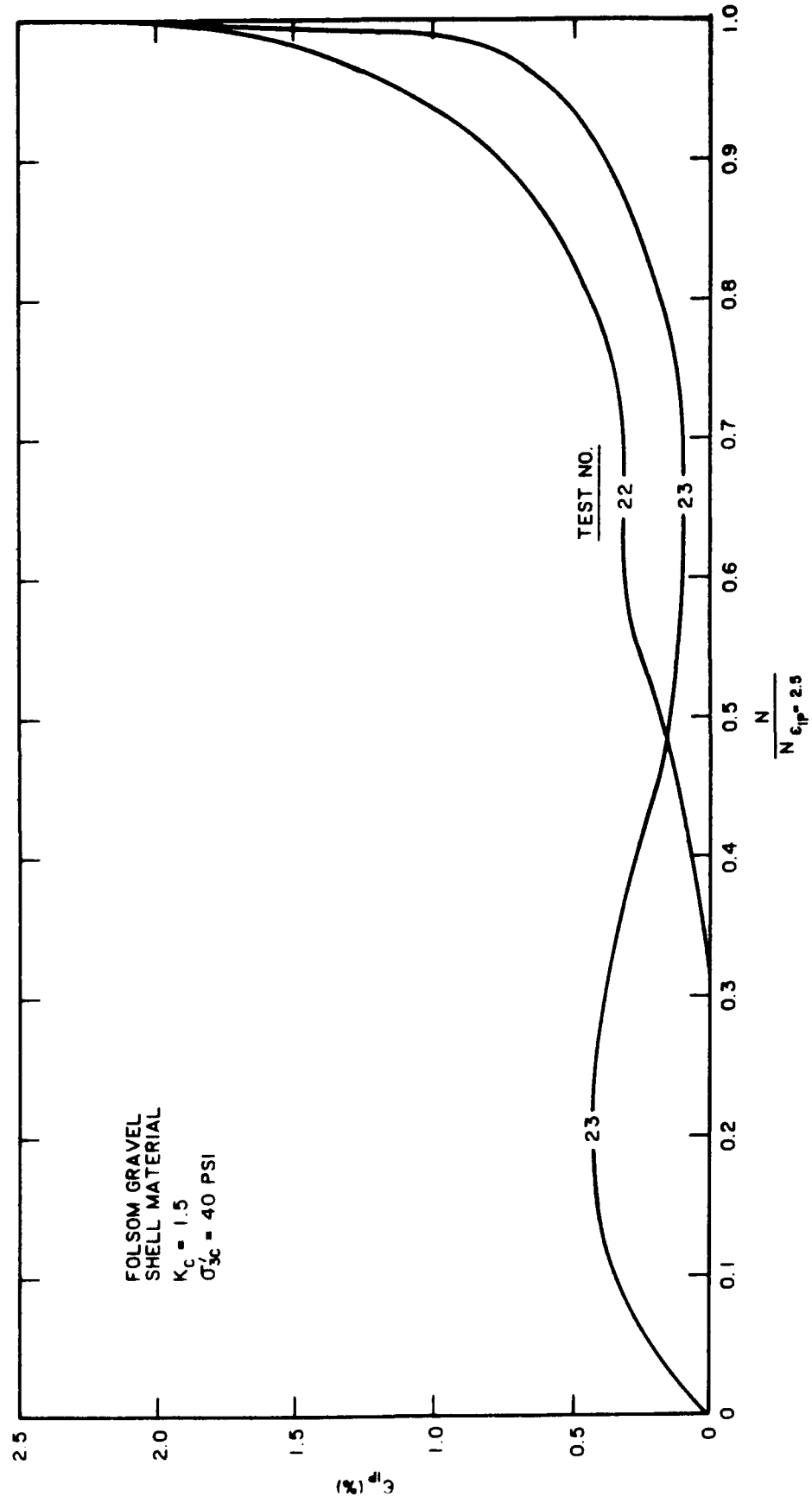


Figure B38. Permanent axial strain versus normalized stress cycle (Note:  $N_f =$  cycle at which  $\epsilon_{1p} = 2.5$  percent)

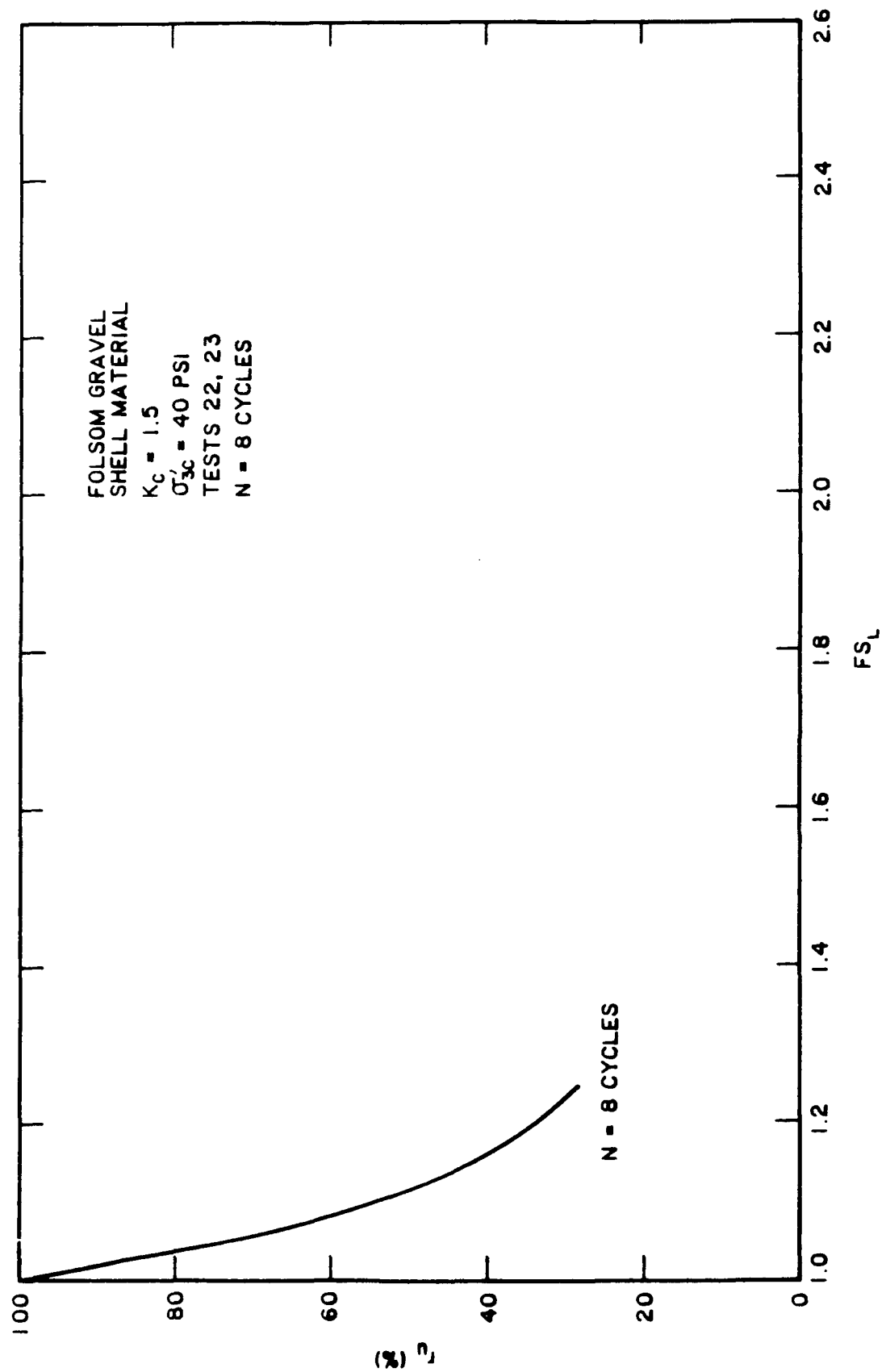


Figure B39. Relationship between residual excess pore pressure ratio and safety factor against liquefaction



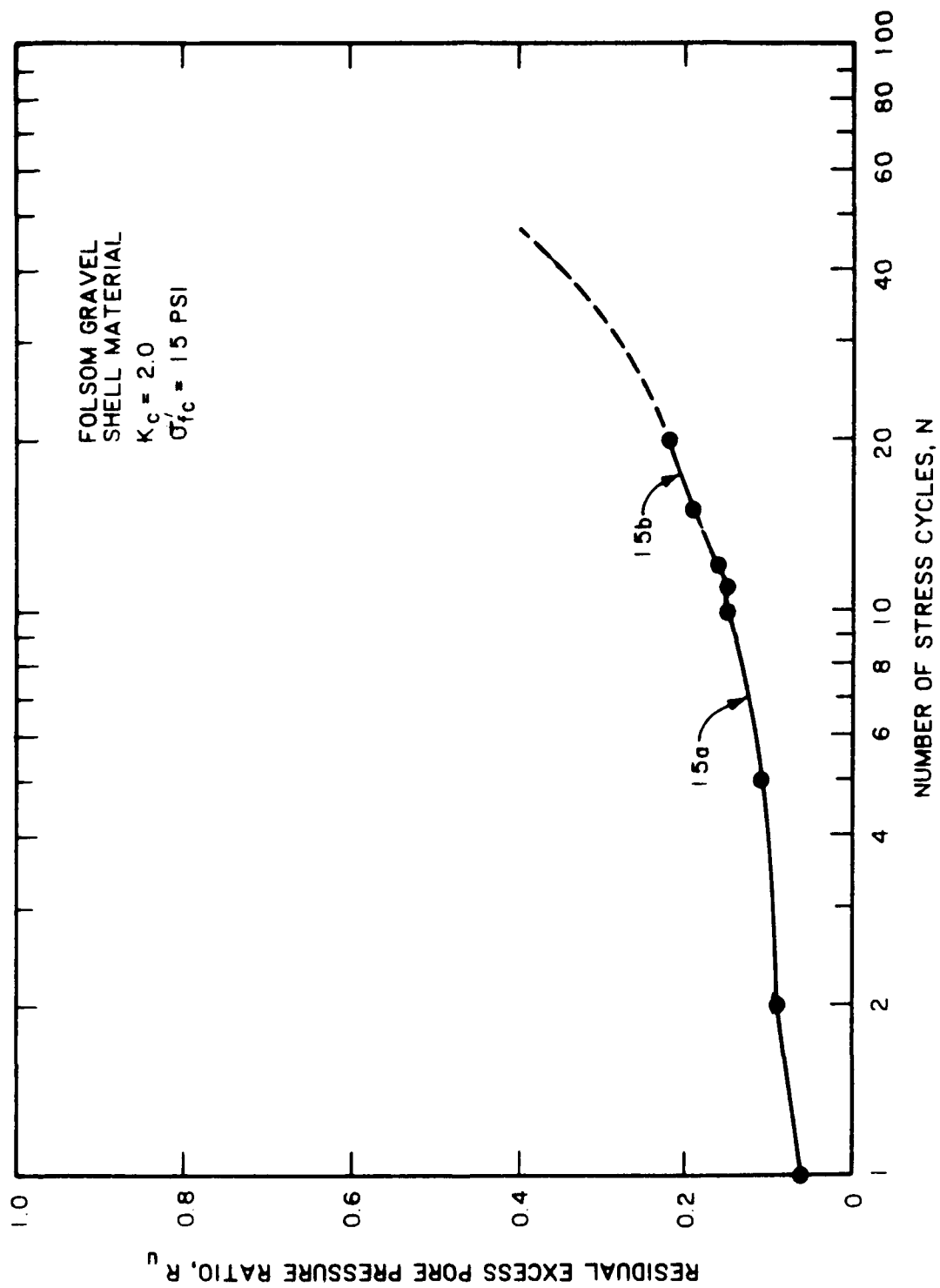


Figure B40. Development of residual excess pore pressure with each stress cycle

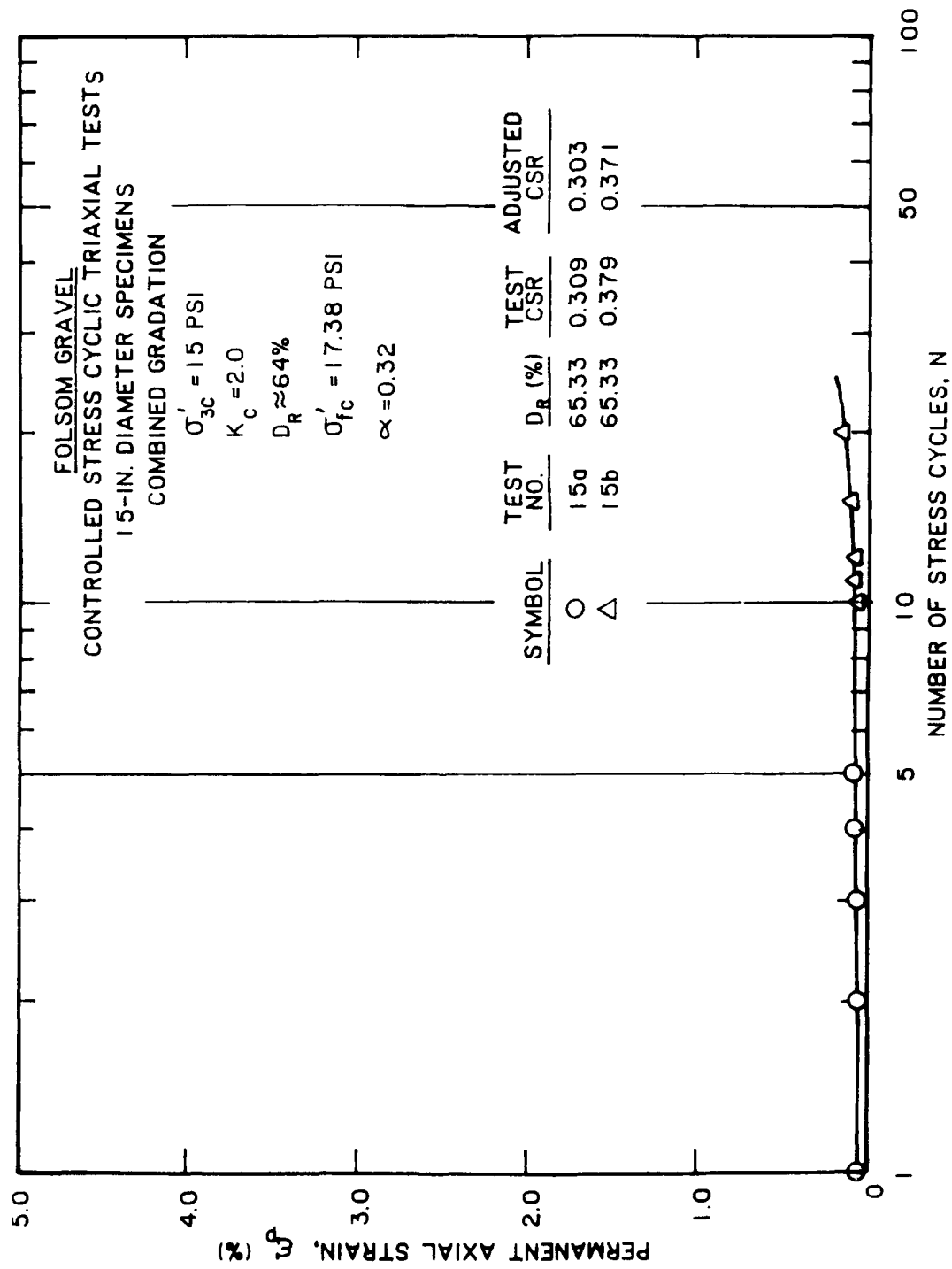


Figure B41. Development of permanent axial strain with each stress cycle

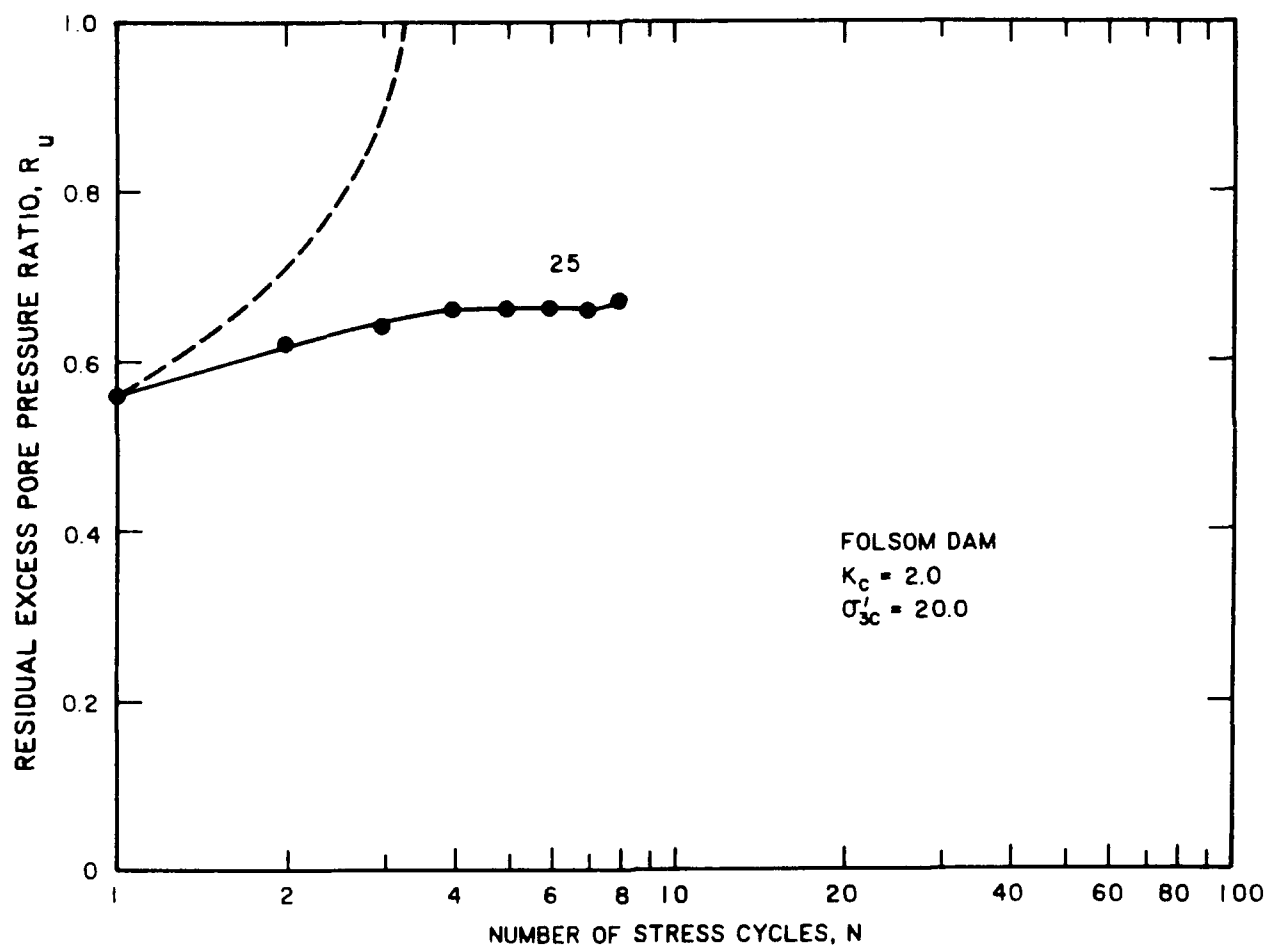


Figure B42. Development of residual excess pore pressure with each stress cycle

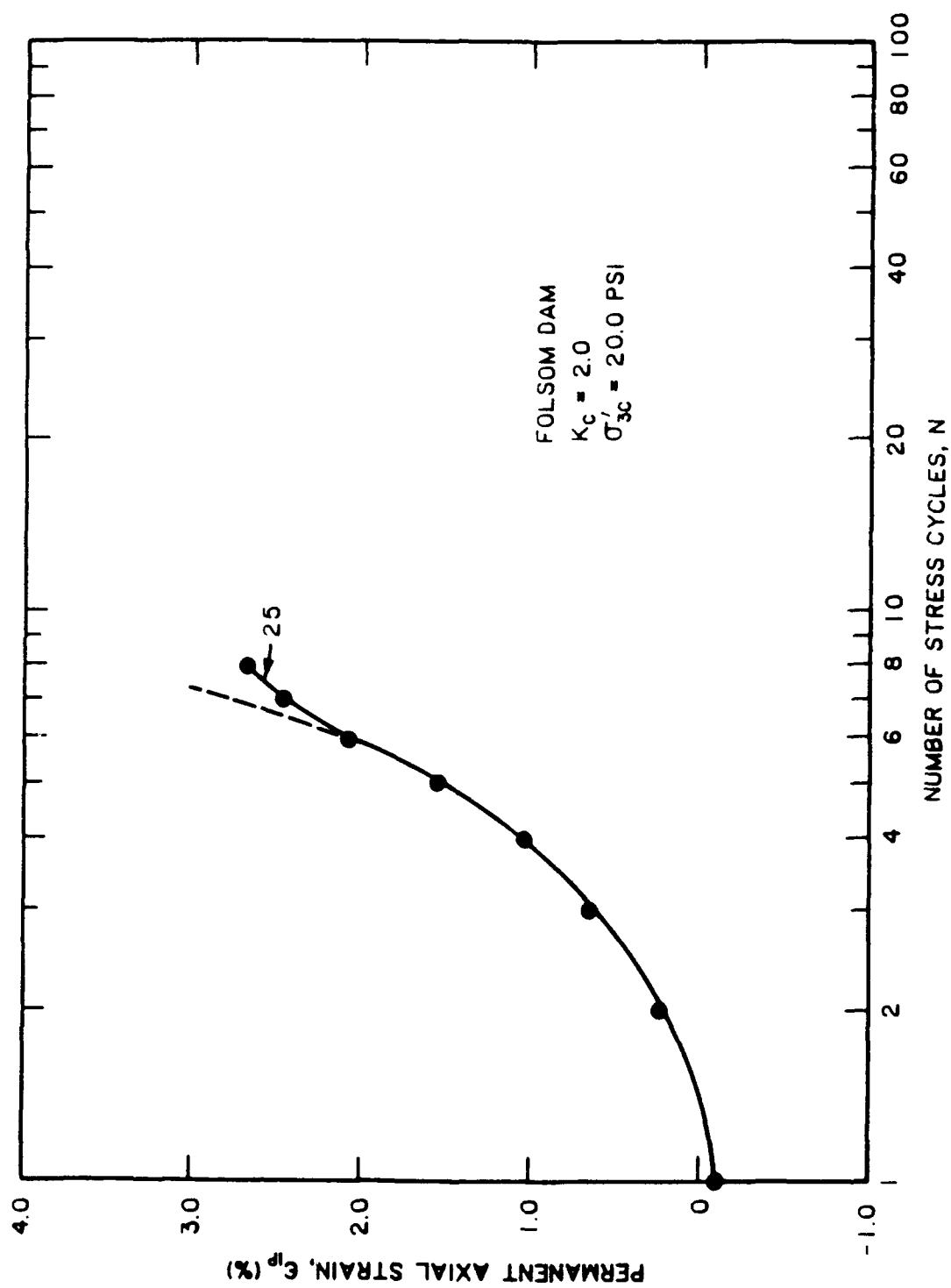


Figure B43. Development of permanent axial strain with each stress cycle

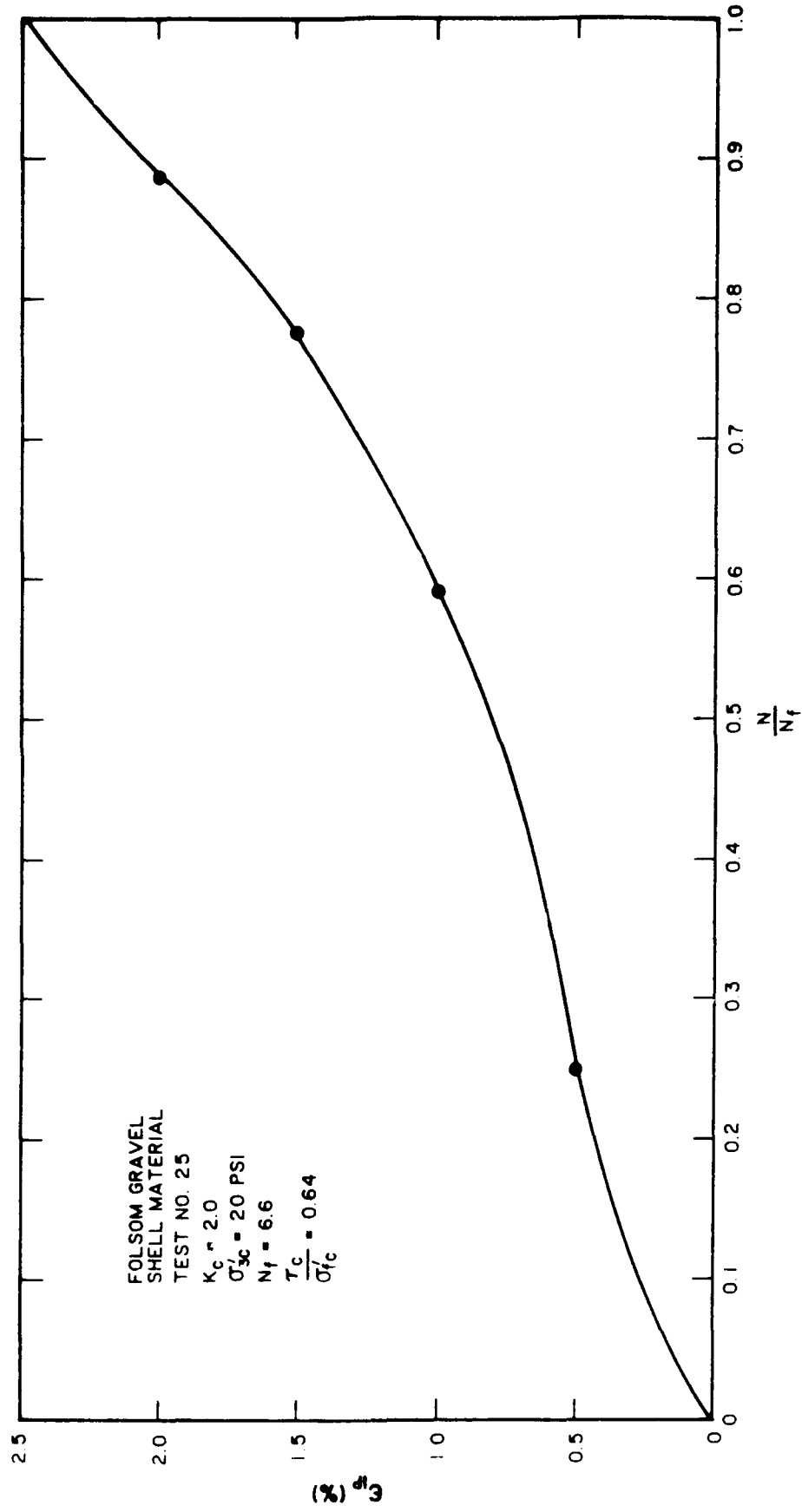


Figure B44. Permanent axial strain versus normalized stress cycle (Note:  $N_f$  = cycle at which  $\pm \epsilon_{1p} = 2.5$  percent)

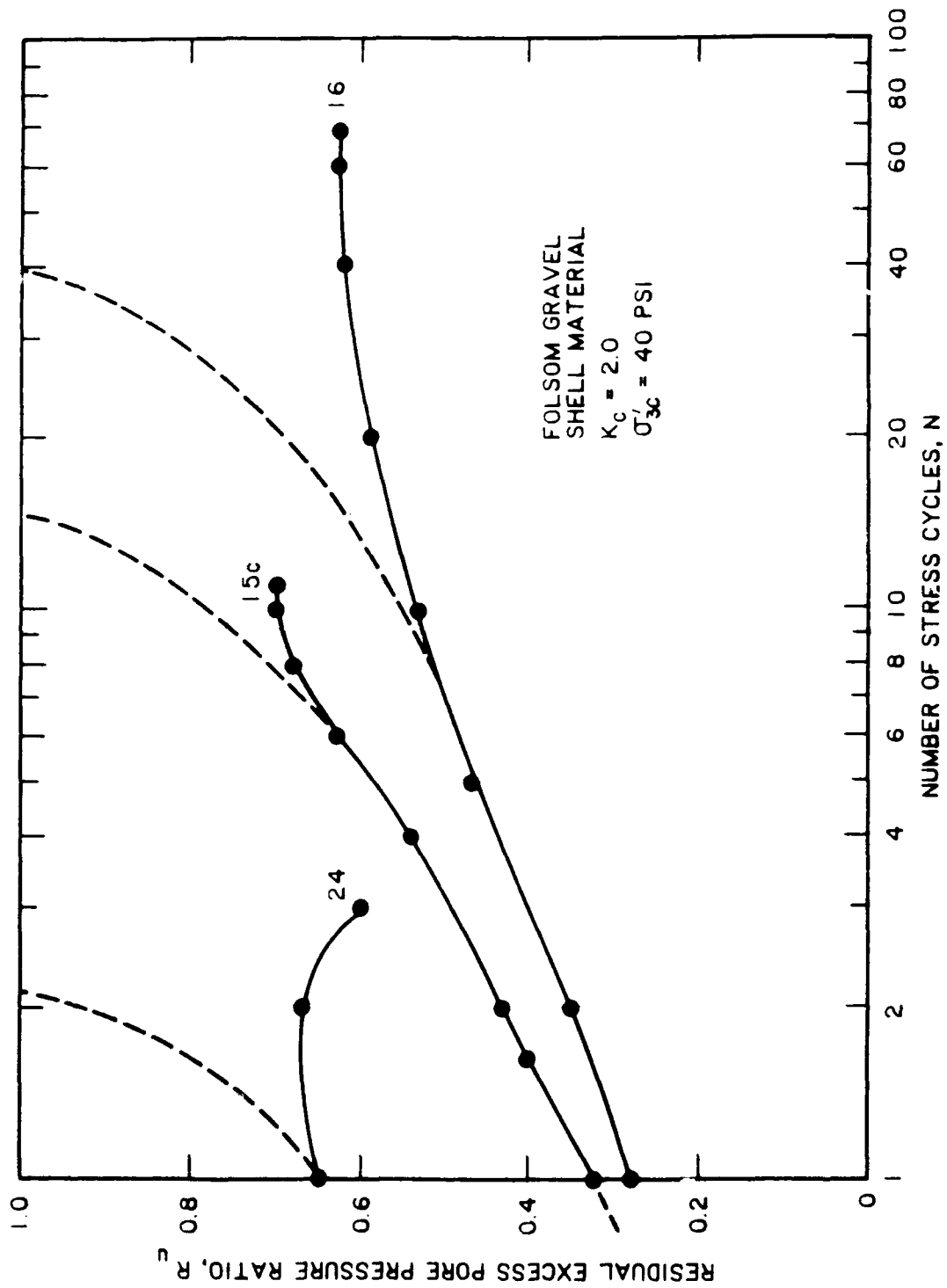


Figure B45. Development of residual excess pore pressure with each stress cycle

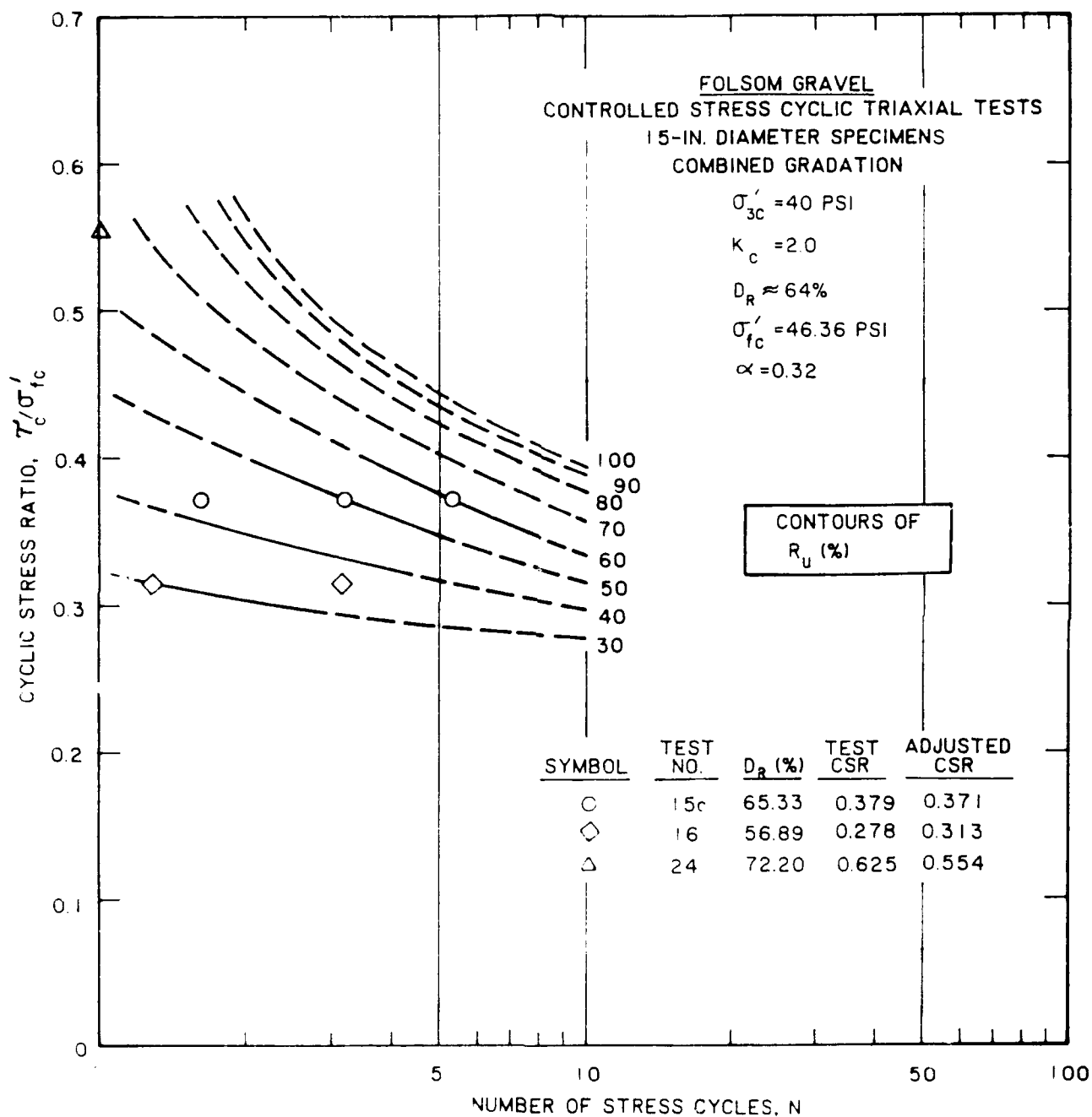


Figure B46. Contours of residual excess pore pressure ratio

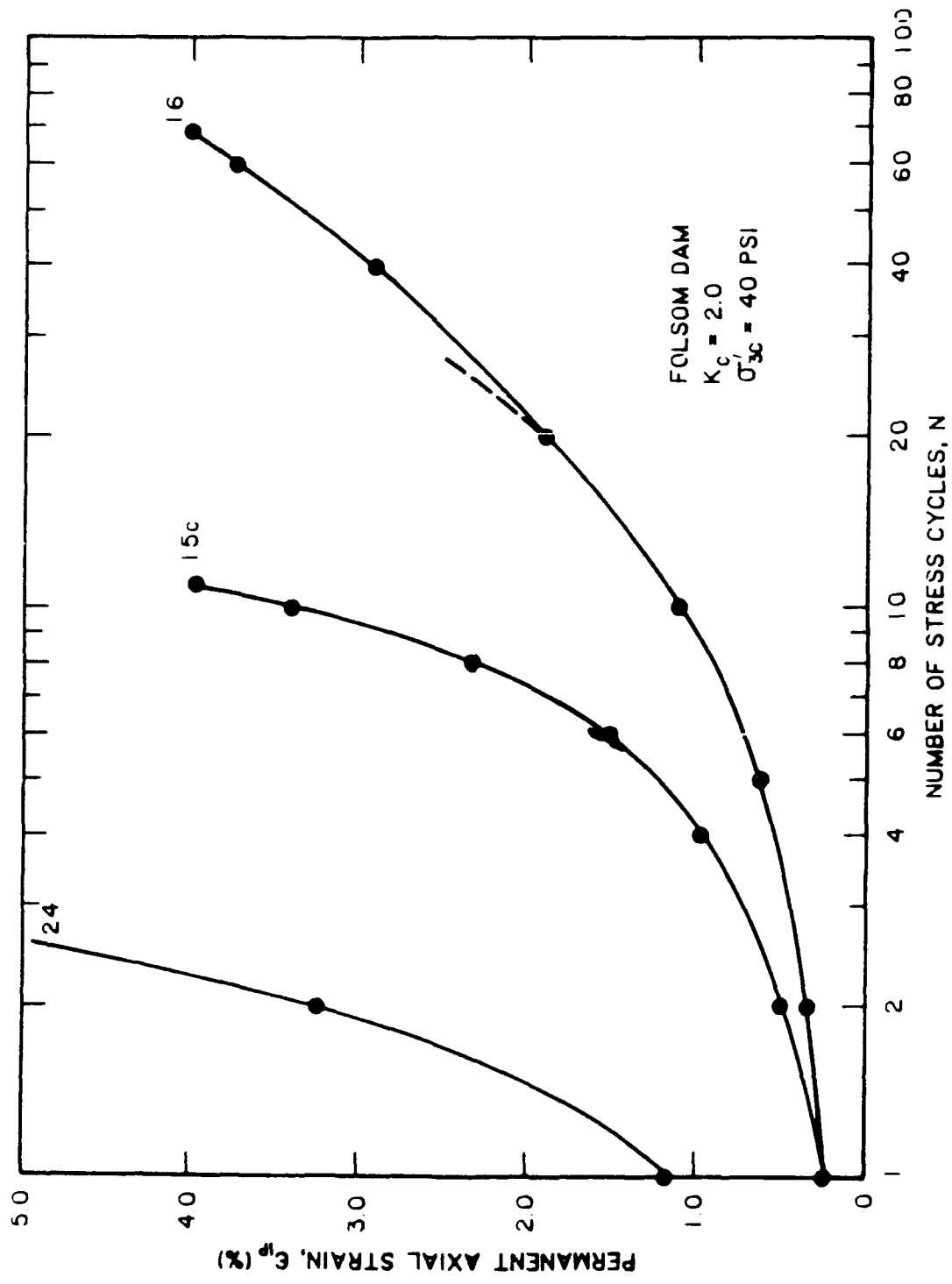


Figure B47. Development of permanent axial strain with each stress cycle



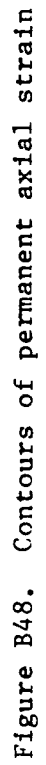


Figure B48. Contours of permanent axial strain

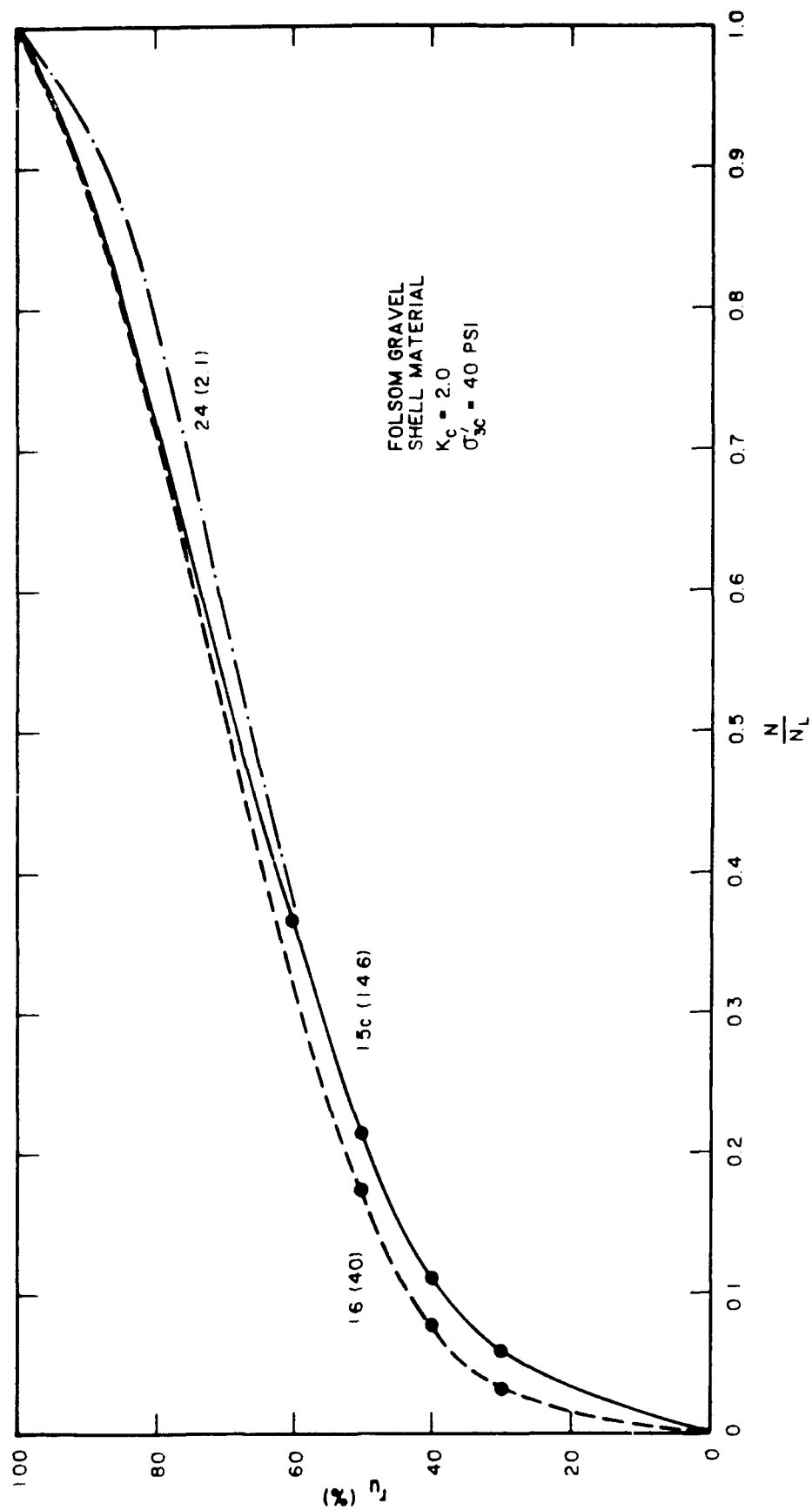


Figure B49. Residual excess pore pressure versus normalized stress cycle

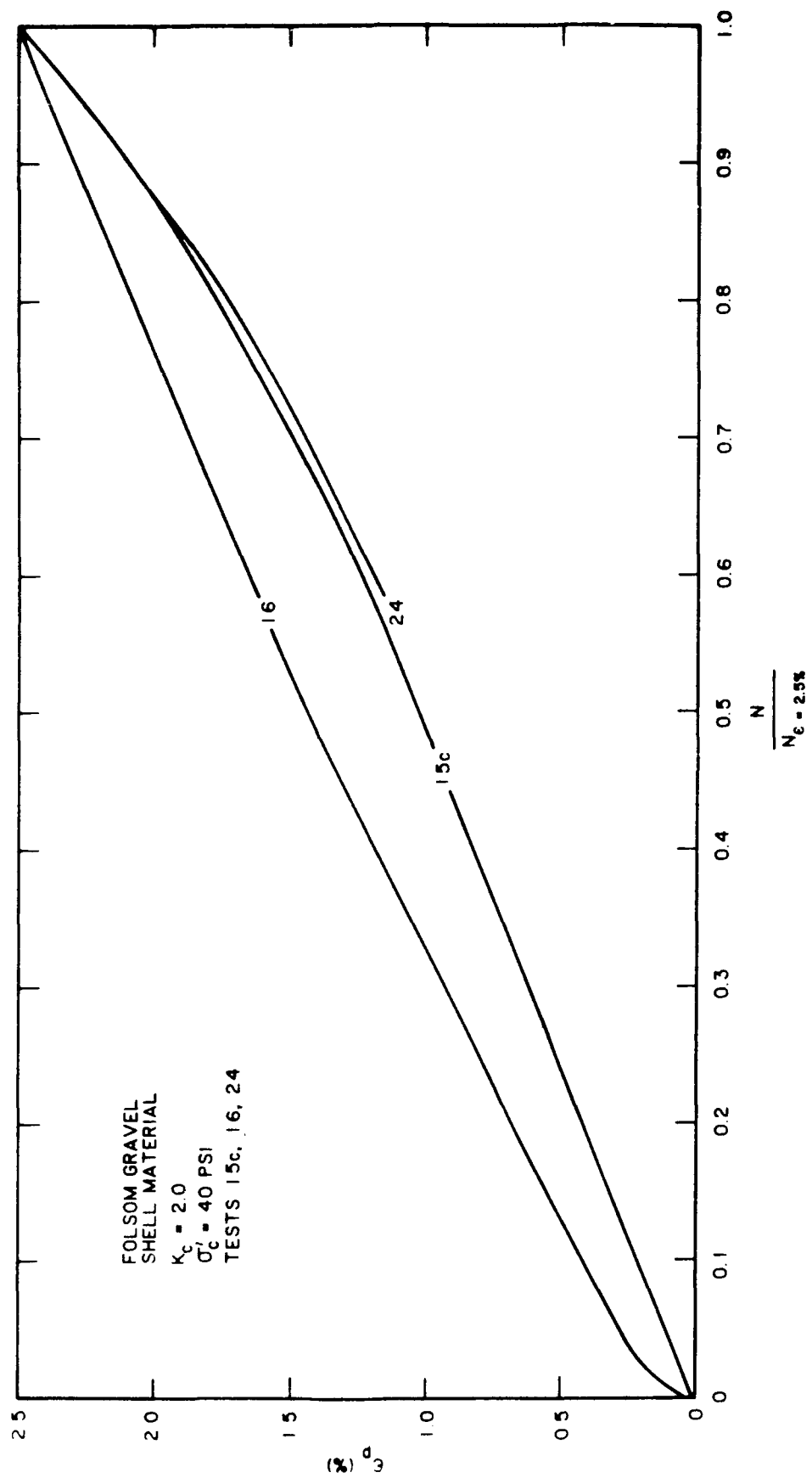


Figure B50. Permanent axial strain versus normalized stress cycle (Note:  $N_f = \text{cycle}$  at which  $\epsilon_{lp} = 2.5$  percent)

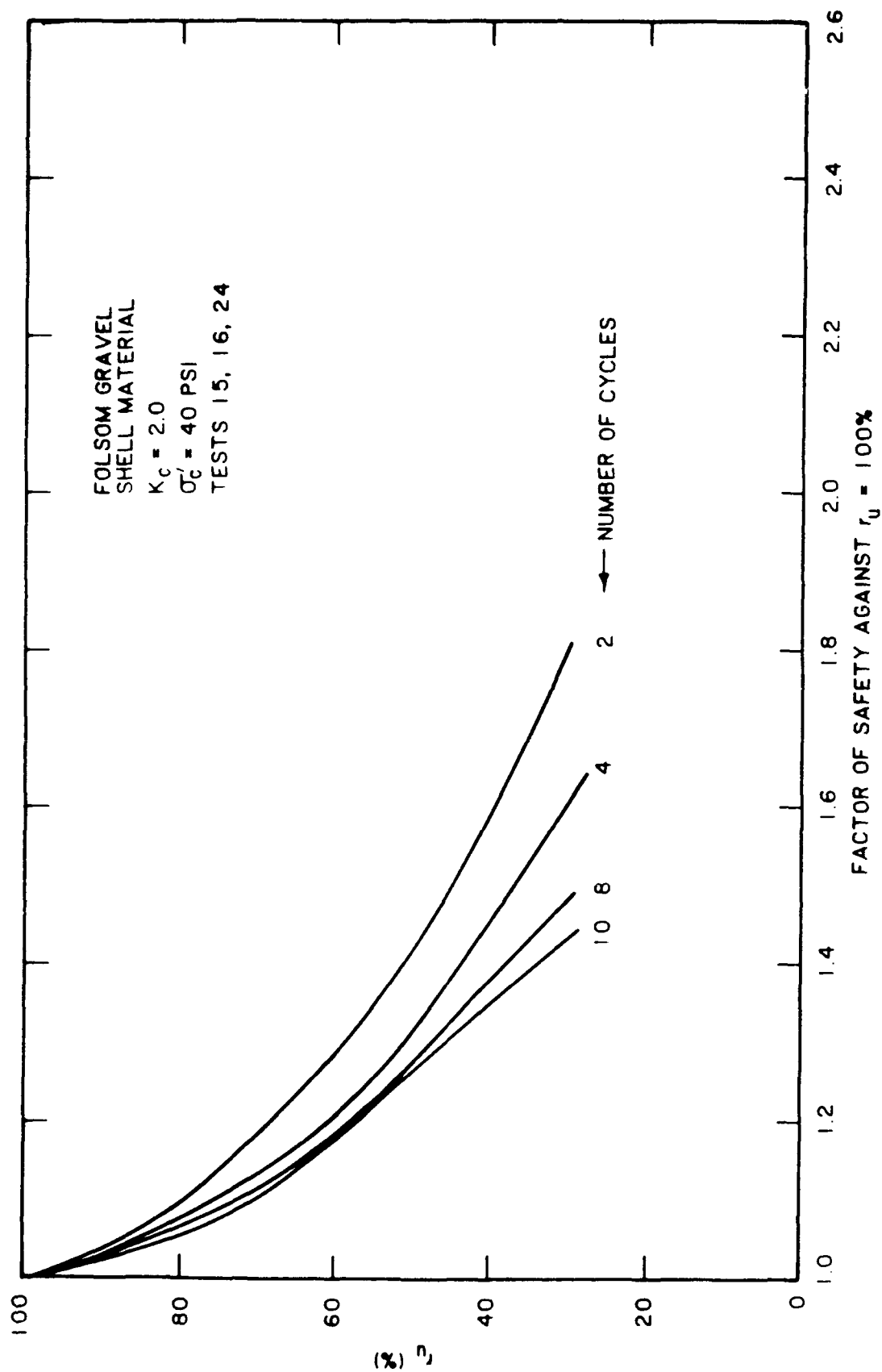


Figure B51. Relationship between factor of safety against liquefaction and residual excess pore pressure ratio

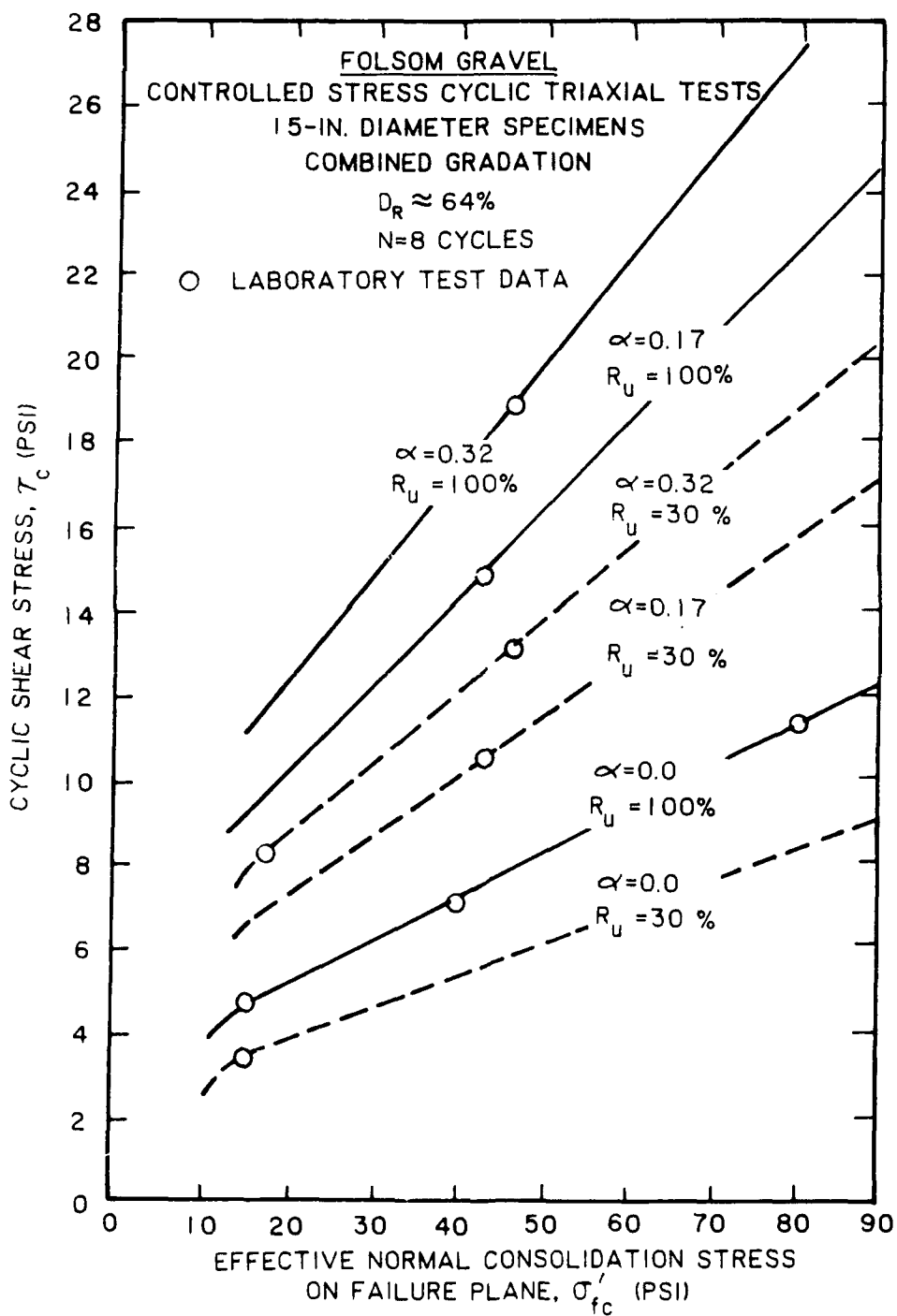


Figure B52. Cyclic strength envelopes for Folsom Dam shell gravels determined from cyclic triaxial laboratory tests

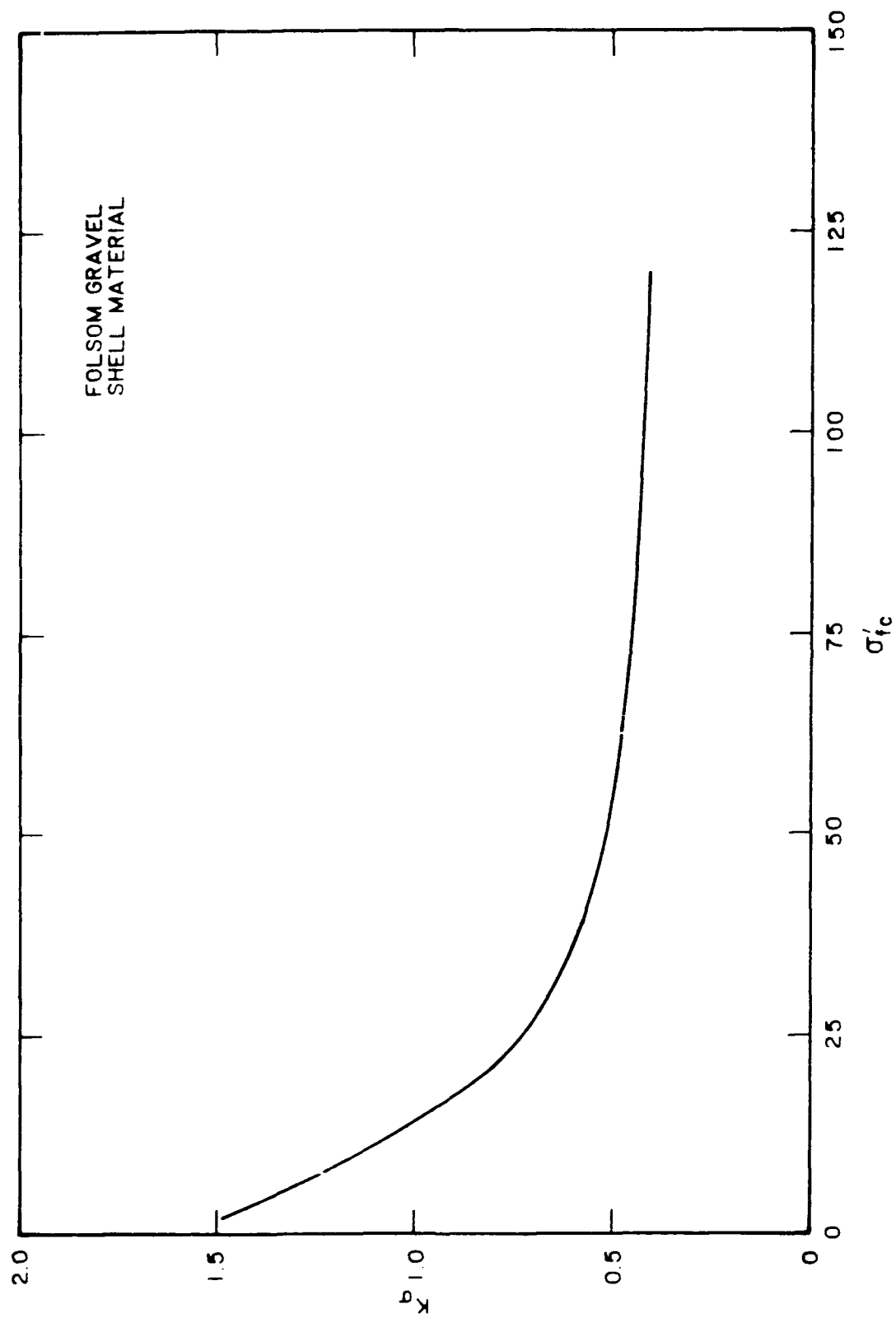


Figure B53. Overburden correction for Folsom shell gravel determined from laboratory tests

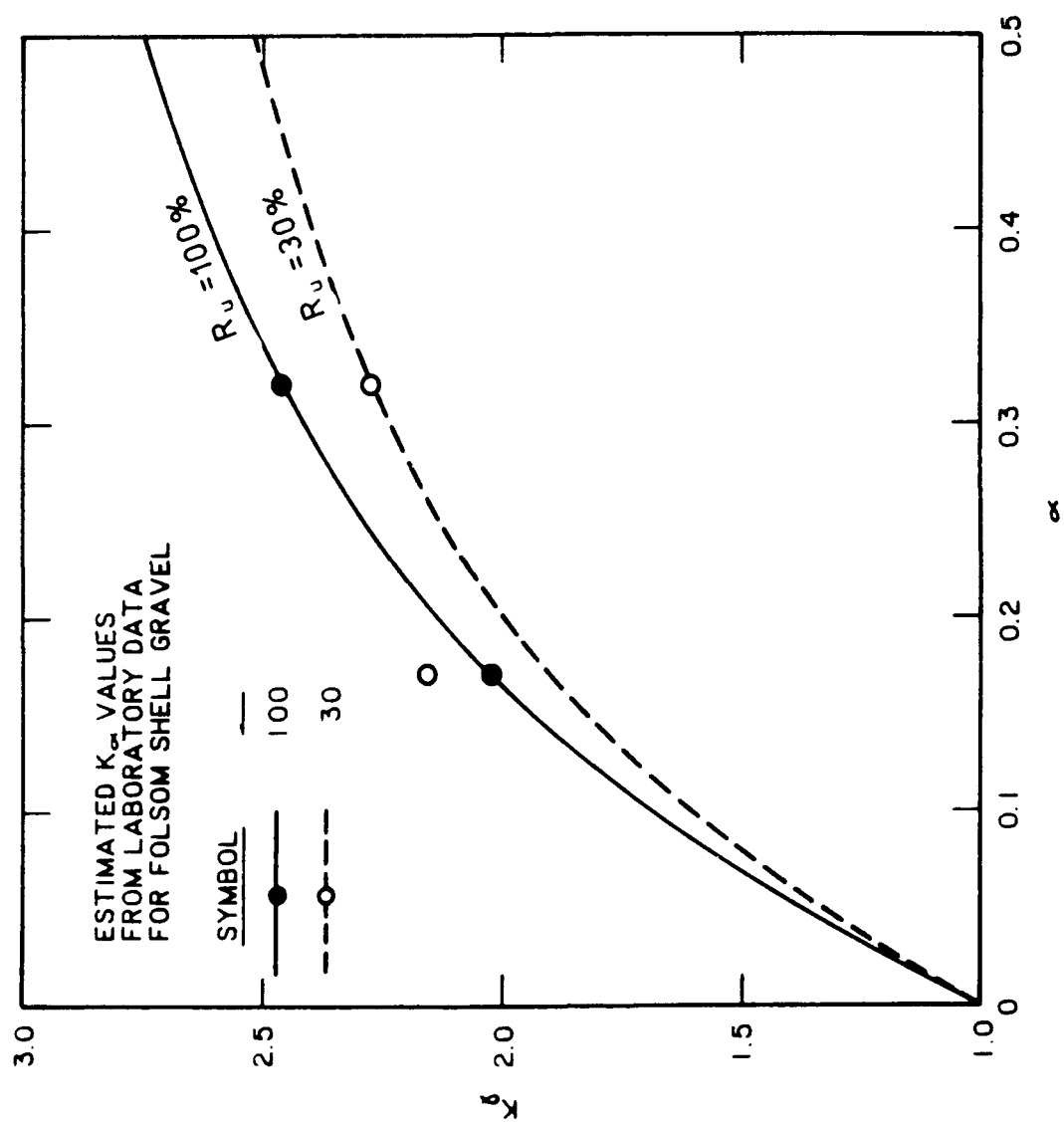


Figure B54. Initial stress ratio correction factors for Folsom shell gravel determined from laboratory tests

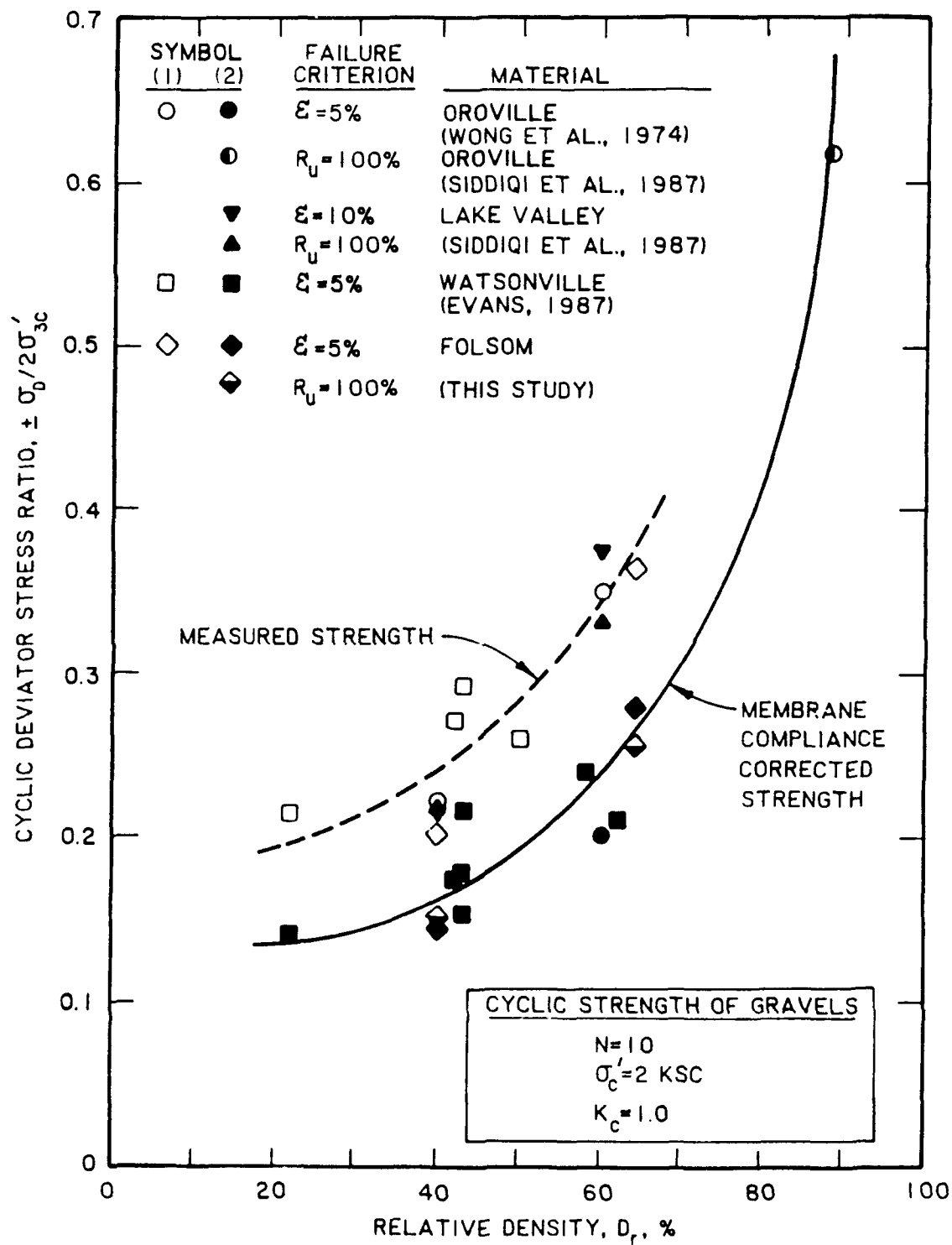
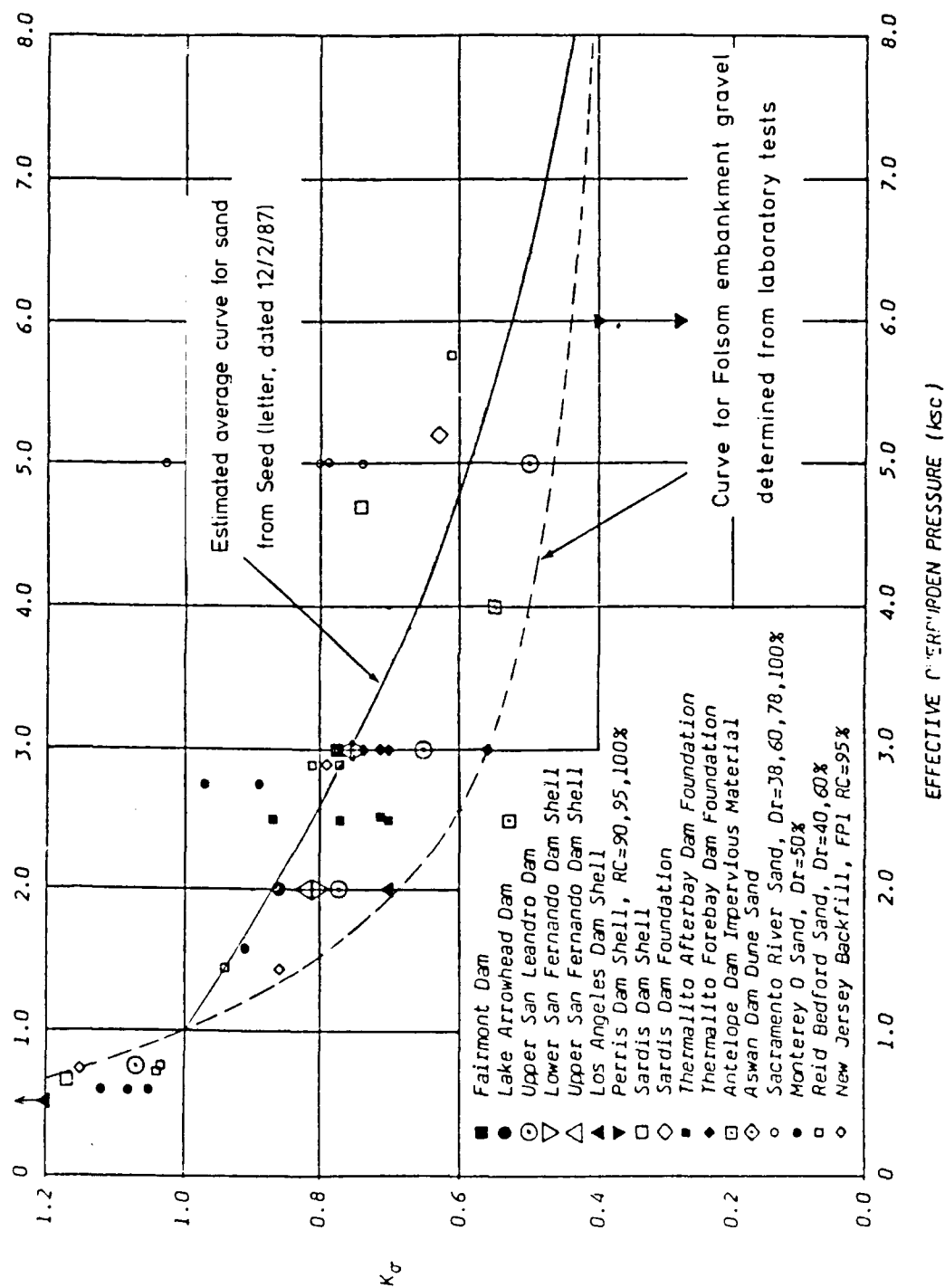


Figure B55. Comparison of cyclic strength for Folsom gravels with other gravels (based on laboratory tests)





Data compiled by Leslie F. Harder

Figure B56. Comparison of laboratory determined  $K_\sigma$  curve for Folsom gravels with other data

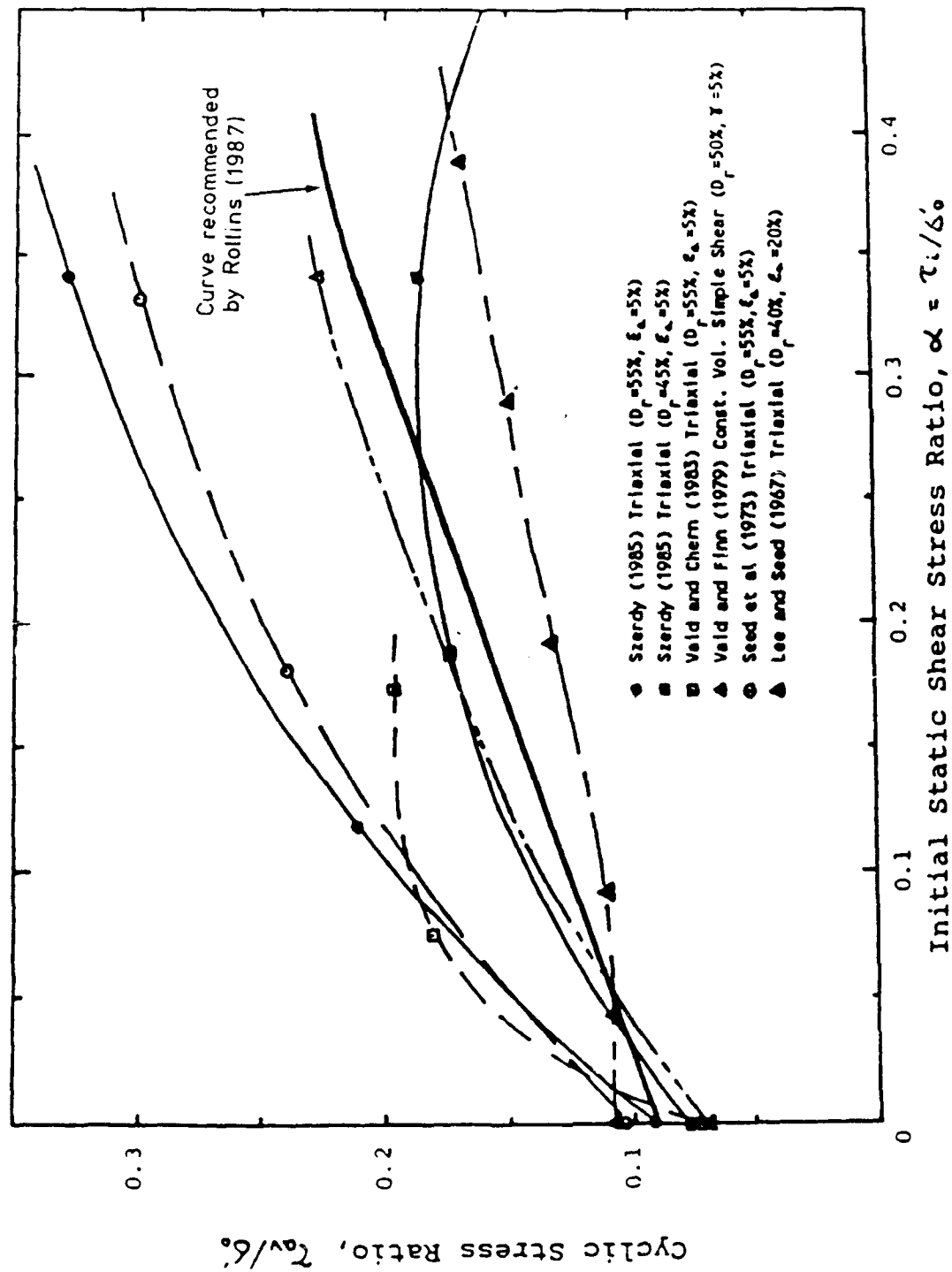


Figure B57a. Applied cyclic stress ratio versus initial static stress ratio for failure in 10 cycles in moderately dense sand samples (from Rollins, 1987)

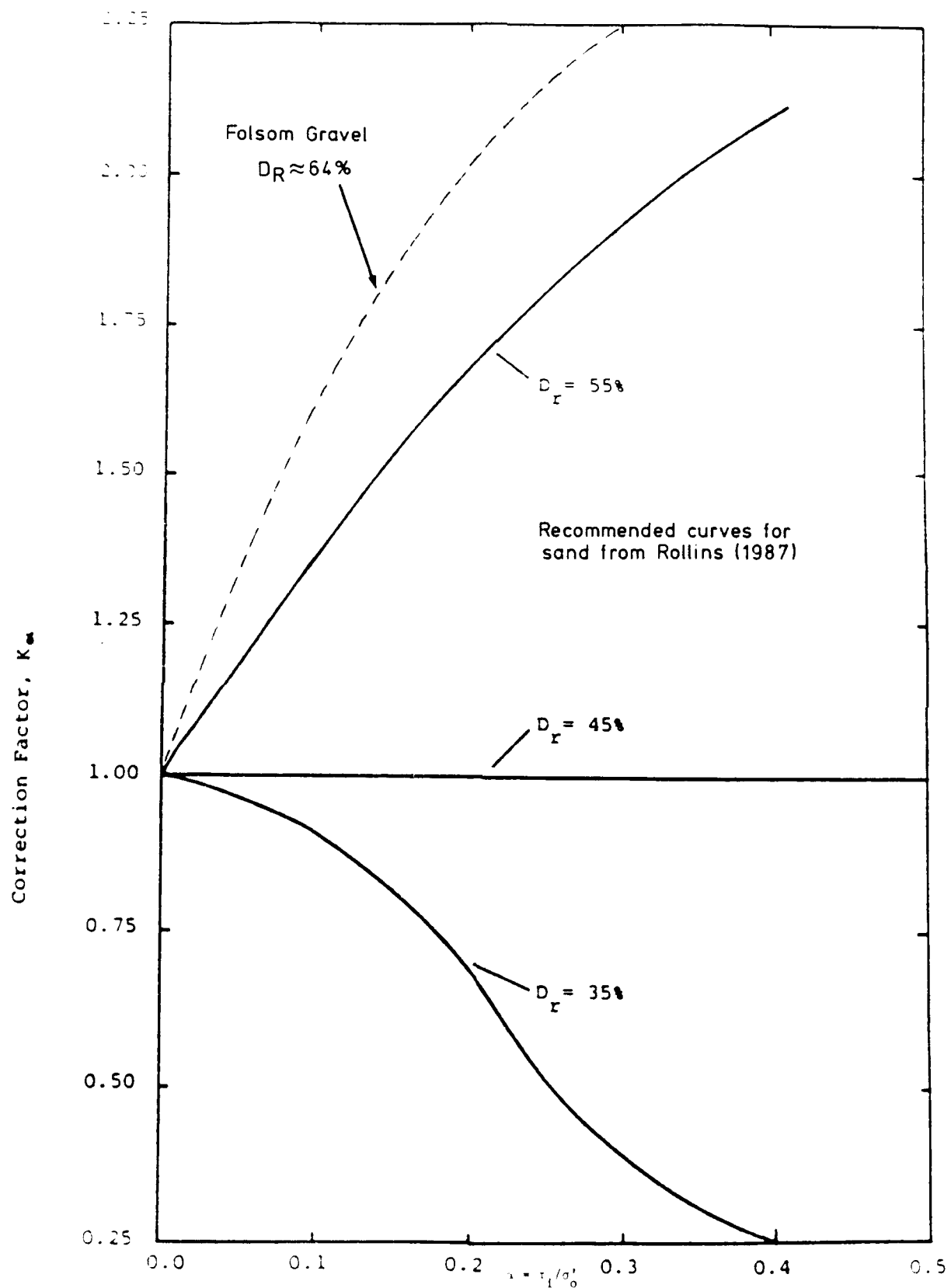


Figure B57b. Initial static stress ratio,  $\alpha = \tau_1/\sigma'_0$  versus initial static stress correction factor,  $K_\alpha$  (from Rollins, 1987)

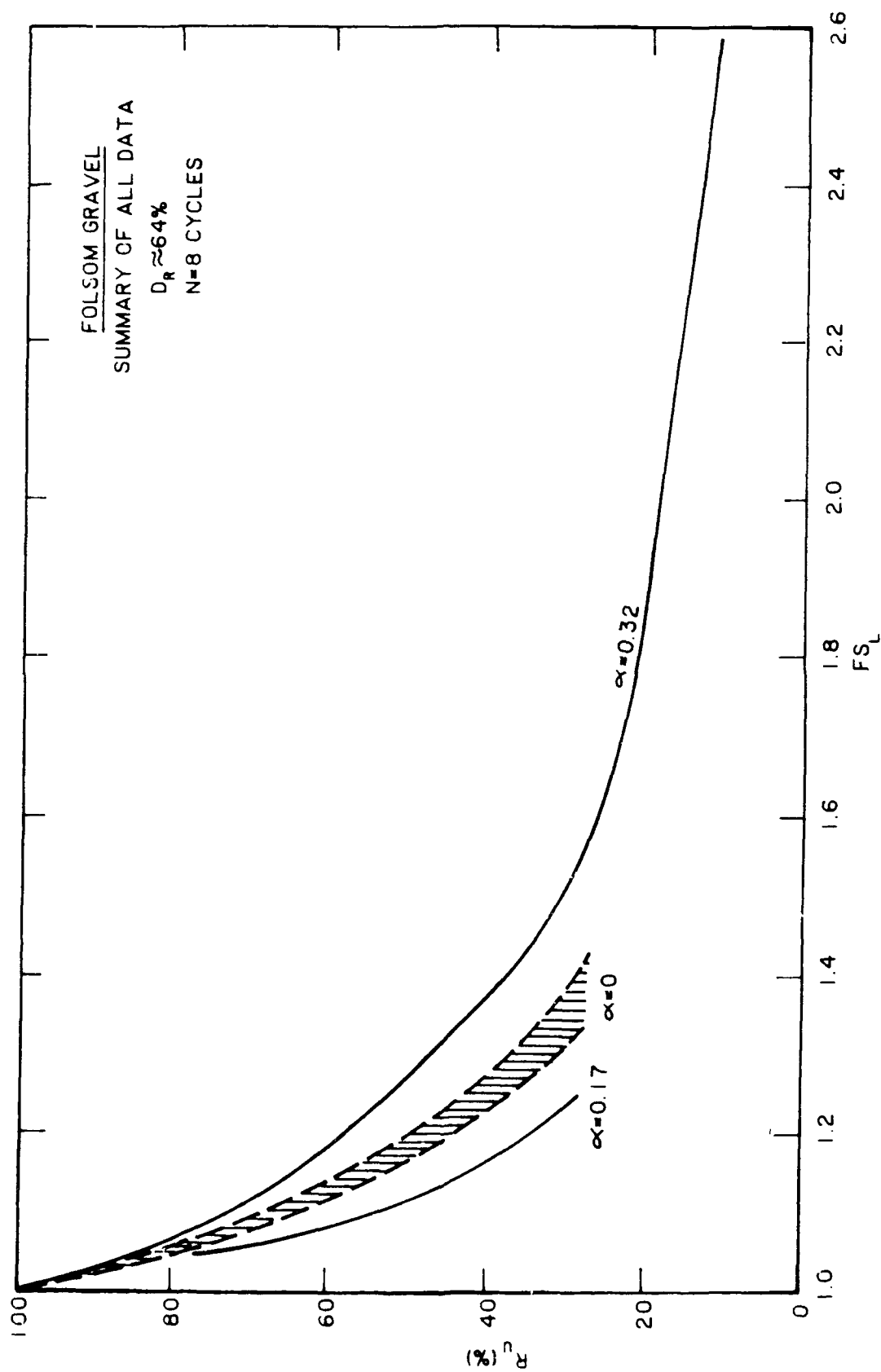


Figure B58. Residual excess pore pressure ratio versus factor of safety against liquefaction, summary of all data for Folsom shell gravel

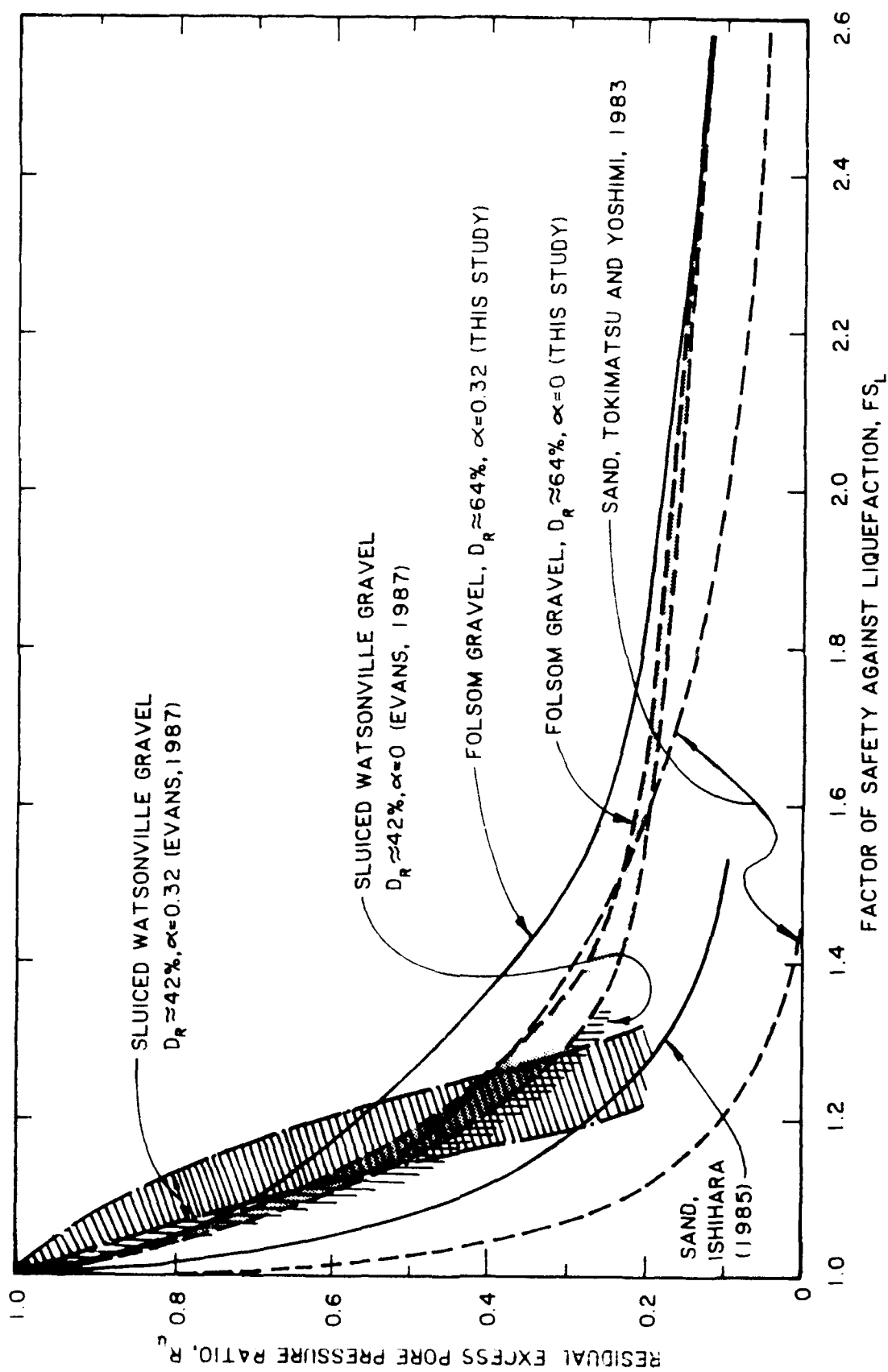


Figure B59. Comparison of  $R_u$  versus  $FS_L$  for Folsom shell gravel with other data for sands and gravel

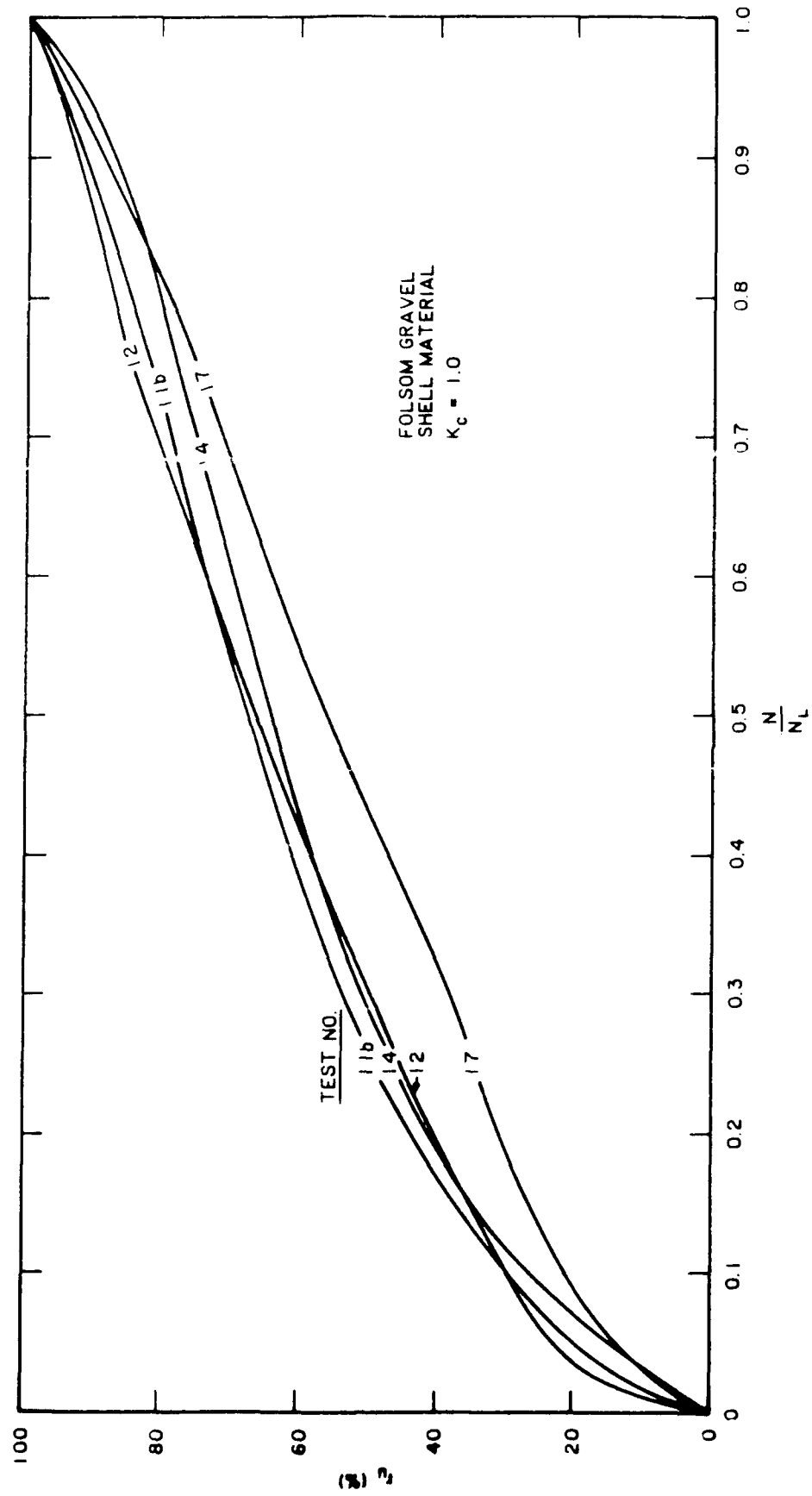


Figure B60. Residual excess pore pressure versus normalized stress cycle

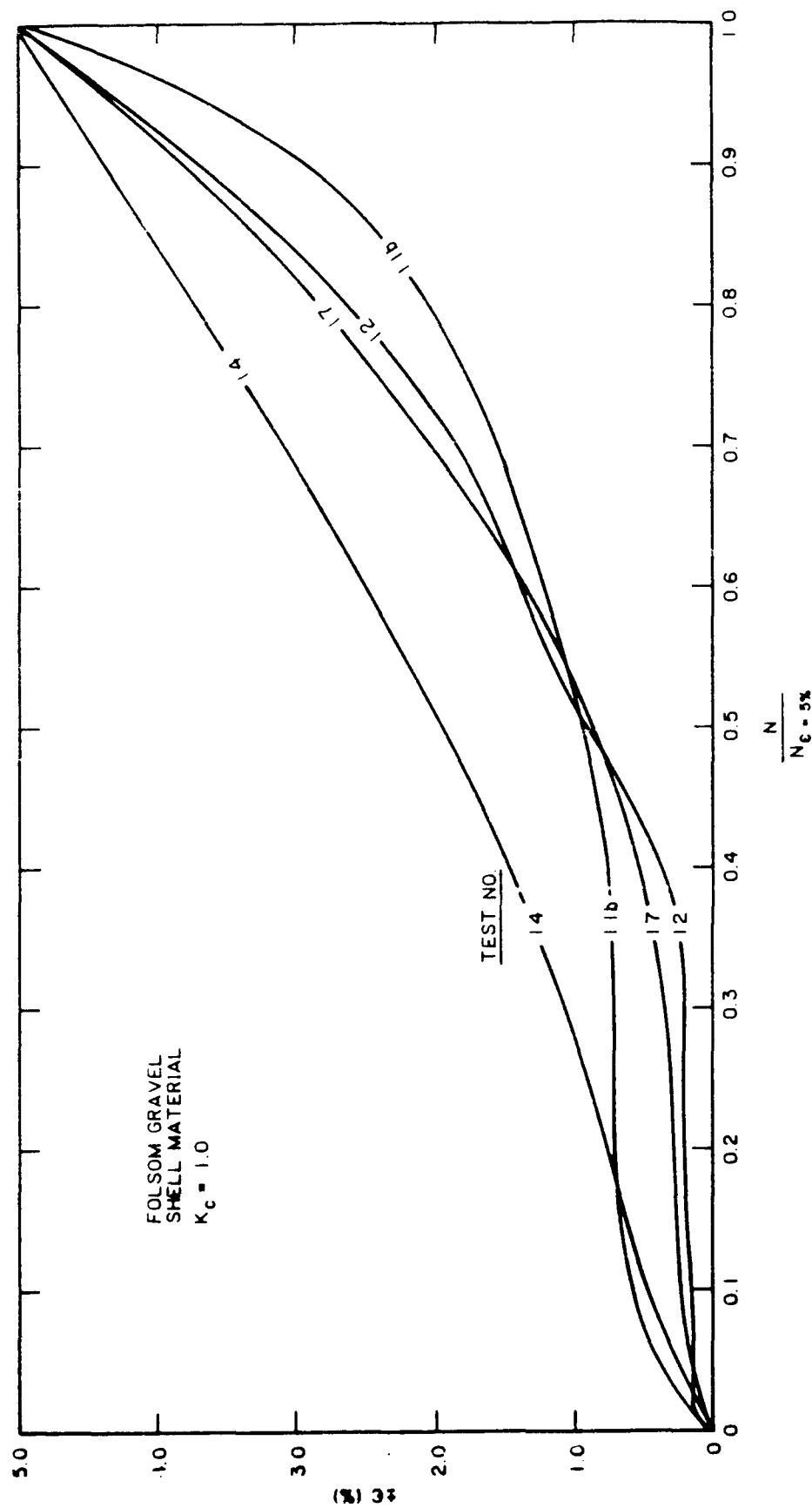


Figure B61. Peak to peak cyclic strain versus normalized stress cycle (Note:  $N_f = \text{cycle}$  at which  $\pm \epsilon = 5 \text{ percent}$ )

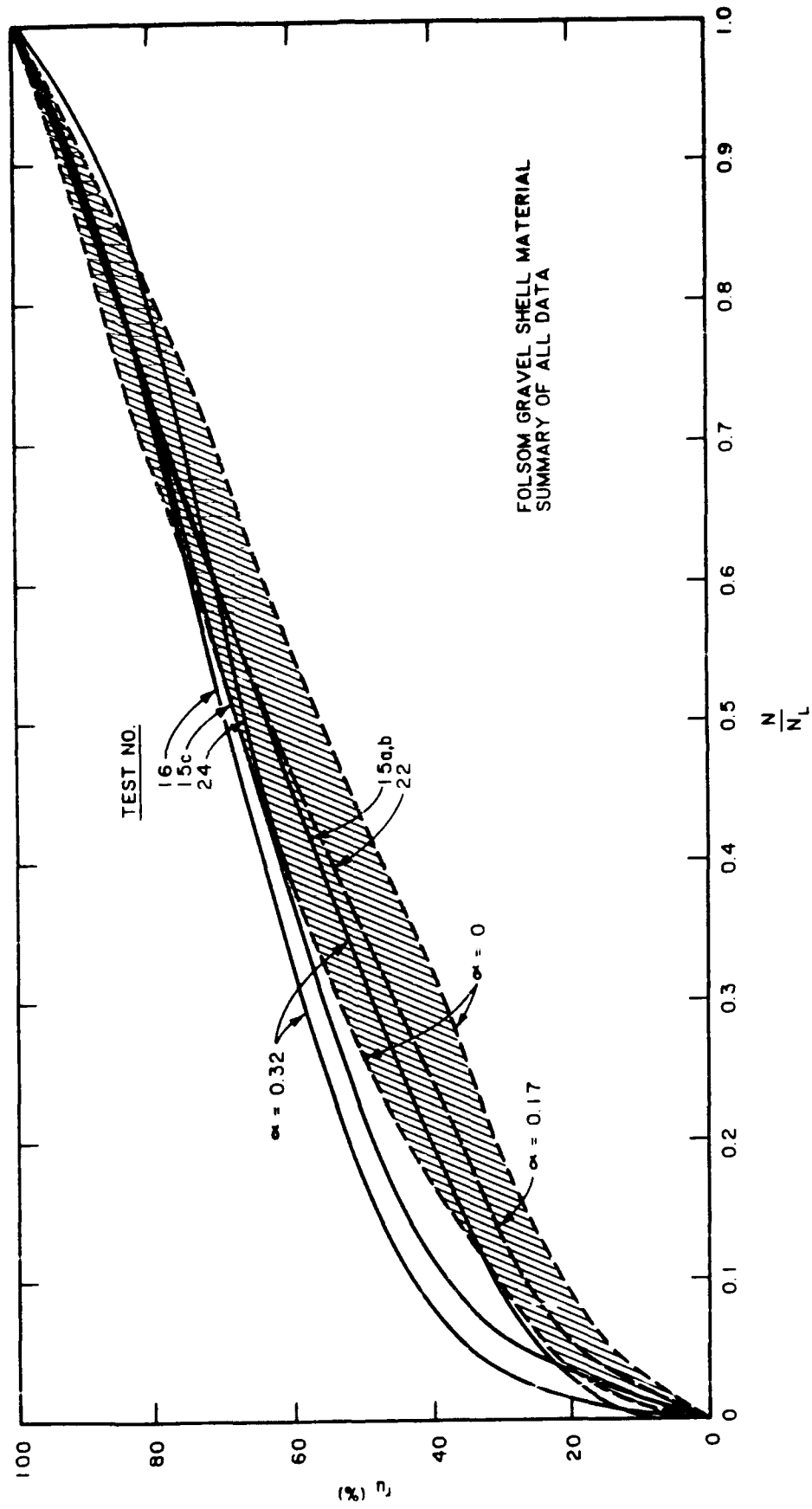


Figure B62. Residual excess pore pressure versus normalized stress cycle, summary of all data



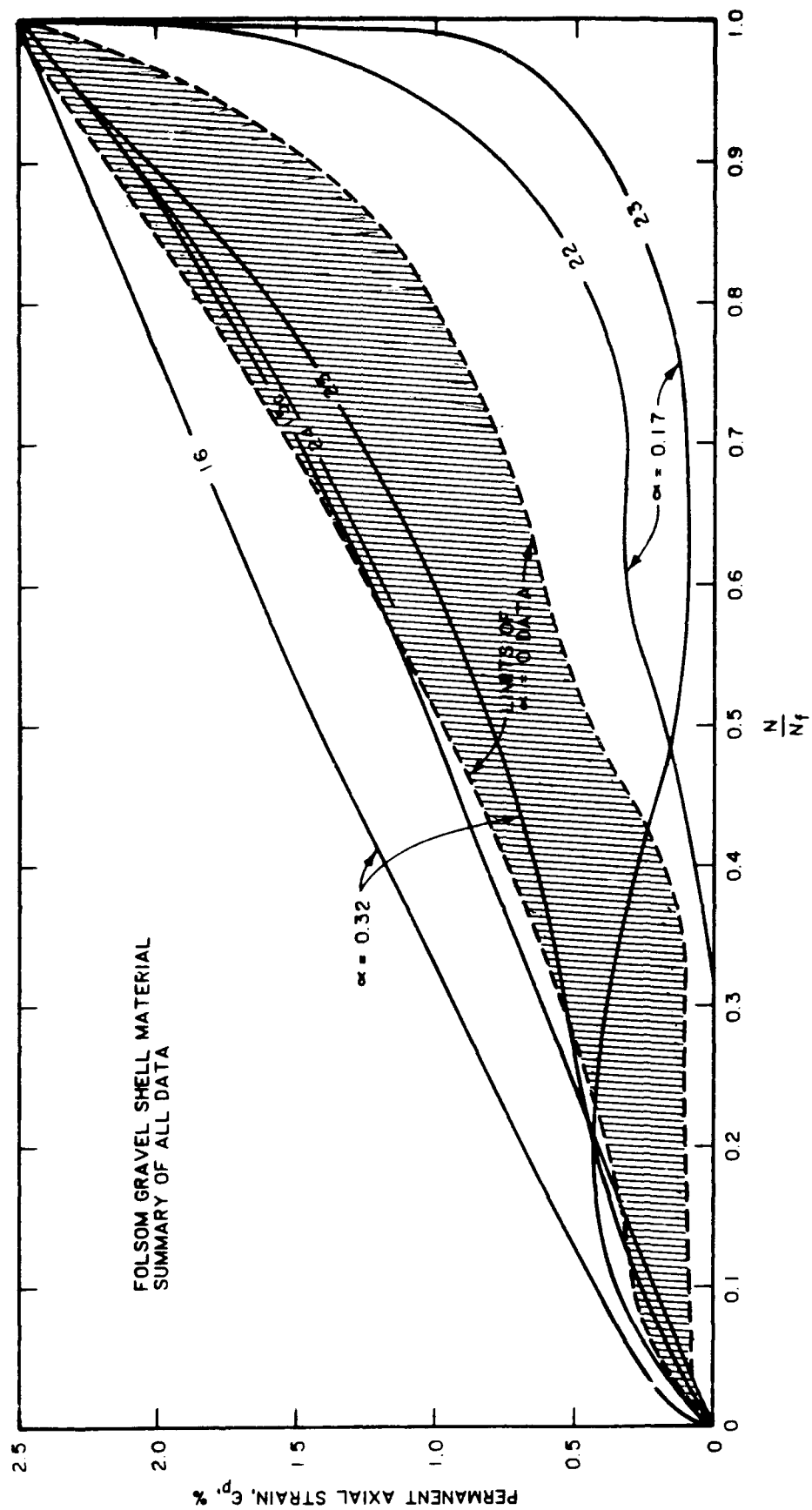


Figure B63. Permanent axial strain versus normalized stress cycle (Note:  $N_f$  = cycle at which  $\epsilon_{lp} = 2.5$  percent), summary of all data

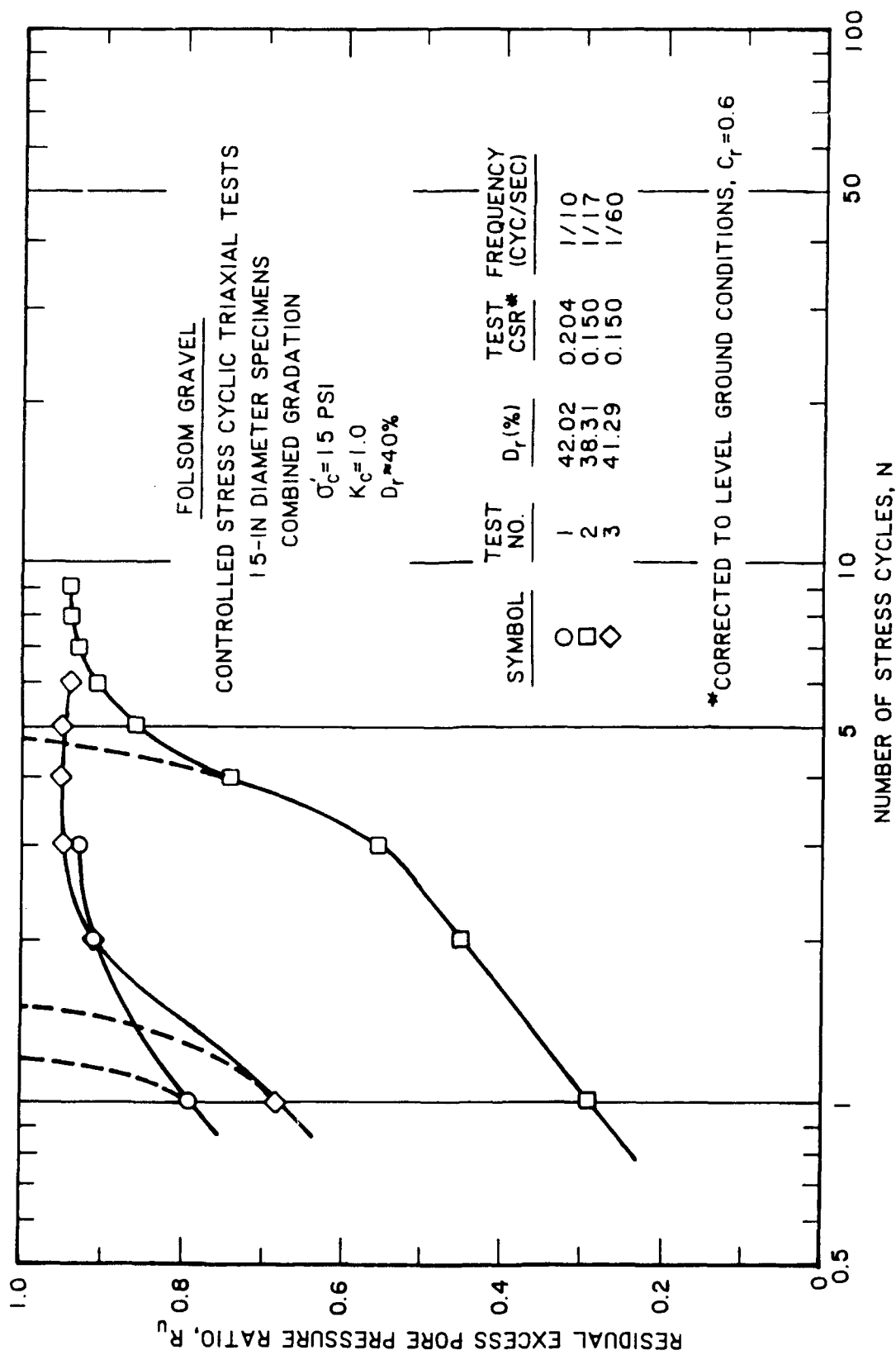


Figure B64. Development of residual excess pore pressure with each stress cycle

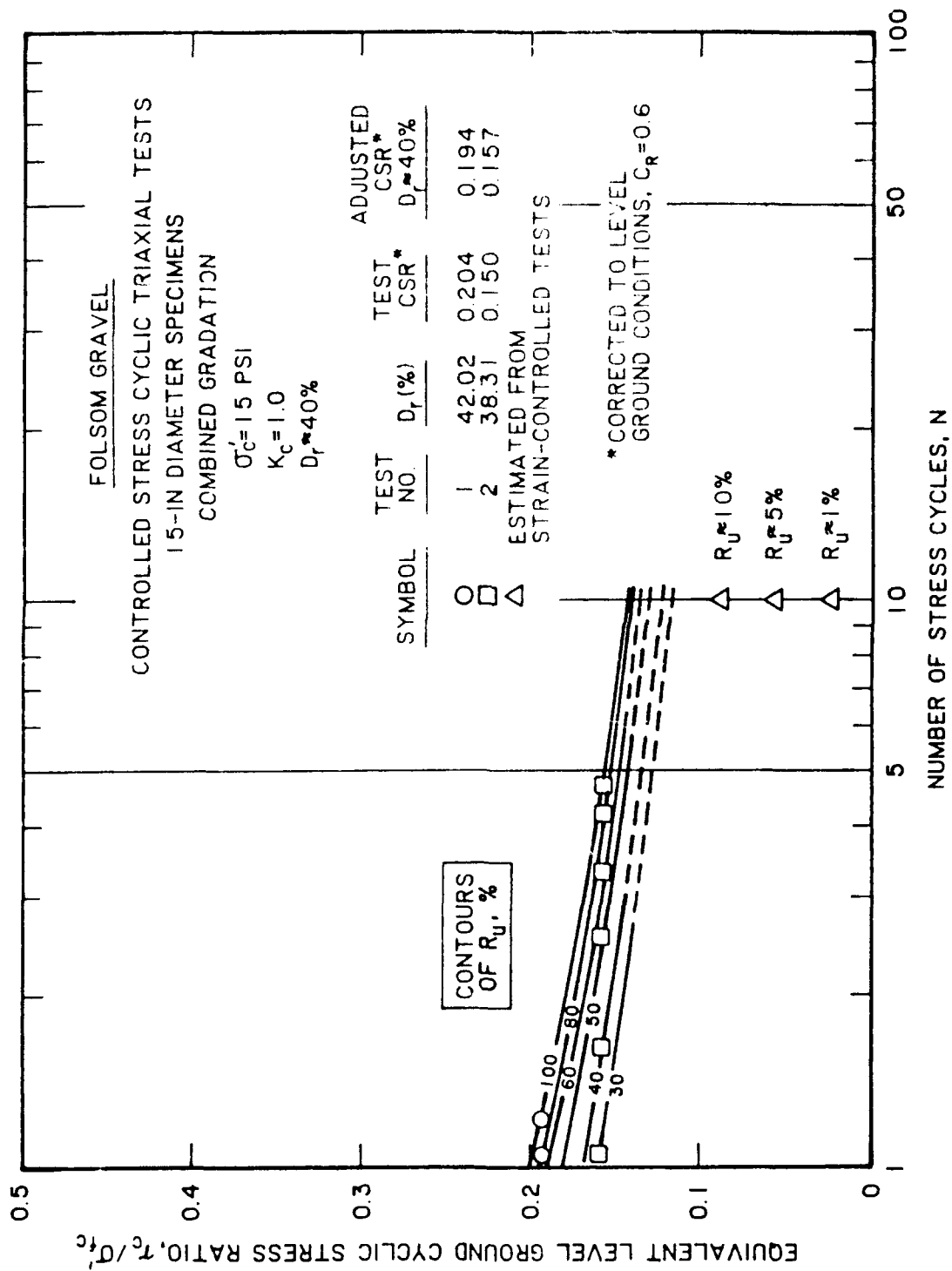


Figure B65. Contours of residual excess pore pressure ratio

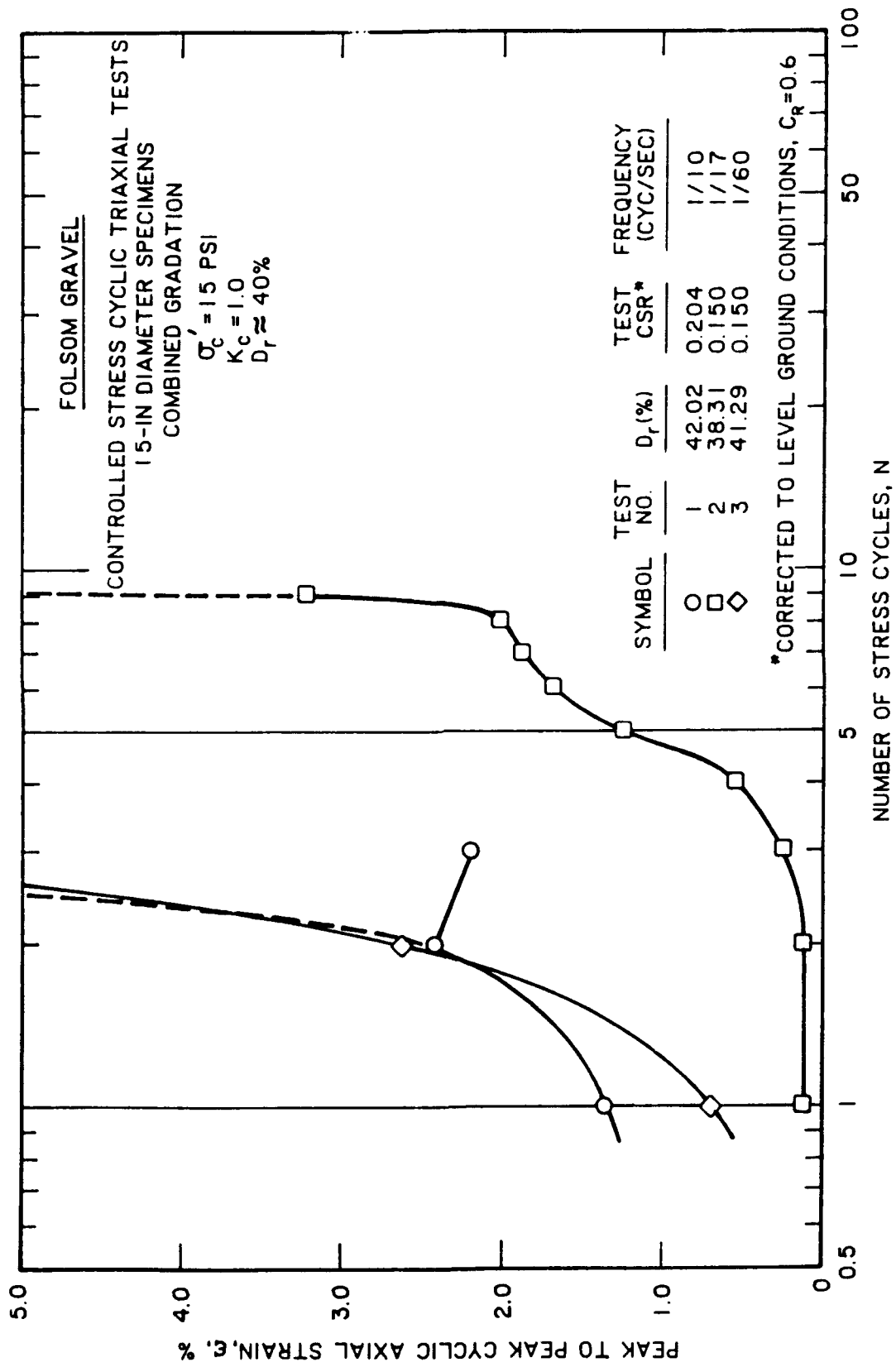


Figure B66. Development of peak to peak cyclic strain with each stress cycle

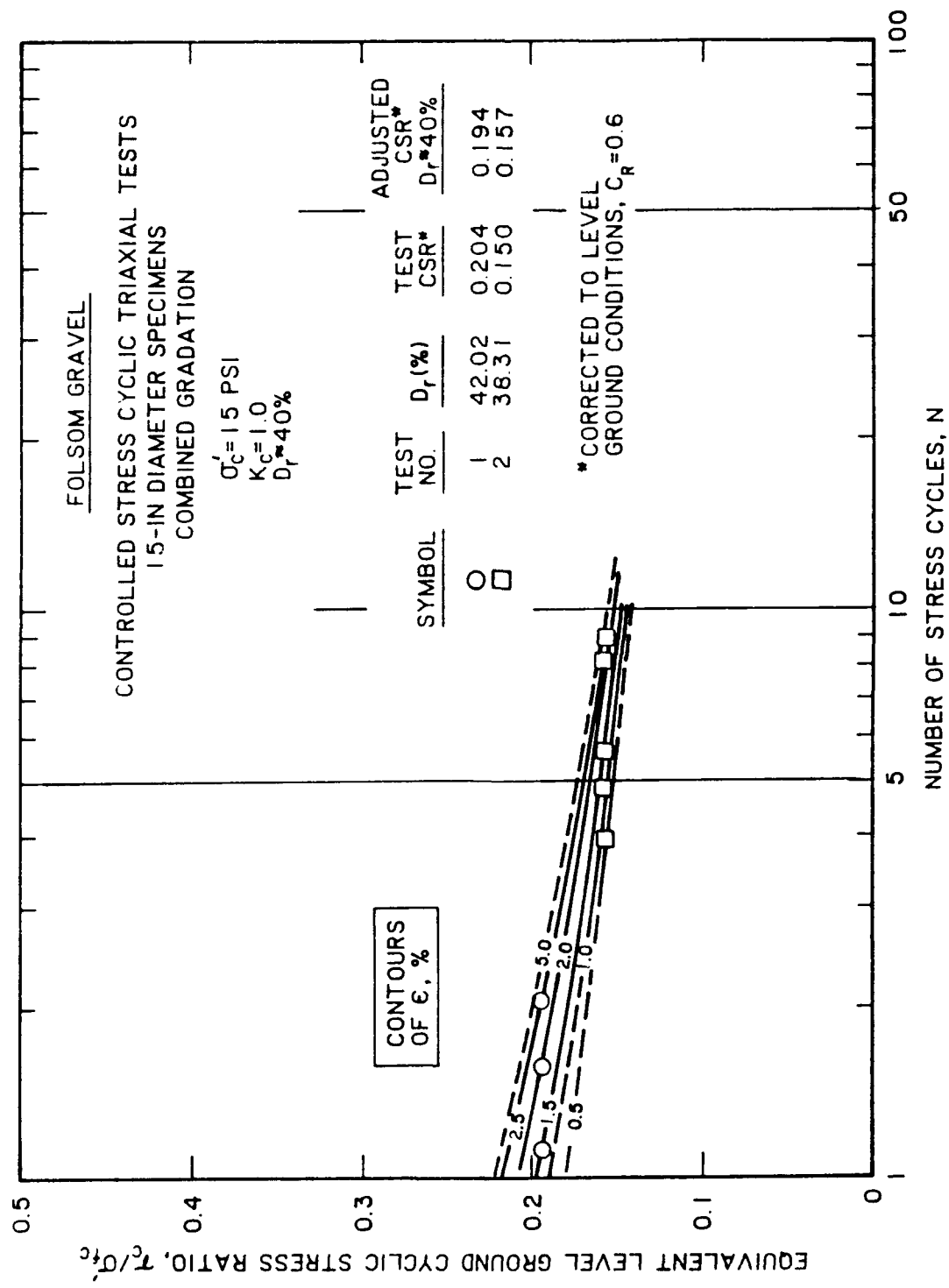


Figure B67. Contours of peak to peak cyclic strain

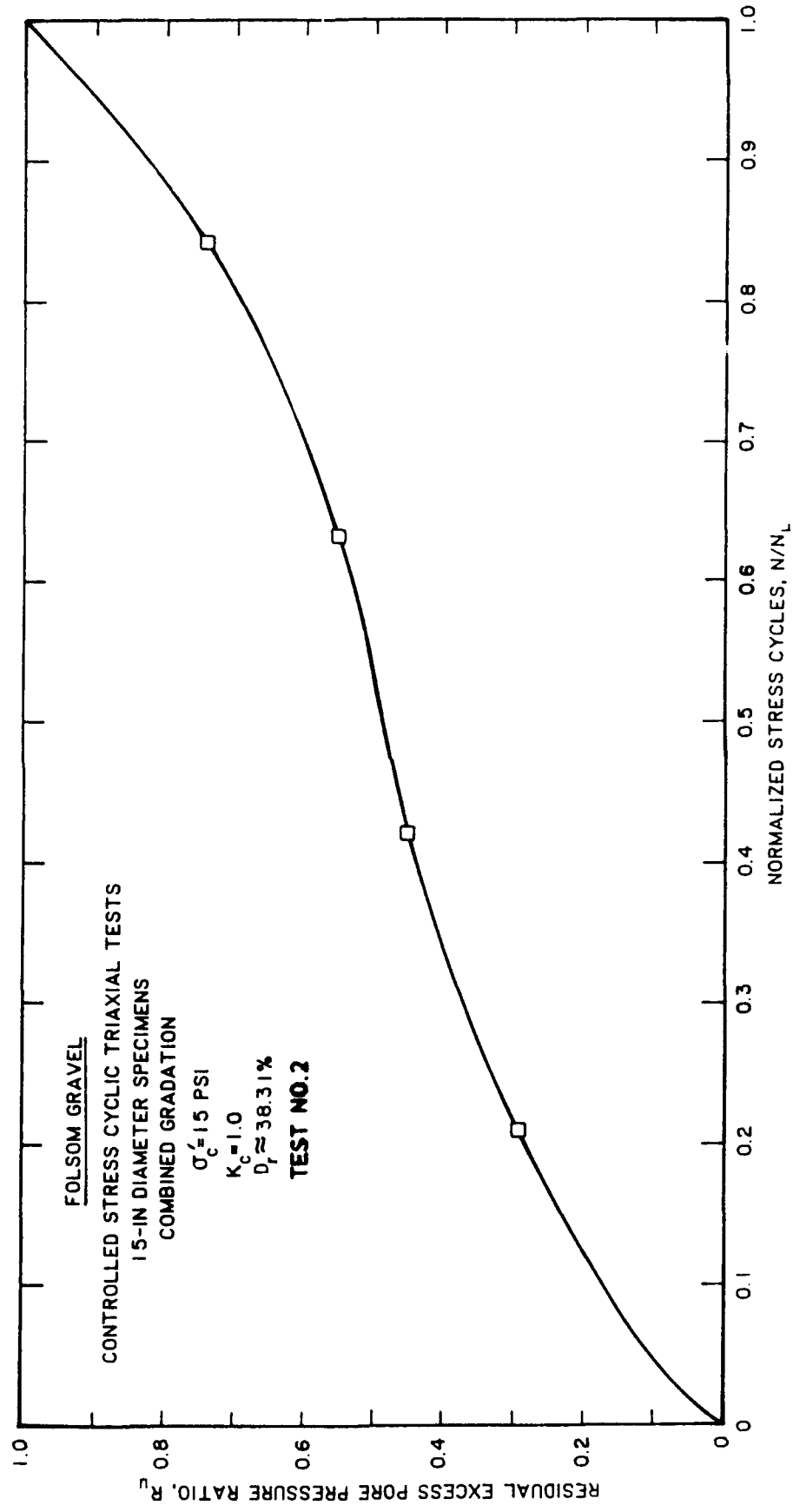


Figure B68. Residual excess pore pressure versus normalized stress cycle

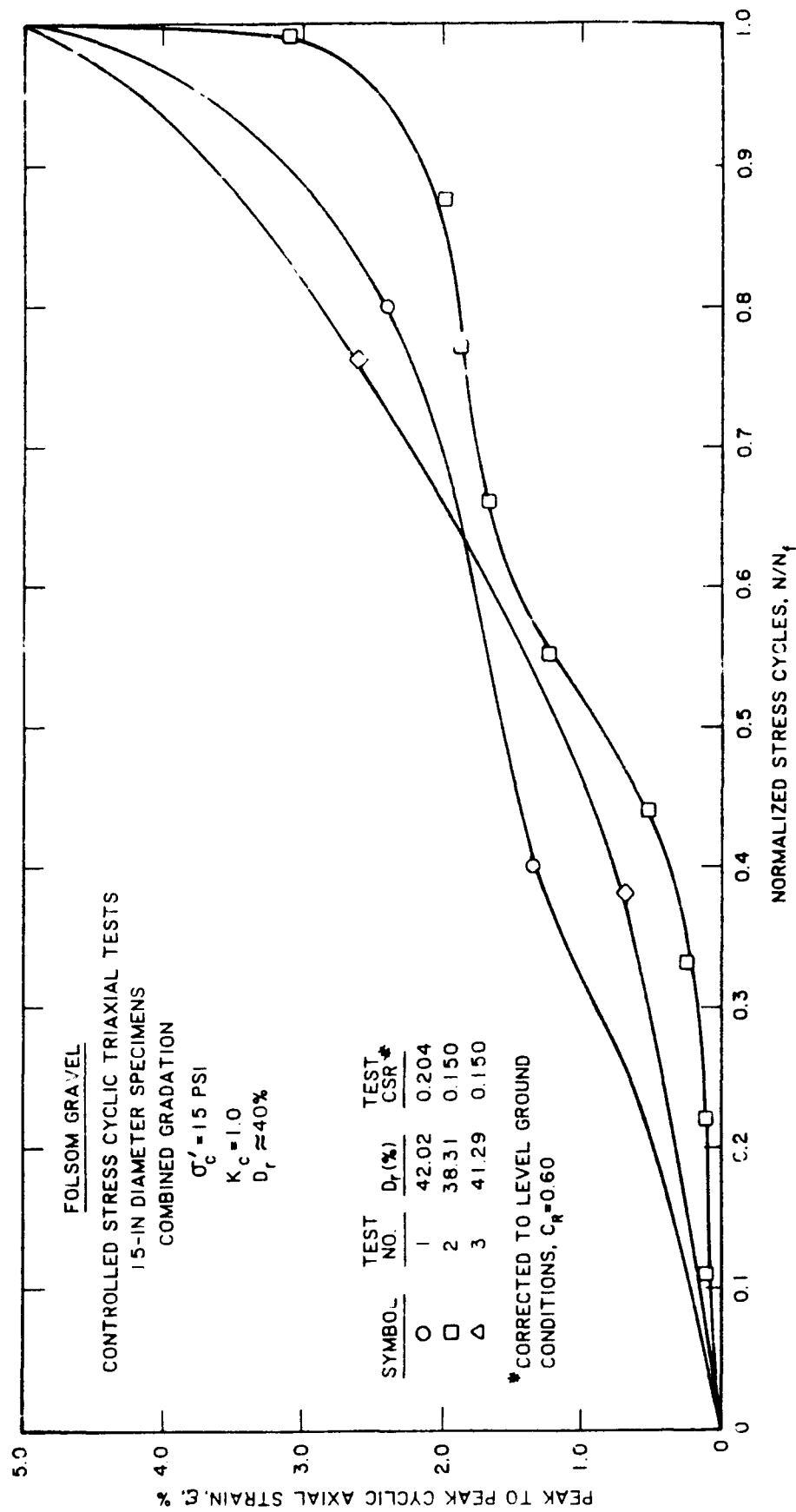


Figure B69. Peak to peak cyclic strain versus normalized stress cycle (Note:  $N_f$  = cycle at which  $\pm \epsilon = 5$  percent)

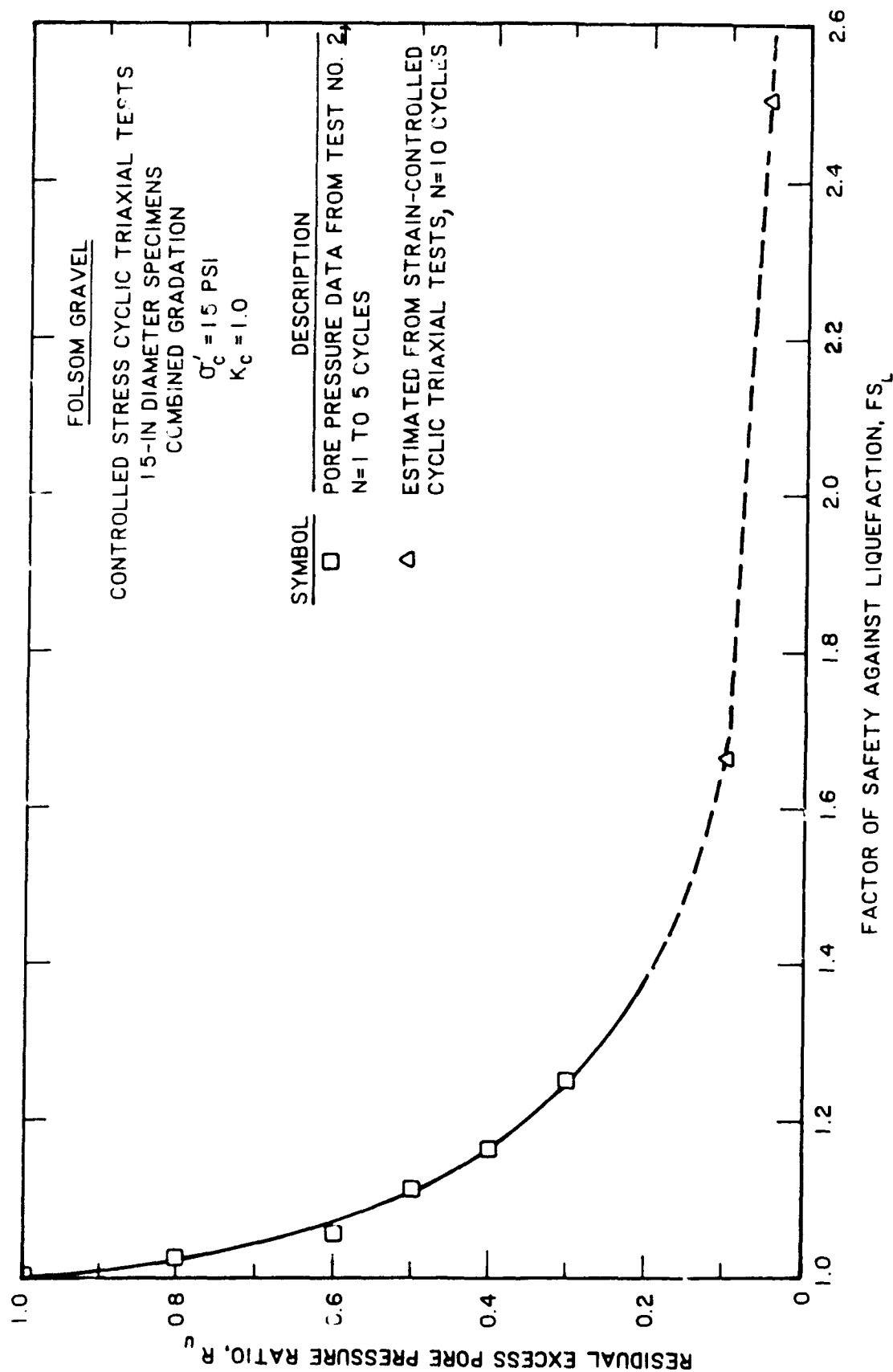


Figure B70. Relationship between factor of safety against liquefaction and residual excess pore pressure ratio



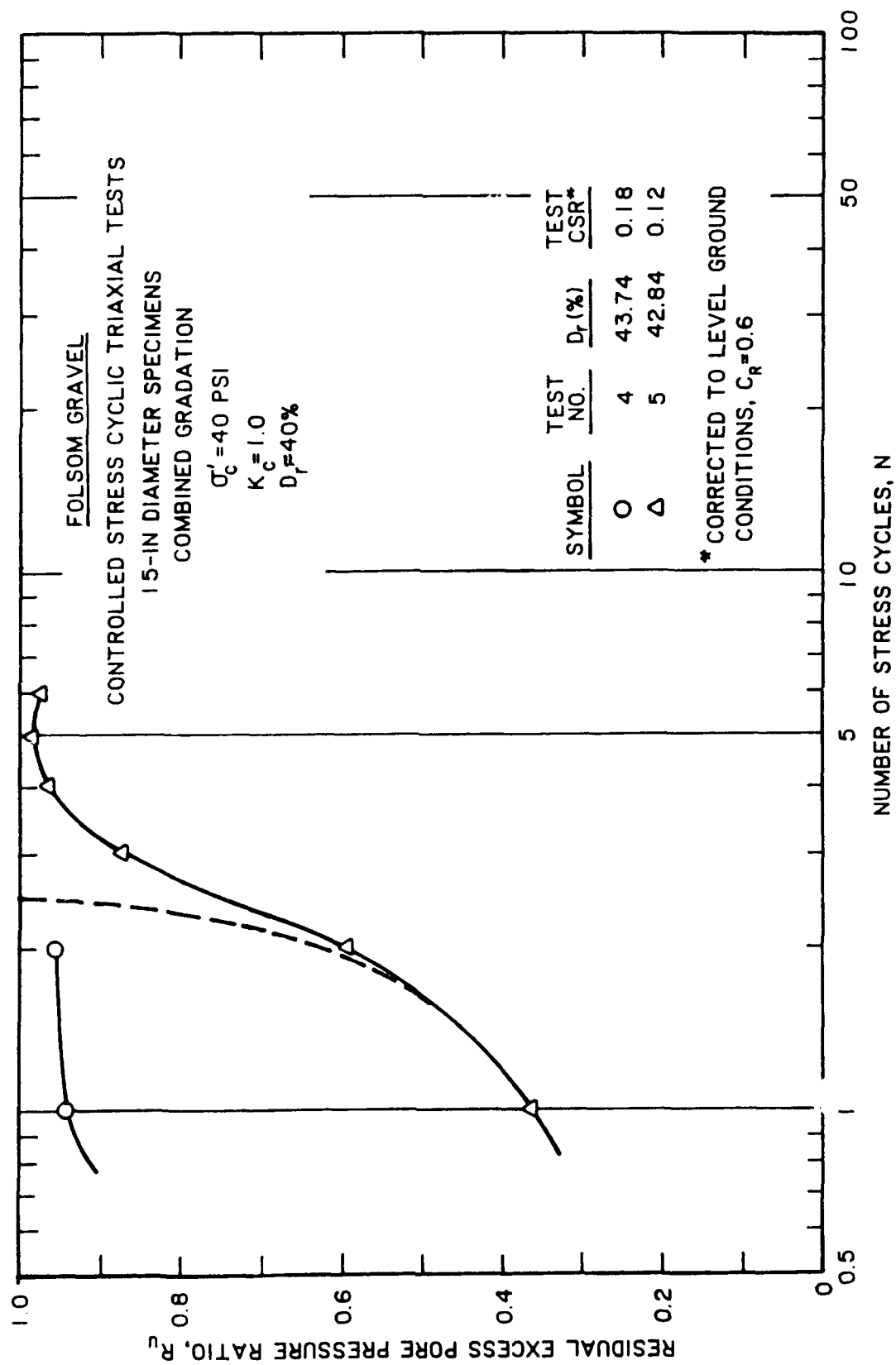


Figure B71. Development of residual excess pore pressure with each stress cycle

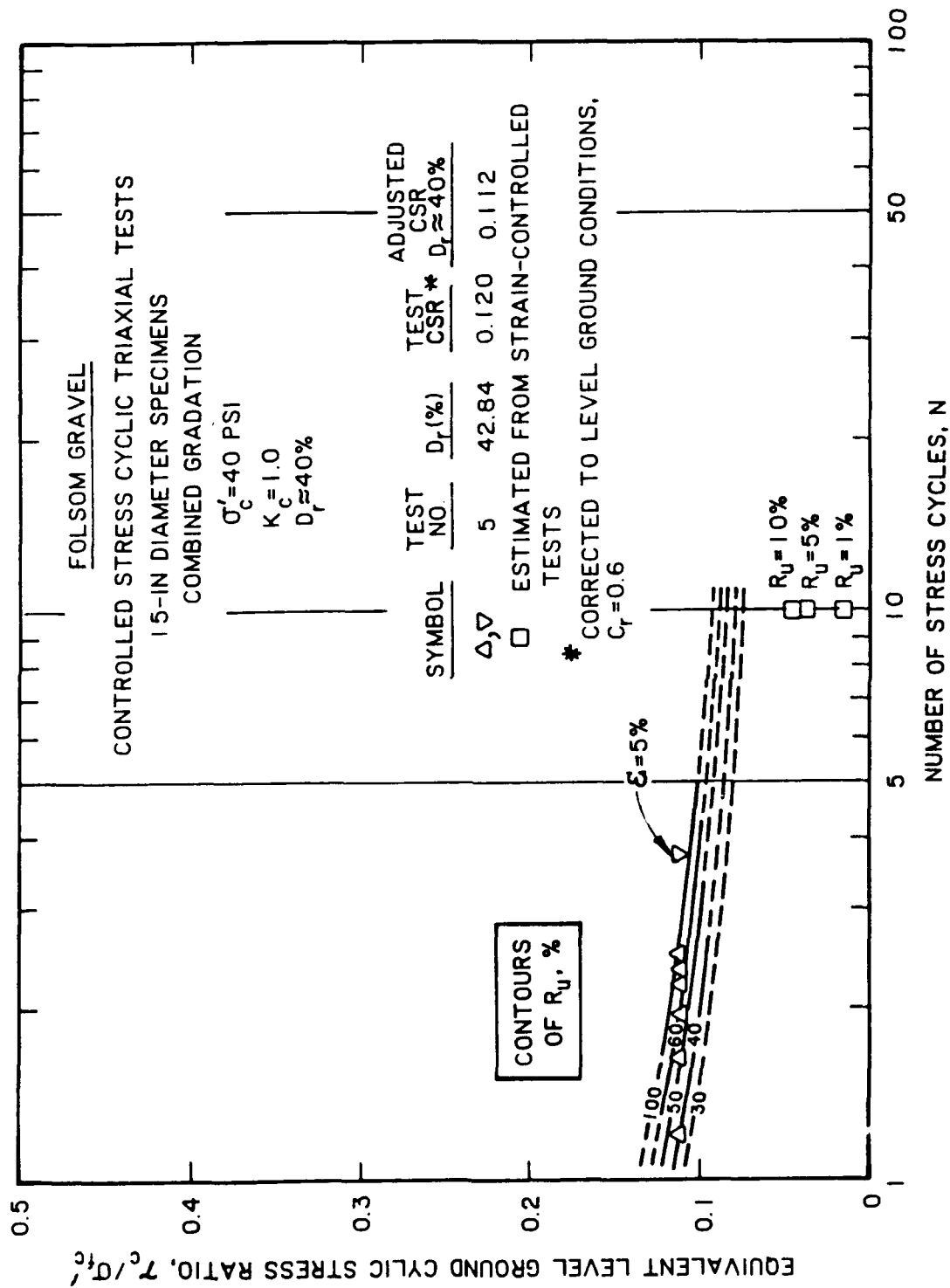


Figure B72. Contours of residual excess pore pressure ratio

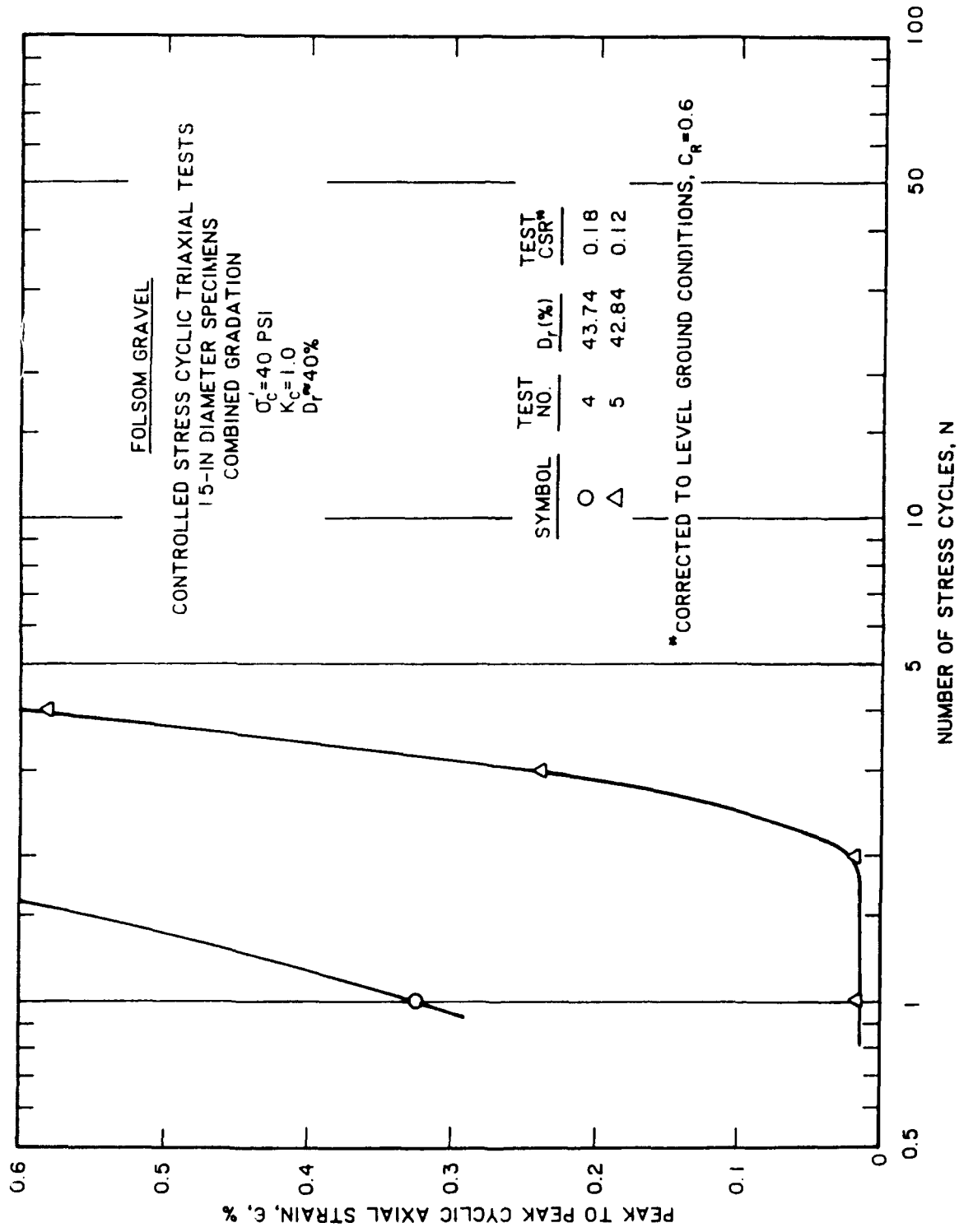


Figure B73. Development of peak to peak cyclic strain with each stress cycle

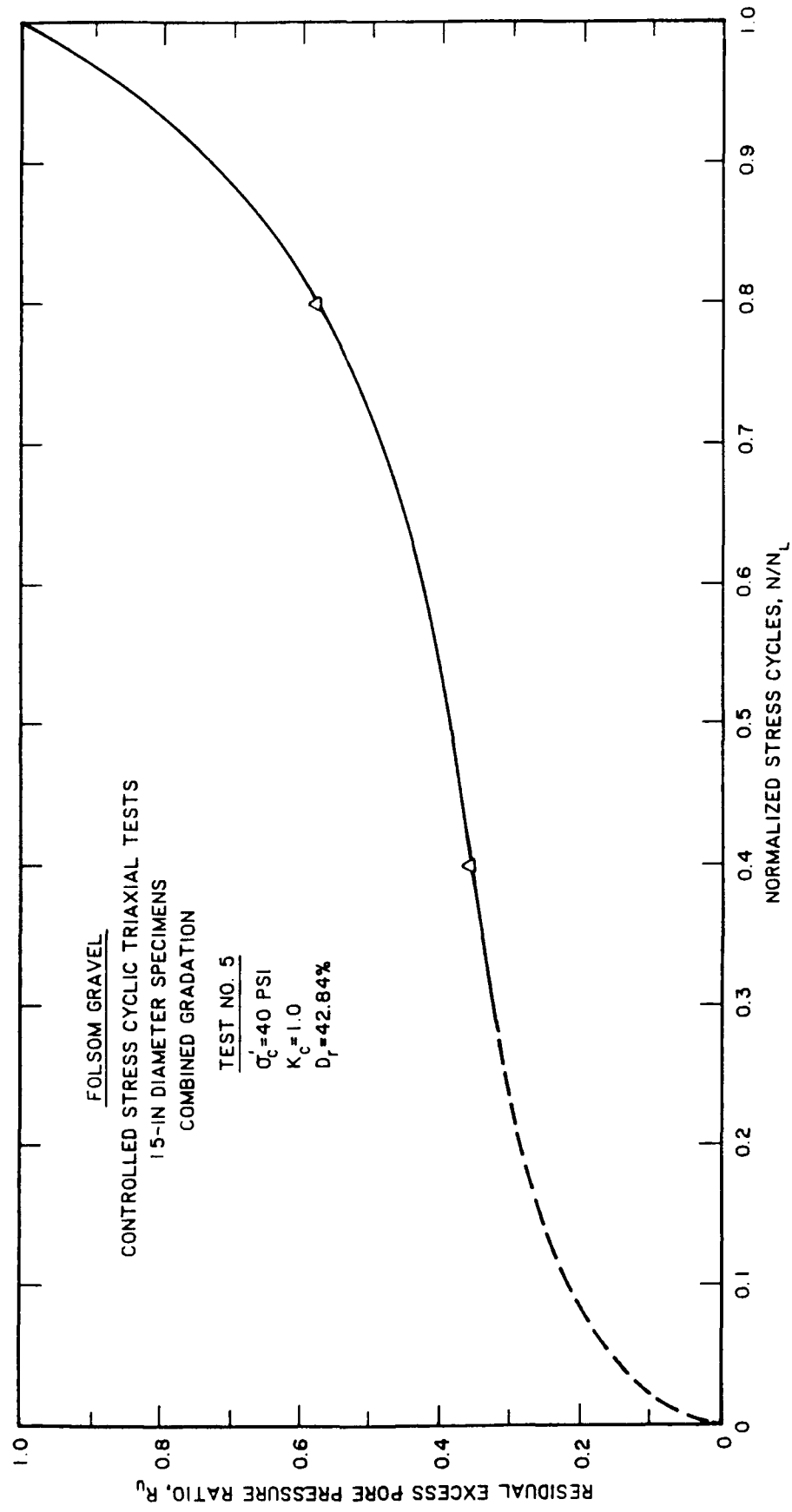


Figure B74. Residual excess pore pressure versus normalized stress cycle

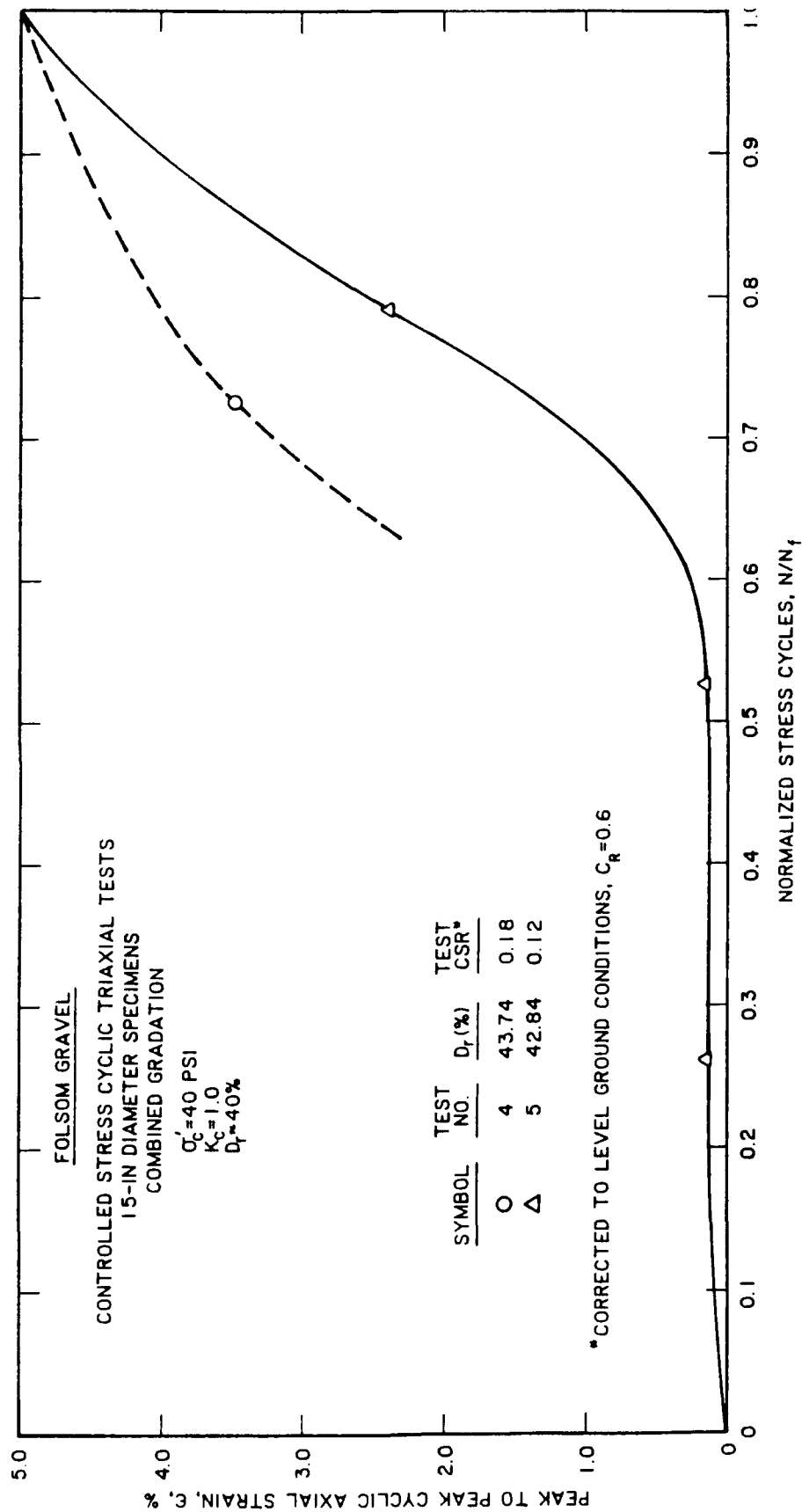


Figure B75. Peak to peak cyclic strain versus normalized stress cycle (Note:  $N_f$  = cycle at which  $\pm \epsilon = 5$  percent)

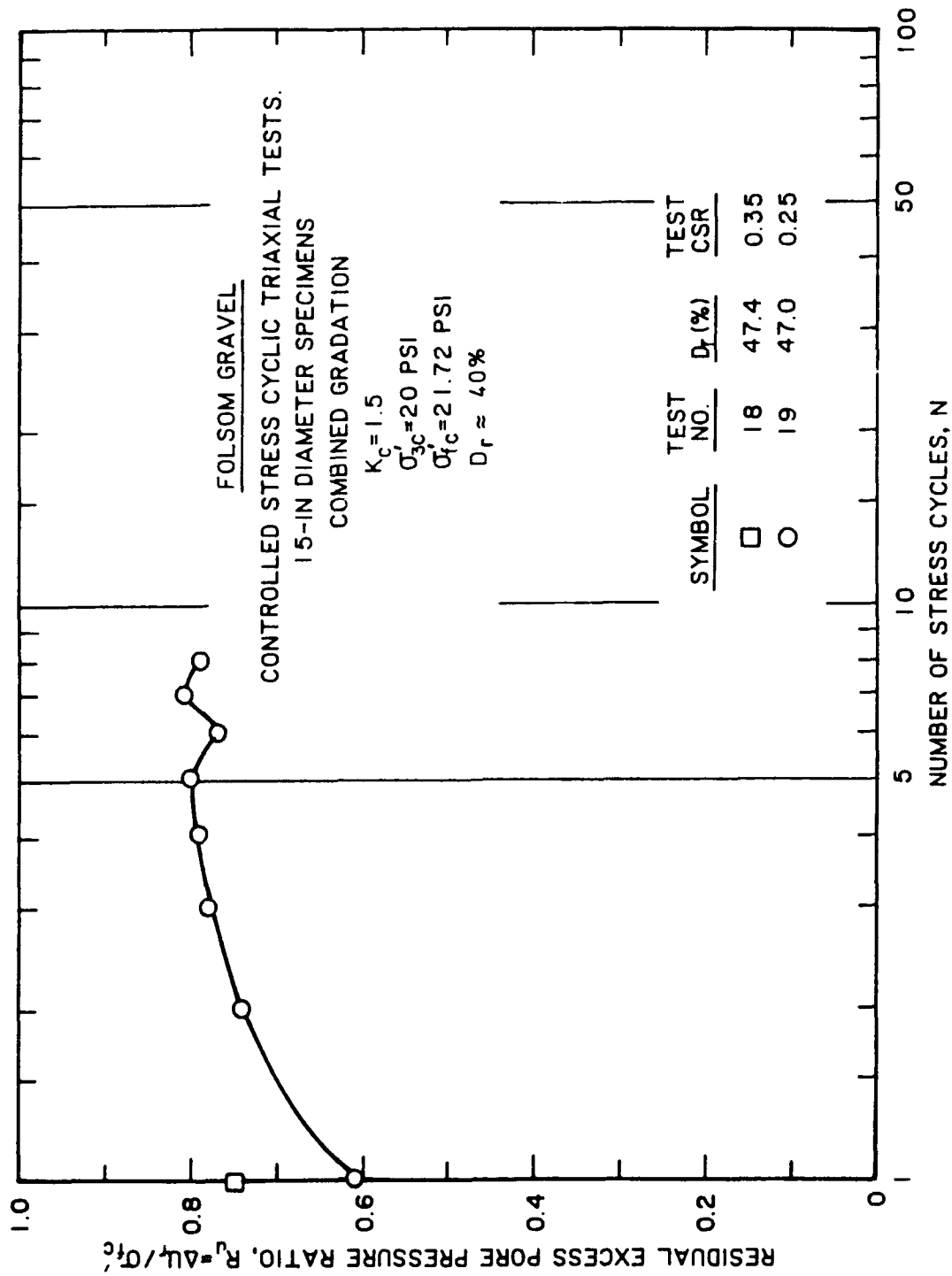


Figure B76. Development of residual excess pore pressure with each stress cycle

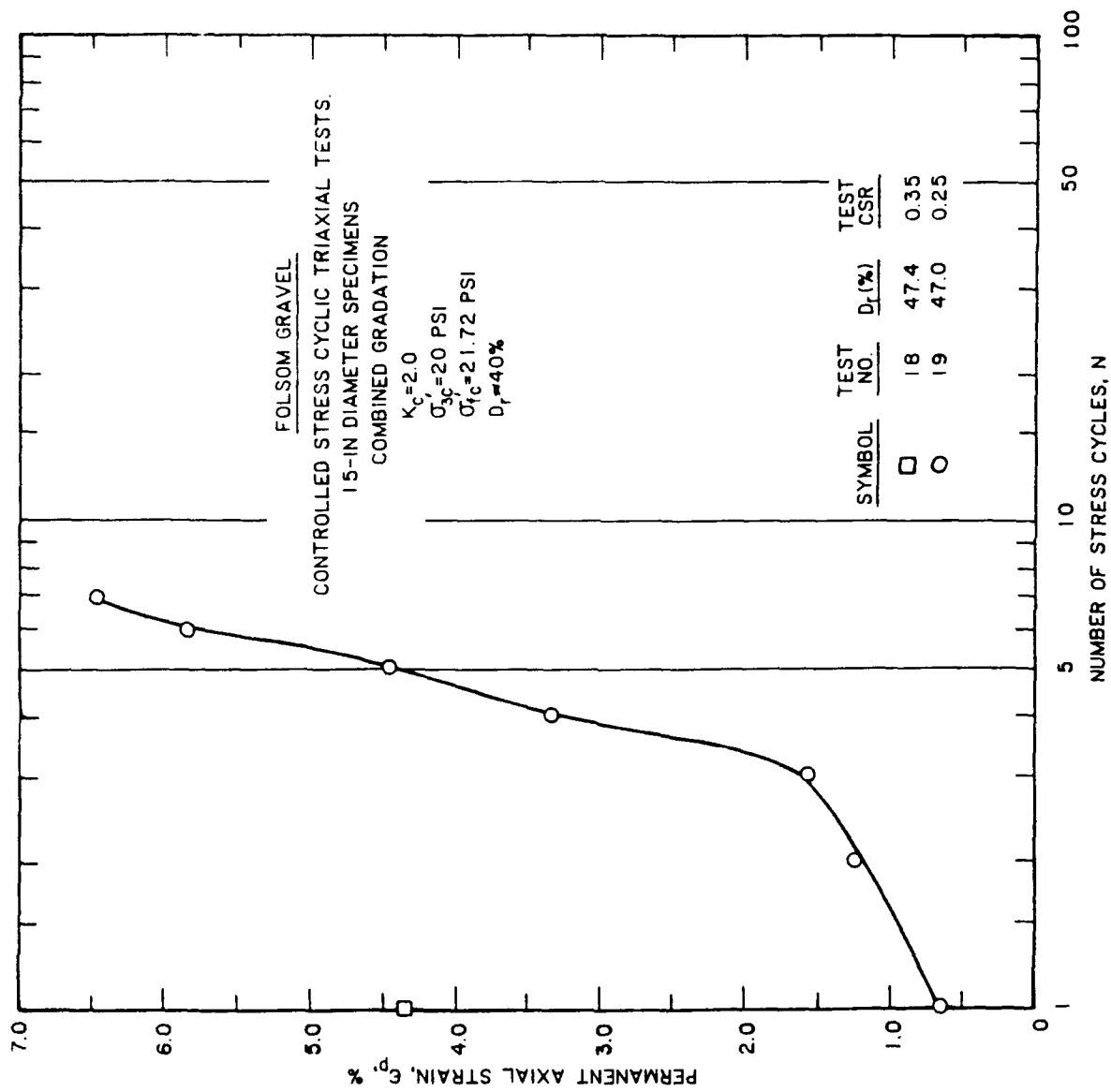


Figure B77. Development of permanent axial strain with each stress cycle

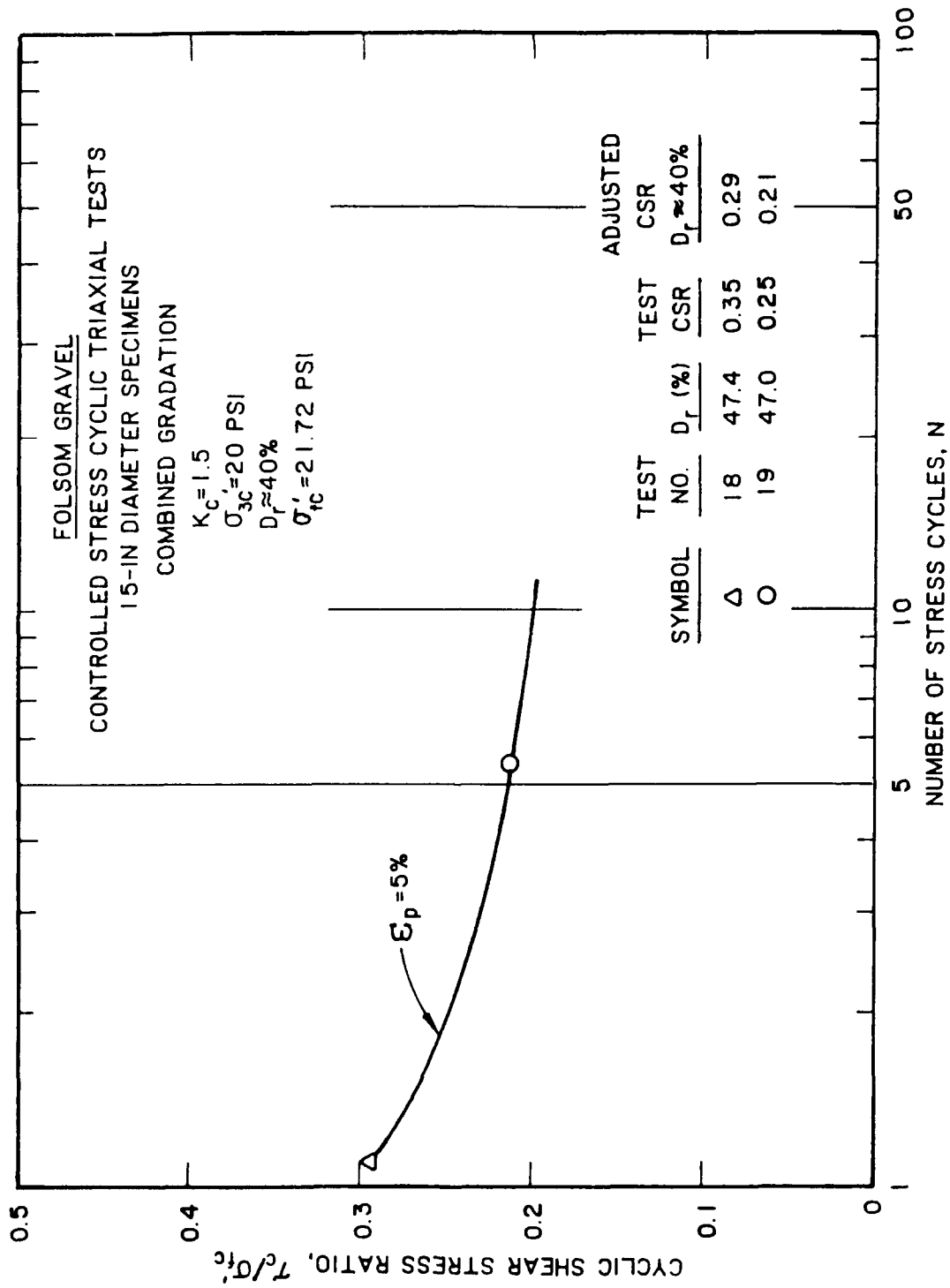


Figure B78. Contours of permanent axial strain



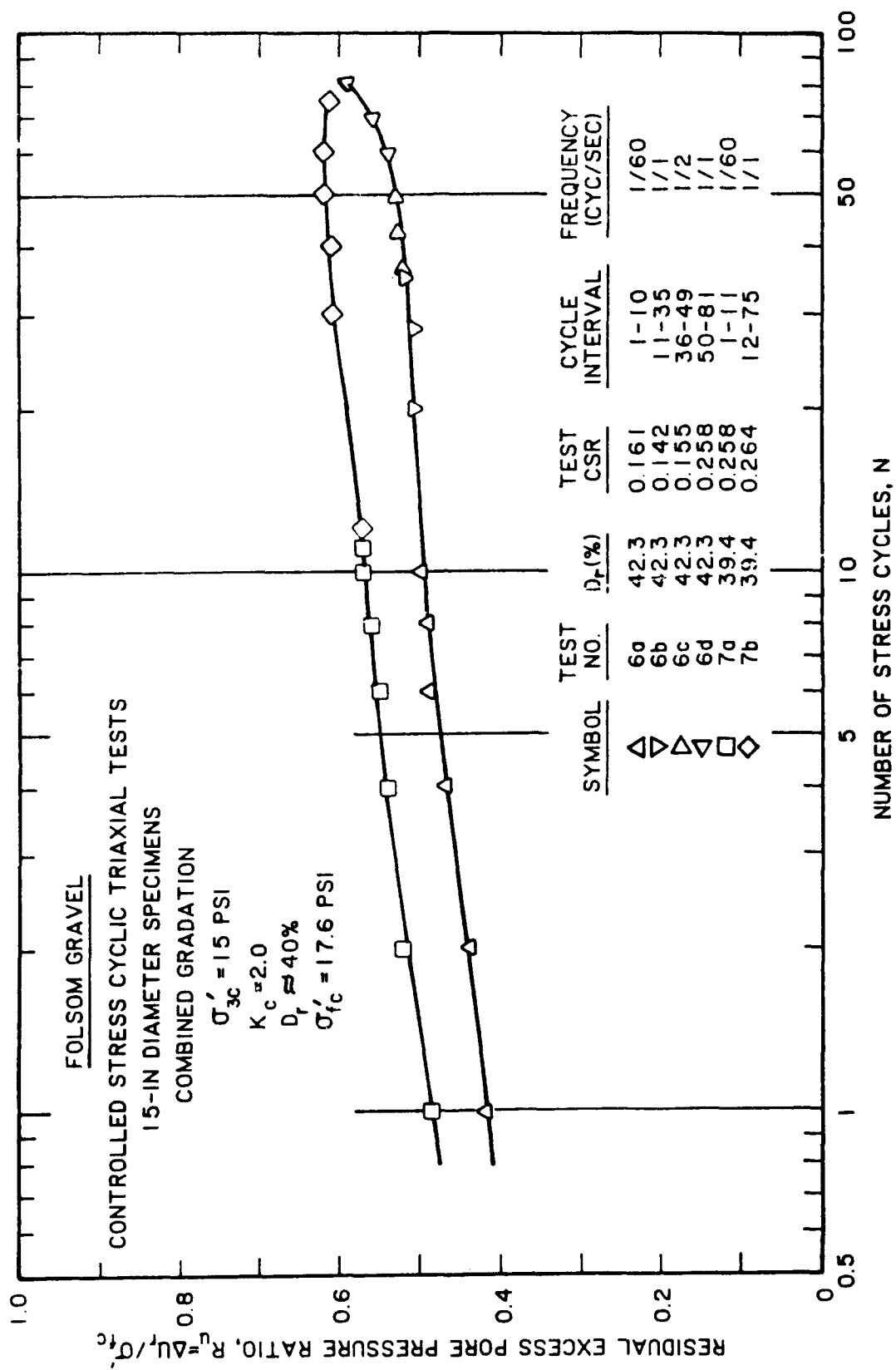


Figure B79. Development of residual excess pore pressure with each stress cycle

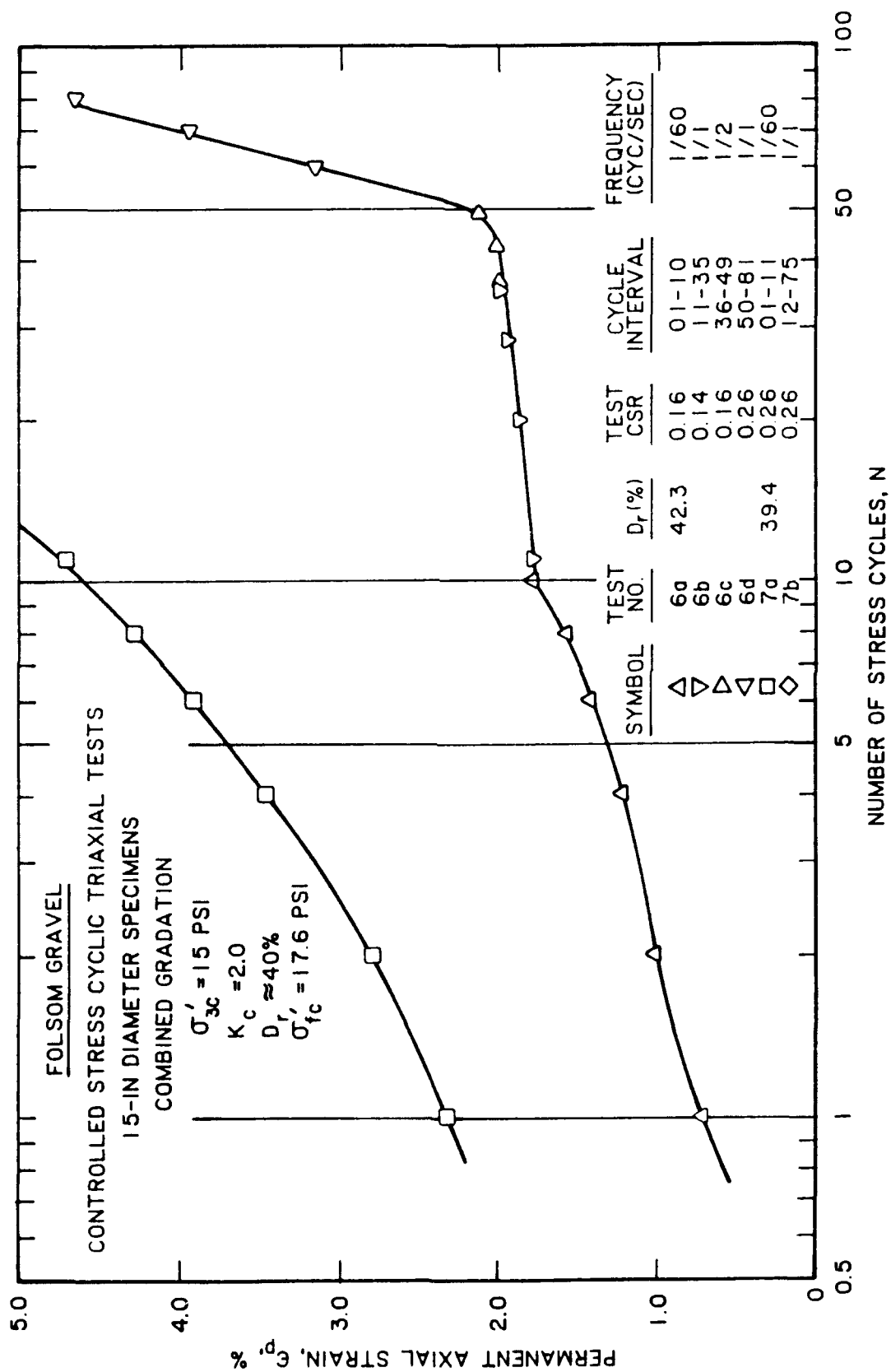


Figure B80. Development of permanent axial strain with each stress cycle

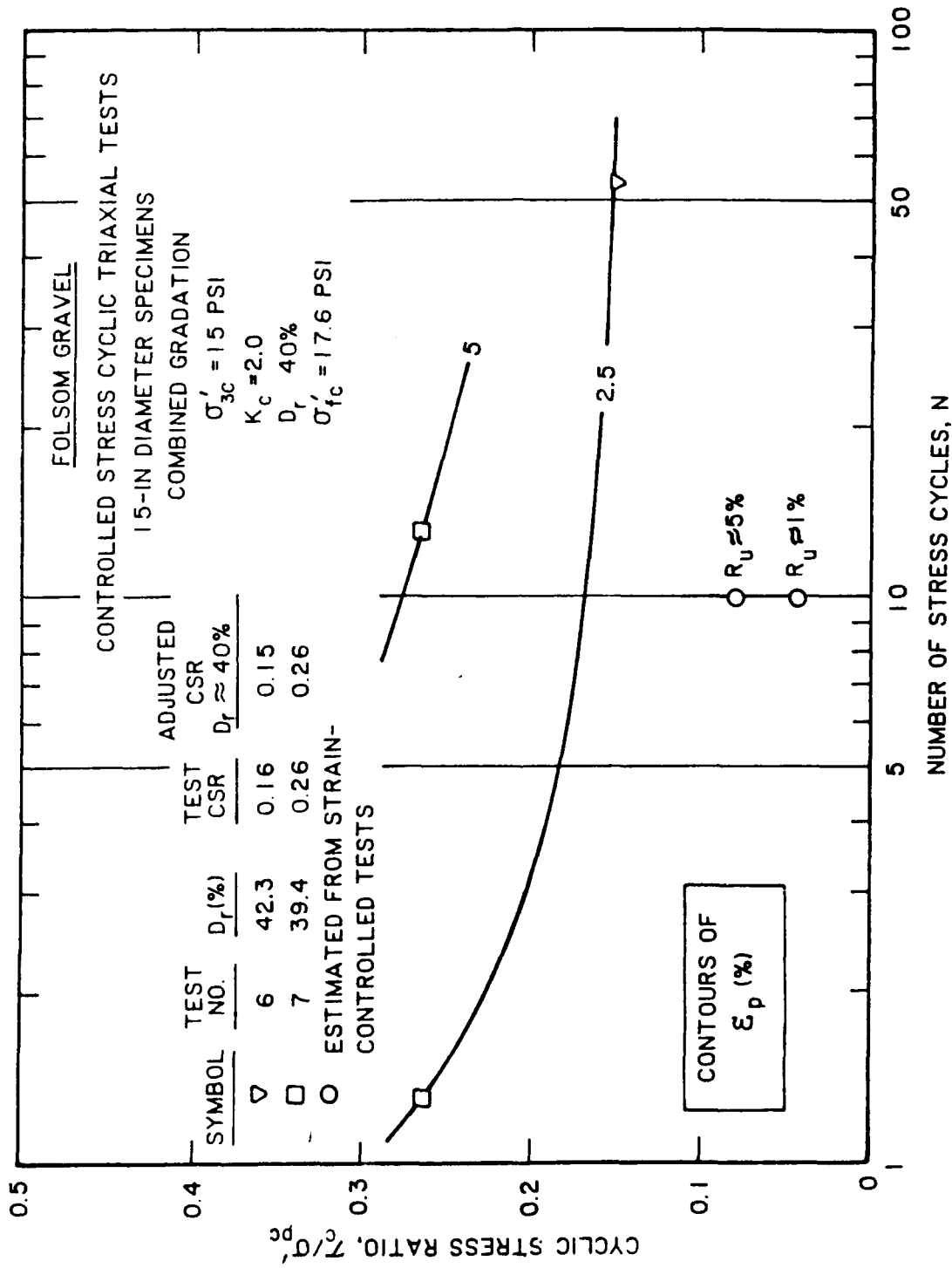


Figure B81. Contours of permanent axial strain

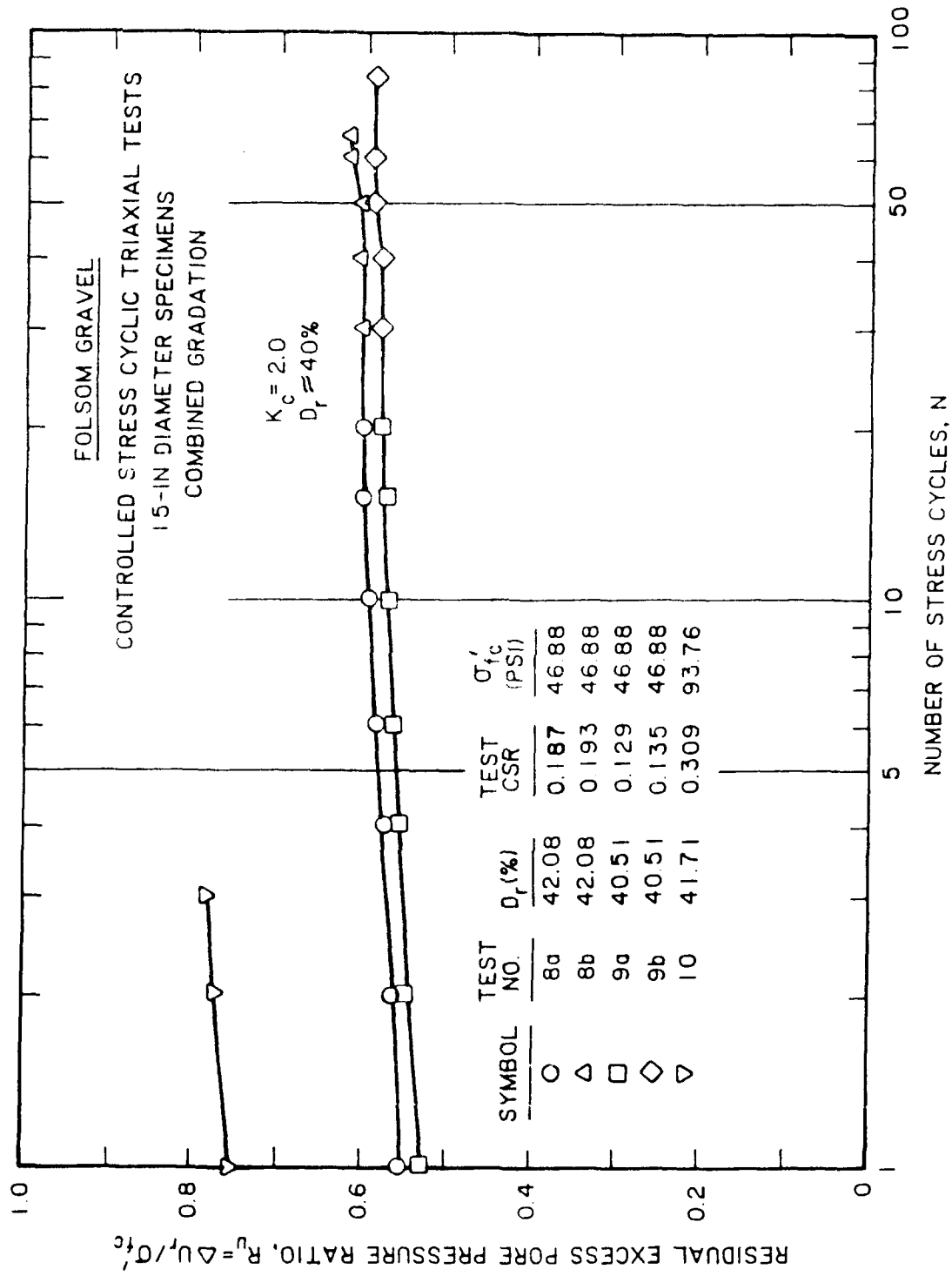


Figure B82. Development of residual excess pore pressure with each stress cycle

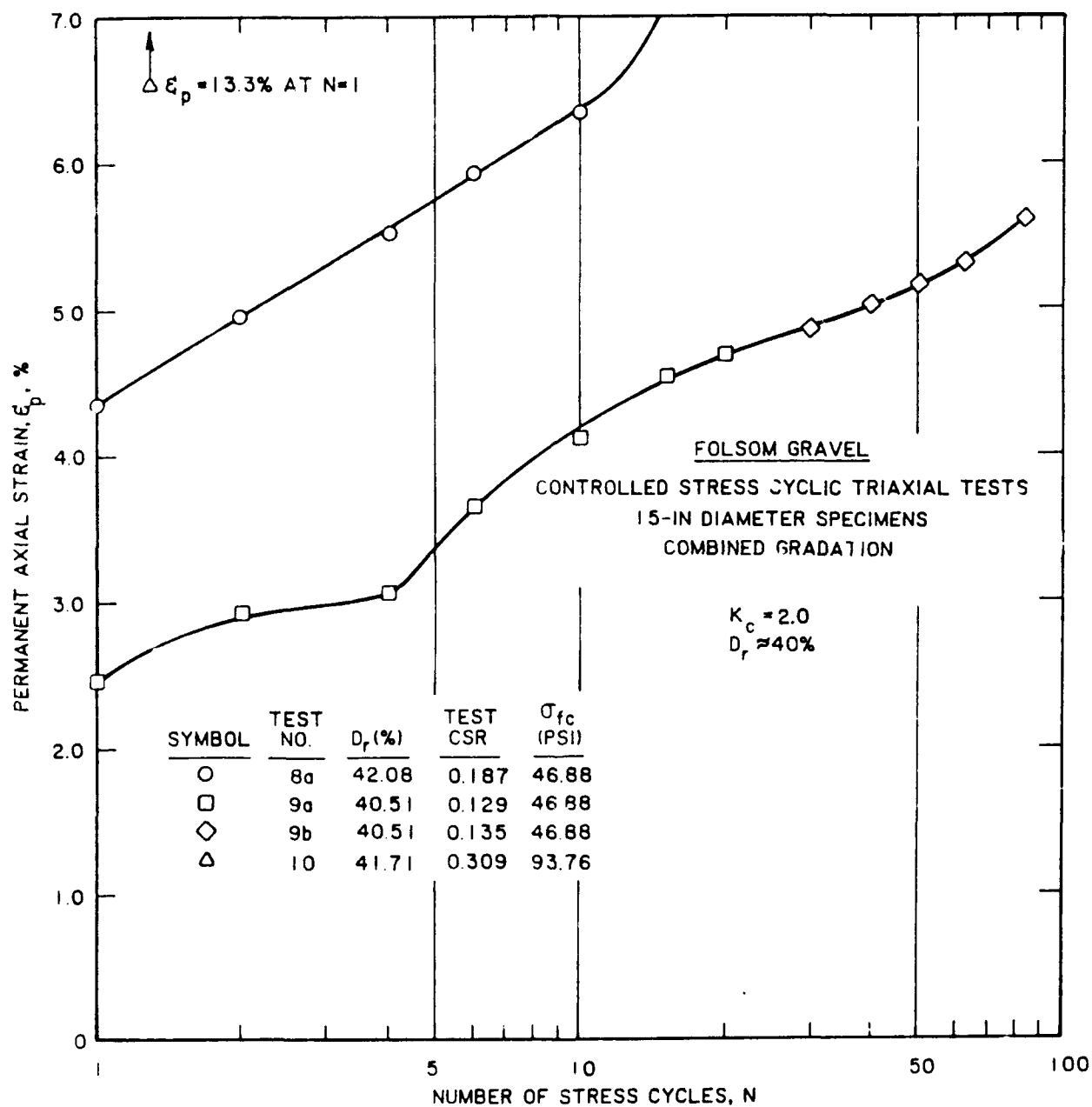


Figure B83. Development of permanent axial strain with each stress cycle

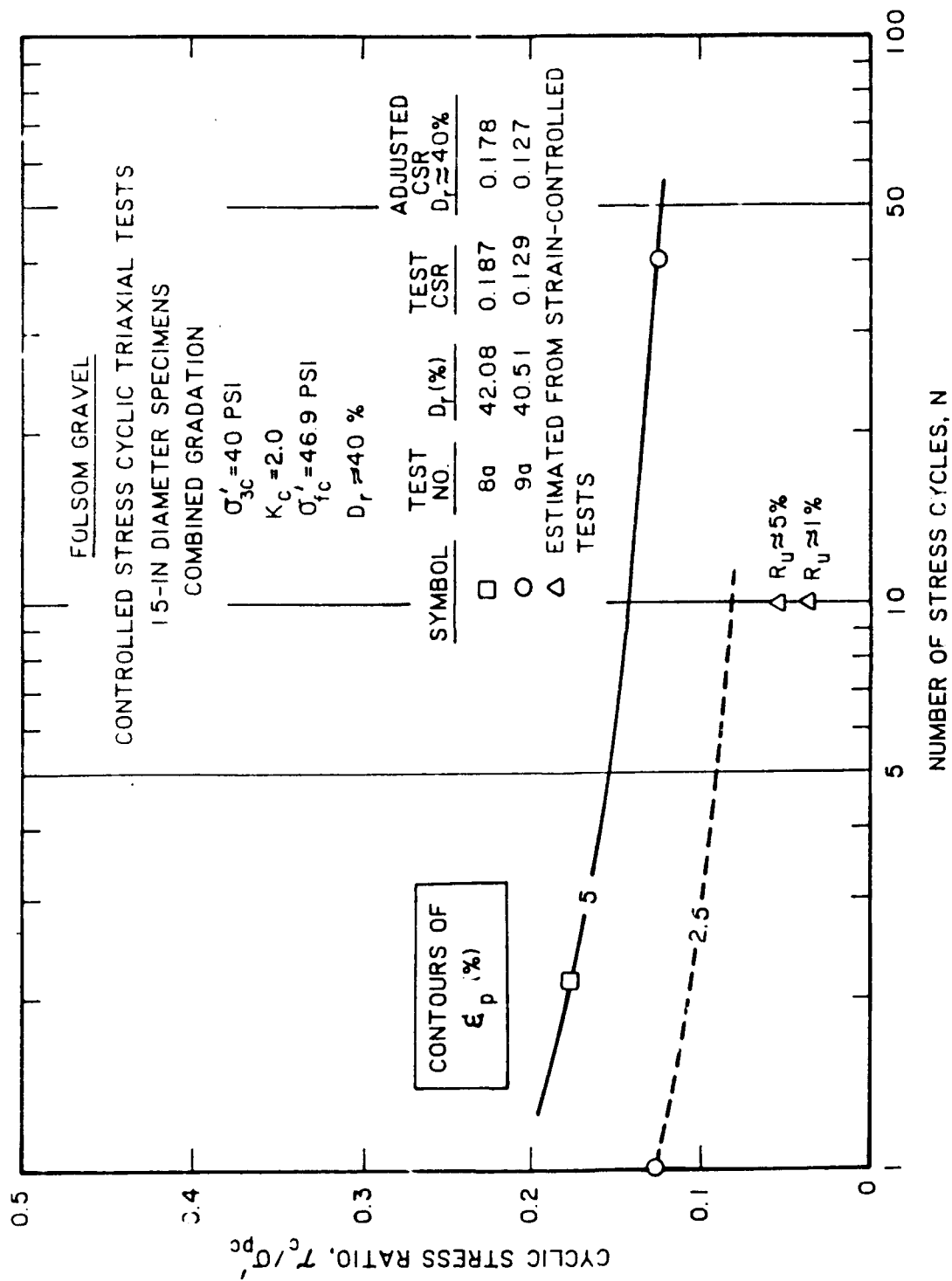


Figure B84. Contours of permanent axial strain

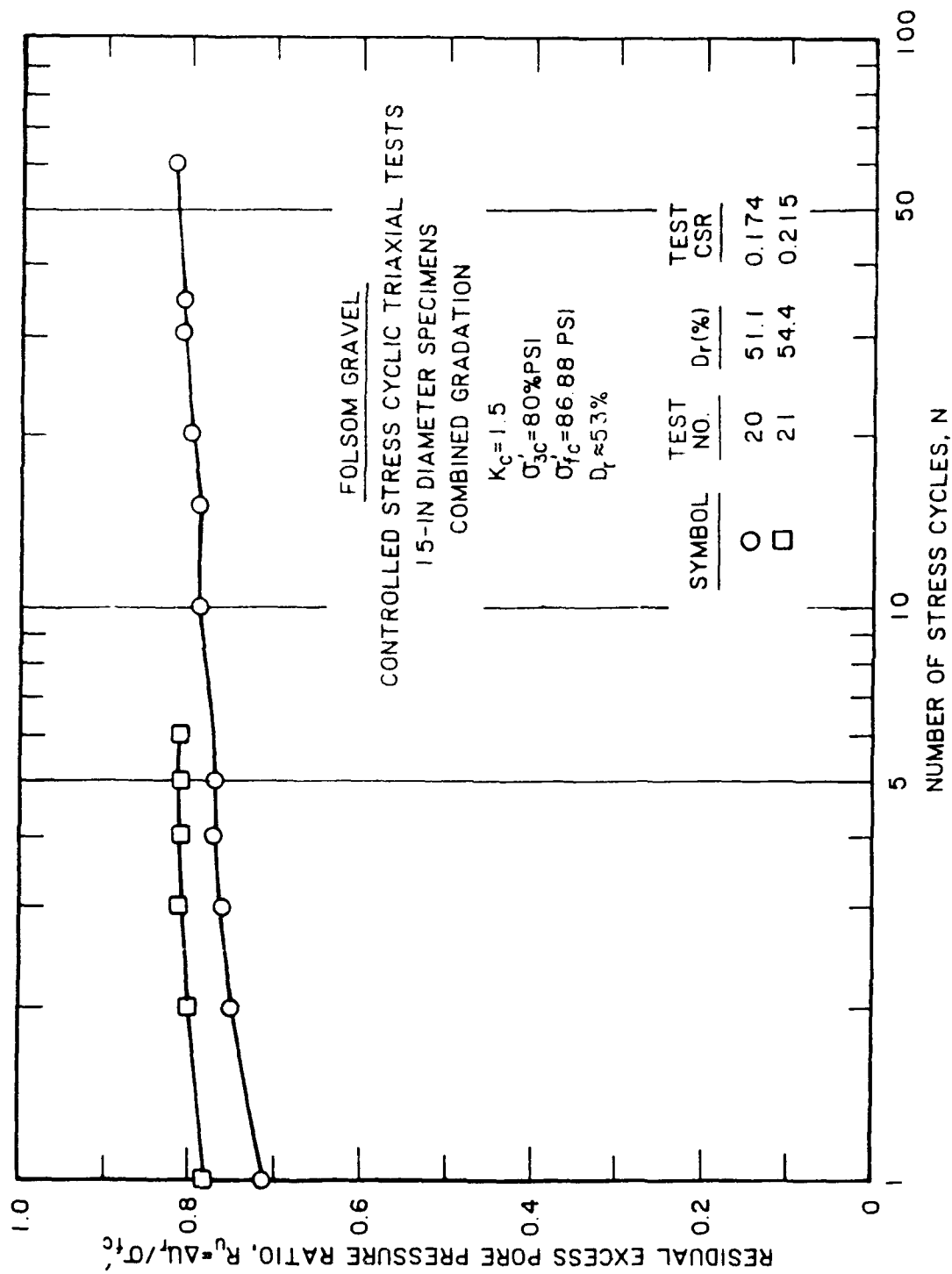


Figure B85. Development of residual excess pore pressure with each stress cycle

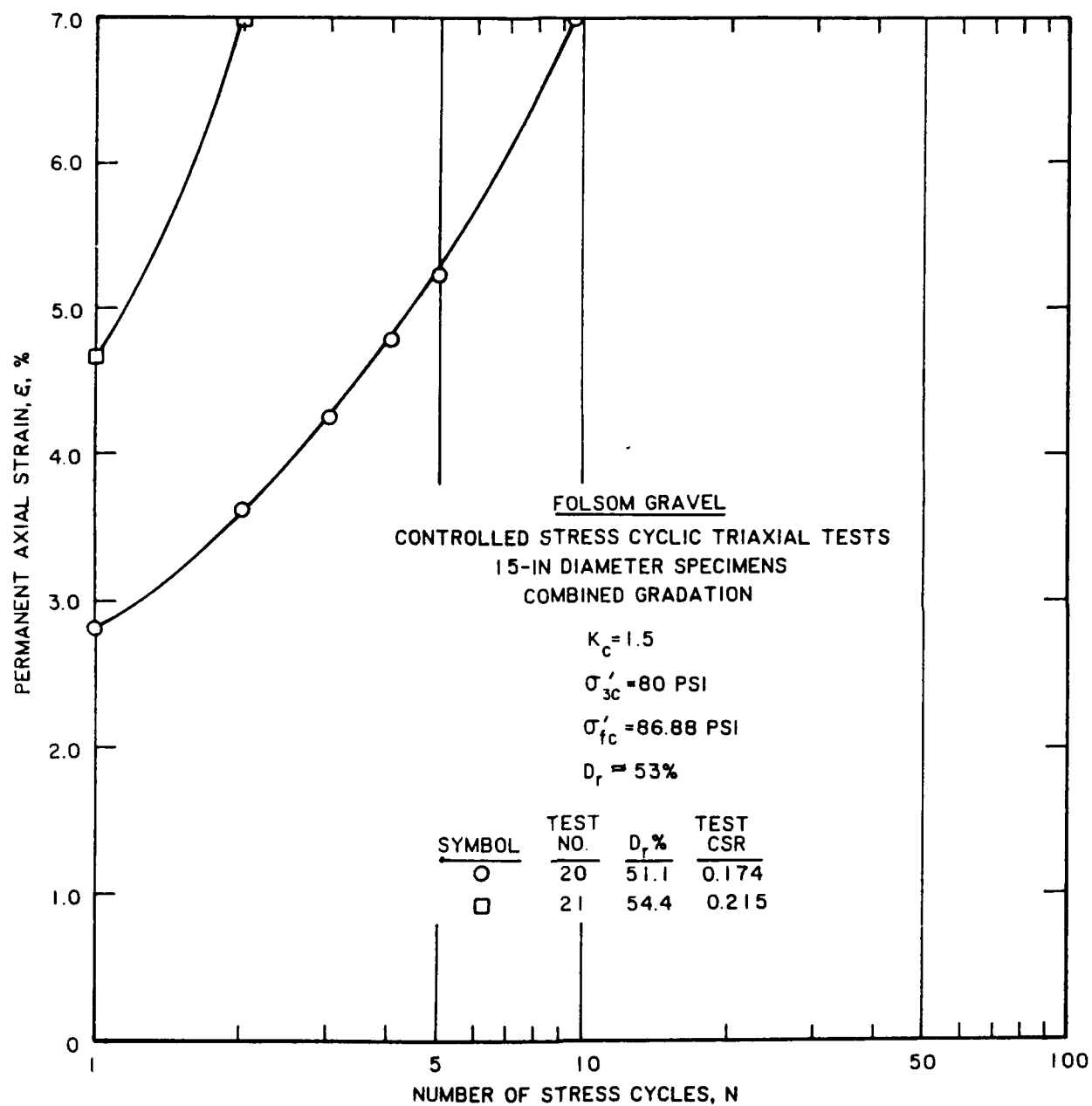


Figure B86. Development of permanent axial strain with each stress cycle



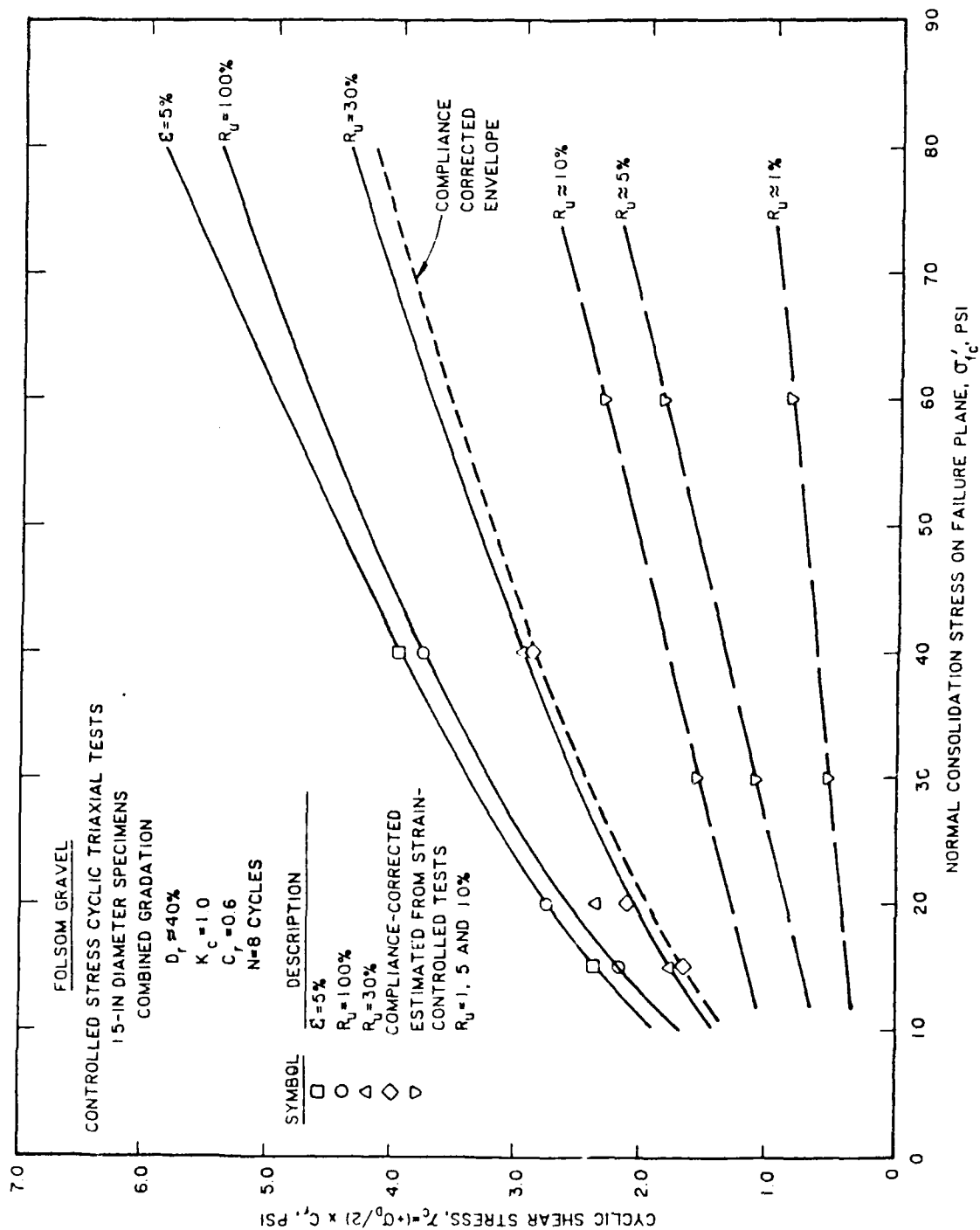


Figure B87. Cyclic strength envelopes for Folsom gravel ( $D_R \approx 40$  percent) determined in laboratory tests

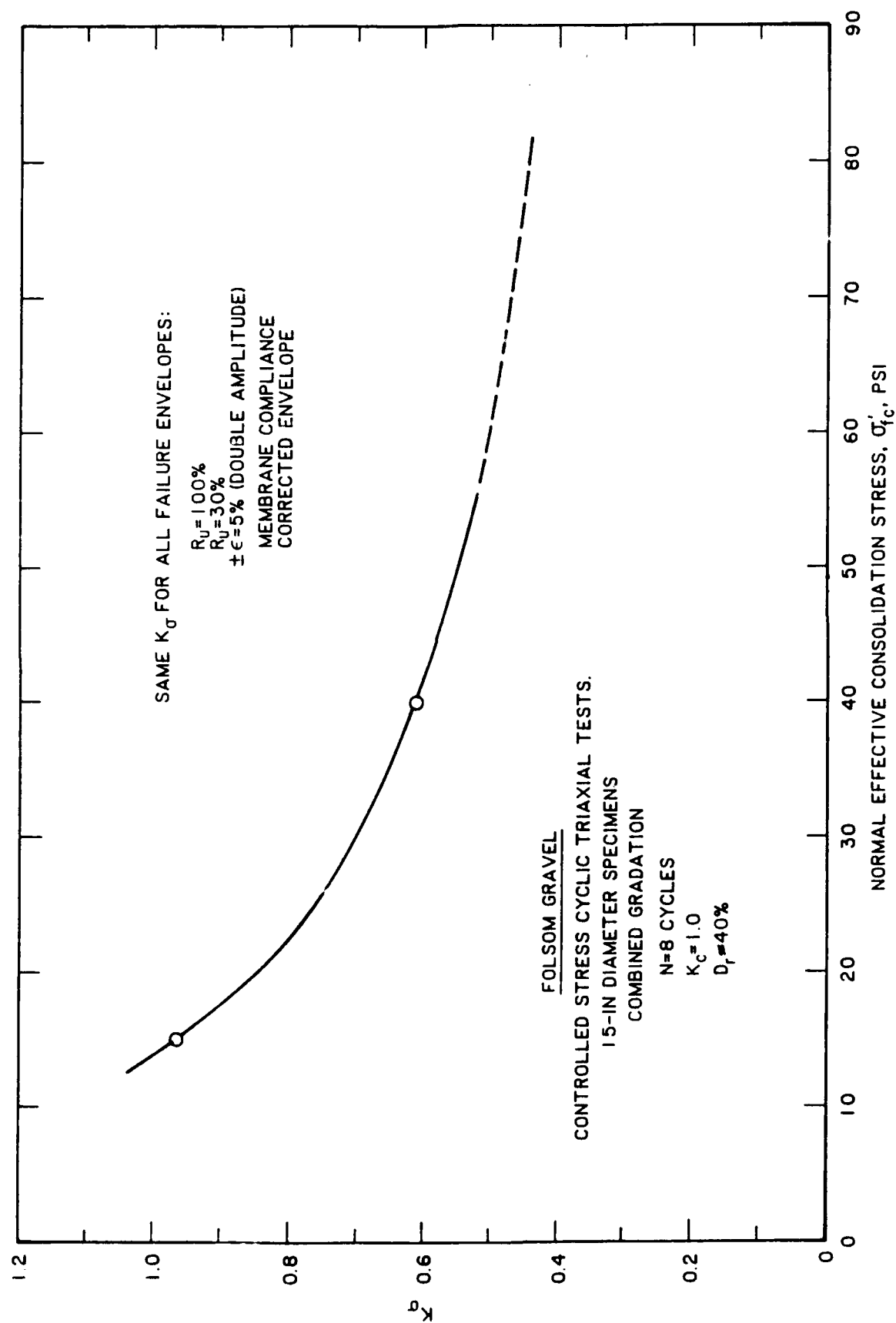


Figure B88. Overburden connection factor,  $K_\sigma$ , for Folsom gravel ( $D_R \approx 40$  percent) determined in laboratory tests

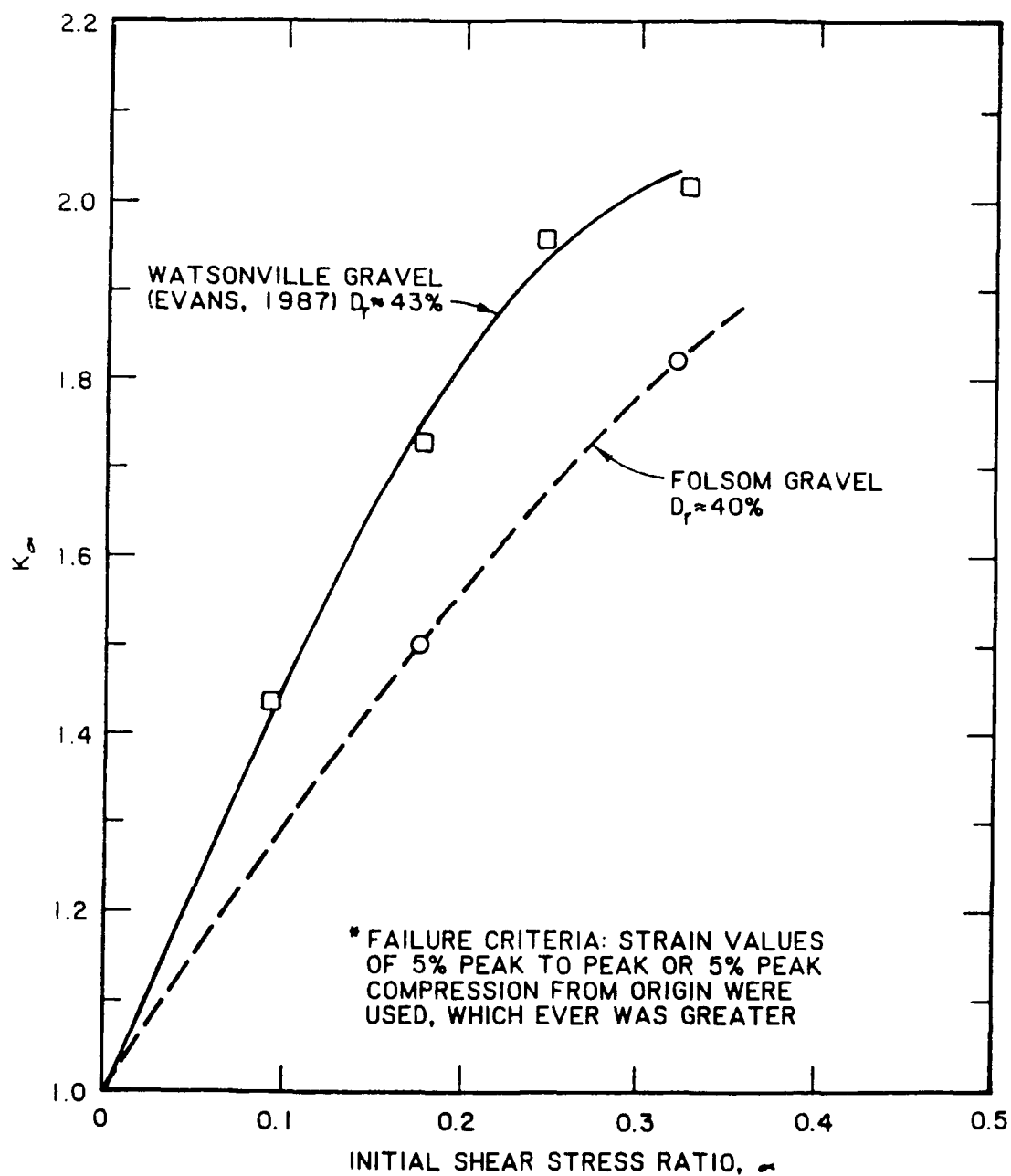


Figure B89. Initial stress ratio correction factor,  $K_\alpha$ , for Folsom gravel ( $D_R \approx 40$  percent) for failure criterion of 5 percent permanent axial strain. Data from Evans (1987) shown for comparison

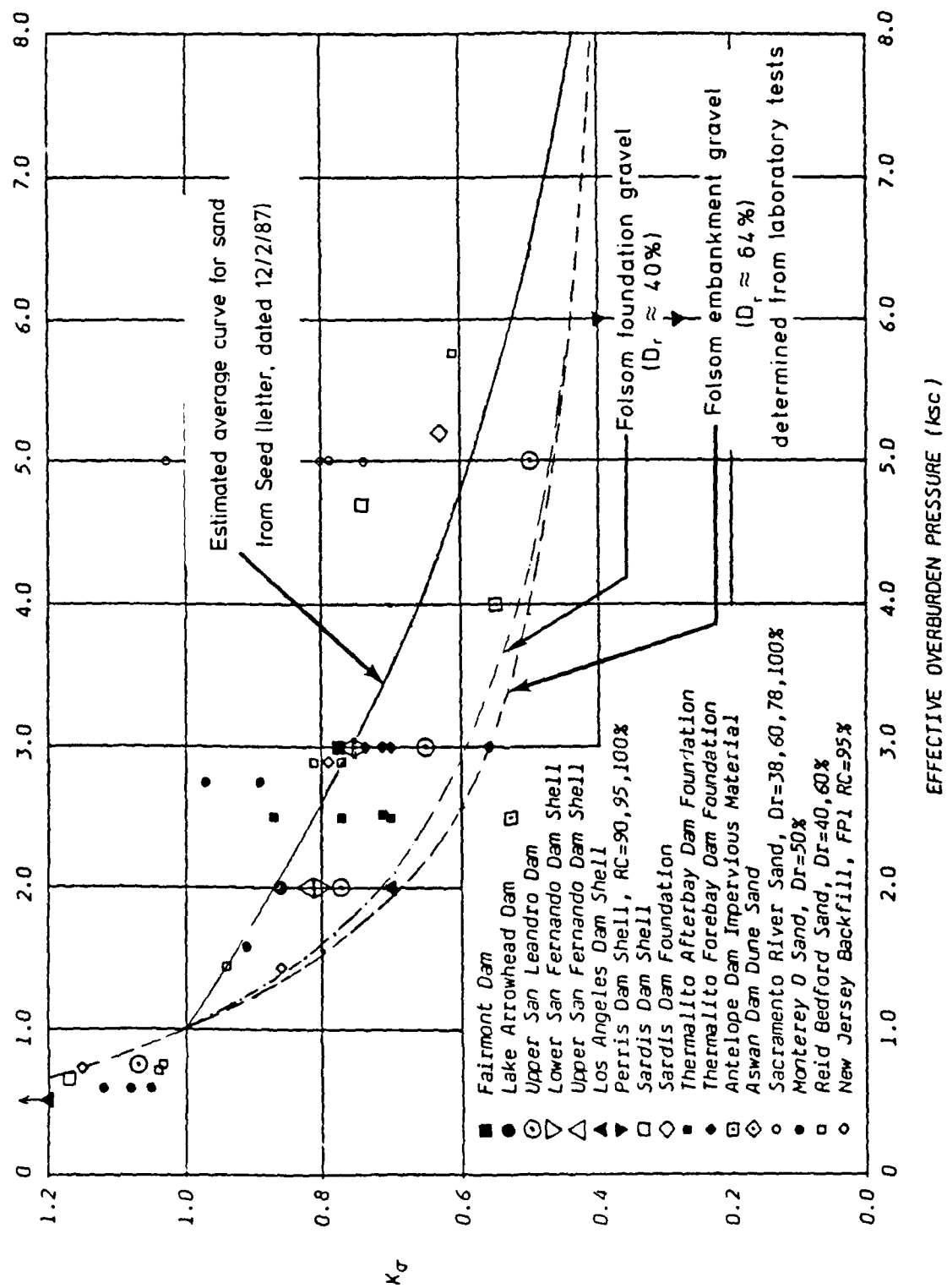


Figure B90. Comparison of laboratory-determined  $K_\sigma$  curve for Folsom gravels with other data  
Data compiled by Leslie F. Harder

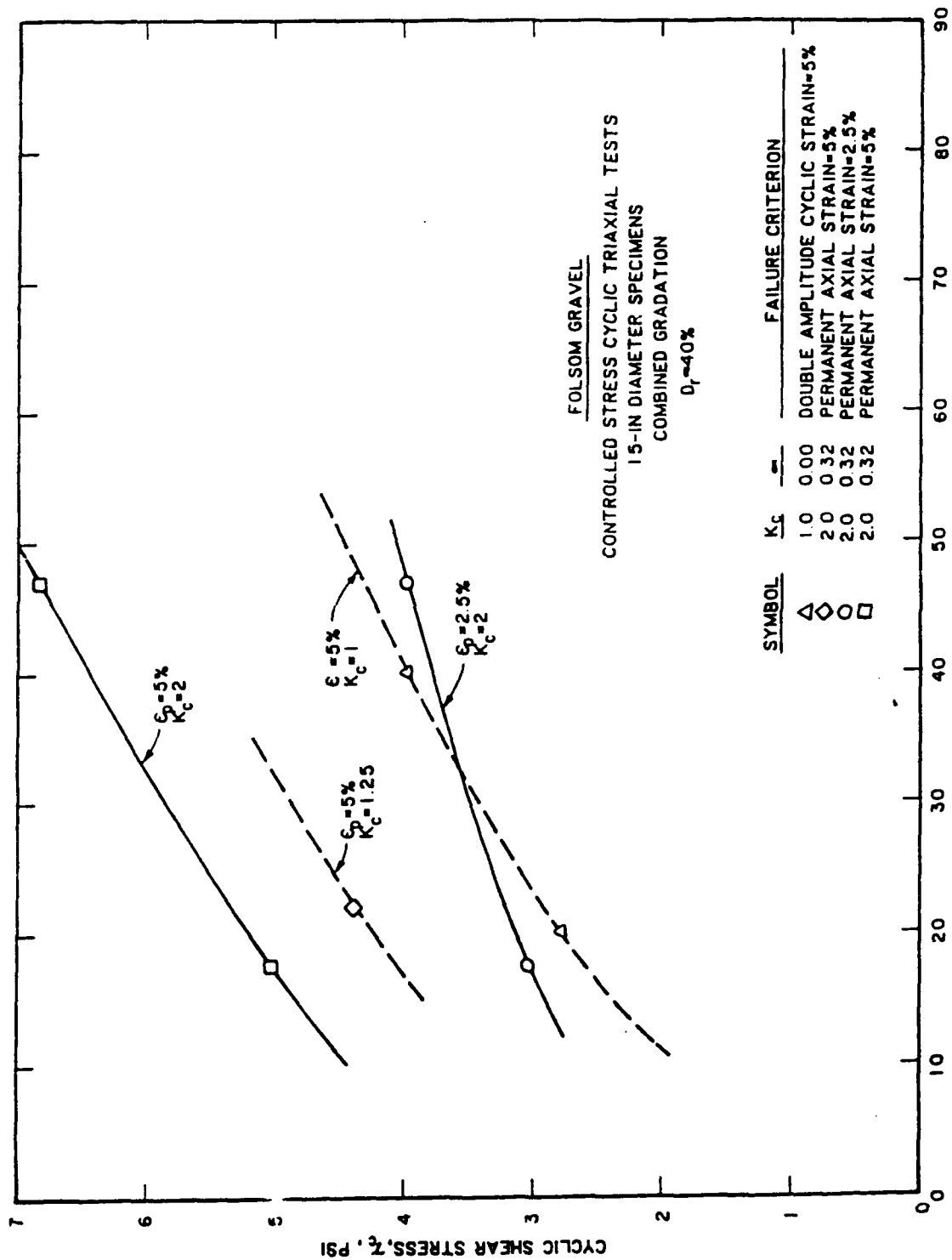


Figure B91. Comparison of cyclic strength envelopes for Folsom gravel ( $D_r \approx 40$  percent) determined in laboratory tests

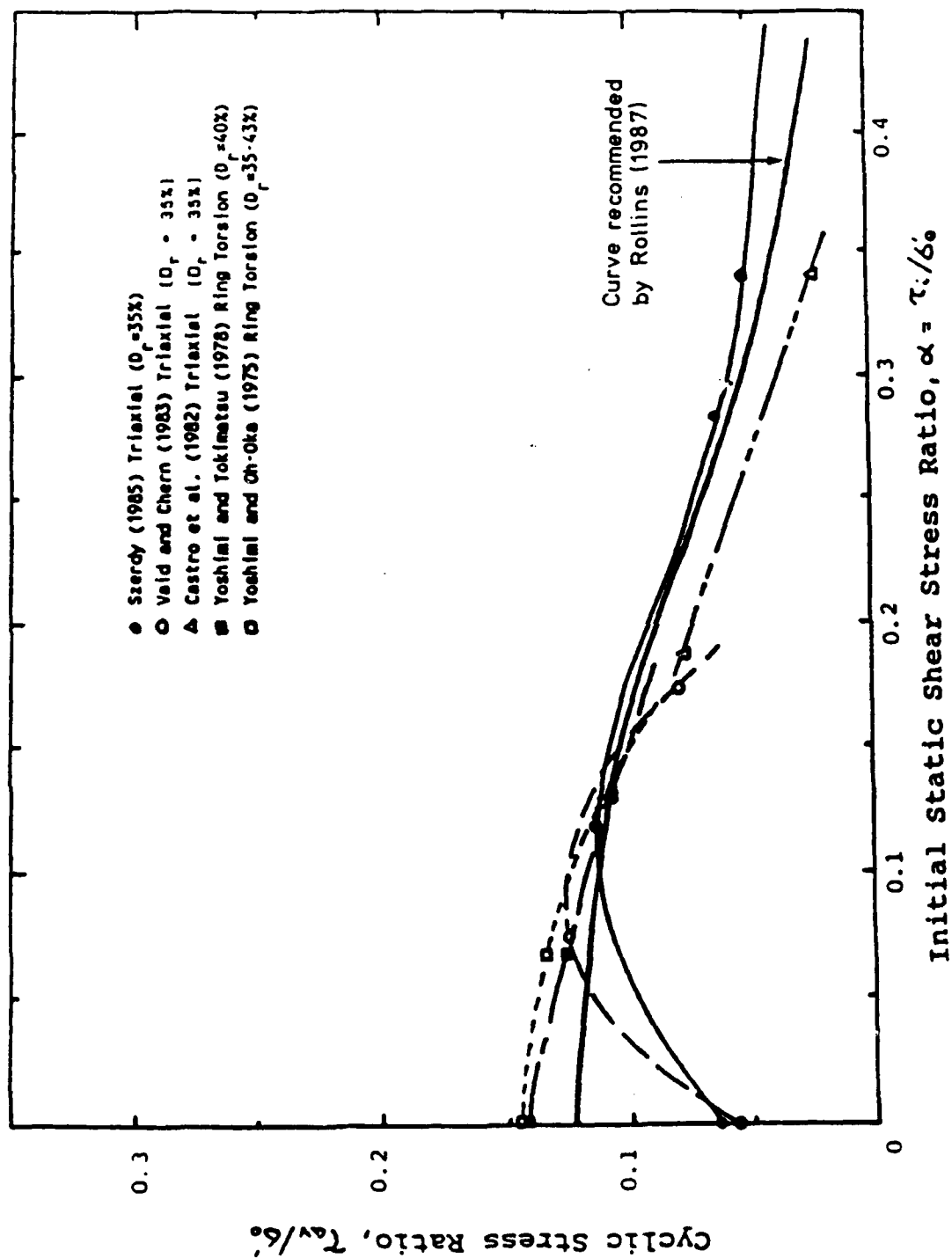


Figure B92a. Applied cyclic stress ratio versus initial static stress ratio for failure in 10 cycles in loose sand samples (from Rollins, 1987)

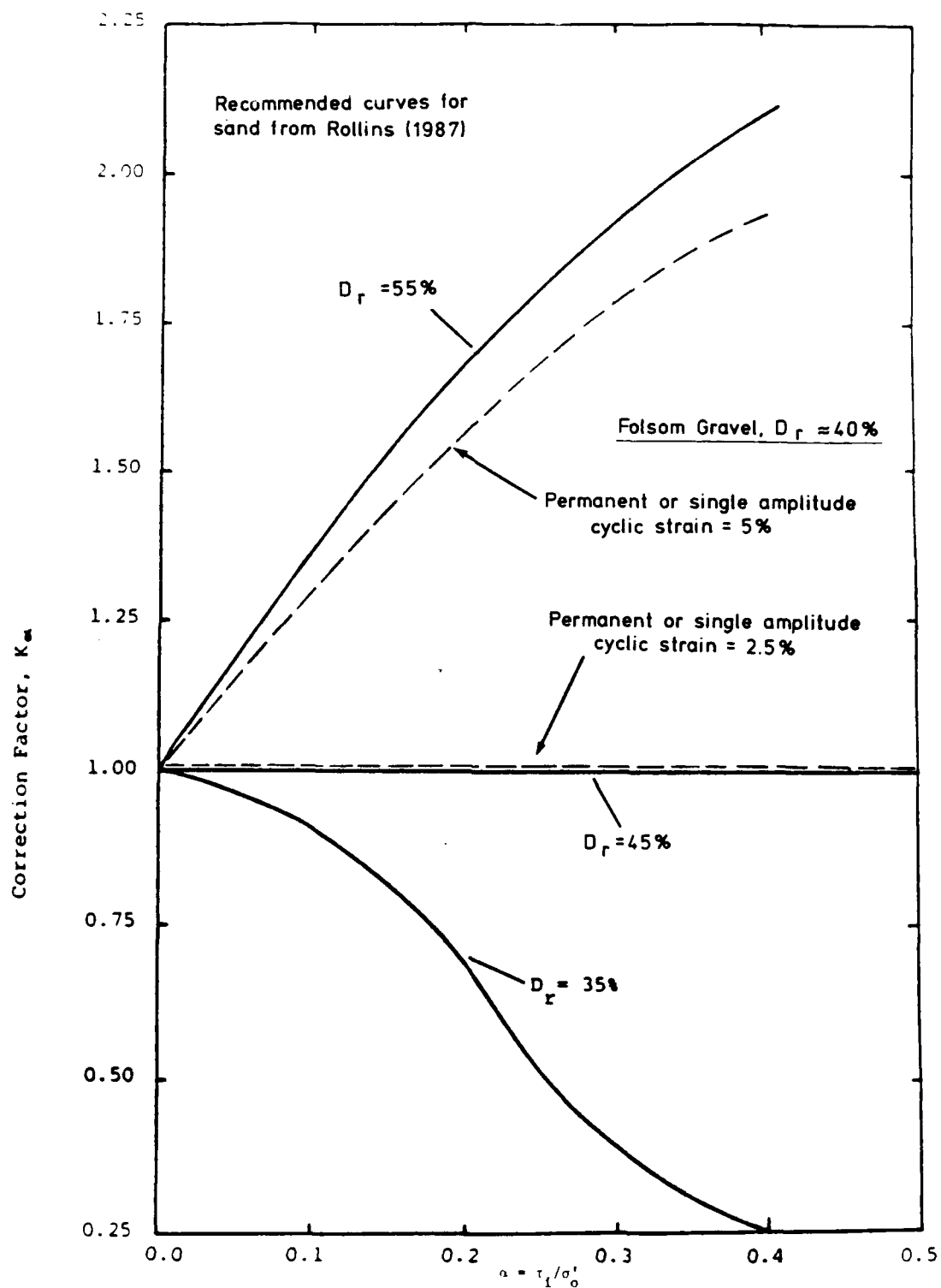


Figure B92b. Initial static stress ratio,  $\alpha = \tau_1/\sigma'_0$  versus initial static stress correction factor,  $K_\alpha$  (from Rollins, 1987)

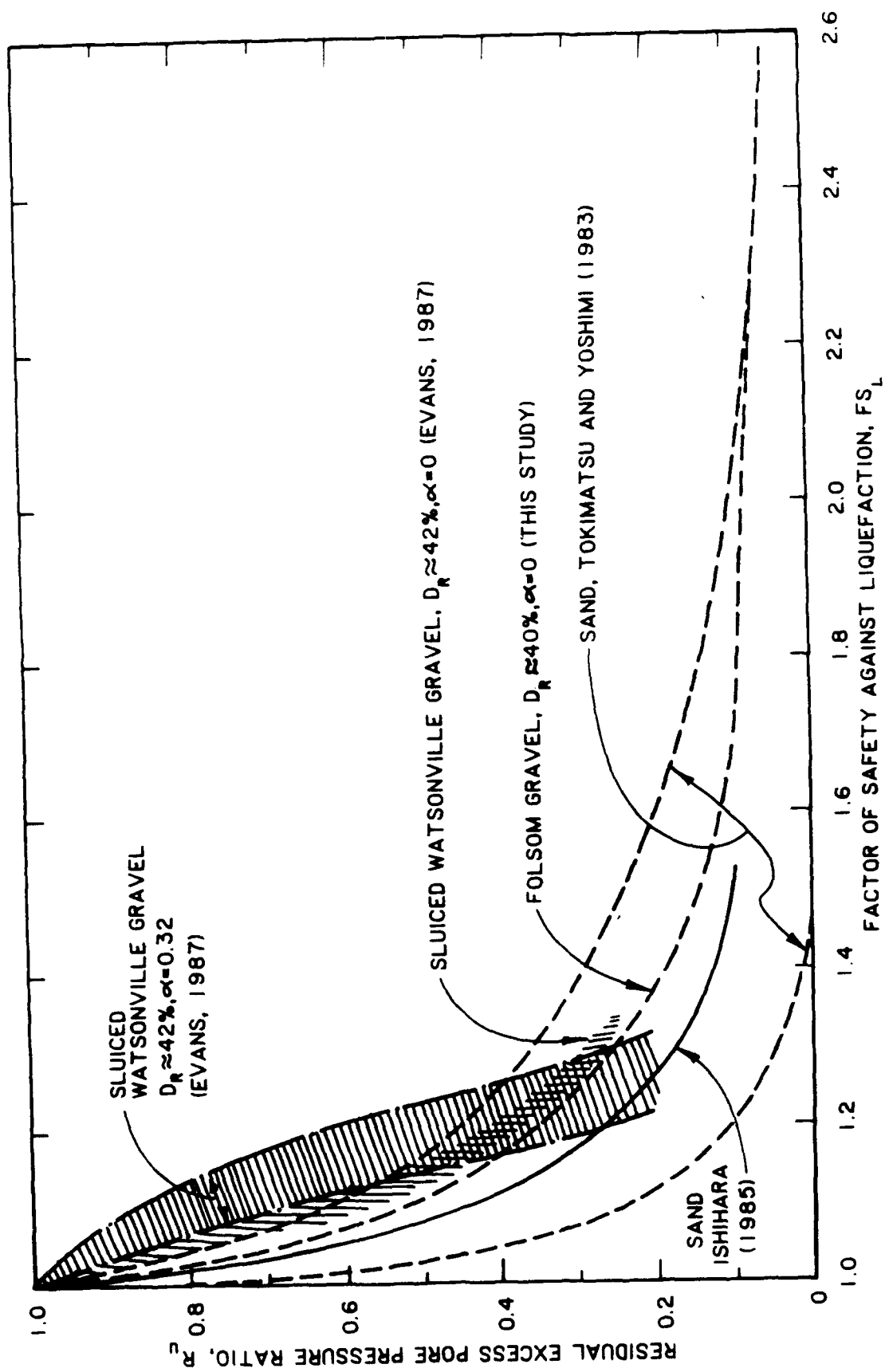


Figure B93. Comparison of  $R_u$  versus  $FS_L$  relationship for Folsom gravel ( $D_R \approx 40$  percent) with other data for sands and gravel



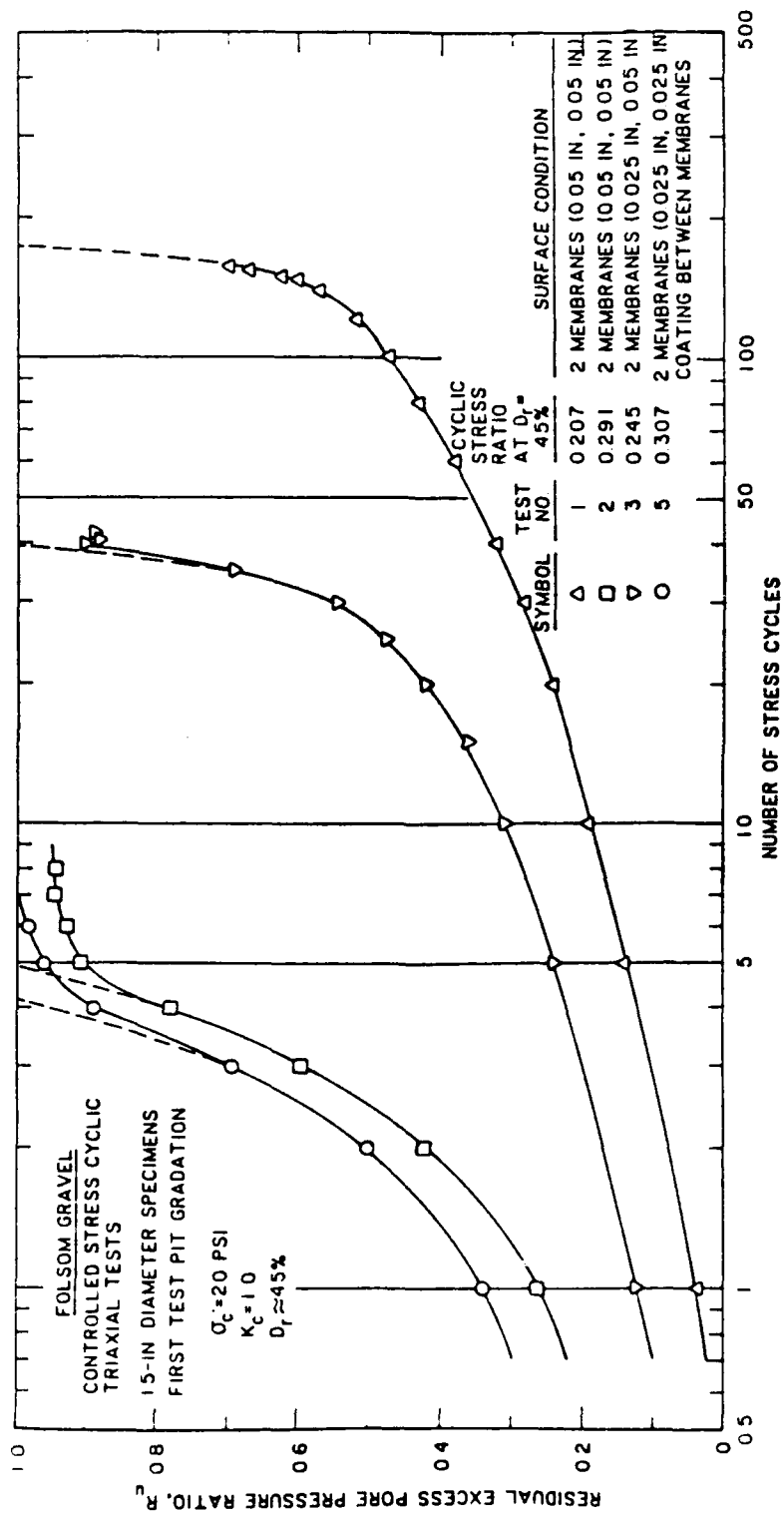


Figure B94. Residual excess pore pressures developed in Tests 1, 2, 3, and 5

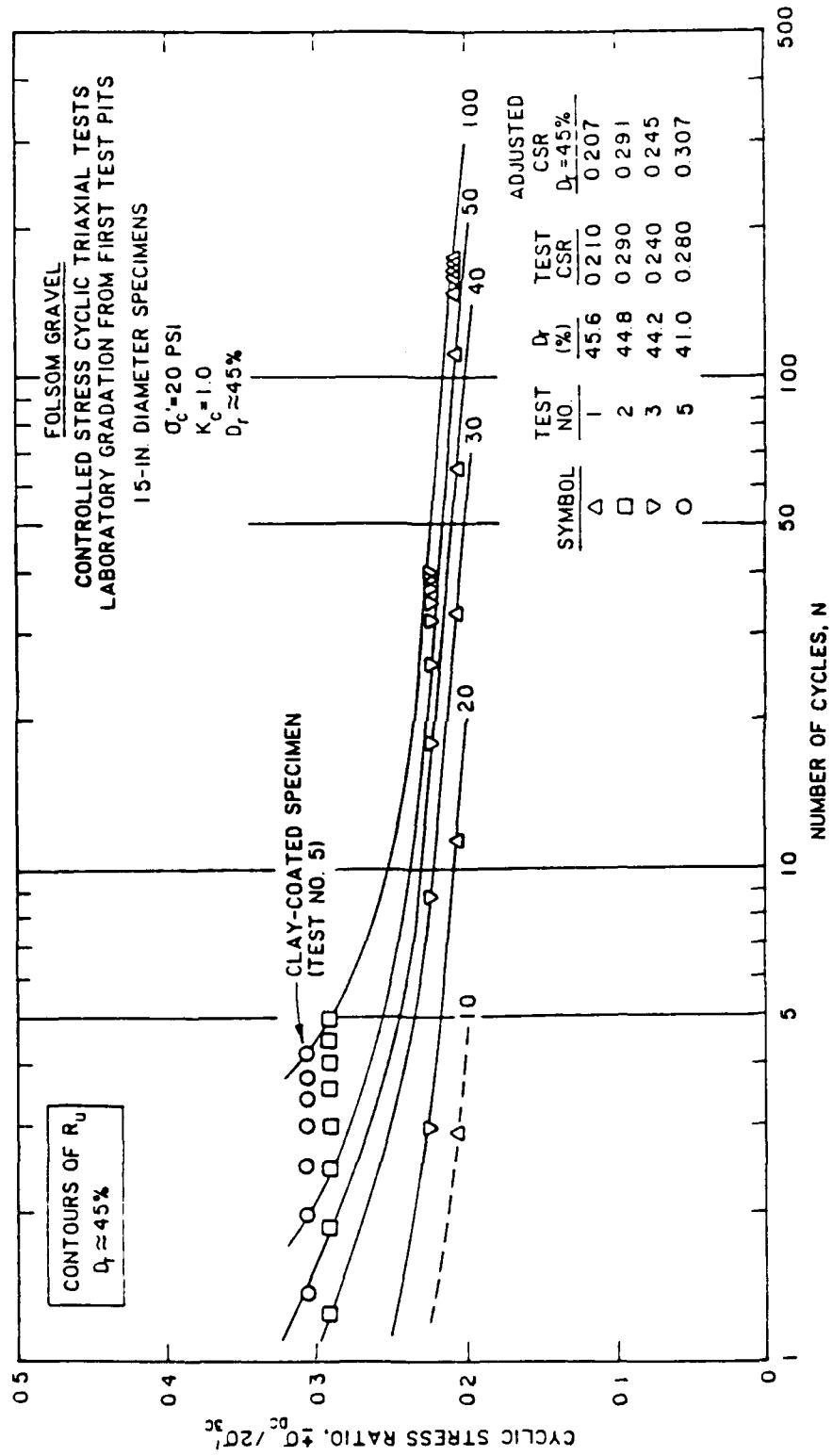


Figure B95. Residual excess pore pressure contours for Tests 1, 2, 3, and 5

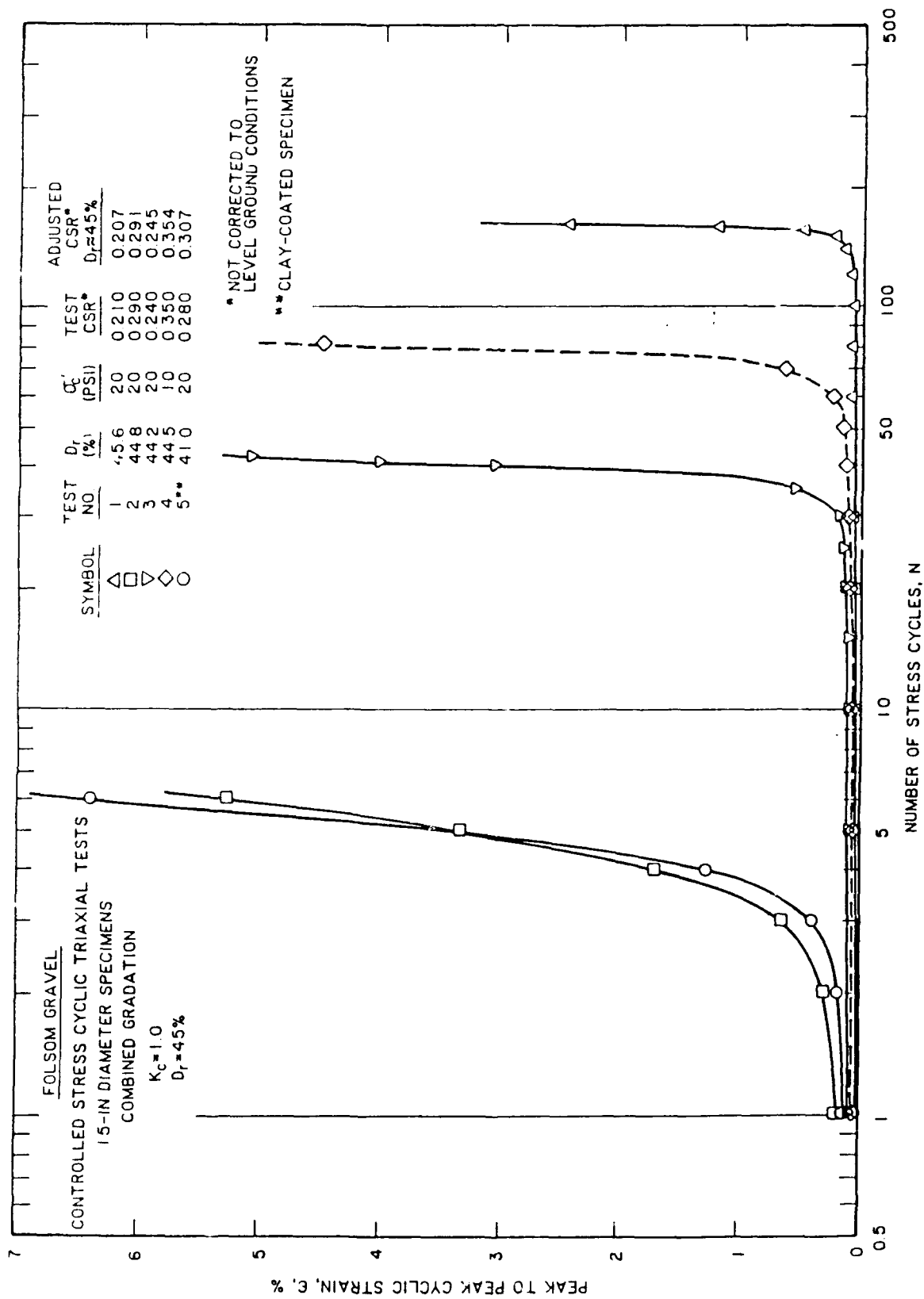


Figure B96. Development of peak to peak cyclic strain with each stress cycle

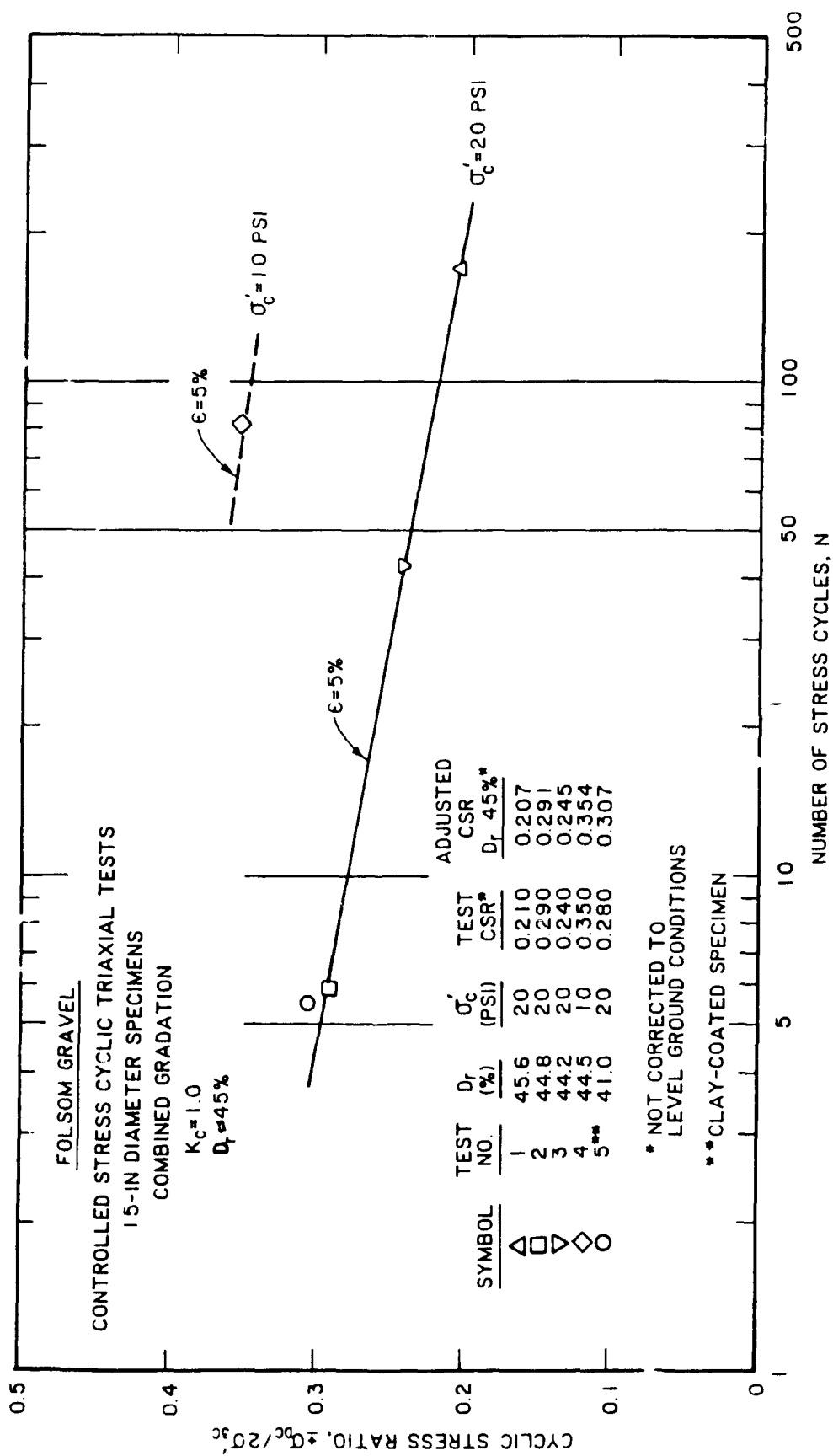


Figure B97. Contours of peak to peak cyclic strain

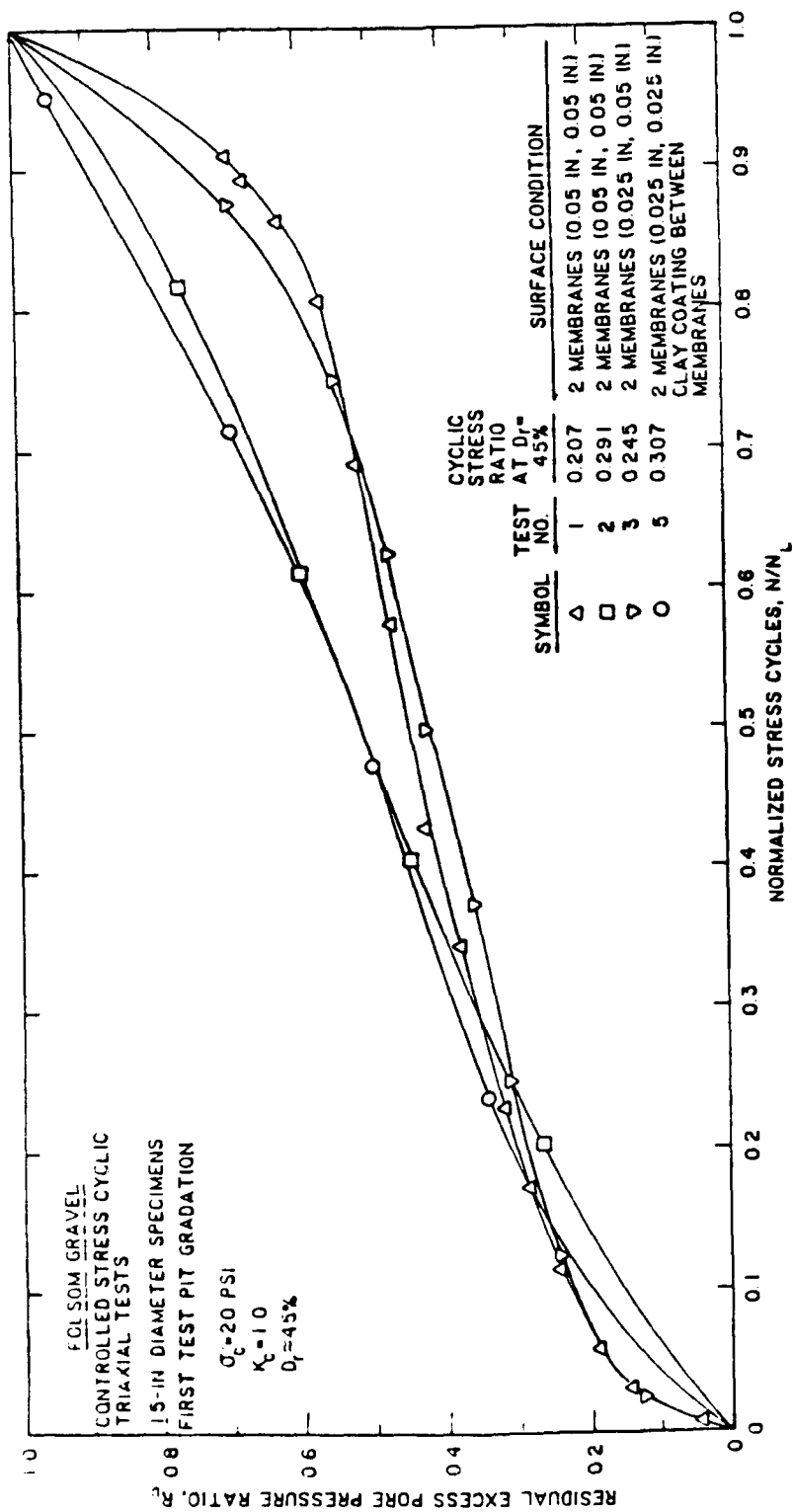


Figure B98. Residual excess pore pressure ratios versus normalized stress cycles for Test 1, 2, 3, and 5

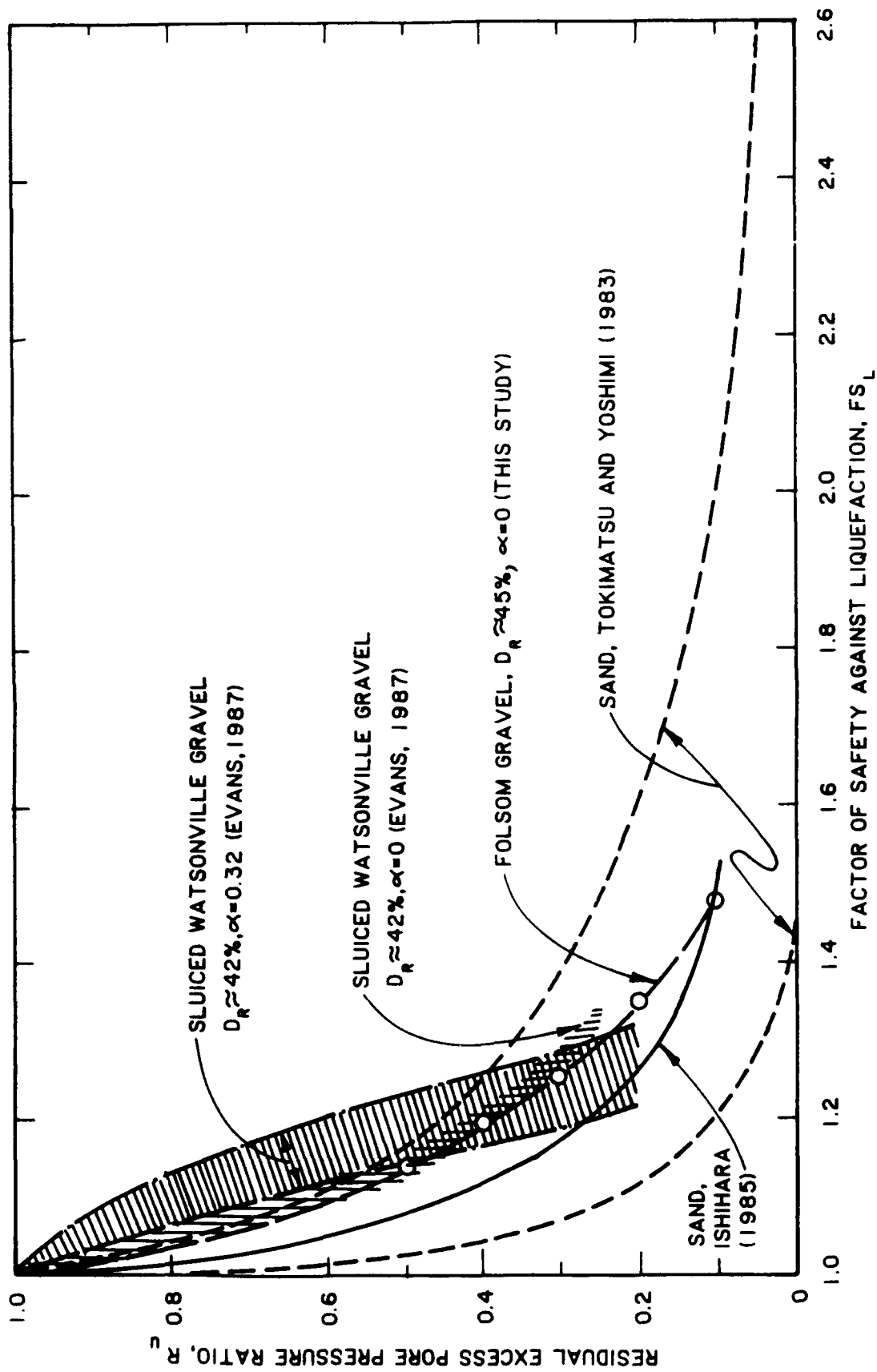


Figure B99. Comparison of  $R_u$  versus  $FS_L$  relationship for Folsom gravel ( $D_R \approx 45$  percent) with other data for sands and gravel